Wheel Speed Distribution Control and its Effect on Vehicle Handling

by

Mahmoud Attia Mohamed El-Bayoumi, *MSc., BSc.*

Submitted in accordance with the
Requirements of the degree of
Doctor of Philosophy

The University of Leeds
School of Mechanical Engineering

May 2007

To my Parents, Eisha,

Merna, Mayar,

Maya and Marwa

Abstract

The current work aims at bridging the gap between the current vehicle handling characteristics and the future demands of higher vehicle handling performance, required to guarantee higher safety and facilitate the application of autonomous driving, platooning and automated highways systems. For this task a state of the art vehicle chassis control system known as "Wheel Speed Distribution Control" (WSDC) has been proposed.

WSDC in principle relies on controlling the vehicle driven wheel speeds to enforce better vehicle handling performance. The WSDC system capacity has been investigated using numerical simulation. Therefore, an innovative vehicle handling simulation model has been developed from first principles. It employs the Magic Formula (MF) tyre model for combined slip, has 23 degrees of freedom and includes more than 60 vehicle handling parameters.

The vehicle handling model has been developed using the novel Cartesian Geometric Translation (CGT) technique which employs geometry, trigonometry, Cartesian coordinates and finite difference approximation in the time domain to facilitate development of high speed models. The model has been built using the BASIC© programming code in the DOS© environment and optimised to meet the novel Model Predictive Control (MPC) based feedforward WSDC yaw rate controller requirements, such as small code size (less than 35 kb) and processing speed faster than real time. The simulation results validated the WSDC principles as it showed the capacity of WSDC to enforce the desired yaw rates, with acceptable driven wheel longitudinal forces.

To put WSDC into practice, an original hardware "Wheel Speed Distribution Differential" (WSDD) design has been developed and optimised for lower speed, torque, power, production and maintenance requirements. It has the capacity to precisely differentiate the driven wheels speed under the influence of a DC motor with relatively small power requirements. It has linear speed and torque characteristics, which facilitate its control. It also has been developed to allow many beneficial differential modes. The simulation results of the whole WSDC system have clearly demonstrated that it can in fact achieve its development target of feasibly enhancing vehicle handling performance.

BLANK IN ORIGINAL

Acknowledgement

I would like to thank my supervisor Prof. David Barton for his guidance and support and my previous supervisors, Prof. David Crolla and Dr. Michel Brown. Thanks must go to the members of Egyptian Student Society in Leeds University for their support and encouragement. Also, thanks should go to various friends in room G54b in School of Mechanical Engineering for their support.

Outside work, thanks go to my family and friends for their long-term support and encouragement. Also, admiration goes to the Egyptian poet Callimachus (300-240 BC) for his inspiration "Do not drive your chariot upon the common tracks of others, nor down a road that is wide, but along untrodden paths, though yóu'll drive a narrower course".

ALL MISSING
PAGES ARE
BLANK
IN
ORIGINAL

Table of Contents

List of Figures

List of Tables

Abbreviations

4WD	Four Wheel Drive
4WS	Four Wheel Steering
ABS	Anti-lock Braking System
AYC	Active Yaw Control
B&B	Branch and Bound optimisation technique
BASIC	Beginners All purpose Symbolic Instruction Code
BFDC	Brake Force Distribution Control
CG	Centre of Gravity
CGT	Cartesian Geometric Translation
CVT	Continuous Variable Transmission
DC	Direct Current
DOS	Disk Operating System
DYC	Direct Yaw Control
DSA	Dynamic Spark Advance
FWD	Front Wheel Drive
FWS	Front Wheel Steering
IP	Ignition Point
LSD	Limited Slip Differential
MF	Magic Formula tyre model for combined slip
MPC	Model Predictive Control
RWD	Rear Wheel Drive
RWS	Rear Wheel Steering
SSF	Static Stability Factor
TC	Traction Control
TCS	Traction Control System
TFD	Traction Force Distribution
TFDC	Traction Force Distribution Control
WSD	Wheel Speed Distribution
WSDC	Wheel Speed Distribution Control
WSDD	Wheel Speed Distribution Differential

Nomenclature

Symbol	Description
$\Delta\theta_{CG}$	vehicle rotation angle during time frame
ΔT	torque difference between driven wheels torque
Δt	time frame step
ΔF_x	half the driven wheels control force
Δx_{Fl}	front-left wheel longitudinal translations in its local coordinates
Δx_{Fr}	front-left wheel longitudinal translations in its local coordinates
Δx_{Rl}	front-right wheel longitudinal translations in its local coordinates
Δx_{Rr}	front-right wheel longitudinal translations in its local coordinates
Δy_{Fl}	rear-left wheel lateral translations in its local coordinates
Δy_{Fr}	rear-left wheel lateral translations in its local coordinates
Δy_{Rl}	rear-right wheel lateral translations in its local coordinates
Δy_{Rr}	rear-right wheel lateral translations in its local coordinates
Θ	vehicle axle to X axis angle
Θ_{CG0}	time frame initial vehicle axle angle to global X axis
Θ_{CG1}	time frame final vehicle axle angle to global X axis
Φ	total manoeuvre angle
Φ_i	instantaneous manoeuvre angle
Ω_{Rl}	rear left wheel rotation speed
Ω_{Rr}	rear right wheel rotation speed
α_F	front axle slip angle
α_{Fl}	slip angle of front-left tyre
α_{Fr}	slip angle of front-right tyre
α_R	rear axle slip angle
α_{Rl}	slip angle of rear-left tyre
α_{Rr}	slip angle of rear-right tyre
γ	wheel camber angle
δ	steering angle
δ_f	nominal front wheel steering angle
δ_{Fl}	front left wheel steering angle

δ_{Fr}	front right wheel steering angle
δ_{Rl}	rear left wheel steering angle
δ_{Rr}	rear right wheel steering angle
δ_i	instantaneous steering angle
ζ_2	vehicle yaw angle within a time frame Δt
θ_0	time frame initial angle between vehicle axle and local x axis
θ_1	time frame final angle between vehicle axle and local x axis
θ_A	vehicle yaw angle according to Ackerman steering in X-Y coordinates
θ_{Fl}	front-left tyre travelling direction angle to local x coordinate
θ_{Fr}	front-right tyre travelling direction angle to local x coordinate
θ_{Rl}	rear-left tyre travelling direction angle to local x coordinate
θ_{Rr}	rear-right tyre travelling direction angle to local x coordinate
$\dot{\theta}$	yaw rate
$\dot{\theta}_0$	time frame final vehicle yaw rate
$\dot{\theta}_1$	time frame final vehicle yaw rate
$\dot{\theta}_A$	vehicle yaw rate according to Ackerman steering
$\dot{\theta}_e$	the yaw rate error from Ackerman
$\ddot{\theta}$	time frame vehicle yaw acceleration
$\ddot{\theta}_C$	correction yaw acceleration
σ_y	tyre relaxation length
σ^*_y	tyre relaxation distance
ψ	angle to x axis
ψ_0	initial time frame angle to x axis
ψ_1	final time frame angle to x axis
$\ddot{\psi}_z$	angular acceleration around z axis
ω_{Cn}	rotational speed of differential case number n, (n=1, 2 ..etc)
ω_{Gn}	rotational speed of gear number n, (n=1, 2 ..etc)
ω_{Rr}	rear right wheel rotational speed
ω_{Rl}	rear left wheel rotational speed
ω_{Sn}	rotational speed of shaft number n, (n=1, 2 ..etc)
ω_t	nominal vehicle wheel speed
a	front axle to vehicle CG distance
b	rear axle to vehicle CG distance

$C_{\alpha f}$	front axle cornering stiffness
$C_{\alpha r}$	rear axle cornering stiffness
C_n	differential case number n, (n=1, 2 ..etc)
$d\omega$	wheel rotational speed percentage difference
deg	degree
F_{xCG}	longitudinal force at the vehicle CG
F_{xCG0}	time frame initial longitudinal force at the vehicle CG
F_{xCG1}	time frame final longitudinal force at the vehicle CG
F_{xFl0}	time frame initial forces of front left tyre in its x direction
F_{xFr0}	time frame initial forces of front right tyre in its x and y direction
F_{xRl0}	time frame initial forces of rear left tyre in its x direction
F_{xRlC}	rear left driven wheel traction force with control ΔF_x
F_{xRr0}	time frame initial forces of rear right tyre in its x direction
F_{xRrC}	rear right driven wheel traction force with control ΔF_x
F_{yCG}	lateral force at the vehicle CG
F_{yCG0}	time frame initial lateral force at the vehicle CG
F_{yCG1}	time frame final lateral force at the vehicle CG
F_{yf}	front lateral force
F_{yFl}	front left tyre lateral force
F_{yFl0}	time frame initial forces of front left tyre in its y directions
F_{yFr}	front right tyre lateral force
F_{yFr0}	time frame initial forces of front right tyre in its y directions
F_{yr}	rear lateral force
F_{yRl}	rear left tyre lateral force
F_{yRl0}	time frame initial forces of rear left tyre in its y directions
F_{yRr}	rear right tyre lateral force
F_{yRr0}	time frame initial forces of rear right tyre in its y directions
F_{zFl1}	time frame final vertical load of front left tyre
F_{zFr1}	time frame final vertical load of front right tyre
F_{zRl1}	time frame final vertical load of rear left tyre
F_{zRr1}	time frame final vertical load of rear right tyre
Gn	gear number n, (n=1, 2 ..etc)
I	moment of inertia

k_{Fl}	longitudinal slip of front
k_{Fr}	longitudinal slip of front
k_{Rl}	longitudinal slip of rear
k_{Rr}	longitudinal slip of rear
L	wheel base
M_{CG}	moment about CG
M_{CG0}	time frame initial moment at the vehicle CG
md	maximum steering angle of the manoeuvre
mt	manoeuvre time
n	time frame number
N_{Gn}	number of teeth of gear no. n, (n=1, 2 ..etc)
R	radius
R_0	unloaded tyre radius
R_F	radius of turn at front axle of RWS vehicle
R_R	radius of turn at rear axle of FWS vehicle
r_{Fl}	front left wheel distance to vehicle CG
r_{Fr}	front right wheel distance to vehicle CG
r_{Rl}	rear left wheel distance to vehicle CG
r_{Rr}	rear right wheel distance to vehicle CG
Sn	shaft number n, (n=1, 2 ..etc)
T_{Cn}	torque of differential case no. n, (n=1, 2 ..etc)
TCS	traction Control Systems
T_C	torque of control shaft
T_D	drive shaft torque
T_{D1}	conventional component of the differential drive shaft torque
T_{D2}	control component of the differential drive shaft torque
T_{Fl}	distance travelled by front left tyre
T_{Fr}	distance travelled by front right tyre
T_{Gn}	torque of gear no. n, (n=1, 2 ..etc)
T_L	left driven wheel torque
T_R	right driven wheel torque
T_{Rl}	distance travelled by rear left tyre
T_{Rr}	distance travelled by rear right tyre

T_{Sn}	torque of shaft no. n, (n=1, 2 ..etc)
t_l	lateral CG to left wheel distance
t_r	lateral CG to right wheel distance
U_{Fl1}	time frame final longitudinal velocity of front-left wheel
U_{Fr1}	time frame final longitudinal velocity of front-right wheel
U_{Rl1}	time frame final longitudinal velocity of rear-left wheel
U_{Rr1}	time frame final longitudinal velocity of rear-right wheel
U_{RlS}	rear left wheel longitudinal slip velocity
U_{RrS}	rear right wheel longitudinal slip velocity
u	longitudinal velocity
$\dot{u}$	longitudinal acceleration
u_0	Initial vehicle forward velocity
u_0	initial longitudinal velocities of a time frame
u_1	final longitudinal velocities of a time frame
u_v	vehicle time frame velocity
v	lateral velocity
v_0	time frame initial vehicle lateral velocity
$\dot{v}$	time frame vehicle lateral acceleration
v_0	time frame initial lateral velocity
v_1	time frame final lateral velocity
v_A	vehicle lateral velocity according to Ackerman steering
V_{Fl1}	time frame final lateral velocity of front-left tyre
V_{Fr1}	time frame final lateral velocity of front-right tyre
V_{Rl1}	time frame final lateral velocity of rear-left tyre
V_{Rr1}	time frame final lateral velocity of rear-right tyre
X_{CG}	vehicle CG location on global X coordinate
X_{CG0}	time frame initial vehicle CG location on global X coordinate
X_{CG1}	time frame final vehicle CG location on global X coordinate
x_{CG0}	time frame initial vehicle CG location on local x coordinate
x_{CG1}	time frame final vehicle CG location on local x coordinate
x_{f0}	time frame initial vehicle front location on local x coordinate
x_{f1}	time frame final vehicle front location on local x coordinate
x_{Fl0}	time frame initial front left wheel x location

x_{Fr0}	time frame initial front right wheel x location
x_{Fl1}	time frame final front left wheel x location
x_{Fr1}	time frame final front right wheel x location
x_{r0}	time frame initial vehicle rear location on local x coordinate
x_{r1}	time frame final vehicle rear location on local x coordinate
x_{Rl0}	time frame initial rear left wheel x location
x_{Rr0}	time frame initial rear right wheel x location
x_{Rl1}	time frame final rear left wheel x location
x_{Rr1}	time frame final rear right wheel x location
Y_{CG}	vehicle CG location on global Y coordinate
Y_{CG0}	time frame initial vehicle CG location on global Y coordinate
Y_{CG1}	time frame final vehicle CG location on global Y coordinate
y_{CG0}	time frame initial vehicle CG location on local y coordinate
y_{CG1}	time frame final vehicle CG location on local y coordinate
y_{f0}	time frame initial vehicle front location on local y coordinate
y_{f1}	time frame final vehicle front location on local y coordinate
y_{Fl0}	time frame initial front left wheel y location
y_{Fr0}	time frame initial front right wheel y location
y_{Fl1}	time frame final front left wheel y location
y_{Fr1}	time frame final front right wheel y location
y_{r0}	time frame initial vehicle rear location on local y coordinate
y_{r1}	time frame final vehicle rear location on local y coordinate
y_{Rl0}	time frame initial rear left wheel y location
y_{Rr0}	time frame initial rear right wheel y location
y_{Rl1}	time frame final rear left wheel y location
y_{Rr1}	time frame final rear right wheel y location

Chapter 1

Introduction

1.1 Background

The motor vehicle is one of the most important and successful products in the 20th century, as it has transformed many aspects of human life, [1]. Consequently a lot of attention has been paid to its problems and huge efforts made towards its development, yet there is still the need for more research. With casualties of 271,017 on Britain's roads in 2005, of which 3,201 were fatalities, motor vehicles were declared among the most life threatening transportation facilities, [2]. Human factors were always questionable in vehicle accidents as 65% of all accidents in the UK in 2005 were caused by human error alone, and in another 30% of accidents human error was associated with another factor, [2].

Researchers have thought an answer to the safety issue would be the introduction of advanced driving technologies, such as vehicle autonomous driving in which a computer would drive the vehicle aided by a set of sensors, [3] [4] [5]. Others suggested employing platooning concepts, in which vehicles would travel on highways as a closely packed platoon, [6] [7] [8]. Platooning demonstrations were held in Japan in 1996, [9], and US in 1997 with 22 vehicles carrying passengers and driving autonomously, [2]. Platooning and convoy demonstrations held in Japan, US and other countries showed that automatic driving technology has reached the level of practical application, so long as road safety and vehicle reliability are assured, [9].

In both autonomous driving and platooning systems, the vehicle has to be able to travel under computer control at high speeds. Vehicles travelling at high speeds raise issues about the reliability of the response to steering commands, termed "vehicle handling". This issue has always been known but it has not been as compelling in human driving especially at low driving speeds.

The main factors affecting the quality of vehicle handling are vehicle dynamics, tyre characteristics and road factors. For a vehicle to negotiate a road turn, it needs to travel laterally and to rotate around its CG; to develop lateral and yaw accelerations requires lateral force and yaw moments respectively. As the vehicle turns at higher speeds or higher steering angles, it needs to develop higher lateral forces and higher yaw moments. Regrettably the tyre, by its basic design, deviates non linearly from its intended path to generate the lateral forces and the larger the lateral force required, the larger the deviation is.

In the conventional vehicle, the driver can only influence the steering angles of steered wheels. By applying a steering angle to the wheels, the tyre heading direction is shifted from its travelling direction, causing the development of lateral force. Consequently, the vehicle develops yaw moment and lateral forces at the non-steered wheels.

On the other hand, the potential role of longitudinal tyre forces in vehicle handling is prevented by the vehicle conventional differential that insures, by design, that both driven wheels receive the same amount of longitudinal traction forces. Accordingly, they can not generate a yaw moment, so the vehicle yaw moment is the result of front and rear wheel axle lateral force moments about the vehicle CG. This link is not constructive as they are both needed for turning and the levels of lateral forces required would not, necessarily, result in the required yaw moment. Also this link increases the burden of front wheel axle lateral forces and reduces the rear wheel axle lateral load. This leads to the poor allocation of the available wheel lateral force generating capacity.

The gap between the generated and required lateral forces and yaw moments is usually much more apparent at higher steering angles or higher vehicle speeds. This gap results in the vehicle deviating from its intended path, which causes problems to autonomous driving techniques. The problems come from the computational overhead needed to track the vehicle path, detect the path deviation and correct it at high speed with only very small margin of error allowed. This correction would be done through manipulating the steering angle. This would be further complicated by the tyre characteristics that are affected non-linearly by the large number of vehicle, road and tyre related factors and are accordingly blamed for the majority of vehicle handling problems.

Many approaches to solve this problem have been made. Some researchers focused on bridging the gap between needed and available lateral forces and yaw moments, through reducing the vehicle need for lateral forces and yaw moments. This was done by limiting engine traction forces available, by means of "Traction Control Systems" (TCS), which are reviewed in section 2.2.1.

Other researchers focused on decoupling yaw moment from lateral forces, through developing a supporting yaw moment to enhance vehicle handling, using different approaches. Some distributed the vehicle traction forces between the left and right vehicle sides, through "Traction Force Distribution Control" (TFDC). Other researchers apply braking force to the appropriate left or right vehicle sides, so-called "Brake Force Distribution Control" (BFDC), to generate the required yaw moment. Others employed different hardware to directly control the yaw rate, such as in "Direct Yaw Control" (DYC). All these systems, reviewed in section 2.2.2, were found to enhance vehicle handling, but they also have difficulties.

The TCS technique relies on limiting the vehicle speed, therefore it may not be acceptable for the futuristic vehicle demands. Also, BFDC would eventually reduce the vehicle speed and accordingly may also not be acceptable, while the TFDC would not function in the case of no traction forces being applied to the driven wheels. Some researchers coordinate both systems to achieve a better performance, but again a traction force is required to have such coordination. DYC systems vary

in performance according to their hardware design but they suffer from the nonlinearity of their components. Therefore all the different systems, TFDC, BFDC and DYC, suffer from different hardware deficiencies and control problems, and consequently have not been widely employed.

1.2 Current Work

The current research is focused on developing a much more coherent concept, termed as "Wheel Speed Distribution Control" WSDC. In this concept the left and right side driven wheels speeds are differentiated under computer control around their mean rotational speed to generate different longitudinal force / yaw moment with the aim of enhancing vehicle handling performance. In this system the driven wheel would apply traction or braking forces depending on their speeds relative to the vehicle speed.

The individual wheel speeds differentiating around the mean vehicle speed would allow WSDC to function with and without traction or braking forces and without self induced acceleration or deceleration. Also, the WSDC system's use of mean wheel speed, Ackerman steering geometry and Ackerman path as references, would simplify the control requirements and facilitate the application of control constraints, which would help in developing a fail safe system. Also, given that rotational speed measurement and control is more established than torque measurement and control, the WSDC system would be in general much more feasible than force based systems to control and adapt.

This technique would also allow for the comprehensive use of the full tyre longitudinal forces range to enhance vehicle handling. It would enable the generation of the maximum possible yaw moment, as one wheel would develop maximum traction force while the other (on the other track) develops the maximum braking force. This torque level would surpass the capacity of competitive systems. The WSDC system's high capacity to follow a steering command would greatly facilitate

autonomous driving and would also be beneficial to human drivers in terms of better control of vehicle handling.

The first stage of the work has been dedicated to prove the above concepts. To achieve this task a vehicle handling simulation model has been developed to investigate the WSDC performance benefits. Also, to allow the model the capacity to be used as an onboard control model through Model Predictive Control (MPC) strategy, this model has been developed using a novel Cartesian Geometric Translation (CGT) modelling technique. The Finite Difference Approximation (FDA) technique was employed in the time domain, along with geometric and trigonometric equations to investigate the vehicle incremental translations in the Cartesian coordinates.

In the second stage, a novel WSDC controller based on the MPC strategy has been introduced. This controller employs the previously mentioned vehicle handling model, along with inverse dynamics, Ackerman steering geometry and a Magic Formula (MF) tyre model to determine the required wheel speeds in a feed forward fashion.

In the third stage, of the work, a novel hardware system, termed the Wheel Speed Distribution Differential (WSDD), has been developed from first principles to allow the application of WSDC principles. This mechanism also facilitates the control task as it exhibits linear performance and has minimal power requirements.

In the fourth stage, the complete WSDC model is demonstrated. In this, the vehicle handling model has been fitted with the WSDC controller and the WSDD hardware model. The complete WSDC model is used to investigate the WSDC vehicle handling performance under a set of standard manoeuvres, in which the benefits are evident.

1.3 Thesis Structure

The thesis is organised into nine Chapters. In this section, a list of the remaining eight Chapters and a brief description of each is given.

Chapter two," Literature review", introduces a review of the related literature. It also defines the current work aims and objectives.

Chapter three, "CGT half vehicle handling model", introduces the novel modelling technique known as Cartesian Geometric Translation (CGT). The technique is proved through building a bicycle (half vehicle) handling model and comparing its results with published data.

Chapter four, "The tyre model", presents the Magic Formula (MF) tyre model used for combined slip and its treatment to suit the current work.

Chapter five, "CGT full vehicle handling model", presents the development of the half vehicle handling model into a full vehicle handling model.

Chapter six, "Wheel speed distribution controller", presents the development of the MPC based WSDC controller.

Chapter seven, "Wheel speed distribution hardware", presents the development of the novel hardware, WSDD. It also describes its speed and torque characteristics, its power requirements and its potential benefits.

Chapter eight, "Wheel speed distribution control system", presents the full vehicle handling model equipped with the WSDD. A Full set of results for the whole system is presented to prove the capability of this system.

Chapter nine, "Conclusions and recommendations", presents the conclusions and recommendations for future work.

Chapter 2

Literature Review

2.1 Vehicle Handling Dynamics

Vehicle handling is the field that investigates vehicle response to various driving commands under different governing conditions. Accordingly it is concerned with all factors affecting the vehicle directional response. Although modern vehicles are equipped with improved handling systems, they still experience many handling performance short comings, especially at high speeds, due to the large number of factors that affect vehicle handling

The safety issues involved with vehicle handling have led to a great deal of research about the parameters affecting vehicle handling [10]. Key vehicle parameters like mass, geometry and mass distribution affect the handling performance. Also, tyre non-linear properties and tyre-road interface, with the large number of factors involved, have been found to cause many handling problems. Vehicle handling proved to be a very sensitive issue as unexpected factors have been found to affect it, such as vehicle body stiffness [11] and, even, the stiffness of the rubber bushings of the steering housing [12]. In the next section a review of the factors that most affect vehicle handling is presented.

2.1.1 Vehicle Related Factors

Mass

Increase in vehicle mass was found to affect the vehicle handling response, especially at high speeds, and cause many of the problems associated with vehicle handling [13] [14]. The higher the vehicle mass, the higher the centrifugal force in cornering, and accordingly the higher the tyre lateral forces required for turning. On the other hand, increase of mass increases the tyre vertical loads and accordingly the tyre roadholding ability. Also, both lateral and vertical tyre forces were found to affect non linearly the tyre slip angle, which affects the vehicle travelling direction, Fig (2.1), [15]. Given that slip angle is the deviation angle between tyre travelling and intended directions, it is one of the most important parameters affecting vehicle directional control and stability [16].

As high vehicle mass causes handling problems especially at high speeds, recent trends in vehicle design have inclined towards its reduction. Various vehicle mass reduction techniques have been investigated to enforce improved handling performance along with fuel economy, such as, employing lightweight materials [17] and advanced mass optimisation of vehicle component design [18].

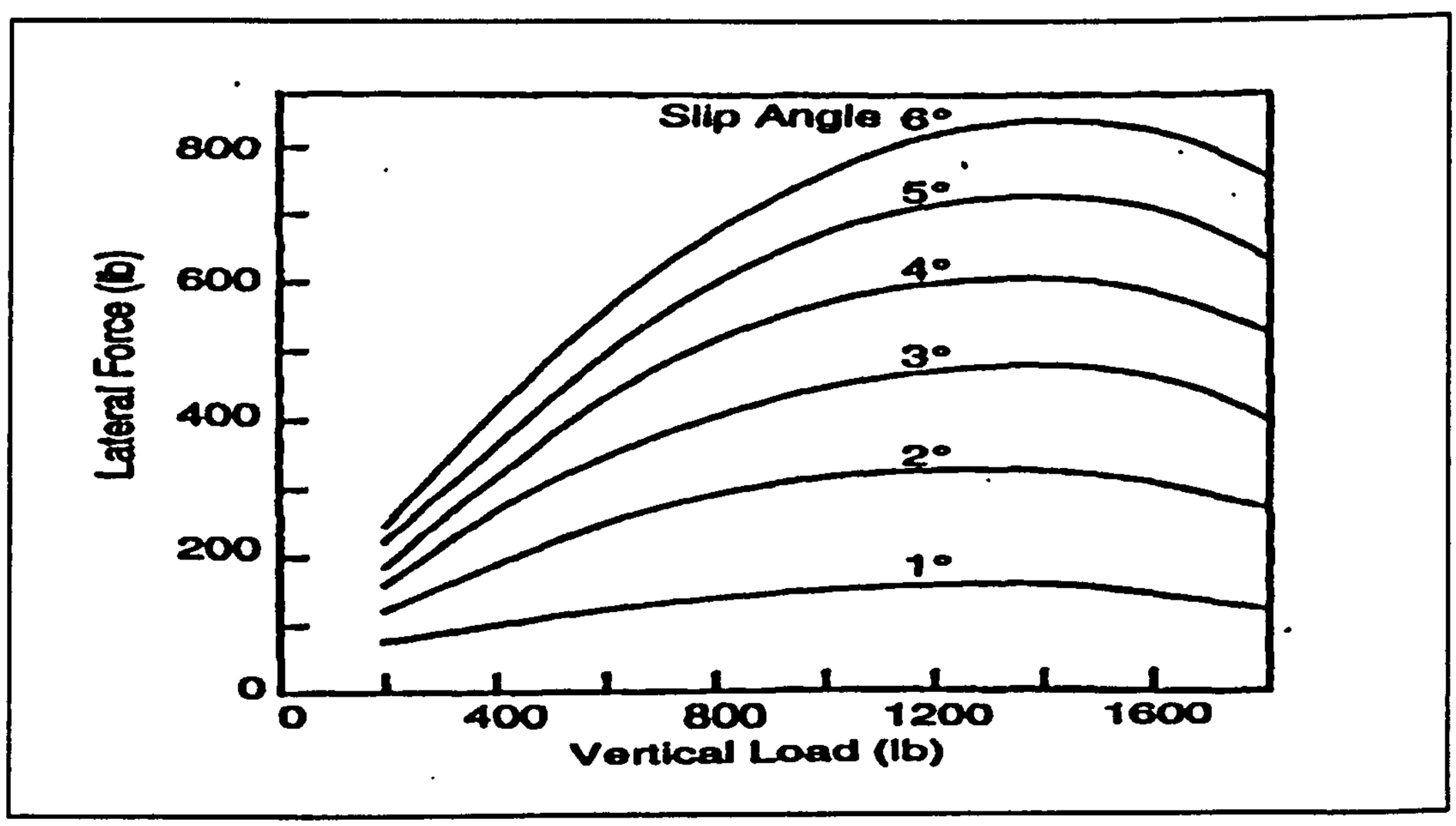

Fig (2.1) Lateral force / vertical load relation with slip angle [15]

On the other hand, vehicle mass reduction increases the ratio between payload mass and the total vehicle mass. This implies that a heavy load may cause a considerable change to vehicle CG location, which, in turn, could result in an unexpected vehicle handling response up to and inducing rollover, especially at high speeds, [19] [20].

Vehicle Geometry

Vehicle body geometry and vehicle mass distribution were found to affect handling performance as they affect vehicle yaw moment of inertia I, tyre vertical loads and CG position. Although a high moment of inertia maintains vehicle stability during straight line travelling at high speeds, it causes high yaw moment requirements in turns, [21]. Figure (2.2), [21] shows the calculation method of vehicle moment of inertia that is evaluated as: -

$$I = \Sigma (m R^2) \qquad (2.1)$$

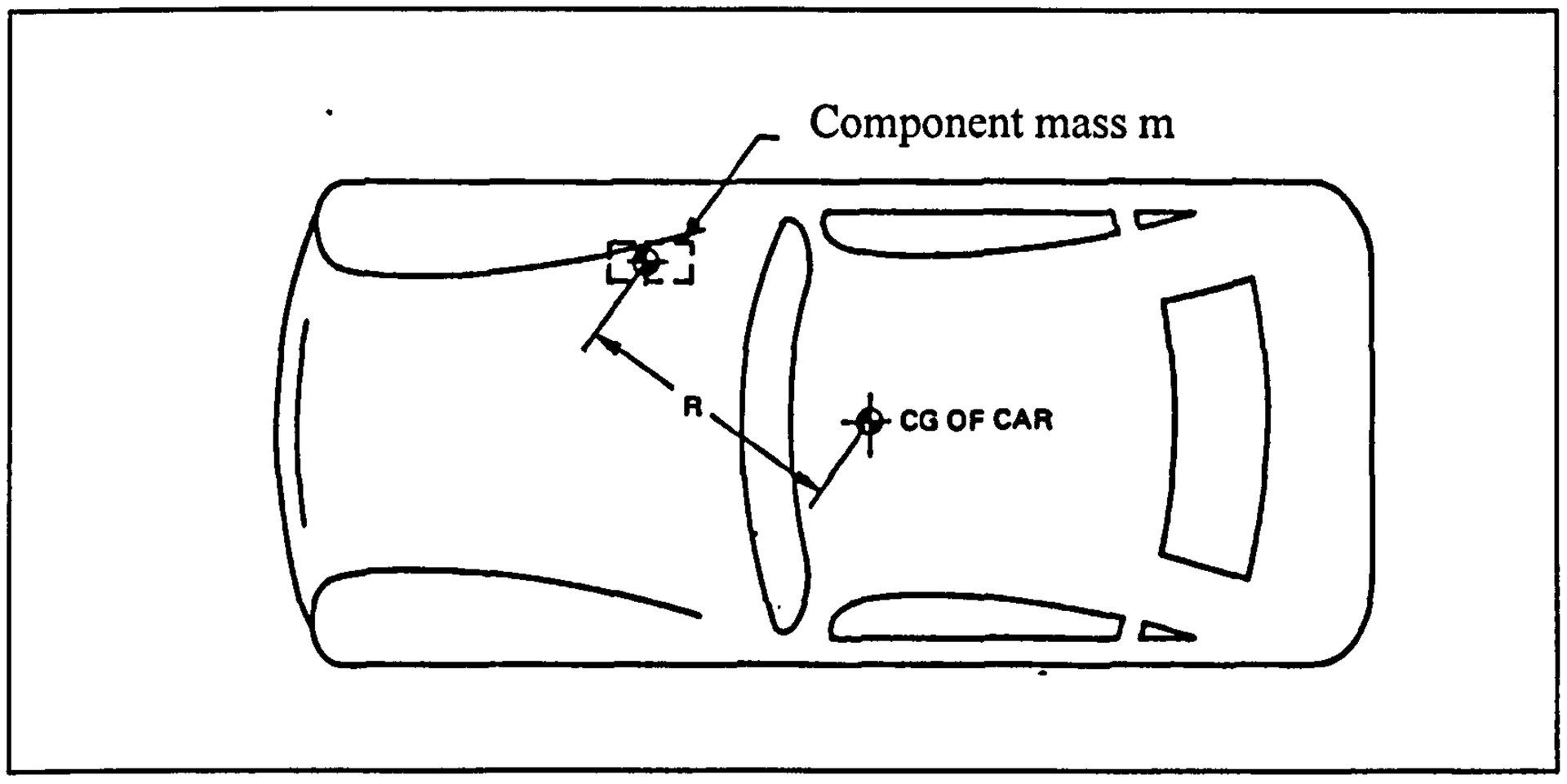

Fig (2.2) Vehicle moment of yaw inertia calculation [21]

Also, unbalanced vehicle mass distribution causes the vehicle CG position to deviate from the longitudinal centre line. This leads to unequal tyre vertical loads, which affect tyre slip angles and accordingly would affect vehicle handling [22] [23]. The lateral deviation of the CG position causes a vehicle steering bias during acceleration and braking, due to the moment the traction and braking forces generate about the vehicle CG. Also, rearward position of vehicle CG, despite tending to increase the traction forces in RWD vehicles [21], causes the vehicle to oversteer in turns, whilst a forward CG position causes it to understeer [15]. Both understeer and oversteer represent vehicle deviation towards larger and smaller turn radius at higher speeds respectively, which degrades vehicle handling performance.

An increase of vehicle CG height also contributes to vehicle handling problems. It increases both lateral and longitudinal load transfer, which degrades vehicle handling characteristics, and could cause the vehicle to roll over. Unfortunately, this effect increases for high speed turns [24] [22] [25].

A theoretical vehicle, with all its mass concentrated at the CG, would not need any yaw moment during turning. Accordingly, the typical vehicle configuration with the engine located far away from vehicle CG does not to help reduce tyre forces resulting from high yaw moment demand.

Suspension specifications

Although suspension springing and damping operates chiefly on the vehicle vertical oscillations, it influences vehicle handling through the distribution of tyre vertical load against the road surface as the tyre loads fluctuate [13]. Also, highly damped suspensions enhance vehicle handling at high speeds, Fig (2.3), [26].

Another important property of a suspension system that directly influences vehicle handling is the roll centre. The roll centre is the location where lateral forces developed by the wheels are transmitted to the sprung mass. Its location affects the behaviour of both sprung and unsprung masses, and therefore directly influences

vehicle handling [15]. It is determined through either the suspension geometry or investigation of forces applied to the vehicle body and its resulting moments [27].

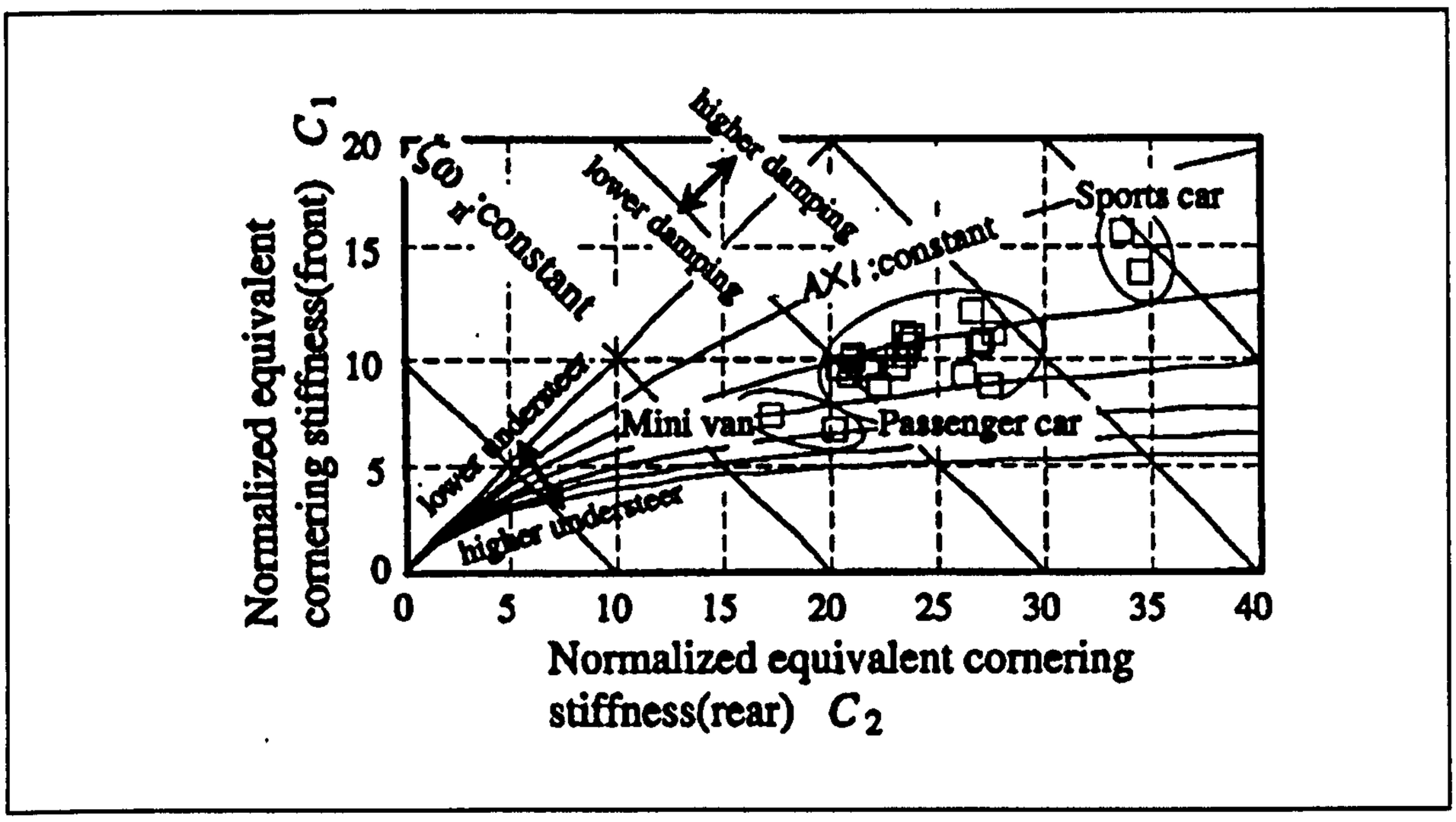

Fig (2.3) Damping effects on vehicle handling [16]

Suspension can play an important role in enhancing vehicle handling through controlled springing, damping and roll moment. On the other hand, its design should always be concerned with passenger feel, which is outside the scope of the current work. Accordingly suspension system designs are not considered in the current work.

2.1.2 Tyre Related Factors

The tyre forms the link between the vehicle and the road, therefore its characteristics are a dominant factor in vehicle handling stability, Fig (2.4), [15] [28] [29] [30]. The non linear nature of tyre properties, along with the delayed response to various external inputs, cause many problems to the vehicle handling in terms of deviation from the intended path [31].

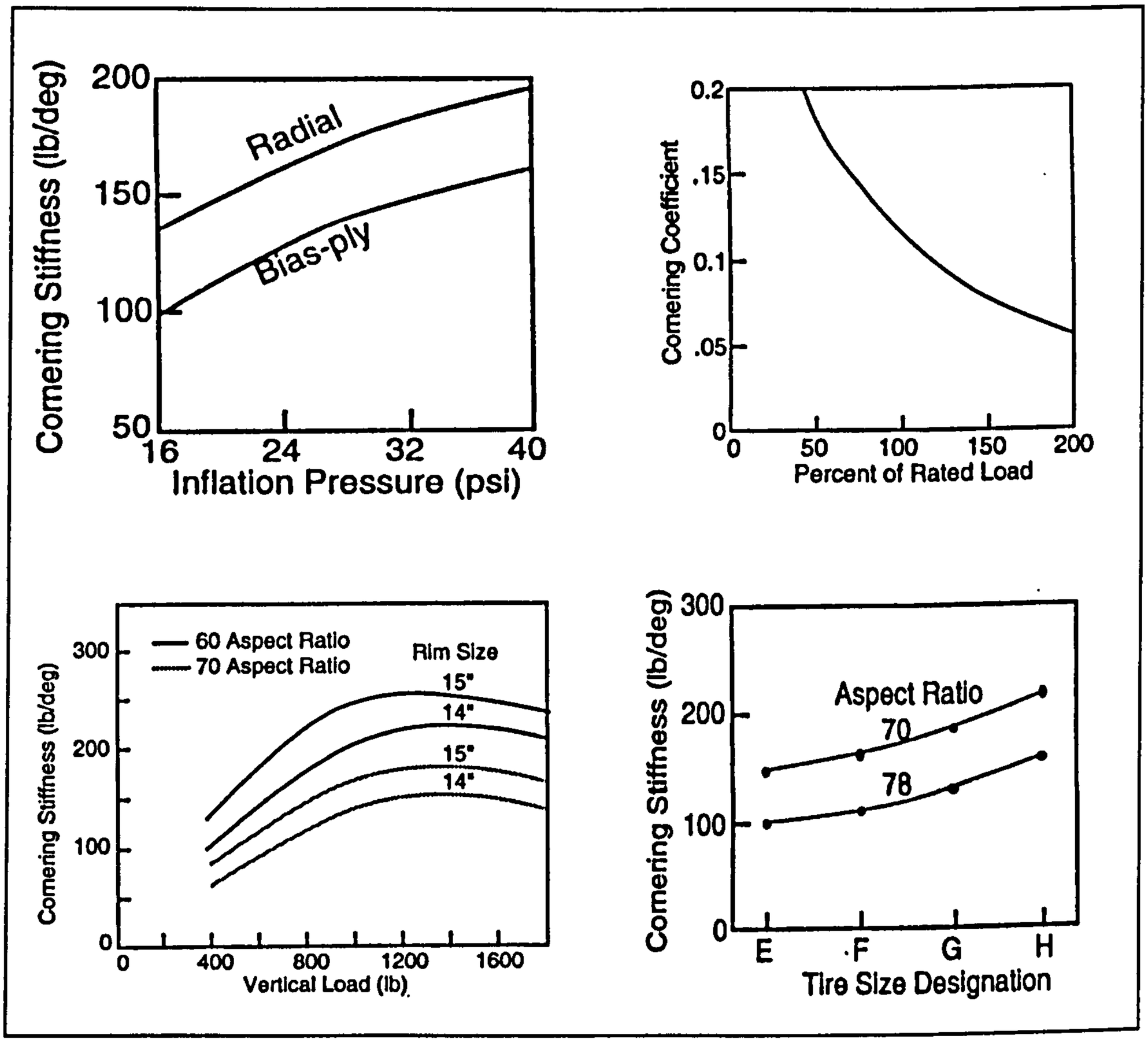

Fig (2.4) Different tyre properties effect on tyre lateral forces and slip angles [15]

Accordingly, researchers recommend that a vehicle should be tested under stability sensitive manoeuvring conditions to make the final tyre selection including size and pressure [28]. This is because the larger the tyre and the lower its profile the more aggressive its response. Consequently such tyres would only suit highly stable vehicles with high Static Stability Factor (SSF) and low roll gradient [28]. Where SSF is a measure to vehicle resistance to rollover and is equal to half the vehicle track divided by its CG height (t/2h). The higher the vehicle's SSF the lower its rollover risks [28].

The tyre inflation pressure is an important factor as it affects the tyre road friction. Although the higher the tyre pressure the higher its cornering stiffness, researchers

found that reducing the tyre inflation pressure would improve its traction on slippery surfaces [32]. The tyre construction also affects the tyre characteristics, as tyre lateral forces were found to be highly influenced by the lateral deformation of the tyre carcass and to a lower degree by its tread deformation [31]. However, the tread depth further affects vehicle handling as it influences the contact pressure distribution between the road and tyre [33]. It also influences the reduction of the tyre-road coefficient of friction caused by wet weather [13].

To evaluate these effects, different tyre models have been proposed for vehicle handling simulations with different considerations, levels of accuracy and mathematical complexity, which are reviewed in section 2.3.5. The Magic Formula tyre model for combined slip is currently recognised for its realistic estimation of tyre forces under combined slip condition [34]. This combined slip condition occurs as the tyre applies traction or brake forces as well as the lateral forces in a turn, which is a common vehicle handling condition.

2.1.3 Road Related Factors

Although road and motorway radius of turns and elevations are optimised for current speed limits, the major problems that face vehicle handling are in turns. The smaller the road turn radius, the greater the vehicle handling problems especially at high speeds. Although straight roads reduce high speed handling problems, it is unrealistic to recommend reconstruction of the entire road network. However, new road network design should be more considerate to future vehicle handling characteristics.

The coefficient of friction between the tyre and the road affects the vehicle handling, as the vehicle roadholding adhesion cannot exceed that of its tyres, and the tyres cannot transmit forces beyond their frictional limit [35]. Regrettably, the coefficient of friction varies according to the nature and condition of the road surface [33] [36], accordingly the exact state of road friction would be unavailable to the driver or to

vehicle control systems [29]. However, different methods to estimate the coefficient of friction between road and tyre have been proposed [29] [32].

Coefficient of friction between tyre and road has been found to be dramatically affected by rain and improperly drained roads [13]. This effect is due to the water wedge that builds up between the tyre and road especially at high speed travelling and small tyre tread depth. Also, " black ice" aggressively reduces the coefficient of friction. Table (2.1) shows these relations as well as the influence of tyre condition. However, a cross wind adds a high lateral force to a travelling vehicle, causing much handling instability, especially at high travelling speeds.

Vehicle speed km/h	Tyre condition	Road condition				
		Dry	Wet water approx. 0.2 mm	Deep rainfall water approx. 1 mm	Puddles water approx. 2 mm	Iced (black ice)
		Coefficient of static friction μ				
50	new	0.85	0.65	0.55	0.5	0.1 and less
	worn	1	0.5	0.4	0.25	
90	new	0.8	0.6	0.3	0.05	
	worn	0.95	0.2	0.1	0.05	
130	new	0.75	0.55	0.2	0	
	worn	0.9	0.2	0.1	0	

Table (2.1) Coefficient of static friction for pneumatic tires on various surfaces [13]

The contradictions between the current high demand for safety [37] and the future demand of higher vehicle travelling speeds [35] coupled with the large number of non manageable, non linear factors affecting vehicle handling have forced the development of advanced chassis control systems that attempt to bridge this gap. In the next section, a review of handling oriented chassis control systems is given.

2.2 Chassis Control Systems

Chassis control systems aim to enhance different aspects of the performance of a vehicle, such as handling and ride. In this section, a review is given of those systems involved in controlling tyre traction forces to enhance vehicle handling performance at high speeds.

These systems aim at enhancing vehicle handling in a number of different ways. This section is divided into two sub-sections. The first reviews the systems that influence traction forces through controlling the engine output. The second reviews the systems that employ traction force distribution to generate a supporting yaw moment.

2.2.1 Traction Control Systems TCS

Developing the vehicle engine by increasing its power is a trend in the automotive industry as a marketing point, Fig (2.5). This occurs regardless of whether the roadholding ability under different handling conditions is sufficient to match the power of the engine [35]. As traction utilisation should be a function of tyre design, load, slip angle, longitudinal slip and road conditions, the driver power demand may at any time exceed the tyre roadholding available.

Traction Control Systems (TCS) were introduced to reduce the engine power output whenever it was sensed to cause vehicle handling instability. The main aim of the TCS is to maintain roadholding and so increase tracking on slippery or μ-split roads without considerable deterioration of either handling or traction performance [38]. Fig (2.6) shows the range of conditions considered by TCS [38].

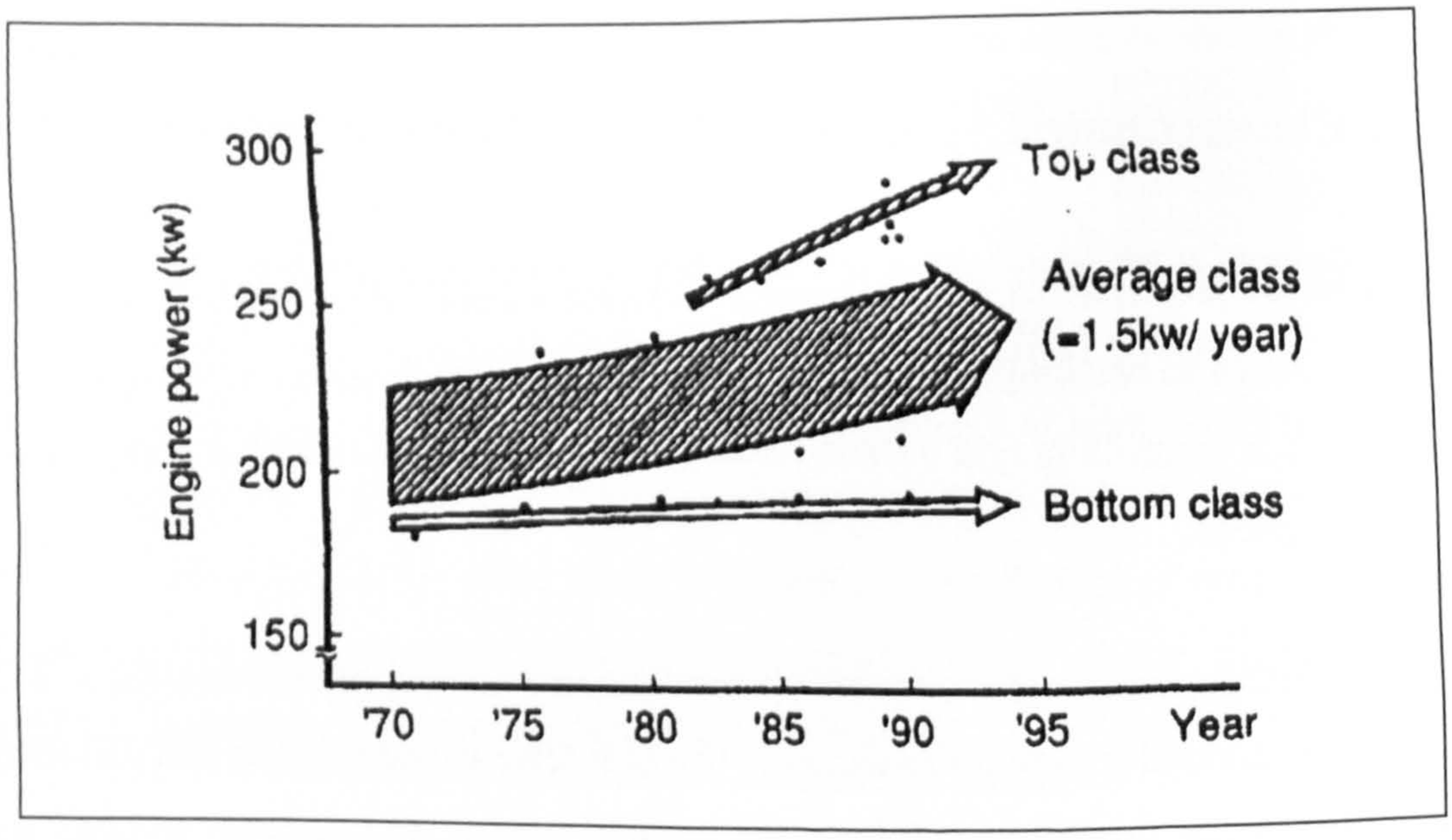

Fig (2.5) The large-sized vehicle engine power trend in Japan [35].

Traction control systems intervene by reducing the engine output through employing different techniques. Some systems reduce the engine output through reducing the throttle opening [38] and [39], while other systems shift the engine ignition point (IP) away from its optimum position [38] and [40]. The reduction of traction forces allows the vehicle to maintain stable handing and traction performance.

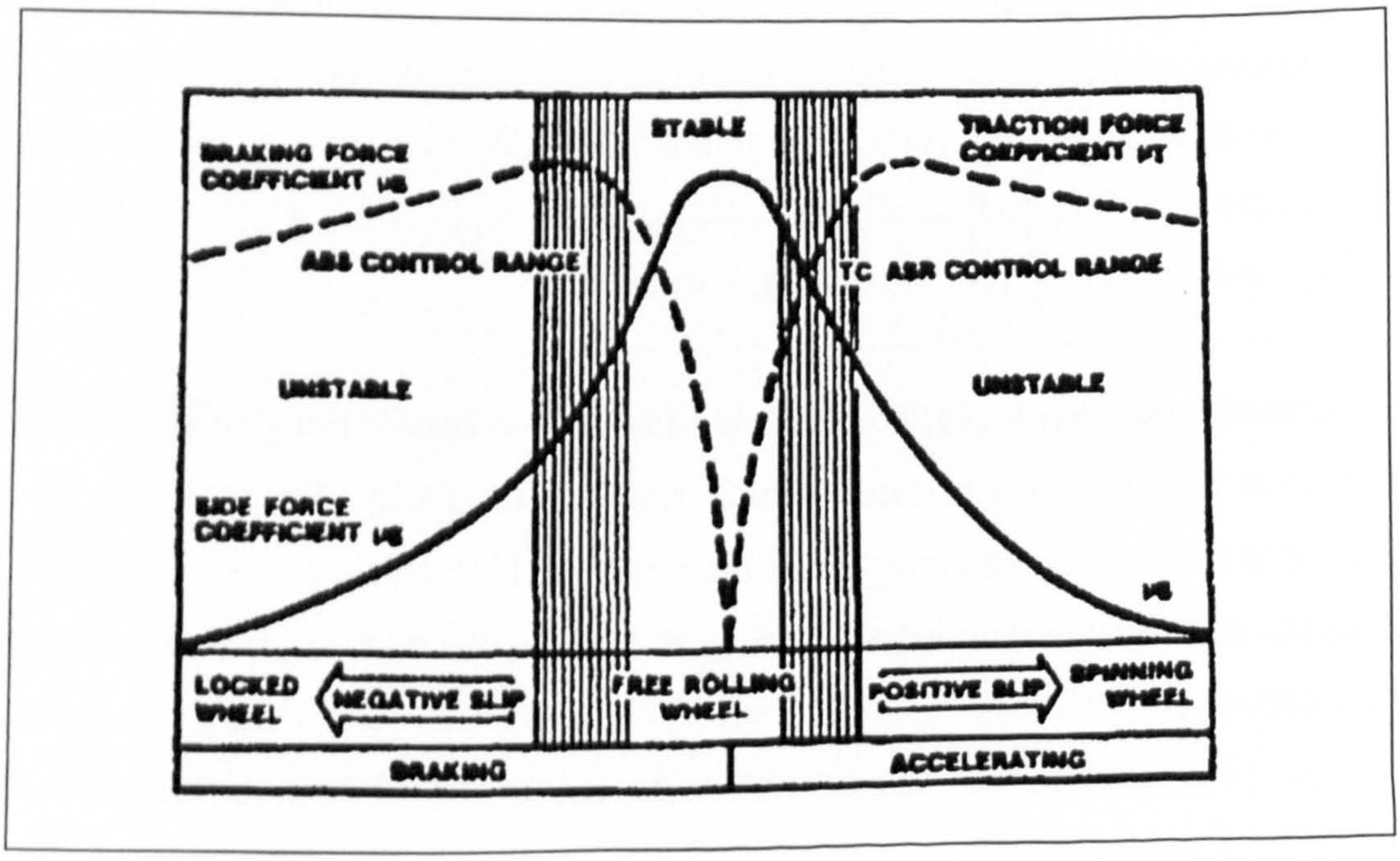

Fig (2.6) Traction, Braking and Lateral forces as a function of wheel slip [38]

Traction control systems limit the engine power to the maximum available tyre roadholding, regardless of the driver power demand. The overall contribution is a higher acceleration and lower wheel slip under adverse conditions.

Throttle Control Systems

Throttle control aims mainly at reducing the engine power available to the driver if the driver power demands, along with the tyre roadholding condition and the current vehicle dynamic condition would cause deterioration of either traction or handling performance. The throttle control systems rely on reducing the engine throttle opening, demanded by the driver, allowing less fuel supply to the engine. This results in a reduction of the engine power output, which limits the maximum traction force delivered to the driven wheels.

Much research has been conducted to evaluate and enhance throttle control systems. Some introduced advanced electronic throttle control systems [39], while others proposed advanced traction controllers [41]. Several proposed the integration of throttle control and other chassis control systems. Augmenting the TCS with Limited Slip Differential (LSD) was evaluated and found to influence handling performance better than or equal to TCS with an open differential [42]. Also, brake force employment, as an addition to the throttle control system, was proposed to reduce excessive steering effort in the case of lateral force saturation when turning on a slippery road [43]. Although throttle control systems are capable of improving vehicle handling, they do reduce vehicle speed.

Dynamic Spark Advance, DSA

Dynamic Spark Advance (DSA) system reduces the engine power available to the driver, when the driver power demand might force the vehicle into an unsafe dynamic condition. The main objective of DSA is enhancing the vehicle tyre

roadholding ability through optimising driven wheels relative slip [40]. Accordingly, it can enhance vehicle handling performance on μ-split surfaces and reduce both lateral slip and skidding in turns.

The DSA system relies on changing the engine ignition point, by advancing or retarding the spark timing, which influence the efficiency of the engine. This results in a reduction in the power output of the engine, as the ignition point is usually set to achieve the maximum fuel efficiency. Through controlling the spark timing, the control system is able to restrict the maximum engine torque available to the driver [40].

As the vehicle ignition point satisfies different requirements, including maximum engine performance and clean exhaust gas, modifying it could result in excess pollution. As major industrial nations are moving towards implementing the stringent American exhaust emission regulations (or have already implemented them) [13], spark advance systems could soon fail to meet the legal requirements. Moreover, both throttle and spark advance systems are criticised for reducing vehicle speed and this could be fatal in emergency manoeuvres.

Others researchers proposed the integration of throttle control, engine spark retard, LSD and brake intervention systems to help the driver in maintaining vehicle directional control [38]. The integrated system was found to enable unskilled drivers to approach the ability of skilled drivers in driving on a μ-split surface. However, since the use of traction control systems alone is usually criticised for the reduction of the vehicle speed, using it in conjunction with braking forces will cause a further speed reduction.

As the focus of the current work is to enhance the handling performance of a vehicle, especially at high speed, traction control systems have been considered inappropriate for the required task, due to the speed reduction effect.

2.2.2 Traction Force Distribution Control TFDC

Traction Force Distribution Control (TFDC) systems are mainly developed to enhance vehicle handling performance through generating a yaw moment at the vehicle CG by distributing engine traction force between driven wheels. Both magnitude and direction of this moment are regulated to support the vehicle handling. It also helps maintain the required lateral forces within the available tyre roadholding ability. Accordingly, TFDC enhances the vehicle handling response and reduces its side slip and path deviation. Therefore, it also enhances vehicle safety.

These systems consist of TFD hardware and the TFD control system. The TFD hardware is usually a purely mechanical system that is capable of influencing the traction forces. It should be able to govern the distribution of traction forces between the driven wheels. Different traction force distribution techniques have been proposed and investigated in the literature [44], [45], [46], [47], [48] and [49].

The TFD control systems are, usually, pure electronic systems. They employ sets of sensors to gather vehicle performance data. These data vary from one system to another. It is usually a collection of driven wheel speeds, non driven wheel speeds, vehicle speeds and yaw rate. The control system processes this data to estimate the vehicle handling performance. If the performance is not considered satisfactory, the control system influences the TFD hardware to redistribute the traction forces delivered to the driven wheels. Accordingly, it generates a yaw moment at the vehicle CG. This moment is regulated to enhance the vehicle handling performance.

The main problem of previous TFD systems arises from criticism of its hardware as a result of its complexity and power losses. Although research has shown its potential to enhance vehicle handling and safety, quite a few different systems have been proposed. Because of this hardware problem, special concentration has been given to the TFD hardware. The TFD hardware history and recent trends are reviewed, to describe the different approaches to design.

TFD hardware design

The idea of differentiating the vehicle left and right side traction forces to induce a steering moment started, primarily, in track laying vehicles such as tractors (skid steer). In these systems, a clutch and brake system was used to apply traction to one side while braking the other side of the tractor [45]. Different design approaches were developed to improve this concept and facilitate its use. Some were primarily dedicated to skid steer tractors, while others were devoted to improve vehicle handling. A review for both types of systems is given to illustrate TFD hardware design concepts.

Van der Lely hardware

In 1981, "Van der Lely" [44] proposed the so-called "Torque Converter", in which two Continuously Variable Transmission (CVT) belt-system and a hydraulic system were employed to differentiate the driving torque of tractor left and right sides. In this system two CVT belt systems, two elliptical gear trains, a mechanical lever system and a hydraulic system were employed. The lever system controls the valves of the hydraulic system, which in turn controls the pressure applied to the CVT elements to influence the required torque ratio.

Van der Lely hardware suites its application in the skid-steering of track-laying trucks. The system hardware is an excellent piece of mechanical design. However, it is rather complicated and slow acting due to the use of different interacting systems, some of which would be slow for vehicle applications such as elliptical gear trains and the belt and pulley arrangement.

It should also be noted that all the traction forces are transmitted to the driven wheels through belt and pulley systems. For passenger vehicles this is unfeasible from power requirements, maintenance requirements and system life time point of views. Accordingly it would not suit the current vehicle application.

Gleasman hardware

In 1983/85/87 Gleasman et al, [45], proposed and improved the design of the so-called "No-Slip, Imposed Differential Reduction Drive" to skid steer track laying trucks. In this system, a second differential was connected in parallel to the ordinary open differential through a set of gears. The second differential was driven by either a DC motor or by the main engine power through clutches, worm and worm wheel. The aim was to control the speed difference between left and right tracks and to prevent tracks from slipping unless slippage occurred on both tracks at the same time.

This hardware achieved its design goals but it would be not feasible for the current vehicle application for many reasons. First, its size would not fit normal road vehicles due to its need for a second axle and gearing system. Second, it would not be possible to power it through the main engine due to the differences in rotational speed requirements. Third, this design would lock the wheels in case of failure, without any means of disengagement, due to the use of worm and worm gear, which are usually criticised for their reliability and manufacturing problems. Finally, the DC motor would have to supply all the power required for turning, which could be significant. Accordingly this system might only suit low speed applications, such as tractors.

Steiger hardware

In 1990, Steiger [46] proposed a so called "Differential drive and steering system" for tractors that employ skid steer. This system featured a CVT system and a control link connected to the tractor direction control lever. The control link adjusts the CVT transmission ratio, which influences the torque delivered to left and right tracks.

The system is capable of differentiating traction torque, for tractors, but applying this system for normal road vehicles is not possible for many reasons. The first reason is that the lever type steering mechanism would not be acceptable for normal vehicles.

The second reason is that continuous running of the CVT belt system, even in straight line driving, would cause durability problems. The belt in this design would have to transmit the difference between the left and right traction forces, which might be quite high in some cases. Accordingly, this system has also been considered unfeasible for the current vehicle application.

Motoyama hardware

In 1993, Motoyama et al [47] introduced a TFD hardware system designed for 4WD passenger vehicles. In this system, the traction forces were distributed to the four wheels. This task was carried out through employing a dedicated controlled clutch for each wheel, a control unit and set of sensors, Fig (2.7).

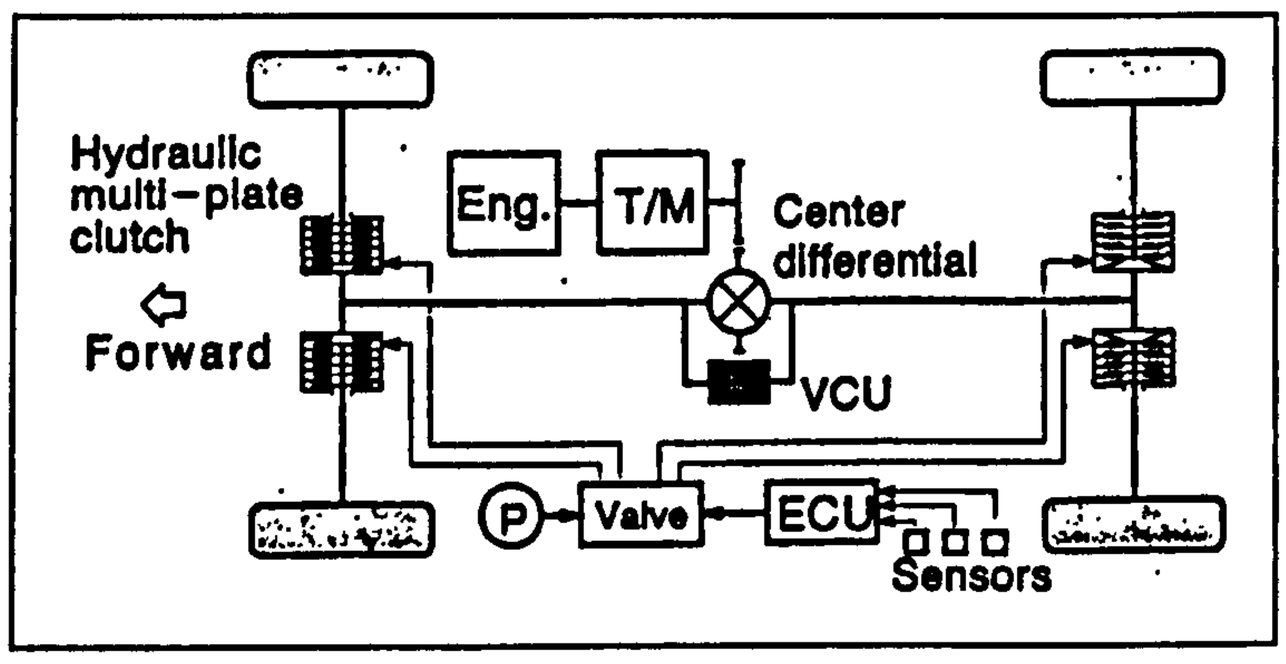

Fig (2.7) Configuration of Motoyama hardware [47]

Motoyama et al., investigated the effect of traction force distribution between individual wheels on vehicle handling, using both simulation and an experimental vehicle test [47]. The experimental vehicle and simulation model employed a 4WD vehicle design with 50:50 front to rear distribution, enforced by a central open differential. The test vehicle has a hydraulic system and multiplate clutches installed at all wheels.

In this system, the traction force distribution ratio α for the front, rear and centre differentials, Fig (2.8), were varied continuously within 0.0 to 1.0 in order to investigate the effect of front/rear and left/right traction force distribution on vehicle handling. Both the experimental test and simulation results showed that the left/right TFD has the capacity to improve vehicle handling performance, Fig (2.9), while front/rear TFD has a minimal effect, Fig (2.10).

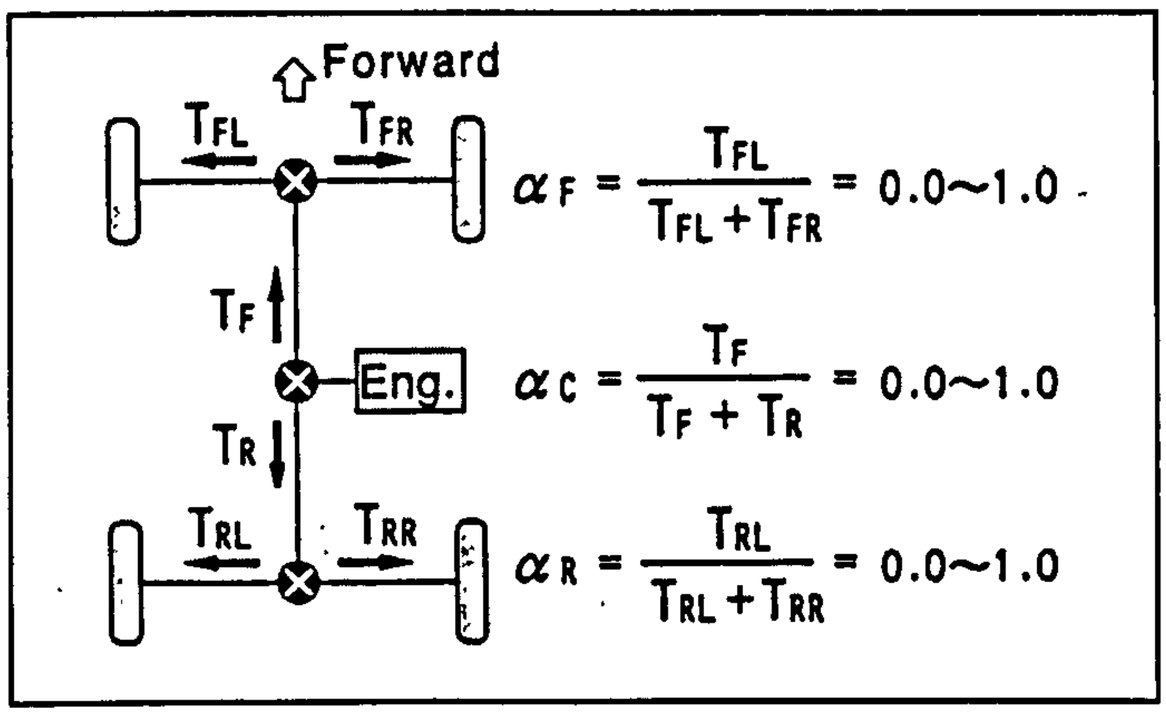

Fig (2.8) Simulation model of drive train [47]

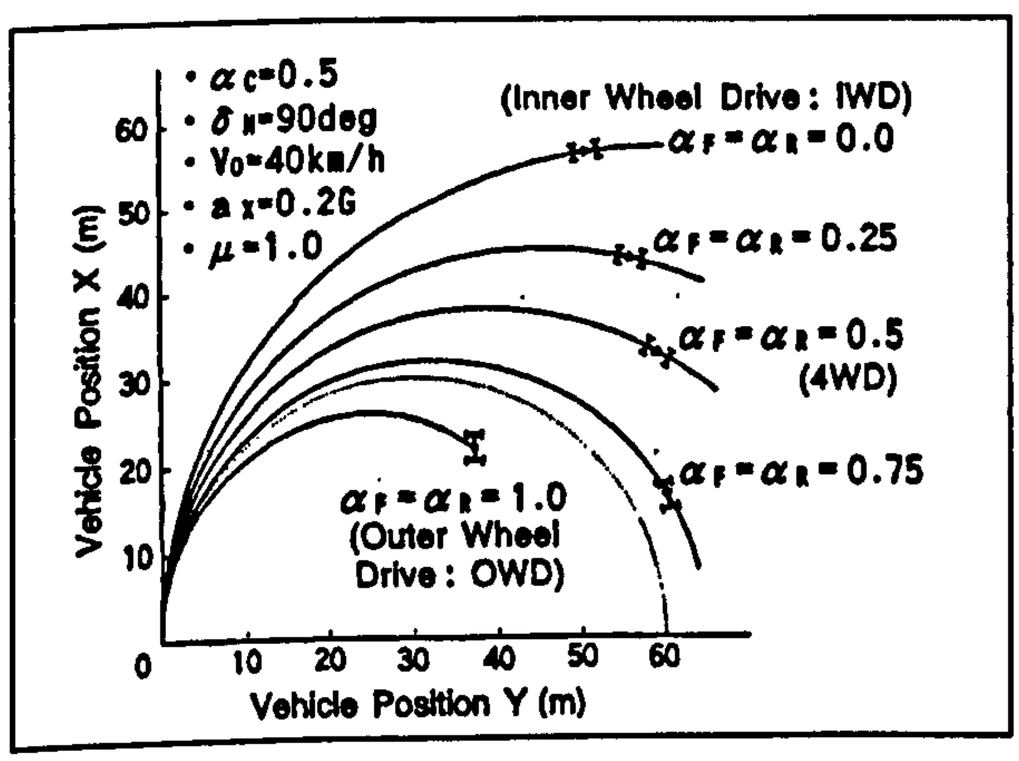

Fig (2.9) Left to right torque distribution [47]

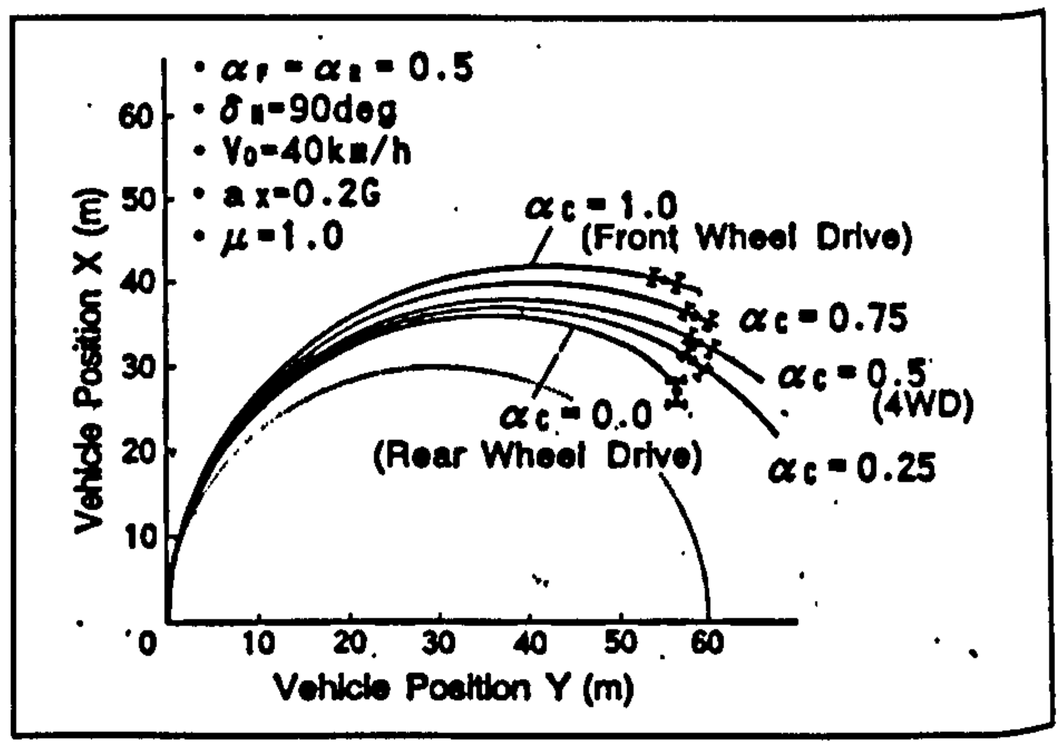

Fig (2.10) Rear to front torque distribution [47]

The Motoyama system's excessive use of clutches in slipping mode would lead to huge power losses, frequent maintenance requirements and a short life time. Power

loses are due to the slip between the clutch plates, and the power needed to engage and disengage the clutches, as they would have to be engaged all the time, especially in straight runs. Another criticism of this hardware is the complexity of employing five multiplate hydraulic clutches, and their required, delicate, hydraulic system.

However, the vehicle in free running would have no traction forces to distribute. Also, it should be noted that the system was tested under acceleration condition, which would not be the common driving condition in a turn. Accordingly, the system would not enhance free running vehicle handling performance. Due to the hardware and functionality problems, the system has been considered not feasible for the current application.

Ikushima hardware

In 1995, Ikushima & Sawase [48] proposed a new TFD hardware based on CVT. The so called "Right/Left Torque Control System" aimed at improving vehicle handling performance through producing a yaw moment. The new mechanism, Fig (2.11), consists of an ordinary open differential and the so called "torque transmitter mechanism", which employed a continuously variable transmission (CVT) and a torque transfer shaft. The CVT element A is directly connected to the right wheel axle, while CVT element B is connected to the left wheel axle, by means of a shaft and gearing system with 1:1 gear ratio. The compressive forces on the CVT elements A and B are controlled individually by means of a hydraulic system.

A control system to drive the proposed hardware consisted of a control unit and a set of sensors. The control unit calculates the difference between the required and actual vehicle yaw rate (yaw rate error), then corrects the yaw error through applying suitable compressive forces to CVT elements A and B to control the CVT transmission ratio, Fig (2.12) b and c. When yaw moment is not required, the control unit applies equal compressive forces to the CVT elements to produces equal traction forces and therefore no yaw moment, Fig (2.12) a.

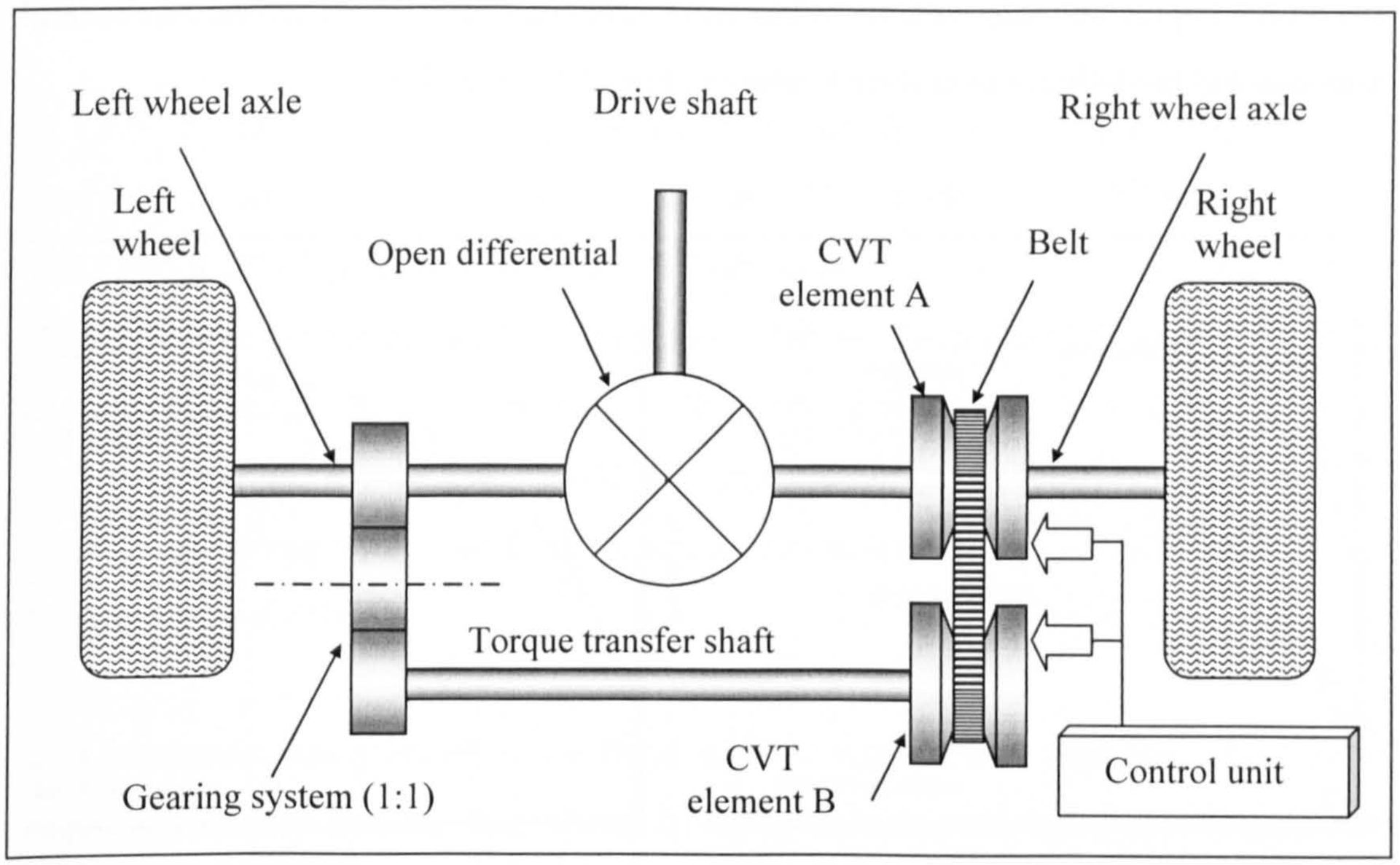

Fig (2.11) Configuration of Ikushima [48] hardware

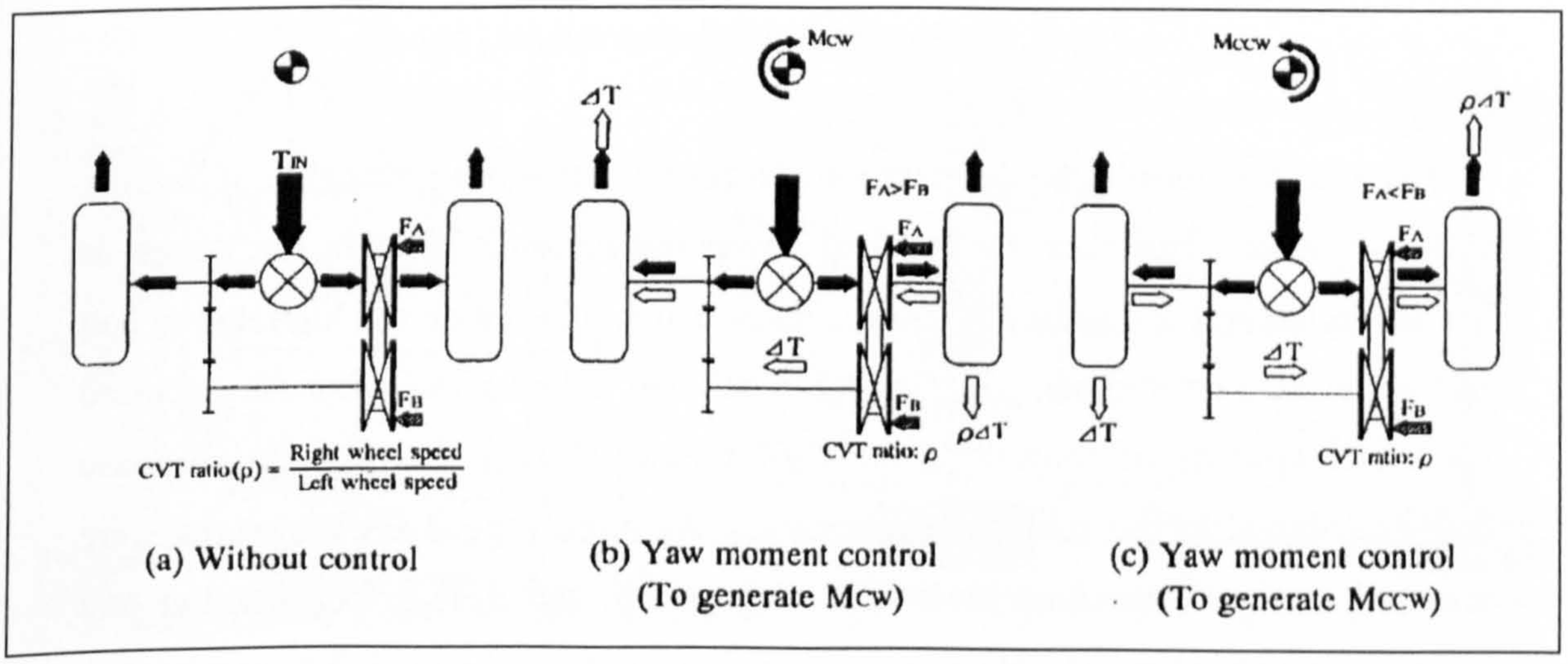

Fig (2.12) Illustration of the right/left torque control mechanism [48]

The proposed hardware and yaw moment controller were evaluated through simulation [48]. In the simulation test, the vehicle steering angle was fixed so that it drove in a circle with a radius of 30 m at constant velocity. It was then suddenly accelerated in the first test and suddenly decelerated in the second to investigate the change in vehicle path upon such acceleration and deceleration. The system was found to enhance the vehicle handling performance in cornering under acceleration

through suppressing the vehicle understeer tendency, and in deceleration through suppressing the vehicle oversteer tendency, Fig (2.13) a and b.

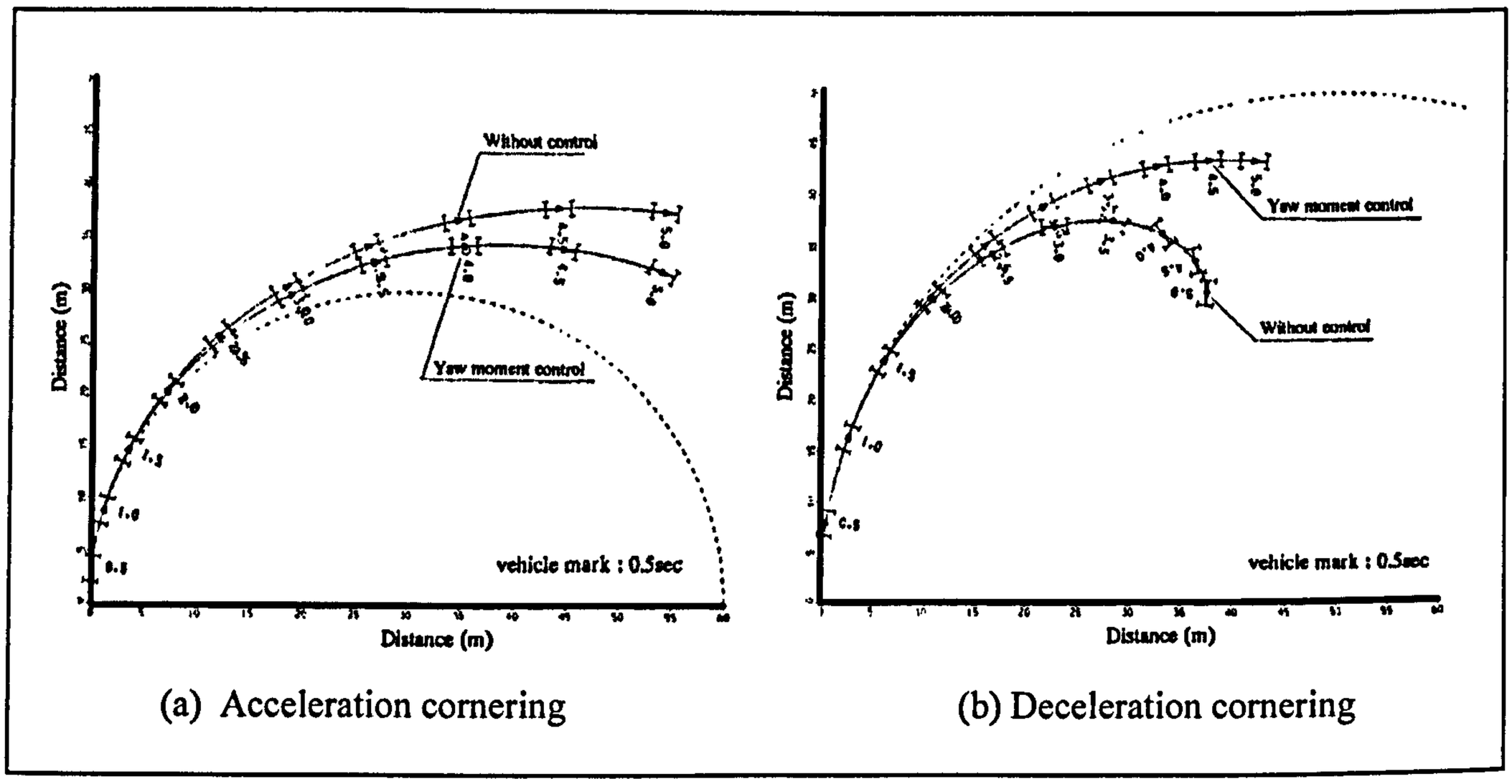

(a) Acceleration cornering (b) Deceleration cornering

Fig (2.13) Ikushima simulation results [48]

The system response in the deceleration test revealed that it was capable of braking the outer wheel. However, the level of power transmission between the wheels is limited to the belt and pulley frictional forces that would not be too high due to belt and pulley size constraints. Also, the CVT belt and pulley systems can be criticised for the complexity of controlling the CVT pressures. This is due to the response delay attributed to the rubber characteristics. As more rugged CVT systems were required, many researchers have been engaged in the design, construction and development of enhanced CVT systems [50], [51], [52], [53] and [54]. However they would not be able to transmit enough power for the current application.

Also the permanent engagement of the Ikushima system would cause high CVT component wear and increase the controller load, leading to durability problems. Furthermore, belt and pulley systems are known to be sensitive to both oil and dust contamination, which would considerably increase system maintenance requirements and reduce its life. Accordingly, this system has also been considered unfeasible for the current application.

Sawase hardware

In 1999, Sawase & Sano [49] proposed the so called "Active Yaw Control" TFD hardware system which employed two controllable clutches, two differential bypass axles and a set of gears to distribute the traction forces, Fig (2.14). One bypass axle is geared to rotate faster than the mean driven wheels speed and the second is geared to rotate slower, with a maximum rotational speed difference of 5%, Fig (2.14) a. Either differential bypass axles could be connected by progressively closing its fitted clutch under computer control, which allows controlling the speed ratio between left and right half-shafts.

This hardware was planned to be fitted to four wheel drive vehicles. The system implementation within the four wheel driven vehicle as well as a block diagram for the control system is shown in Fig (2.14) b.

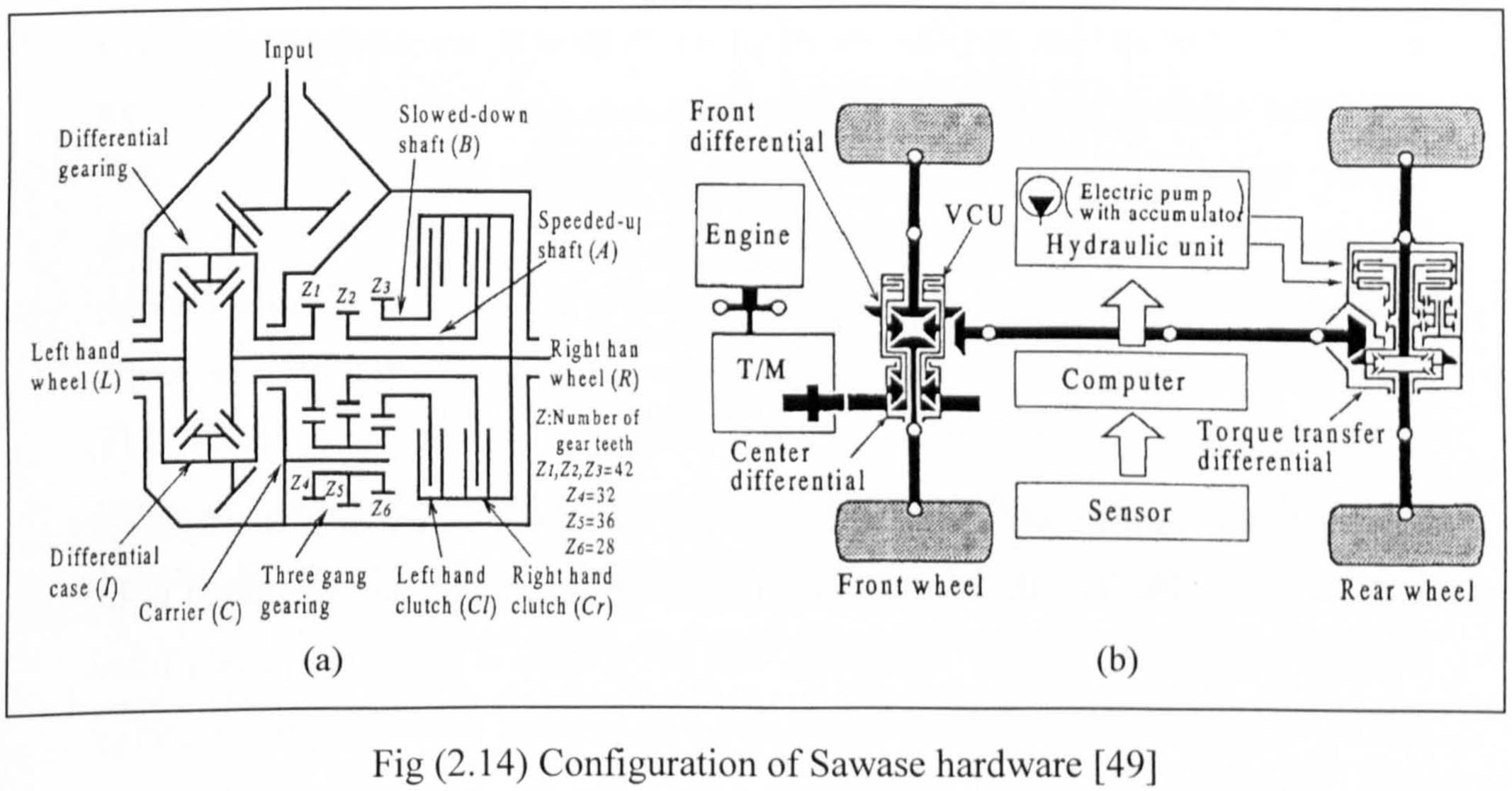

Fig (2.14) Configuration of Sawase hardware [49]

This system was said to achieve similar results to the CVT based systems, with a less complex hardware installation [55]. Its effect on vehicle handling was investigated through simulation with five degrees of freedom (DOF) model. The employed DOF were longitudinal, lateral, and yaw motions, the torque transfer between front wheels and the torque transfer between rear wheels. Three types of drivetrain layout were

tested, front wheel drive, rear wheel drive and 4WD. In this simulation 4WD was said to produce near perfect performance, Fig (2.15) c. In both rear wheel drive and front wheel drive models, transferring the torque between the driven wheels was more effective than transferring it between the non driven wheels, Fig (2.15) a and b.

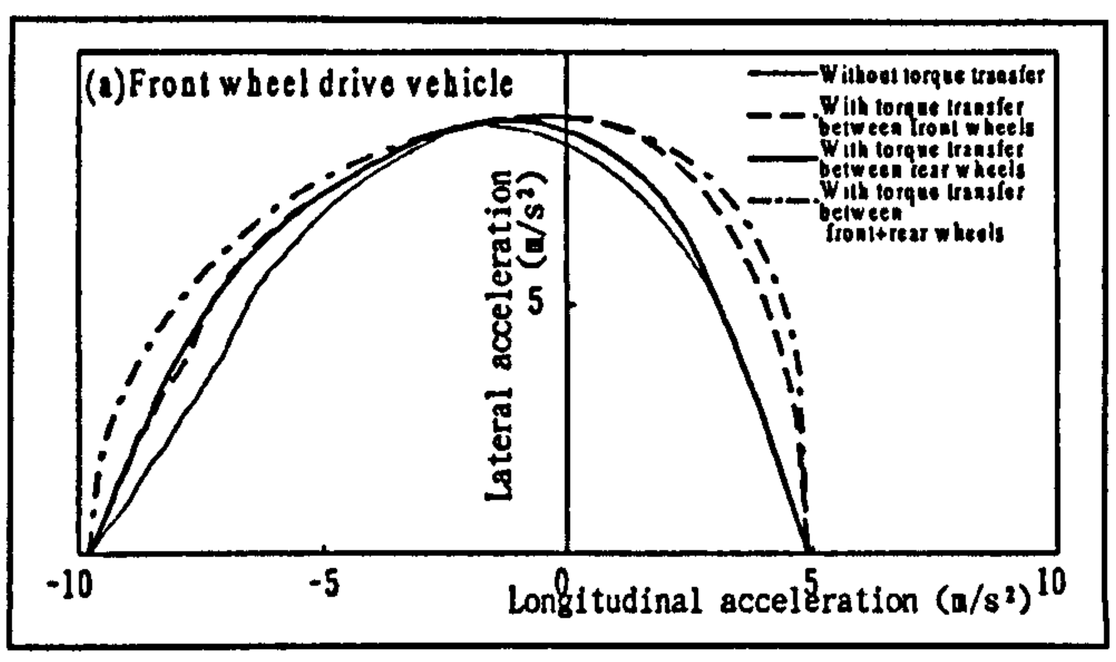

(a) Front wheel drive

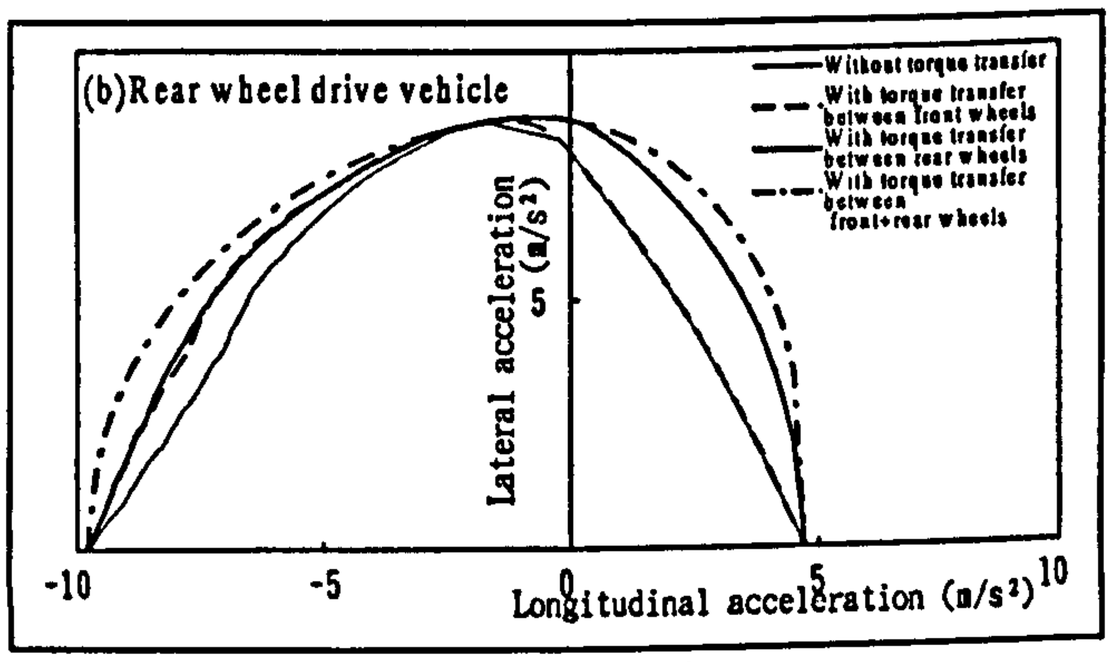

(b) Rear wheel drive

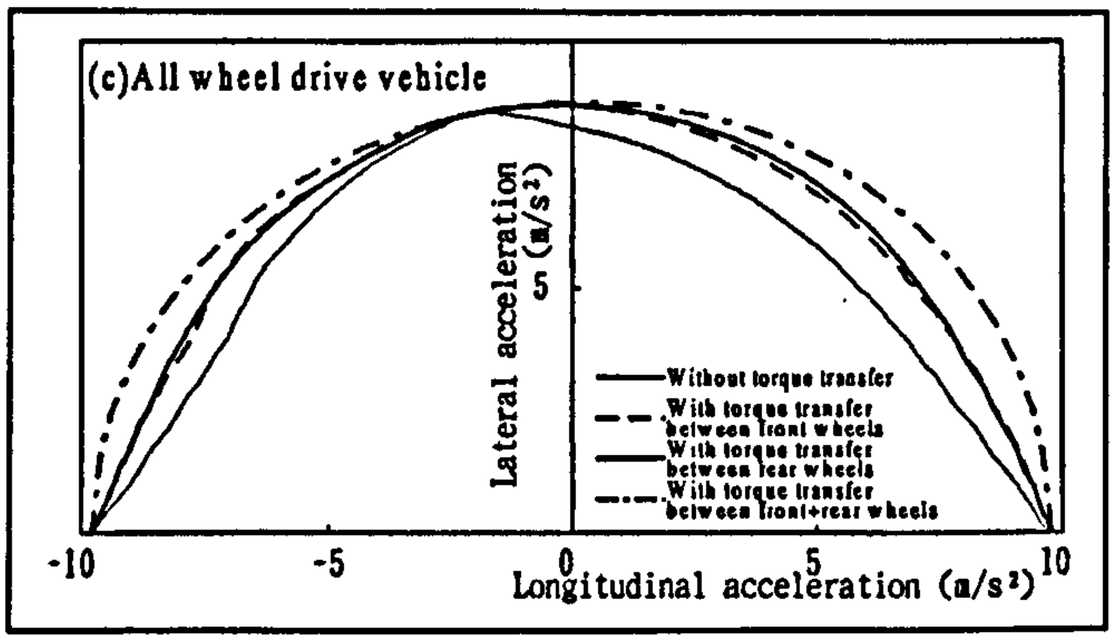

(c) Four wheel drive

Fig (2.15) Sawase simulation results [49]

This system is refined and could be considered the most feasible available system. Accordingly, it has already been adopted by Mitsubishi Motors and was fitted in its Mitsubishi Lancer Evolution© 4x4 series, Evo IV in 1996. It was subsequently fitted in Evo VI in 2000, Evo VII in 2001 and Evo VIII in 2004. However, greater energy consumption was apparent due to the slip of one clutch when the system is active. Although the system is disengaged when not needed, clutch slip is likely to result in wear and consequently high maintenance requirements and short life time. Also control over clutch slip with its nonlinearity would have to be added to the controller tasks. Also the 5% difference could be insufficient in small radius turns. Accordingly, a more feasible system is considered to be required for the current application.

2.2.3 Wheel Speed Distribution Control, WSDC

In this work a novel Wheel Speed Distribution Control (WSDC) vehicle chassis system is proposed, with the aim of enhancing vehicle handling performance. In WSDC, the vehicle driven wheel speeds are forced to run faster or slower than the Ackerman reference values, which are theoretical inner and outer wheel speeds obtained from vehicle velocity, wheel diameter, track and "Ackerman steering configuration", which is a theoretical relation between vehicle radius of turn, steering angles and wheel base. This control of wheel speed compels the wheels to develop homogeneous longitudinal slip, which, in turn, produces the forces that generate the supporting yaw moment, required to enhance the vehicle handling.

Although WSDC is related to TFDC as both systems differentiate forces between the vehicle sides, the force generating means in WSD are the controlled wheel rotational speeds. Accordingly, WSDC has many benefits over TFDC. The first is that rotational speeds are easier to control than forces. Also, in contrast to TFDC that has no reference to how much controller output would cause vehicle instability, Ackerman steering offers a good reference to the required wheel speeds. Accordingly, the amount of imposed wheel longitudinal slip can be estimated through advanced tyre models, checked against the available tyre roadholding and its effect on vehicle handling evaluated before applying the designated wheel speeds. This would allow more vehicle speed smoothness in contrast to TFDC that could encounter force discontinuities due to tyre force delay. Another benefit is that if the vehicle, for any reason, lost its roadholding, the tyres could be forced to rotate at speeds that match the road speed, so that no slip with the road is experienced and the roadholding is regained.

The principle of Wheel Speed Distribution (WSD) has never been proposed for road vehicle handling. However, in 2004, Besselink [56] has described a four-wheeled agricultural equipments (ride-on lawn mower) having two independent manually controlled driven wheels, and so called "steering-drive system". When both the left-drive wheel and right-drive wheel are driven at equal and opposite speeds the lawn mower rotates about the centre of the drive axle

The steering-drive system was achieved by replacing the two castors of the conventional system with two steerable non-driven wheels [56]. These are positively turned to steer angles appropriate to the radius of curvature produced by the manually controlled speeds of the two independently driven wheels. A microprocessor is used to determine the appropriate steer angles, using an algorithm based on the mathematical relationship between the wheel speeds of the two independently driven rear wheels and the Ackerman steer angles of the two front steerable wheels.

The test-bed vehicle, Fig (2.17), is based on the John Deere Z-Trak 757 lawn mower, Fig (2.16), which has a zero turn radius (ZTR) for studying the integration of the steering system of a wheeled vehicle with the drive system. The integrated steering-drive system of the test-bed vehicle used a computer to co-ordinate the steer angles of the non-driven steerable wheels, Fig (2.18) (a), with the independently driven wheel speeds of the drive system, which is the primary steering system, to produce a beneficial secondary steering effect.

This steering-drive system can be considered to be the opposite of WSD in the sense that the controller in the steering-drive system would sense the driven wheel speeds and control the steering angle. In contrast, the WSD controller would sense the steering angle, amongst the other vehicle handling parameters, and control the driven wheel speeds.

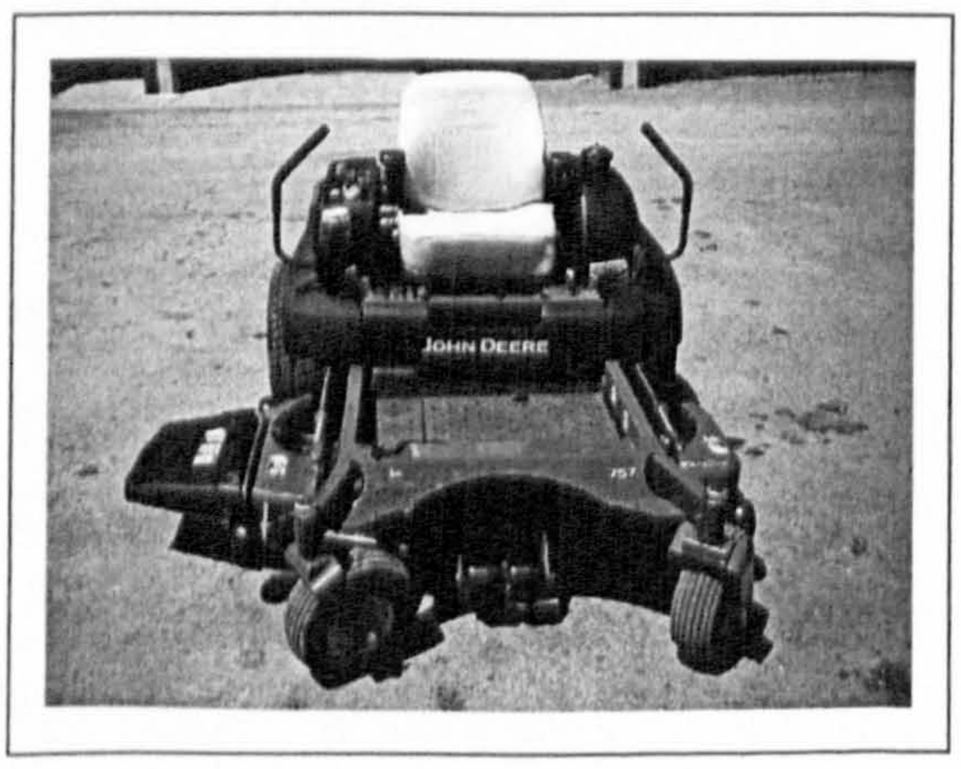

Fig (2.16) Z-Trak 757 lawn mower [56]

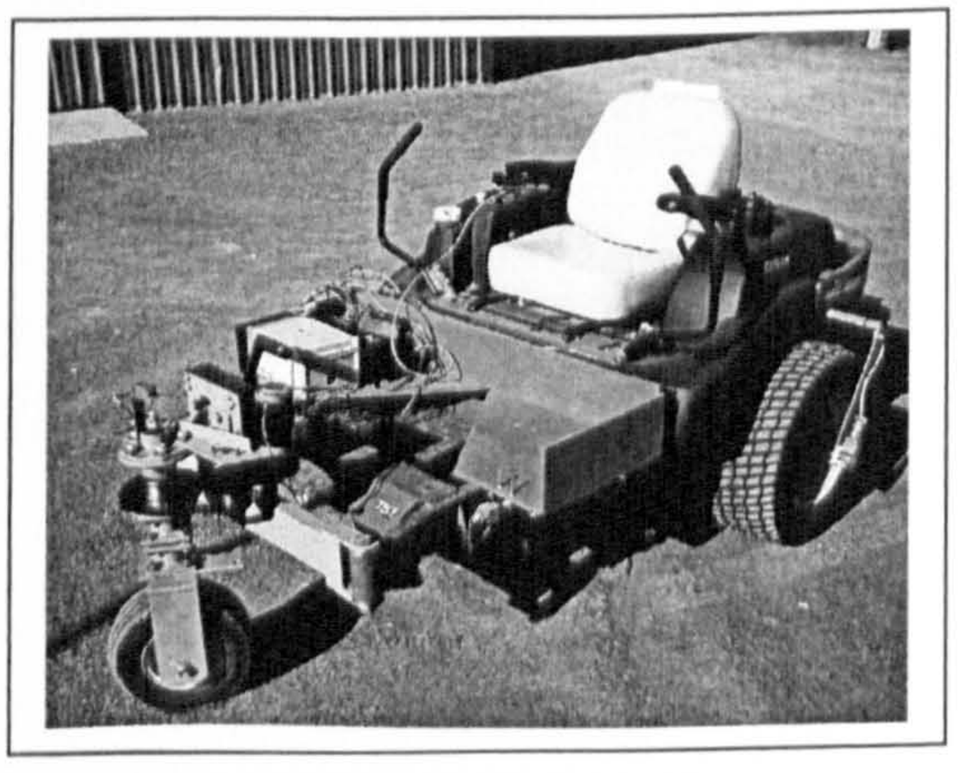

Fig (2.17) Z-Trak 757 after modification [56]

The hydraulically driven lawn mower was chosen because of its potential for reconfiguration compared to a mechanically driven vehicle. The hydraulic drive, Fig (2.19), could be configured for independent drive, Fig (2.19) (a), constant left and right torque, Fig (2.19) (b), and constant left and right speeds, Fig (2.19) (c). The original drive system of the test-bed vehicle was an independent drive system with one variable displacement hydraulic pump matched with one fixed displacement hydraulic motor for each drive wheel, Fig (2.19) (a). This choice emphasises the problems that face available mechanical drive systems in terms of both flexibility and ability to adjust driven wheel speeds independently.

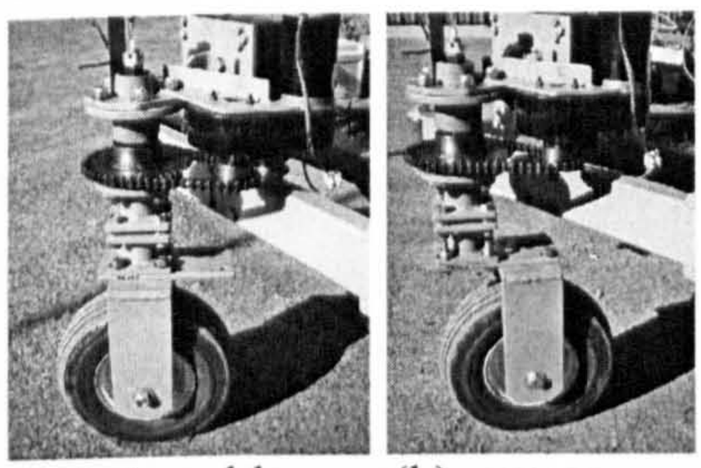

Fig (2.18) Front wheel sets [56]

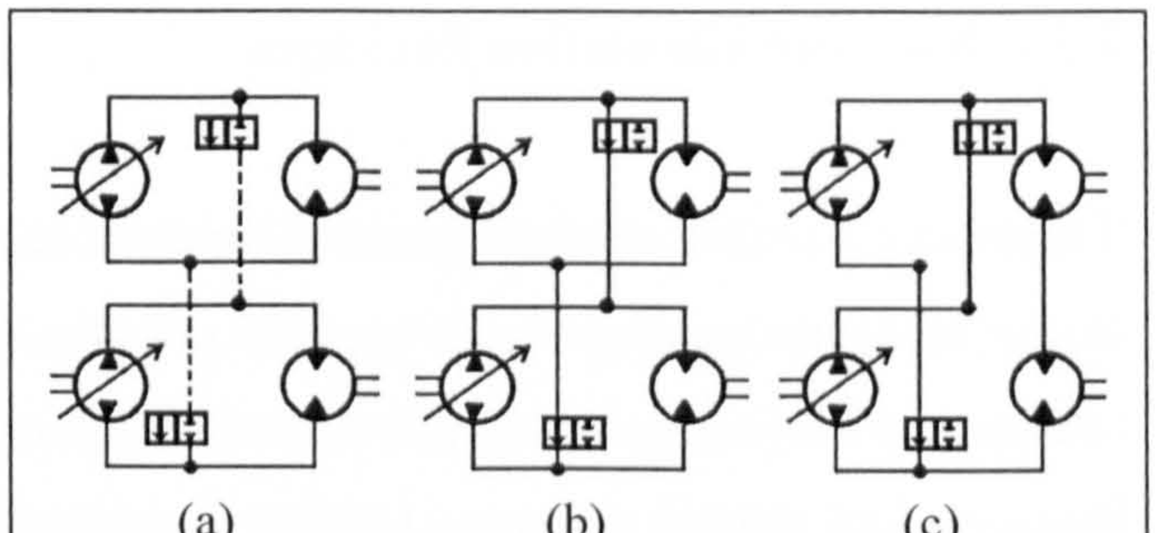

Fig (2.19) Hydraulic dive configurations [56]

Besselink [56] found that a wheeled vehicle having the tractive advantages of two independent drive wheels but having steerable non-driven wheels has greater design possibilities with respect to weight distribution, space considerations, and wheel sizes. It also benefits from improved tractive ability, mobility and safety on slopes and slippery surfaces.

Accordingly it has been concluded that WSD would be easier to implement and control. It would enhance vehicle handling at high speeds. It also would remove the force discontinuities encountered by TFD systems and would give better feel through adjusting the level of wheel acceleration, which would be further smoothed by the natural tyre rubber damping. Accordingly, the decision has been taken to investigate the high potentials of WSD control through the current work.

2.3 Vehicle Modelling

In the current vehicle production industry the need to develop more competitive vehicles is a matter of survival. The new vehicle designs are facing challenges in different fields such as cost, safety, handling, comfort, size, weight, fuel economy and style. This survival competition is quite hard as the interlocked relations between all these factors are not easy to investigate in design stage. Therefore, computer simulations are used to facilitate the investigation of vehicle performance and to speed up the vehicle design process. A number of approaches have been developed for the vehicle simulations. The most common approach involves the employment of academic and commercial packages.

2.3.1 Software Simulation Packages

There are a number of packages available for developing vehicle simulation models. Some of these packages are general purpose dynamic modelling packages, like Automated Dynamic Analysis of Mechanical Systems (ADAMS), Dynamic Analysis and Design System (DADS) and MatLab® Simulink™. Also a number of packages were developed specifically for vehicle modelling like Vehicle Dynamics Analysis Software (VDAS), AUTOSIM and Advanced Vehicle Simulator (ADVISOR™).

ADAMS (Automated Dynamic Analysis of Mechanical Systems) from "MSC Software" started as commercially available package in 1980. Since then, it has become one of the most widely used packages in vehicle dynamic simulation.

ADAMS incorporates a powerful set of software modules capable of simulating three dimensional motion of a wide range of multi-body mechanical systems. It, also, employs specific modules with special libraries to simulate vehicles dynamics such as ADAMS/car, ADAMS/chassis, ADAMS/driveline and ADAMS/driver. It generates sets of numerical equations of motion that represent the three dimensional movement of each part of the multi-body mechanical system, and then solves them in time domain to investigate their movements [57].

Unfortunately, ADAMS© is not capable of developing the required onboard vehicle handling model with real time capacity [57] [58]. In research carried out by Villec, 1998 at Ford Motors Company using ADAMS, eight seconds of vehicle simulation with output time step of 0.000125 second took 2245 seconds to complete, and with output time step of 0.001 second took 435 seconds to complete. Although, the second run was more than 50 times slower than real time, it was considered "the most computationally efficient run" [59]. This shows the incapacity of ADAMS to develop real time vehicle simulation models.

DADS (Dynamic Analysis and Design System) is a lumped parameter simulation package from CADSI. It is based on matrix method of formulating kinematics and dynamics of mechanical systems that was developed by Haug, 1989 [60] at the University of Iowa, US.

DADS is widely used to predict the dynamics of multi-body mechanical systems. It also can perform inverse dynamic, static, quasi-static and kinematic analysis to investigate load, acceleration, velocity and position of mechanical system components. However, in vehicle simulations carried out using DADS by Perera and Romano, 2006, DADS was found unable to create real-time models [61].

VDAS (Vehicle Dynamics Analysis Software) is a lumped parameter software package for vehicle dynamics analysis. It is capable of performing standard range of investigations of vehicle ride and handling performance, [62]. It was developed by Crolla et al., at the University of Leeds in 1994 and is not available commercially. However, its capacity to develop real time simulation models was not claimed.

ADVISOR^{tm} (Advanced Vehicle Simulator) is a package written in the MatLab® Simulink^{tm} environment. It was developed at the U.S. National Renewable Energy Laboratory (NREL) in 1997 and commercially available from AVL Powertrain Engineering Inc.

ADVISOR^{tm} was developed to investigate hybrid vehicles performance with focus on energy consumption and emissions, but it can be used to simulate and analyze

conventional, light and heavy vehicles performance, including hybrid electric and fuel cell vehicles. ADVISOR^{tm} investigates the continuous behaviors of the modeled vehicle in the form of a series of discrete steps. During these step the vehicle components are assumed to be at steady state [63]. However, ADVISOR has not claimed capacity to develop real time vehicle handling simulation models.

AUTOSIM is a symbolic code generation language that was built on top of the standardised artificial intelligence language COMMONLISP and used for multi-body dynamics analysis, [64]. It is capable of generating a stand alone code for simulation of multi-body dynamic systems.

It was commercially released in 1996 and was originally developed for vehicle simulation but it has the capacity of general purpose multi-body dynamics simulation. It also employs a range of optimisation techniques to produce what is claimed to be computationally efficient computer programs. For this purpose it simplifies the mathematical equations to create code that is claimed to have similar run time and accuracy as the hand written programs, [65]. However, AUTOSIM capacity to develop real time simulation models has not been claimed.

MatLab® Simulink^{tm}. MatLab® (Matrix Laboratory) from "The MathWorks" company is an integrated computing environment. It is equipped with Simulink^{tm}, a platform that can perform multi-domain simulation and analysis of mechanical systems. It is, also, featured with a customisable set of libraries and advanced graphics and visualisation capacity.

As recognition of the importance of real time application requirements, MatLab® has introduced "Real-Time Workshop" a package that relies on ANSI C and C++ to transform Matlab® Simulink^{tm} models into faster running codes [66], which confirm the original Matlab® Simulink^{tm} slow model speeds. This package claims to be a general real time application developer. It can produce stand alone C language codes for developing and testing algorithms modelled in Simulink^{tm}. Nevertheless, it can not convert a whole vehicle simulation model into a real time capable model.

The "Real-Time Workshop" package relying on computer code development proves the importance of code programming to real time systems development. On the other hand, its claim of being general real time application developer is not accurate as there are dynamic systems that are too complicated to have real time simulations by any current available computational means. Also, real time complicated dynamic systems need a clear system understanding and special mathematical formulation [67]. Accordingly, real time vehicle handling models have to be built using specially developed mathematical formulations and real time oriented code programming.

2.3.2 Real Time Modelling

The task of developing a real time capable onboard vehicle handling simulation model and control system was described by Najmi and Mahran, 1994 as "Infinity too complex" [68]. Real time simulation of vehicles has always required extensive development effort by experts. It also required special hardware to provide the computational speed necessary to synchronise the simulated vehicle response with the dynamic operation of physical vehicle. The equations of motion are required to be derived by hand and fine tuned to run in real time. [69].

Although processor speeds have since improved and simulation methodology and knowledge have developed, real time capable onboard vehicle handling simulation models development still poses a challenge. Even, the advanced simulation packages like "ADAMS and other multi-body packages are not capable of real time operation and have no provision for connecting to hardware", [69].

The processing time of onboard real time vehicle handling simulation model, is essential as a vehicle moving at 110 km/hr travels more than 30 m in each second. This is a very small processing time available for the onboard simulation model and a very long travelled distance, given that the vehicle could face grave dangers in this distance. Accordingly, the decision has been taken to develop a vehicle modelling technique that would have the capacity to develop faster than real time vehicle simulation models, as "The most sophisticated software provides no match for the mental activity that leads to invention. Otherwise, inventions would become programmable", [70]

2.3.3 Modelling Environment

PC's are currently attracting a lot of attention due to their fast control capabilities. This is because of their current high performance and high performance to cost ratio in the large competitive market. Also PC's can be fitted with large data storage and Random Access Memory (RAM) allowing models and programmed controllers to include large sets of dedicated situation handling routines. Furthermore, using PC programming, would facilitate both model and controller further development, which could be as simple as adding a few lines of code.

As this research is not about the operating systems, only the widely available operating systems have been considered, as long as they prove to be satisfactory. Given that, Microsoft operating systems are currently dominating the PC market, only Windows© and the older Disk Operating System DOS© have been investigated.

Windows© is an operating system developed to allow a user friendly graphical interface between the user and the PC hardware. Its superior points of functionality are multitasking, multi-user, networking, object oriented programming, and multimedia. However, its multitasking features prevent its based programs from controlling the PC hardware directly and allow them only a share of the PC resources, which causes them to run slower than programs of non-multitasking operating systems. This prevents the Windows© based programs from meeting the tight time commitments of real time applications, given that violation of the timing requirements of the current real time system is a failure whose consequences may be catastrophic [71].

DOS© is widely regarded as an old non-multitasking operating system, yet it is very stable with high processing speed and small memory requirements. It also allows the programs to control all the PC hardware resources. As one of the current work aims is high speed real time model development, the need for high processing speed is evident, therefore, full control over the PC hardware resources is a requirement for the further controller development. Accordingly, DOS© could be considered the most suitable, widely available, operating system for real time model development.

Although there are a large number of programming languages that work under DOS© and some of these languages offer ready made advanced mathematical libraries, the model simplicity criteria favours the employment of Beginners All purpose Symbolic Instruction Code (BASIC©) programming language, even though its simplicity would add to the efforts required for model development due to its lack of mathematical libraries. On the other hand, BASIC© is widely understood programming language that offers near plain English commands, which facilitate model understanding and subsequently further development by other researchers. Also its compiler is widely available and is included in all DOS© versions, with a more advanced menu driven version included, free of charge, in latest versions of DOS© and so called QBasic©.

The employment of BASIC© Programming language under DOS© operating system meets the guidelines of Simulation Model Portability (SMP), developed by European Space Agency (ESA) [72] to promote reuse of developed models through minimising models interactions with programming environments and making the models understandable for other developers.

2.3.4 Tyre Modelling

The current trend in both research and industry is biased towards investigation of vehicle performance in the design phase through simulation to reduce cost and enhance performance and safety. As the tyre forms an integral part of the vehicle road interface where all the vehicle handling and ride forces pass through, its characteristics affect the vehicle handling performance. Unfortunately, tyre characteristics are affected non-linearly by a large number of factors, which complicate its simulation. Therefore, a variety of tyre models have been introduced. These models differ in the principles on which they were developed, the number of factors taken into consideration and the amount of computation required.

In physical tyre models, physical relations are used to represent the tyre characteristics, while in empirical tyre models, tyre test results and curve fitting techniques are used to generate the set of equations that represent the tyre

characteristics. In some tyre models, both approaches are combined to develop the equations that represent the tyre characteristics (semi-empirical models).

Dugoff tyre model is a physical tyre model. It was introduced by Dugoff et al., 1970, [73] for use in vehicle handling dynamics modelling. Since its introduction, it has gained popularity in vehicle dynamics research due to its relatively simple equations. On the other hand, the physical analysis of tyre characteristics is a complex problem. "This kind of analysis includes many problems related to deformable solid mechanics, such as: complex geometry and heterogeneity of the material, large displacements and strains, hyperelasticity, variable properties of the cord-rubber composite and contact simulation", [74]. Accordingly, analytical methods of tyre modelling are not accurate enough, especially at high levels of tyre force, due to the too many simplifying assumptions, [74].

Magic Formula (MF) tyre model development was started in the 1980's by Bakker et al., 1989, and since then a number of versions have been introduced. Although, the model equations were originally derived using an innovative curve fitting technique from a large set of tyre experimental data, the MF model also considers the evaluation of tyre longitudinal and lateral forces in the combined slip condition from a physical point of view (semi-empirical) [34].

In 1993 Bayle et al. introduced a purely empirical method based on the MF functions. This model was validated using experimental test data and proved to be satisfactory due to its realistic prediction of the tyre lateral and longitudinal forces the in the case of the combined slip condition, [34]. MF tyre model development was later carried out by Pacejka and Besselink, 1997 in which a physically based tyre model extension was introduced [75].

As the current work focus on the vehicle handling performance through manipulation of wheel speeds that influence tyre longitudinal forces, the capacity of the tyre model to accurately investigate high tyre lateral and longitudinal forces under combined slip conditions has been considered the most important feature. As the MF tyre model, Bayle et al., [34] version, was considered to accurately fulfil this task it has been considered the most suitable for the current work, although its tyre data are not

widely available and its equations are somehow lengthy and complicated. A further investigation into the suitability of this MF tyre model for employment in the current work is presented in Chapter 4.

2.4 Vehicle Handling Control Strategies

As the WSD system will be evaluated through simulation, a precise vehicle handling model must be developed. Accordingly, a control strategy known as Model Predictive Control (MPC) that can make good use of this model has been investigated and found to be suitable.

2.4.1 Model Predictive Control (MPC) Strategy

MPC is an advanced method of control that was developed in the 1970s. The term MPC does not designate a specific control strategy. It, rather, refers to its explicit employment of a dynamic model for the controlled system to obtain a control signal, through minimisation of an objective function.

MPC has been in use in the chemical industry since the 1980s, [76]. Its success in the chemical industry was attributed to the slow rate of change in chemical processes, which enables the computer model employed to be faster than the process under control. As the computer computational power developed, capacity of MPC was investigated in vehicle automation and control field. For example, MPC was employed to analyse vehicle trajectories in order to investigate optimal emergency obstacle avoidance, [77]. It was employed to control multi-vehicle cooperation, [78] and [79], and to stabilise multi-vehicle formation, [80]. It was also introduced to the field of highway automation, through highway dynamic speed control, [81].

The most important features of MPC are summarised as: -

- Explicit use of a model to predict the output of the controlled system at some point in the future.
- Calculation of control sequences to minimise an objective function.

The MPC has many advantages over other control methods. The most important of these are: -

- It can be used to control system with complex dynamics.
- It can deal easily with multivariable systems.
- It facilitates the employment of feed forward control in a natural way to enforce better performance
- Its developed controllers are easy to implement.
- It is particularly useful when a future reference is available.
- It is an open methodology that allows further development.

On the other hand, its drawbacks are: -

- It needs a precise model for the control system.
- Systematic analysis of stability and robustness measurements does not apply.
- The complexity of its control law derivation compared to classical PID controllers.
- High amount of computation required.

The advantages of MPC and the capacity to reduce its disadvantages through careful design of the employed simulation model and its controller have weighted its employment in the current application. A precise vehicle handling model with carefully reduced computational requirements will avoid most of the disadvantages of MPC. Also, a carefully designed controller with well defined future reference points could reduce the controller complexity and facilitate its stability. Accordingly MPC has been chosen for control of the present WSDC system. As MPC facilitates the employment of feedforward control in a natural way, feedforward control has been considered.

2.4.2 Feedforward Control Strategy

Feedforward controllers are controllers that employ knowledge about the controlled system response to inputs to enforce the desired response. Feedforward control has

the advantage of managing system performance drift before it actually takes place and therefore it has been applied to vehicle handling control, [82] and [83]. On the other hand the accuracy of its function relies on the accuracy of the knowledge available about the controlled system. As MPC controllers employ a precise model for the controlled system to investigate its future response, feedforward employment under MPC would be highly convenient for the current application.

To apply feedforward control, the controlled system must meet a set of requirements, namely: -

1- Inputs and / or disturbances must be defined and measurable.

2- Time required for the controlled system to exhibit the undesired performance must be longer than the time required for the controller to evaluate and respond to the inputs or disturbances.

For the current work steering inputs to the vehicle handling model are well defined and easily measurable. On the other hand the time required for the controller to evaluate and respond to the steering angle input, under MPC, is highly dependent on the processing time of the employed vehicle handling model. In general the vehicle handling model processing time has to be faster than real time to allow feasible feedforward control.

2.5 Cartesian Geometric Translation (CGT)

The vehicle handling model is required to work as a real time onboard model to facilitate the control task. It is also required to investigate the contribution of the new proposed Wheel Speed Distribution Control technique on vehicle handling performance. Accordingly, it requires a faster than real time speed as well as monitoring of a wide range of parameters involved in the simulation task, as all the available modeling software packages fail to achieve real time model development [71].

A novel technique of formulating and solving the vehicle simulation model equations to allow higher processing speeds has been introduced. The novel technique, Cartesian Geometric Transition (CGT), allows the use of programming languages to solve the model equations directly, which allows faster running models [71]. This technique employs Newtonian equations, Finite Difference Approximation (FDA) kinematical equations along with geometrical and trigonometrical relations in consecutive finite time frames to investigate the vehicle translation in both local and global Cartesian coordinates. The CGT technique is described in detail through developing half and full vehicle handling models in Chapter 3 and Chapter 5 respectively.

2.6 Conclusions

There is a considerable volume of research linked to vehicle handling problems due to the high impact of this subject on safety. These problems proved hard to overcome due to the high number of nonlinearities. Different systems have been developed to control force distribution across the vehicle track to influence the vehicle yaw rate and consequently improve vehicle directional response. However, all the developed solutions had limitations or drawbacks that limited their implementation.

Although TFD systems enforce changes in wheel speeds to generate force differences, controlling vehicle wheel speeds have not been investigated, even though wheel speeds are easier to measure than wheel forces. Such systems do not encounter force discontinuities that would be experienced with TFD systems. In this research a novel chassis subsystem "Wheel Speed Distribution Control" (WSDC) has been developed and its effect on vehicle handling has been investigated using simulation.

Advanced simulation packages and other multi-body packages were found incapable of real time operation and have no provision for connecting to hardware, [69]. Accordingly, a different approach had to be investigated. In order to deliver a simulation model with a faster than real time speed, a small size to permit onboard model features, ease of understanding, lower interaction with modelling environment

and more comprehensiveness, the novel modelling CGT technique has been developed. This technique was used to develop the WSDC full vehicle handling model.

The main problem in utilising wheel speed control in vehicle handling systems, is linked to the non linear characteristics of the tyre that lead to uncertainty about how much rotational speed would be required to generate the required longitudinal force under a given condition of longitudinal speed and lateral slip. However, the development of the MF tyre model for combined slip, which accurately estimates the forces generated due to given longitudinal slip and slip angle could be considered a step towards the removal of this barrier. However, a tyre model that estimates tyre longitudinal slip and slip angle due to applied forces would be more appropriate for wheel speed distribution control. The suitability of MF tyre model for combined slip and its adaptation to fit in the current research has been investigated.

Another problem is the controller output accuracy as there is no direct means to check it. Accordingly, in most systems, measuring vehicle yaw rate is the only method to check the controller output. Given that yaw rate needs time to develop, if it was found that the wrong yaw rate had been developed, it would be too late to manage a correction efficiently. Given the vehicle high speed, high safety requirements and tyre response delay, systems that rely on yaw rate feedback control would not be appropriate, yet current systems rely on yaw rate feedback control, [48] and [49]. Accordingly, the onboard real time vehicle handling model has been considered necessary to estimate the vehicle response and give the control unit an early indication of the handling situation. For this purpose, a MPC strategy has been employed, in feedforward fashion, to facilitate the employment of, the developed, real time onboard model to achieve better control and save precious time for vehicle handling performance improvement.

As there is currently no chassis subsystem capable of employing WSDC, dedicated hardware has been developed "Wheel Speed Distribution Differential" WSDD. It was developed with the aims of facilitating WSDC and solving the drawbacks associated with reviewed systems in order to promote its implementation.

2.7 Aims and Objectives

The aims of the current work are to introduce a novel WSDC vehicle chassis system, to prove its capacity to enhance vehicle handling performance, and to facilitate its application.

To carry out these aims a number of objectives have been put forward: -

1. To develop a modelling technique with high processing speed, in order to facilitate the vehicle handling simulation and its control. This system will be validated through development of the well known half vehicle (bicycle) handling model and comparison of its predictions with published data.

2. To adapt the Magic Formula tyre model for employment in the validated vehicle handling model.

3. To upgrade the developed half vehicle handling model to a full vehicle handling model fitted with the adapted MF tyre model and the capacity to regulate the driven wheel speeds.

4. To design a vehicle handling controller based on MPC and feedforward strategies to apply the WSDC, to integrate this in the validated vehicle handling model and to investigate the vehicle handling performance improvements due to WSDC employment.

5. Upon the establishment of the WSDC benefits, to design feasible hardware that can put the theoretical WSDC into practice, and to analyse its performance, production, maintenance and control requirements.

6. To incorporate the hardware model into the developed WSDC vehicle handling model and to demonstrate the full WSDC system potential to enhance vehicle handling performance.

Chapter 3

CGT Half Vehicle Handling Model

3.1 Introduction

A model is software, hardware or software and hardware tool which is used to investigate the performance of a specific system under different working conditions. The models are usually used in the design stage of a system to reduce the cost of hardware development, through investigation of its functionality and performance before production. Also the models can be used in the control stage as onboard models that would feed the controller its prediction of the system performance under a given situation in advance, to give Model Predictive Control (MPC).

A vehicle handling model is usually developed to investigate the effect of its different sub-systems upon the handling performance. These vehicle handling models usually incorporate a set of equations that represent the vehicle performance in handling situations. This set of equations describes the dynamic relationships governing the vehicle movement in global (fixed) X-Y plane with local x-y axis, Fig (3.1). It also may include the effect of vehicle dynamics in other planes that influence the vehicle handling. By solving this set of equations using a set of vehicle parameters and a handling situation, the vehicle handling performance and how it is affected by different vehicle subsystems can be investigated.

For the current work the developed vehicle handling model aims at two targets. The first is to investigate the effect of the proposed Wheel Velocity Distribution Control (WSDC) system upon the vehicle handling performance. The second is to meet the requirements of onboard models as required for the MPC based controller planned for the WDSC system. The onboard models should be small sized, capable of being integrated with actual controllers and be able to run faster than real time to facilitate the control process.

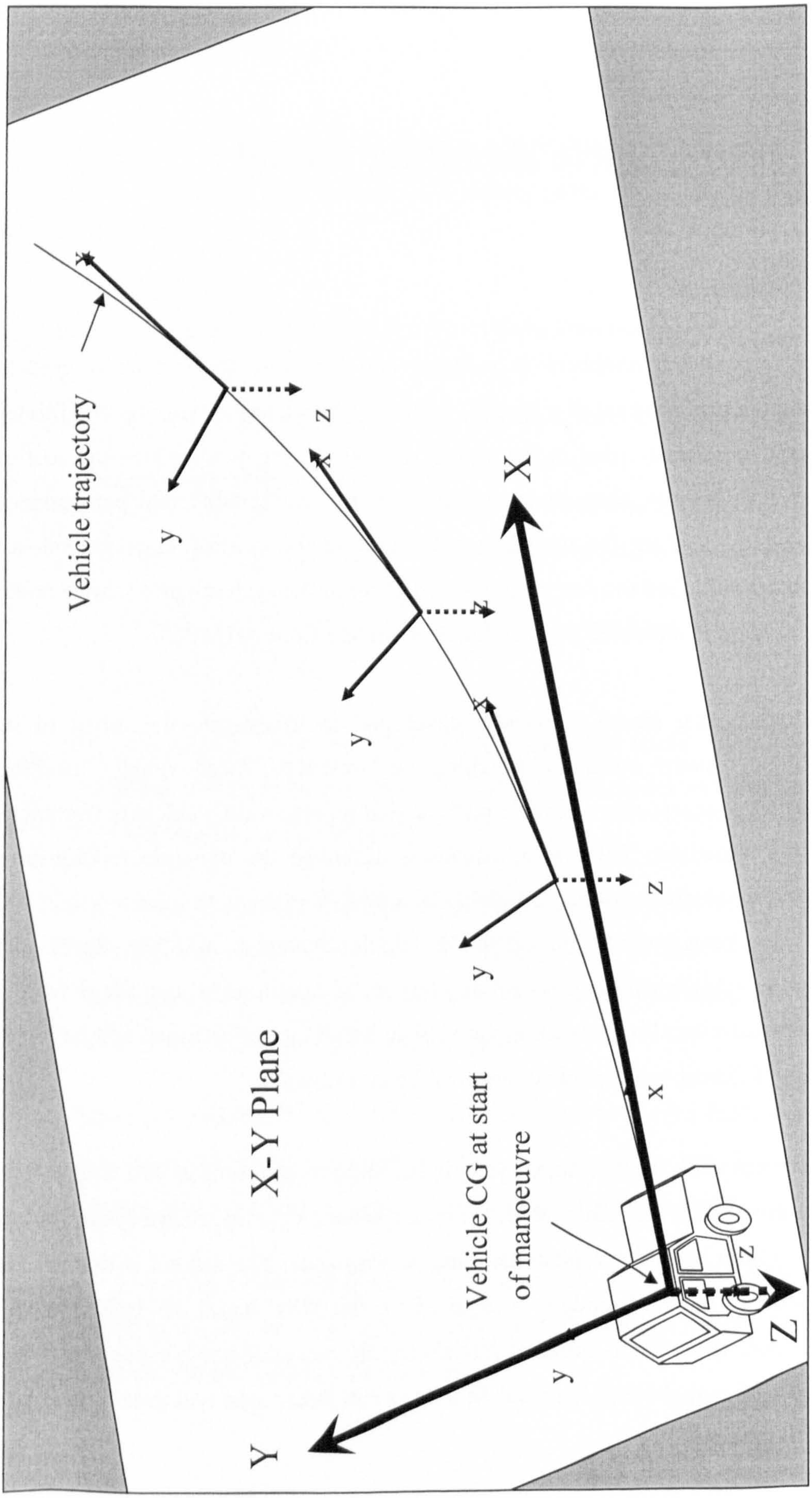

Fig (3.1) Global (fixed) and local (moving) axis systems of vehicle during a manoeuvre

In this chapter, the environment used for simulation and the simulation technique is presented and tested through a case study of the well known half vehicle (bicycle) handling model. For this purpose, a half vehicle handling model has been derived and tested through comparison with the reviewed results.

3.2 Software Issue

As the vehicle handling model is usually a set of equations that represent the vehicle dynamics, there is always the issue of how accurate these equations represent the true behaviour. The trade off between model accuracy and model simplicity has been a subject of much debate. A simple, inaccurate, model is small and fast but may produce misleading results, which would violate the basic requirements of the modelling. On the other hand a complex model will take longer to develop, longer time to run and take up more computer resources, even though there is not an assurance of achieving more realistic results.

Although high model accuracy is desirable, it requires a larger and more complicated set of equations, which would in turn require a significant effort to develop. Also the different numerical techniques and software packages used to solve this model will restrict the number of factors employed in the model. Another important factor is the model running time as the onboard model is required to run faster than real time, which all the available modelling software packages fail to achieve [68]. Therefore, a new technique will be used to formulate the vehicle model equations to allow greater flexibility has been introduced and tested in this chapter. The novel technique, Cartesian Geometric Translation (CGT) allows the use of programming languages to solve the model equations directly, and this facilitates its rapid execution [68].

The CGT technique is also meant to meet the new objectives of Simulation Model Portability (SMP) developed by the European Space Agency (ESA) [71], to promote portability of models among different simulation environments and operating systems, and to promote the reuse of simulation models. These objectives are mainly: -

- Minimise model interactions with environment
- Make the model understandable for other developers

To develop a faster running model, as a first priority for MPC, the computer has to allocate all its processing capacity to the model. Accordingly, the operating system has to be non-multitasking (non Windows©) as in multitasking operating systems every program is allowed only a share of the computer resources. Also, the operating system would be preferred not to have a Graphical User Interface GUI (non Windows©) because graphics consumes a considerable share of computer resources. Taking these measures into account along with availability, popularity and the size of different operating systems the operating system has been chosen to be the Disk Operating System DOS©.

DOS© is unique among other operating system in its very small footprint. Some DOS© versions are less than a 100 kb in size, which make it highly portable. It is also supported by all PC based computers and embedded in the widely available and popular Windows© based operating systems.

To minimise model interactions with the environment the decision has been taken to use a programming language. Accordingly, the developed model could be compiled to generate an executable code capable of running under a wide range of operating systems. Also, taking into account making the model understandable for other developers, the decision has been taken to use the widely understood programming language Beginners All purpose Symbolic Instruction Code BASIC©. Although the BASIC© language only offers a small set of commands and does not offer libraries to the programmer, which would make the programming task harder, the decision has been taken to employ it, based on Pidd's 1996 principle "Model Simple – Think Complicated" [66].

3.3 Cartesian Geometric Translation Technique

A vehicle handling model is required to study the effect of the new proposed Wheel Velocity Distribution Control technique upon vehicle handling behaviour, and to work as a real time onboard model for its MPC based controller. Accordingly, it requires a handling prediction capability, faster than real time, as well as the ability to monitor all the parameters involved in the simulation task. In order to do this, a novel approach has been introduced, termed the Cartesian Geometric Translation (CGT) technique.

This technique employs Newtonian equations and a Finite Difference Approximation (FDA) set of kinematical equations in consecutive finite time frames. It also employs geometrical and trigonometrical relations to investigate the vehicle Translation in Cartesian coordinates. To use this technique standard sign convention of directions and angles have to be adhered to due to the use of trigonometric functions that are sensitive to direction and angle signs. Accordingly, all angles will be positive in Counter Clock Wise (CCW) direction and negative in Clock Wise (CW) direction.

In the CGT technique, the equations are not combined together to generate a small set of equations that represent the whole system. Instead, all the equations are left in their simplest form. Also, some equations are manipulated to allow the use of geometrical solvers. The set of equations used in this solving technique are introduced in next sections.

3.3.1 Acceleration Calculation

The time frame acceleration is calculated using the Newtonian equations of motion. The acceleration in any given direction is calculated by dividing the time frame initial force acting in this direction by the body mass. For planar motion, accelerations in x and y are given by equations (3.1) and (3.2) respectively. The angular acceleration around z axis, $\ddot{\psi}_z$ is calculated by dividing the time frame initial torque M_z by the body's moment of inertia around this axle, I_z, Eq.(3.3).

$$\ddot{x} = \left(\frac{F_x}{m}\right) \tag{3.1}$$

$$\ddot{y} = \left(\frac{F_y}{m}\right) \tag{3.2}$$

$$\ddot{\psi}_z = \left(\frac{M_z}{I_z}\right) \tag{3.3}$$

3.3.2 Velocity Calculation

The final velocity of a solid body within a time frame is calculated using the Finite Difference Approximation version of the kinematic equations. For both linear and angular motions, the time frame final velocities $\dot{x}_1$, $\dot{y}_1$ and $\dot{\psi}_1$ are calculated by adding the time frame accelerations $\ddot{x}$, $\ddot{y}$ and $\ddot{\psi}$ multiplied by the time frame width Δt to the initial time frame velocities, $\dot{x}_0$, $\dot{y}_0$ and $\dot{\psi}_0$, Eq.(3.4), Eq.(3.5) and Eq. (3.6) respectively.

$$\dot{x}_1 = \dot{x}_0 + \ddot{x}\Delta t \tag{3.4}$$

$$\dot{y}_1 = \dot{y}_0 + \ddot{y}\Delta t \tag{3.5}$$

$$\dot{\psi}_1 = \dot{\psi}_0 + \ddot{\psi}\ \Delta t \tag{3.6}$$

3.3.3 Translation Calculation

The body translation, Δx, Δy and $\Delta \psi$ in the time frame of Δt are calculated using the Finite Difference Approximation version of the kinematic equations. For both linear and angular motions, the translation is calculated by multiplying the mean velocity of the interval by the time step Δt, Eq.(3.7), Eq.(3.8) and Eq.(3.9).

$$\Delta x = \left(\frac{\dot{x}_0 + \dot{x}_1}{2}\right)\Delta t \tag{3.7}$$

$$\Delta y = \left(\frac{\dot{y}_0 + \dot{y}_1}{2} \right) \Delta t \tag{3.8}$$

$$\Delta \psi = \left(\frac{\dot{\psi}_0 + \dot{\psi}_1}{2} \right) \Delta t \tag{3.9}$$

3.3.4 Location Calculation

For a linear movement the new body location in x and y directions, x_1 and y_1 are calculated by adding the linear translations, Δx and Δy, to the initial locations, x_0 and y_0, Eq.(3.10) and Eq.(3.11). The angular location is calculated by adding the angular translation, $\Delta\psi$, to the body initial angle, ψ_0, Eq.(3.12).

$$x_1 = x_0 + \Delta x \tag{3.10}$$

$$y_1 = y_0 + \Delta y \tag{3.11}$$

$$\psi_1 = \psi_0 + \Delta \psi \tag{3.12}$$

3.3.5 Angles Calculation

The angles are calculated from the geometric equation of straight line slope, Eq.(3.13) and equation Eq.(3.14) is used to determine the angle ψ.

$$\tan(\psi) = \left(\frac{y_1 - y_0}{x_1 - x_0} \right) \tag{3.13}$$

$$\psi = \tan^{-1} \left(\frac{y_1 - y_0}{x_1 - x_0} \right) \tag{3.14}$$

This set of equations is used to determine the dynamic state of a solid body in consecutive finite time frames. By transforming the results at the end of each time frame to global coordinates the body path and dynamic performance can be investigated. To clarify and validate the CGT technique a case study has been carried out. In this case study the CGT technique has been used to develop the well known half vehicle (bicycle) handling model. The CGT model parameters and derivation is presented in the next sections.

3.4 Model Parameters

For a vehicle handling model to run, a specific set of input parameters is needed. They describe the vehicle and the handling situation. In this section both the input and output parameters of the current CGT vehicle handling model are presented.

3.4.1 Vehicle Parameters

The set of vehicle parameters required to define the vehicle for the current CGT half vehicle handling model are given in Table (3.1)

Vehicle Parameter	Symbol	Units
Mass	m	kg
Yaw moment of inertia	I	kg m^2
CG to front axle distance	a	m
CG to rear axle distance	b	m
Front axle cornering stiffness	$C_{\alpha f}$	N / rad
Rear axle cornering stiffness	$C_{\alpha r}$	N / rad

Table (3.1) Vehicle parameters

3.4.2 Vehicle Handling Parameters

For the current vehicle handling model, both the vehicle longitudinal velocity and steering angle are required to define the handling condition. The required handling parameters, their symbols and units are shown in Table (3.2).

Handling Parameter	Symbol	Units
Forward velocity	u	m / s
Steering angle	δ	deg

Table (3.2) Vehicle handling parameters

3.4.3 Model Run Parameters

For this technique, a fixed time increment (time frame width) Δt is required for the modelling task, Table (3.3).

Running Parameter	Symbol	Units
Time increment	Δt	s

Table (3.3) Vehicle handling simulation parameters

3.4.4 Model Outputs

The model is capable of defining the vehicle handling simulation through deriving the values of a comprehensive set of parameters. The set of parameters is derived at the end of each time frame. A list of the model outputs, their symbols and units are shown in Table (3.4), noting that adding a small zero as a subscript means a time frame initial value, while adding 1 means a time frame final value.

3.4.5 Axis System

The vehicle local coordinates are used to define the vehicle geometry in which the origin of the local coordinates is taken at the vehicle CG. The x axis lies on the initial

vehicle longitudinal axis. The y axis passes through the vehicle CG in the lateral direction, Fig (3.2). The origin is taken at the vehicle CG to allow better geometrical relations for the vehicle CG movements and the front and the rear wheels. In the initial vehicle position both vehicle local x-y coordinates and global X-Y coordinates are coincident, Fig (3.2).

Model output	Symbol	Units
CG location on X coordinate	X_{CG}	m
CG location on Y coordinate	Y_{CG}	m
Vehicle axle to X axis angle	Θ	rad
Longitudinal velocity	u	m / s
Longitudinal acceleration	$\dot{u}$	m / s^2
Lateral velocity	v	m / s
Lateral acceleration	$\dot{v}$	m / s^2
Yaw velocity	$\dot{\theta}$	rad / s
Yaw acceleration	$\ddot{\theta}$	rad / s^2
Front slip angle	α_f	rad
Rear slip angle	α_r	rad
Front lateral force	F_{yf}	N
Rear lateral force	F_{yr}	N
CG longitudinal force	F_{xCG}	N
CG lateral force	F_{yCG}	N
CG moment	M_{CG}	Nm

Table (3.4) Vehicle handling simulation outputs

According to Fig (3.2) the vehicle initial location in its local coordinates can be defined, Table (3.5).

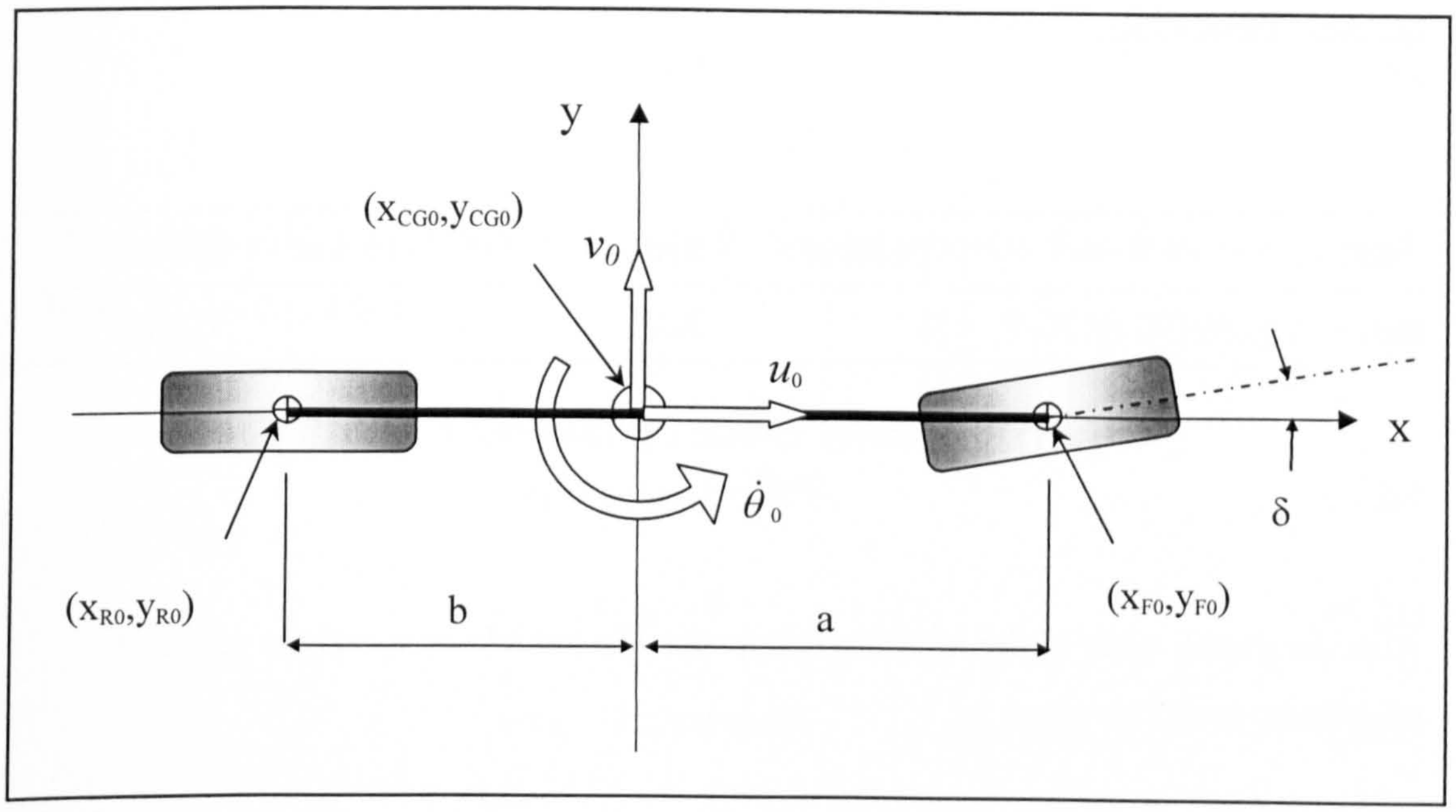

Fig (3.2) Vehicle initial location on the local coordinates

Point	x location	Symbol	y location	Symbol
Initial rear axle centre	-b	x_{r0}	0	y_{r0}
Initial vehicle CG	0	x_{CG0}	0	y_{CG0}
Initial front axle centre	a	x_{f0}	0	y_{f0}

Table (3.5) Vehicle initial location on the local coordinates

Also from Fig (3.2): -

$$\theta_0 = 0 \tag{3.15}$$

Where: -

θ_0 The initial angle between local x axis and vehicle axle

In the first step, the local coordinates are coincident with the global coordinates. Accordingly, the starting vehicle CG location in the global coordinates are easily defined, Table (3.6).

Point	X location	Symbol	Y location	Symbol
Initial vehicle CG on X-Y	0	X_{CG0}	0	Y_{CG0}

Table (3.6) Initial vehicle CG location on X-Y

Also the initial value of the total angle between the vehicle axle and the global X coordinate could be given as: -

$$\Theta_{CG0} = 0 \tag{3.16}$$

Where: -

Θ_{CG0} Initial angle between the vehicle axle and X axis

3.5 Model Derivation

To clarify the model and the solving technique, the model flowchart is presented in Fig (3.3). Also, the derivation of the model equations is presented in the next sections. The model equations have been arranged to follow and hence clarify the model data processing steps.

3.5.1 Vehicle Initial Conditions

The vehicle initial conditions at the start of the simulation are given in Eq.(3.17), Eq. (3.18) and Eq.(3.19).

$$u_0 = Initial\ vehicle\ forward\ velocity \tag{3.17}$$

$$v_0 = 0 \tag{3.18}$$

$$\dot{\theta}_0 = 0 \tag{3.19}$$

The vehicle initial conditions that apply at the start of every time frame are given in Eq.(3.20) to Eq.(3.24).

$$(x_{CG0}, y_{CG0}) = (0,0) \tag{3.20}$$

$$\theta_{CG0} = 0 \tag{3.21}$$

$$(x_{F0}, y_{F0}) = (a,0) \tag{3.22}$$

$$(x_{R0}, y_{R0}) = (-b,0) \tag{3.23}$$

$$\delta = \textit{Given steering angle} \tag{3.24}$$

3.5.2 CG Forces and Moments

At the start of every time frame the CG longitudinal and lateral forces are calculated as the resultant of tyre forces, Fig (3.4), Eq.(3.25) and Eq. (3.26). Also, the moment of the forces at the vehicle CG is calculated using Eq.(3.27), Fig (3.4).

$$F_{xCG0} = F_{xR0} - F_{yF0}\sin(\delta) \tag{3.25}$$

$$F_{yCG0} = F_{yR0} + F_{yF0}\cos(\delta) \tag{3.26}$$

$$M_{CG0} = aF_{yF0}\cos(\delta) - bF_{yR0} \tag{3.27}$$

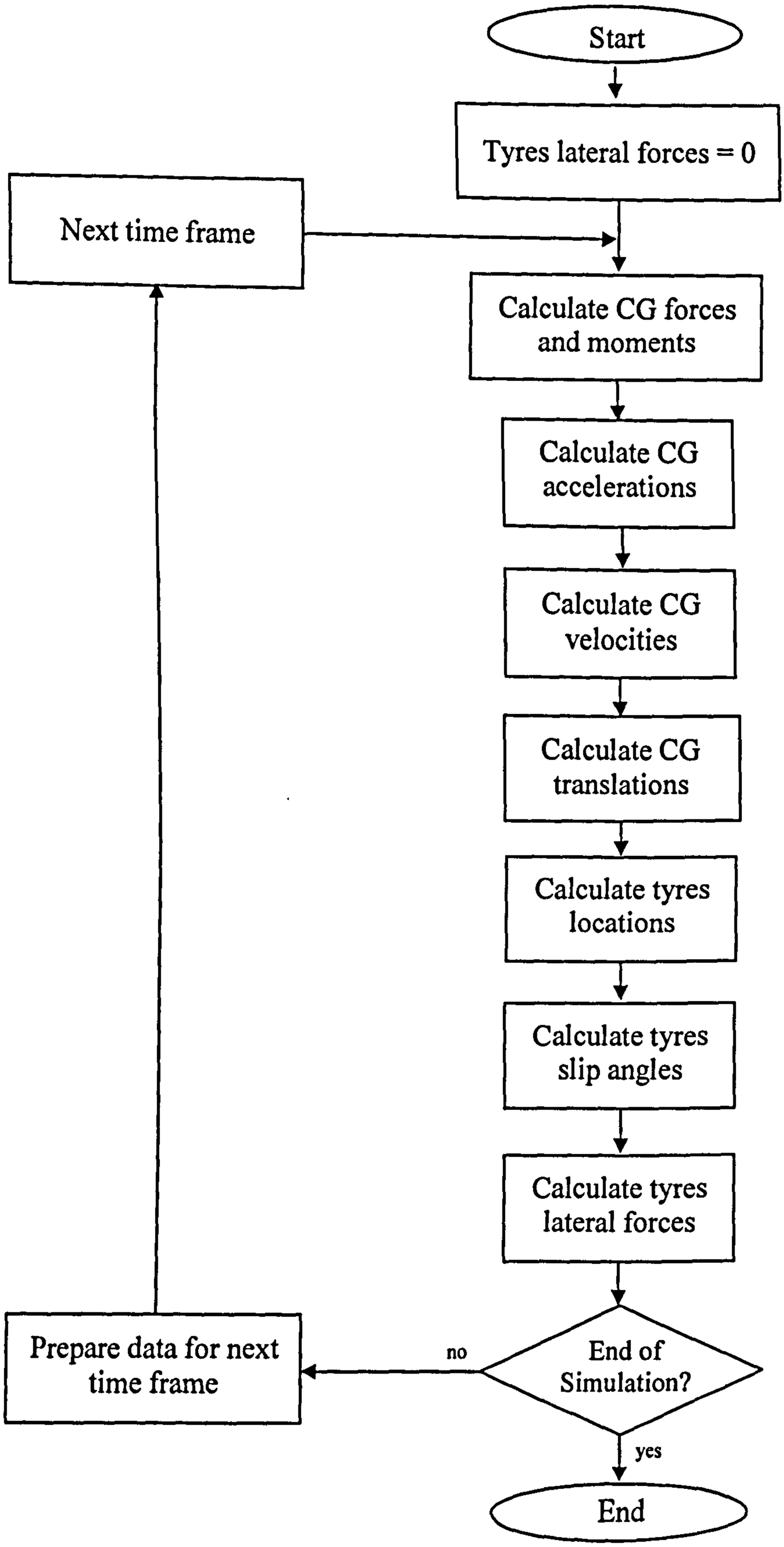

Fig (3. 3) Vehicle handling model flowchart

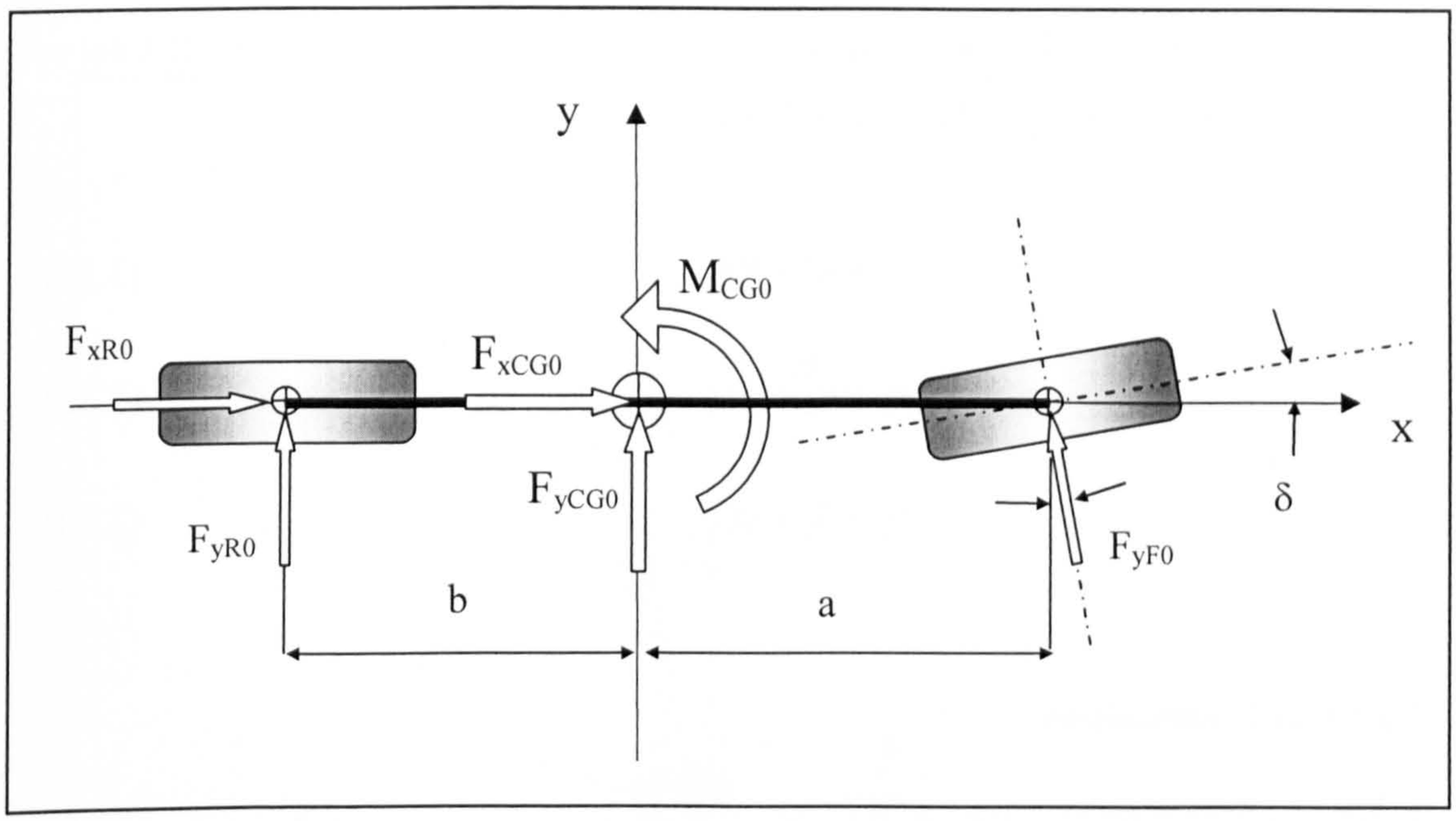

Fig (3.4) Forces and moments acting on the vehicle

3.5.3 CG Accelerations

The vehicle CG accelerations are calculated using Newtonian equations. Longitudinal and lateral accelerations are calculated by dividing the initial frame force in the longitudinal and lateral directions respectively by the vehicle mass (m), Eq.(3.28) and Eq.(3.29). The yaw acceleration is calculated by dividing the initial frame moments around the vehicle CG by the vehicle yaw moment of inertia (I), Eq.(3.30).

$$\dot{u} = \left(\frac{F_{xCG0}}{m} \right) \tag{3.28}$$

$$\dot{v} = \left(\frac{F_{yCG0}}{m} \right) \tag{3.29}$$

$$\ddot{\theta} = \left(\frac{M_{CG0}}{I} \right) \tag{3.30}$$

3.5.4 Final CG Velocity

The final velocities at the end of each time frame are calculated using the FDA set of kinematics equations Eq.(3.31), Eq.(3.32) and Eq.(3.33).

$$u_1 = u_0 + \dot{u}\Delta t \tag{3.31}$$

$$v_1 = v_0 + \dot{v}\Delta t \tag{3.32}$$

$$\dot{\theta}_1 = \dot{\theta}_0 + \ddot{\theta}\Delta t \tag{3.33}$$

3.5.5 CG Translations

As the vehicle initial and final velocities of the time frame are defined the vehicle translation during this time frame can also be defined, Fig (3.5). For both linear and angular translations the amount of translation is calculated from the FDA set of kinematic equations by multiplying the mean velocity of the time frame by the time frame width Δt, Eq.(3.34), Eq.(3.35) and Eq.(3.36).

$$\Delta x_{CG} = \left(\frac{u_0 + u_1}{2}\right)\Delta t \tag{3.34}$$

$$\Delta y_{CG} = \left(\frac{v_0 + v_1}{2}\right)\Delta t \tag{3.35}$$

$$\Delta \theta_{CG} = \left(\frac{\dot{\theta}_0 + \dot{\theta}_1}{2}\right)\Delta t \tag{3.36}$$

3.5.6 CG Final Location

The vehicle final location in local x-y coordinates, Fig (3.5) is defined by adding the vehicle translations to its initial location in the same x-y coordinates, Eq.(3.37), Eq.(3.38) and Eq.(3.39).

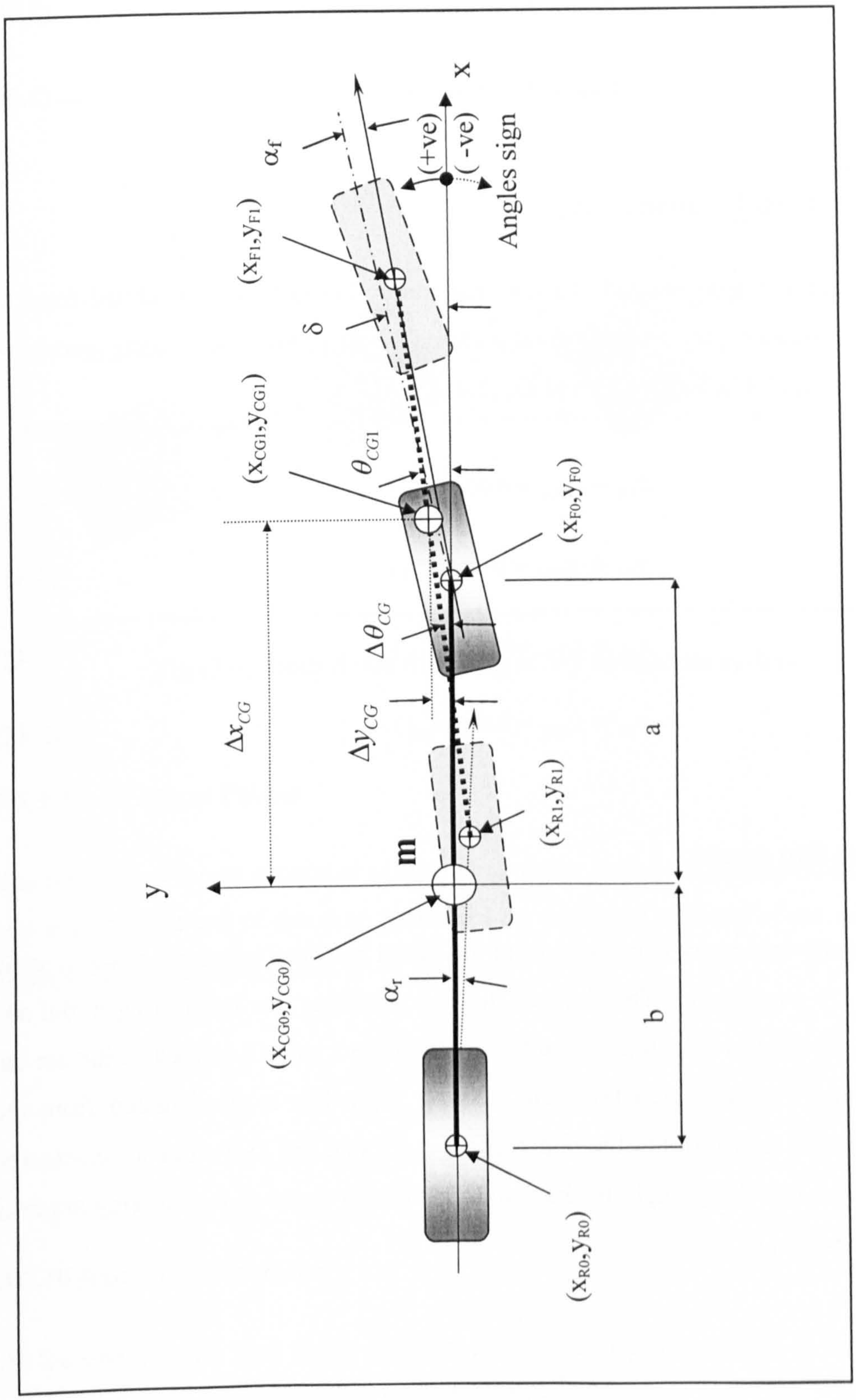

Fig (3.5) Representation of the vehicle translation on the x-y plane

$$x_{CG1} = x_{CG0} + \Delta x_{CG} \tag{3.37}$$

$$y_{CG1} = y_{CG0} + \Delta y_{CG} \tag{3.38}$$

$$\theta_{CG1} = \theta_{CG0} + \Delta \theta_{CG} \tag{3.39}$$

3.5.7 Tyre Final Locations

The tyres locations at the end of each time frame, Fig (3.5) are calculated from the CG final location, the vehicle final yaw angle θ_{CG1} and the vehicle geometry, Eq.(3.40), Eq.(3.41), Eq.(3.42), and Eq.(3.43).

$$x_{F1} = x_{CG1} + a\cos(\theta_{CG1}) \tag{3.40}$$

$$y_{F1} = y_{CG1} + a\sin(\theta_{CG1}) \tag{3.41}$$

$$x_{R1} = x_{CG1} - b\cos(\theta_{CG1}) \tag{3.42}$$

$$y_{R1} = y_{CG1} - b\sin(\theta_{CG1}) \tag{3.43}$$

3.5.8 Tyre Slip Angles

The tyres slip angles are calculated from the initial and final locations of the tyres in the local x-y coordinates. The slope of the tyre travelling line connecting initial and final tyre location is calculated, then the angle to the x axis is derived as the arc tan of the slope. For a steered tyre, the steering angle has to be deduced from the obtained angle to determine the slip angle, Eq. (3.44), Fig (3.6). For a non-steered tyre, the tyre travelling angle to the x axis is the slip angle as the steering angle is equal to zero, Eq.(3.45).

$$\alpha_F = \tan^{-1}\left(\frac{y_{F1} - y_{F0}}{x_{F1} - x_{F0}}\right) - \delta \tag{3.44}$$

$$\alpha_R = \tan^{-1}\left(\frac{y_{R1} - y_{R0}}{x_{R1} - x_{R0}}\right) \tag{3.45}$$

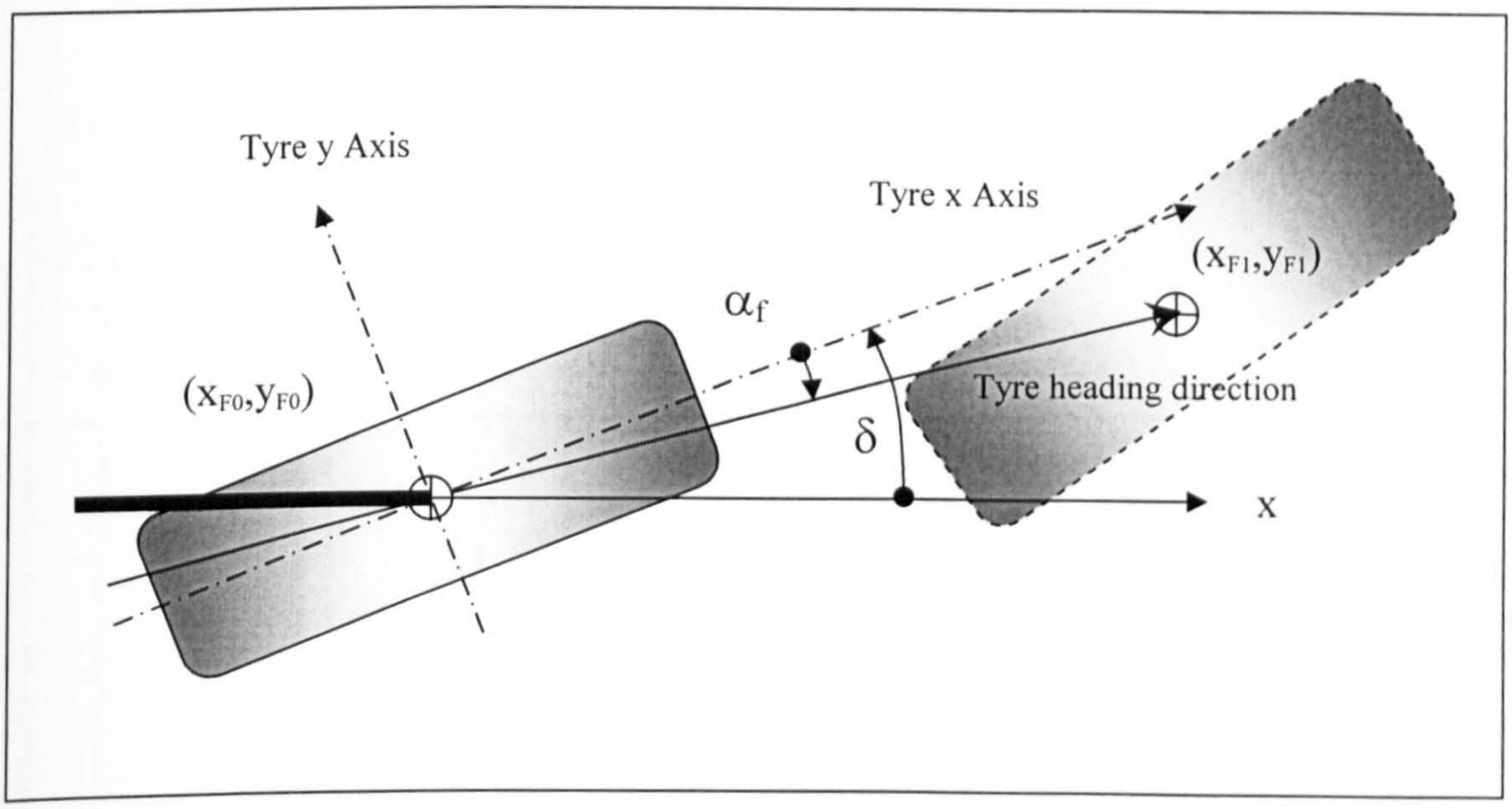

Fig (3.6) Steered tyre travelling in x-y coordinate system

3.5.9 Tyre Lateral Forces

The tyre lateral forces generated at the end of a time frame are calculated from the slip angles at the end of that time frame and the cornering stiffness of the vehicle tyres, Eq.(3.46) and Eq.(3.47).

$$F_{yF1} = -\alpha_F C_{\alpha F} \tag{3.46}$$

$$F_{yR1} = -\alpha_R C_{\alpha R} \tag{3.47}$$

3.5.10 Axis Transformation

At the end of each time frame the vehicle CG translations defined in the local x-y coordinates are transformed to global X-Y coordinates, Fig (3.7). The vehicle translation in local x-y coordinates along with the local coordinates location are used

to determine the final vehicle CG location and yaw in the global coordinate system, Eq.(3.48), Eq.(3.49) and Eq.(3.50).

$$X_{CG1} = X_{CG0} + x_{CG1}\cos(\Theta_{CG0}) - y_{CG1}\sin(\Theta_{CG0}) \tag{3.48}$$

$$Y_{CG1} = Y_{CG0} + y_{CG1}\cos(\Theta_{CG0}) + x_{CG1}\sin(\Theta_{CG0}) \tag{3.49}$$

$$\Theta_{CG1} = \Theta_{CG0} + \theta_{CG1} \tag{3.50}$$

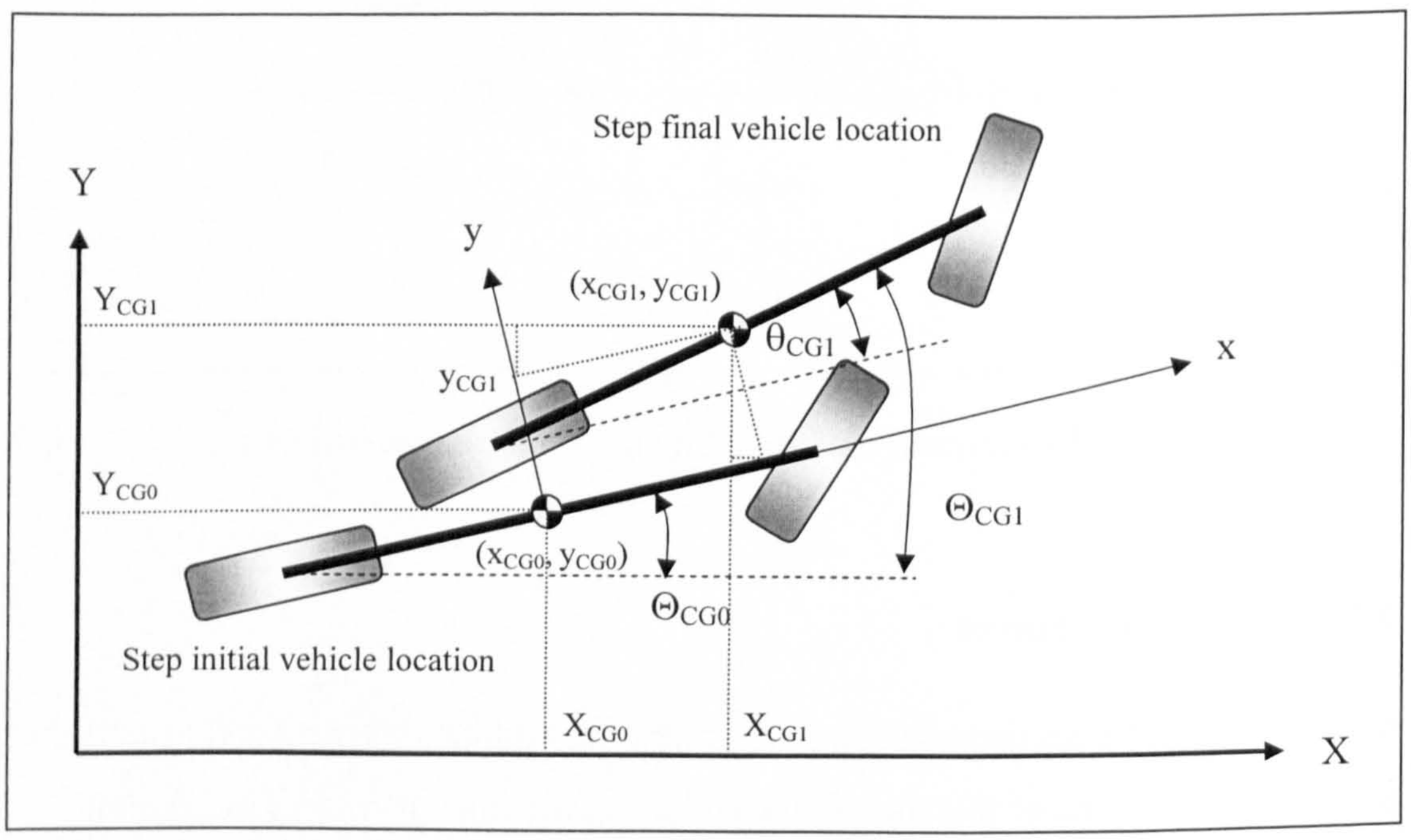

Fig (3.7) Vehicle handling results transfer to global coordinates

3.5.11 Initial Velocities of Next Time Frame

In preparation for the next time frame, the vehicle velocities in x and y directions at the end of each time frame are transformed to the new vehicle local coordinates, Fig (3.8). The main factor affecting this transformation is the yaw angular displacement $\Delta\theta_{CG}$. The new linear velocities are calculated using Eq.(3.51) and Eq.(3.52), while the yaw rate is untransformed, Eq.(3.53). The vehicle velocities u_0, v_0 and $\dot{\theta}_0$ in Eq. (3.51), Eq.(3.52) and Eq.(3.53) refer to the initial values of the next time frame.

$$u_0 = u_1 \cos(\Delta\theta_{CG}) + v_1 \sin(\Delta\theta_{CG}) \tag{3.51}$$

$$v_0 = v_1 \cos(\Delta\theta_{CG}) - u_1 \sin(\Delta\theta_{CG}) \tag{3.52}$$

$$\dot{\theta}_0 = \dot{\theta}_1 \tag{3.53}$$

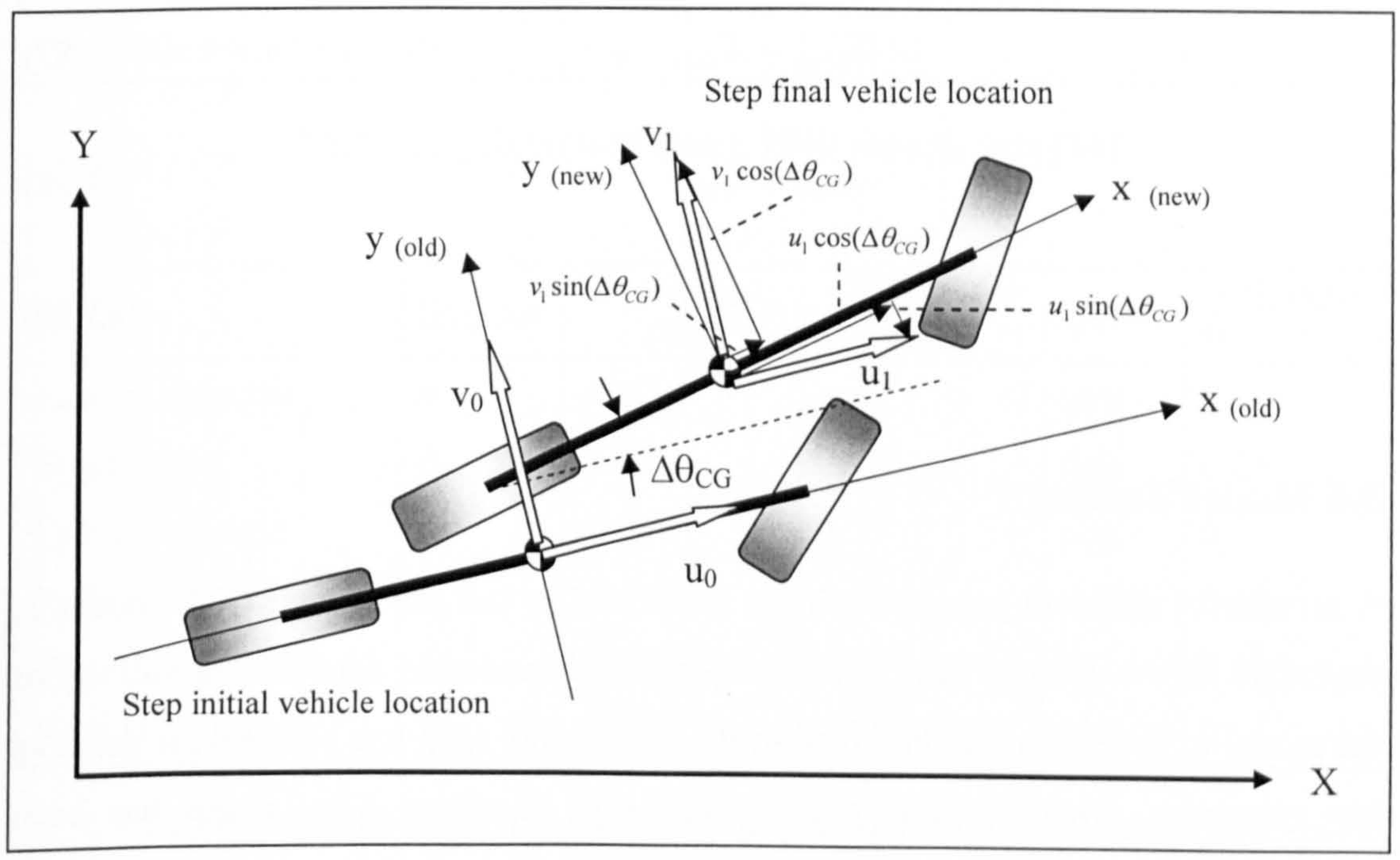

Fig (3.8) Vehicle parameters transfer to new local coordinates

3.5.12 Initial Forces of Next Time Frame

The initial lateral tyre forces of the next time frame are the same tyre forces resulting from the slip angles at the end of the current time frame, Eq.(3.54) and Eq.(3.55), while the longitudinal driven tyre force would remain as that applied by the vehicle engine, Eq.(3.56),

$$F_{yF0} = F_{yF1} \tag{3.54}$$

$$F_{yR0} = F_{yR1} \tag{3.55}$$

$$F_{xR0} = F_{xR1} \tag{3.56}$$

3.5.13 Initial CG Position of Next Time Frame

In the global coordinate system the final vehicle CG location and orientation in a time frame become the initial vehicle CG location and orientation of the next time frame, Eq.(3.57), Eq.(3.58) and Eq.(3.59).

$$X_{CG0} = X_{CG1} \tag{3.57}$$

$$Y_{CG0} = Y_{CG1} \tag{3.58}$$

$$\Theta_{CG0} = \Theta_{CG1} \tag{3.59}$$

3.6 Model Testing

A number of different procedures have been used to test the current CGT model as described below. Results have been compared with reviewed data. The sensitivity of the model to the parameter involved in the simulation, (Δt), has been investigated as has symmetry, when evaluating CCW and CW handling. Also, a test has been carried out to investigate the CGT model compliance with vehicle understeer, oversteer and neutral steer behaviour. Finally, a demonstration of the wide range of model outputs is presented.

3.6.1 Comparison with Reviewed Data

In these tests typical published vehicle data and handling conditions have been used to derive the corresponding vehicle handling results. Then the model results, using Δt = 0.001 s, have been compared to the published results.

The first reviewed vehicle is a Buick 1949 vehicle, Table (3.7) [84]. The reviewed vehicle model was driven at 0.3g rightward turn at a fixed forward velocity of 20 m/s. The reviewed results and the new CGT model results are summarised in Table (3.8).

Parameter	Symbol	Buick 1949	Units
Mass	m	2045	kg
Yaw Inertia	I	5428	kg m^2
CG to front axle	a	1.488	m
CG to rear axle	b	1.712	m
Front axle cornering stiffness	C_{af}	77850	N/rad
Rear axle cornering stiffness	C_{ar}	76510	N/rad

Table (3.7) Reviewed Buick 1949 vehicle data [84]

Results	Symbol	Reviewed [84]	CGT model results	Units	Difference %
Lateral velocity	v	-0.48	0.48	m/s	0
Steer angle	δ_f	1.62	-1.62	deg	0.25
Front slip angle	α_f	-2.37	2.37	deg	0
Rear slip angle	α_r	-2.09	2.1	deg	0.48
Front lateral force	F_{yf}	3220	-3223	N	0.09
Rear lateral force	F_{yr}	2800	-2800	N	0

Table (3.8) Reviewed and CGT handling model results of Buick 1949

The second reviewed vehicle is a Ferrari Monza vehicle, Table (3.9) [84]. The reviewed vehicle model was driven at 0.3g rightward turn at a fixed forward velocity of 20 m/s. The reviewed results and the new CGT model results are summarised in Table (3.10).

Parameter	Symbol	Ferrari Monza	Units
Mass	m	1008	kg
Yaw Inertia	I	1031	kg m^2
CG to front axle	a	1.234	m
CG to rear axle	b	1.022	m
Front axle cornering stiffness	C_{af}	117440	N/rad
Rear axle cornering stiffness	C_{ar}	144930	N/rad

Table (3.9) Reviewed Ferrari Monza vehicle data [84]

Results	Symbol	Reviewed [84]	CGT model results	Units	Difference %
Lateral velocity	v	-0.07	0.07	m/s	0
Steer angle	δ_f	0.96	-0.97	deg	1.04
Front slip angle	α_f	-0.66	0.66	deg	0
Rear slip angle	α_r	-0.64	0.64	deg	0
Front lateral force	F_{yf}	1340	-1344	N	0.3
Rear lateral force	F_{yr}	1620	-1622	N	0.12

Table (3.10) Reviewed and CGT handling results model of Ferrari Monza

The CGT vehicle handling model results are highly comparable to the reviewed results with a percentage difference mostly in the range of less than 0.5%. The sign differences are due to the CGT model employment of standard coordinate sign convention. Since the CGT model has to adapt standard sign convention due to its employment of trigonometric functions that are sensitive to these signs.

In the third test the CGT model has been tested for higher vehicle velocities. For the reviewed vehicles (Buick and Ferrari), the yaw rate response at 0.3g rightward turn and 50 m/s forward velocity has been plotted against time for comparison [84], Fig (3.9). The new CGT model has been used to investigate the yaw rate response for the same vehicles at the same driving conditions, Fig (3.10). Ferrari and Buick yaw rate response curves derived from the CGT model are highly comparable to the reviewed curves, Fig (3.9), taking into account the different sign convention.

In the light of these testing results, the new CGT model results have been considered as validation of the new modelling technique and therefore the model is able to form a strong base for further development. To further validate this result the model sensitivity to Δt values has been investigated in the next section. This test is designed to make sure that the system results are reliable over a range of Δt and not only for the one employed.

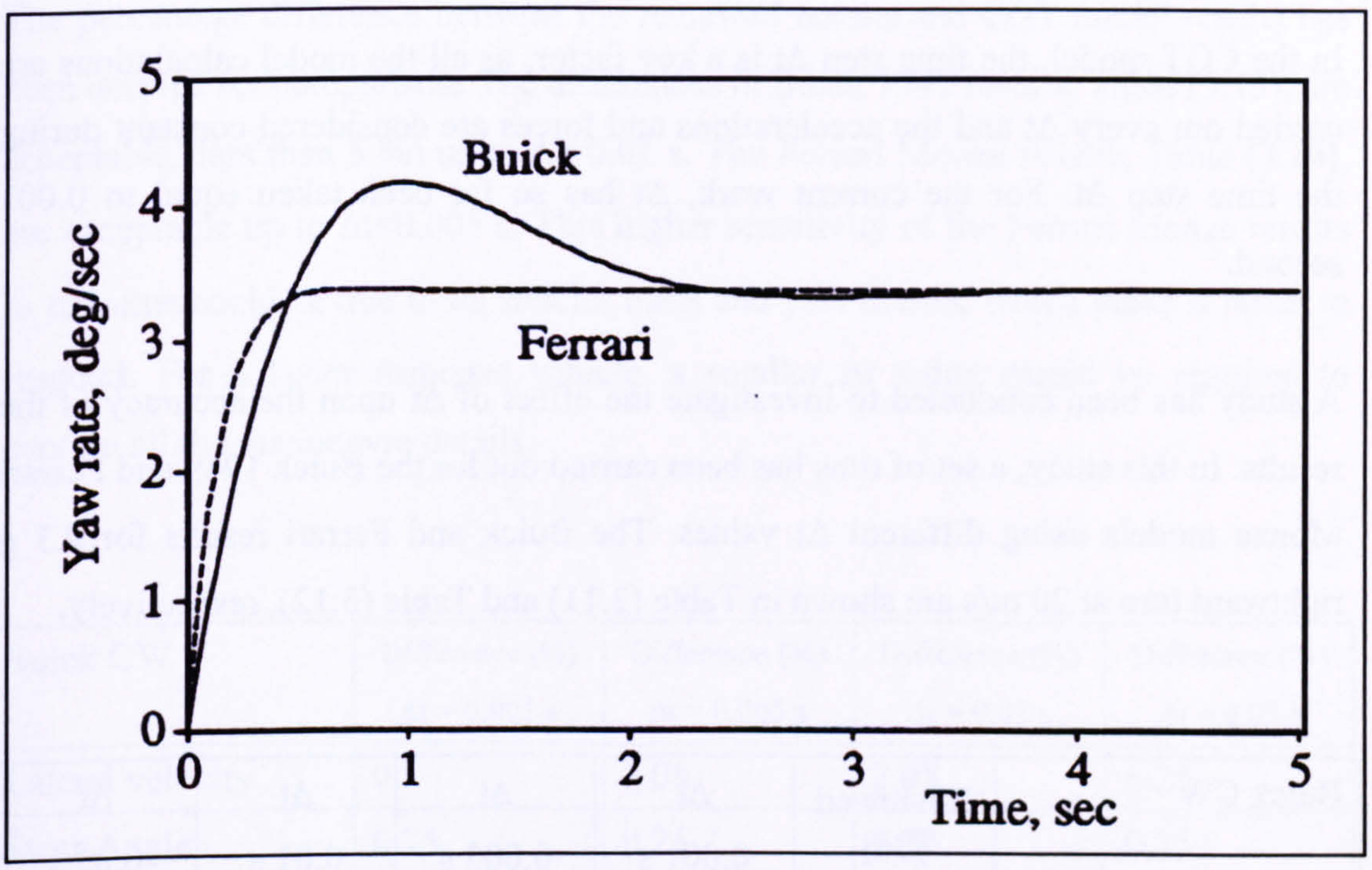

Fig (3.9) Reviewed yaw rate response of the Buick and Ferrari [84]

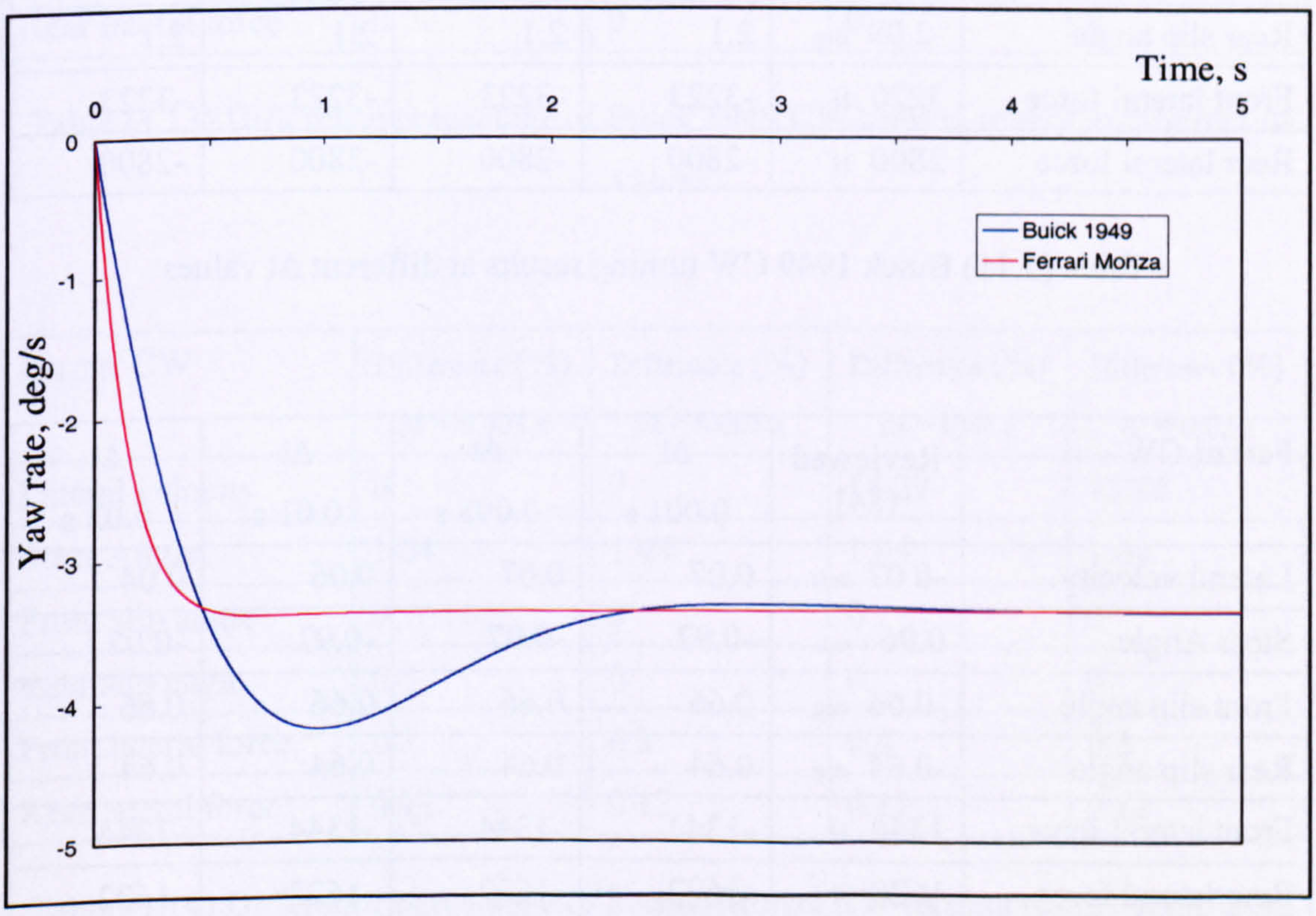

Fig (3.10) CGT model yaw rate response results of the Buick and Ferrari

3.6.2 Sensitivity Test

In the CGT model, the time step Δt is a key factor, as all the model calculations are carried out every Δt and the accelerations and forces are considered constant during the time step Δt. For the current work, Δt has so far been taken equal to 0.001 second.

A study has been conducted to investigate the effect of Δt upon the accuracy of the results. In this study, a set of runs has been carried out for the Buick 1949 and Ferrari Monza models using different Δt values. The Buick and Ferrari results for 0.3 g rightward turn at 20 m/s are shown in Table (3.11) and Table (3.12), respectively.

Buick CW	Reviewed [84]	Δt 0.001 s	Δt 0.005 s	Δt 0.01 s	Δt 0.02 s
Lateral velocity	-0.48 m/s	0.48	0.47	0.47	0.45
Steer Angle	1.62 m/s	-1.62	-1.62	-1.62	-1.62
Front slip angle	-2.37 deg	2.37	2.37	2.37	2.37
Rear slip angle	-2.09 deg	2.1	2.1	2.1	2.1
Front lateral force	3220 N	-3223	-3223	-3223	-3223
Rear lateral force	2800 N	-2800	-2800	-2800	-2800

Table (3.11) Buick 1949 CW turning results at different Δt values

Ferrari CW	Reviewed [84]	Δt 0.001 s	Δt 0.005 s	Δt 0.01 s	Δt 0.02 s
Lateral velocity	-0.07 m/s	0.07	0.07	0.06	0.04
Steer Angle	0.96 m/s	-0.97	-0.97	-0.97	-0.97
Front slip angle	-0.66 deg	0.66	0.66	0.66	0.66
Rear slip angle	-0.64 deg	0.64	0.64	0.64	0.64
Front lateral force	1340 N	-1344	-1344	-1344	-1344
Rear lateral force	1620 N	-1622	-1622	-1622	-1622

Table (3.12) Ferrari Monza CW turning results at different Δt values

The percentage difference between the reviewed results and CGT model results has been derived for comparison. The differences in Buick 1949 results, Table (3.13), are acceptable (less than 5 %) up to Δt=0.01 s. The Ferrari Monza results, Table (3.14), are acceptable up to Δt=0.005 s. This higher sensitivity of the Ferrari Monza results to Δt value could be due to its smaller mass and yaw inertia, which make it faster to respond. For a faster response vehicle, a smaller Δt value would be required to capture all the manoeuvre details.

Buick CW	Difference (%) Δt = 0.001 s	Difference (%) Δt = 0.005 s	Difference (%) Δt = 0.01 s	Difference (%) Δt = 0.02 s
Lateral velocity	0	2.08	2.08	6.25
Steer Angle	0.25	0.25	0.25	0.25
Front slip angle	0	0	0	0
Rear slip angle	0.48	0.48	0.48	0.48
Front lateral force	0.09	0.09	0.09	0.09
Rear lateral force	0	0	0	0

Table (3.13) Difference percentage of Buick 1949 CW turning results at different Δt values

Ferrari CW	Difference (%) Δt = 0.001 s	Difference (%) Δt = 0.005 s	Difference (%) Δt = 0.01 s	Difference (%) Δt = 0.02 s
Lateral velocity	0	0	14.29	42.86
Steer Angle	1.04	1.04	1.04	1.04
Front slip angle	0	0	0	0
Rear slip angle	0	0	0	0
Front lateral force	0.3	0.3	0.3	0.3
Rear lateral force	0.12	0.12	0.12	0.12

Table (3.14) Difference percentage of Ferrari Monza CW turning results at different Δt values

3.6.3 Model Symmetry Test

As the model depends on geometrical and trigonometric formulas, the model results would possibly be sensitive to the turn direction. The model has been tested for the same reviewed Buick and Ferrari vehicles 0.3 g turn at 20 m/s forward velocity but in the CCW (leftward) direction. Also, the accuracy of results have been investigated at different Δt values to investigate the sensitivity of the model CCW turning to Δt, Table (3.15) and Table (3.16).

Buick CCW	Δt 0.001 s	Δt 0.005 s	Δt 0.01 s	Δt 0.02 s
Lateral velocity	-0.48	-0.47	-0.47	-0.45
Steer Angle	1.624	1.624	1.624	1.624
Front slip angle	-2.37	-2.37	-2.37	-2.37
Rear slip angle	-2.1	-2.1	-2.1	-2.1
Front lateral force	3223	3223	3223	3223
Rear lateral force	2800	2800	2800	2800

Table (3.15) Buick 1949 CCW turning results at different Δt values

Ferrari CCW	Δt 0.001 s	Δt 0.005 s	Δt 0.01 s	Δt 0.02 s
Lateral velocity	-0.07	-0.07	-0.06	-0.04
Steer Angle	0.97	0.97	0.97	0.97
Front slip angle	-0.66	-0.66	-0.66	-0.66
Rear slip angle	-0.64	-0.64	-0.64	-0.64
Front lateral force	1344	1344	1344	1344
Rear lateral force	1622	1622	1622	1622

Table (3.16) Ferrari Monza CCW turning results at different Δt values

For both the Ferrari and the Buick vehicle models, the CCW results are identical to the CW results with the only difference in the signs due to the difference in turning direction. This has been considered a further proof of the CGT model validity to undertake the required handling simulations.

3.6.4 Understeer Gradient Test

In this test, the performance of the modelled vehicle is investigated to prove the consistency of the new modelling technique with the known understeer gradient effect on vehicle handling performance.

The understeer gradient (K) is a factor that relates the vehicle parameters to indicate the degree of vehicle understeer or oversteer:

$$K = \left(\frac{W_f}{C_{\alpha f}}\right) - \left(\frac{W_r}{C_{\alpha r}}\right) \tag{3.60}$$

Where: -

W_f Load at front axle

W_r Load at rear axle

$C_{\alpha f}$ Cornering stiffness of front axle

$C_{\alpha r}$ Cornering stiffness of rear axle

Neutral Steer

When K value is equal to zero the vehicle is said to be neutral steering. A neutral steering performance indicates that the vehicle in the steady state will turn at the nominal radius of turn indicated by equation (3.61) regardless of the travelling velocity.

$$R = \left(\frac{L}{\tan(\delta)}\right) \tag{3.61}$$

Where: -

R Nominal radius of turn

L Wheel base (m)

δ Steering angle

Understeer

When K is greater than zero the vehicle is said to understeer. Understeer performance indicates that the vehicle under steady state cornering will turn at the

nominal radius only at very low longitudinal velocity, while increase of the vehicle velocity would increase its turn radius in the steady state.

Oversteer

When K is less than zero the vehicle is said to oversteer. Oversteer performance indicates that the vehicle under steady state cornering will turn at the nominal radius only at very low longitudinal velocity, while increase of the forward velocity would decrease its turn radius in the steady state.

To test the model compliance, a set of runs has been carried out investigating this known phenomenon. The Ferrari vehicle parameters have been used for this test. The vehicle CG has been moved forward and backward to enforce oversteer and understeer behaviour. The vehicle has been tested at three K values of 0, 1, and –1. To evaluate the CG location that enforces a certain K value, the following derivation has been carried out.

For any vehicle

$$W_f = mg\left(\frac{b}{L}\right) \tag{3.62}$$

$$W_r = mg\left(\frac{a}{L}\right) \tag{3.63}$$

Substituting in equation (3.60) and rearranging

$$K = \left(\frac{mg}{L}\right)\left(\left(\frac{b}{C_{\alpha f}}\right) - \left(\frac{a}{C_{\alpha r}}\right)\right) \tag{3.64}$$

The wheelbase definition gives:-

$$L = a + b \tag{3.65}$$

Rearranging

$$b = L - a \tag{3.66}$$

Substituting in equation (3.64) and rearranging

$$a = \left(LC_{\alpha r}\left(\frac{KL}{mg}\right)\right)\left(\frac{C_{\alpha r}C_{\alpha f}}{C_{\alpha r}+C_{\alpha f}}\right) \tag{3.67}$$

From equation (3.67) and (3.66) the location of the vehicle CG that produces a certain K value could be evaluated. This principle has been used to produce different K values for the Ferrari, by assuming movement of its CG. Although the modified vehicles can not be considered the same as the reviewed Ferrari, the results adequately test the model functionality.

Using equation (3.67) and (3.66) the vehicle parameters that would produce understeer, neutral steer and oversteer have been defined, Table (3.17).

	Reviewed Ferrari [84]	K = -1	K = 0	K = 1
m (kg)	1008	1008	1008	1008
I (kg m^2)	1031	1031	1031	1031
a (m)	1.234	1.505	1.246	0.988
b (m)	1.022	0.751	1.01	1.268
L (m)	2.256	2.256	2.256	2.256
$C_{\alpha f}$ (N/rad)	117440	117440	117440	117440
$C_{\alpha r}$ (N/rad)	144930	144930	144930	144930

Table (3.17) Vehicles parameters used in the understeer-oversteer gradient test

To evaluate the effect of understeer gradient on vehicle handling, a set of runs have been carried out. Each set modelled one set of vehicle parameters at 3^{o} degree steering step input and different forward velocities (1, 10 and 20 m/s).

The neutral steer vehicle (K = 0) results for a 3^{o} step steer input for different forward velocities, Fig (3.11), reveal many points. The first point is that the paths of the vehicle under different velocities show a constant radius of turn, which validates

the model compliance to steer gradient. The second point is that even though the steady state radius of the turns are constant, transients at the start of the turn still exist and the CGT model investigated it.

The transients are caused by the momentary under developed turning radius at the start of a manoeuvre, specially the step steer manoeuvres. This is due to the high demand of lateral and yaw accelerations at the start of a manoeuvre in contrast to the lag of lateral forces development and, consequently, lag of yaw rate development. This is manifest as a translation of the vehicle turn centre away from the theoretical centre. This translation increases with vehicle velocity, Fig (3.11). The capacity of CGT technique to investigate this vehicle transient handling dynamics justifies the need for the current CGT model with its strong handling prediction capacity.

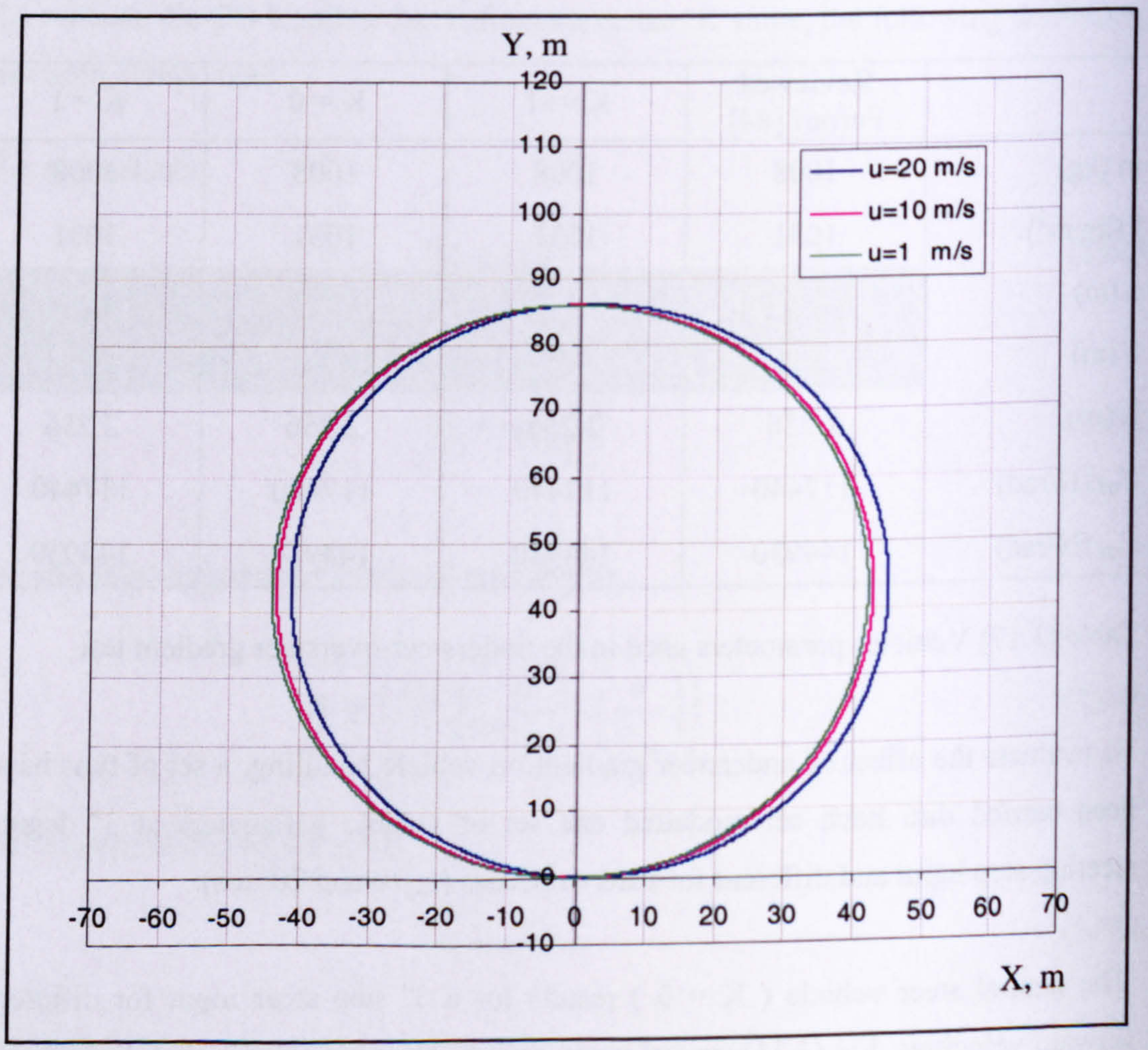

Fig (3.11) Neutral steer vehicle path after 3° step steer at different forward velocities

The understeer vehicle (K = 1) path after a 3° step steer input under different forward velocities is shown in Fig (3.12). The results show that the turn diameter at 1 m/s is comparable to the turn diameter of the neutral steer vehicle, which proves the principle and so validates the CGT model. Also, it shows that the vehicle follows a larger turning radius as the forward velocity increases, which further proves the principle of an understeering vehicle and so validates the CGT based model.

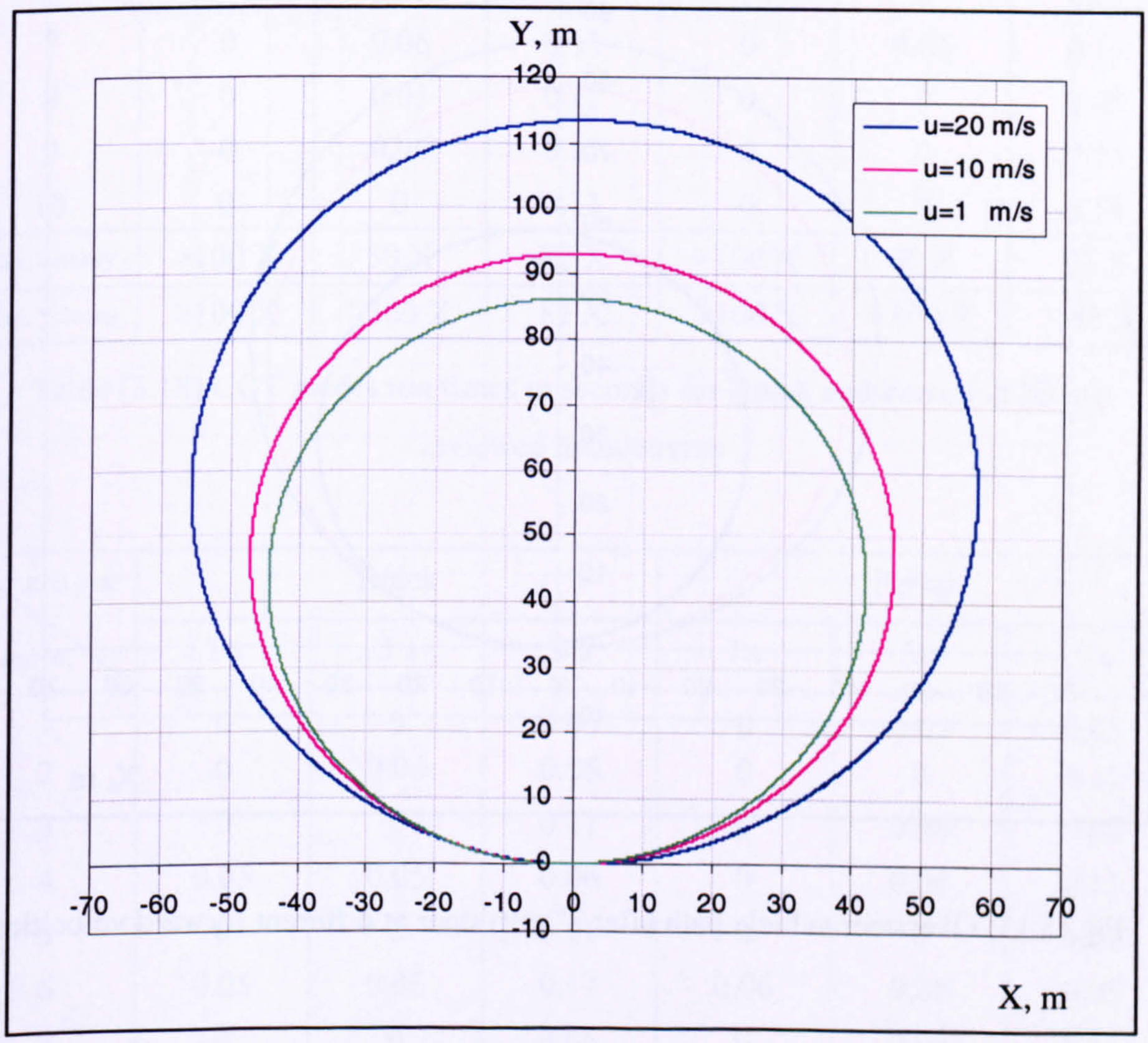

Fig (3.12) Understeer vehicle path after 3° step steer at different forward velocities

The oversteer vehicle (K = -1) path after a 3° step steer input under different forward velocities is shown in Fig (3.13). The results show that the turn diameter at 1 m/s is comparable to the turn diameter of the neutral steer and understeer vehicles, which proves the principle and so validates the CGT model. It also shows that the vehicle follows a smaller turning radius as the forward velocity increases, which

proves the principle of an oversteering vehicle and so further validates the CGT based model.

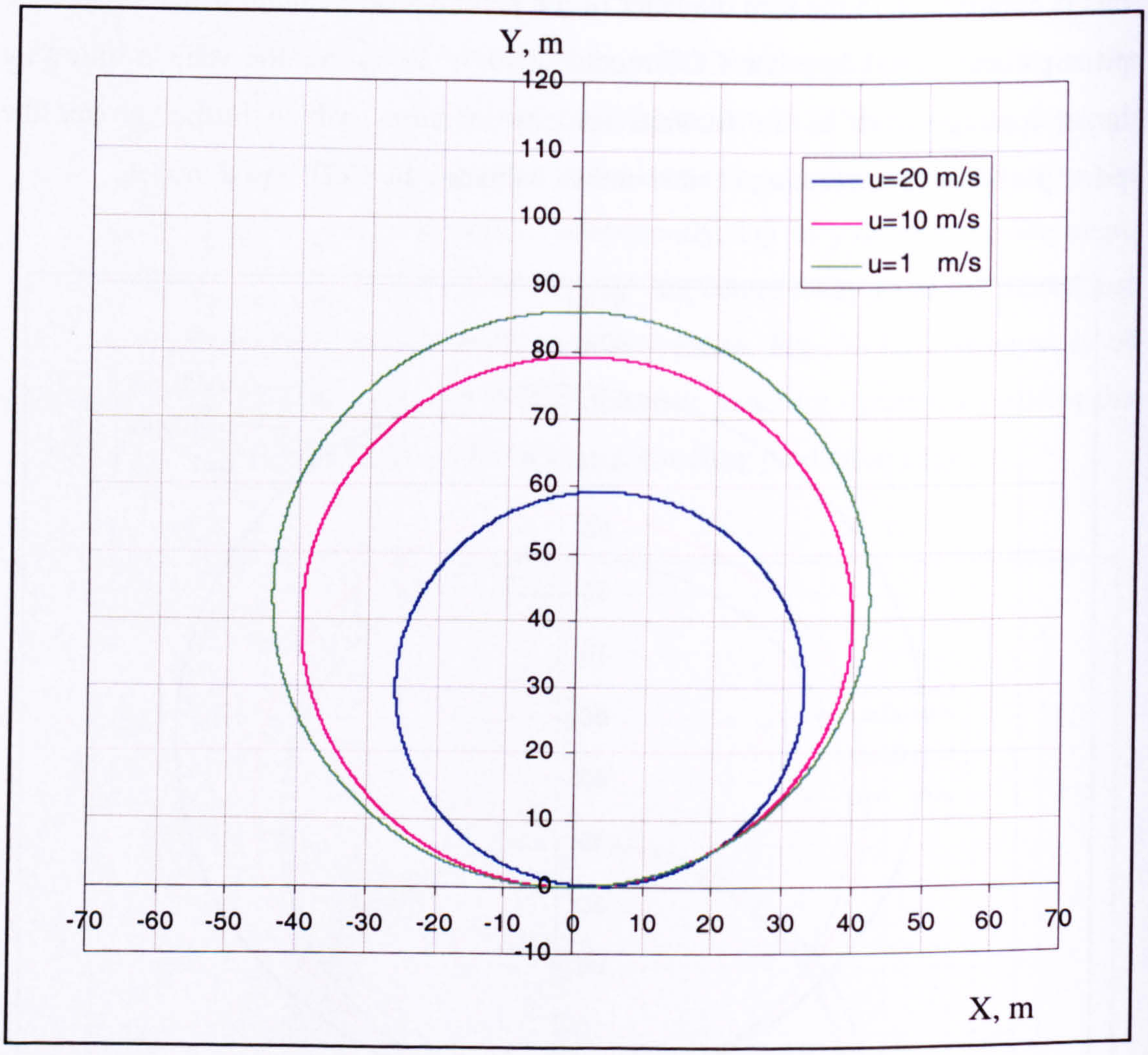

Fig (3.13) Oversteer vehicle path after 3° step steer at different forward velocities

3.7 CGT Model Speed

In this stage of the test the model processing speed has been investigated on a PC equipped with 2200 MHz AMD Barton© processor. The test has been carried out for both Buick and Ferrari vehicle under the 20 m/s reviewed handling manoeuvre, Table (3.18) and 50 m/s reviewed handling manoeuvre, Table (3.19).

Real time / Run No.	Buick			Ferrari		
	1 s	3 s	9 s	1 s	3 s	9 s
1	0	0	0.11	0	0	0.11
2	0	0	0.11	0	0.05	0.11
3	0	0	0.11	0	0.05	0.11
4	0	0	0.11	0	0.05	0.11
5	0	0.06	0.11	0	0	0.05
6	0	0.05	0.11	0	0	0.11
7	0	0.06	0.11	0	0.06	0.11
8	0	0.05	0.11	0	0	0.05
9	0	0.06	0.11	0	0	0.11
10	0	0	0.11	0	0	0.11
Min. Velocity	>100 X	50 X	82 X	>100 X	50 X	82 X
Max. Velocity	>100 X	>300 X	82 X	>100 X	>300 X	180 X

Table (3.18) CGT model run times in seconds for Buick and Ferrari at 20 m/s reviewed manoeuvres

Real time / Run No.	Buick			Ferrari		
	1 s	3 s	9 s	1 s	3 s	9 s
1	0	0	0.05	0	0.05	0.05
2	0	0.06	0.05	0	0	0.11
3	0	0	0.11	0	0.06	0.05
4	0.05	0.05	0.06	0	0.06	0.11
5	0	0	0.11	0	0	0.11
6	0.05	0.06	0.17	0.06	0.06	0.05
7	0	0	0.05	0	0.06	0.11
8	0	0.05	0.06	0	0.06	0.11
9	0	0	0.11	0	0.06	0.11
10	0	0	0.05	0	0.05	0.11
Min. Velocity	20 X	50 X	53 X	>17 X	50 X	82 X
Max. Velocity	>100 X	>300 X	180 X	>100 X	>300 X	180 X

Table (3.19) CGT model run times in seconds for Buick and Ferrari at 50 m/s reviewed manoeuvres

The results in Table (3.18) and Table (3.19) demonstrated the high potential of the developed model as high running velocities up to more than 300 times faster than real time were achieved, given that a 0 means less than 0.01 s which is the smallest time division measurable in BASIC. A minimum model velocity of at least 17 times faster than real time has also been achievable. Although the minimum velocity should be considered the limiting factor at the current stage, the variation step patterns indicate that it is a PC hardware issue with the PC dynamic memory refresh cycle involved. This refresh cycle is a characteristic of PC hardware. During this cycle the computer has no access to its memory.

Although attributing this high velocity solely to the CGT modelling technique would require further investigations using different programming languages, the achieved velocity using CGT with BASIC can be considered very satisfactory.

To further develop the model velocity, a special hardware with more expensive static memory would be required. This will enable a more consistent higher running velocity. The model's very small memory requirement (less than 640 kB) facilitates its velocity development through either employing a small static memory module or loading it into the high velocity processor cache memory (512 MB), which would rule out the need for a special memory to achieve higher velocity.

3.8 Sample of Model Results

As further validation of the modelling technique, the model code is given in Appendix A to allow close examination to the novel CGT technique simplicity. Also, a demonstration of the wide range of the developed model outputs is presented in Appendix B to show the capability of the developed model. In this demonstration, the model outputs for the "Ferrari Monza" and "Buick 1949" vehicle simulations at 20 m/s and 50 m/s forward velocity manoeuvres are detailed.

3.9 Conclusions

In this chapter, a half vehicle handling model has been developed and tested. In the first stage, a novel model solving technique employing Cartesian geometry, trigonometry and finite difference approximations has been laid out and the model equations have been formulated. In this technique the vehicle moves forward in fixed consecutive finite time steps Δt. The model has been constructed using QBasic© programming language in the DOS© operating environment to allow fast standalone models to be developed.

In the second stage, the model results have been compared with published data of "Buick 1949" and "Ferrari Monza" vehicles for $\Delta t = 0.001$ s. Although the current model and the published model have been built using completely different techniques and equations, the results have been impressively comparable. The majority of results demonstrate a very close match between the two techniques.

In the third stage, the model sensitivity has been investigated. First, the model sensitivity to the time step, Δt, has been investigated to further assure the validity of the solution solving technique. In this test the developed model has been used to derive the reviewed results at different Δt values, typically 0.001, 0.005, 0.01 and 0.02 s. Both vehicle models showed considerable insensitivity up to $\Delta t = 0.005$ s and the Buick model showed this insensitivity up to $\Delta t = 0.01$ s.

Second, the model sensitivity to CW and CCW direction of turn has been investigated. The same CW results have been produced through steering the vehicles in the CCW direction. The results have also been checked against Δt sensitivity and found to typically match the CW direction results with the only difference being the signs due to the difference in turning directions

In the fourth stage, the model prediction of understeer gradient (K) has been tested. In this test the vehicle data has been manipulated to enforce neutral steer, understeer and oversteer with understeer gradient values of 0, 1 and -1 respectively. The data

has been input to the model and the results proved that the model accurately predicts the understeer gradient effect on vehicle handling. The model is also capable of predicting the transients at the start of the manoeuvres.

As the results demonstrated excellent comparison with previously published results and the model proved stable under different working parameters in both CW and CCW directions, both the CGT model and its implementation have been considered satisfactory. Consequently the modelling technique is considered a strong base for further model development.

The next stage of model development involves incorporating the vehicle handling model with the Magic Formula (MF) tyre model for combined slip to investigate the tyre longitudinal force effects on lateral forces and slip angles on vehicle handling. Also it is necessary to upgrade the half vehicle handling model to a full vehicle handling model to observe the lateral and longitudinal load transfer effect on vehicle handling. However, as the MF tyre model requires some treatment before incorporating it into the vehicle handling model, the next chapter is devoted to the MF tyre model itself.

Chapter 4

The Tyre Model

4.1 Introduction

The tyre at the vehicle road interface is responsible for developing all the required longitudinal and lateral forces, so it plays a very important role in vehicle handling, but it causes some problems too. Its main problem is that it has to slip laterally and longitudinally to generate lateral and longitudinal forces respectively. This slip is a physical deviation from the intended tyre path and influences the vehicle handling performance. Tyre slip is difficult to predict due its non-linear relation with the generated forces and the large number of tyre related parameters.

For a vehicle handling simulation, the effect of the tyre is often characterised through a mathematical model, which is a set of equations that represent the tyre behaviour at various conditions. These equations are usually derived from a physical point of view, empirical point of view or both (semi-empirical). The equations represent the relation between the tyre slip in different directions and the forces generated. There are many different tyre models, each with its own level of complexity, accuracy, advantages, disadvantages and limitations. Therefore the proper selection of a suitable tyre model can be considered a key factor in achieving a realistic simulation of vehicle handling.

For the current work, a tyre model that considers the effect of combined tyre slip has been considered essential. The combined slip condition occurs as the tyre deals with the demands of simultaneous lateral and longitudinal forces and accordingly undergoes a combination of longitudinal and lateral slip. These force demands are required when a vehicle accelerates or decelerates in a turn. It is also required when longitudinal right or left driven tyre forces are applied during a vehicle manoeuvre to generate an additional yaw moment in order to implement a better vehicle handling performance.

The main problem in the combined slip condition is that the tyre tends to generate a lower force to slip ratio in any direction when it suffers slip in the other direction. As improving the vehicle handling performance through influencing the driven tyre forces represents the focus of the current work, a tyre model that includes the effect of combined slip situations has to be chosen.

The aim of this chapter is to select a tyre model that is fit for the purpose of the current research and facilitates its application. It also aims to investigate and solve any problem that would hinder the tyre model implementation in the current CGT vehicle handling model.

4.2 Magic Formula Tyre Model for Combined Slip

The "Magic Formula" (MF) tyre model for combined slip [34] has been chosen for the current simulation task. The MF tyre model development started in the mid eighties and a number of versions have been introduced. Although, the model equations were originally derived using an innovative curve fitting technique from a large set of tyre experimental data, it also considered the combined slip condition from a physical point of view (semi-empirical).

In 1993 Bayle et al introduced a purely empirical method based on Magic Formula functions [34]. This model was validated and proved to be satisfactory due to its realistic estimation of the tyre forces in the case of combined lateral and longitudinal

slip, [34]. Accordingly, it has been considered suitable for the current work, although data for particular tyres are not widely available and the model equations are somewhat lengthy and complicated.

4.2.1 Magic Formula Tyre Model Implementation

The MF tyre model equations have been written in BASIC© format along with the available Goodyear 205/60 R15 tyre data. The model equations have been rearranged to meet programming requirements, so no factor would appear in the execution line before it is assigned its value. The equations have been manipulated to develop the tyre results using the ISO tyre axis system in contrast to the published results that employed the adapted SAE tyre axis system [34], Appendix C. The ISO axis system has been adopted to facilitate the use of Cartesian coordinates and trigonometric functions, as they are sensitive to direction and angle signs. Due to the difference in the sign convention employed, the tyre simulation results show an opposite F_y sign to the published work. The MF tyre model equations are given in Appendix D.

4.2.2 Magic Formula Tyre Model Testing

Testing of the model has been carried out by comparing Goodyear 205/60 R15 tyre predicted results with published results [34]. A set of tyre performance results at different conditions has been derived. These results have been compared against the reviewed model and test results.

In the first test, the relation between slip angle α and the lateral force F_y developed has been investigated at different vertical loads F_z with $\gamma = 0$ and longitudinal slip k = 0, Fig (4.1). The results have been compared with the reviewed results, Fig (4.2).

The effect of different γ values on the lateral force F_y relation with slip angle α has been investigated at a vertical load $F_z = 7000$ N, Fig (4.3). The results have been compared to the reviewed results Fig (4.4). The comparison showed good comparability. The slight difference could be due to the difference in tyre width, as the wider tyre would show higher sensitivity to camber angle change.

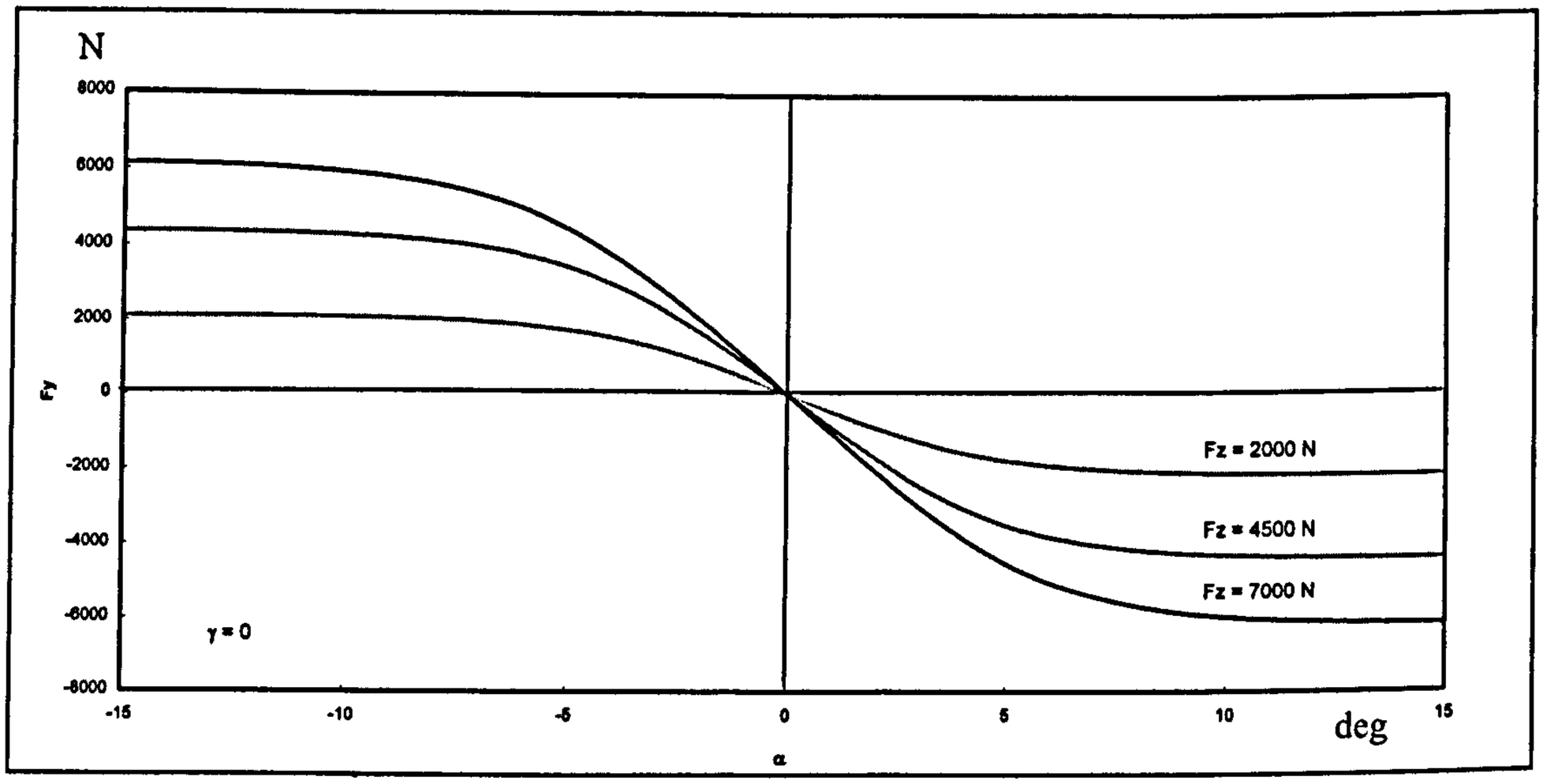

Fig (4.1) Achieved F_y - α relations at different F_z of a 205/60 R15 car tyre

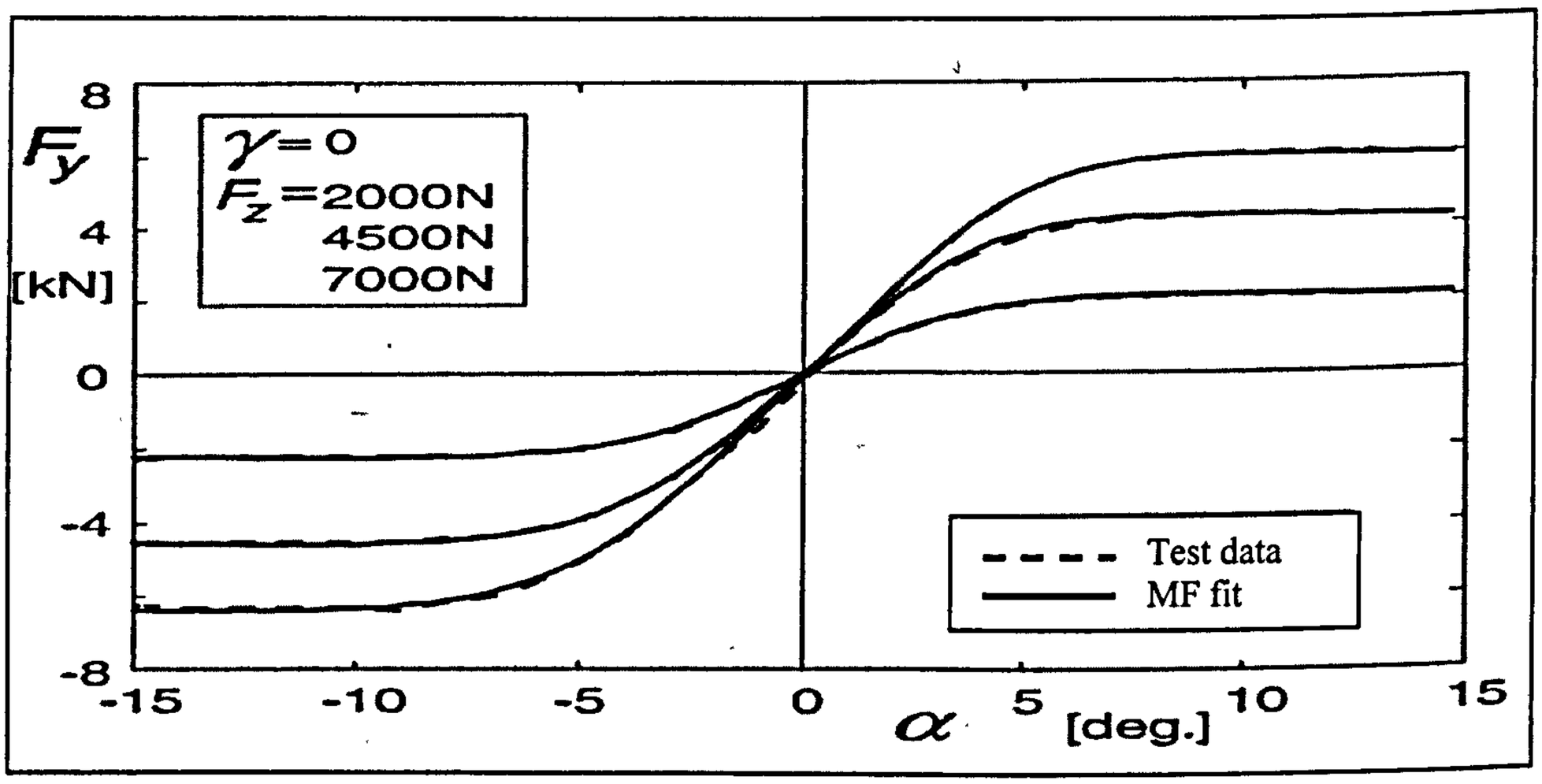

Fig (4.2) Reviewed F_y - α relations at different F_z of a 195/65 R15 car tyre [34]

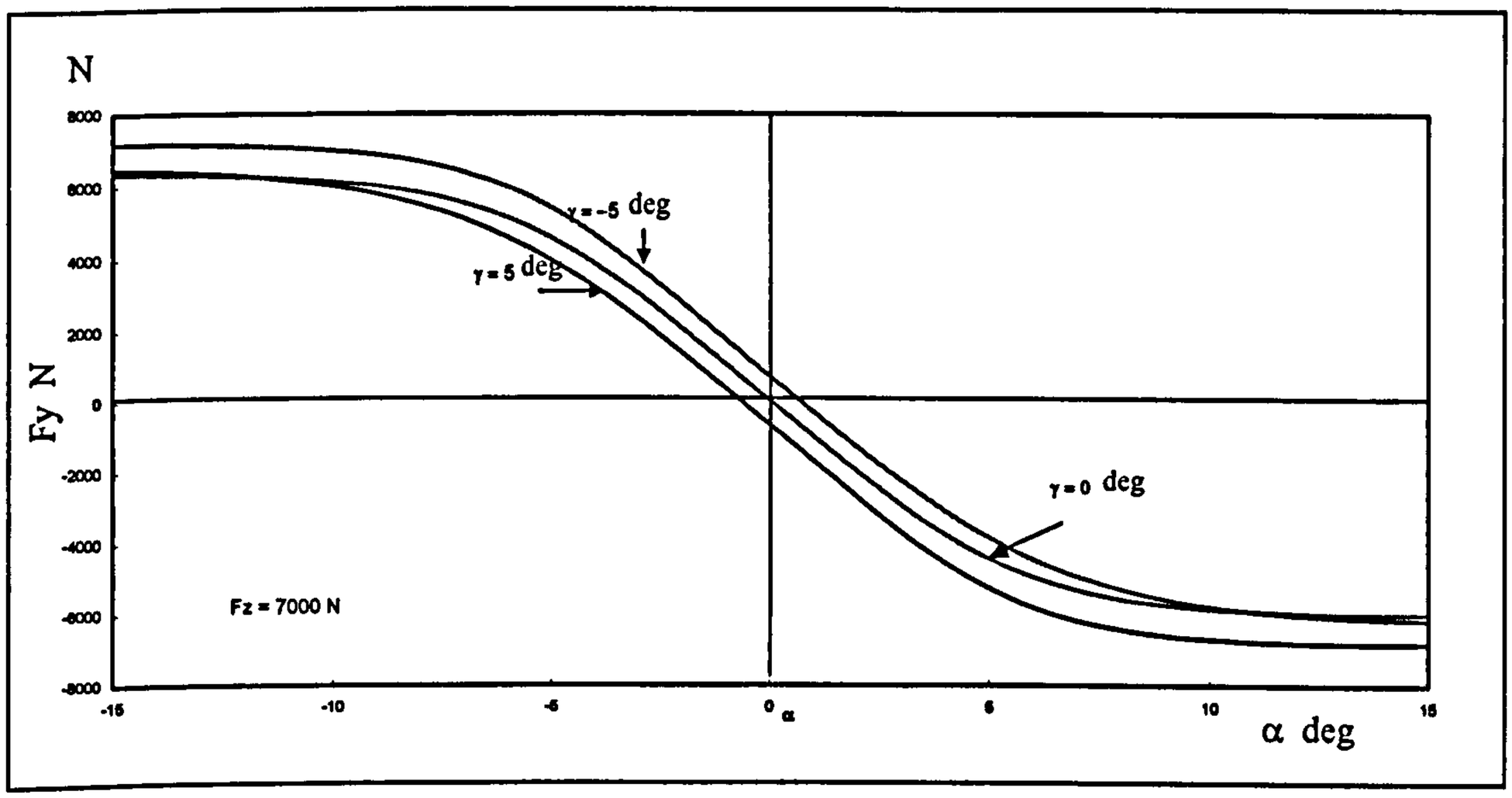

Fig (4.3) Achieved F_y - α relations at different γ of a 205/60 R15 car tyre

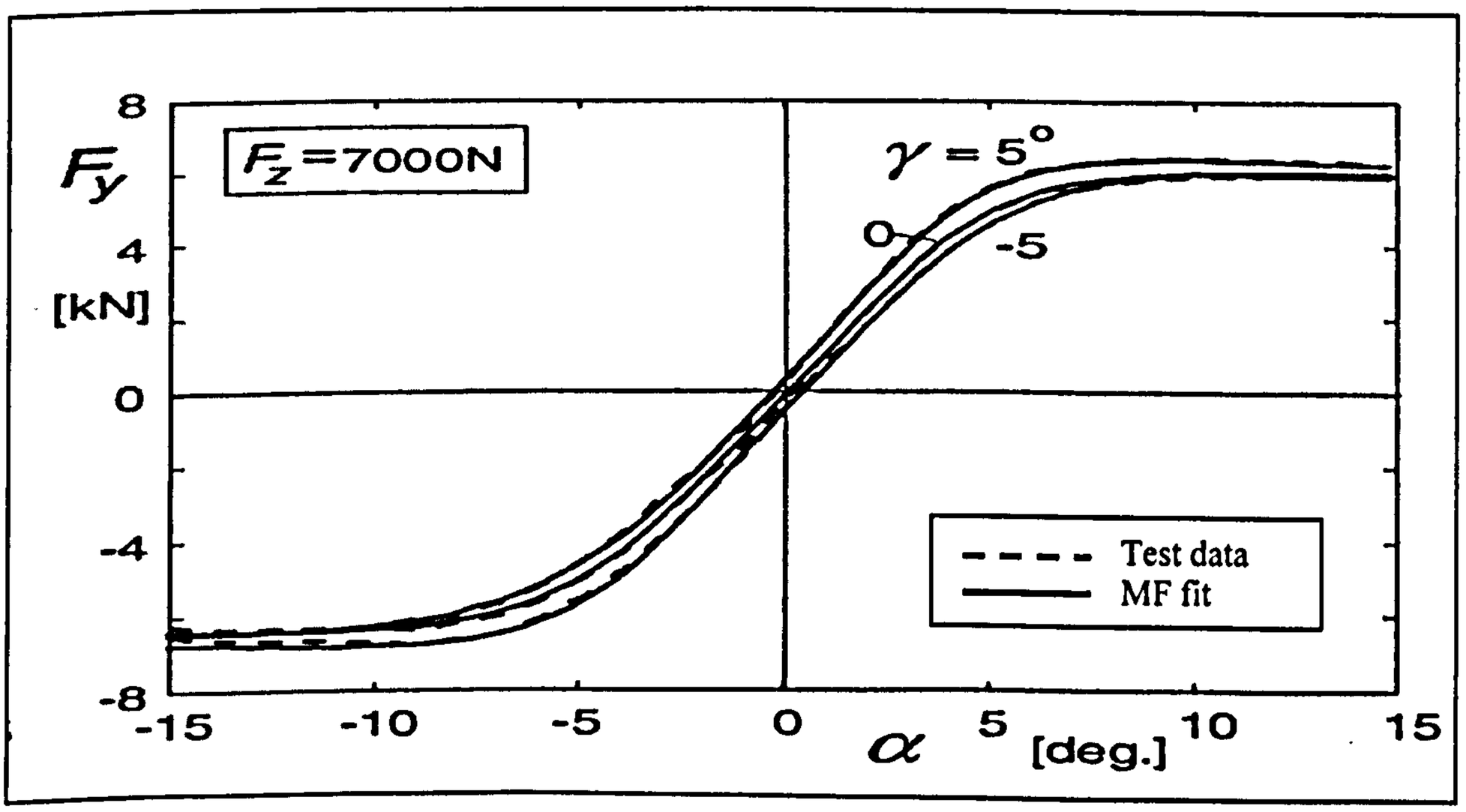

Fig (4.4) Reviewed F_y - α relation at different γ of a 195/65 R15 car tyre [34]

The relation between longitudinal force F_x and the longitudinal slip k has been investigated at different vertical loads F_z with $\gamma = 0$ and $\alpha = 0$ degrees, Fig (4.5). The results have been found to be very comparable with the reviewed results, Fig (4.6).

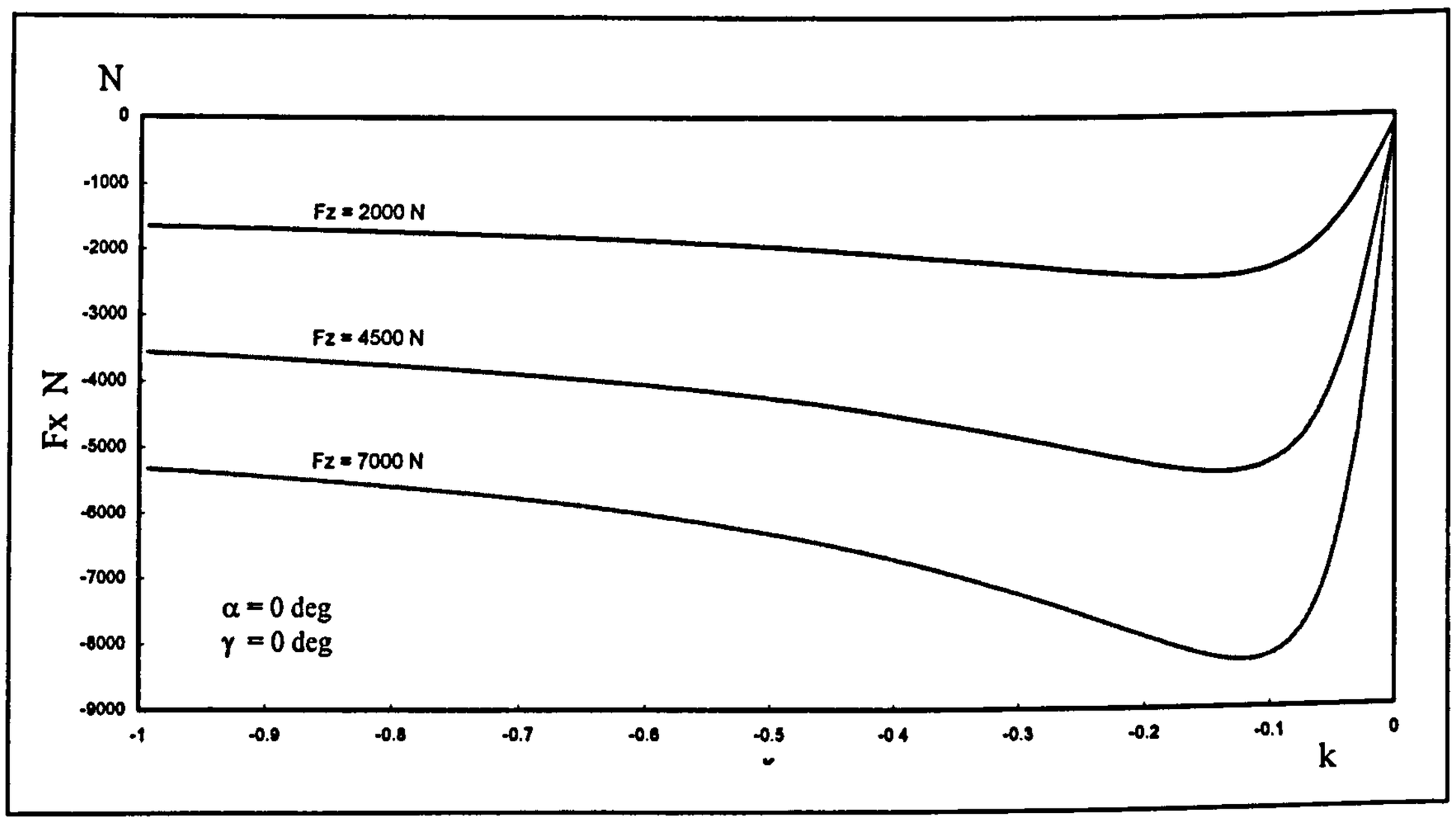

Fig (4.5) Achieved F_x - k relation at different F_z of a 205/60 R15 car tyre

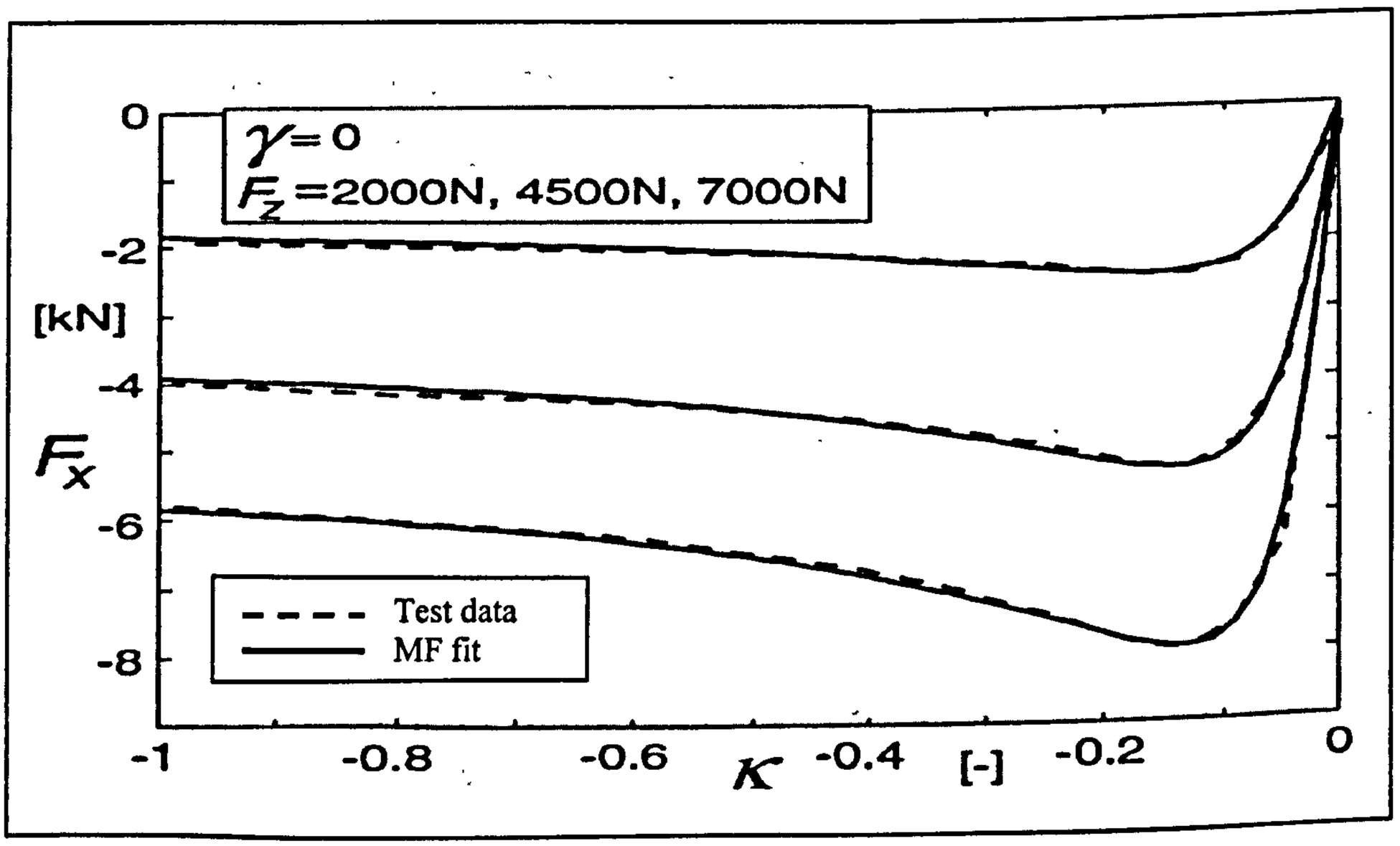

Fig (4.6) Reviewed F_x - k relation at different F_z of a 195/65 R15 car tyre [34]

The combined slip effect of different slip angle α values on the longitudinal force F_x relation with longitudinal slip k has been investigated at a vertical load F_z = 7000 N and γ = 0, Fig (4.7). The results have again been found to be very comparable with the reviewed results, Fig (4.8).

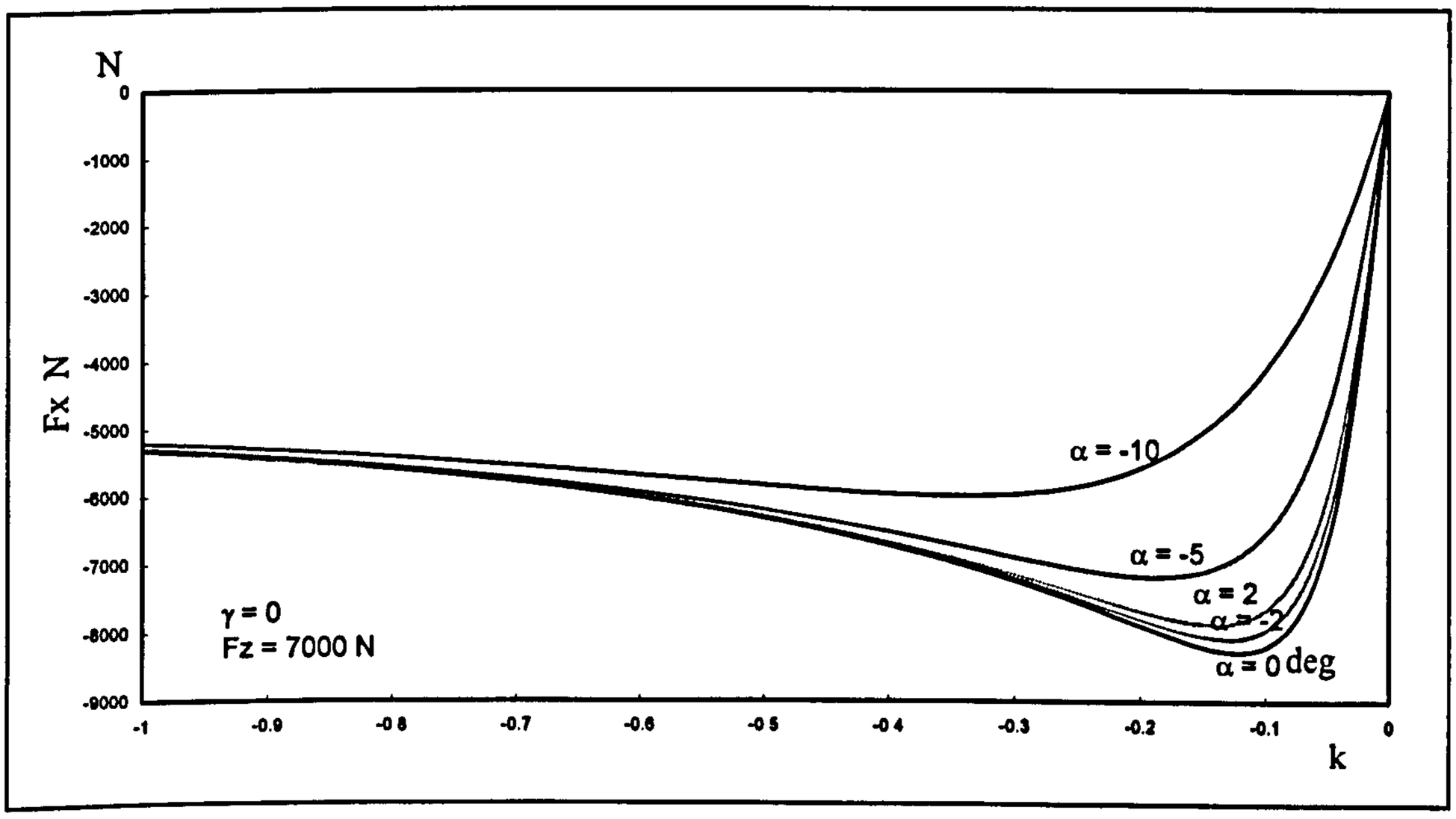

Fig (4.7) Achieved F_x - k relation at different α of a 205/60 R15 car tyre

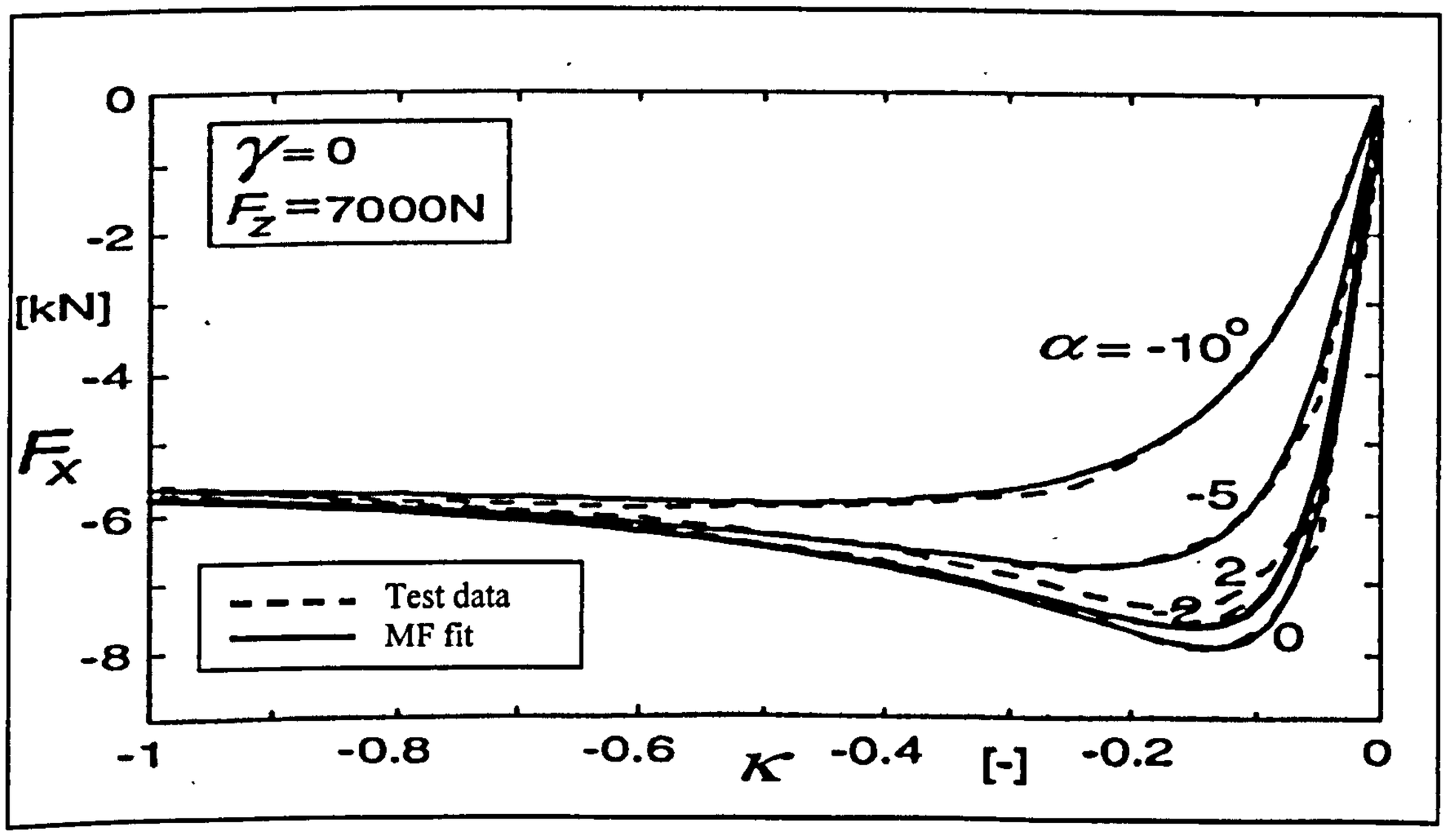

Fig (4.8) Reviewed F_x - k relation at different F_z of a 195/65 R15 car tyre [34]

The model prediction of tyre combined slip condition has also been tested through evaluating the effect of longitudinal slip k on the achievable lateral force F_y for a set of α values, Fig (4.9). The results have been found to be very comparable with the reviewed results, Fig (4.10).

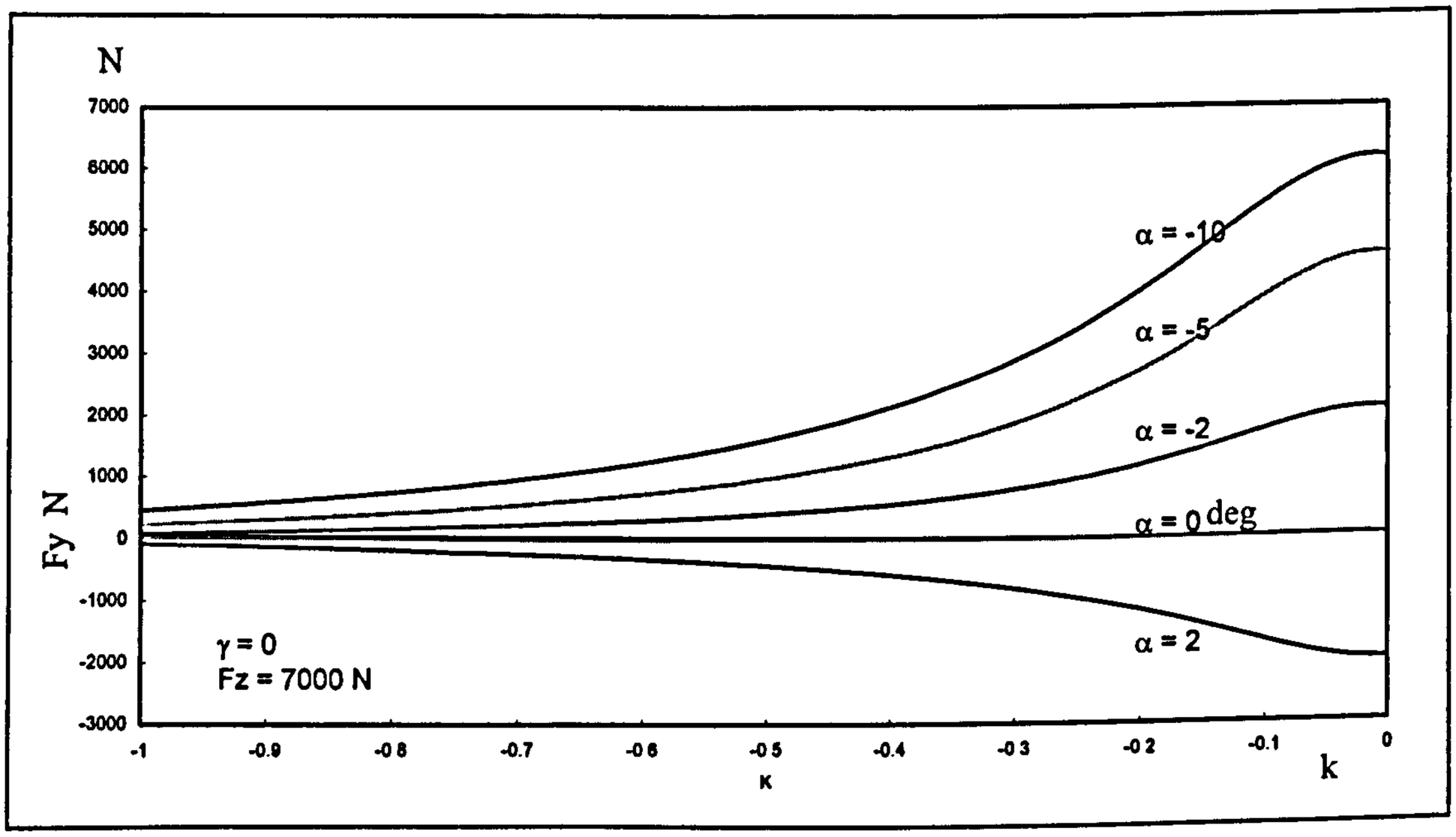

Fig (4.9) Achieved F_y - k relation at different α of a 205/60 R15 car tyre

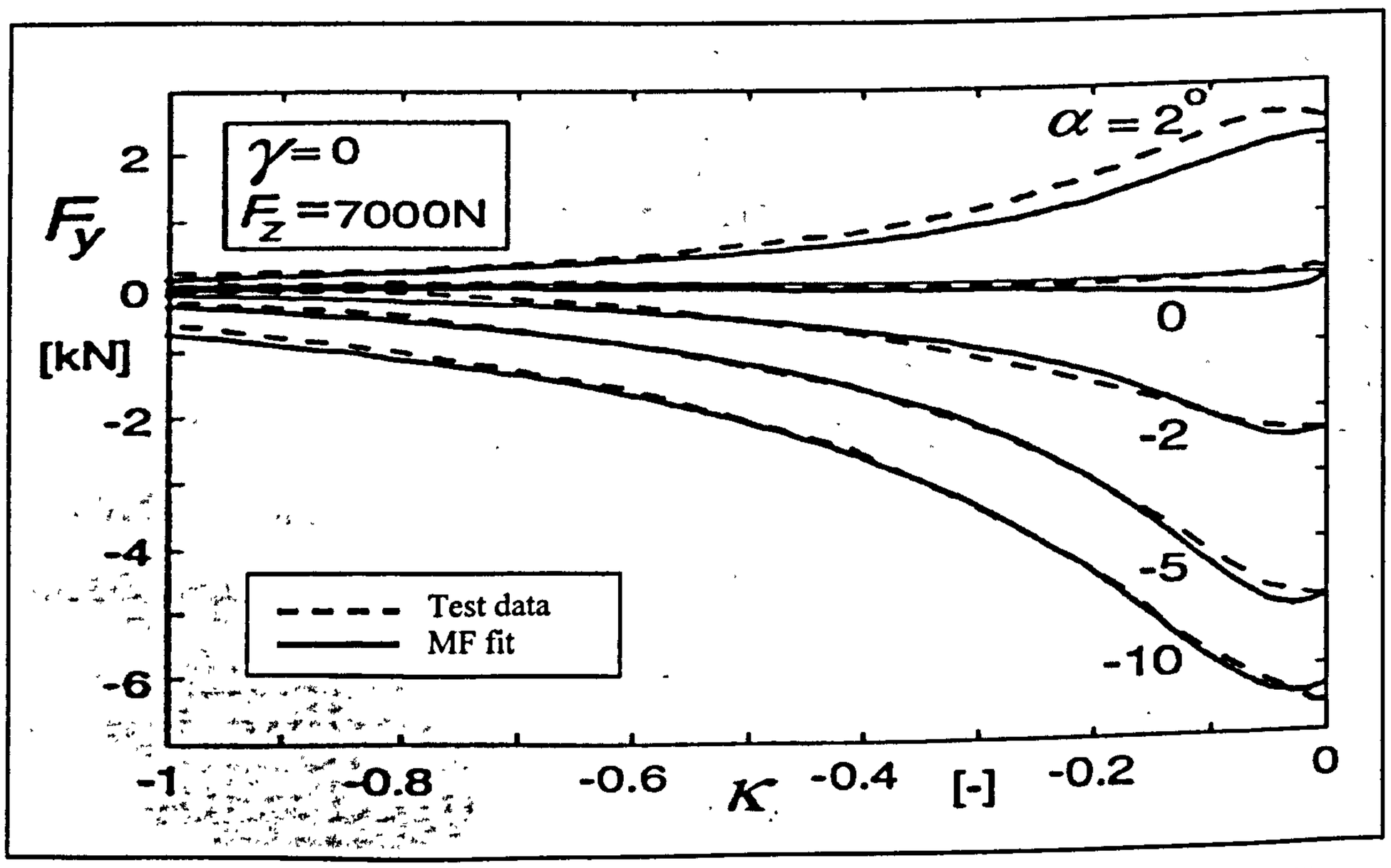

Fig (4.10) Reviewed F_y - k relation at different α of a 195/65 R15 car tyre [34]

The model prediction of tyre combined slip condition has been further tested through evaluating the longitudinal force F_x relation with the lateral force F_y at different slip angle α values, with a vertical load F_z = 7000 N and γ = 0, Fig (4.11). The results have been compared with the reviewed results, Fig (4.12) and a good level of agreement has been shown.

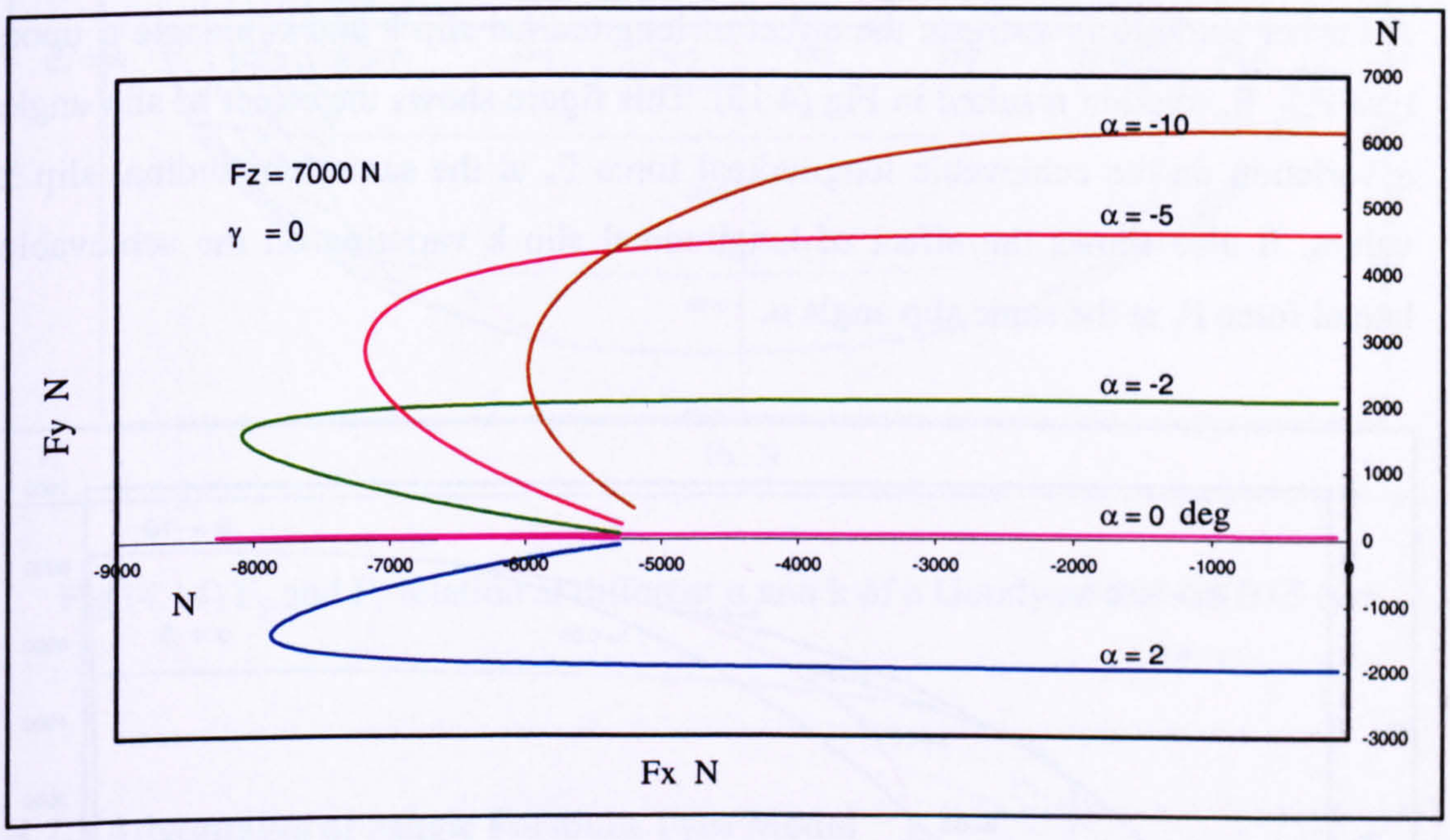

Fig (4.11) Achieved F_y - F_x relation at different α of a 205/60 R15 car tyre

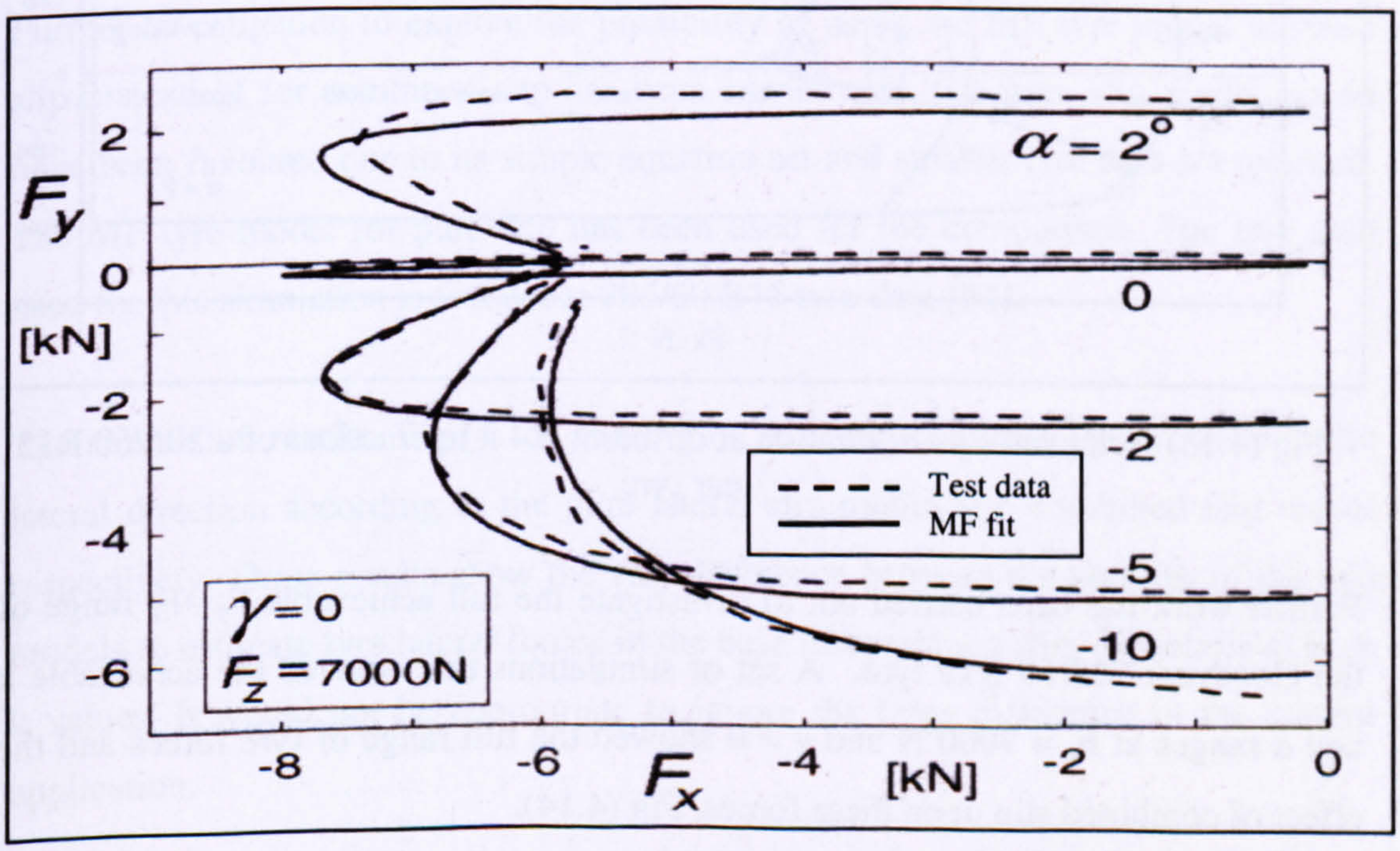

Fig (4.12) Reviewed F_y - F_x relation at different α of a 195/65 R15 car tyre [34]

The comparison between the results achieved with the present model and the reviewed demonstrated good agreement. Also the model equations have already been validated against experimental results [34]. The current comparison has been conducted to prove the functionality of the MF based BASIC© tyre simulation model developed for use in the present work.

A further study to investigate the effect of longitudinal slip k and slip angle α upon tyre $F_y - F_x$ relation resulted in Fig (4.13). This figure shows the effect of slip angle α variation on the achievable longitudinal force F_x at the same longitudinal slip k values. It also shows the effect of longitudinal slip k variation on the achievable lateral force F_y at the same slip angle α.

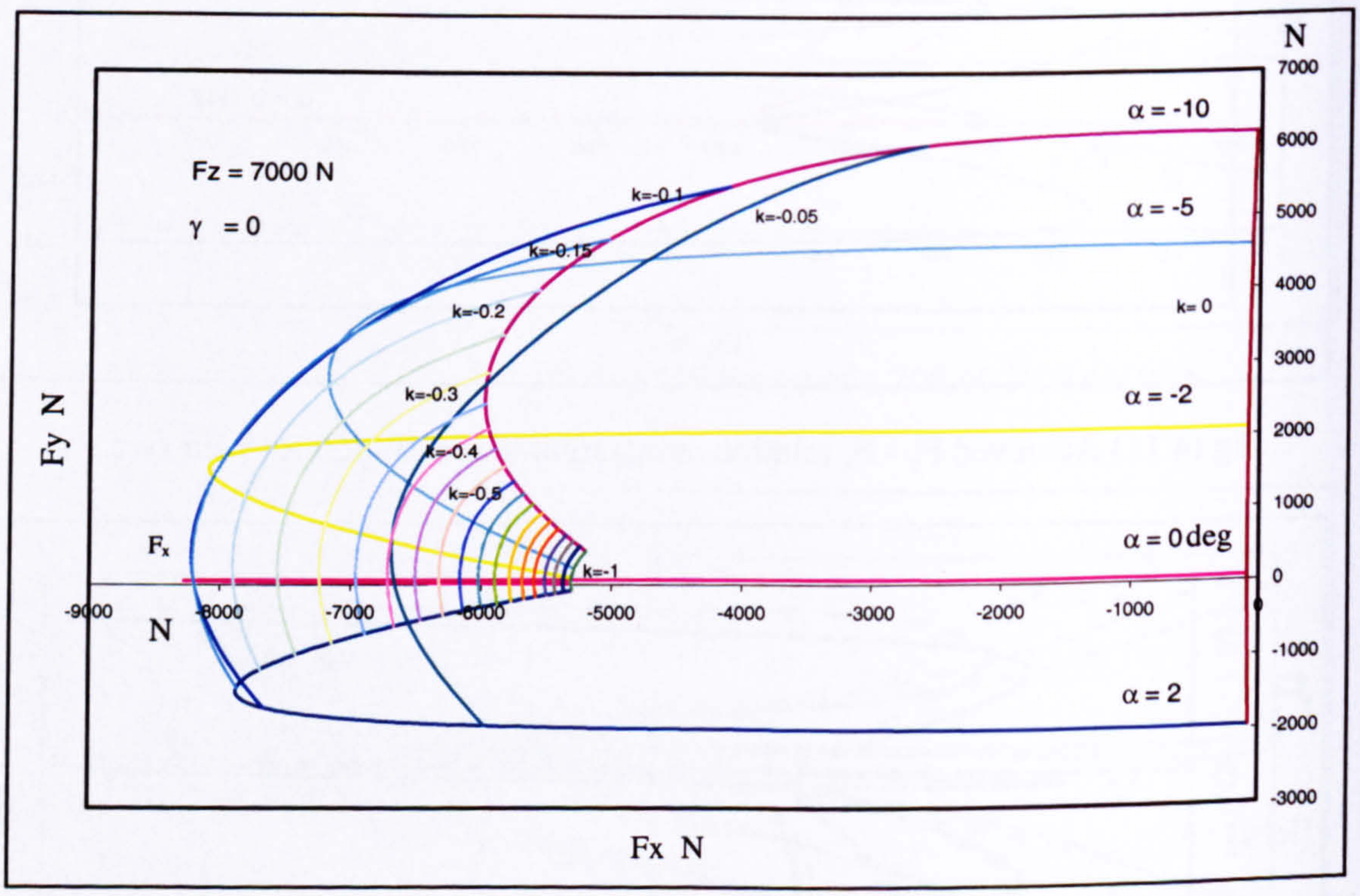

Fig (4.13) Achieved F_y - F_x relation at different α – k interactions of a 205/60 R15 car tyre

Further work has been carried out to investigate the full achievable F_y –F_x range of the Goodyear 205/60 R15 tyre. A set of simulations that covered the achievable k and α ranges at F_z = 7000 N and γ = 0 showed the full range of tyre forces and the effect of combined slip upon these forces, Fig (4.14).

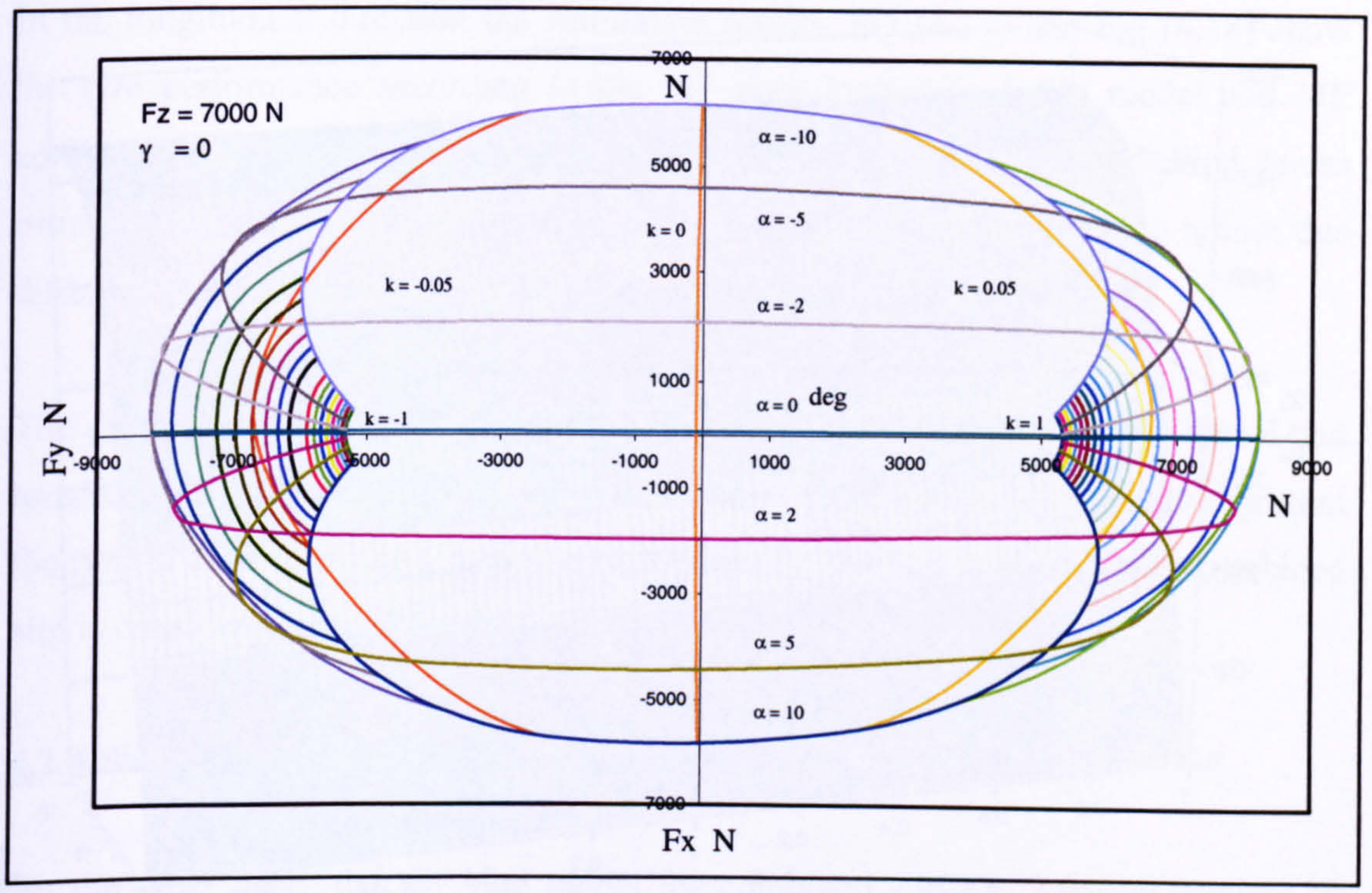

Fig (4.14) F_y and F_x relation at different α and k of a Goodyear 205/60 R15 tyre

4.2.3 Advantages of Magic Formula Tyre Model

Further investigation to explore the possibility of using the MF tyre model for pure slip instead of for combined slip has been carried out. The pure slip model would have been favoured due to its simple equation set and smaller tyre data set required. The MF tyre model for pure slip has been used for the comparison. The tyre data used for this simulation is Goodyear 205/60 R15 tyre data [34].

The simulation results, Fig (4.15) and Fig (4.16), show the tyre performance in the lateral direction according to the pure lateral slip model and combined slip model respectively. These results show the vast difference between the abilities of the two models to estimate tyre lateral forces in the case of combined slip, especially at high k values. It would not be appropriate to ignore the large difference in the current application.

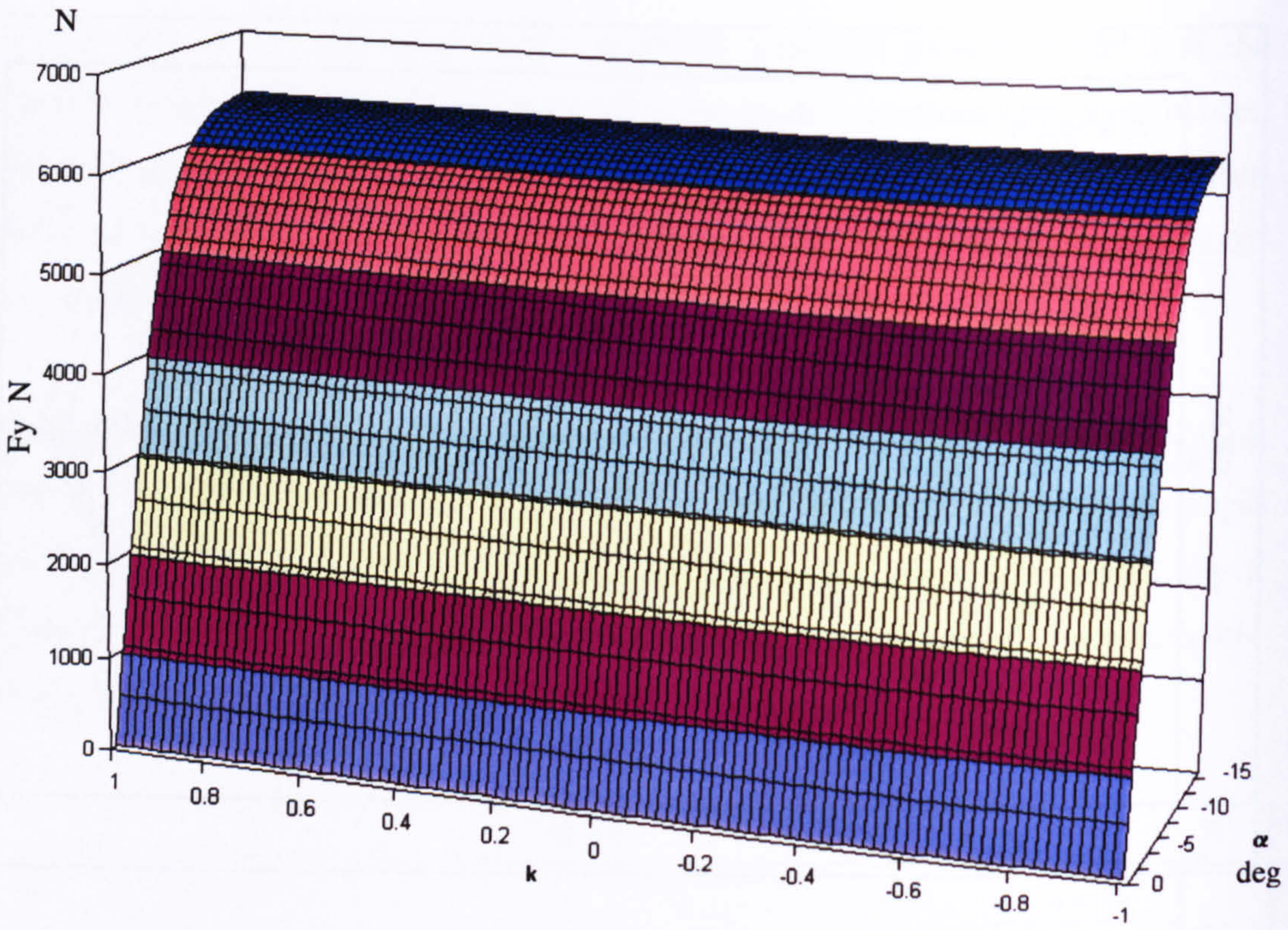

Fig (4.15) $F_y - \alpha$ relation at different k values according to pure lateral slip model

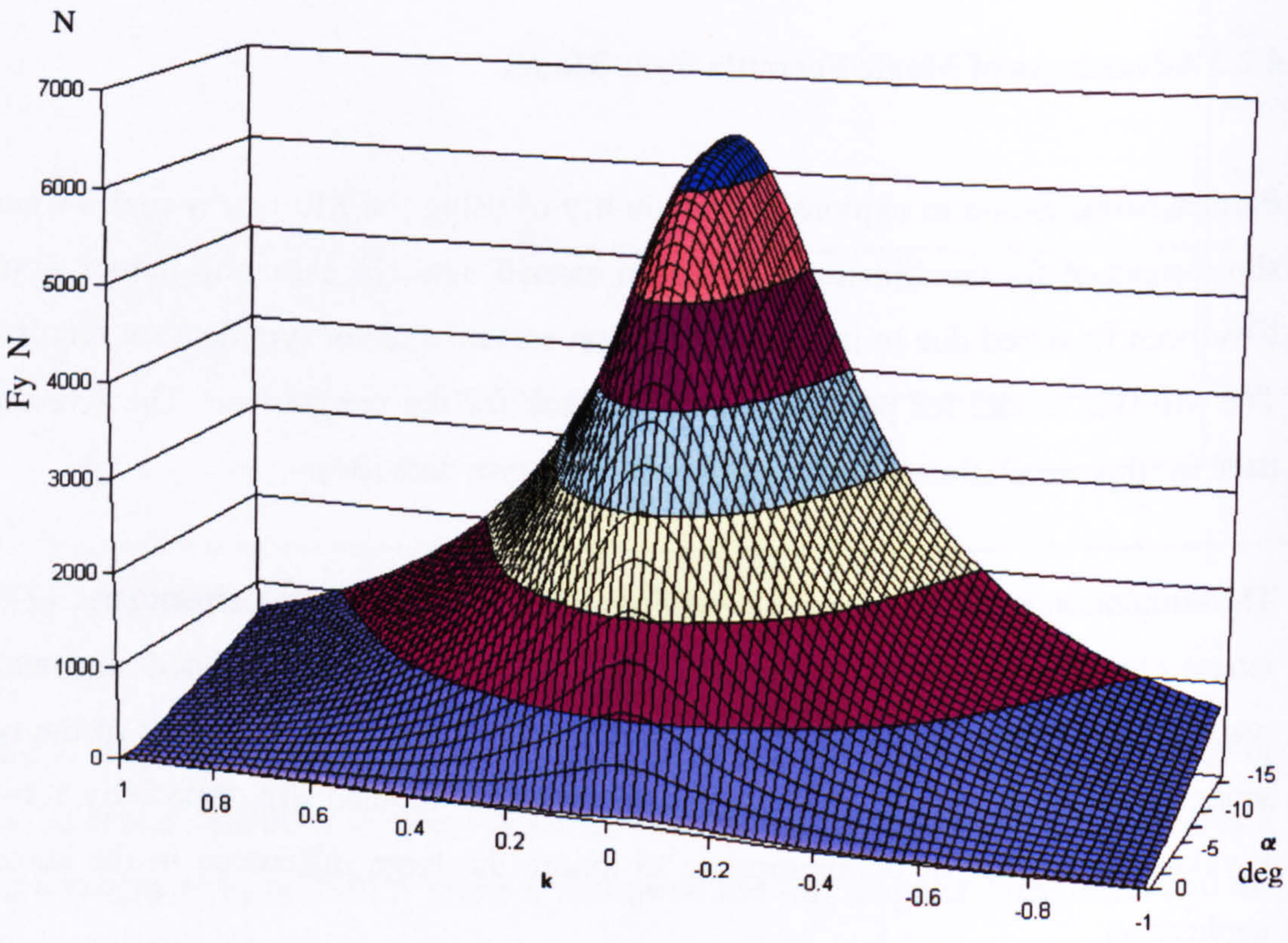

Fig (4.16) F_y - α relation at different k values according to combined lateral slip model

In the longitudinal direction the simulation results, Fig (4.17) and Fig (4.18) show the tyre performance according to the MF pure longitudinal slip model and MF combined slip model respectively. The difference between the longitudinal forces estimated by the two models is large and it would not be appropriate to ignore this difference in the current application.

The differences between the MF pure and combined slip results for both lateral and longitudinal slip prove that the MF pure slip tyre model does not properly represent the tyre in combined slip situations. Consequently, the MF tyre model for combined slip is considered crucial for the current work.

4.2.4 Shortcomings of Magic Formula Tyre Model

On the other hand, the MF tyre model for combined slip has some drawbacks. It consists of a large set of equations, and requires a large set of, often unavailable, tyre data. This complication could compromise its adaptation for real time systems due to the large processing time required. Also the nature of the equations makes mathematical manipulation difficult.

The MF tyre model set of equations is written in a way such that input values for α and k produces output values for F_y and F_x which resembles tyre testing machines where α and k are imposed inputs while F_x and F_y are the measured output. This causes problems in the current CGT vehicle handling model where F_x and slip angle α are predicted from the CGT model, while F_y and k are the unknowns. Therefore the current CGT model requires a modified version of the MF tyre model for combined slip.

A short investigation of different solution possibilities has been carried out. It was concluded that there are three different alternatives: -

1. Change the vehicle model.
2. Analytically reverse the MF tyre model equations.
3. Use an iteration technique to treat the model inputs and outputs.

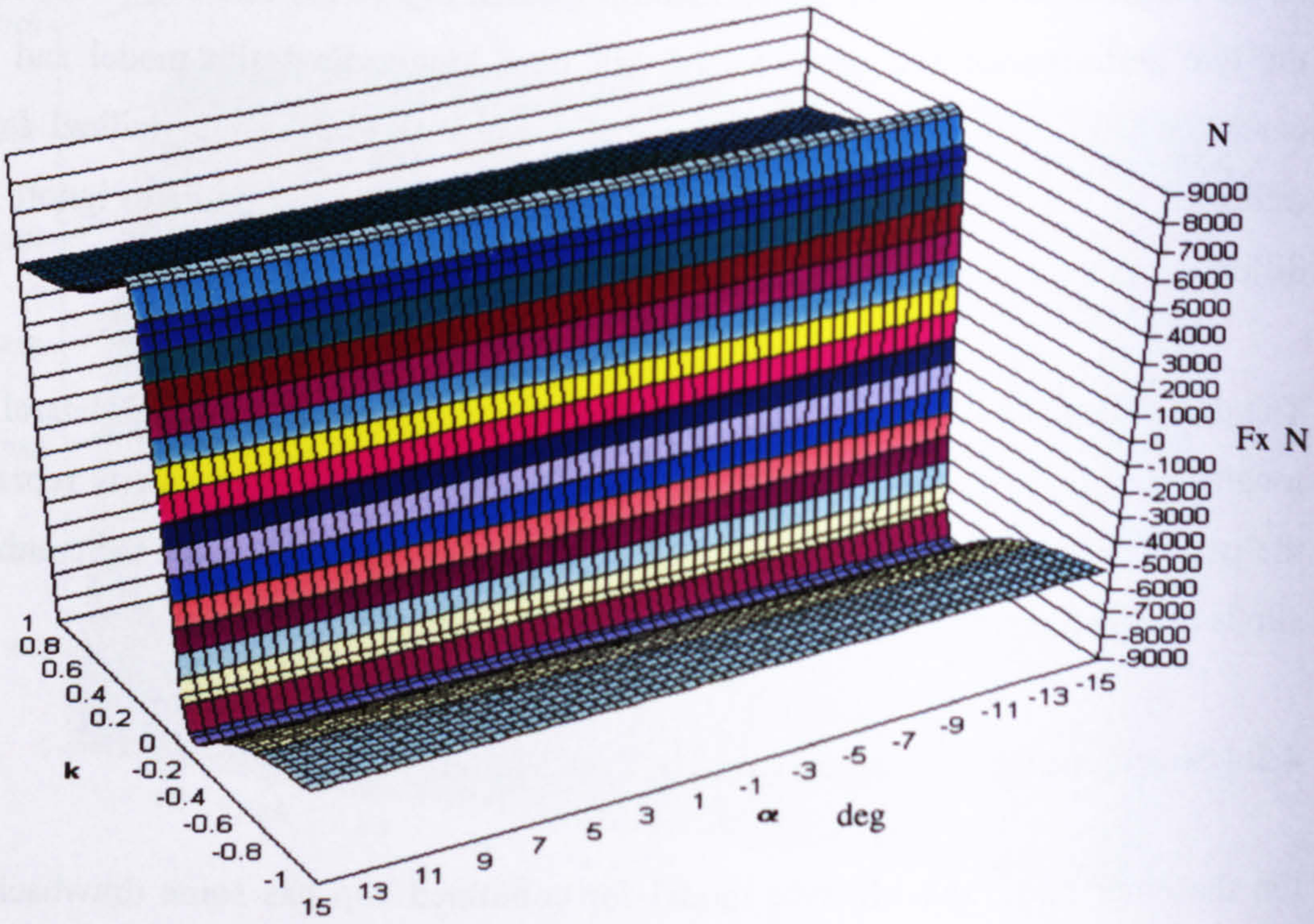

Fig (4.17) F_x – k relation at different α values according to pure longitudinal slip model

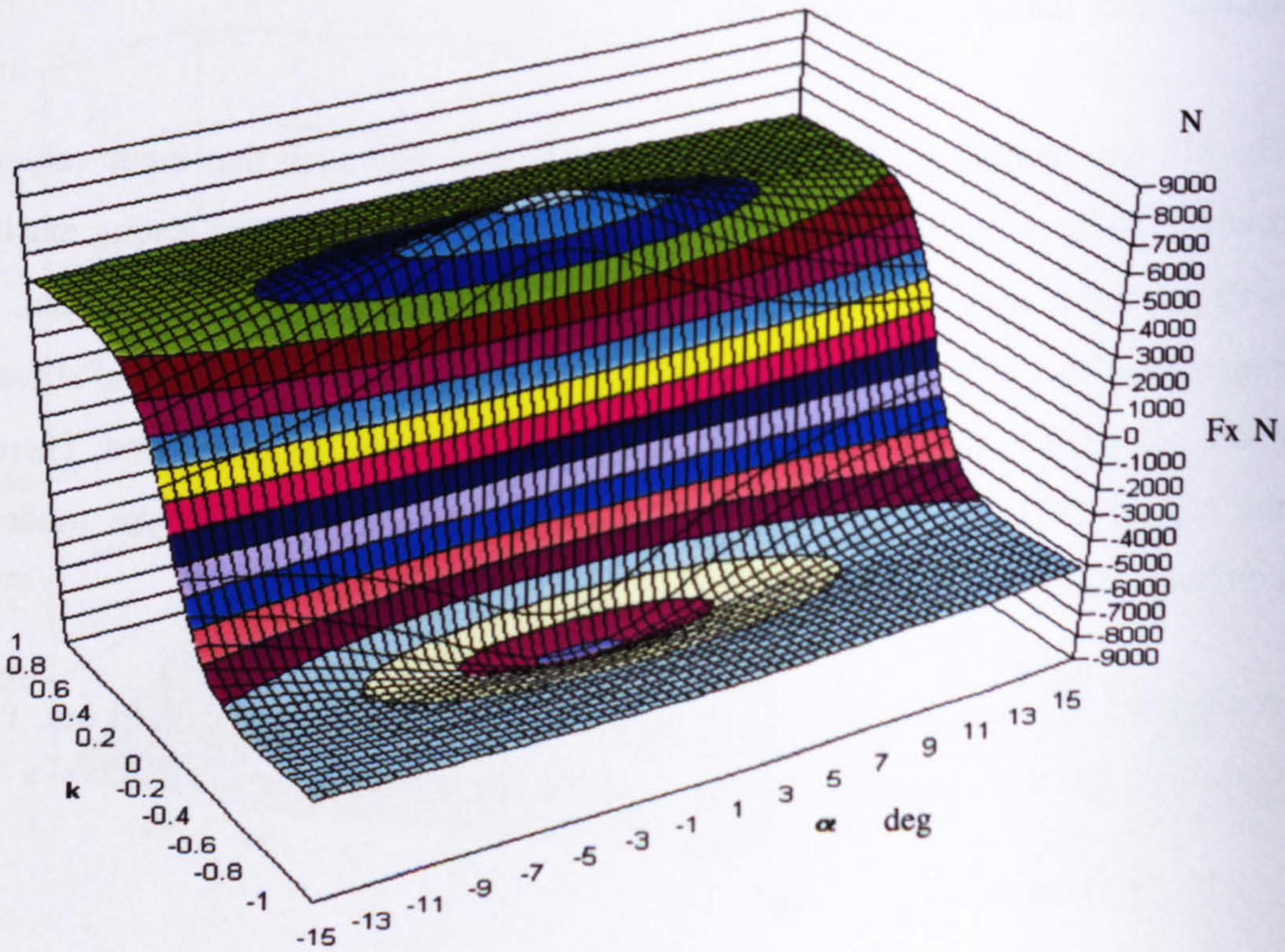

Fig (4.18) F_x – k relation at different α values according to combined longitudinal slip model

The first option to change the vehicle model has not been considered due to the promising results model so far.

The second option to analytically reverse the MF tyre model for combined slip equations has been considered unrealistic as the nature of the tyre characteristics, Fig (4.14), shows that at some F_x and F_y combinations there are two different sets of α and k values while at other F_x and F_y combinations there are no defined values for α and k, which would add to the reversed model mathematical complexity. In addition, the MF model equations are written with nested α and k factors that will lead to difficult reversed model equations, requiring iteration techniques to solve. On the other hand, the use of iteration techniques would in itself solve the situation as in the third option. So the second option has not been chosen.

The third option, involves the use of an iteration technique to treat the inputs and outputs of the MF tyre model for combined slip has been considered the more feasible option, even though it has been considered a relatively hard task due to the nature of the surface representing the tyre characteristics, Fig (4.14).

4.3 Longitudinal Slip Calculation Routine (kcal)

This routine has been developed to match the CGT vehicle handling model requirements and the MF tyre model outputs, Fig (4.19). It employs the MF tyre model for combined slip through iteration to investigate longitudinal slip k value at a given F_x and α. Then, α and k values are fed to the MF tyre model to predict F_y values.

The kcal routine is the only iterative technique to be employed in the current CGT vehicle handling model. Hence, an investigation towards its run time reduction has been carried out. In this investigation a fast iteration process has been developed. This development evolved from knowledge of the tyre performance chart, Fig (4.14)

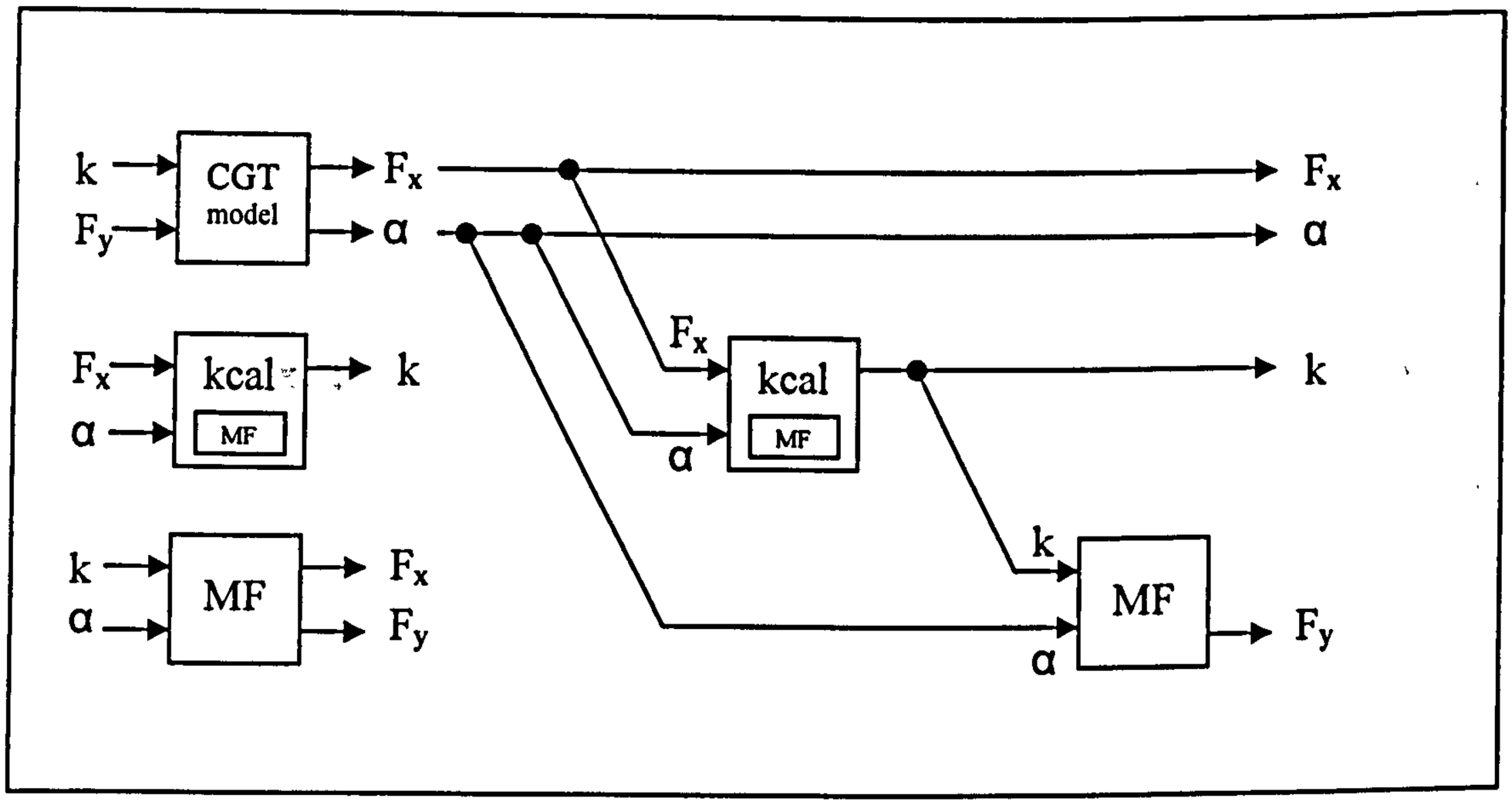

Fig (4.19) kcal matching between CGT model and MF tyre model

In the kcal routine, the branch and bound iteration technique, [85] has been employed to investigate the two k values, 0.01 spaced, surrounding the required k value. These two values are the closest k values that have F_x estimation errors with opposite signs Fig (4.20). The surrounding k values along with the errors of F_x estimations are then fed to a specially developed module based on the false position iteration technique, [86], Fig (4.20). The combined iteration technique has the capability of achieving the required k value accuracy in a small number of cycles, which yields short processing time and hence a fast iteration process. The kcal algorithm flow chart is given in Appendix E.

The kcal routine has been tested to investigate its functionality. In the first test, a large set of random F_y and α pairs (50,000 pairs) were fed to the kcal routine. F_x ranged between 0 and 9000 N while the α values ranged between 0 and –10 degrees. A vertical load Fz of 7000 N has been employed to match the published MF results. The kcal routine is capable of differentiating between the F_y and α pairs that are within the tyre working range, Fig (4.21), and the pairs that lie outside the tyre working range, Fig (4.22). The estimation errors for the in range pairs are plotted against the calculated k in Fig (4.23). The characteristic shape of the error chart is due to the nature of the iteration technique employed.

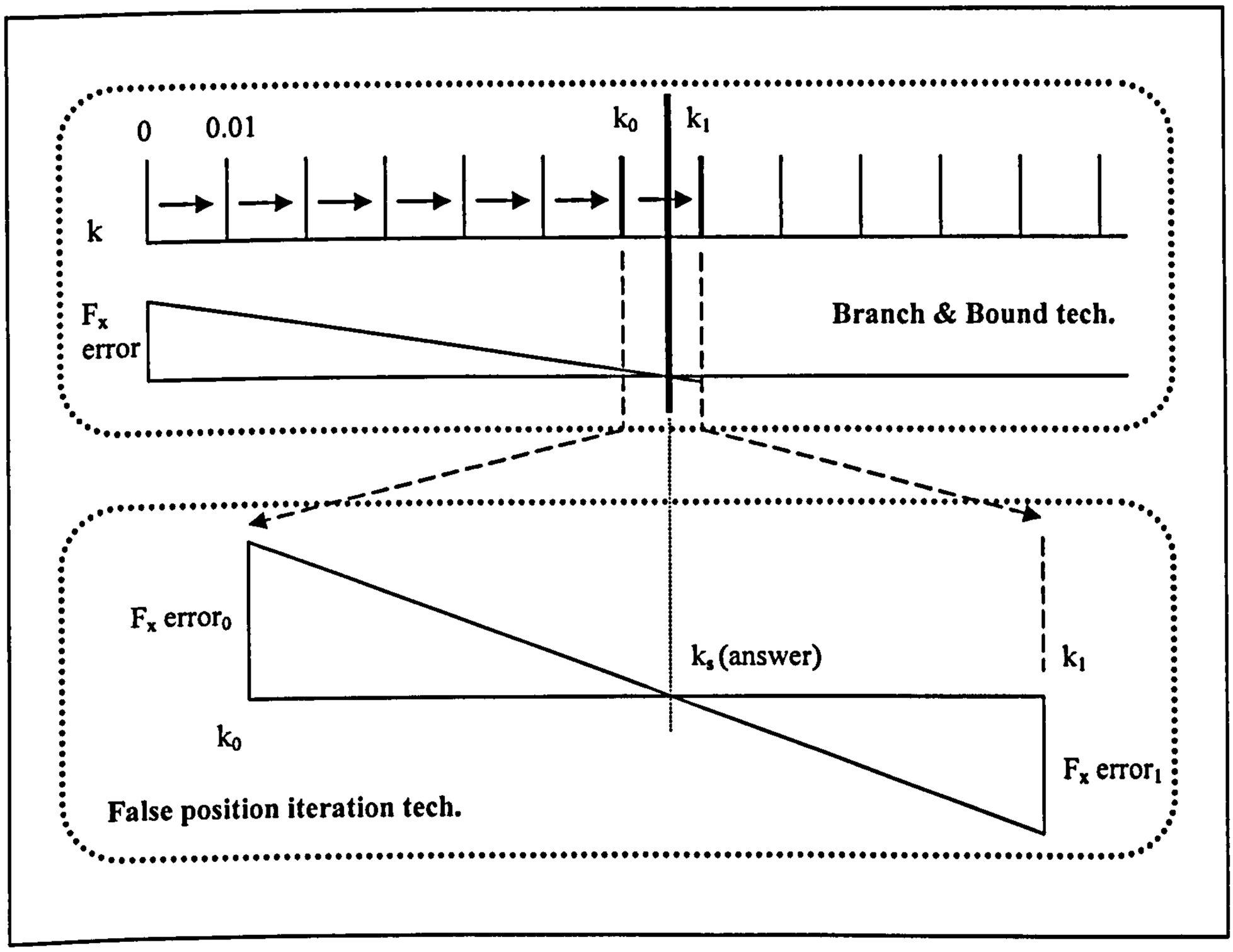

Fig (4.20) Outline of the iteration techniques used in kcal routine

In the second test a set of 1 N spaced F_x values from 0 N to 9000 N were fed to the kcal routine at α values of 0, -2, -5 and –10, for a vertical load F_z of 7000 N. The resulting in-range k values were plotted against the corresponding F_x values, Fig (4.24). The highest F_x and k values were comparable to the MF tyre model results. Finally, the effect of α on k and F_x was investigated using the kcal routine to further proof its functionality, Fig (4.25). The test results from the kcal routine proved its functionality, accuracy and suitability to perform its objective.

During the kcal routine development, a fully reversed MF tyre model for combined slip has been developed and tested. In this iteration-based reversed MF tyre model, F_y and F_x are the inputs while α and k are the outputs, Appendix F.

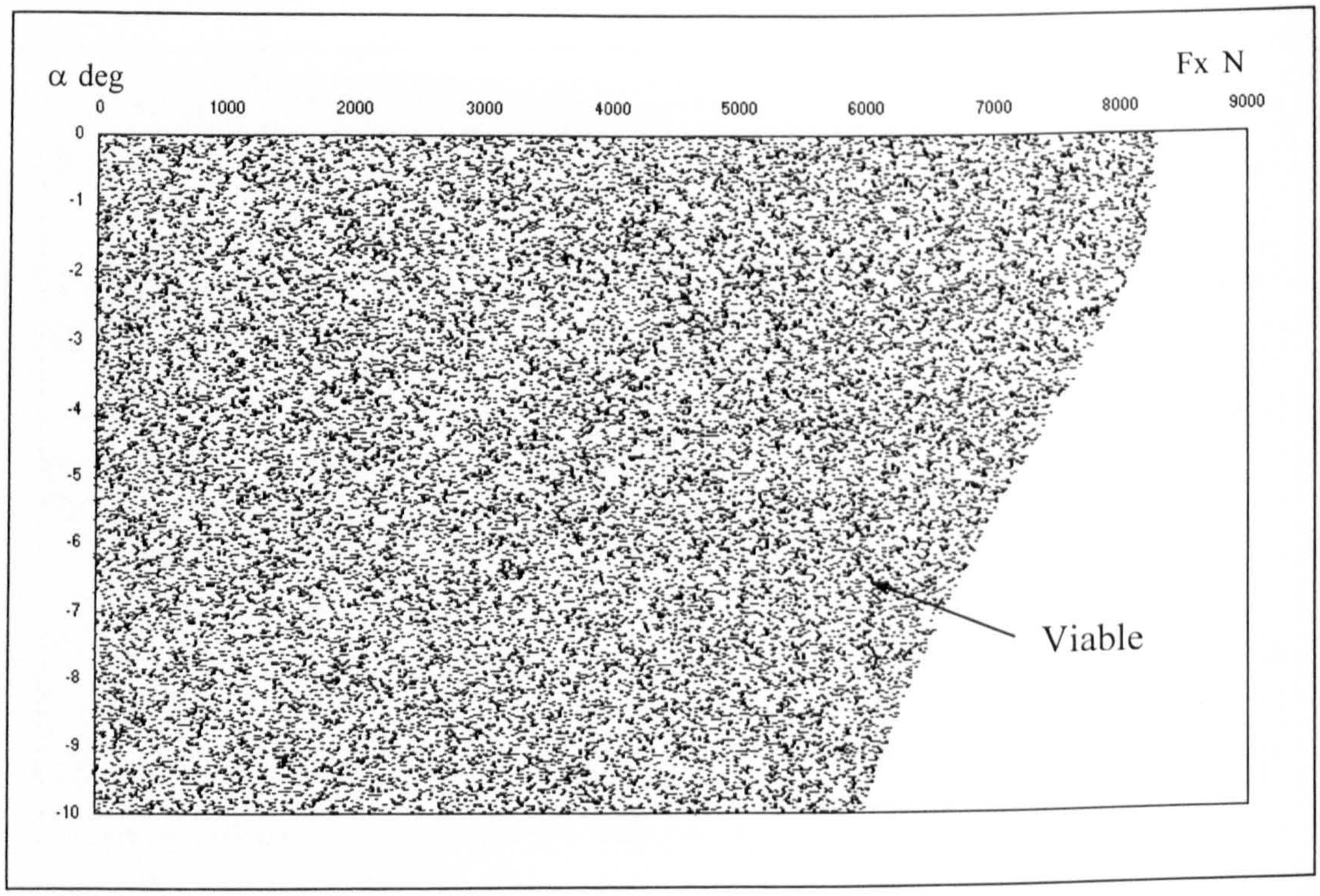

Fig (4.21) kcal routine test results, random in-range F_x-α pairs

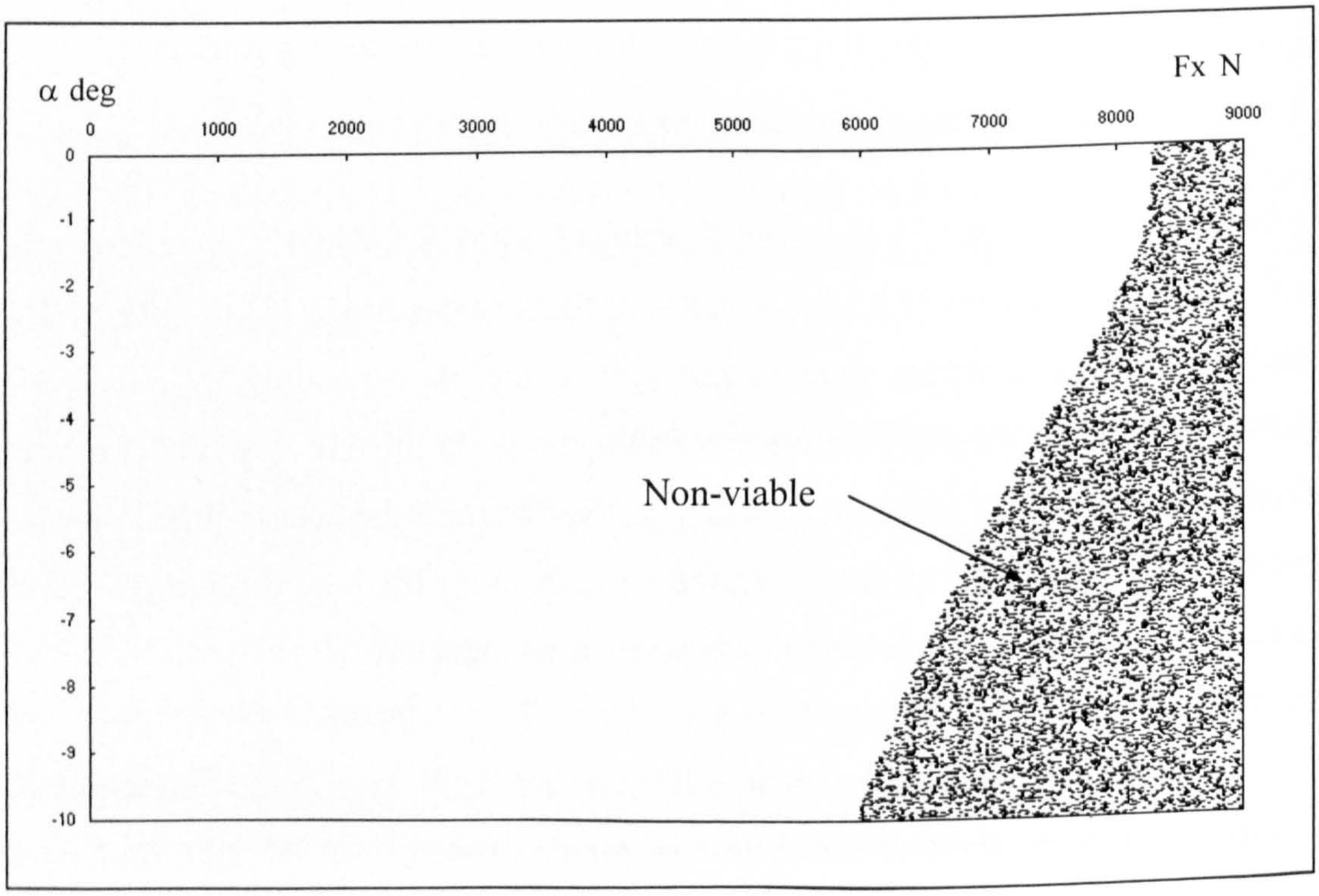

Fig (4.22) kcal routine test results, random out-of-range F_x-α pairs

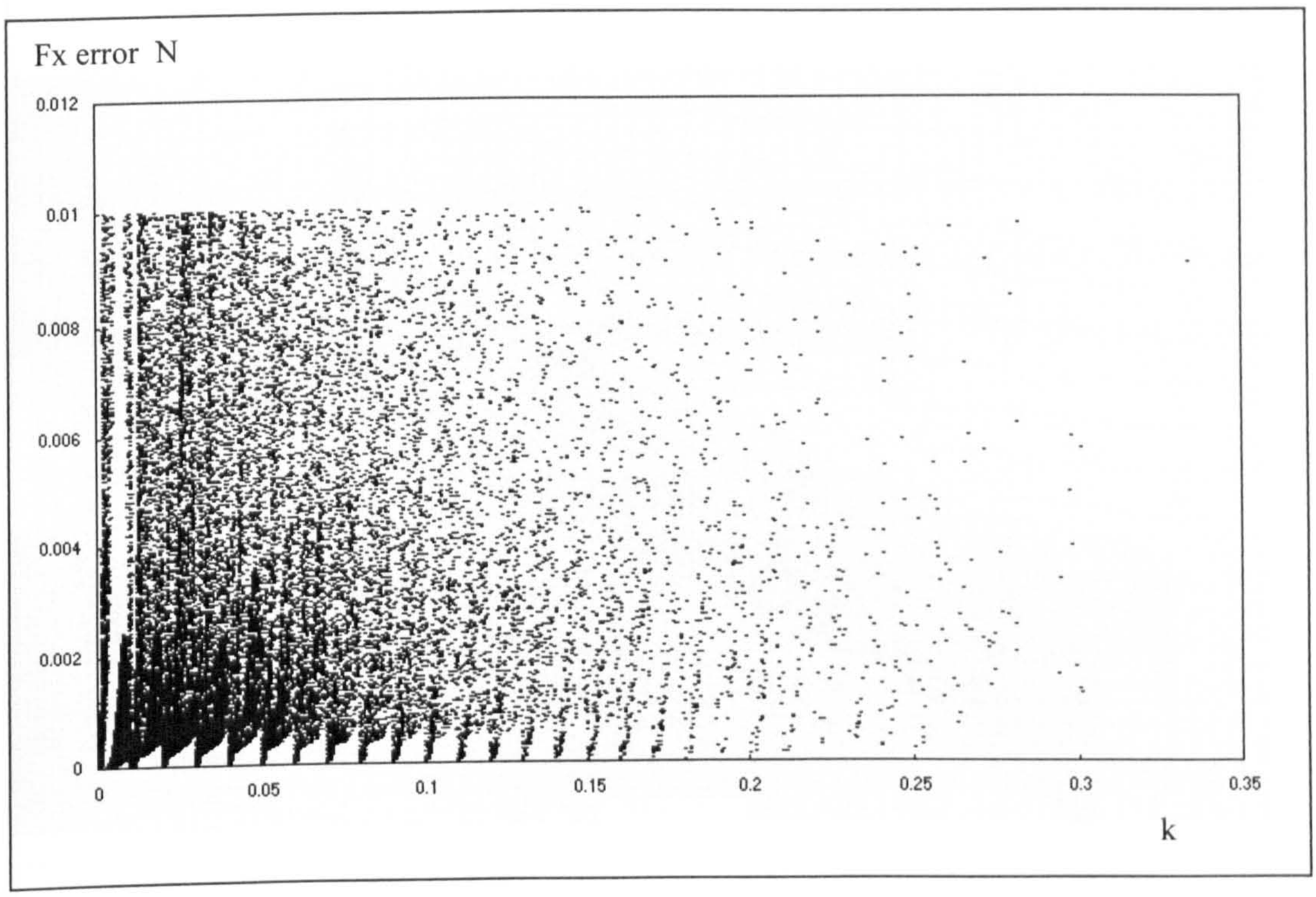

Fig (4.23) kcal routine test results, errors of random in-range pairs

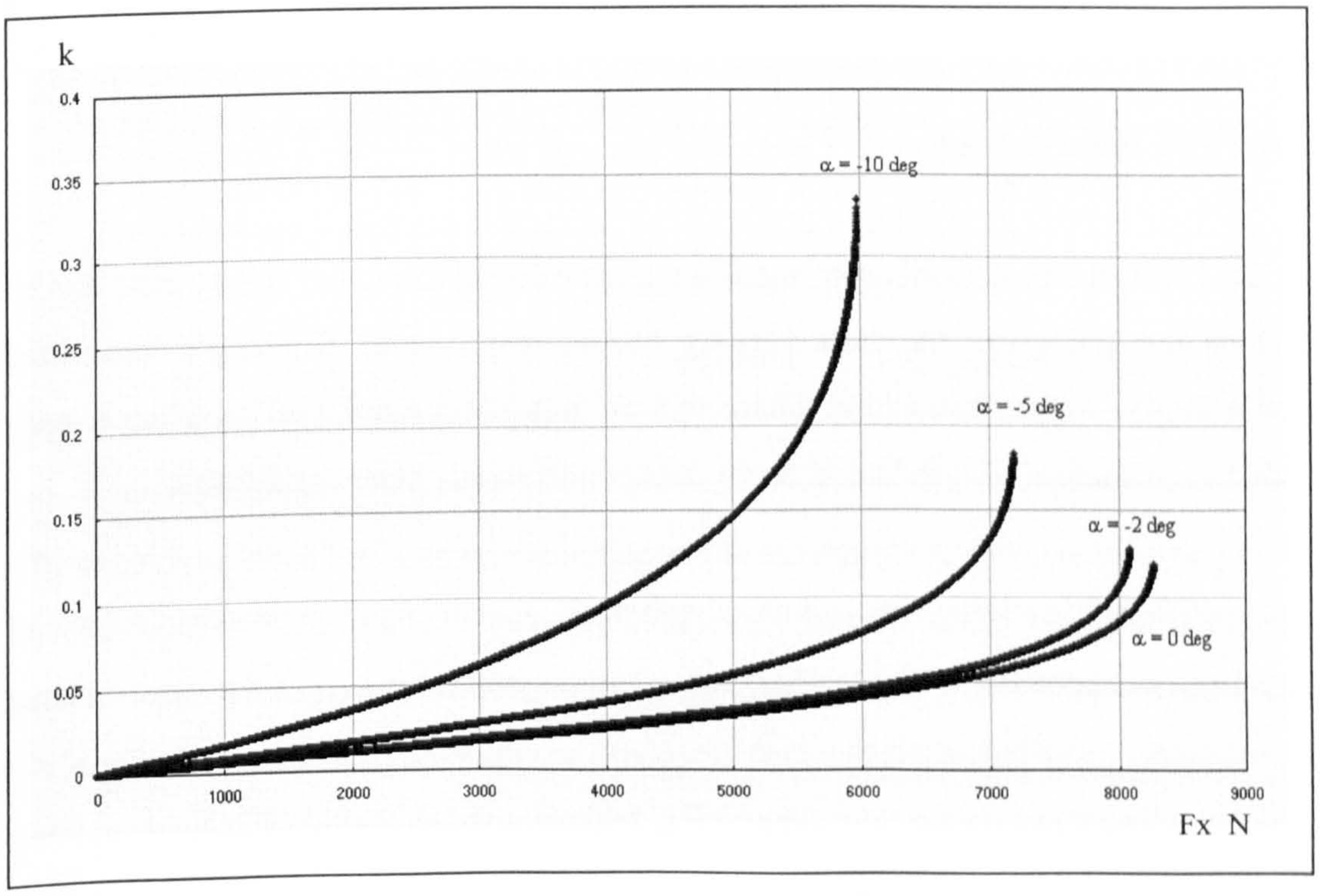

Fig (4.24) kcal routine test results at different α values

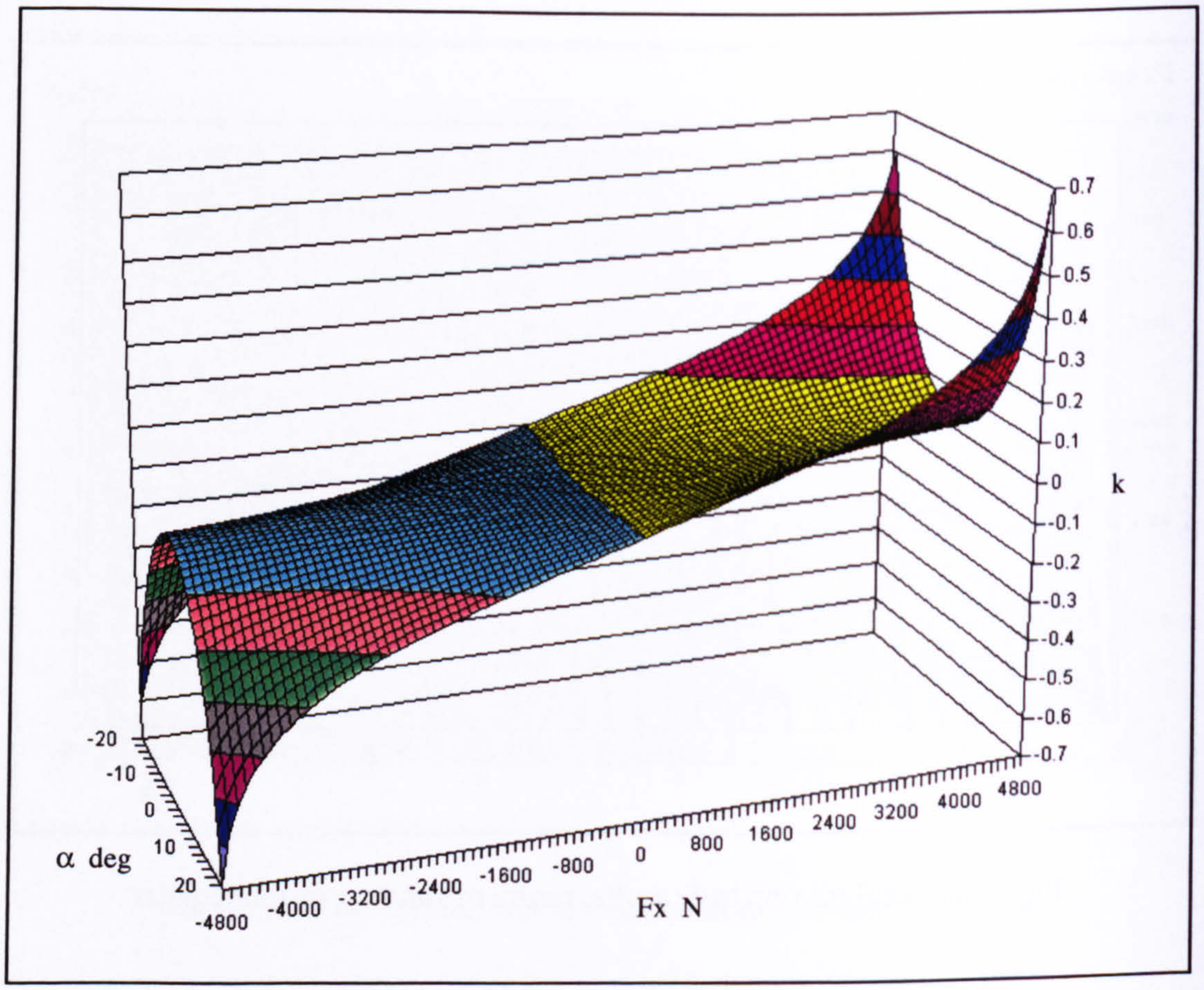

Fig (4.25) kcal routine test results showing effect of α on k-F_x relation

4.4 Tyre Relaxation

As the MF tyre model for combined slip was developed to predict steady state forces, it does not recognise the time-varying rubber response to slip angle variations. Accordingly, a tyre relaxation characteristic has been employed to give a more realistic estimation of tyre lateral forces under non steady state conditions.

The tyre relaxation length σ_y is a characteristic tyre property. It represents a forward travelling distance delay for the tyre lateral force generation. This forward distance σ_y must be travelled after the tyre develops a slip angle α before 63 % of the corresponding steady state lateral force F_{yss} is developed [87], Fig (4.26).

The tyre relaxation length is affected by many vehicle handling factors. It increases as the tyre vertical load increases, and decreases as the steering angle and slip angle

increase. Figure (4.27) shows tyre relaxation lengths at different F_z and α values [88].

The existence of relaxation lengths means that the lateral force F_y developed at the end of a CGT model time frame is the result of slip angles α already developed and known from previous time frames and the slip angle at the end of this time frame.

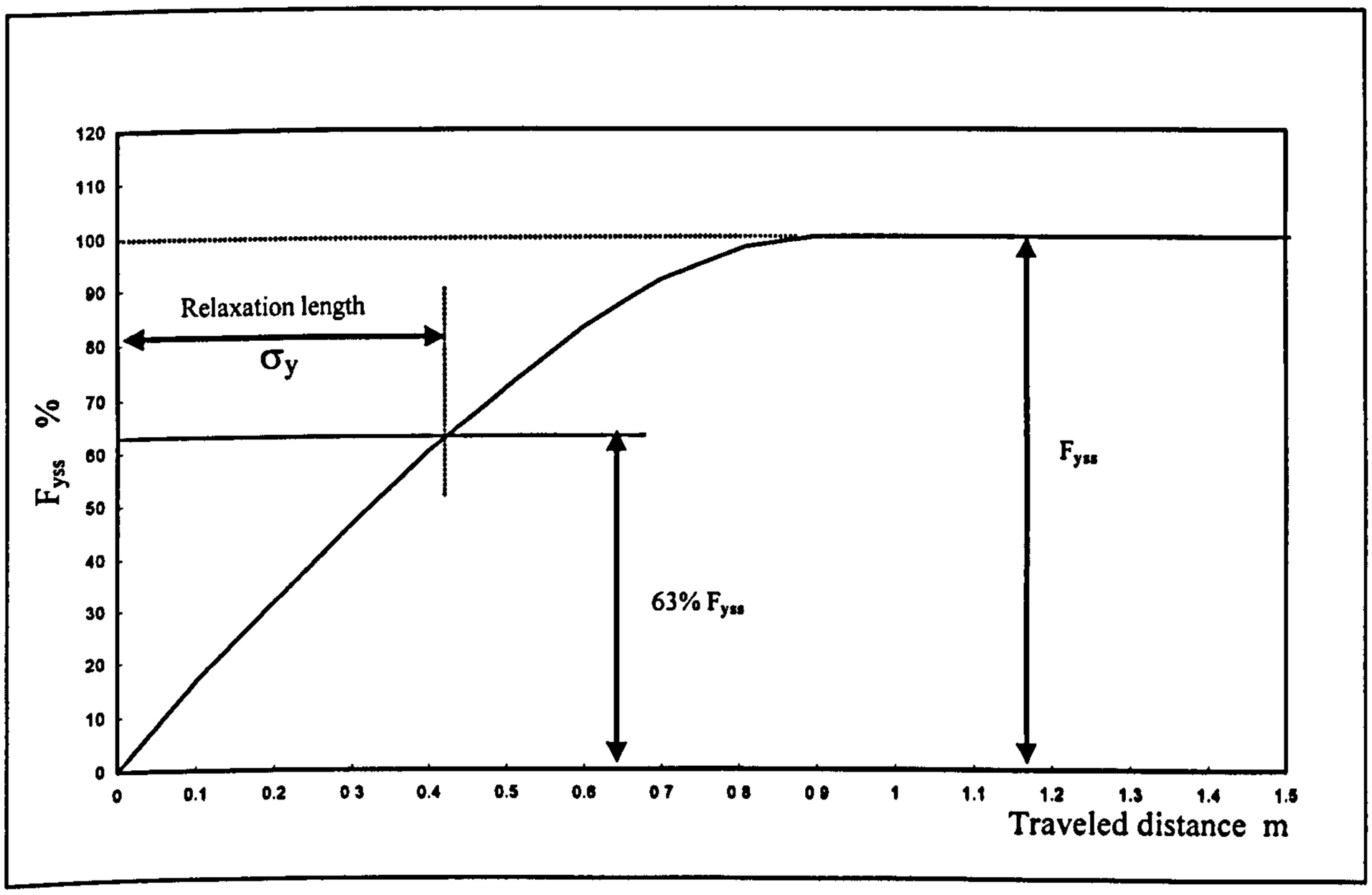

Fig (4.26) Tyre relaxation length σ_y

4.4.1 Tyre Relaxation Adaptation

The employment of tyre relaxation length in the current CGT vehicle handling model caused some difficulties. The first difficulty was that the lateral force development and forward distances relation is not given. The second was that the total length required for the tyre to develop the steady state lateral force is not given. For the current model an average value for the tyre relaxation length has been employed. This value is averaged for the tyre relaxation lengths deduced from Figure (4.27) and given in Table (4.1).

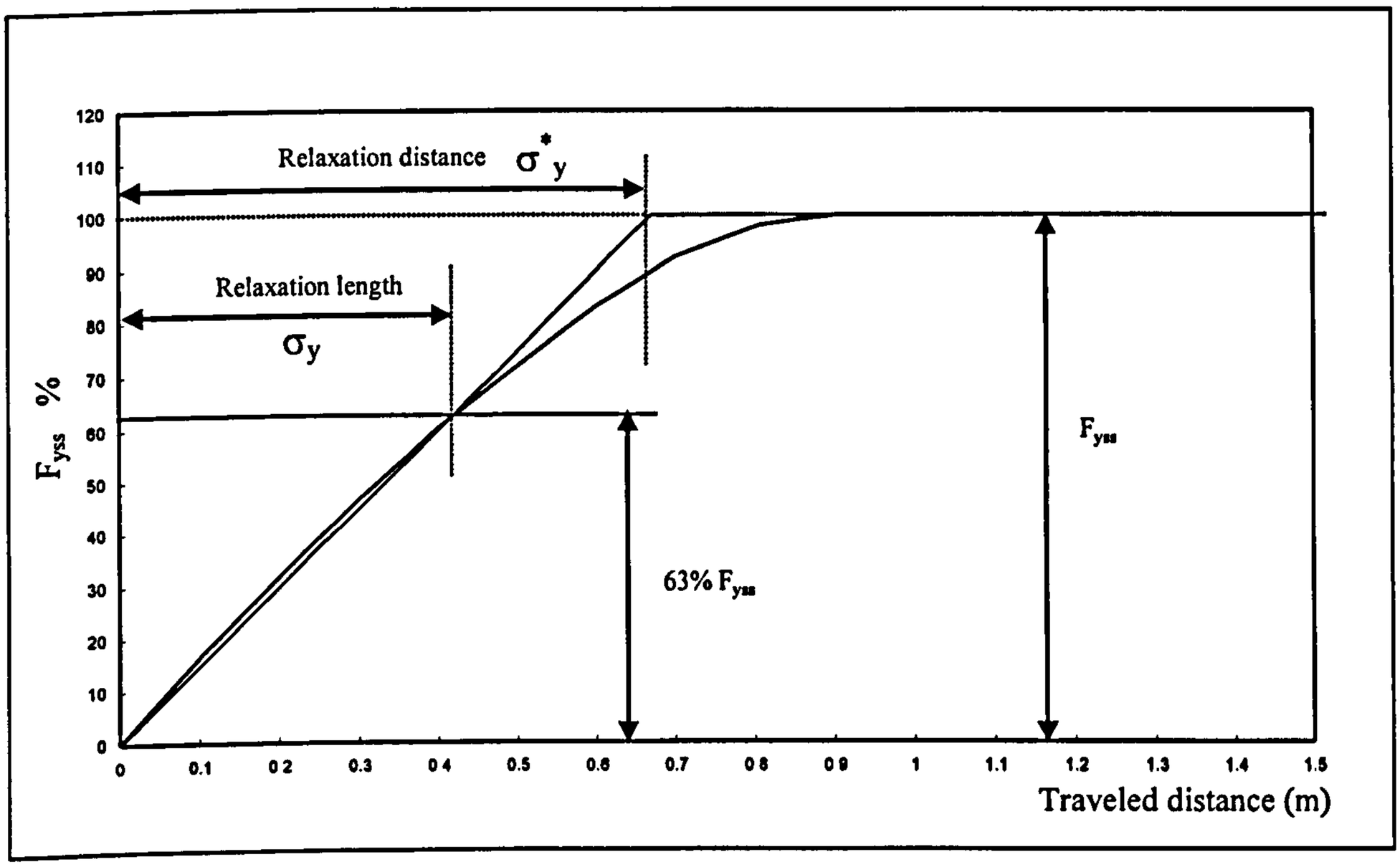

Fig (4.28) Tyre relaxation distance σ^*_y

4.4.2 Tyre Relaxation Application

To allow recognition of the lateral tyre relaxation characteristics in the vehicle handling models a special routine has been developed. A calculated tyre lateral force at the end of a CGT model time frame is fed to this routine, where it is used along with the history of the tyre lateral forces from previous time frames to investigate the applied tyre lateral force. This force is then added to the previous tyre lateral force history for use in the next time frame. Figure (4.29) shows the relaxation length routine.

The routine starts by calculating the number of time frames required for the tyre to develop the full lateral force that corresponds to its developed slip angle.

$$i = \left| \frac{\sigma^*_y}{u\Delta t} \right| \tag{4.2}$$

Where: -

i Number of time intervals ($i \geq 1$)

σ^*_y Lateral relaxation distance

In this routine the lateral forces corresponding to the tyre slip angles developed at the end of the different time frames are stored to form the tyre lateral force history. To evaluate the lateral force at time frame n, the forces that have been developed during the last *i* frames are then taken into account. The average of these forces represents the tyre lateral force produced, Fig (4.29).

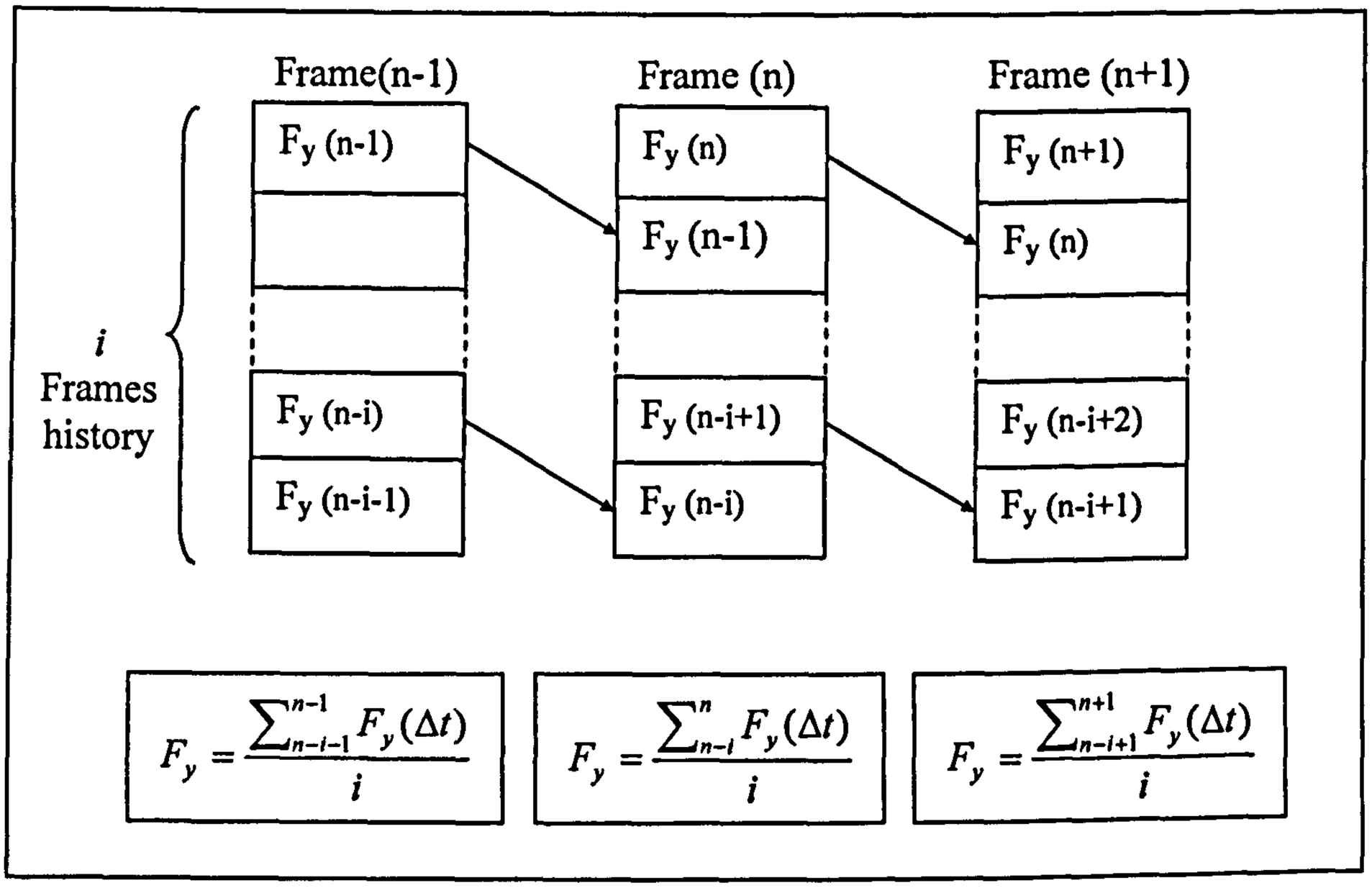

Fig (4.29) Lateral force evaluation form lateral forces history

4.5 Conclusions

In this chapter, the choice of the Magic Formula tyre model for combined slip has been discussed. Also the BASIC© code developed for the Magic Formula tyre model has been tested through comparison with published results.

The performance differences between the MF pure slip tyre model and the MF model for combined slip have been investigated. The MF pure slip has been found to poorly estimate the lateral force at high longitudinal slip conditions. The error in longitudinal force estimation, due to slip angles, has been found to be smaller. These

results support the employment of the MF tyre model for combined slip for the CGT vehicle handling simulations, as high levels of longitudinal slip are unavoidable.

The advantages and shortcomings of employing the Magic Formula tyre model for combined slip have been investigated and the tyre model interface problem with the developed vehicle CGT handling model has been discussed along with the different alternatives. As a result the decision has been taken to treat the Magic Formula tyre model inputs and outputs using the Branch and Bound iteration technique and false position iteration technique. Accordingly the kcal routine has been developed, tested and found capable of predicting k values that correspond to longitudinal force F_x and α pairs.

The kcal routine employing the Magic Formula tyre model for combined slip has been developed in the BASIC© code. It has been tested through solving large random set of 50,000 longitudinal force and slip angle pairs, to evaluate their corresponding k values. The results proved both the functionality and precision of the algorithm, as no points were outside its range. Also the k and α results were fed to the MF tyre model and the errors of reversed MF tyre model estimation of F_x were below 0.01 N. Accordingly, the kcal routine has been considered ready for integration with the already developed CGT vehicle handling model.

In the final stage, the tyre relaxation characteristic has been employed to give a more realistic estimation of tyre lateral forces at non steady state conditions. To take the relaxation length into account, the time frame force and the history of the tyre lateral forces from previous time frames have been employed to investigate the applied tyre lateral force. The time frame force is then added to this tyre lateral forces history for use in the next time frames.

Chapter 5

CGT Full Vehicle Handling Model

5.1 Introduction

In this chapter the CGT half vehicle (bicycle) handling model developed in Chapter 3 is upgraded to a novel CGT full vehicle handling model. The upgrade includes the model's ability to investigate the full effect of individual wheel longitudinal force regulation (TFDC) and their effect on vehicle longitudinal, lateral and yaw accelerations and velocities. It also includes individual wheel steering (4WS), employment of MF tyre model for combined slip and adaptation of tyre relaxation length characteristics. The CGT full vehicle handling model has also been featured with Ackerman steering and an enhanced manoeuvre capacity.

These improvements have considered the extra processing load applied to the model and therefore increase its processing time. Hence, they have been considered an essential step towards the development of the WSDC vehicle handling model and the onboard model for the MPC controller.

The CGT vehicle handling model upgrade to steer the front wheels, rear wheels or all four wheels has been developed. Although this increases the model processing time, it is intended to facilitate investigation of the WSDC effect on different vehicle configurations and to facilitate further research.

5.2 WSDC CGT Full Vehicle Handling Model Outline

The CGT full vehicle handling model has been developed as an upgrade to CGT half vehicle handling model. It also, capitalises on the demonstrated success of the CGT vehicle modelling technique. In this model the vehicle is simulated in successive time frames. In each time frame the vehicle starts at an initial position on local coordinates and ends at a final position, Fig. (5.1).

In order to make the developed CGT vehicle handling model understandable, the different stages of the model solving have been clearly defined and organised in the order processed by the computer. The model is designed in open architecture manner. Accordingly, any stage or equation could be further developed without need to modify other stages. The CGT model development took into account the need to avoid any conflict between inputs and outputs at different solving stages, as this would enforce the use of iteration techniques. The resulting model outline, Fig (5.2), managed to reduce the need for iterations to only one process; the calculation of tyre longitudinal slip k (kcal routine).

For the current model every modelled time frame has three inputs. The first input is the tyre longitudinal force F_x, with the possibility to be controlled externally to allow TFDC. The second input is the tyre lateral force F_y that resulted from the previous slip angle history, managed through the tyre relaxation length routine. The third input is the vehicle longitudinal, lateral velocities and yaw rate at the end of the preceding time frame.

The model solving stages start by employing the input tyre longitudinal and lateral forces along with vehicle parameters and steering angles to calculate the forces and moment at the vehicle CG. The developed forces and moments are then used along with vehicle mass and rotational moment of inertia to calculate the CG longitudinal, lateral and yaw accelerations. The calculated CG accelerations are used in two different ways. First, the accelerations are used along with the input initial velocities and the time frame width Δt to calculate the time frame final CG velocities. Second the accelerations are used with vehicle mass and CG location within the vehicle to evaluate the tyre vertical loads, F_z.

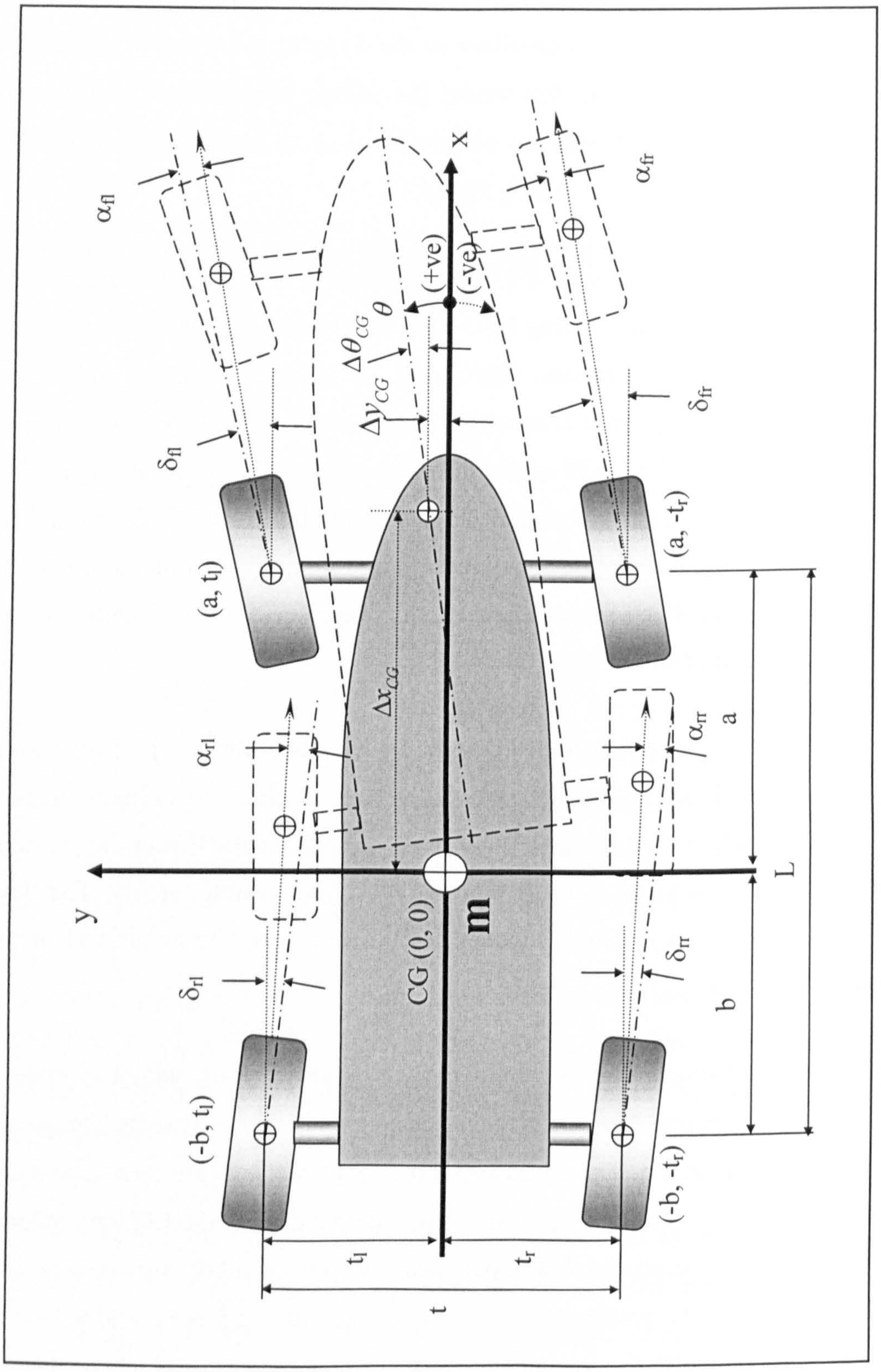

Fig (5.1) Representation of the vehicle travelling on the x-y plane

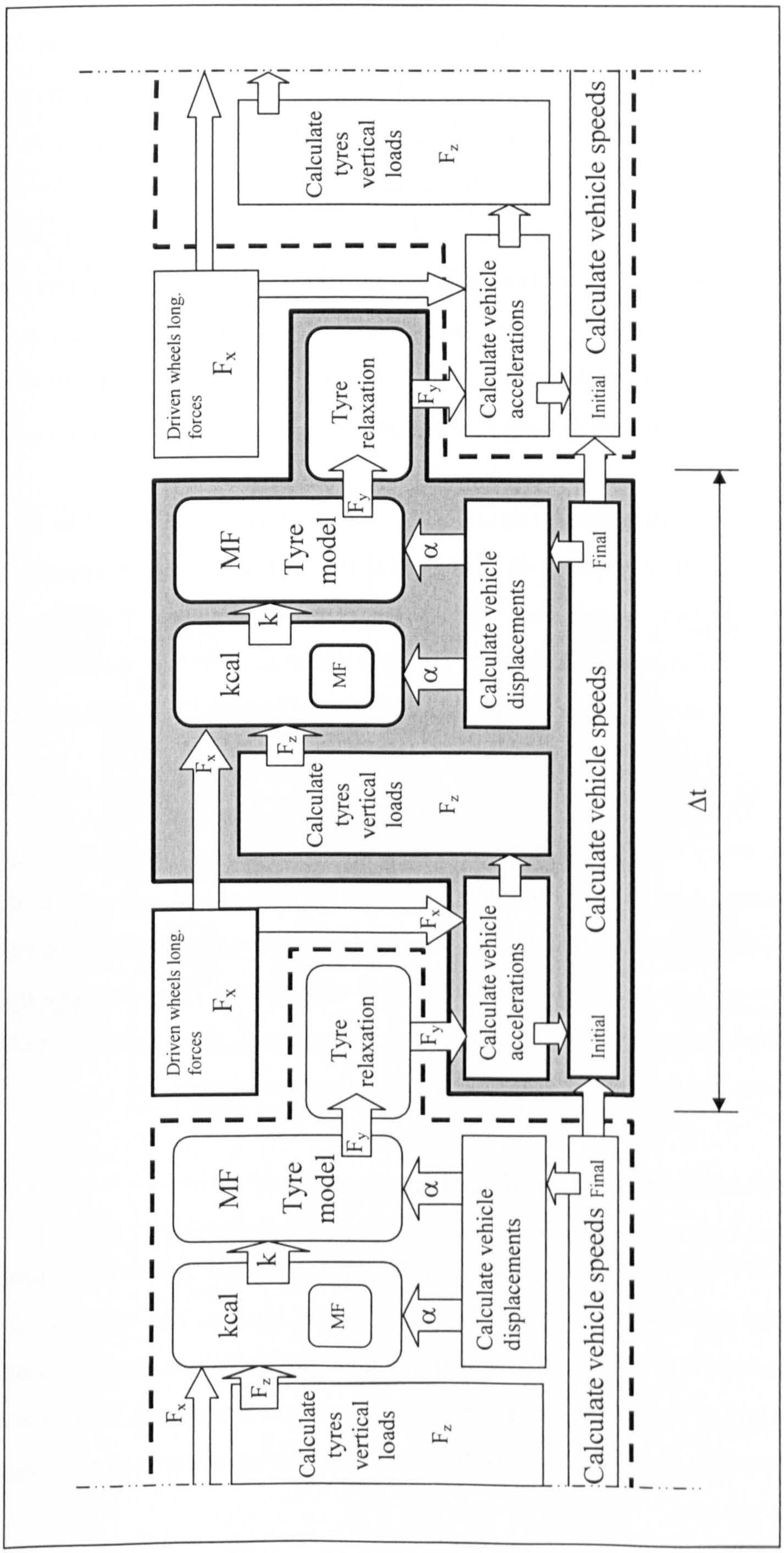

Fig (5.2) Block diagram of full WSDC CGT vehicle handling model time frame

The initial and final time frame velocities associated with the vehicle CG are used with the time frame width Δt to calculate the CG rotation and translation in x-y coordinates. The rotation and translations are employed with vehicle parameters to calculate the new tyre x-y locations. These locations along with the initial tyre locations and steering angles are used to calculate the tyre slip angles. The developed tyre slip angles along with the calculated tyre vertical loads and the input tyre longitudinal forces F_x are fed to the kcal routine, which employs the MF tyre model to evaluate, through iteration, the corresponding tyre longitudinal slip k. The developed tyre longitudinal slip along with calculated slip angles are fed to the MF tyre model, which evaluates the tyre lateral forces F_y.

For each tyre, the lateral force calculated by the MF tyre model is fed to the tyre relaxation routine that employs it, along with the tyre lateral force history from previous time frames, to calculate the current time frame lateral force F_y output based on tyre relaxation characteristics. The time frame also outputs the final vehicle CG velocities. At this point the vehicle handling model is ready to start the next time frame.

At the end of every time frame the vehicle displacements are transferred to the global X-Y coordinates. Also the vehicle x-y coordinates are rotated and moved to initialise the vehicle CG position in local x-y coordinates for the next time frame. The vehicle CG velocities are also transferred to the new x-y coordinates. Through repeating the developed time frame solution for successive time frames, the required simulation time is covered and the vehicle handling performance investigated.

5.3 CGT Vehicle Handling Model Derivation

The novel CGT technique used in developing the novel CGT full vehicle handling model and the model equations are presented in this section. The objective of the solving technique is to evaluate the vehicle translations, velocities, accelerations and forces at the end of each time frame. The model equations are presented in an orderly fashion to describe, clarify and justify the technique through describing the stages of a time frame solution.

5.3.1 Stage One: Vehicle Initial Conditions

At the start of each time frame, the vehicle CG is located at (0,0) in the local x-y coordinates and the vehicle axle falls on the local x coordinate, so the initial vehicle rotation angle θ_{CG0} is equal to zero, Fig (5.3). The tyre locations at this initial position are evaluated as function of the vehicle geometry and CG location. The initial CG and tyre locations in x-y local coordinates are given as follows: -

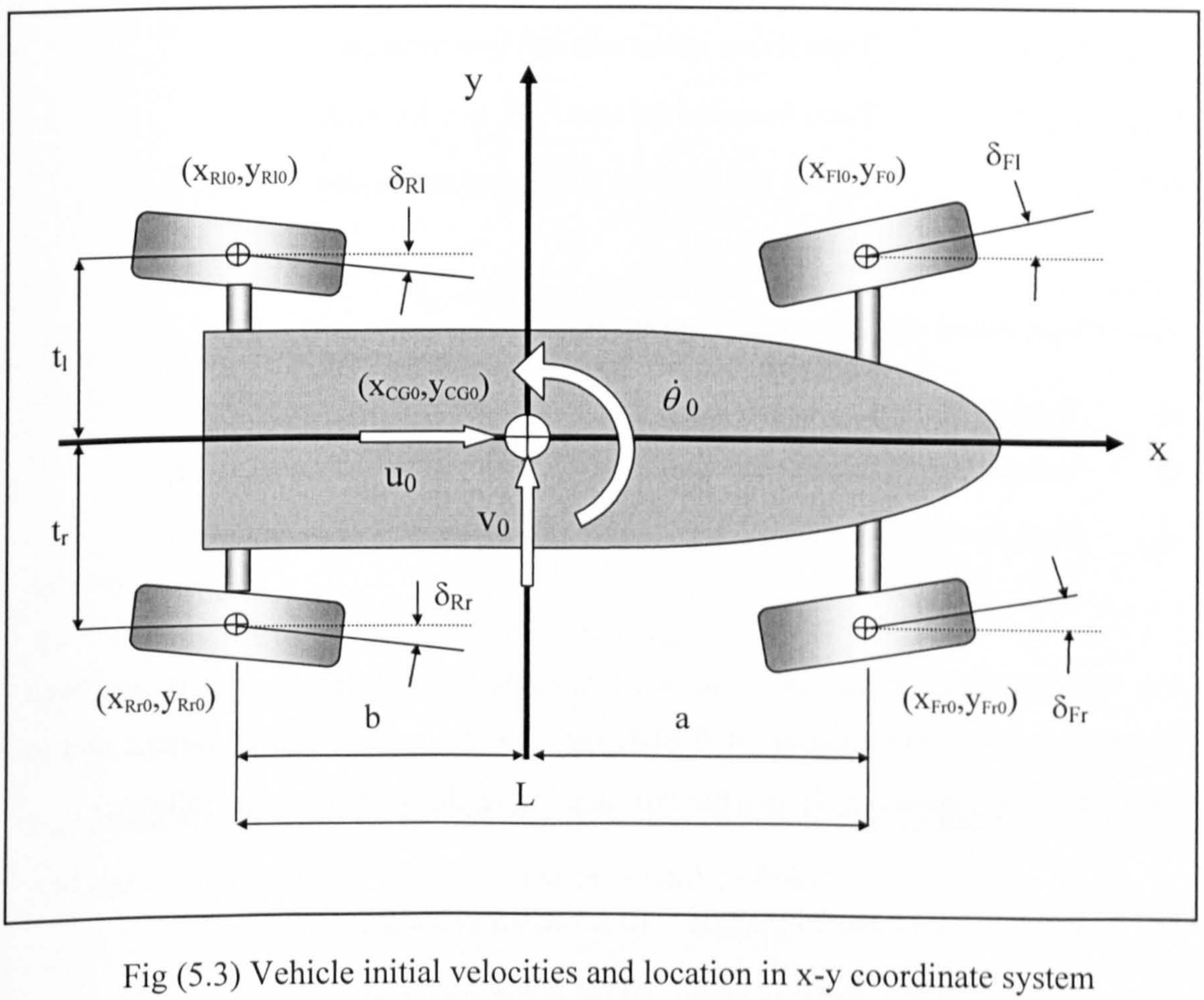

Fig (5.3) Vehicle initial velocities and location in x-y coordinate system

$$(x_{Fl0}, y_{Fl0}) = (a, t_l) \tag{5.1}$$

$$(x_{Fr0}, y_{Fr0}) = (a, -t_r) \tag{5.2}$$

$$(x_{Rl0},\ y_{Rl0}) = (-b, t_l) \tag{5.3}$$

$$(x_{Rr0},\ y_{Rr0}) = (-b, -t_r) \tag{5.4}$$

Where: -

$(x_{CG0},\ y_{CG0})$	Time frame initial CG location = (0, 0)
θ_{CG0}	Time frame initial vehicle axle angle = 0
$(x_{Fl0},\ y_{Fl0})$	Time frame initial front left tyre location
(x_{Fr0}, y_{Fr0})	Time frame initial front right tyre location
$(x_{Rl0},\ y_{Rl0})$	Time frame initial rear left tyre location
$(x_{Rr0},\ y_{Rr0})$	Time frame initial rear right tyre location
t_l, t_r	Lateral CG distance to left and right tyres

The vehicle initial velocities are given as: -

u_0	Vehicle initial forward velocity	
v_0	Vehicle initial lateral velocity	(0 at the start of manoeuvre)
$\dot{\theta}_0$	Vehicle initial yaw rate	(0 at the start of manoeuvre)

For this model an extra ability to independently steer different wheels has been adopted to allow investigation of WSDC for different vehicle configurations and to facilitate further research. Hence the tyre steering angles δ are given as follows:-

δ_{Fl}	Front left tyre steering angle	(0 for RWS vehicles)
δ_{Fr}	Front right tyre steering angle	(0 for RWS vehicles)
δ_{Rl}	Rear left tyre steering angle	(0 for FWS vehicles)
δ_{Rr}	Rear right tyre steering angle	(0 for FWS vehicles)

The equations used to evaluate these tyre steering angles are given in the next section.

5.3.2 Stage Two: Full Vehicle Ackerman Steering

To allow the developed vehicle handling model to follow the standard Ackerman steering, the steering angles of left and right steered wheels have been differentiated for FWS and RWS vehicles. The steering angles of the Four Wheel Steering (4WS) vehicles are not considered in this phase as there is a lack of standardisation of this vehicle configuration. According to the Ackerman steering geometry, the radius of turn at rear axle and left and right tyre steering angles for a front wheel steering vehicle, Fig (5.4) are calculated as follows: -

$$R_R = \left(\frac{L}{\tan(\delta_F)}\right) \tag{5.5}$$

$$\delta_{Fl} = \arctan\left(\frac{L}{R_R - t_l}\right) \tag{5.6}$$

$$\delta_{Fr} = \arctan\left(\frac{L}{R_R + t_r}\right) \tag{5.7}$$

Where: -

R_R Radius of turn at rear axle of FWS vehicle

δ_F Nominal front wheel steering angle

For a rear wheel steering vehicle, Fig (5.5), the radius of turn at front axle and left and right rear wheel steering angles are calculated as follows: -

$$R_F = -\left(\frac{L}{\tan(\delta_R)}\right) \tag{5.8}$$

$$\delta_{Rl} = -\arctan\left(\frac{L}{R_F - t_l}\right) \tag{5.9}$$

$$\delta_{Rr} = -\arctan\left(\frac{L}{R_F + t_r}\right) \tag{5.10}$$

Where: -

R_F Radius of turn at front axle of RWS vehicle

δ_R Nominal rear wheel steering angle

As shown from the above equations, in the current model the turn radius has been assigned a sign. For a CCW turn, the radius is positive, while it has a negative sign for CW turns. The equations have been applied and protected from singularity, preventing the R_R and R_F values from going to infinity. Also R_R and R_F values have been restricted to a range of ± 10,000,000 m to prevent program overflow. The flowchart of the routine used to achieve this task is shown in Fig (5.6).

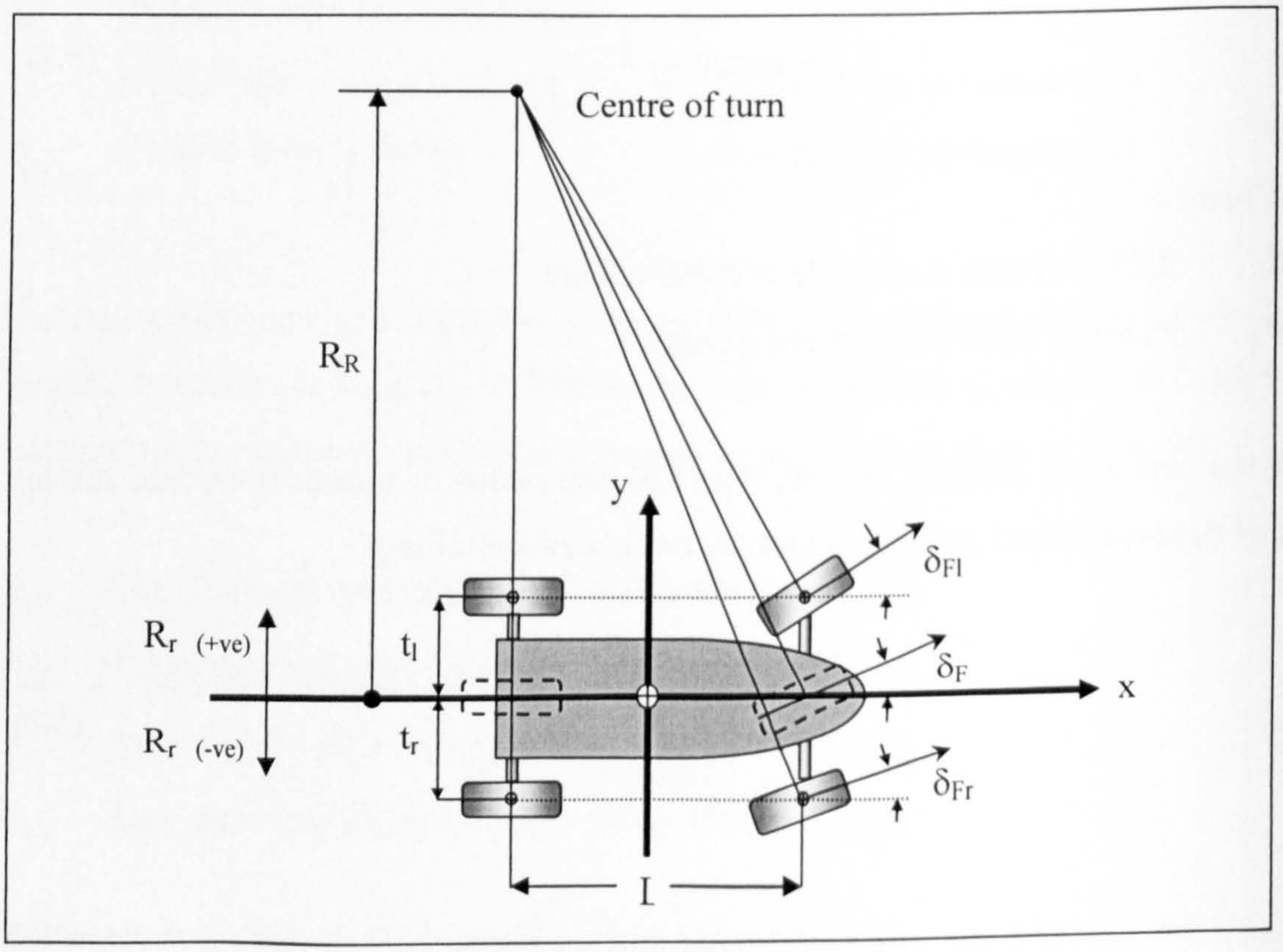

Fig (5.4) Ackerman steering geometry of a FWS vehicle

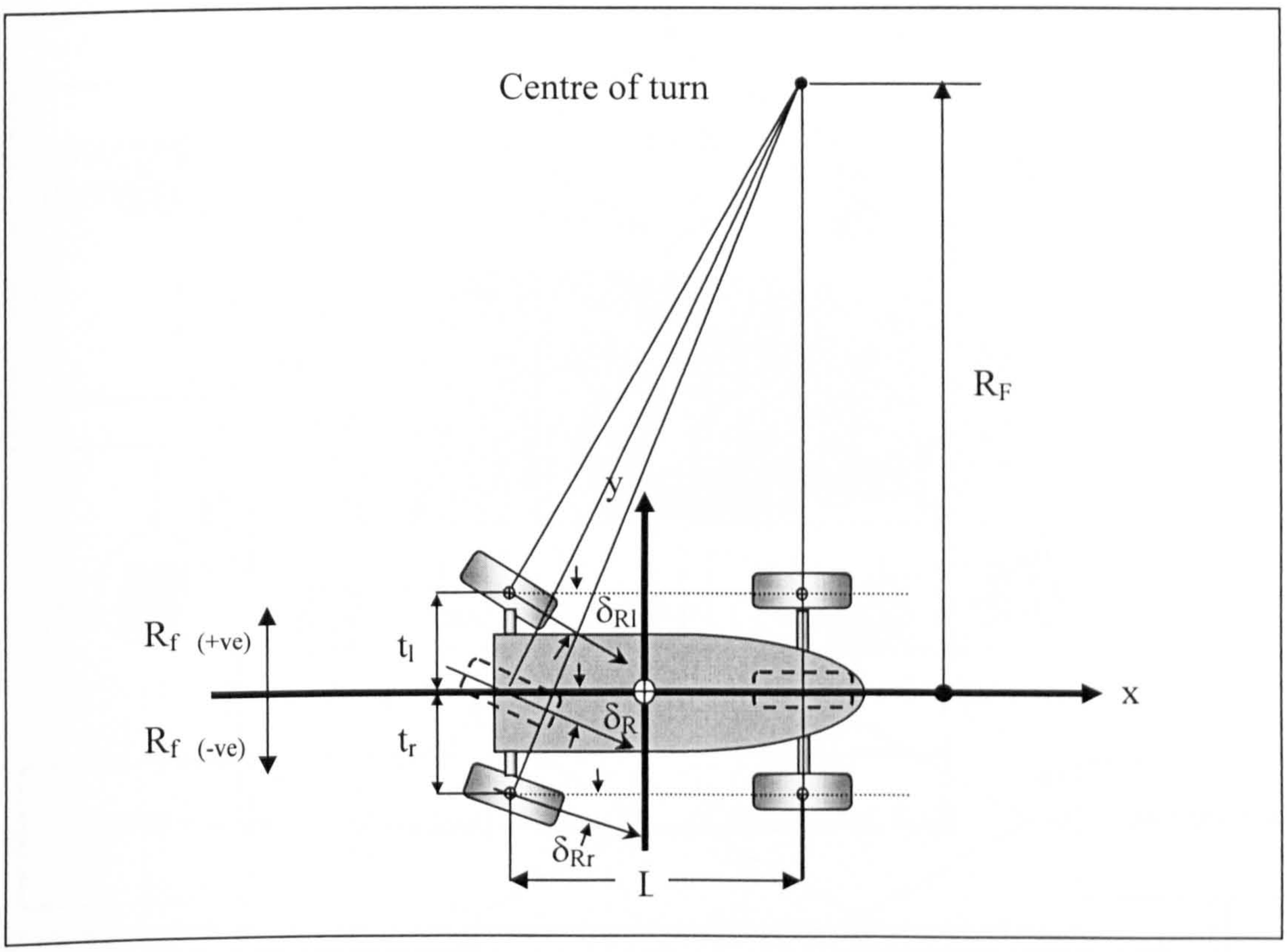

Fig (5.5) Ackerman steering geometry of RWS vehicle

5.3.3 Stage Three: CG Forces and Moments

At the start of every time frame, the forces and moments applied to the tyres from the previous time frame, Fig (5.7), are resolved into their x-y components, summed and used to calculate the current time frame initial longitudinal force, lateral force and moment at the vehicle CG. Although, a rear wheel drive, front wheel steering vehicle is considered for the current work the equations have been formulated to allow application of Four Wheel Drive (4WD) and Four Wheel Steering (4WS) vehicles to facilitate further research.

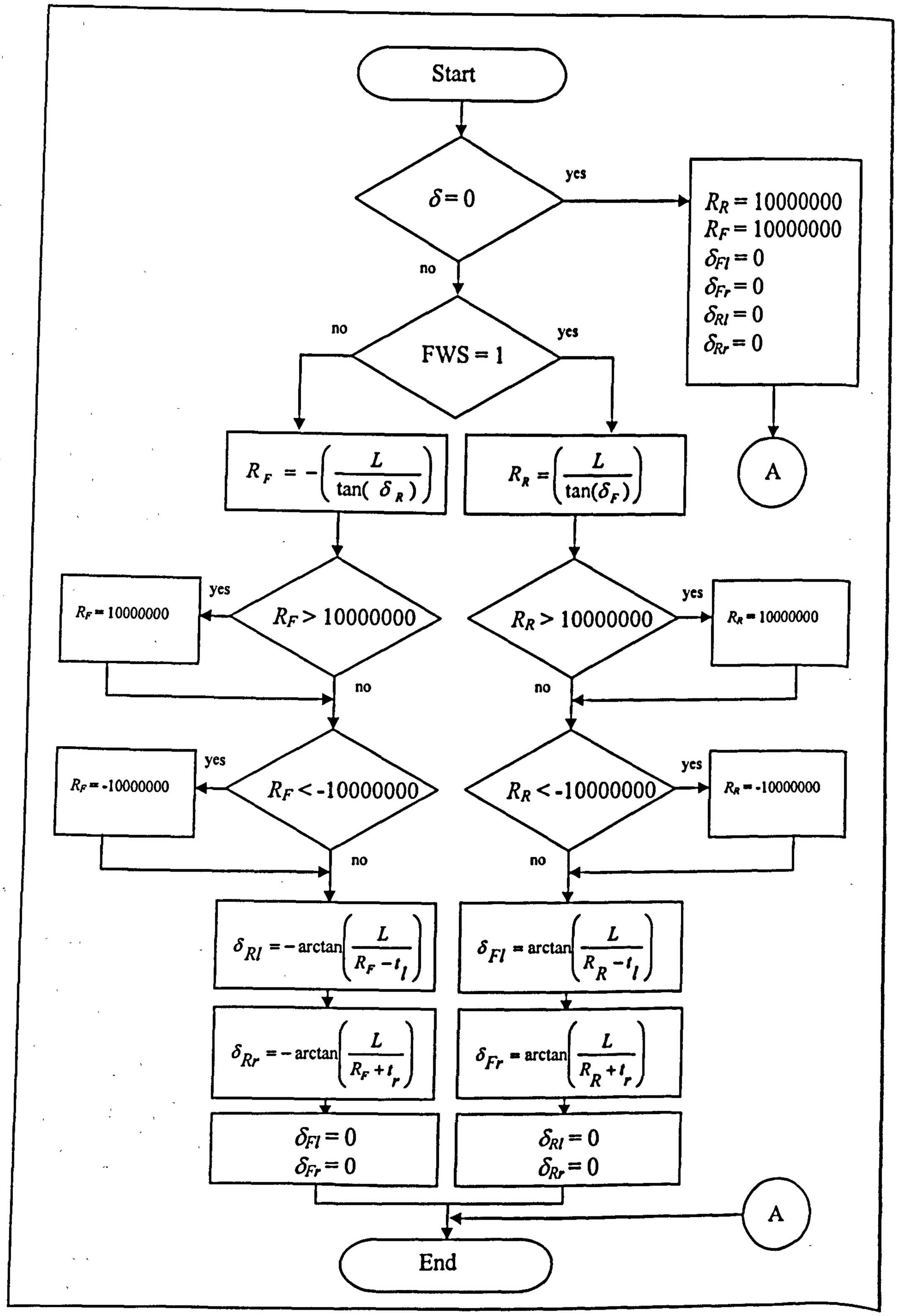

Fig (5.6) Flowchart of right and left wheel steering angle calculation routine

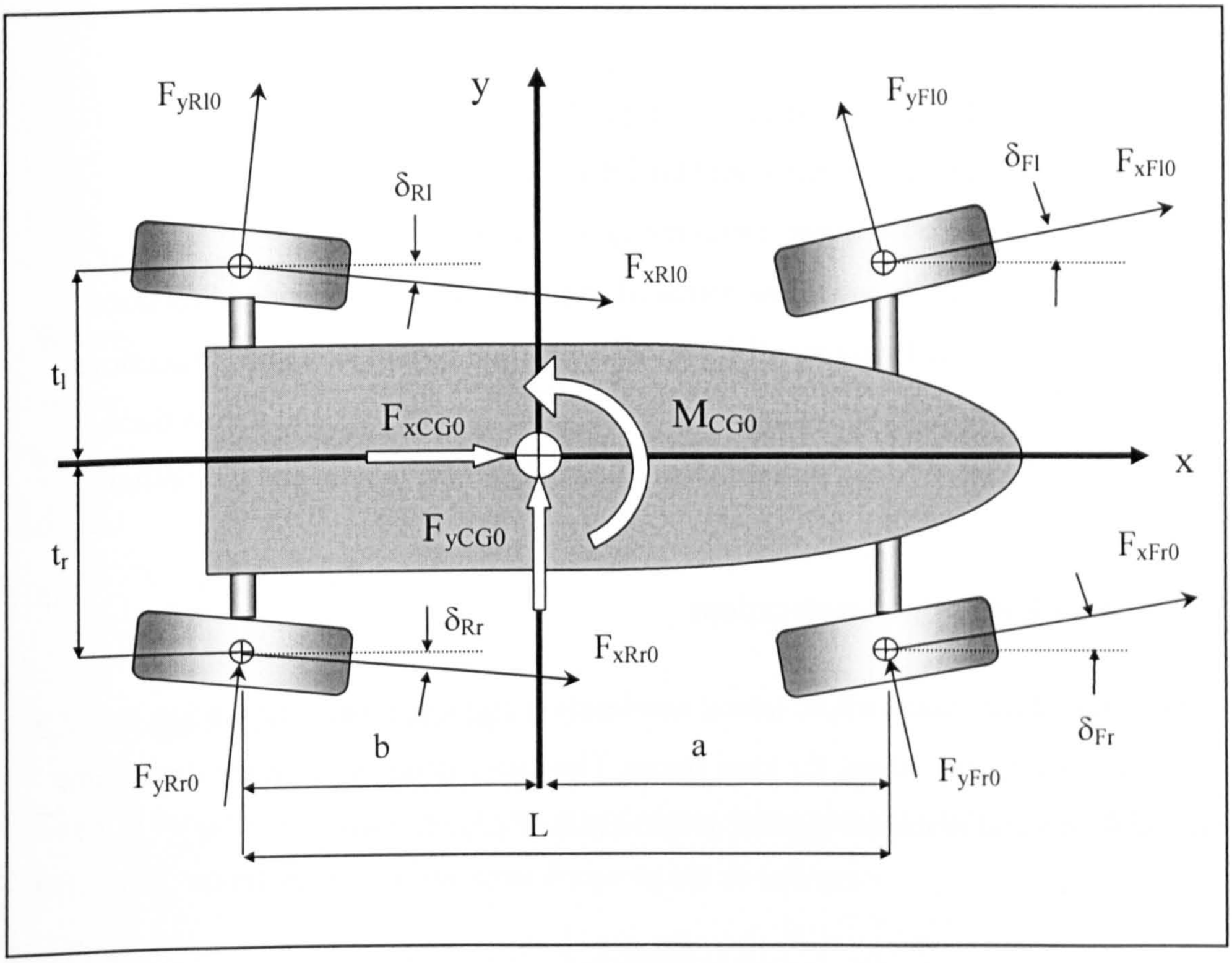

Fig (5.7) Forces and moments acting on the vehicle

At the start of every time frame the forces and moments at the vehicle CG are given as follows:-

$$\begin{aligned} F_{xCG0} = {} & F_{xFl0}\cos(\delta_{Fl}) - F_{yFl0}\sin(\delta_{Fl}) + F_{xFr0}\cos(\delta_{Fr}) - F_{yFr0}\sin(\delta_{Fr}) \\ & + F_{xRl0}\cos(\delta_{Rl}) - F_{yRl0}\sin(\delta_{Rl}) + F_{xRr0}\cos(\delta_{Rr}) - F_{yRr0}\sin(\delta_{Rr}) \end{aligned} \tag{5.11}$$

$$\begin{aligned} F_{yCG0} = {} & F_{yFl0}\cos(\delta_{Fl}) + F_{xFl0}\sin(\delta_{Fl}) + F_{yFr0}\cos(\delta_{Fr}) + F_{xFr0}\sin(\delta_{Fr}) \\ & + F_{yRl0}\cos(\delta_{Rl}) + F_{xRl0}\sin(\delta_{Rl}) + F_{yRr0}\cos(\delta_{Rr}) + F_{xRr0}\sin(\delta_{Rr}) \end{aligned} \tag{5.12}$$

$$\begin{aligned} M_{CG0} = {} & t_r\left(F_{xRr0}\cos(\delta_{Rr}) - F_{yRr0}\sin(\delta_{Rr}) + F_{xFr0}\cos(\delta_{Fr}) - F_{yFr0}\sin(\delta_{Fr})\right) \\ & - t_l\left(F_{xFl0}\cos(\delta_{Fl}) - F_{yFl0}\sin(\delta_{Fl}) + F_{xRl0}\cos(\delta_{Rl}) - F_{yRl0}\sin(\delta_{Rl})\right) \\ & + a\left(F_{yFl0}\cos(\delta_{Fl}) + F_{xFl0}\sin(\delta_{Fl}) + F_{yFr0}\cos(\delta_{Fr}) + F_{xFr0}\sin(\delta_{Fr})\right) \\ & - b\left(F_{yRl0}\cos(\delta_{Rl}) + F_{xRl0}\sin(\delta_{Rl}) + F_{yRr0}\cos(\delta_{Rr}) + F_{xRr0}\sin(\delta_{Rr})\right) \end{aligned} \tag{5.13}$$

Where :-

F_{xCG0}	The time frame initial longitudinal force at the vehicle CG
F_{yCG0}	The time frame initial lateral force at the vehicle CG
M_{CG0}	The time frame initial moment at the vehicle CG
F_{xFl0}, F_{yFl0}	Time frame initial forces of front-left tyre in its x and y directions
F_{xFr0}, F_{yFr0}	Time frame initial forces of front-right tyre in its x and y directions
F_{xRl0}, F_{yRl0}	Time frame initial forces of rear-left tyre in its x and y directions
F_{xRr0}, F_{yRr0}	Time frame initial forces of rear-right tyre in its x and y directions

5.3.4 Stage Four: CG Accelerations

The longitudinal acceleration, lateral acceleration and rotational acceleration are considered constant during the time frame. They are calculated from the time frame initial forces and moments applied at the vehicle CG as follows: -

$$\dot{u} = \frac{F_{xCG0}}{m} \tag{5.14}$$

$$\dot{v} = \frac{F_{yCG0}}{m} \tag{5.15}$$

$$\ddot{\theta} = \frac{M_{CG0}}{I} \tag{5.16}$$

Where :-

$\dot{u}$	Time frame vehicle longitudinal acceleration
$\dot{v}$	Time frame vehicle lateral acceleration
$\ddot{\theta}$	Time frame vehicle yaw acceleration

5.3.5 Stage Five: CG Velocity

The final velocities at the end of a time frame are evaluated using CG initial velocities, accelerations and the time frame width Δt as follows: -.

$$u_1 = u_0 + \dot{u}\Delta t \tag{5.17}$$

$$v_1 = v_0 + \dot{v}\Delta t \tag{5.18}$$

$$\dot{\theta}_1 = \dot{\theta}_0 + \ddot{\theta}\Delta t \tag{5.19}$$

Where:-

$u_{0,}$ u_1 Vehicle CG initial and final longitudinal velocities of a time frame

v_0, v_1 Vehicle CG initial and final lateral velocities of a time frame

$\dot{\theta}_0$, $\dot{\theta}_1$ Vehicle CG initial and final yaw rates of a time frame

Δt Time frame width

5.3.6 Stage Six: CG Translations

The CG longitudinal, lateral and yaw translations are evaluated using CG final velocities, initial velocities and time frame width as follows:-

$$\Delta x_{CG} = \left(\frac{u_0 + u_1}{2}\right)\Delta t \tag{5.20}$$

$$\Delta y_{CG} = \left(\frac{v_0 + v_1}{2}\right)\Delta t \tag{5.21}$$

$$\Delta \theta_{CG} = \left(\frac{\dot{\theta}_0 + \dot{\theta}_1}{2}\right)\Delta t \tag{5.22}$$

Where:-

Δx_{CG} Vehicle CG translation on local x coordinate during the time frame

Δy_{CG} Vehicle CG translation on local y coordinate during the time frame

$\Delta \theta_{CG}$ Vehicle longitudinal axle rotation angle during the time frame

The new CG location and vehicle axle angle are calculated by adding Δx_{CG}, Δy_{CG} and $\Delta \theta_{CG}$ to the CG time frame initial positions.

$$x_{CG1} = x_{CG0} + \Delta x_{CG} \tag{5.23}$$

$$y_{CG1} = y_{CG0} + \Delta y_{CG} \tag{5.24}$$

$$\theta_{CG1} = \theta_{CG0} + \Delta \theta_{CG} \tag{5.25}$$

Where:-

x_{CG0}, x_{CG1} Time frame initial and final vehicle CG x location

y_{CG0}, y_{CG1} Time frame initial and final vehicle CG y location

θ_{CG0}, θ_{CG1} Time frame initial and final vehicle θ location

5.3.7 Stage Seven: Tyres Translations

The tyre locations at the end of the time frame are a function of the new CG location x_{CG1}, y_{CG1} and θ_{CG1}, and the vehicle parameters a, b, t_l and t_r. The different tyre locations are evaluated as follows: -

$$x_{Fl1} = x_{CG1} + a\cos(\theta_{CG1}) - t_l \sin(\theta_{CG1}) \tag{5.26}$$

$$y_{Fl1} = y_{CG1} + a\sin(\theta_{CG1}) + t_l \cos(\theta_{CG1}) \tag{5.27}$$

$$x_{Fr1} = x_{CG1} + a\cos(\theta_{CG1}) + t_r \sin(\theta_{CG1}) \tag{5.28}$$

$$y_{Fr1} = y_{CG1} + a\sin(\theta_{CG1}) - t_r \cos(\theta_{CG1}) \tag{5.29}$$

$$x_{Rl1} = x_{CG1} - b\cos(\theta_{CG1}) - t_l \sin(\theta_{CG1}) \tag{5.30}$$

$$y_{Rl1} = y_{CG1} - b\sin(\theta_{CG1}) + t_l \cos(\theta_{CG1}) \tag{5.31}$$

$$x_{Rr1} = x_{CG1} - b\cos(\theta_{CG1}) + t_r \sin(\theta_{CG1}) \tag{5.32}$$

$$y_{Rr1} = y_{CG1} - b\sin(\theta_{CG1}) - t_r \cos(\theta_{CG1}) \tag{5.33}$$

Where:-

(x_{Fl1}, y_{Fl1}) Time frame final front left tyre x-y location

(x_{Fr1}, y_{Fr1}) Time frame final front right tyre x-y location

(x_{Rl1}, y_{Rl1}) Time frame final rear left tyre x-y location

(x_{Rr1}, y_{Rr1}) Time frame final rear right tyre x-y location

Using the initial and final tyre locations, the distance travelled by each tyre is evaluated as follows: -

$$T_{Fl} = \sqrt{(x_{Fl1} - x_{Fl0})^2 + (y_{Fl1} - y_{Fl0})^2} \tag{5.34}$$

$$T_{Fr} = \sqrt{(x_{Fr1} - x_{Fr0})^2 + (y_{Fr1} - y_{Fr0})^2} \tag{5.35}$$

$$T_{Rl} = \sqrt{(x_{Rl1} - x_{Rl0})^2 + (y_{Rl1} - y_{Rl0})^2} \tag{5.36}$$

$$T_{Rr} = \sqrt{(x_{Rr1} - x_{Rr0})^2 + (y_{Rr1} - y_{Rr0})^2} \tag{5.37}$$

Where: -

T_{Fl} Distance travelled by front left tyre

T_{Fr} Distance travelled by front right tyre

T_{Rl} Distance travelled by rear left tyre

T_{Rr} Distance travelled by rear right tyre

Tyre lateral and longitudinal translations in the local coordinates are given as follows:-

$$\Delta x_{Fl} = T_{Fl} \cos(\alpha_{Fl}) \tag{5.38}$$

$$\Delta y_{Fl} = T_{Fl} \sin(\alpha_{Fl}) \tag{5.39}$$

$$\Delta x_{Fr} = T_{Fr} \cos(\alpha_{Fr}) \tag{5.40}$$

$$\Delta y_{Fr} = T_{Fr} \sin(\alpha_{Fr}) \tag{5.41}$$

$$\Delta x_{Rl} = T_{Rl}\cos(\alpha_{Rl}) \tag{5.42}$$

$$\Delta y_{Rl} = T_{Rl}\sin(\alpha_{Rl}) \tag{5.43}$$

$$\Delta x_{Rr} = T_{Rr}\cos(\alpha_{Rr}) \tag{5.44}$$

$$\Delta y_{Rr} = T_{Rr}\sin(\alpha_{Rr}) \tag{5.45}$$

Where: -

$\Delta x_{Fl}, \Delta y_{Fl}$ Front-left tyre longitudinal and lateral translations in its local coordinates

$\Delta x_{Fr}, \Delta y_{Fr}$ Front-right tyre longitudinal and lateral translations in its local coordinates

$\Delta x_{Rl}, \Delta y_{Rl}$ Rear-left tyre longitudinal and lateral translations in its local coordinates

$\Delta x_{Rr}, \Delta y_{Rr}$ Rear-right tyre longitudinal and lateral translations in its local coordinates

5.3.8 Stage Eight: Tyres Slip Angles

The tyre initial locations and new locations, Fig (5.8) are used to calculate the tyre travelling angles to vehicle x coordinate. These angles are used along with the steering angles to evaluate the slip angles. The tyre travelling direction angles are given as follows: -

$$\theta_{Fl} = \arctan\left(\frac{y_{Fl1} - y_{Fl0}}{x_{Fl1} - x_{Fl0}}\right) \tag{5.46}$$

$$\theta_{Fr} = \arctan\left(\frac{y_{Fr1} - y_{Fr0}}{x_{Fr1} - x_{Fr0}}\right) \tag{5.47}$$

$$\theta_{Rl} = \arctan\left(\frac{y_{Rl1} - y_{Rl0}}{x_{Rl1} - x_{Rl0}}\right) \tag{5.48}$$

$$\theta_{Rr} = \arctan\left(\frac{y_{Rr1} - y_{Rr0}}{x_{Rr1} - x_{Rr0}}\right) \tag{5.49}$$

Where:-

θ_{Fl} Front-left tyre travelling direction angle to local x coordinate

θ_{Fr} Front-right tyre travelling direction angle to local x coordinate

θ_{Rl} Rear-left tyre travelling direction angle to local x coordinate

θ_{Rr} Rear-right tyre travelling direction angle to local x coordinate

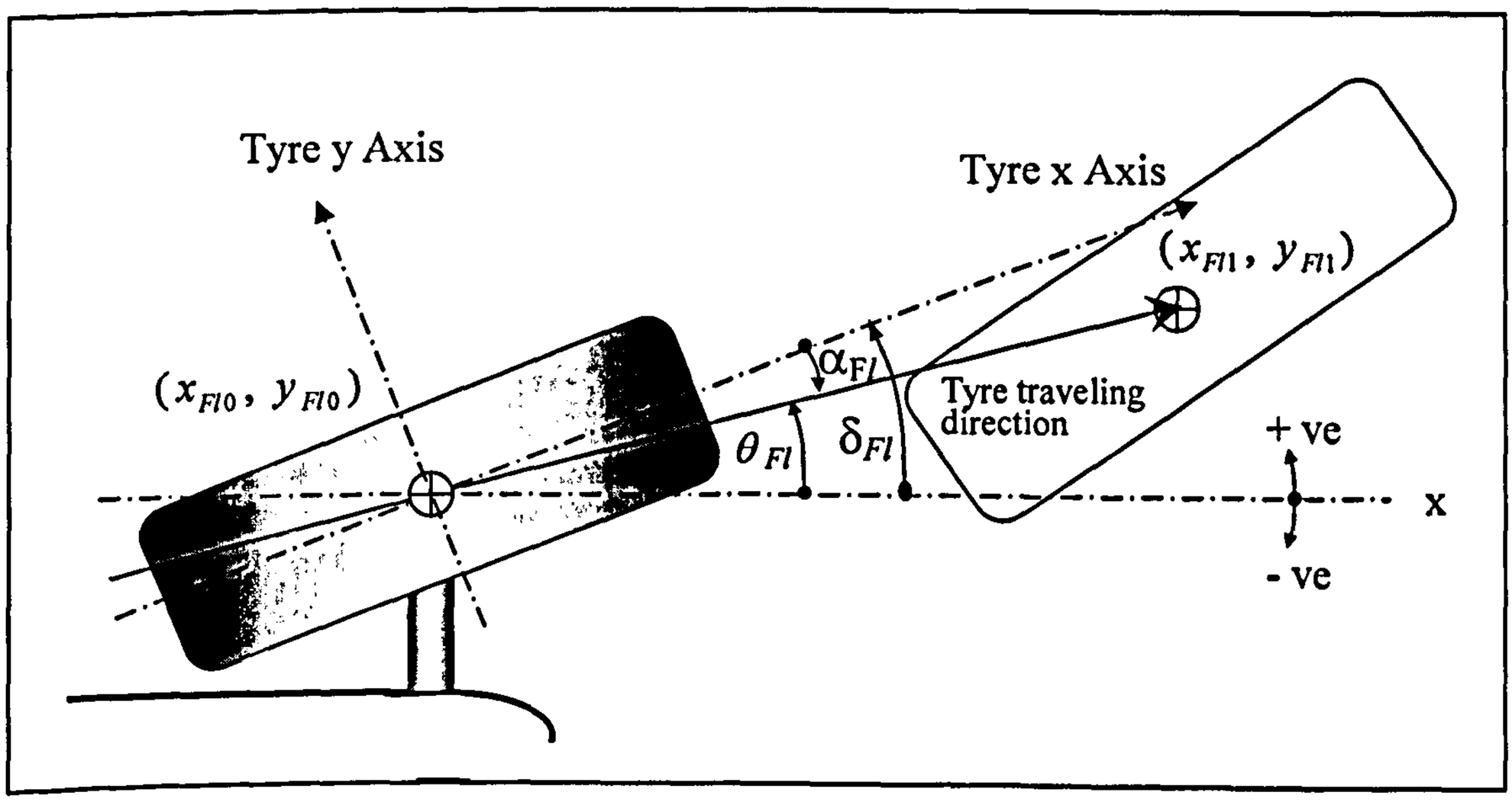

Fig (5.8) Front left tyre travelling in x-y coordinate system

The slip angles are calculated by subtracting the tyre steering angle from the vehicle x axis angle to tyre travelling direction, Fig (5.8), as follows: -

$$\alpha_{Fl} = \theta_{Fl} - \delta_{Fl} \tag{5.50}$$

$$\alpha_{Fr} = \theta_{Fr} - \delta_{Fr} \tag{5.51}$$

$$\alpha_{Rl} = \theta_{Rl} - \delta_{Rl} \tag{5.52}$$

$$\alpha_{Rr} = \theta_{Rr} - \delta_{Rr} \tag{5.53}$$

Where:-

α_{Fl} Slip angle of front-left tyre

α_{Fr} Slip angle of front-right tyre

α_{Rl} Slip angle of rear-left tyre

α_{Rr} Slip angle of rear-right tyre

5.3.9 Stage Nine: Tyres Velocities

The tyre longitudinal and lateral velocities are calculated from CG velocities and vehicle geometry, Fig (5.9). The tyres velocities are calculated for two purposes. The first is required for WSDC to evaluate the required tyre rotational speeds. The second is required for the MF to calculate the tyre forces. Tyre longitudinal and lateral velocities are given as follows:-

$$U_{Fl1} = u_1 \cos(\Delta\theta_{CG} + \delta_{Fl}) + v_1 \sin(\Delta\theta_{CG} + \delta_{Fl}) + \dot{\theta}_{CG} r_{Fl} \cos(\phi_{Fl}) \quad (5.54)$$

$$V_{Fl1} = v_1 \cos(\Delta\theta_{CG} + \delta_{Fl}) - u_1 \sin(\Delta\theta_{CG} + \delta_{Fl}) + \dot{\theta}_{CG} r_{Fl} \sin(\phi_{Fl}) \quad (5.55)$$

$$U_{Fr1} = u_1 \cos(\Delta\theta_{CG} + \delta_{Fr}) + v_1 \sin(\Delta\theta_{CG} + \delta_{Fr}) + \dot{\theta}_{CG} r_{Fr} \cos(\phi_{Fr}) \quad (5.56)$$

$$V_{Fr1} = v_1 \cos(\Delta\theta_{CG} + \delta_{Fr}) - u_1 \sin(\Delta\theta_{CG} + \delta_{Fr}) + \dot{\theta}_{CG} r_{Fr} \sin(\phi_{Fr}) \quad (5.57)$$

$$U_{Rl1} = u_1 \cos(\Delta\theta_{CG} + \delta_{Rl}) + v_1 \sin(\Delta\theta_{CG} + \delta_{Rl}) + \dot{\theta}_{CG} r_{Rl} \cos(\phi_{Rl}) \quad (5.58)$$

$$V_{Rl1} = v_1 \cos(\Delta\theta_{CG} + \delta_{Rl}) - u_1 \sin(\Delta\theta_{CG} + \delta_{Rl}) + \dot{\theta}_{CG} r_{Rl} \sin(\phi_{Rl}) \quad (5.59)$$

$$U_{Rr1} = u_1 \cos(\Delta\theta_{CG} + \delta_{Rr}) + v_1 \sin(\Delta\theta_{CG} + \delta_{Rr}) + \dot{\theta}_{CG} r_{Rr} \cos(\phi_{Rr}) \quad (5.60)$$

$$V_{Rr1} = v_1 \cos(\Delta\theta_{CG} + \delta_{Rr}) - u_1 \sin(\Delta\theta_{CG} + \delta_{Rr}) + \dot{\theta}_{CG} r_{Rr} \sin(\phi_{Rr}) \quad (5.61)$$

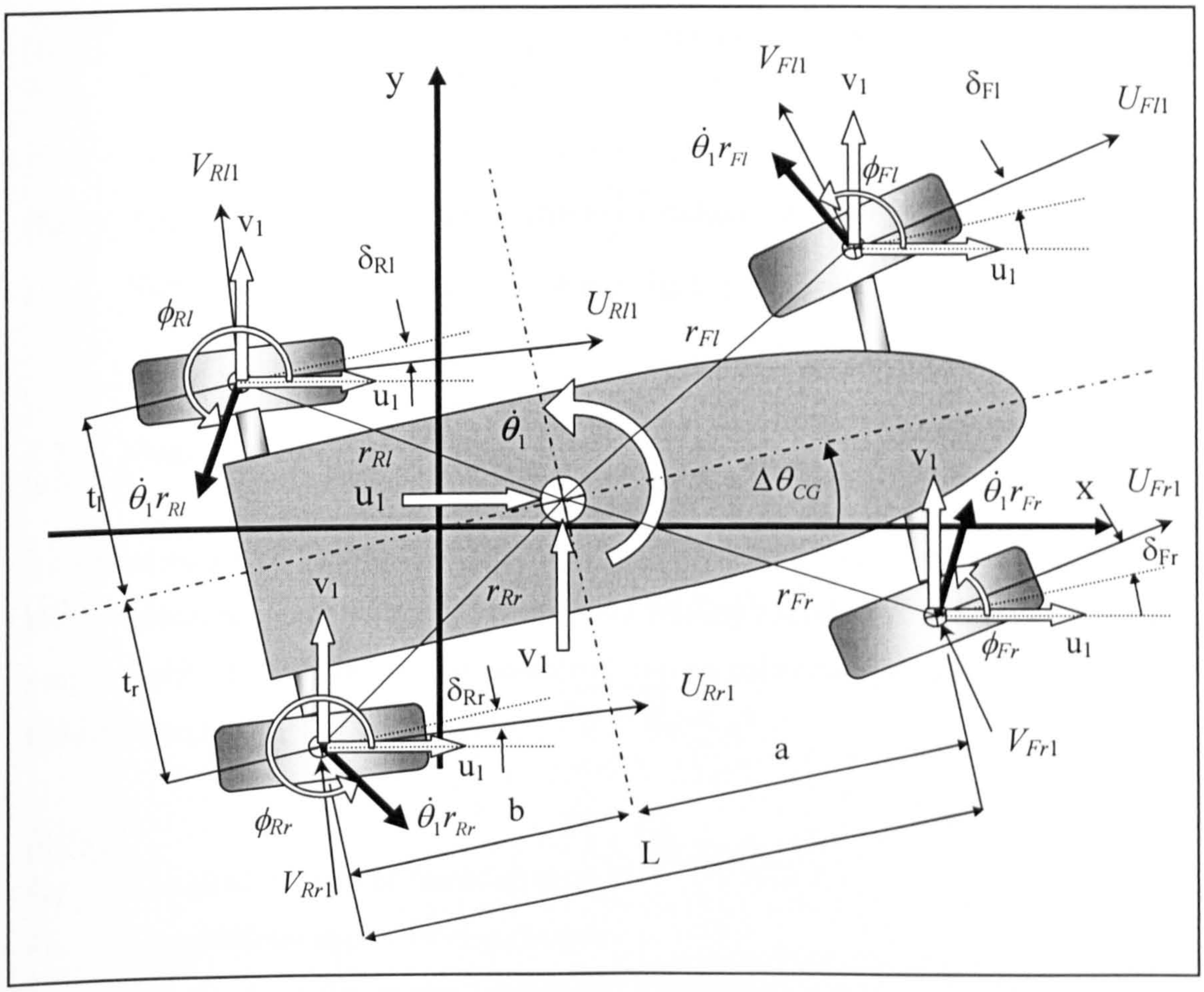

Fig (5.9) Tyre velocities at the end of a time frame

Where: -

U_{Fl1}, V_{Fl1} Time frame final longitudinal and lateral velocities of front-left tyre

U_{Fr1}, V_{Fr1} Time frame final longitudinal and lateral velocities of front-right tyre

U_{Rl1}, V_{Rl1} Time frame final longitudinal and lateral velocities of rear-left tyre

U_{Rr1}, V_{Rr1} Time frame final longitudinal and lateral velocities of rear-right tyre

Where: -

$$\phi_{Fl} = \left(\frac{1}{2}\pi + \arctan(\frac{t_1}{a}) - \delta_{Fl} + \Delta\theta_{CG} \right) \tag{5.62}$$

$$\phi_{Fr} = \left(\frac{1}{2}\pi + \arctan(\frac{-t_r}{a}) - \delta_{Fr} + \Delta\theta_{CG} \right) \tag{5.63}$$

$$\phi_{Rl} = \left(\frac{3}{2}\pi + \arctan(\frac{t_l}{-b}) - \delta_{Rl} + \Delta\theta_{CG}\right) \tag{5.64}$$

$$\phi_{Rr} = \left(\frac{3}{2}\pi + \arctan(\frac{-tr}{-b}) - \delta_{Rr} + \Delta\theta_{CG}\right) \tag{5.65}$$

Where: -

$$r_{Fl} = \sqrt{a^2 + t_l^{\,2}} \tag{5.66}$$

$$r_{Fr} = \sqrt{a^2 + t_r^{\,2}} \tag{5.67}$$

$$r_{Rl} = \sqrt{b^2 + t_l^{\,2}} \tag{5.68}$$

$$r_{Rr} = \sqrt{b^2 + t_r^{\,2}} \tag{5.69}$$

5.3.10 Stage Ten: Tyres Vertical Loads

The different tyre vertical loads are calculated from the vehicle mass m, vehicle geometry (t, t_l, t_r, a, b and h) and the vehicle accelerations ($\dot{u}$ and $\dot{v}$) as follows: -

$$F_{zFl1} = mg\left(\frac{b}{L}\right)\left(\frac{t_r}{t}\right) - 0.5m\dot{u}_1\left(\frac{h}{L}\right) - 0.5m\dot{v}_1\left(\frac{h}{t}\right) \tag{5.70}$$

$$F_{zFr1} = mg\left(\frac{b}{L}\right)\left(\frac{t_l}{t}\right) - 0.5m\dot{u}_1\left(\frac{h}{L}\right) + 0.5m\dot{v}_1\left(\frac{h}{t}\right) \tag{5.71}$$

$$F_{zRl1} = mg\left(\frac{a}{L}\right)\left(\frac{t_r}{t}\right) + 0.5m\dot{u}_1\left(\frac{h}{L}\right) - 0.5m\dot{v}_1\left(\frac{h}{t}\right) \tag{5.72}$$

$$F_{zRr1} = mg\left(\frac{a}{L}\right)\left(\frac{t_l}{t}\right) + 0.5m\dot{u}_1\left(\frac{h}{L}\right) + 0.5m\dot{v}_1\left(\frac{h}{t}\right) \tag{5.73}$$

Where :-

F_{zFl} Time frame final vertical load of front left tyre

F_{zFr} Time frame final vertical load of front right tyre

F_{zRl} Time frame final vertical load of rear left tyre

F_{zRr} Time frame final vertical load of rear right tyre

5.3.11 Stage Eleven: Tyres Longitudinal Slip

To calculate a tyre longitudinal slip k, its tyre slip angle, velocities, vertical load F_z and longitudinal force F_x are fed to the kcal routine (developed in Chapter 4). This employs the MF tyre model for combined slip to calculate tyre longitudinal slip k through iteration.

Where: -

k_{Fl} Longitudinal slip of front-left tyre

k_{Fr} Longitudinal slip of front-right tyre

k_{Rl} Longitudinal slip of rear-left tyre

k_{Rr} Longitudinal slip of rear-right tyre

5.3.12 Stage Twelve: Tyres Lateral Forces

Each tyre lateral force F_y is calculated through feeding its calculated longitudinal slip k, slip angle, velocities, vertical load F_z and longitudinal force F_x to the Magic Formula (MF) tyre model for combined slip.

Where: -

F_{yFl} Front left tyre lateral force

F_{yFr} Front right tyre lateral force

F_{yRl} Rear left tyre lateral force

F_{yRr} Rear right tyre lateral force

5.3.13 Stage Thirteen: Relaxation Length Application

To allow the vehicle handling model to recognise the lateral tyre relaxation characteristics, a special routine has been developed in Chapter 4. For each tyre, the calculated lateral force is fed to the tyre relaxation routine, where it is used along with the tyre history of lateral forces to investigate the applied tyre lateral force. These tyre applied lateral forces are used as tyre initial lateral forces for the next time frame.

5.3.14 Stage Fourteen: Local Axis Transfer

At the end of each time frame, in preparation for the next time frame, the vehicle local coordinates are positioned to align with the vehicle initial location condition at the start of the next time frame. For the current solving technique, the factors that require transferring to the new local coordinates are the vehicle velocities, Fig (5.10). The velocities are transferred to the vehicle local axes as follows: -

$$u_0 = u_1 \cos(\Delta\theta_{CG}) + v_1 \sin(\Delta\theta_{CG}) \tag{5.74}$$

$$v_0 = v_1 \cos(\Delta\theta_{CG}) - u_1 \sin(\Delta\theta_{CG}) \tag{5.75}$$

$$\dot{\theta}_0 = \dot{\theta}_1 \tag{5.76}$$

Where: -

u_0 Initial longitudinal velocity of next time frame

v_0 Initial lateral velocity of next time frame

$\dot{\theta}_0$ Initial yaw rate of next time frame

The vehicle CG velocities along with the tyre lateral forces are then ready to be input to the next time frame.

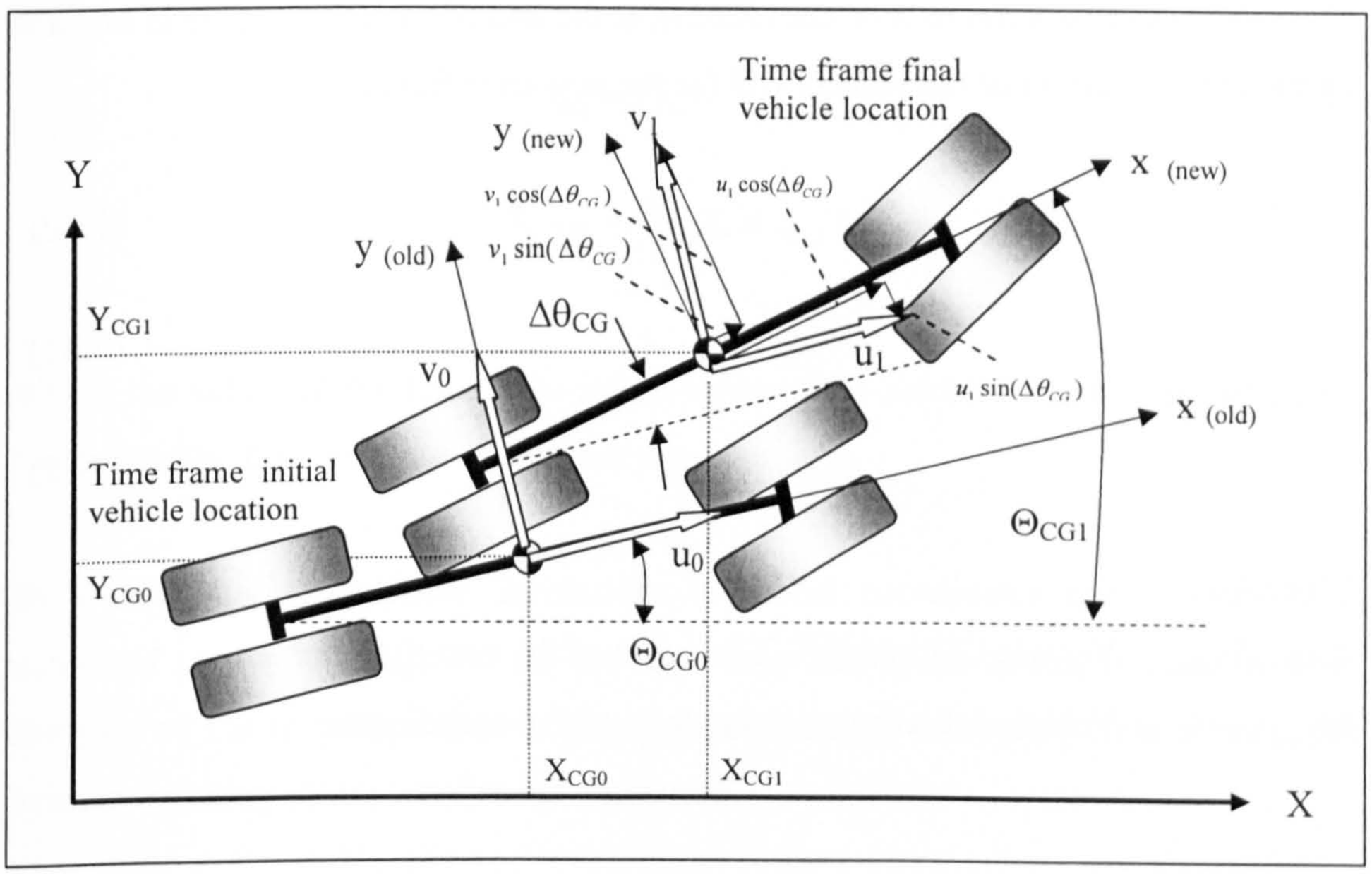

Fig (5.10) Vehicle parameters transfer at the end of a time frame

5.3.15 Stage Fifteen: Results Transfer to X-Y Coordinates

To capture the vehicle handling performance, the vehicle translations in its local coordinates are transferred to the X-Y global coordinates at the end of each time frame. These are then summed with the previous vehicle translations with respect to global X-Y coordinates. The vehicle new location in global X-Y coordinates is given as follows:-

$$X_{CG1} = X_{CG0} + x_{CG1}\cos(\Theta_{CG0}) - y_{CG1}\sin(\Theta_{CG0}) \tag{5.77}$$

$$Y_{CG1} = Y_{CG0} + y_{CG1}\cos(\Theta_{CG0}) + x_{CG1}\sin(\Theta_{CG0}) \tag{5.78}$$

$$\Theta_{CG1} = \Theta_{CG0} + \theta_{CG1} \tag{5.79}$$

Where: -

X_{CG1}, Y_{CG1} Vehicle new X-Y location in global coordinates

X_{CG0}, Y_{CG0} Vehicle previous location in global coordinates

Θ_{CG0}, Θ_{CG1} Vehicle previous and new rotation angle in global coordinates

The vehicle CG location in X-Y coordinates at the end of each time frame is taken to be the initial location of the vehicle CG for the new time frame.

$$X_{CG0} = X_{CG1} \tag{5.80}$$

$$Y_{CG0} = Y_{CG1} \tag{5.81}$$

$$\Theta_{CG0} = \Theta_{CG1} \tag{5.82}$$

Where: -

X_{CG0}, Y_{CG0} Vehicle CG initial X-Y location of the next time frame

Θ_{CG0} Vehicle initial rotation angle to global coordinates

5.3.16 Stage Sixteen: Initial Conditions of Next Time Frame

At the end of each time frame, a set of the time frame final parameters values are passed as initial conditions to the next time frame as follows: -

$$F_{xFl0} = F_{xFl1} \tag{5.83}$$

$$F_{yFl0} = F_{yFl1} \tag{5.84}$$

$$F_{xFr0} = F_{xFr1} \tag{5.85}$$

$$F_{yFr0} = F_{yFr1} \tag{5.86}$$

$$F_{xRl0} = F_{xRl1} \tag{5.87}$$

$$F_{yRl0} = F_{yRl1} \tag{5.88}$$

$$F_{xRr0} = F_{xRr1} \tag{5.89}$$

$$F_{yRr0} = F_{yRr1} \tag{5.90}$$

$$X_{CG0} = X_{CG1} \tag{5.91}$$

$$Y_{CG0} = Y_{CG1} \tag{5.92}$$

$$\Theta_{CG0} = \Theta_{CG1} \tag{5.93}$$

Where the subscript 0 refers to the initial value of the next time frame and subscript 1 refers to the final value of the current time frame.

By transferring the vehicle translations to global coordinates and setting initial values of parameters required for the next time frame, the model is ready to start analysis of the next time frame. Through analysis of successive time frames, the vehicle handling characteristics are evaluated.

5.4 Ackerman Path

The Ackerman path is supposed to be followed by the vehicle. However, due to deviation from the intended path at high longitudinal velocities, the vehicle only follows the Ackerman path at low longitudinal velocities. It has been developed as a tool to validate the WSDC CGT full vehicle handling model. The Ackerman path has also been developed as a reference for the WSDC MPC controller as it predicts the ideal vehicle path during a manoeuvre. As it is formulated to respond to vehicle handling parameters in successive time frames, it is also able to predict the ideal path for any intricate vehicle manoeuvre.

To find out the Ackerman steering path, the yaw angle and X-Y locations of the vehicle CG are derived from the Ackerman steering geometry, Fig (5.11). Also the Ackerman steering yaw rate is evaluated in this section. The Ackerman vehicle yaw angle to X coordinate is given as: -

$$\theta_{A(n)} = \theta_{A(n-1)} + \varsigma_2 \tag{5.94}$$

Where: -

θ_A Vehicle yaw angle according to Ackerman steering in X-Y coordinates

ζ_2 Vehicle yaw angle within a time frame Δt

n Time frame number

As Δy_R is very small in comparison to R_R, ζ_2 is evaluated as: -

$$\zeta_2 = \arctan\left(\frac{u_v \Delta t}{R_R}\right) \tag{5.95}$$

Where: -

u_v Vehicle time frame velocity

Substituting for R_R: -

$$\zeta_2 = \arctan\left(u_v \Delta t\left(\frac{\tan(\delta_F)}{L}\right)\right) \tag{5.96}$$

Substitution for ζ_2 in Eq. (6.78): -

$$\theta_{A(n)} = \theta_{A(n-1)} + \arctan\left(u_v \Delta t\left(\frac{\tan(\delta_{F(n)})}{L}\right)\right) \tag{5.97}$$

Accordingly, the vehicle yaw rate and lateral velocity are evaluated as: -

$$\dot{\theta}_{A(n)} = \left(\frac{\theta_{A(n)} - \theta_{A(n-1)}}{\Delta t}\right) \tag{5.98}$$

$$v_A = \left(\frac{\Delta y_{CG}}{\Delta t}\right) \tag{5.99}$$

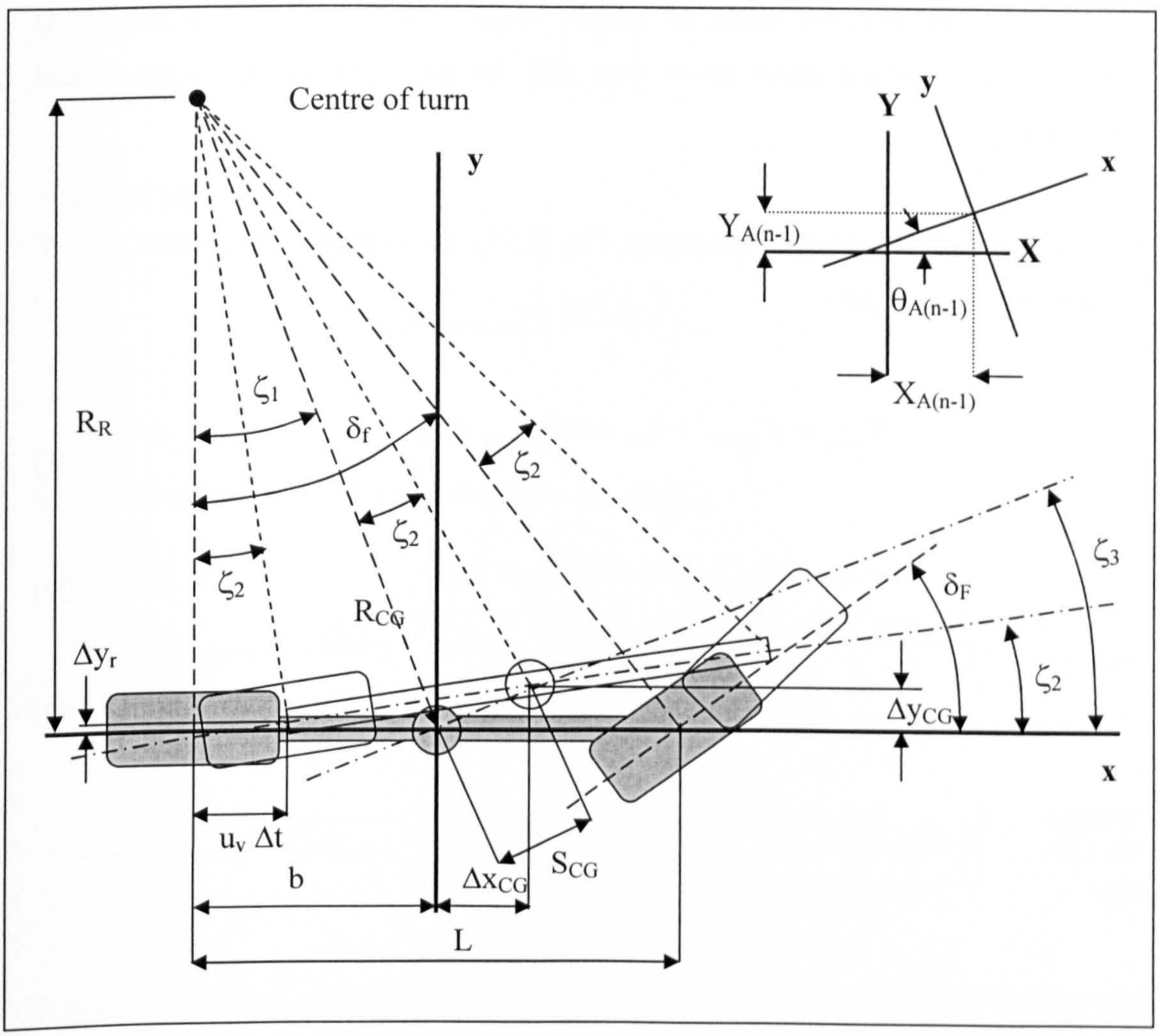

Fig (5.11) Vehicle ideal movement according to Ackerman steering applied to bicycle vehicle

Where: -

$\dot{\theta}_A$ Vehicle yaw rate according to Ackerman steering

v_A Vehicle lateral velocity according to Ackerman steering

Substituting for $\theta_{A(n+1)}$ and simplifying, the Ackerman yaw rate is given as: -

$$\dot{\theta}_{A(n)} = \frac{\arctan\left(u_v \Delta t\left(\frac{\tan\left(\delta_{F(n)}\right)}{L}\right)\right)}{\Delta t} \qquad (5.100)$$

This equation reflects the effect of vehicle length upon its yaw rate response, as longer vehicles would show lower yaw rate for the same vehicle velocity and steering angle.

From the Ackerman steering geometry, Fig (5.11), the vehicle CG location in X-Y coordinates is given as: -

$$X_{A(n)} = X_{A(n-1)} + S_{CG}\cos(\theta_{A(n-1)} + \varsigma_3) \tag{5.101}$$

$$Y_{A(n)} = Y_{A(n-1)} + S_{CG}\sin(\theta_{A(n-1)} + \varsigma_3) \tag{5.102}$$

$$S_{CG} = \sqrt{(\Delta x_{CG})^2 + (\Delta y_{CG})^2} \tag{5.103}$$

Where:-

S_{CG} Vehicle CG total translation

The vehicle CG translations Δx is derived as: -

$$\Delta x_{CG} = u_v \Delta t + b\cos(\zeta_2) - b \tag{5.104}$$

Using circle segment geometry, Δy is derived as: -

$$\Delta y_{CG} = u_v \Delta t \tan\left(\frac{\varsigma_2}{2}\right) + b\sin(\zeta_2) \tag{5.105}$$

Also from geometry, the angles ζ_3 and ζ_1 are given as: -

$$\varsigma_3 = \varsigma_1 + \frac{\pi}{2} - \left(\frac{\pi - \varsigma_2}{2}\right) \tag{5.106}$$

$$\varsigma_1 = \arctan\left(\frac{b}{R_R}\right) \tag{5.107}$$

Substituting for R_R: -

$$\varsigma_1 = \arctan\left(b\frac{\tan(\delta_F)}{L}\right) \tag{5.108}$$

Substituting in the $X_A - Y_A$ equations for S_{CG} and ζ_3: -

$$X_{A(n)} = X_{A(n-1)} + \sqrt{(\Delta x_{CG})^2 + (\Delta y_{CG})^2}\cos\left[\theta_{A(n-1)} + \varsigma_1 + \frac{\pi}{2} - \left(\frac{\pi - \varsigma_2}{2}\right)\right] \tag{5.109}$$

$$Y_{A(n)} = Y_{A(n-1)} + \sqrt{(\Delta x_{CG})^2 + (\Delta y_{CG})^2}\sin\left[\theta_{A(n-1)} + \varsigma_1 + \frac{\pi}{2} - \left(\frac{\pi - \varsigma_2}{2}\right)\right] \tag{5.110}$$

Substituting for Δx_{CG} and Δy_{CG}: -

$$X_{A(n)} = X_{A(n-1)} + \sqrt{(u_v\Delta t + b\cos(\zeta_2) - b)^2 + (u_v\Delta t\tan\left(\frac{\varsigma_2}{2}\right) + b\sin(\zeta_2))^2}$$
$$\cos\left[\theta_{A(n-1)} + \arctan\left(b\frac{\tan(\delta_{F(n)})}{L}\right) + \frac{\pi}{2} - \left(\frac{\pi - \varsigma_2}{2}\right)\right] \tag{5.111}$$

$$Y_{A(n)} = Y_{A(n-1)} + \sqrt{(u_v\Delta t + b\cos(\zeta_2) - b)^2 + (u_v\Delta t\tan\left(\frac{\varsigma_2}{2}\right) + b\sin(\zeta_2))^2}$$
$$\sin\left[\theta_{A(n-1)} + \arctan\left(b\frac{\tan(\delta_{F(n)})}{L}\right) + \frac{\pi}{2} - \left(\frac{\pi - \varsigma_2}{2}\right)\right] \tag{5.112}$$

Substituting for ζ2: -

$$X_{A(n)} = \sqrt{\left(u_v\Delta t + b\cos\left(\arctan\left(u_v\Delta t\left(\frac{\tan\left(\delta_{F(n)}\right)}{L}\right)\right)\right) - b\right)^2 + \left(u_v\Delta t\tan\left(\frac{\arctan\left(u_v\Delta t\left(\frac{\tan\left(\delta_{F(n)}\right)}{L}\right)\right)}{2}\right) + b\sin\left(\arctan\left(u_v\Delta t\left(\frac{\tan\left(\delta_{F(n)}\right)}{L}\right)\right)\right)\right)^2}$$
$$\cos\left[\theta_{A(n-1)} + \arctan\left(b\frac{\tan\left(\delta_{F(n)}\right)}{L}\right) + \frac{\pi}{2} - \left(\frac{\pi - \arctan\left(u_v\Delta t\left(\frac{\tan\left(\delta_{F(n)}\right)}{L}\right)\right)}{2}\right)\right] + X_{A(n-1)} \quad (5.113)$$

$$Y_{A(n)} = \sqrt{\left(u_v\Delta t + b\cos\left(\arctan\left(u_v\Delta t\left(\frac{\tan\left(\delta_{F(n)}\right)}{L}\right)\right)\right) - b\right)^2 + \left(u_v\Delta t\tan\left(\frac{\arctan\left(u_v\Delta t\left(\frac{\tan\left(\delta_{F(n)}\right)}{L}\right)\right)}{2}\right) + b\sin\left(\arctan\left(u_v\Delta t\left(\frac{\tan\left(\delta_{F(n)}\right)}{L}\right)\right)\right)\right)^2}$$
$$\sin\left[\theta_{A(n-1)} + \arctan\left(b\frac{\tan\left(\delta_{F(n)}\right)}{L}\right) + \frac{\pi}{2} - \left(\frac{\pi - \arctan\left(u_v\Delta t\left(\frac{\tan\left(\delta_{F(n)}\right)}{L}\right)\right)}{2}\right)\right] + Y_{A(n-1)} \quad (5.114)$$

Accordingly the Ackerman lateral velocity is given as:-

$$v_{A(n)} = u_v\Delta t\tan\left(\frac{\arctan\left(u_v\Delta t\left(\frac{\tan\left(\delta_{F(n)}\right)}{L}\right)\right)}{2}\right) + b\sin\left(\arctan\left(u_v\Delta t\left(\frac{\tan\left(\delta_{F(n)}\right)}{L}\right)\right)\right) \quad (5.115)$$

It should be noted that these equations were manipulated to avoid any appearance of vehicle radius of turn, as it would cause numerical instability when it reaches infinity. Also the jump of radius of turn value from positive infinity to negative infinity during manoeuvres adds to the problems associated with its employment.

This set of equations has been tested by evaluating vehicle turning diameters (of a step steered vehicle) and comparing these against the calculated turn diameters. A theoretical vehicle of wheelbase equal to 2 m and rear axle to CG distance (b) = 1m has been employed. In this test the vehicle velocity has been fixed at 20 m/s. The X-Y position of vehicle CG has been evaluated at 0.01 s intervals.

The vehicle has been step steered at different δ_F values to investigate the steering angle effect on simulated path accuracy. The turn diameter results have been investigated in both X and Y directions separately to check for any inconsistency. The comparison of simulation results with the calculated turn diameters revealed high accuracy, Table (5.1).

The vehicle Ackerman turn radius has been calculated from geometry as follows: -

$$R_{CG} = \sqrt{\left(\frac{L}{\tan(\delta_F)}\right)^2 + b^2} \tag{5.116}$$

δ_F	Simulated		Calculated		Difference	
	x diameter (m)	y diameter (m)	x diameter (m)	y diameter (m)	x diameter (m)	y diameter (m)
1 deg	229.1709	229.1709	229.1686	229.1686	0.0023	0.0023
2 deg	114.5671	114.5671	114.5625	114.5625	0.0046	0.0046
3 deg	76.3578	76.3577	76.3508	76.3508	0.0070	0.0069
4 deg	57.2470	57.2469	57.2376	57.2376	0.0094	0.0093

Table (5.1) Simulated and calculated turn diameters at different steering angles

To check the equation sensitivity to vehicle forward velocities and simulation intervals, the turn diameter has been simulated at different forward velocities and different time intervals, Table (5.2). This test has been carried out with the vehicle step steered at 2 degrees. The results showed very good consistency with respect to vehicle running velocity and different simulation intervals. Accordingly, the Ackerman path equations have been considered satisfactory and ready to be employed in developing and testing the CGT vehicle model and its manoeuvre ability.

Δt / u_v	0.005 s		0.01 s		0.05 s	
	x diameter (m)	y diameter (m)	x diameter (m)	y diameter (m)	x diameter (m)	y diameter (m)
10 m/s	114.5634	114.5634	114.5645	114.5645	114.5787	114.5786
50 m/s	114.5686	114.5686	114.5787	114.5786	114.7809	114.7816
100 m/s	114.5787	114.5786	114.6104	114.6103	114.4056	114.4094

Table (5.2) Simulated turn diameters at $\delta_f = 2$ deg, for different u_v and different Δt

5.5 Model Manoeuvre

In this section the vehicle handling model has been developed to check the vehicle handling performance for different manoeuvres. The chosen manoeuvres are lane change, cornering and step steer. These manoeuvres are based on a sine wave pattern. For the lane change manoeuvre, the sine wave steering is defined by a maximum value for the steering angle and a manoeuvre time during which the sine wave advances from 0 to 360 degrees, leading to the required lane change pattern. For the cornering manoeuvre, the sine wave advances from 0 to 180 degree leading to the required vehicle turning and finishing the manoeuvre at 0 steering angle. For the step steer, the sine wave steering advances to only 90 degree, leaving the vehicle steered with the maximum steering angle at the end of the manoeuvre time, Fig (5.12).

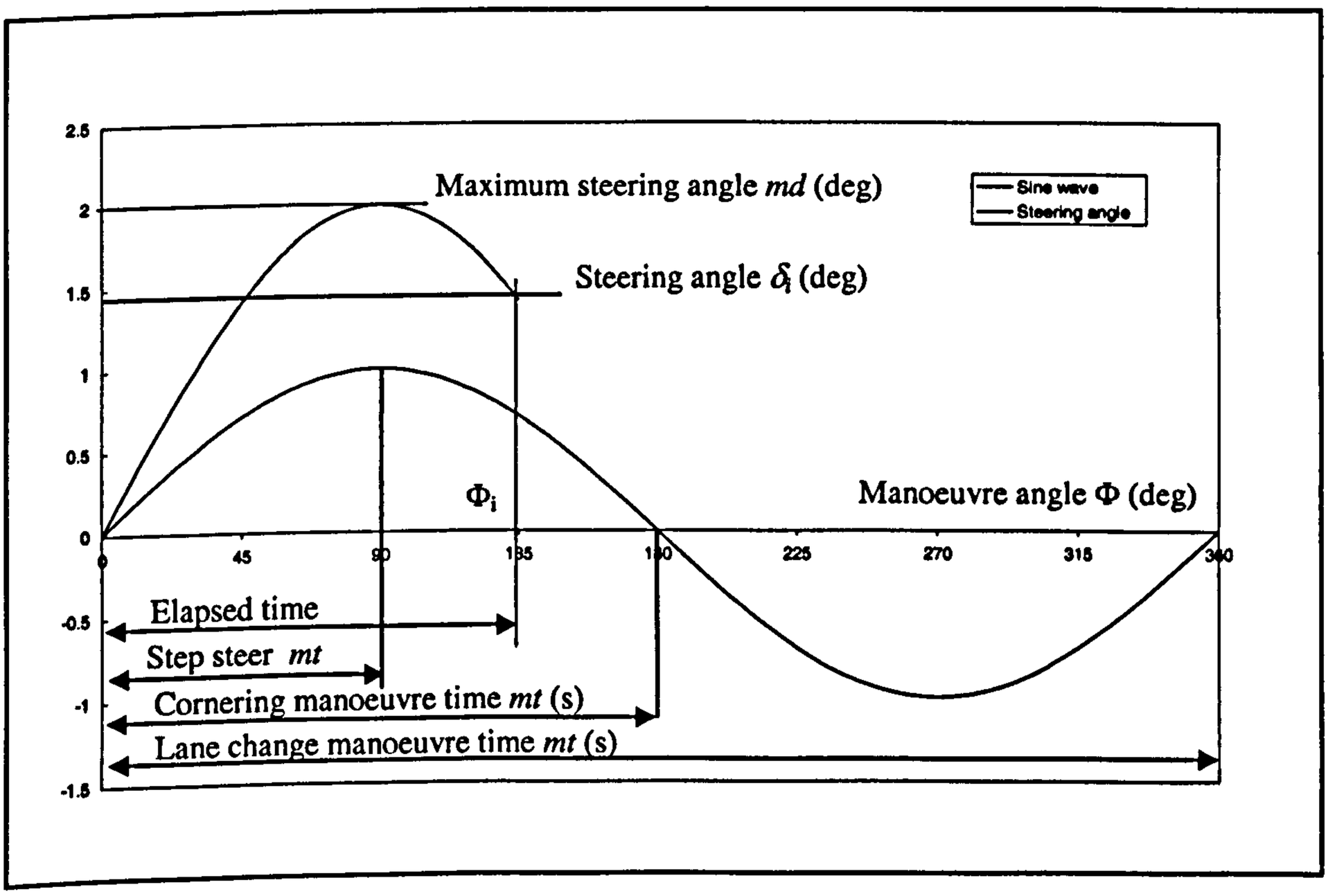

Fig (5.12) Steering angle of for different manoeuvres

The changing steering angle during the manoeuvre time is calculated as a function of the steering angle of the previous time frame, total manoeuvre time, total manoeuvre angle, time frame width Δt and maximum steering angle as follows: -

$$\Phi_{i(n)} = \Phi_{i(n-1)} + \Phi\left(\frac{\Delta t}{mt}\right) \tag{5.117}$$

$$\delta_{i(n)} = md \sin\left(\Phi_{i(n)}\right) \tag{5.118}$$

Where: -

Φ Total manoeuvre angle

Φ_i Instantaneous manoeuvre angle

mt Manoeuvre time

md Maximum steering angle of the manoeuvre

δ_i Instantaneous steering angle

n Time frame number

The manoeuvre routine has been developed based on the Ackerman path equations and the manoeuvre steering angle equations. The routine has been tested through simulating the lane change results at different forward velocities, Fig (5.13). Also it has been tested at different manoeuvre times, Fig (5.14), and at different maximum steering angles, Fig (5.15). The results showed the expected Ackerman paths of lane change manoeuvres and the expected effect of the involved factors.

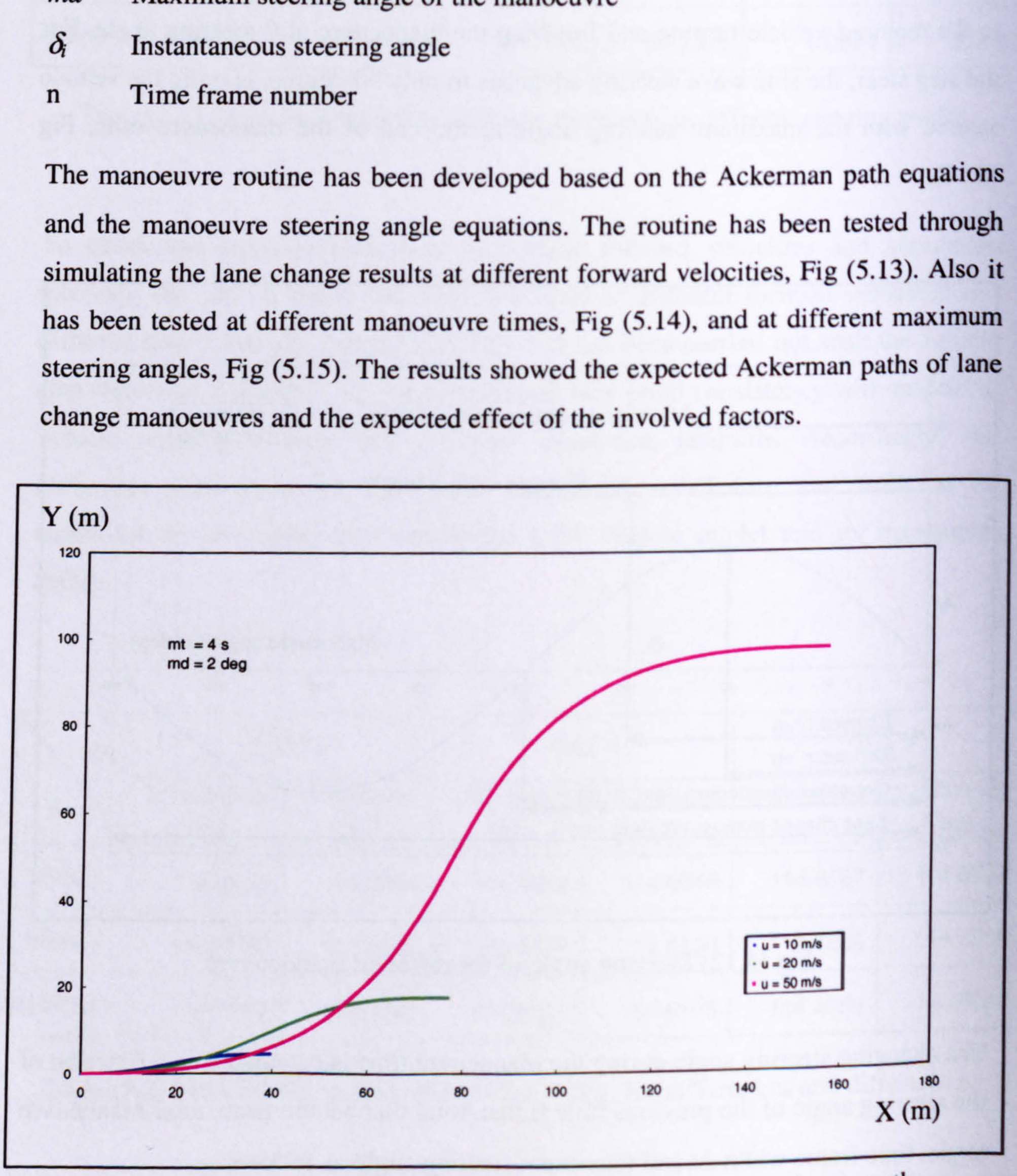

Fig (5.13) Effect of vehicle velocity (u) on Ackerman lane change path

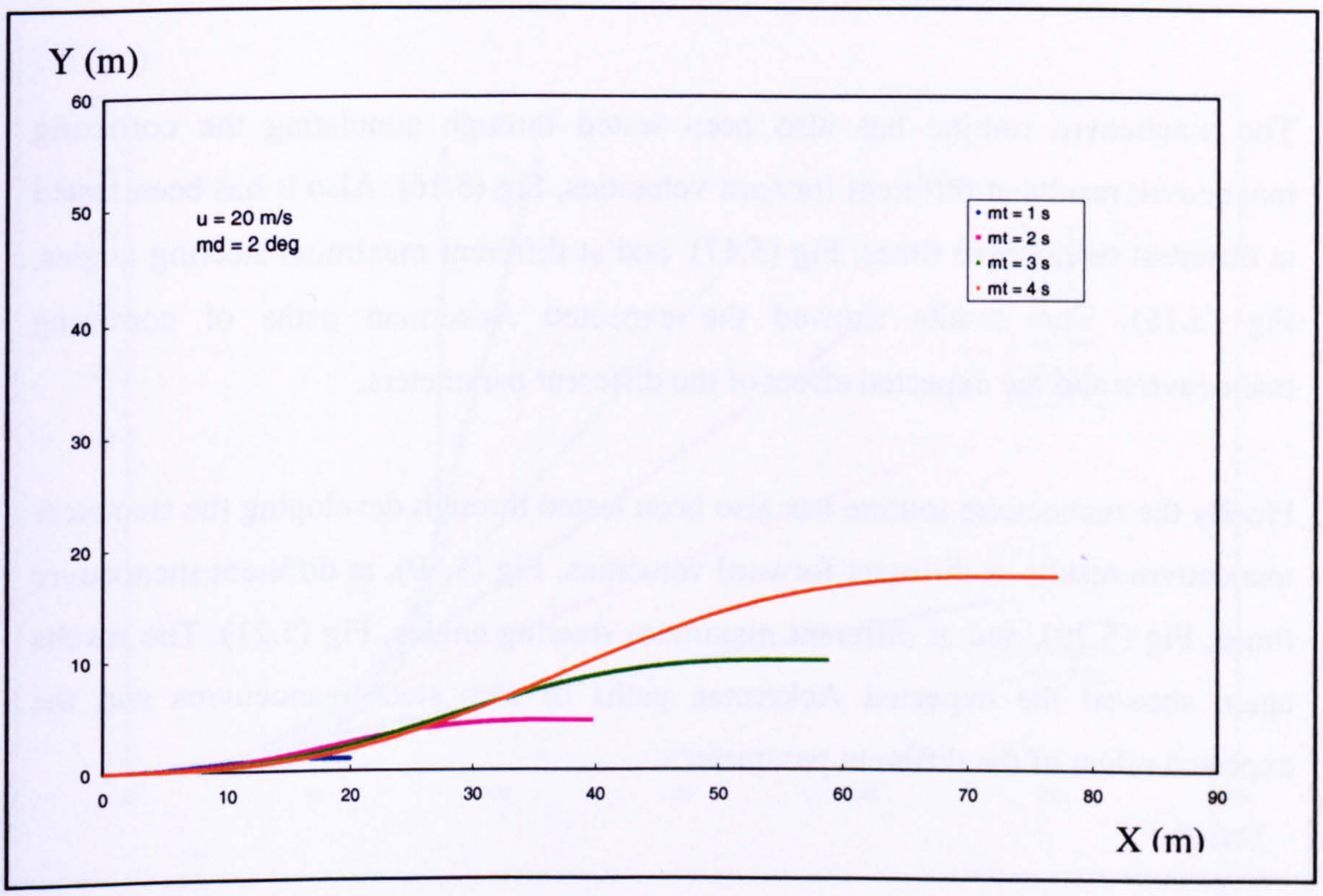

Fig (5.14) Effect of manoeuvre time (mt) on Ackerman lane change path

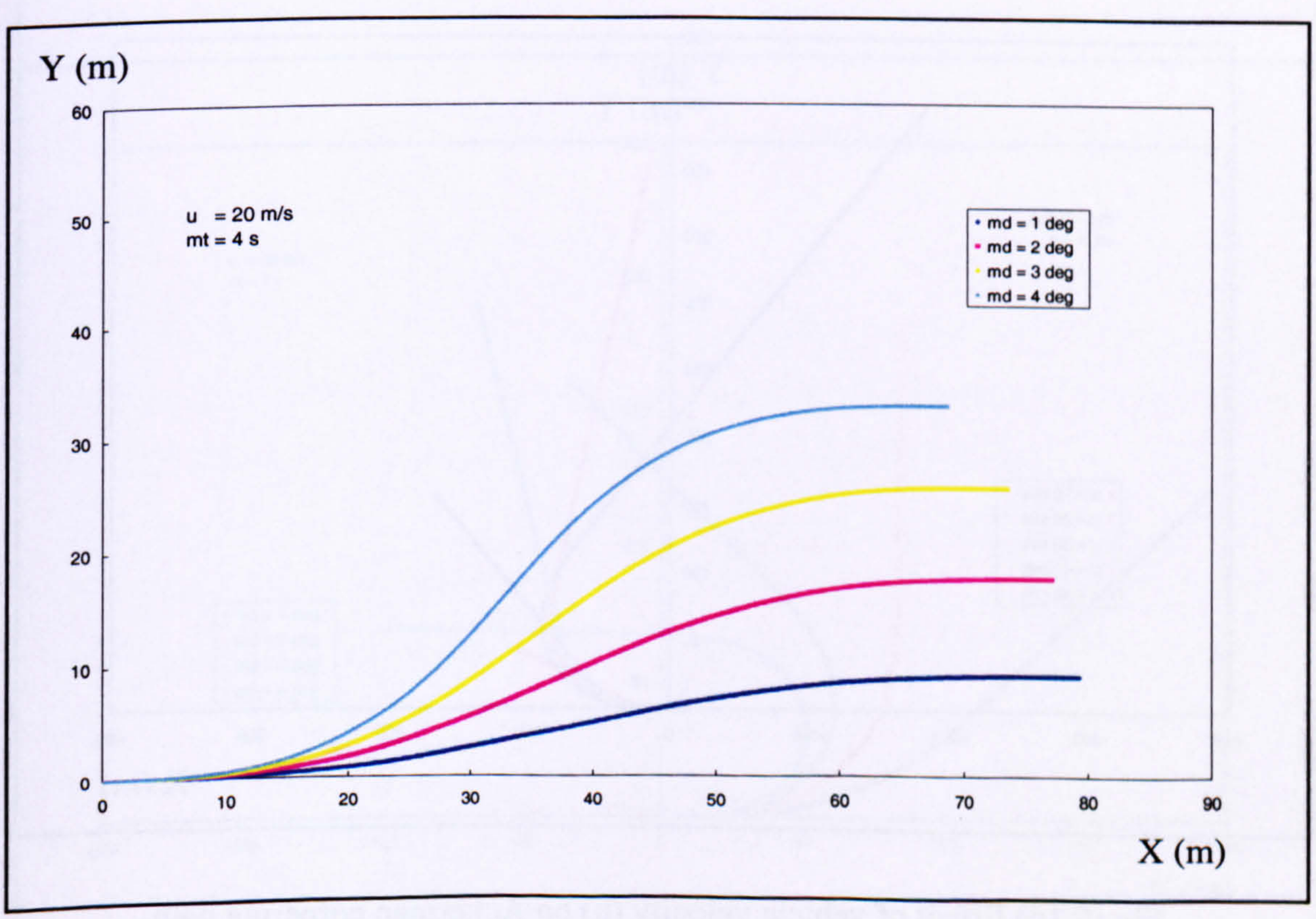

Fig (5.15) Effect of maximum steering angles (md) on Ackerman lane change path

The manoeuvre routine has also been tested through simulating the cornering manoeuvre results at different forward velocities, Fig (5.16). Also it has been tested at different manoeuvre times, Fig (5.17), and at different maximum steering angles, Fig (5.18). The results showed the expected Ackerman paths of cornering manoeuvres and the expected effect of the different parameters.

Finally the manoeuvre routine has also been tested through developing the step steer manoeuvre results at different forward velocities, Fig (5.19), at different manoeuvre times, Fig (5.20), and at different maximum steering angles, Fig (5.21). The results again showed the expected Ackerman paths of step steer manoeuvres and the expected effect of the different parameters.

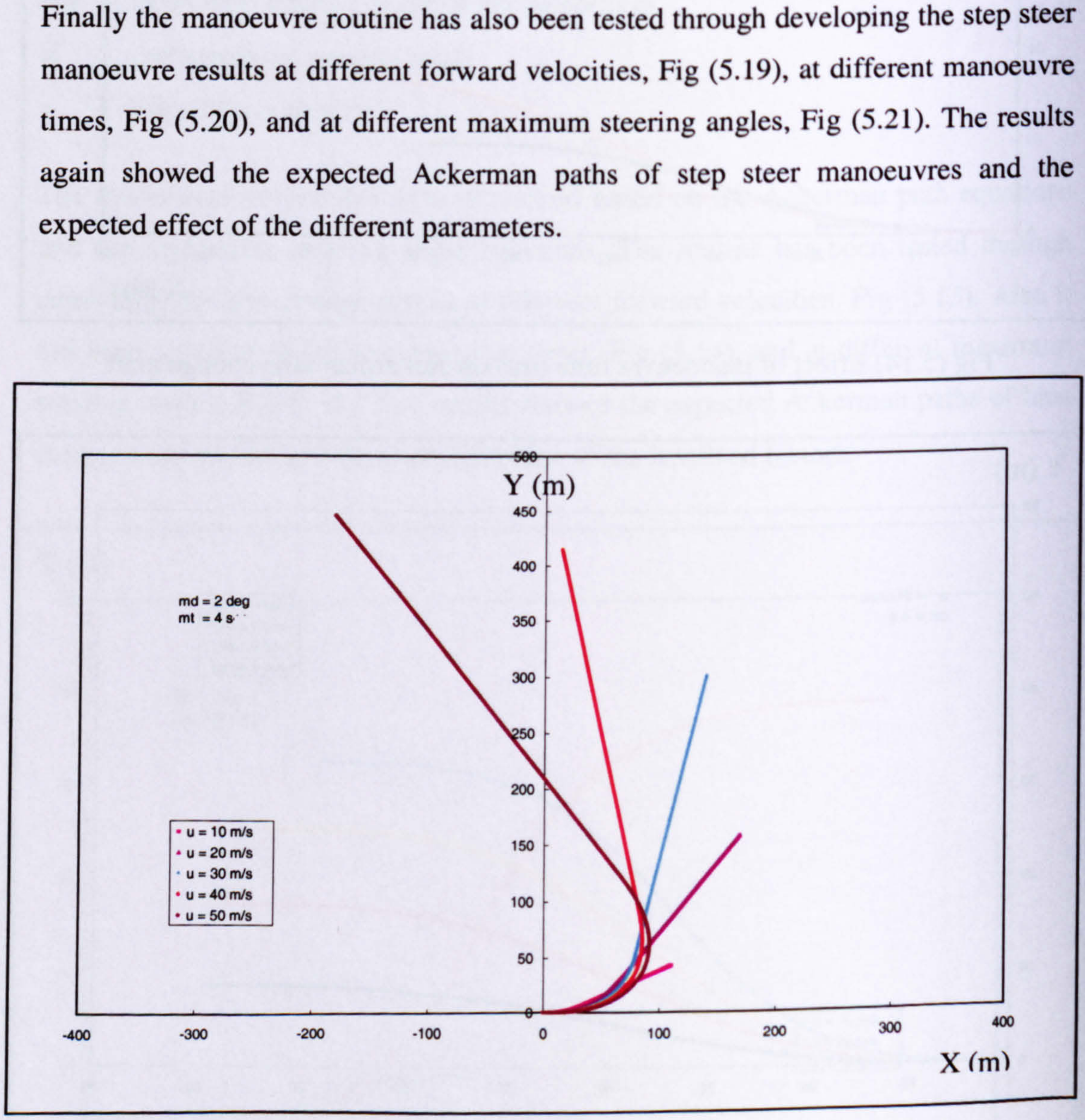

Fig (5.16) Effect of vehicle velocity (u) on Ackerman cornering path

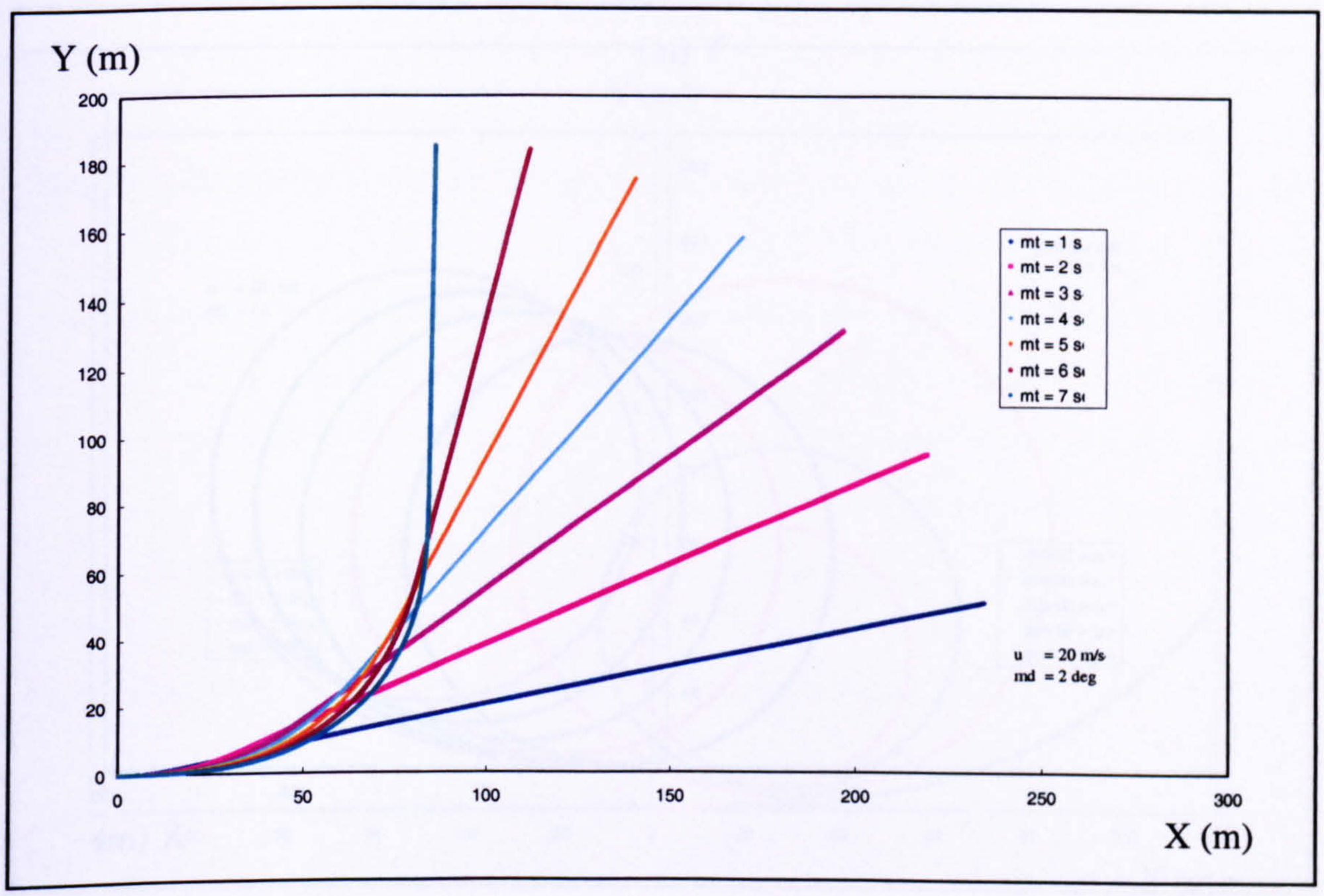

Fig (5.17) Effect of manoeuvre time (mt) on Ackerman cornering path

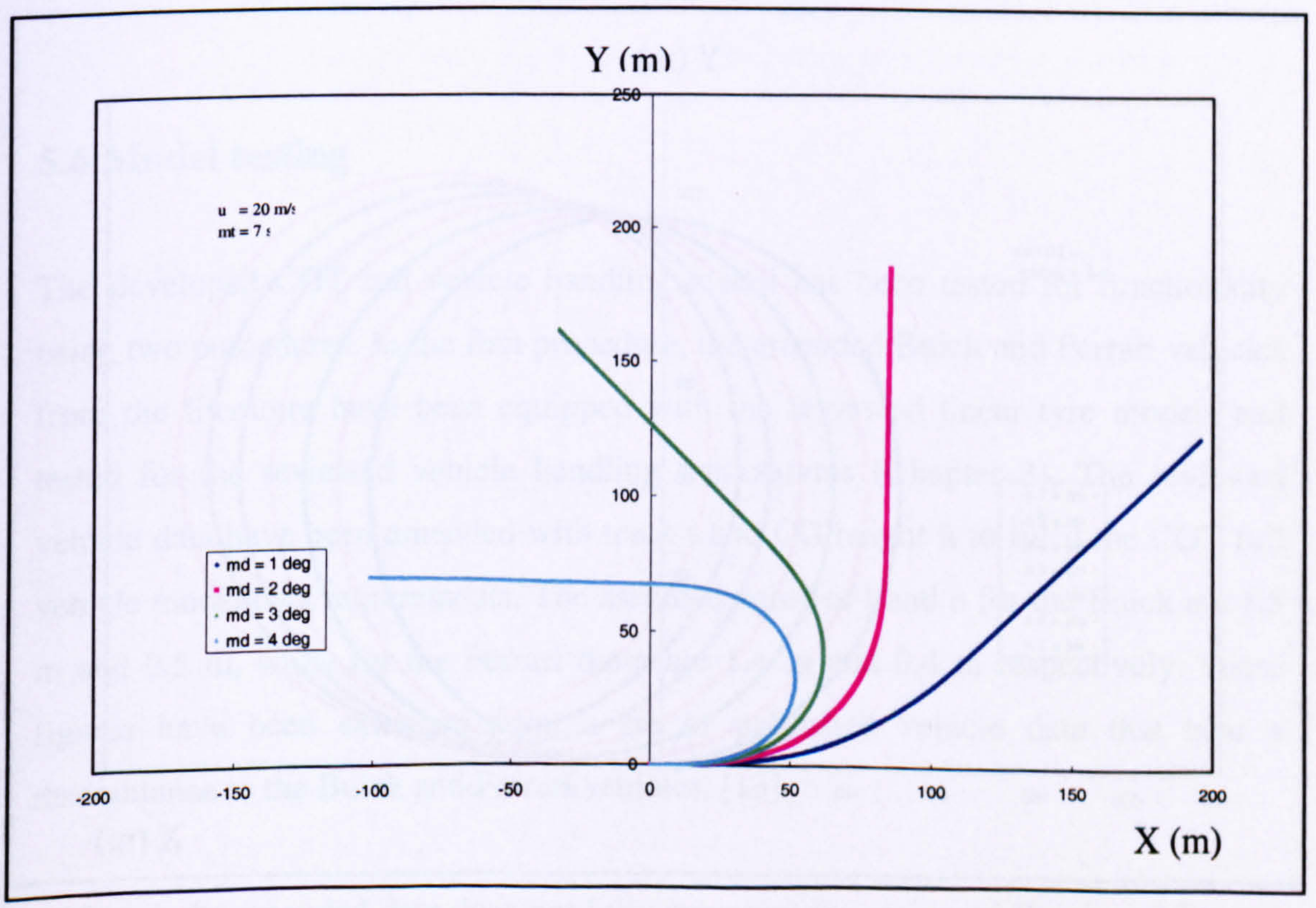

Fig (5.18) Effect of maximum steering angles (md) on Ackerman cornering path

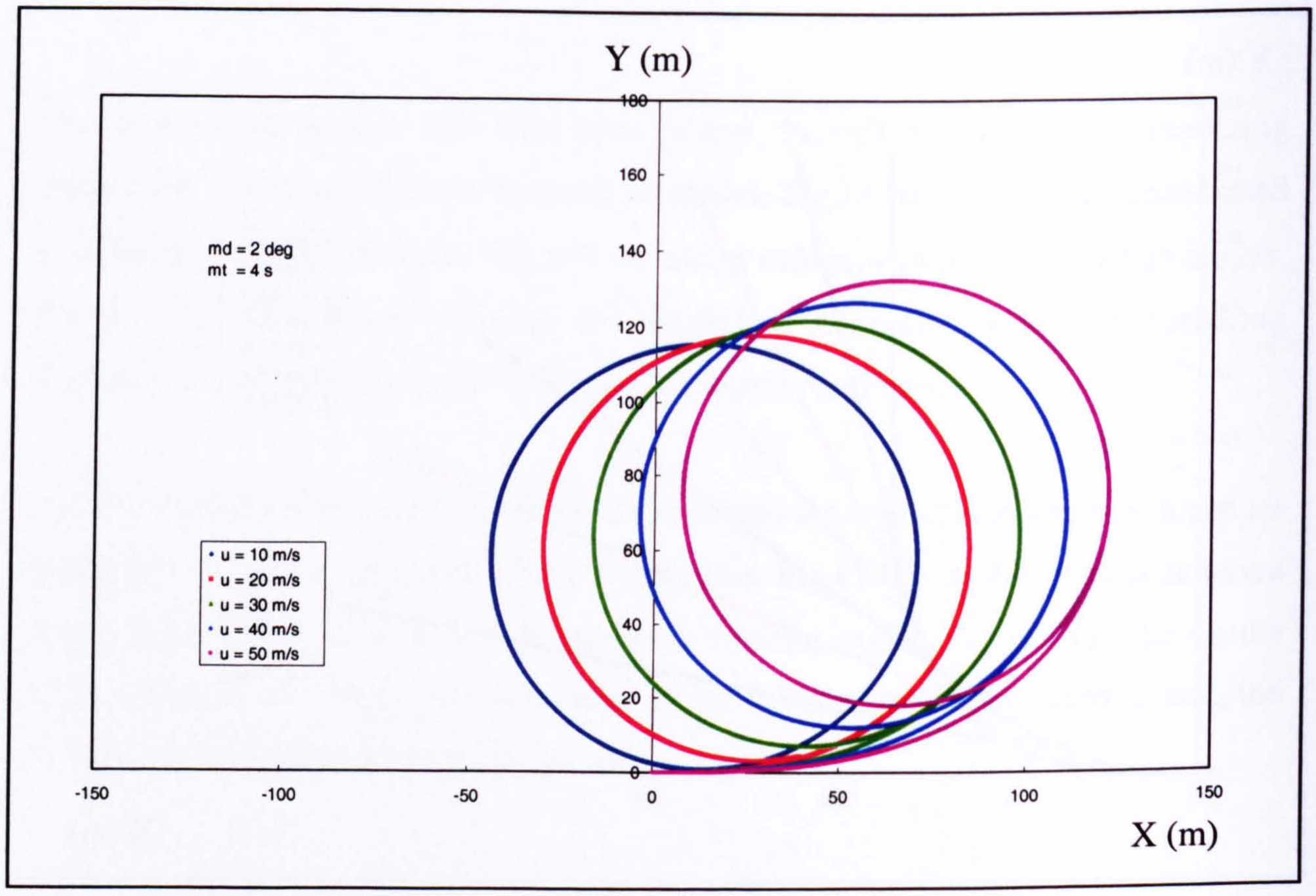

Fig (5.19) Effect of vehicle velocity (u) on Ackerman step steer path

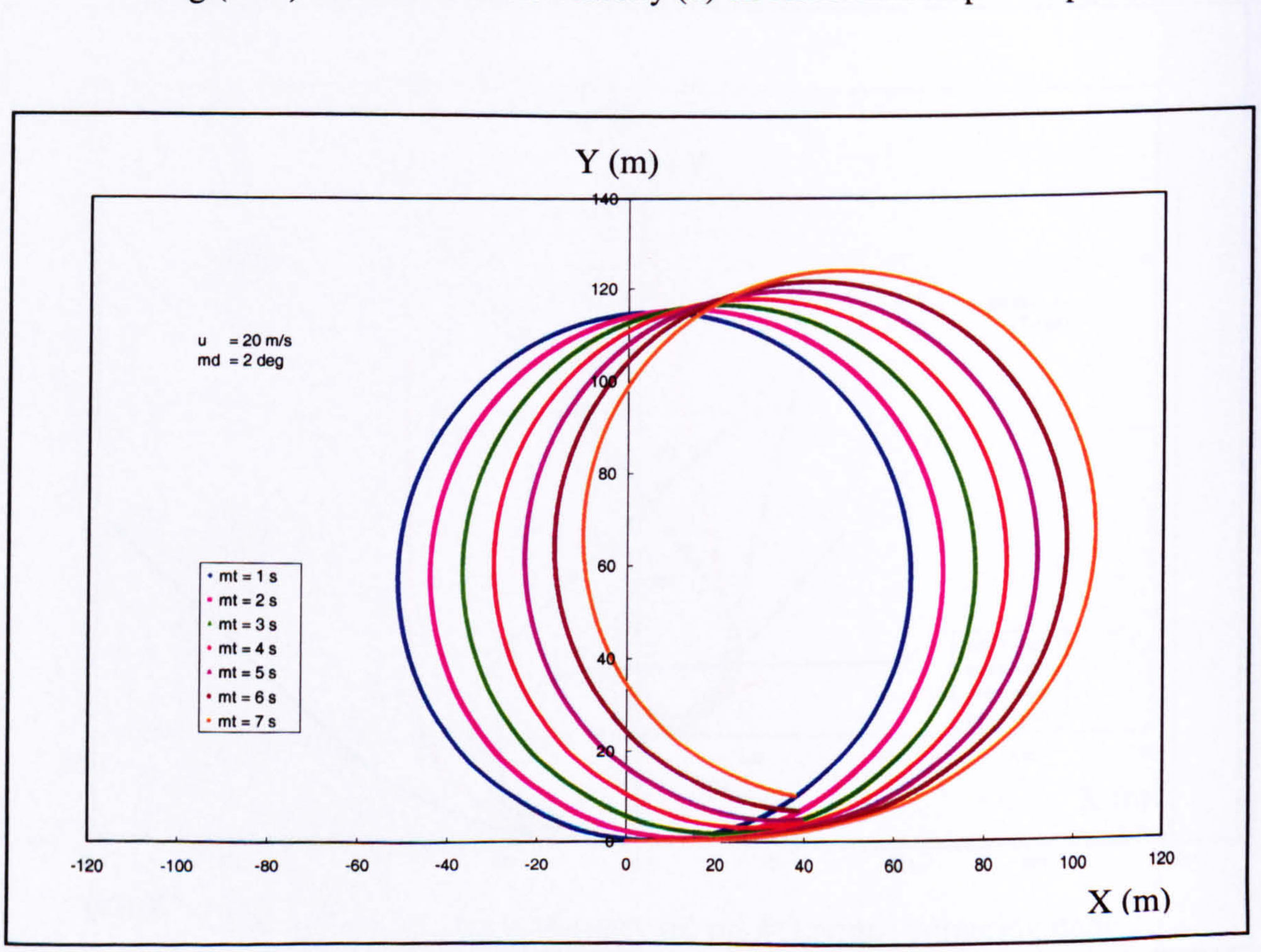

Fig (5.20) Effect of manoeuvre time (mt) on Ackerman step steer path

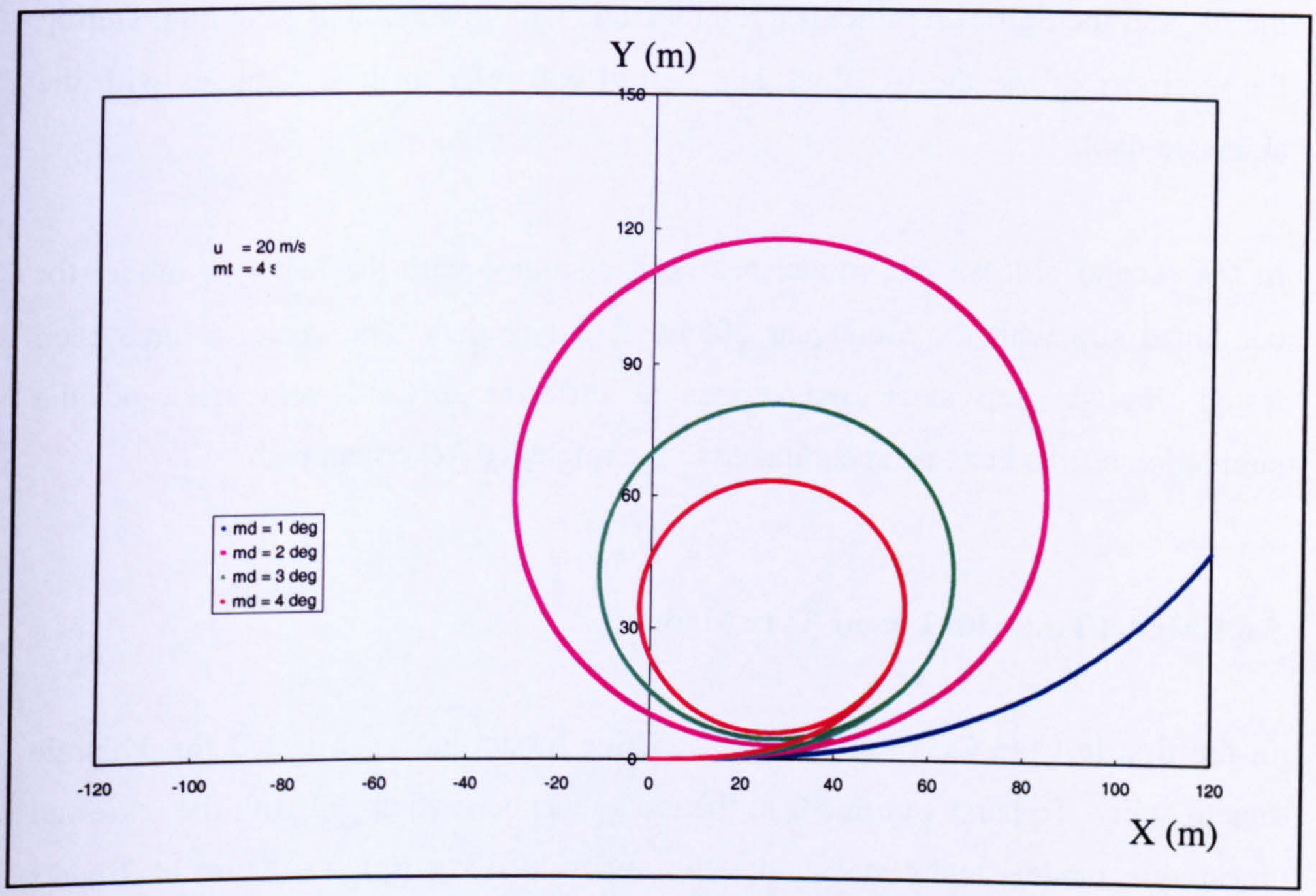

Fig (5.21) Effect of maximum steering angles (md) on Ackerman step steer path

5.6 Model testing

The developed CGT full vehicle handling model has been tested for functionality using two procedures. In the first procedure, the amended Buick and Ferrari vehicles from the literature have been equipped with the reviewed linear tyre models and tested for the reviewed vehicle handling manoeuvres (Chapter 3). The reviewed vehicle data have been amended with track t and CG height h to fulfil the CGT full vehicle model data requirements. The assumed value of t and h for the Buick are 1.5 m and 0.5 m, while for the Ferrari these are 1.4 m and 0.4 m respectively. These figures have been extracted from a set of published vehicle data that bear a resemblance to the Buick and Ferrari vehicles, [13].

Although the amended data does not fully represent the reviewed Buick and Ferrari, it has been considered to fit the purpose of investigating the effect of WSDC on

vehicle handling, as the Buick represents a heavy vehicle with high moment of inertia, and the Ferrari represents a light vehicle with low moment of inertia. During the reminder of the thesis, Buick and Ferrari will refer to these vehicles with the amended data.

In the second process, the model has been equipped with the MF tyre model for combined slip with the Goodyear 205/60 R15 tyre data. The vehicles have been tested through step steer manoeuvres at different forward velocities and the simulation results have been compared to the reference Ackerman path.

5.6.1 Model Test with Linear Tyre Model

In the first test the CGT full vehicle handling model has been tested for dynamic functionality. To carry out this test, the model has been equipped with the reviewed linear tyre models and tested under the reviewed 0.3 g rightward turn at 20 m/s forward velocity. In this manoeuvre the Buick vehicle model has been step steered by -1.624 degrees following a quarter of a sine wave pattern over 0.01 s. The Ferrari has been step steered by -0.965 degrees following the same pattern.

To apply the linear tyre model to the full vehicle, "stage twelve", section 5.3.12, has been replaced. The left and right tyre lateral forces are calculated as follows:-

$$F_{yFl} = \alpha_{Fl}\left(\frac{C_{\alpha f}}{2}\right) \tag{5.119}$$

$$F_{yFr} = \alpha_{Fr}\left(\frac{C_{\alpha f}}{2}\right) \tag{5.120}$$

$$F_{yRl} = \alpha_{Rl}\left(\frac{C_{\alpha r}}{2}\right) \tag{5.121}$$

$$F_{yRr} = \alpha_{Rr}\left(\frac{C_{\alpha r}}{2}\right) \tag{5.122}$$

The results have been plotted against validated CGT half vehicle handling model results (Chapter 3). For the Buick vehicle, the results, Fig (5.22), showed high comparability to the CGT half vehicle Buick model. Also, the Ferrari vehicle results, Fig (5.23), showed high comparability to the CGT half vehicle Ferrari model. This demonstrates the CGT full vehicle handling model dynamic functionality.

To further prove the consistency of the model functionality, the higher velocity reviewed manoeuvres (50 m/s) have also been simulated in which the vehicles are step steered rightward to develop a 0.3 g steady state lateral acceleration. In this manoeuvre the Buick vehicle model has been step steered by -0.49 degrees following a quarter of a sine wave pattern in 0.01 s. The Ferrari has been step steered by -0.116 degrees following the same pattern.

The results have been plotted against validated CGT half vehicle handling model results (Chapter 3). For the 50 m/s manoeuvre, the Buick vehicle yaw results showed good comparability to the Buick CGT half vehicle model results, Fig (5.24). Also, the Ferrari vehicle yaw results showed good comparability to Ferrari CGT half vehicle model results, Fig (5.25). This is considered a further demonstration of the CGT full vehicle handling model dynamic functionality. In the next step the CGT vehicle handling model has been tested while equipped with the MF tyre model for combined slip.

5.6.2 Model Test with MF Combined Slip Tyre Model

This test has been carried out to investigate the proper integration of the MF tyre model for combined slip into the CGT full vehicle handling model. For this test, the original "stage twelve" has been employed. The model has been tested through investigating the Buick and Ferrari vehicles travelling path after 3 degrees leftward step steer following a 90 degrees sine wave pattern over 0.01 s at different forward velocities. The results have been compared with the Ackerman path.

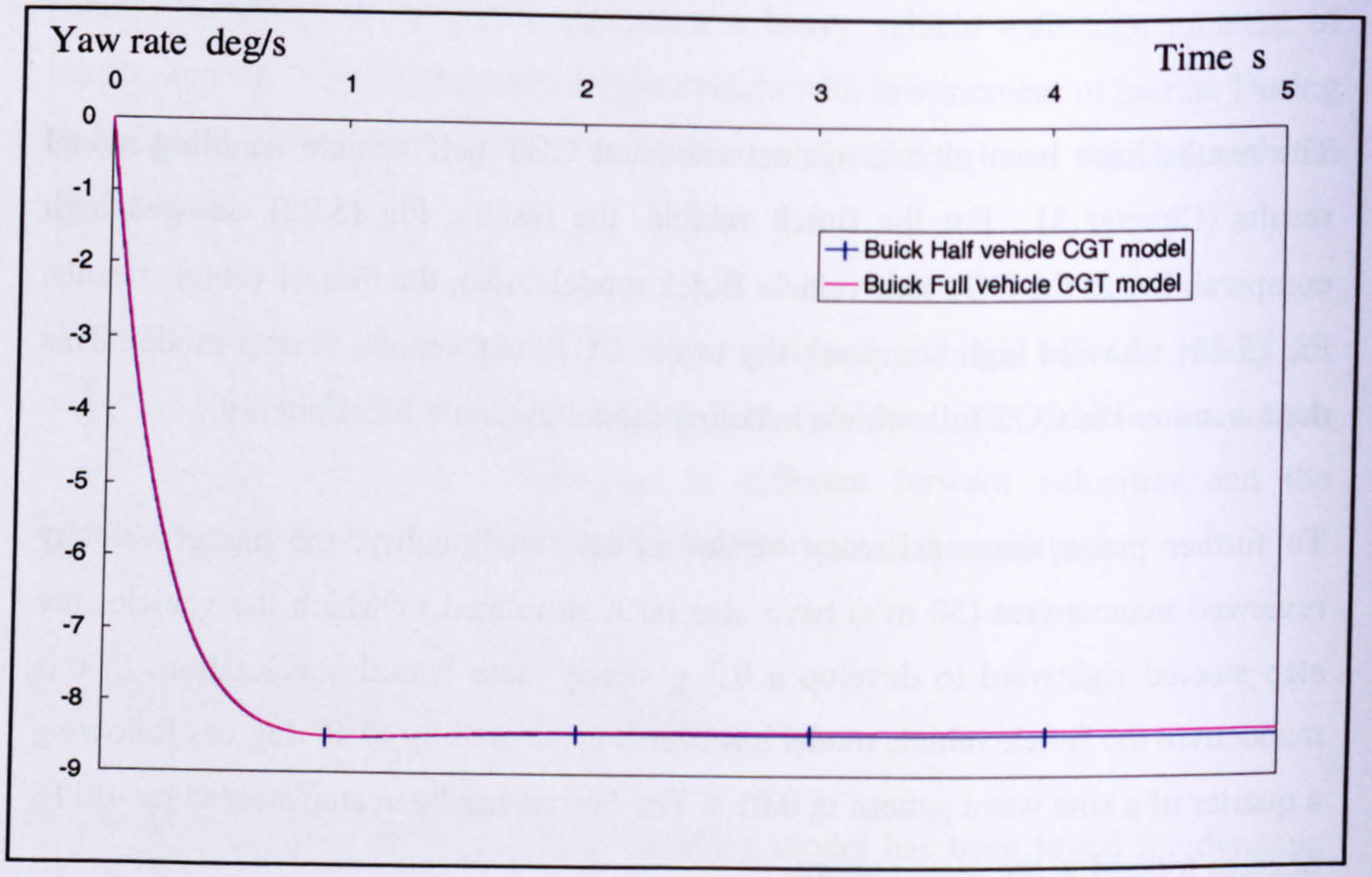

Fig (5.22) Buick CGT full and half vehicle model yaw rates during reviewed 0.3g rightward turn at 20 m/s forward velocity for linear tyre model

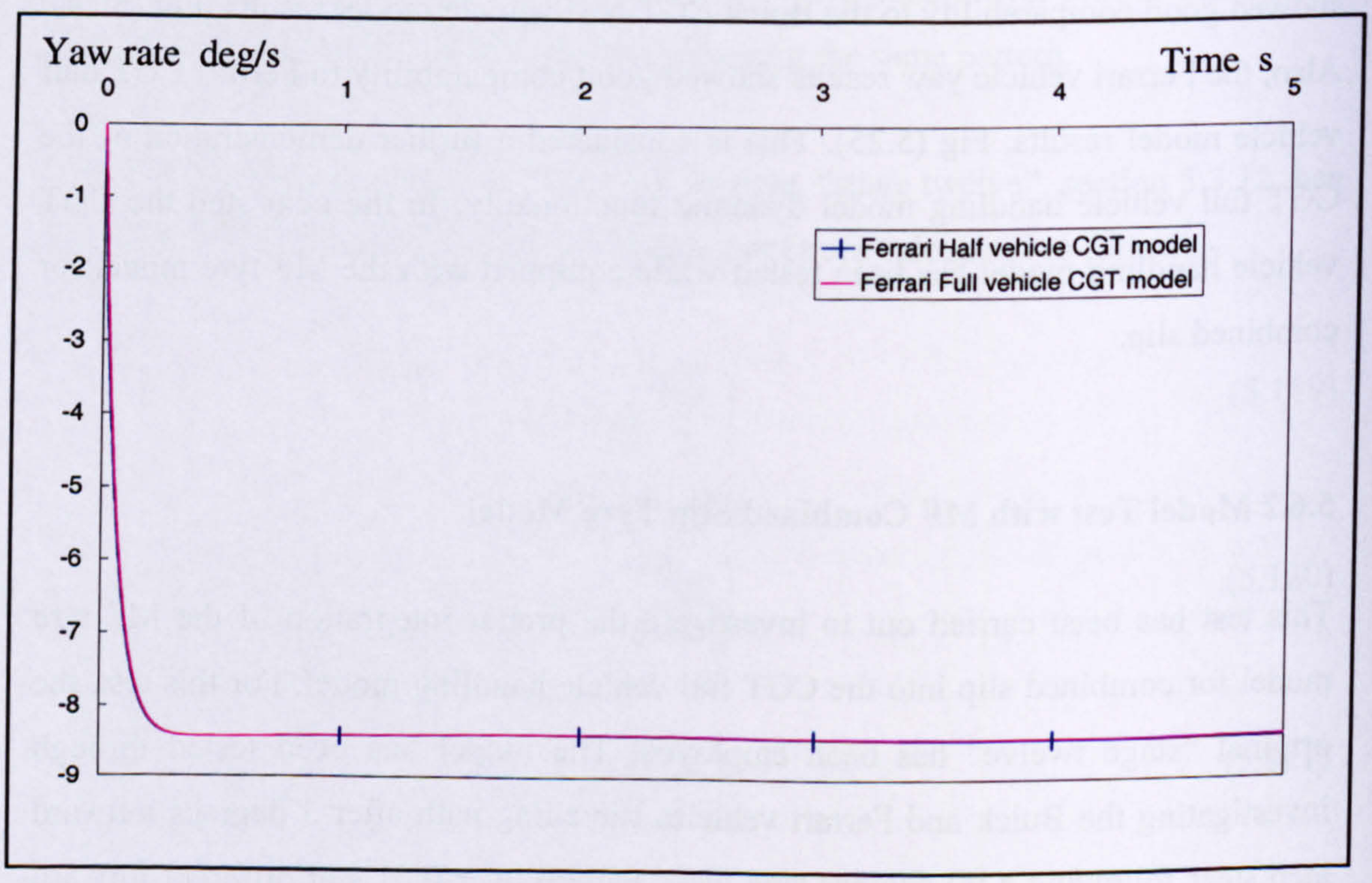

Fig (5.23) Ferrari CGT full and half vehicle models yaw rates during reviewed 0.3g rightward turn at 20 m/s forward velocity for linear tyre model

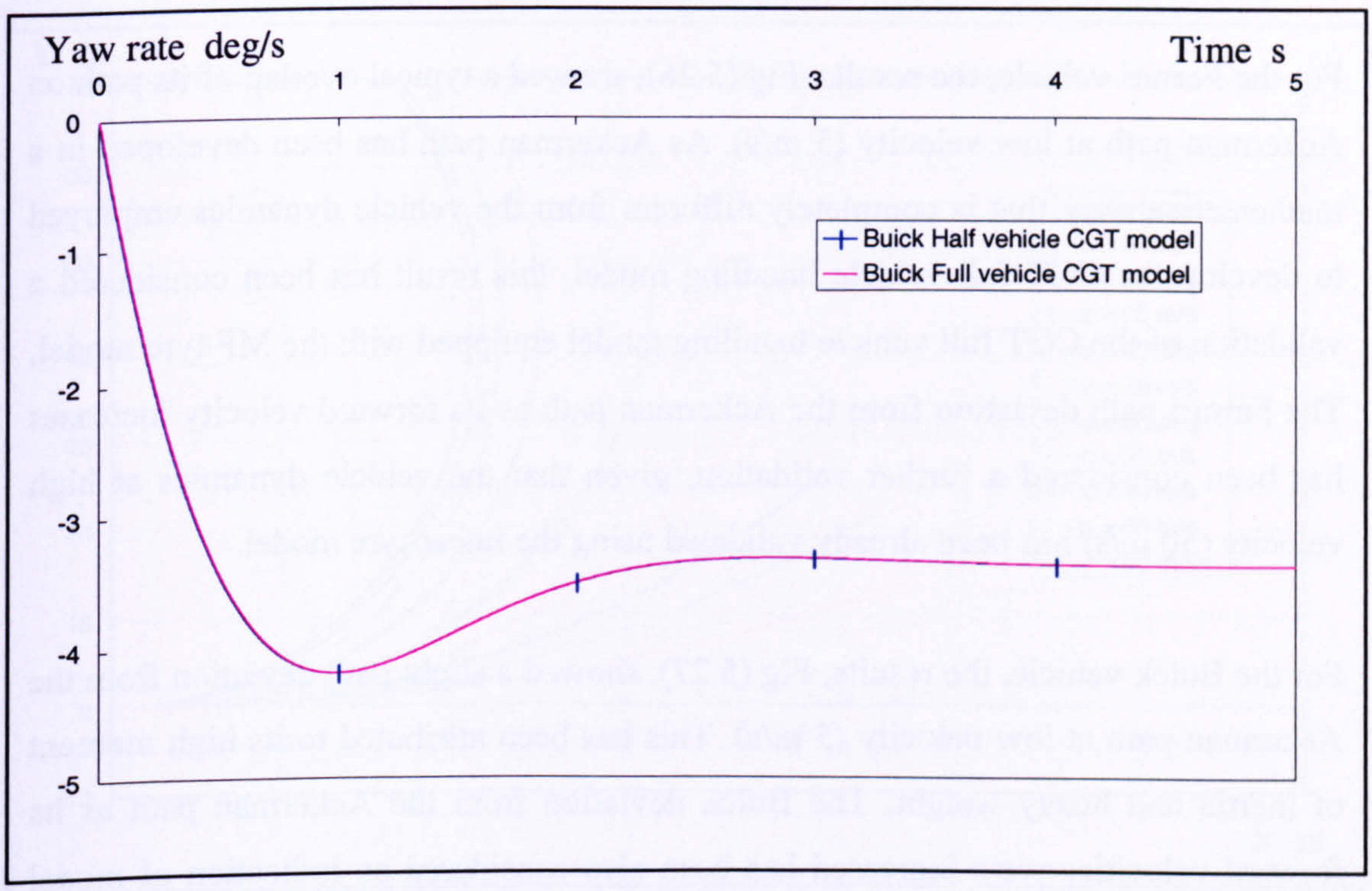

Fig (5.24) CGT full and half Buick vehicles yaw rates during reviewed 0.3g rightward turn at 50 m/s forward velocity for linear tyre model

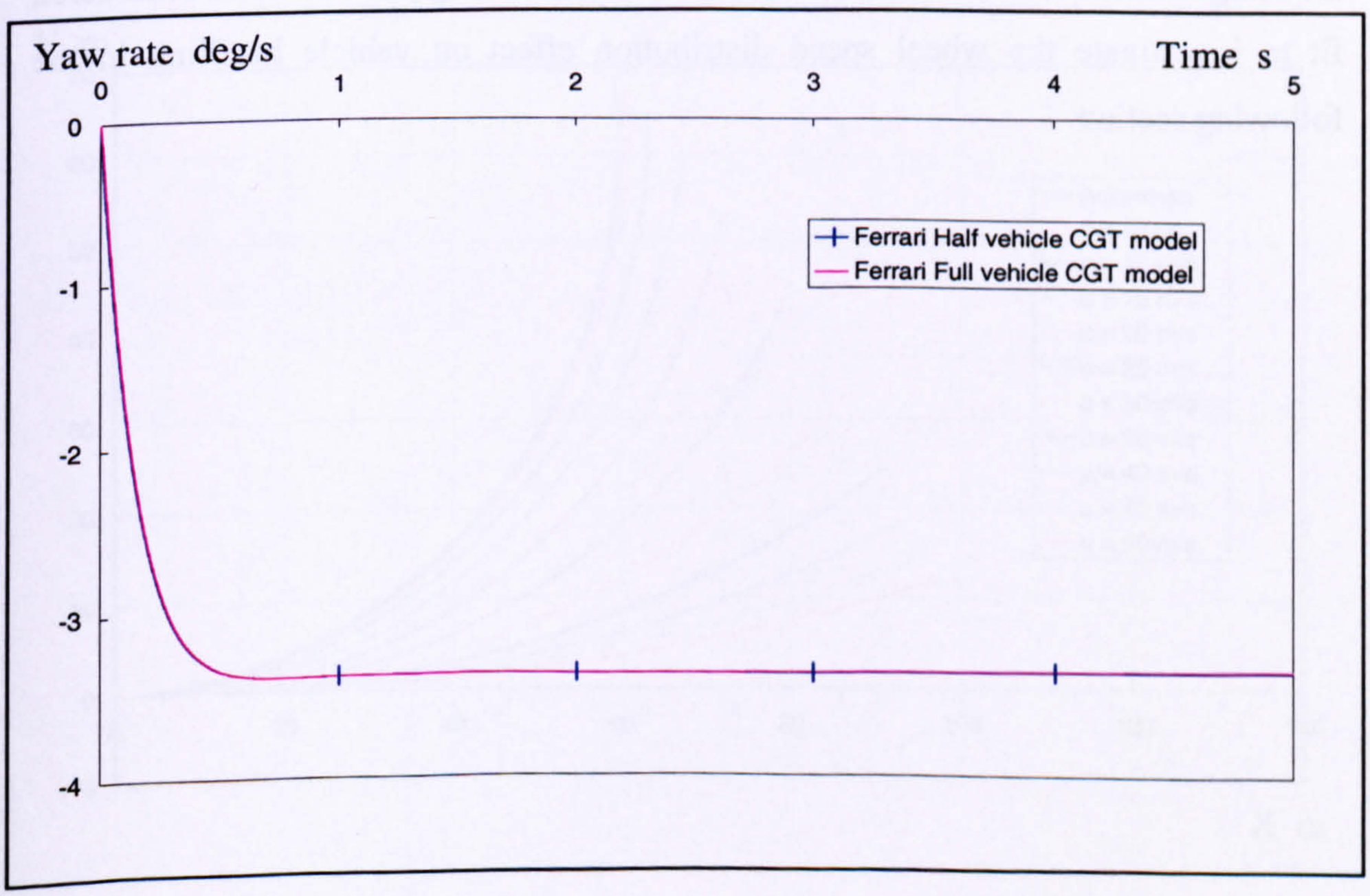

Fig (5.25) CGT full and half Ferrari vehicles yaw rates during reviewed 0.3g rightward turn at 50 m/s forward velocity for linear tyre model

For the Ferrari vehicle, the results, Fig (5.26), showed a typical overlap of its path on Ackerman path at low velocity (5 m/s). As Ackerman path has been developed in a mathematical way that is completely different from the vehicle dynamics employed to develop the CGT full vehicle handling model, this result has been considered a validation of the CGT full vehicle handling model equipped with the MF tyre model. The Ferrari path deviation from the Ackerman path as its forward velocity increases has been considered a further validation, given that the vehicle dynamics at high velocity (50 m/s) has been already validated using the linear tyre model.

For the Buick vehicle, the results, Fig (5.27), showed a slight path deviation from the Ackerman path at low velocity (5 m/s). This has been attributed to its high moment of inertia and heavy weight. The Buick deviation from the Ackerman path as its forward velocities were increased has been also considered an indication of model functionality.

Given the above results for the Buick and Ferrari vehicles, the CGT full vehicle handling model has been considered validated. Accordingly it has been considered fit to investigate the wheel speed distribution effect on vehicle handling in the following section.

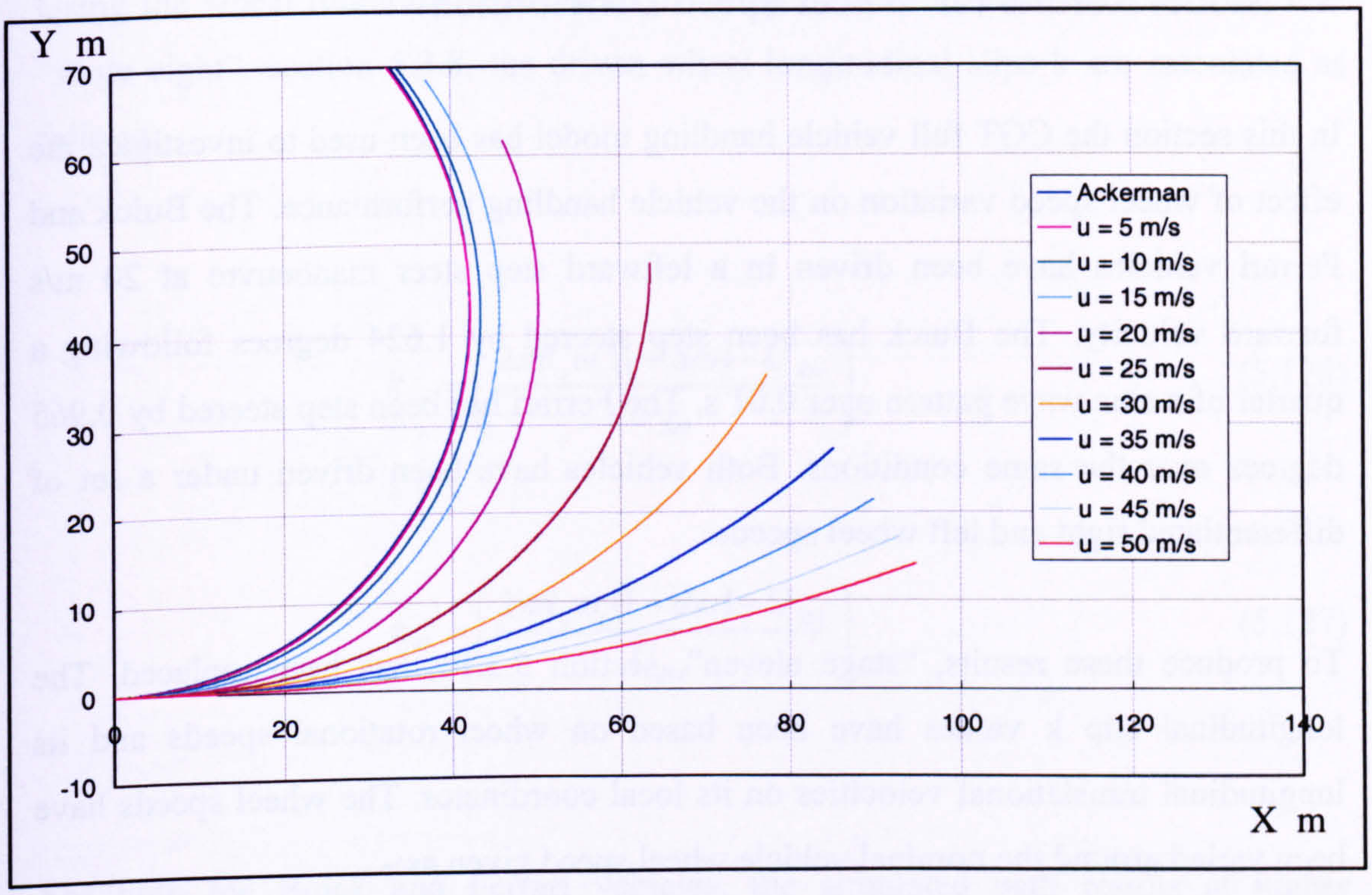

Fig (5.26) Ferrari CGT full vehicle path during 3 degrees leftward sep steer at different forward velocities and the MF tyre model

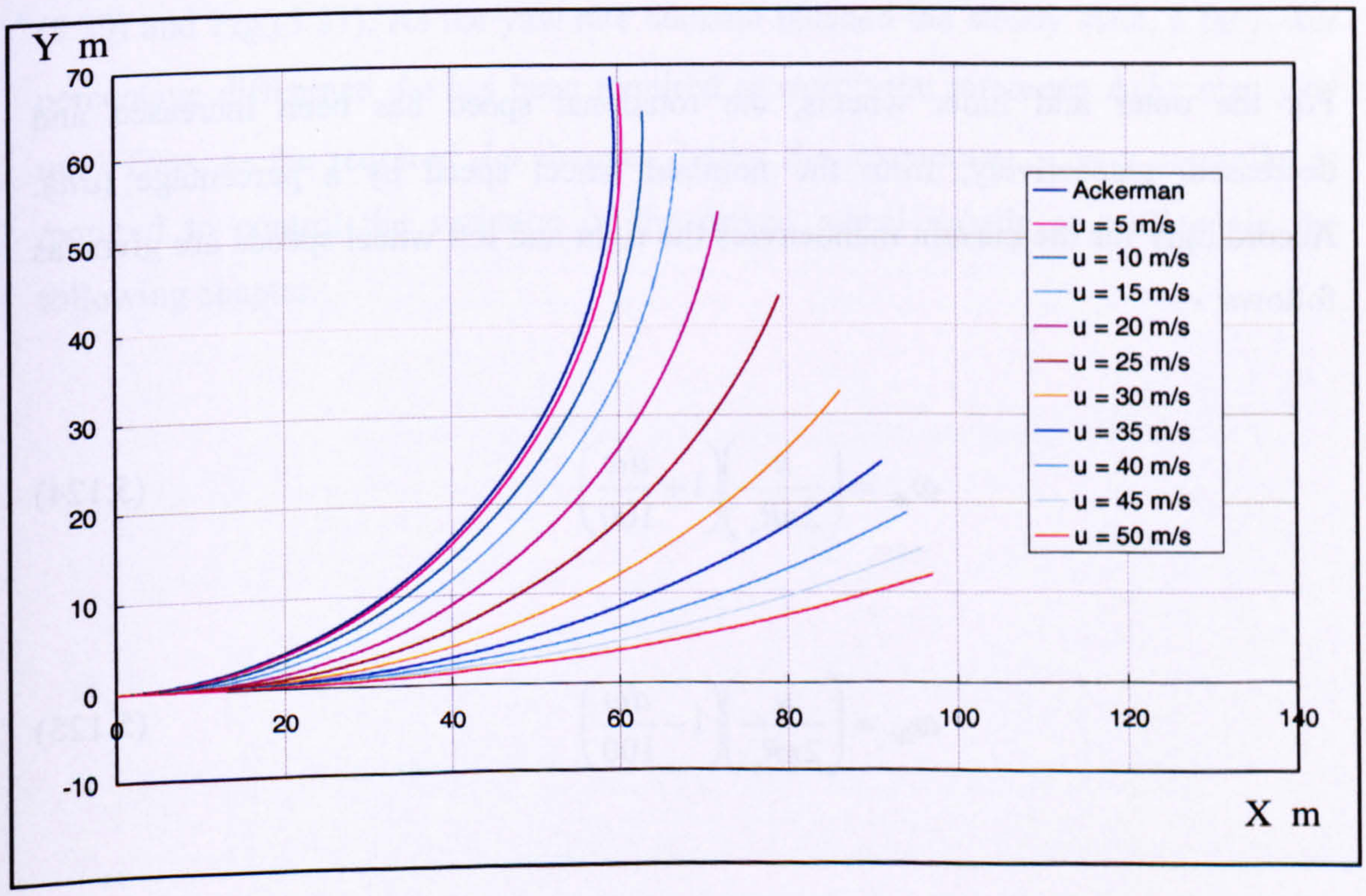

Fig (5.27) Buick CGT full vehicle path during 3 degrees leftward sep steer at different forward velocities and the MF tyre model

5.7 Model Results for Wheel Speed Distribution

In this section the CGT full vehicle handling model has been used to investigate the effect of wheel speed variation on the vehicle handling performance. The Buick and Ferrari vehicles have been driven in a leftward step steer manoeuvre at 20 m/s forward velocity. The Buick has been step steered by 1.624 degrees following a quarter of a sine wave pattern over 0.01 s. The Ferrari has been step steered by 0.965 degrees over the same conditions. Both vehicles have been driven under a set of differentiated right and left wheel speeds.

To produce these results, "stage eleven", section 5.3.11, has been replaced. The longitudinal slip k values have been based on wheel rotational speeds and its longitudinal translational velocities on its local coordinates. The wheel speeds have been varied around the nominal vehicle wheel speed given as:-

$$\omega_t = \left(\frac{u}{2\pi R_o}\right) \tag{5.123}$$

For the outer and inner wheels, the rotational speed has been increased and decreased, respectively, from the nominal wheel speed by a percentage ($d\omega$). Accordingly for the current manoeuvres the right and left wheel speeds are given as follows: -

$$\omega_{Rr} = \left(\frac{u}{2\pi R_o}\right)\left(1+\frac{d\omega}{100}\right) \tag{5.124}$$

$$\omega_{Rr} = \left(\frac{u}{2\pi R_o}\right)\left(1-\frac{d\omega}{100}\right) \tag{5.125}$$

Where: -

$d\omega$ Wheel rotational speed percentage difference from nominal rotational speed

Using the wheel rotational speeds and the longitudinal translational velocities from "stage eight", section 5.3.8, the driven wheel longitudinal slips k are calculated as follows: -

$$k_{Rr} = \left(\frac{2\pi R_o \omega_t (1 + d\omega) - U_{Rrr}}{U_{Rrr}} \right) \tag{5.126}$$

$$k_{Rl} = \left(\frac{2\pi R_o \omega_t (1 - d\omega) - U_{Rl1}}{U_{Rr1}} \right) \tag{5.127}$$

For both the Buick and Ferrari vehicles, the simulated path results at higher percentage difference $d\omega$ are closer to the Ackerman path at the start of the manoeuvre, Fig (5.28) and Fig (5.30). This has been attributed to the high yaw rate required to follow the Ackerman path at the start of the step steer manoeuvre, Fig (5.29) and Fig (5.31). As the yaw rate demand reached the steady state, a far lower percentage difference $d\omega$ has been required to match the reference Ackerman yaw rate. Thus, as the required $d\omega$ changes during the manoeuvre, a yaw controller is required to control the variation of the driven wheel speeds as outlined in the following chapter.

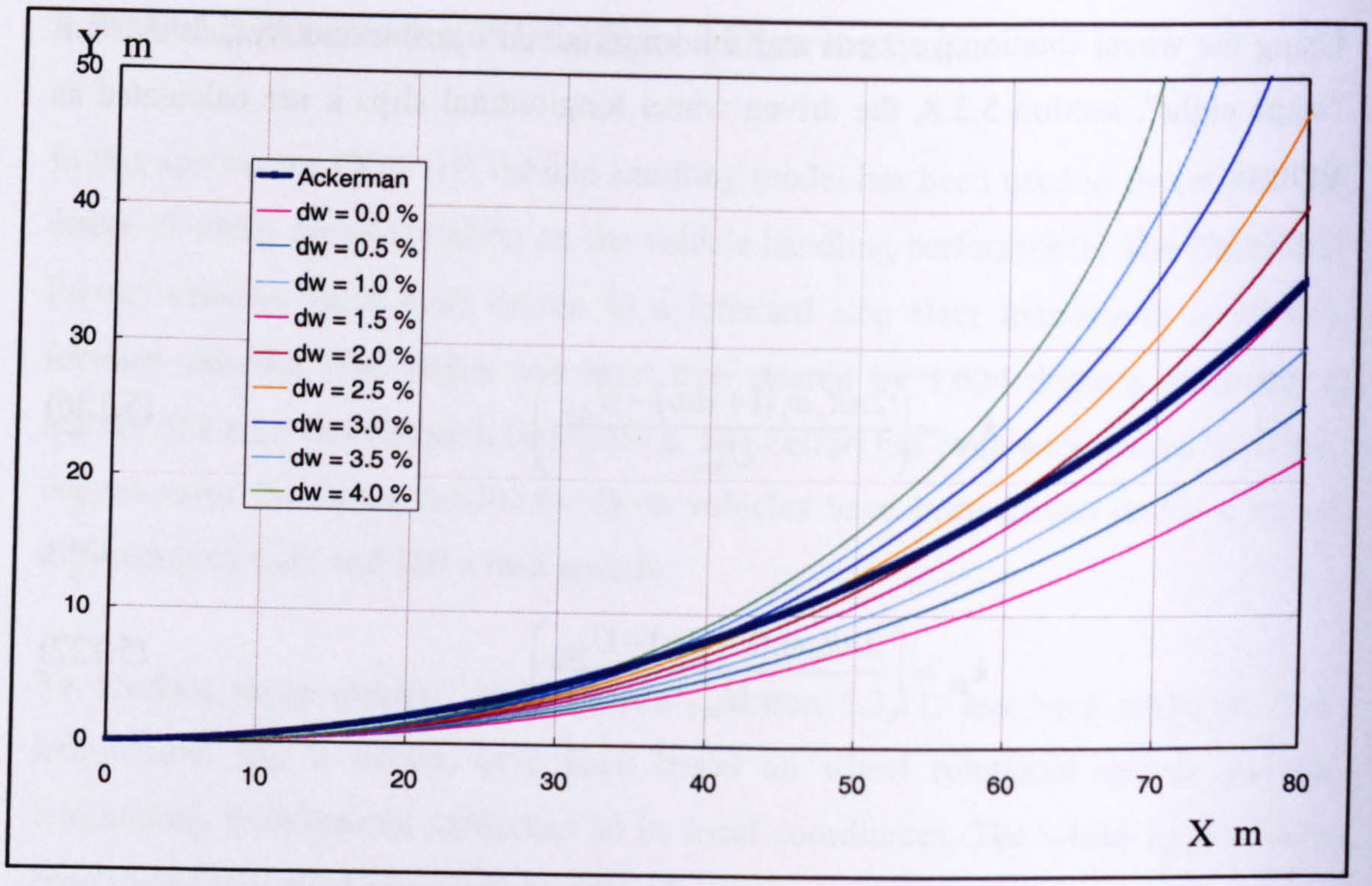

Fig (5.28) Buick path after 1.624 degrees step steer at 20 m/s forward velocity and different $d\omega$

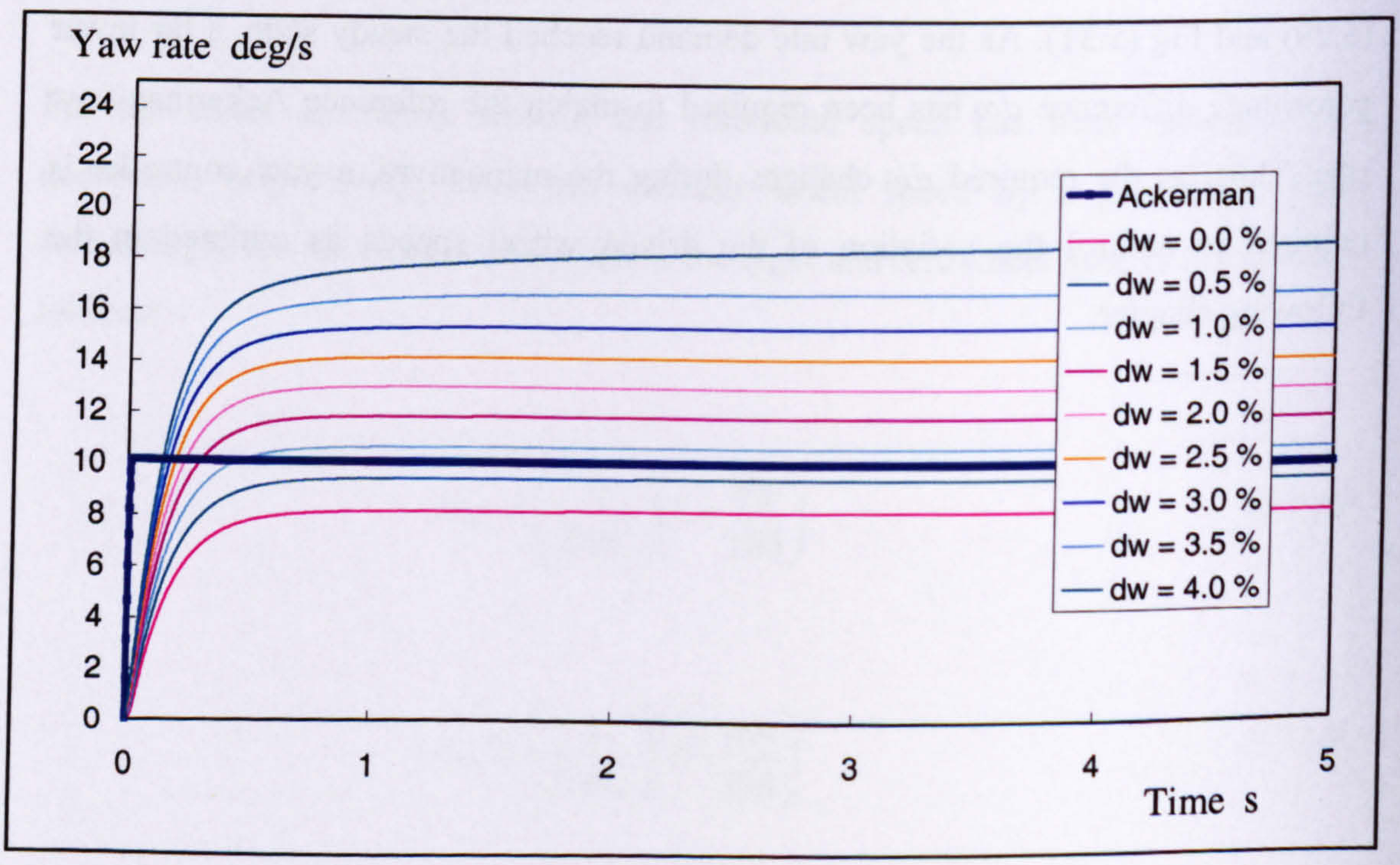

Fig (5.29) Buick yaw rate after 1.624 degrees step steer at 20 m/s forward velocity and different $d\omega$

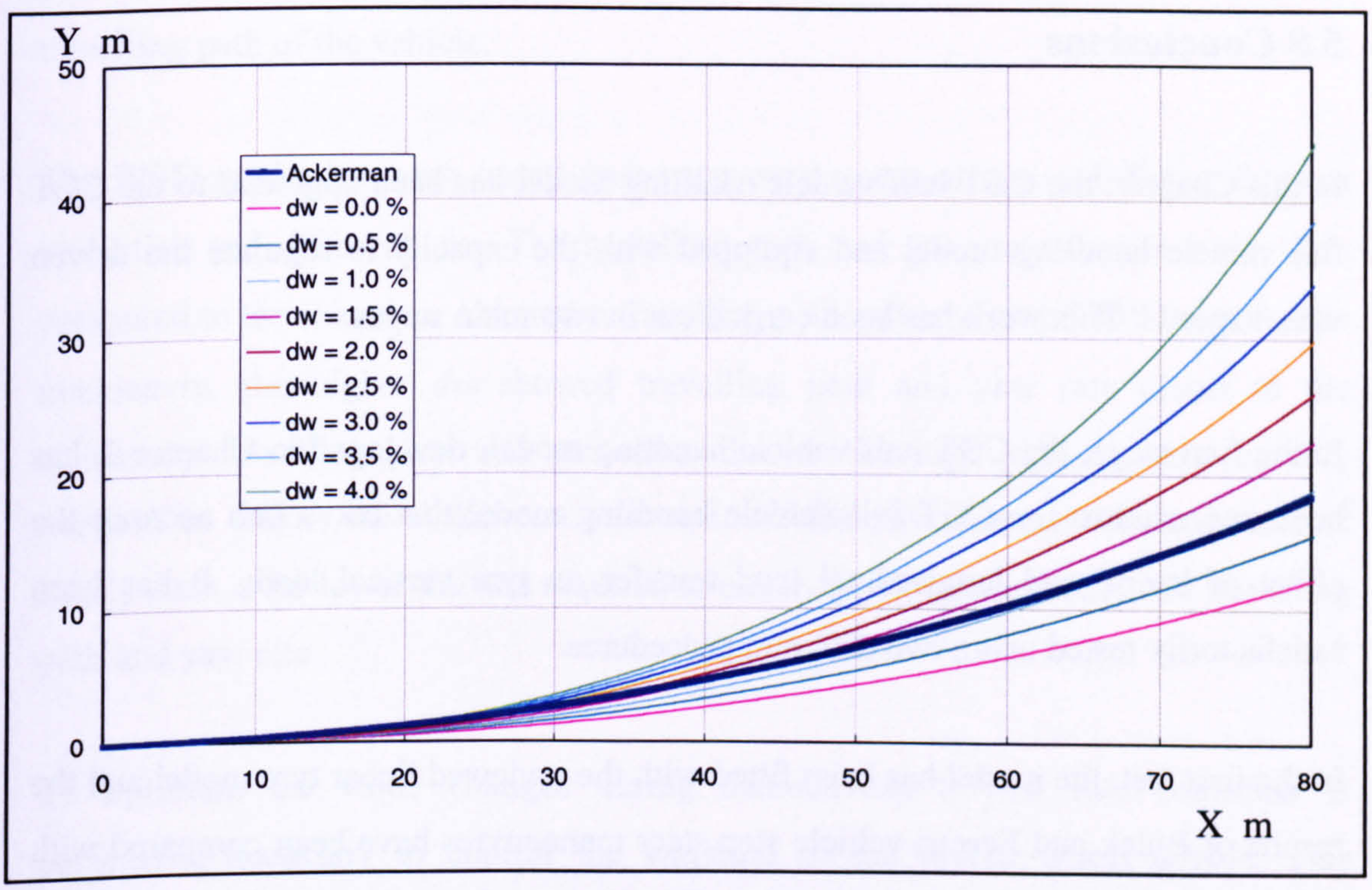

Fig (5.30) Ferrari path after 0.965 degrees step steer at 20 m/s forward velocity and different $d\omega$

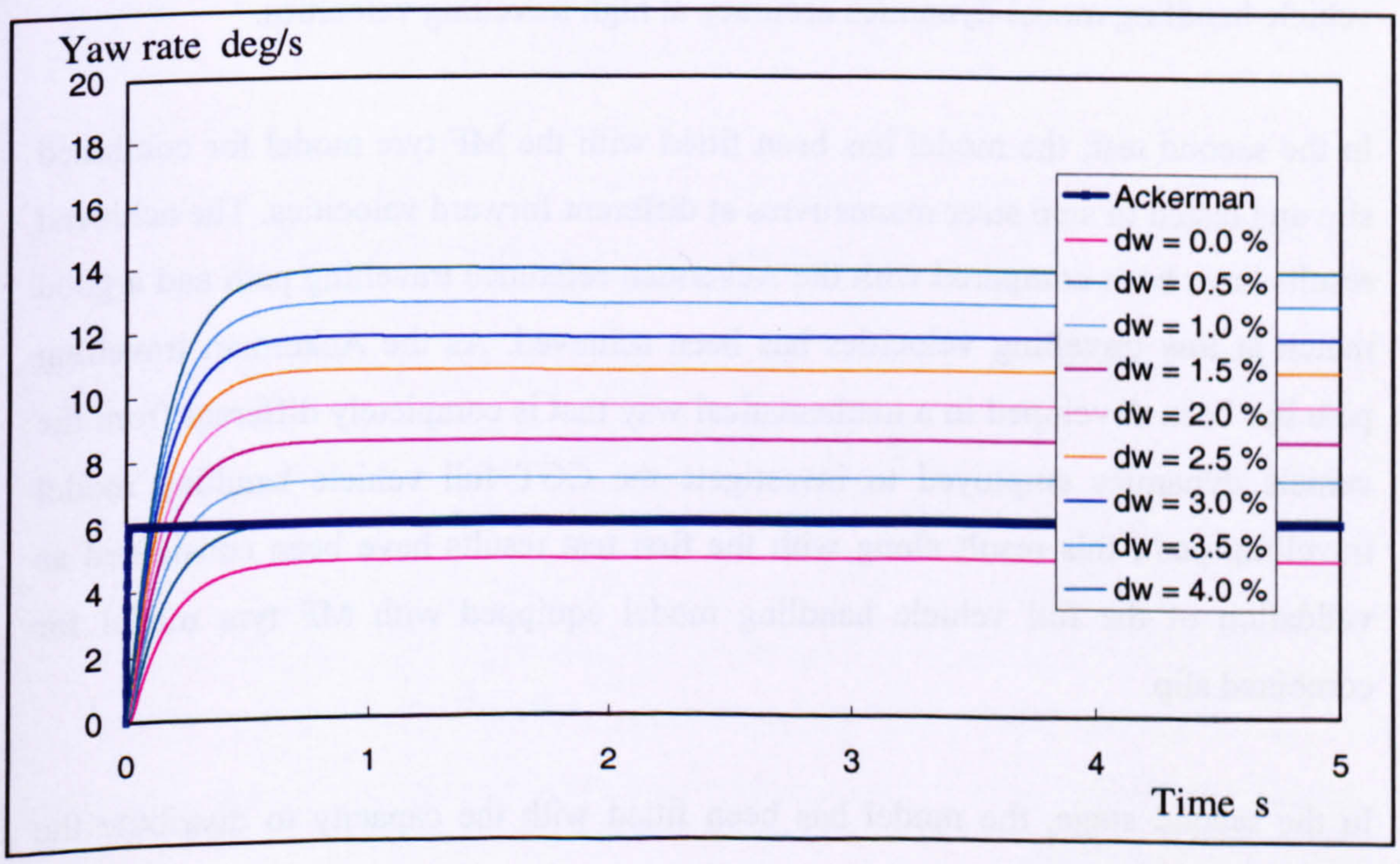

Fig (5.31) Ferrari yaw rate after 0.965 degrees step steer at 20 m/s forward velocity and different $d\omega$

5.8 Conclusions

In this Chapter, the CGT half vehicle handling model has been upgraded to the CGT full vehicle handling model and equipped with the capacity to regulate the driven wheel speeds. This work has been carried out in two main stages.

In the first stage, the CGT half vehicle handling model, developed in Chapter 3, has been upgraded to the CGT full vehicle handling model that takes into account the effect of lateral and longitudinal load transfer on tyre vertical loads. It has been satisfactorily tested using two different procedures.

In the first test, the model has been fitted with the reviewed linear tyre model and the results of Buick and Ferrari vehicle step steer manoeuvres have been compared with the CGT half vehicle handling model results, where a good match has been achieved due to the reviewed linear tyre model insensitivity to the variation of both longitudinal and vertical tyre forces. Accordingly, this test only proves the CGT full vehicle handling model dynamics accuracy at high travelling velocities.

In the second test, the model has been fitted with the MF tyre model for combined slip and tested in step steer manoeuvres at different forward velocities. The achieved results have been compared with the Ackerman reference travelling path and a good match at low travelling velocities has been achieved. As the Ackerman travelling path has been developed in a mathematical way that is completely different from the vehicle dynamics employed to investigate the CGT full vehicle handling model travelling path, this result along with the first test results have been considered as validation of the full vehicle handling model equipped with MF tyre model for combined slip.

In the second stage, the model has been fitted with the capacity to distribute the driven wheel rotational speeds (WSD). These speeds were varied with a rotational speed percentage difference ($d\omega$) around their nominal rotational speed, extracted from the vehicle nominal forward velocity. This WSD model has been used to prove

the wheel speed distribution system's capacity to influence both the yaw rate and travelling path of the vehicle.

The WSD model has been tested under step steer manoeuvres at different forward velocities and different $d\omega$. The travelling path and yaw rate results have been compared to the reference Ackerman travelling path and yaw rates. At the start of the manoeuvre, the higher $d\omega$ showed travelling path and yaw rate closer to the Ackerman travelling path and yaw rate, due to the high yaw moment initially required to follow the Ackerman yaw rate. As the yaw moment demand reached steady state, a far lower $d\omega$ was required to match the reference Ackerman travelling path and yaw rate.

As optimum dω value changes during manoeuvres, a yaw rate controller is considered necessary to control the variation of the driven wheel speeds. This controller is developed, tested and fitted to the CGT full vehicle handling model as described in the next Chapter.

Chapter 6

Wheel Speed Distribution Controller

6.1 Introduction

The driven wheel speed variation effect on vehicle handling performance has been proven through simulation in Chapter 5. Also the need for a controller to regulate the wheel speed distribution is demonstrated. In this Chapter, a WSD yaw rate controller with control constraint is developed and tested. The WSD yaw rate controller is based on comparison between the vehicle yaw rate predicted by the WSD onboard model and the reference Ackerman yaw rate, developed in Chapter 4. The WSD controller has been planned as a yaw rate controller because longitudinal forces resulting from wheel speed variation directly generate a yaw moment about the vehicle CG.

The developed WSD controller is a feedforward yaw rate controller that employs finite difference approximation equations in the time domain and inverse dynamics under the Model Predictive Control (MPC) strategy to determine the optimal vehicle wheel speed distribution. The WSD controller development and integration with the WSD vehicle handling model to form the WSDC vehicle handling model is presented in this chapter. Also, the WSDC simulation results for the Buick and Ferrari vehicles are presented. Finally the improvements of vehicle handling performance due to the WSDC are investigated.

6.2 Controller Development

The WSD controller has been designed to take full advantage of the CGT modelling technique, the finite difference approximation technique, inverse dynamics and the high model processing speed to turn the controller development into an efficient product.

For the current controller the yaw rate of the vehicle, predicted by the onboard model, is compared to the reference Ackerman yaw rate developed in Chapter 5. The yaw rate error is then used to evaluate the extra yaw moment required to minimize the yaw rate error. This moment is used to determine the longitudinal force variation of the right and left driven wheels from their original values, in order to achieve the required correction.

The kcal routine is used to determine the longitudinal slip k values required to generate these tyres longitudinal forces. Subsequently, the calculated k value is used together with the wheel translation velocities in their local x coordinates to calculate the driven wheel rotational speeds that would achieve the required yaw rate correction. Figure (6.1) shows the developed controller block diagram for a rear wheel driven vehicle.

The Ackerman reference yaw rate for a time frame $\dot{\theta}_A$ is given as:-

$$\dot{\theta}_A = \frac{\arctan\left(u_v \Delta t\left(\frac{\tan(\delta_F)}{L}\right)\right)}{\Delta t} \tag{6.1}$$

The yaw rate error, $\dot{\theta}_e$, that is to be minimised is the difference between the reference Ackerman yaw rate and the predicted time frame final yaw rate. This error is given as:-

$$\dot{\theta}_e = \dot{\theta}_A - \dot{\theta}_1 \tag{6.2}$$

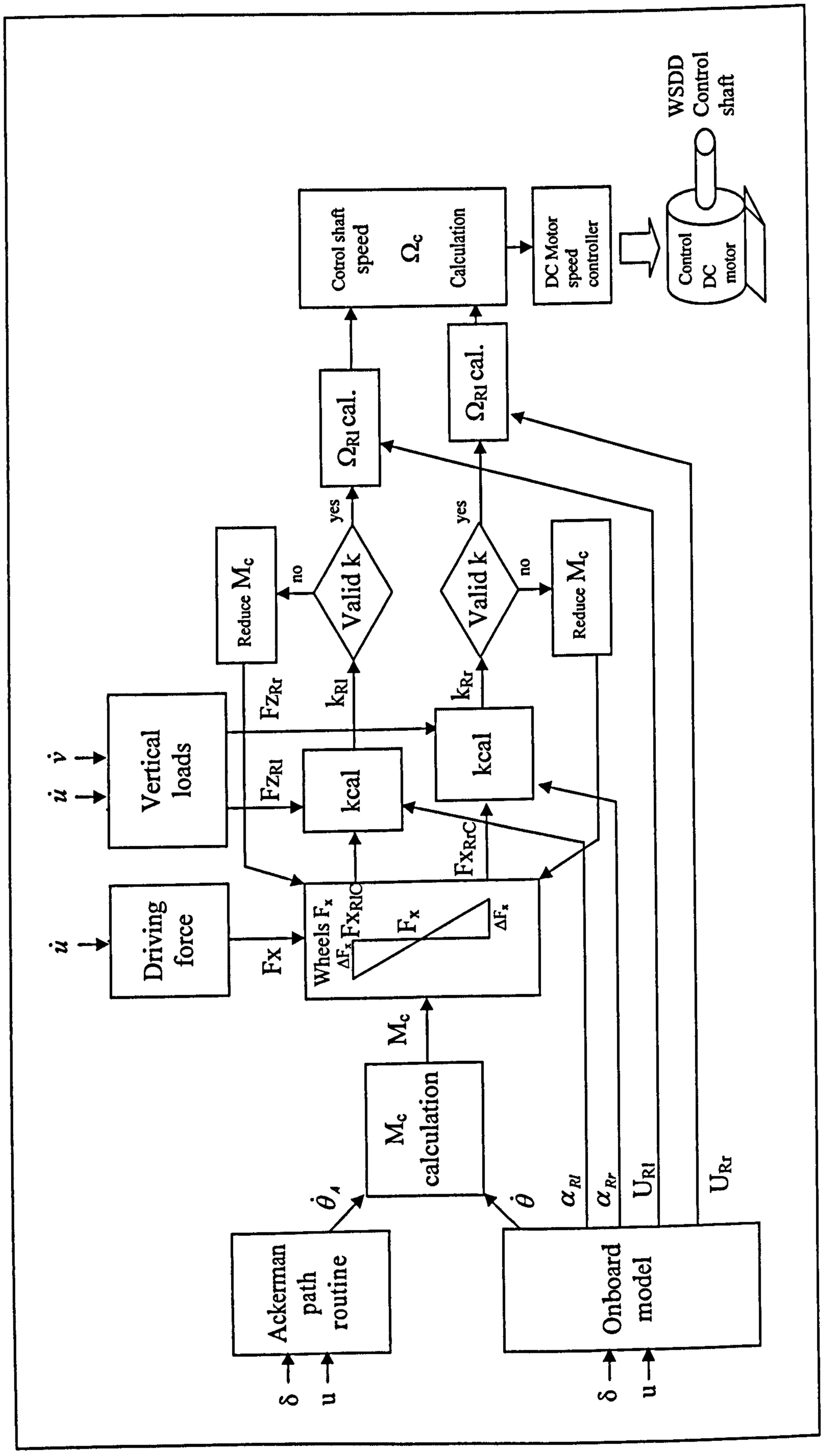

Fig (6.1) The WSD yaw moment controller block diagram

To correct this yaw rate error during the time frame, a finite difference approximation to the kinematics equation has been employed. The required correction yaw rate acceleration, $\ddot{\theta}_C$, is given as:-

$$\ddot{\theta}_C = \left(\frac{\dot{\theta}_e}{\Delta t}\right) \tag{6.3}$$

Using inverse dynamics, the control moment, M_C, required to generate this correction acceleration is given as:-

$$M_C = I\ddot{\theta}_C \tag{6.4}$$

The longitudinal force (ΔF_x) required to be added to the right driven wheel longitudinal force and subtracted from the longitudinal force of the left driven wheel with the aim of generating the required correcting control moment at the vehicle CG is given as:-

$$\Delta F_x = \left(\frac{M_C}{t}\right) \tag{6.5}$$

The vehicle traction force at the CG is the sum of driven wheel traction forces. As the right and left driven wheels traction forces are equal for conventional vehicles, they are given as:-

$$F_{xRr} = \left(\frac{F_{xCG}}{2}\right) \tag{6.6}$$

$$F_{xRl} = \left(\frac{F_{xCG}}{2}\right) \tag{6.7}$$

Through the control process, the traction forces of conventional vehicles driven wheels are altered to produce the required control moment as follows:-

$$F_{xRrC} = F_{xRr} + \Delta F_x \tag{6.8}$$

$$F_{xRlC} = F_{xRl} - \Delta F_x \tag{6.9}$$

Where:-

F_{xRrC} The rear right driven wheel traction force with control ΔF_x

F_{xRlC} The rear left driven wheel traction force with control ΔF_x

Each driven wheel traction force is input along with its slip angle to the kcal routine to calculate the corresponding longitudinal slip k value. Then, the longitudinal slip value, k, is used with the driven wheel translation velocity in the wheel local x coordinate to calculate the wheel control rotational speed.

For the MF tyre, model the slip value for the driven rear wheels is given as:-

$$k_{Rr} = -\left(\frac{U_{RrS}}{U_{Rr1}}\right) \tag{6.10}$$

$$k_{Rl} = -\left(\frac{U_{RlS}}{U_{Rl1}}\right) \tag{6.11}$$

Where:-

k_{Rr} The rear right wheel longitudinal slip

k_{Rl} The rear left wheel longitudinal slip

U_{RrS} The rear right wheel longitudinal slip velocity

U_{RlS} The rear left wheel longitudinal slip velocity

The slip velocities are evaluated as follows:-

$$U_{RrS} = U_{Rr1} - \Omega_{Rr} R_o \tag{6.12}$$

$$U_{RlS} = U_{Rl1} - \Omega_{Rl} R_o \tag{6.13}$$

Where: -

U_{Rr1}	Rear right wheel longitudinal velocity at the end of time the frame
U_{Rl1}	Rear right wheel longitudinal velocity at the end of time the frame
Ω_{Rr}	Rear right wheel rotation speed
Ω_{Rl}	Rear left wheel rotation speed
R_o	Unloaded tyre radius

Substituting for the slip velocities, the driven wheel longitudinal slip values are given as follows:-

$$k_{Rr} = \frac{(\Omega_{Rr} R_o - U_{Rr1})}{U_{Rr1}} \tag{6.14}$$

$$k_{Rl} = \frac{(\Omega_{Rl} R_o - U_{Rl1})}{U_{Rl1}} \tag{6.15}$$

Rearranging the driven wheel longitudinal slip equations, the driven wheel speeds are evaluated as follows:-

$$\Omega_{Rr} = U_{Rr1}\left(\frac{1+k_{Rr}}{R_o}\right) \tag{6.16}$$

$$\Omega_{Rl} = U_{lr1}\left(\frac{1+k_{Rl}}{R_o}\right) \tag{6.17}$$

The driven wheel speeds evaluated by the controller are then applied to the driven wheels to influence the vehicle yaw rate in a feedforward style.

6.3 Controller Constraint

As the vehicle yaw rate error at some point in a manoeuvre might require a longitudinal correction force that is beyond the capacity of the tyre of a particular

drive wheel, a controller constraint has been introduced. This over demand condition is detected within the kcal routine. In case of over demand, it turns out that there is no corresponding k value for the demanded tyre longitudinal force and slip angle pair. This is due to the shape of the tyre characteristic surface discussed in Chapter 4. In this over demand condition, the controller has been developed to reduce the demanded control moment M_C in steps until the corresponding tyre demanded forces fit within the applicable tyre force range. Thus, the maximum possible yaw rate correction is achieved.

6.4 Controller Testing

Although the MPC controller has many benefits, it does have drawbacks in terms of controller tuning and performance analysis. A systematic tuning and analysis of the MPC controller stability and robustness is not possible, [76]. Accordingly, the controller performance has been evaluated through simulation of manoeuvres for the Buick vehicle. The Buick has been selected, as it is higher in weight and moment of inertia than the Ferrari, leading to its yaw control being a more challenging task for the controller.

To test the developed WSD controller's ability to enhance the vehicle yaw rate response, the Buick vehicle WSDC model yaw rate results have been obtained at 30 m/s forward velocity in a lane change manoeuvre with 3 seconds manoeuvre time (mt) and maximum steering angle amplitude (md) of 2 degrees. The yaw rate results for the controlled manoeuvre have been compared with those for the non controlled manoeuvre and the reference Ackerman yaw rate, Fig (6.2).

The results show the high yaw rate correction achieved by the WSD model fitted with the controller (WSDC). The achieved yaw rate results are very close to the derived Ackerman yaw rate. Accordingly, the controller has been considered satisfactory for performing its main task of demonstrating the WSD potential to improve vehicle handling performance. In the following stage, the WSDC effect on vehicle handling performance is investigated.

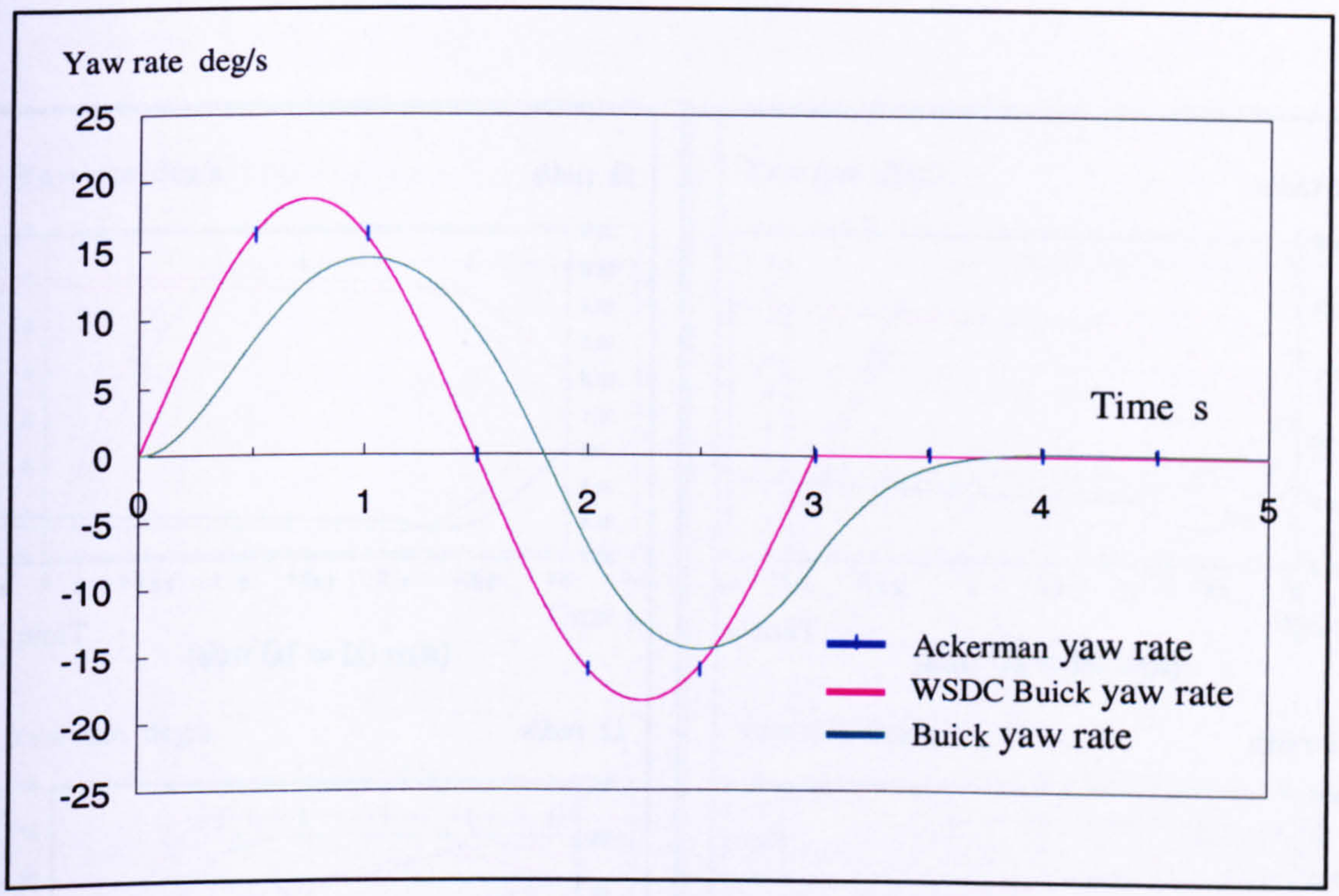

Fig (6.2) Yaw rate results for Buick lane change manoeuvre

6.5 Model Results

To investigate the vehicle handling performance improvement due to the WSDC, the simulation results of the Buick and Ferrari WSDC vehicle handling models have been obtained for step steer and lane change manoeuvres. The manoeuvres results have been compared to the non controlled model manoeuvres and the reference Ackerman yaw rate and path.

In the first test the Buick and Ferrari WSDC vehicle handling models have been tested under a step steer manoeuvre. In this manoeuvre the vehicle models have been step steered from 0 to 2 degrees following a quarter of a sine wave in 1 second. The controlled and non controlled driven wheel rotational speeds have been obtained at different forward velocities, 10, 20 and 30 m/s for the Buick and Ferrari, Fig (6.3) and Fig (6.4) respectively.

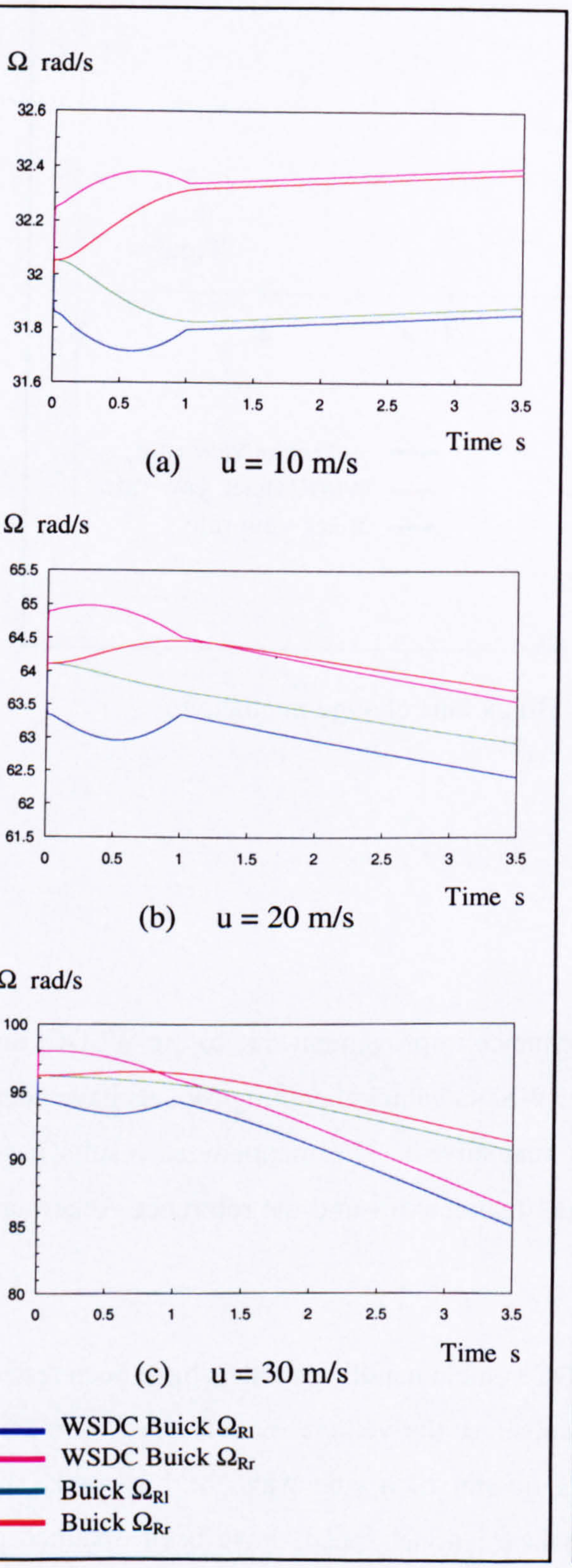

Fig (6.3) Driven wheel speeds of Buick in step steer manoeuvre

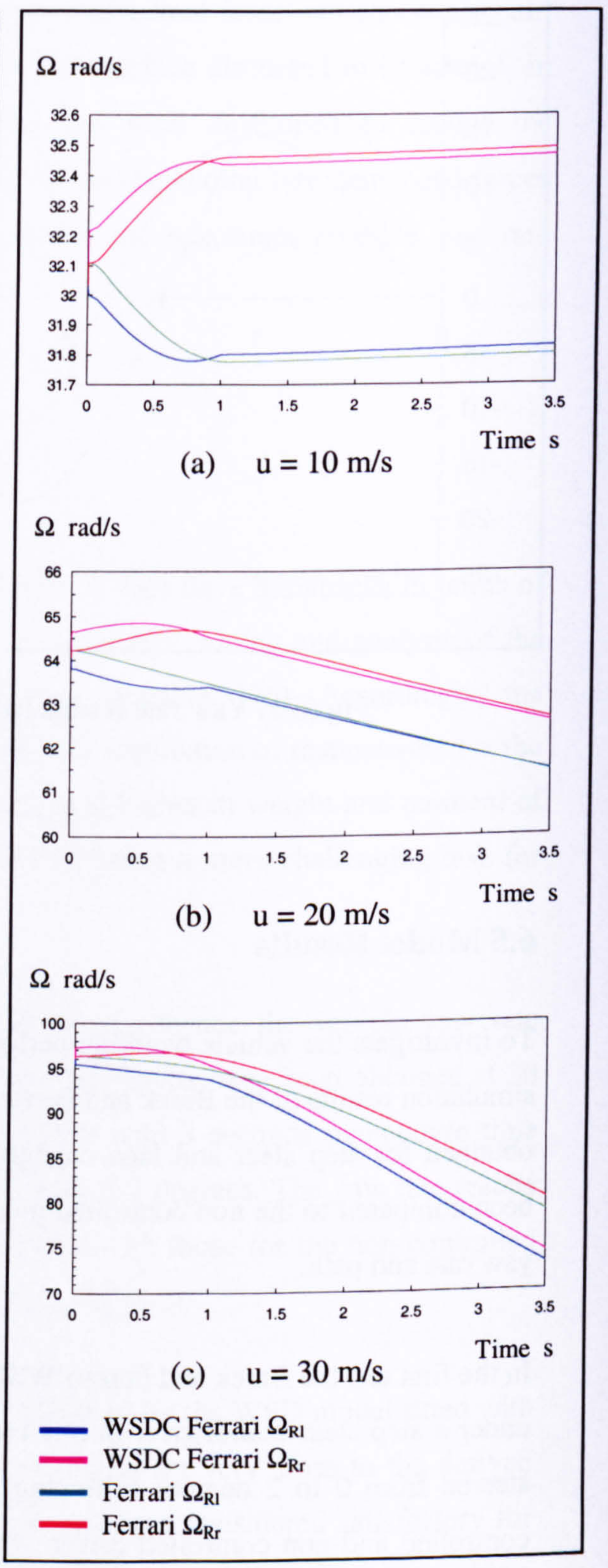

Fig (6.4) Driven wheel speeds of Ferrari in step steer manoeuvre

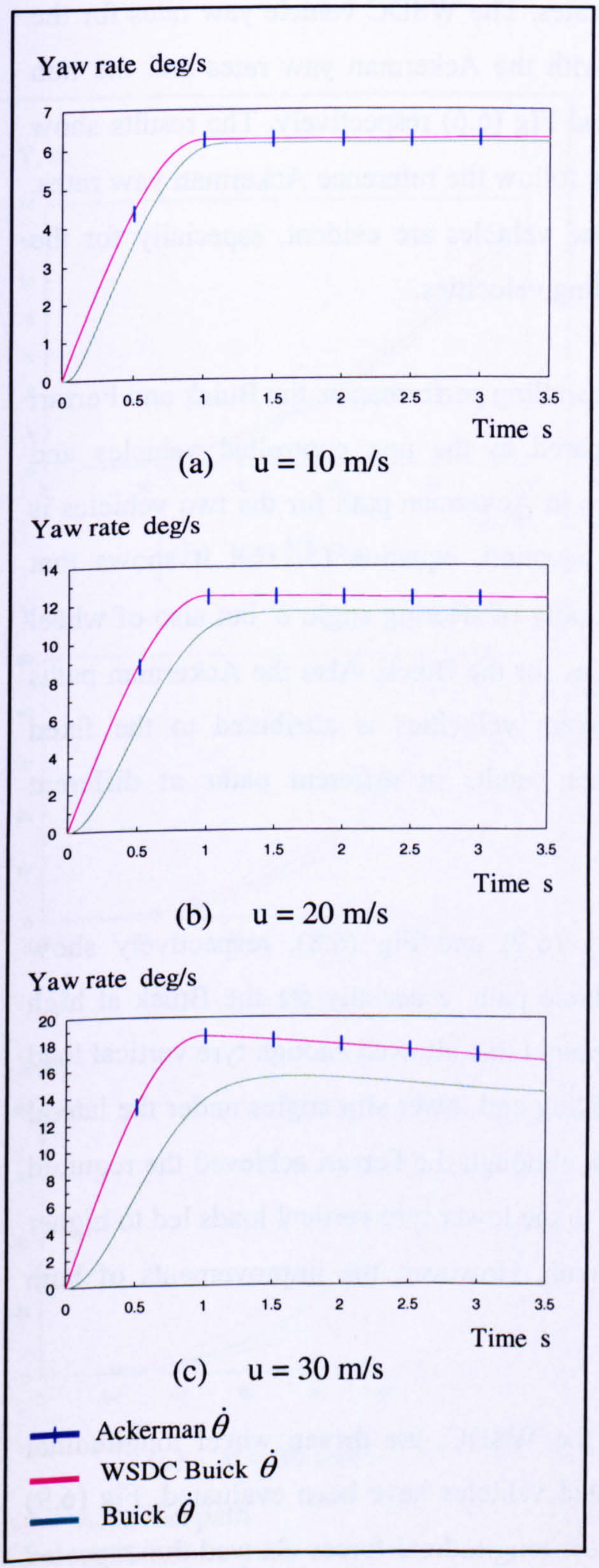

Fig (6.5) Yaw rate response of Buick in step steer manoeuvre

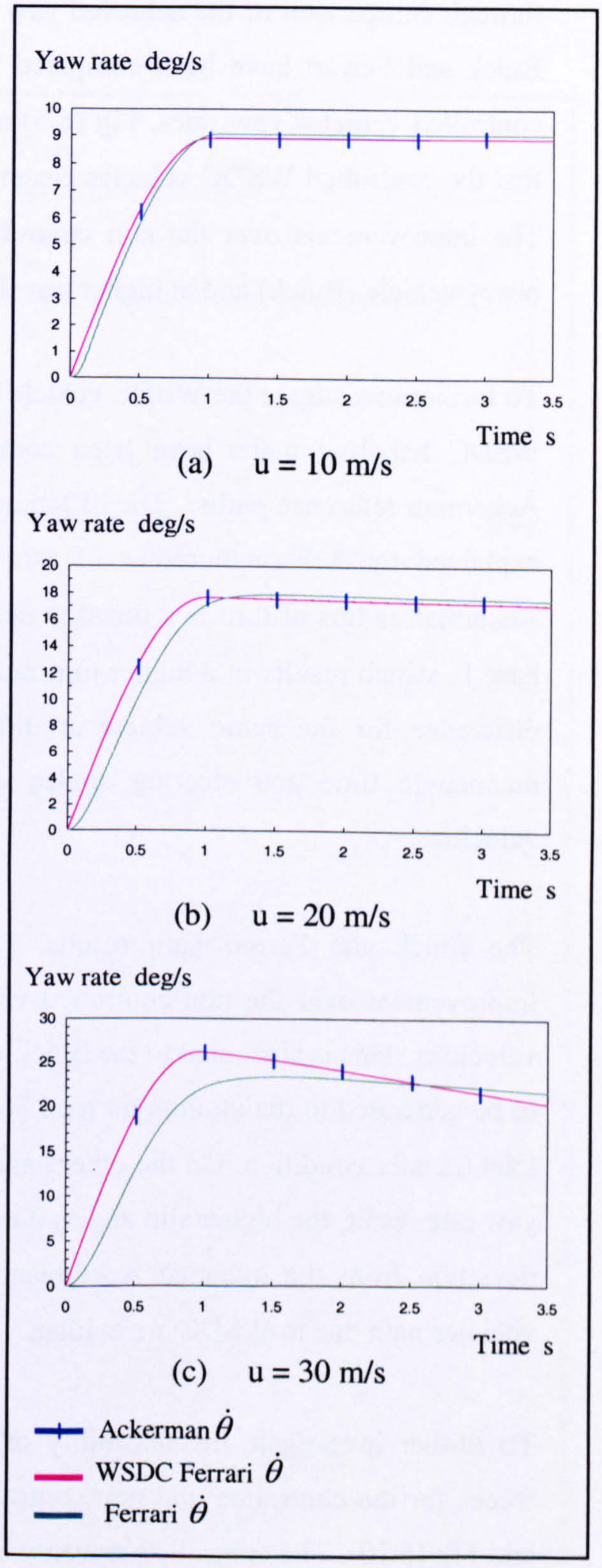

Fig (6.6) Yaw rate response of Ferrari in step steer manoeuvre

The effect of the controlled driven wheel rotational speeds has been investigated through comparison of the achieved yaw rates. The WSDC vehicle yaw rates for the Buick and Ferrari have been compared with the Ackerman yaw rates and the non controlled vehicles yaw rates, Fig (6.5) and Fig (6.6) respectively. The results show that the controlled WSDC vehicles closely follow the reference Ackerman yaw rates. The improvements over the non controlled vehicles are evident, especially for the heavy vehicle (Buick) and at higher travelling velocities.

To further investigate the WSDC vehicle handling performance, the Buick and Ferrari WSDC handling paths have been compared to the non controlled vehicles and Ackerman reference paths. The difference in Ackerman path for the two vehicles is explained by Ackerman radius of turn equation, equation (5.116). It shows that Ackerman radius of turn is a function not only of steering angle δ but also of wheel base L, which results in a higher turn radius for the Buick. Also the Ackerman paths difference for the same vehicle at different velocities is attributed to the fixed manoeuvre time and steering angles that results in different paths at different velocities.

The Buick and Ferrari path results, Fig (6.7) and Fig (6.8), respectively show improvement over the non controlled vehicle path, especially for the Buick at high velocities. This is attributed to the Buick weight that allowed enough tyre vertical load to be generated to maintain good road holding and lower slip angles under the lateral load transfer condition. On the other hand, although the Ferrari achieved the required yaw rate result, the higher slip angles due to the lower tyre vertical loads led to higher deviation from the intended Ackerman path. However, the improvements of both vehicles path due to WSDC are evident.

To further investigate the feasibility of the WSDC, the driven wheel longitudinal forces for the controlled and non controlled vehicles have been evaluated, Fig (6.9) and Fig (6.10). The controlled driven wheel longitudinal forces showed the expected symmetry with respect to the non controlled vehicle forces. The wheel forces were capable of seamlessly moving between positive and negative values. As standard tyre longitudinal force capacity ranges symmetrically between positive and negative

values, the results show good employment of the tyre force range. Consequently, the generated yaw moment has not over loaded either the outer or inner driven wheel

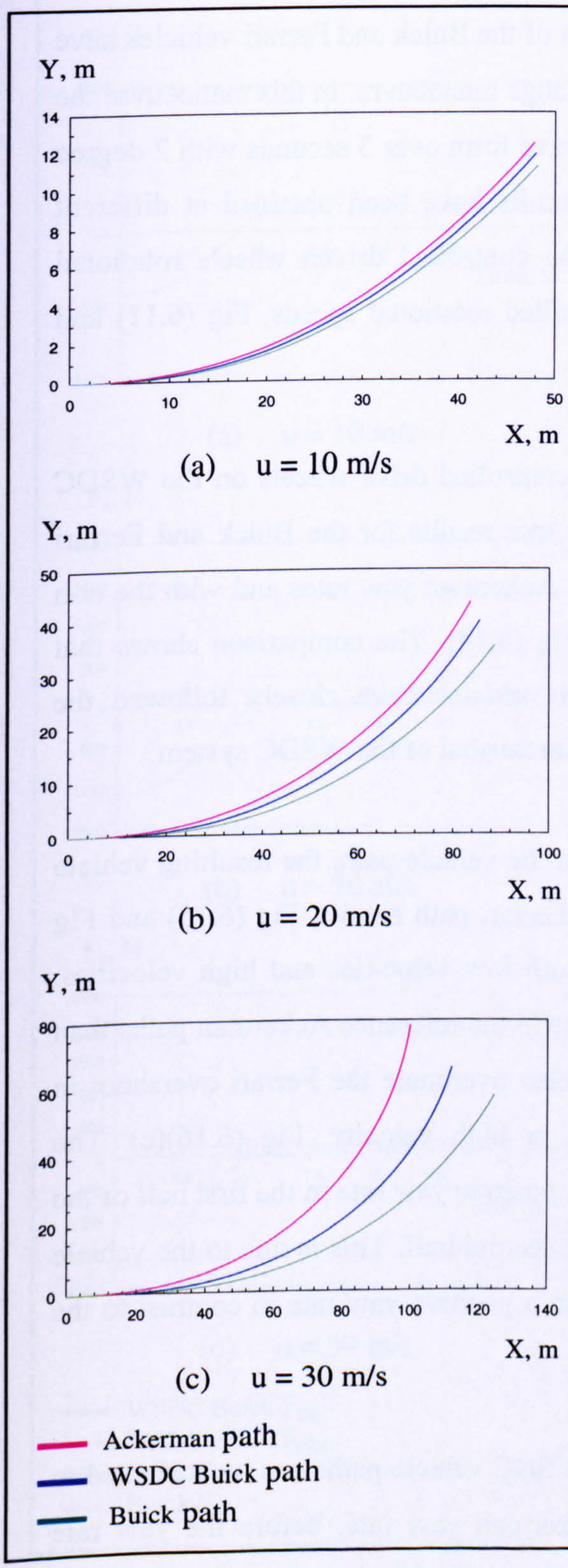

Fig (6.7) Buick path in step steer manoeuvre

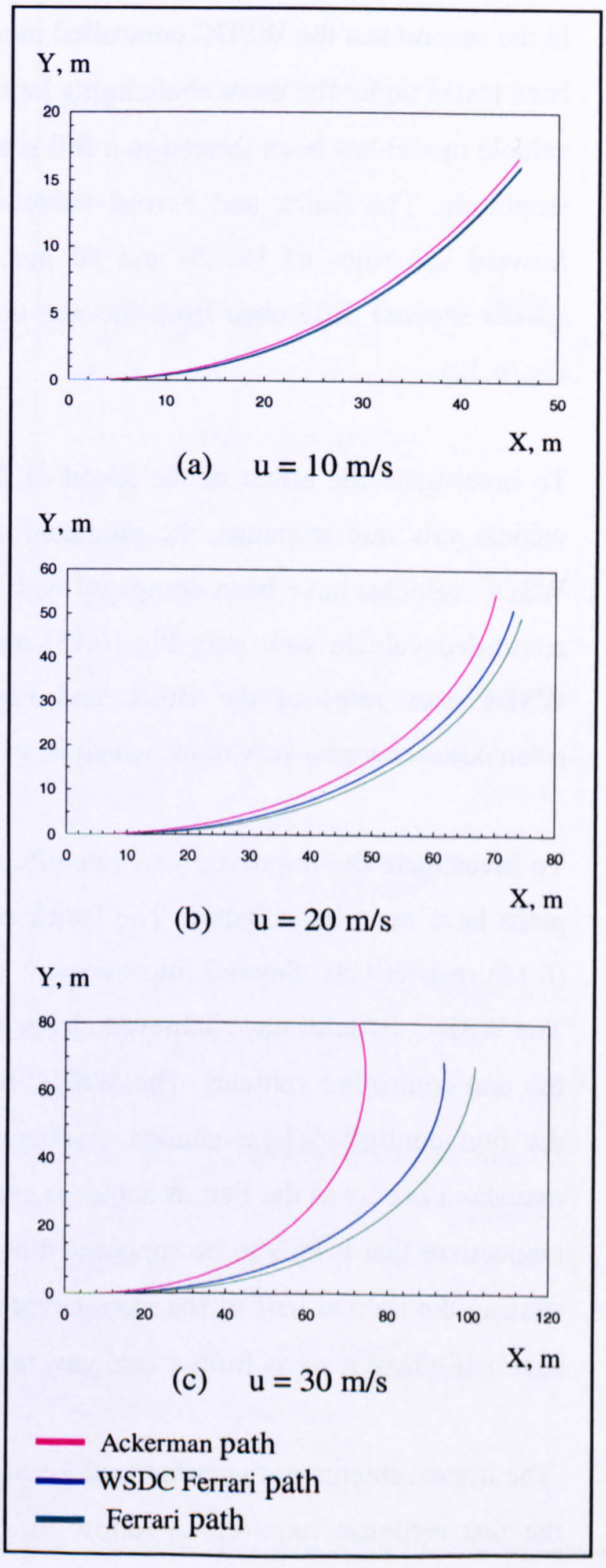

Fig (6.8) Ferrari path in step steer manoeuvre

force. Also the smooth force pattern proved the ease of application to the driven wheels as sharp force spikes would not be desirable due to tyre force lag characteristics.

In the second test the WSDC controlled models of the Buick and Ferrari vehicles have been tested under the more challenging lane change manoeuvre. In this manoeuvre the vehicle model has been steered in a full sine wave form over 3 seconds with 2 degree amplitude. The Buick and Ferrari vehicles results have been obtained at different forward velocities of 10, 20 and 30 m/s. The controlled driven wheels rotational speeds showed difference from the non controlled rotational speeds, Fig (6.11) and Fig (6.12).

To investigate the effect of the speed of the controlled drive wheels on the WSDC vehicle yaw rate response, the predicted yaw rate results for the Buick and Ferrari WSDC vehicles have been compared with the Ackerman yaw rates and with the non controlled vehicle yaw rate, Fig (6.13) and Fig (6.14). The comparison shows that WSDC yaw rates of the Buick and Ferrari vehicles have closely followed the reference Ackerman yaw rates, which is an ultimate goal of the WSDC system.

To investigate the improved yaw rate effect on the vehicle path, the resulting vehicle paths have been investigated. The Buick and Ferrari path results, Fig (6.15) and Fig (6.16) respectively showed improvement at both low velocities and high velocities. The WSDC vehicles have achieved closer paths to the reference Ackerman paths than the non controlled vehicles. The WSDC has also overcome the Ferrari overshoot in the non controlled lane change manoeuvres at high velocity, Fig (6.16)(c). The overshoot occurs as the Ferrari achieves a high positive yaw rate in the first half of the manoeuvre that it fails to be suppressed in the second half. This is due to the vehicle starting the second half of the manoeuvre from a positive yaw rate in contrast to the first half where it starts from a zero yaw rate.

The improvements in the Buick and Ferrari WSDC vehicle paths can be attributed to the fast response required to follow the Ackerman yaw rate, before the yaw rate difference gets large and requires larger moments and so larger tyre forces, that might not be achievable. The achieved WSDC vehicle path results for lane change

manoeuvres can be considered a further assurance of the functionality of the WSDC system.

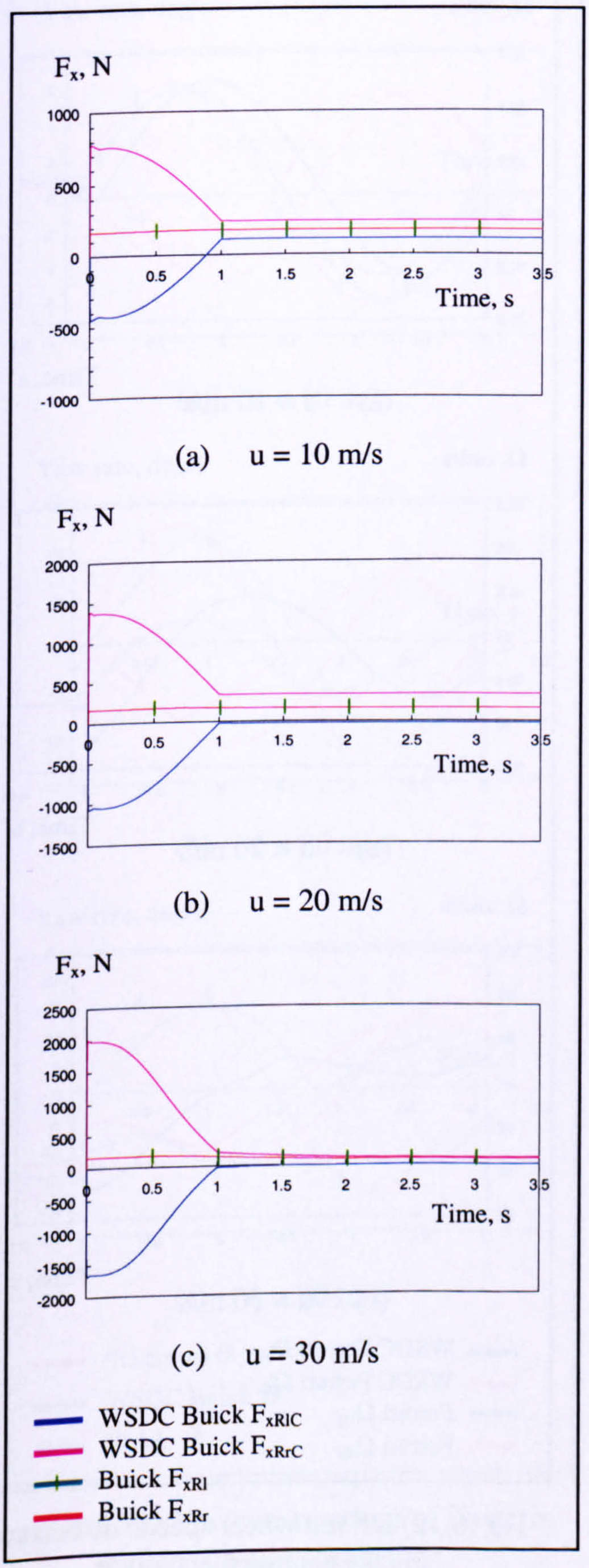

Fig (6.9) Driven wheels F_x of Buick in step steer manoeuvre

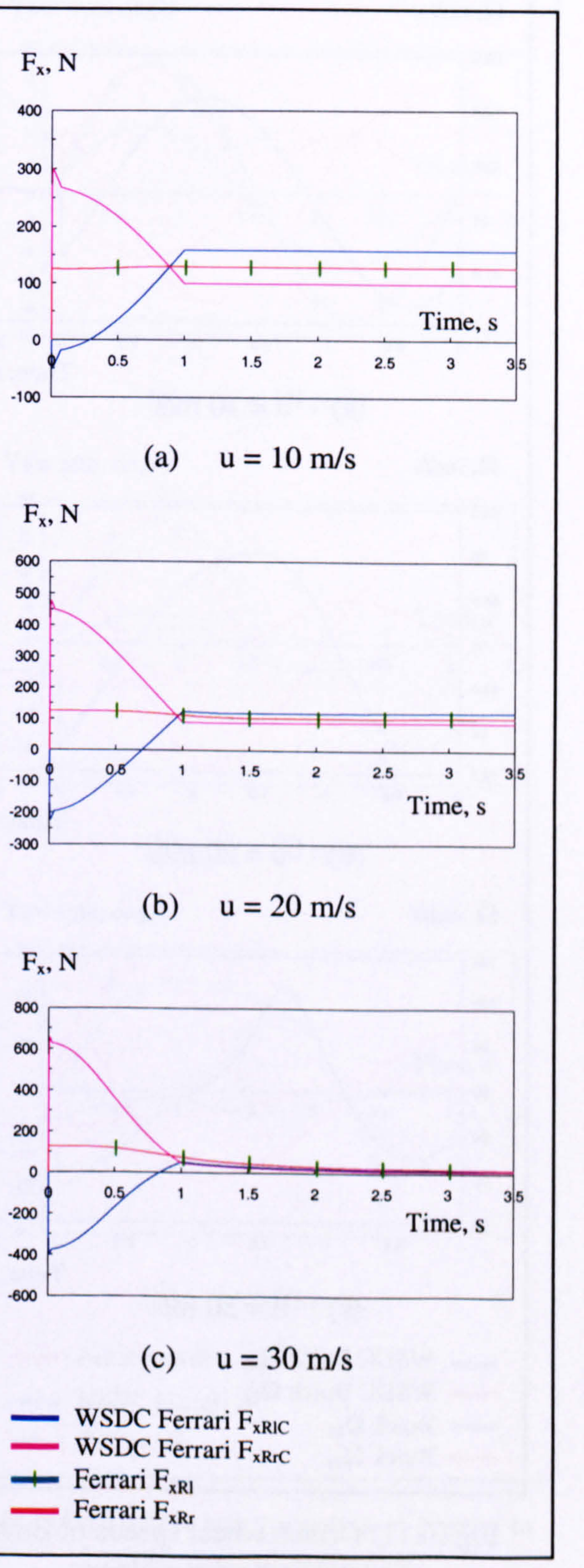

Fig (6.10) Driven wheels F_x of Ferrari in step steer manoeuvre

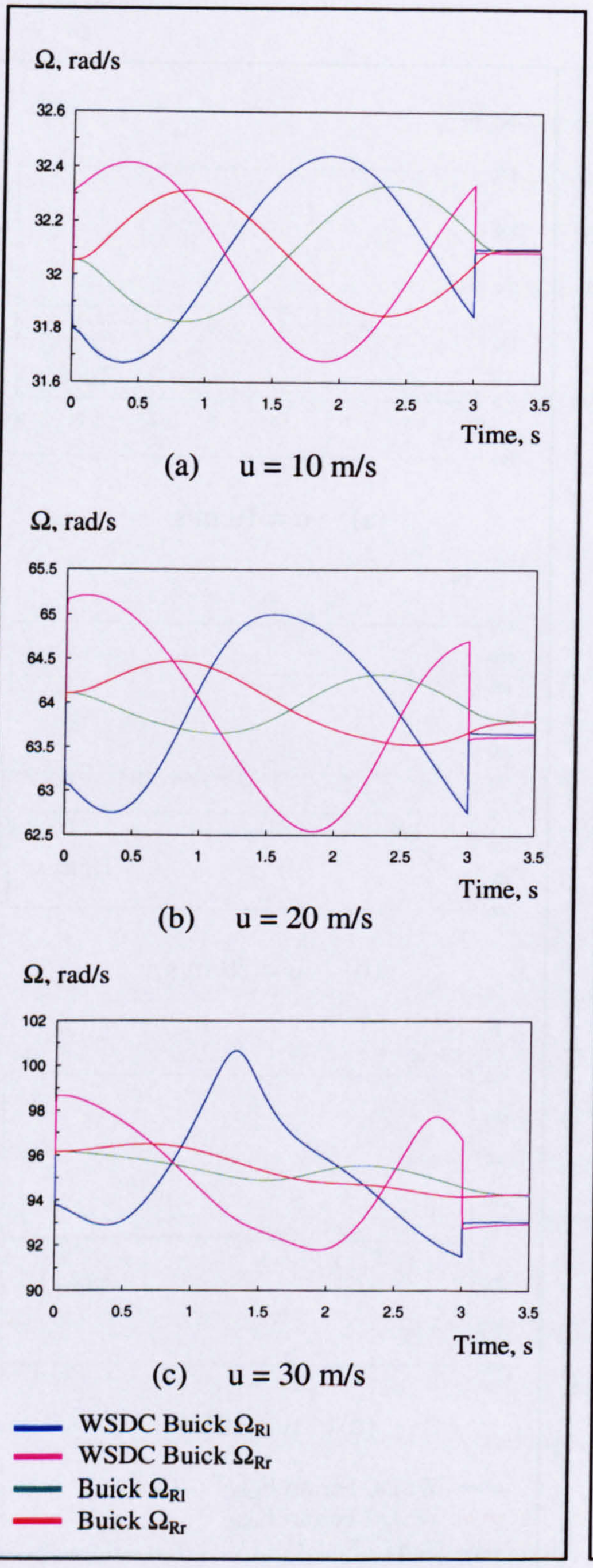

Fig (6.11) Driven wheel speeds of Buick in lane change manoeuvre

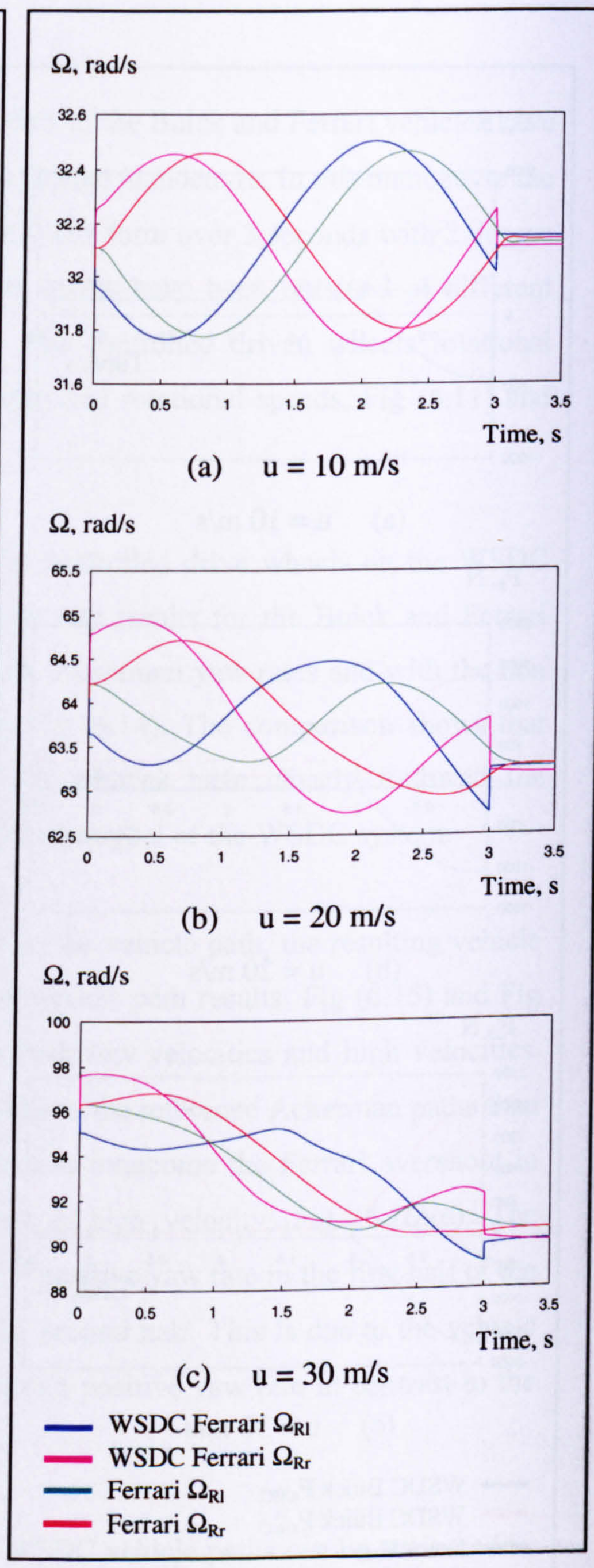

Fig (6.12) Driven wheel speeds of Ferrari in lane change manoeuvre

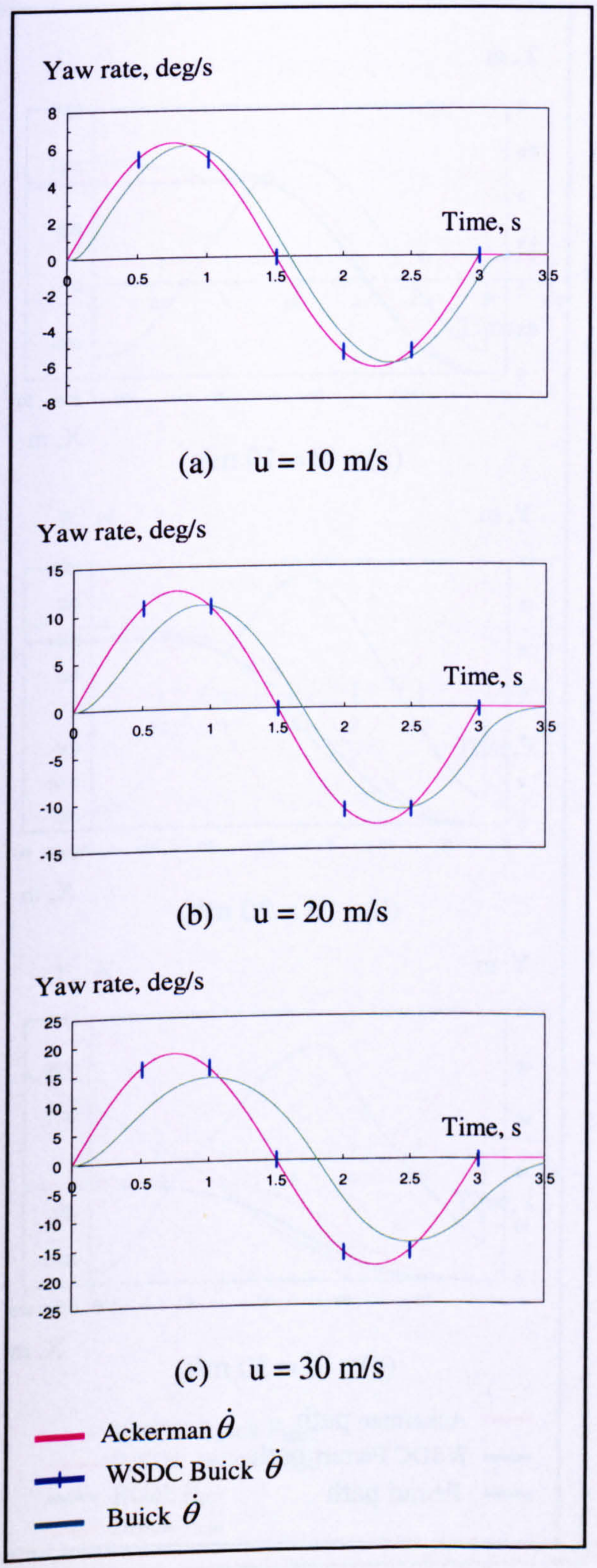

Fig (6.13) Yaw rate response of Buick in lane change manoeuvre

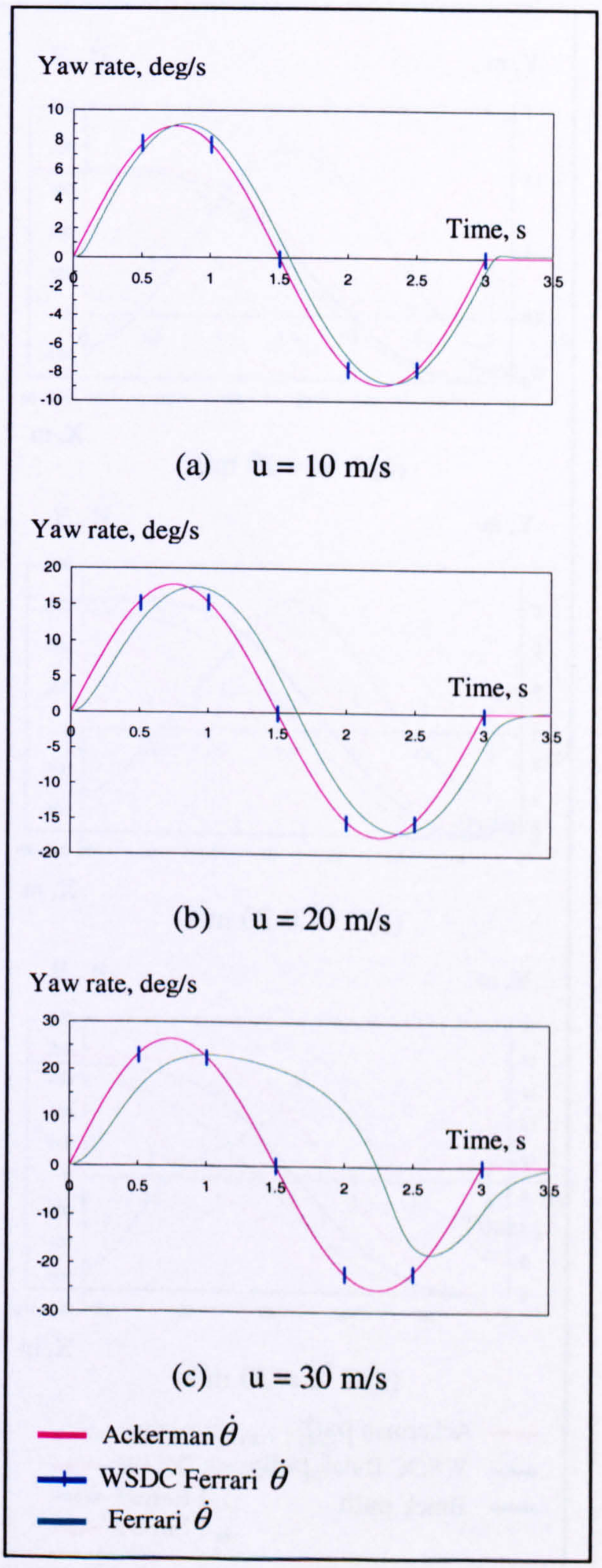

Fig (6.14) Yaw rate response of Ferrari in lane change manoeuvre

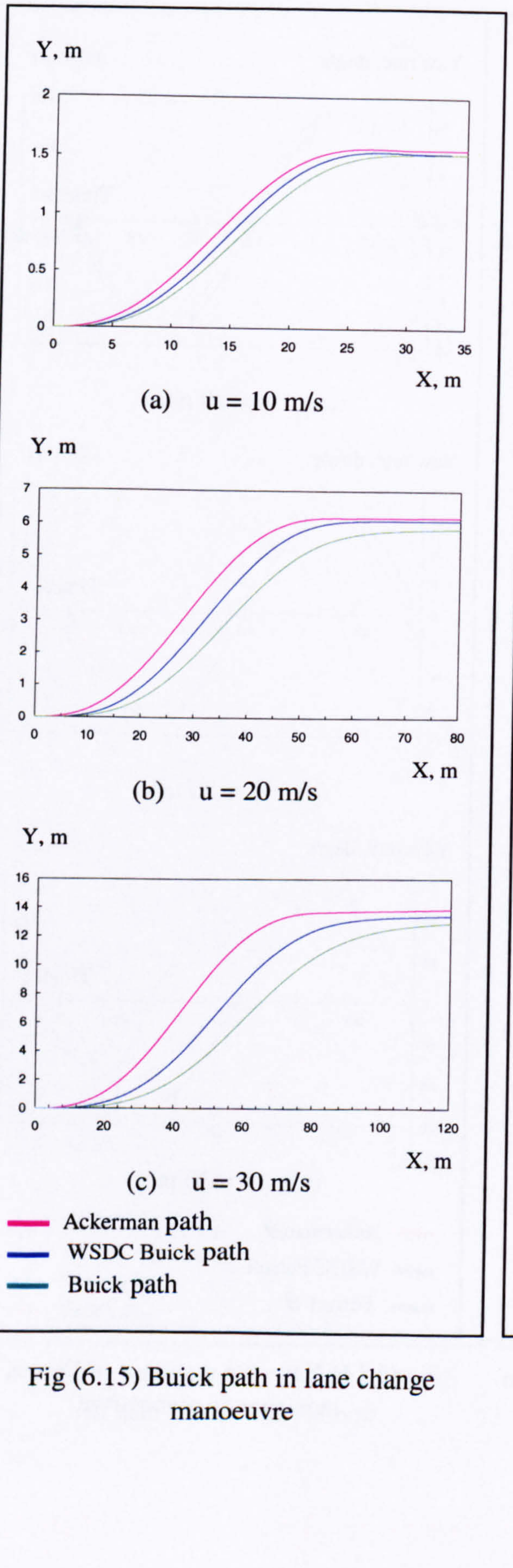

Fig (6.15) Buick path in lane change manoeuvre

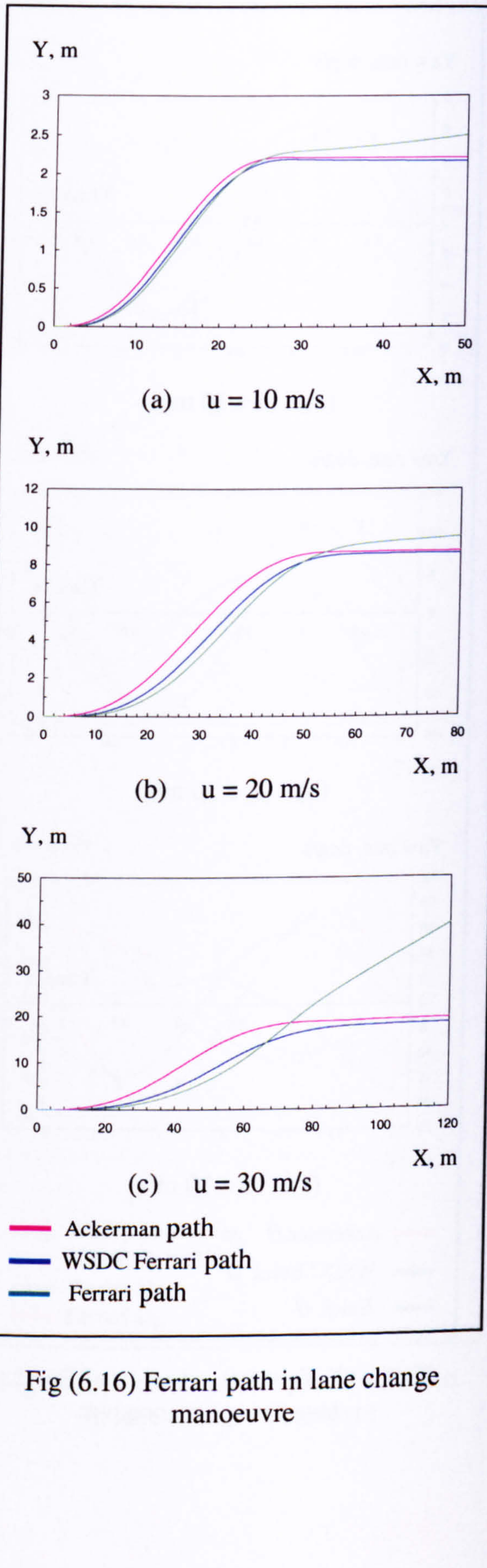

Fig (6.16) Ferrari path in lane change manoeuvre

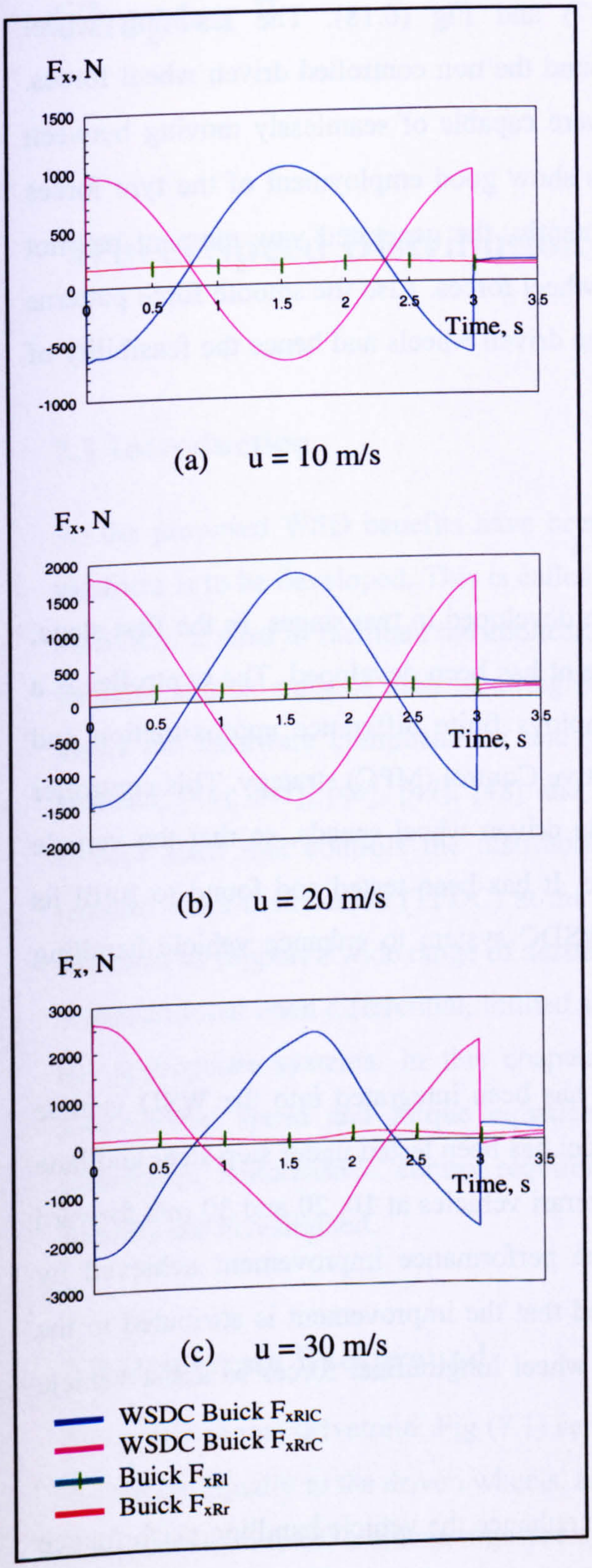

Fig (6.17) Driven wheels F_x of Buick in lane change manoeuvre

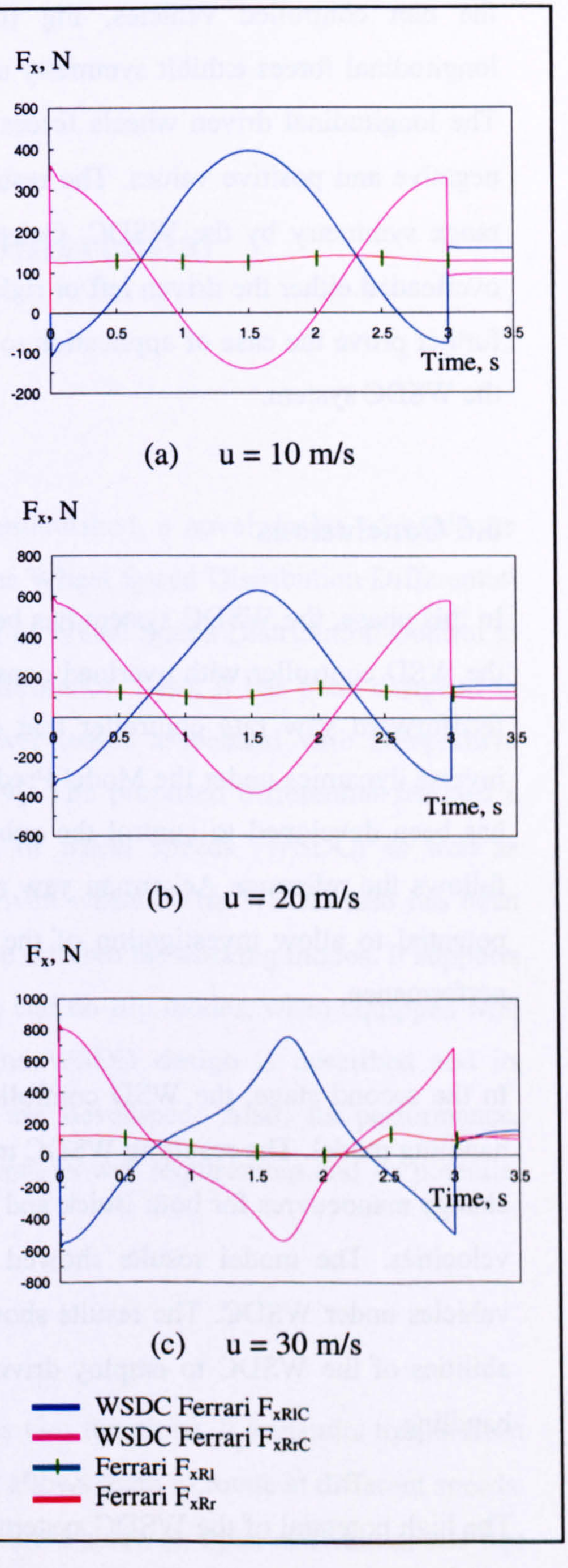

Fig (6.18) Driven wheels F_x of Ferrari in lane change manoeuvre

To further investigate the WSDC feasibility, the applied driven wheel longitudinal forces have been investigated and compared to the driven wheel longitudinal forces of the non controlled vehicles, Fig (6.17) and Fig (6.18). The resulting wheel longitudinal forces exhibit symmetry around the non controlled driven wheel forces. The longitudinal driven wheels forces were capable of seamlessly moving between negative and positive values. The results show good employment of the tyre forces range symmetry by the WSDC. Consequently, the generated yaw moment has not overloaded either the driven left or right wheel forces. Also the smooth force patterns further prove the ease of application to the driven wheels and hence the feasibility of the WSDC system.

6.6 Conclusions

In this phase, the WSDC system has been developed in two stages. In the first stage, the WSD controller with overload constraint has been developed. The controller is a feedforward yaw rate controller that employs finite difference approximation and inverse dynamics under the Model Predictive Control (MPC) strategy. This controller has been developed to control the vehicle driven wheel speeds, so that the vehicle follows the reference Ackerman yaw rate. It has been tested and found to fulfil its potential to allow investigation of the WSDC system to enhance vehicle handling performance.

In the second stage, the WSD controller has been integrated into the WSD vehicle handling model. The resulting WSDC model has been tested under step steer and lane change manoeuvres for both Buick and Ferrari vehicles at 10, 20 and 30 m/s forward velocities. The model results showed the performance improvement achieved by vehicles under WSDC. The results showed that the improvement is attributed to the abilities of the WSDC to employ driven wheel longitudinal forces to assist vehicle handling.

The high potential of the WSDC system to enhance the vehicle handling performance has been demonstrated. However, as there is currently no feasible hardware that would support WSDC, the next phase of the research was to design suitable WSDC hardware as reported in Chapter 7.

Chapter 7

Wheel Speed Distribution Differential

7.1 Introduction

As the proposed WSD benefits have been established, a novel design of hardware platform is to be developed. This is called the Wheel Speed Distribution Differential (WSDD). It aims to facilitate the application of Wheel Speed Distribution Control to vehicles and so enhance their handling performance. Also, it has been designed to avoid the hardware complications and power losses associated with competitive systems, [44], [45], [46], [47], [48] and [49]. The proposed differential features a control shaft that controls the distribution of wheel speeds (WSDC) as well as traction force distribution (TFDC) at the driven wheels. The WSDD also has been designed to support a wide range of desirable differential working modes. It supports a conventional open differential, limited slip and no slip modes, when equipped with the appropriate systems. In this chapter the WSDD design is described and its fundamental speed and torque equations are developed. Also, its performance, production, maintenance, control requirements, power requirement and its potential benefits are investigated.

7.2 Drivetrain Background

The conventional drivetrain, Fig (7.1) serves two functions. It transmits torque from the engine equally to the driven wheels, and allows them to rotate at different speeds. It consists mainly of, a clutch, a gearbox, a drive shaft, an open differential and two half shafts. The components involved in the present work are the drive shaft, the open differential and the two half shafts.

The drive shaft, also called a propeller shaft, is used to transmit the torque from the gearbox to the differential. It is commonly a hollow steel tube with universal joints at its ends. The universal joints connect one end to the gearbox and the other to the differential.

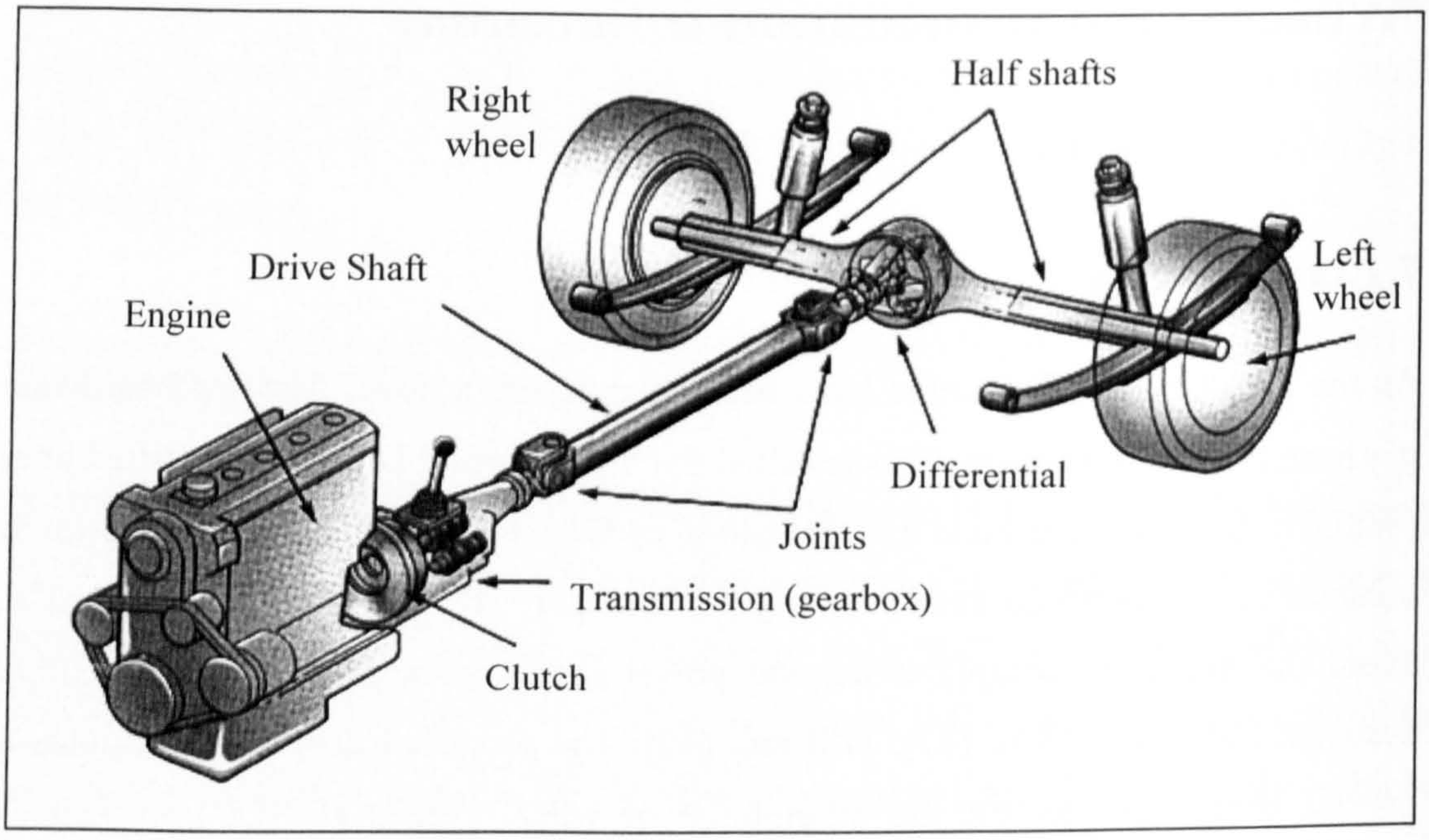

Fig (7.1) Typical vehicle drivetrain [89]

The differential is the device that delivers the drive shaft torque to the driven wheels. While it transmits the driveshaft torque equally to the driven wheels, it allows them to rotate at different speeds to facilitate vehicle cornering, since for a vehicle undertaking a turn, the outer wheels have to rotate faster than the inner wheels, due to the difference in the length of the paths they take.

The half shafts are a set of two shafts, each with a splined end connecting it to the differential side gear. The other end is connected to the corresponding driven wheel. Each half shaft transmits the torque from its differential side gear to its corresponding driven wheel. As the differential is the key component in this work, special attention is given to its construction and function.

7.2.1 Differential Construction

The differential is usually located between the two driven wheels. Four-wheel drive vehicles have a separate differential for each axle. The differential is connected to each wheel by a half-shaft (S_5) and (S_6), Fig (7.2). In the differential, a splined axle side gear is positioned on the splined end of each half-shaft (G_4) and (G_5). The side gears each mesh with a bevel gear (spider gear) (G_3). The spider gear rotates about a point located on a central pivot beam (Spider shaft) (S_3). This spider shaft is connected to the differential case (C_1).

The differential case is a drum-like case, concentric with the side gears. It contains the side gears and the spider gear. It is also fitted with a ring gear (G_2), Fig (7.2), on its outer surface and mounted on two large bearings. Accordingly, it can be rotated about this axis. The differential pinion (G_1) and the ring gear transmit the drive shaft (S_1) torque to the differential case.

7.2.2 Differential Principle of Operation

The drive shaft and two universal joints connect the gearbox output shaft to the drive shaft (S_1) and pinion (G_1), Fig (7.2). As the differential pinion drives the ring gear (G_2) it causes the differential case (C_1) to rotate. As the central spider shaft is connected to the differential case, it rotates in a circular orbit around the axis of rotation of the side gears. The spider gear rotates with the spider shaft while registering between the side gears. Consequently, the spider gear split the radial force (P) applied to it by the spider shaft equally between the side gears (P/2), Fig (7.3) (a). Thus, side gears receive equal torque. This torque is transmitted from the side gears to the half shafts, and so to the driven wheels.

The spider gear and spider shaft configuration delivers equal torque to the side gears even while rotating at different speeds. In case of different side gears rotational speeds the spider gear rotates to compensate their relative movement. Fig (7.3) (b).

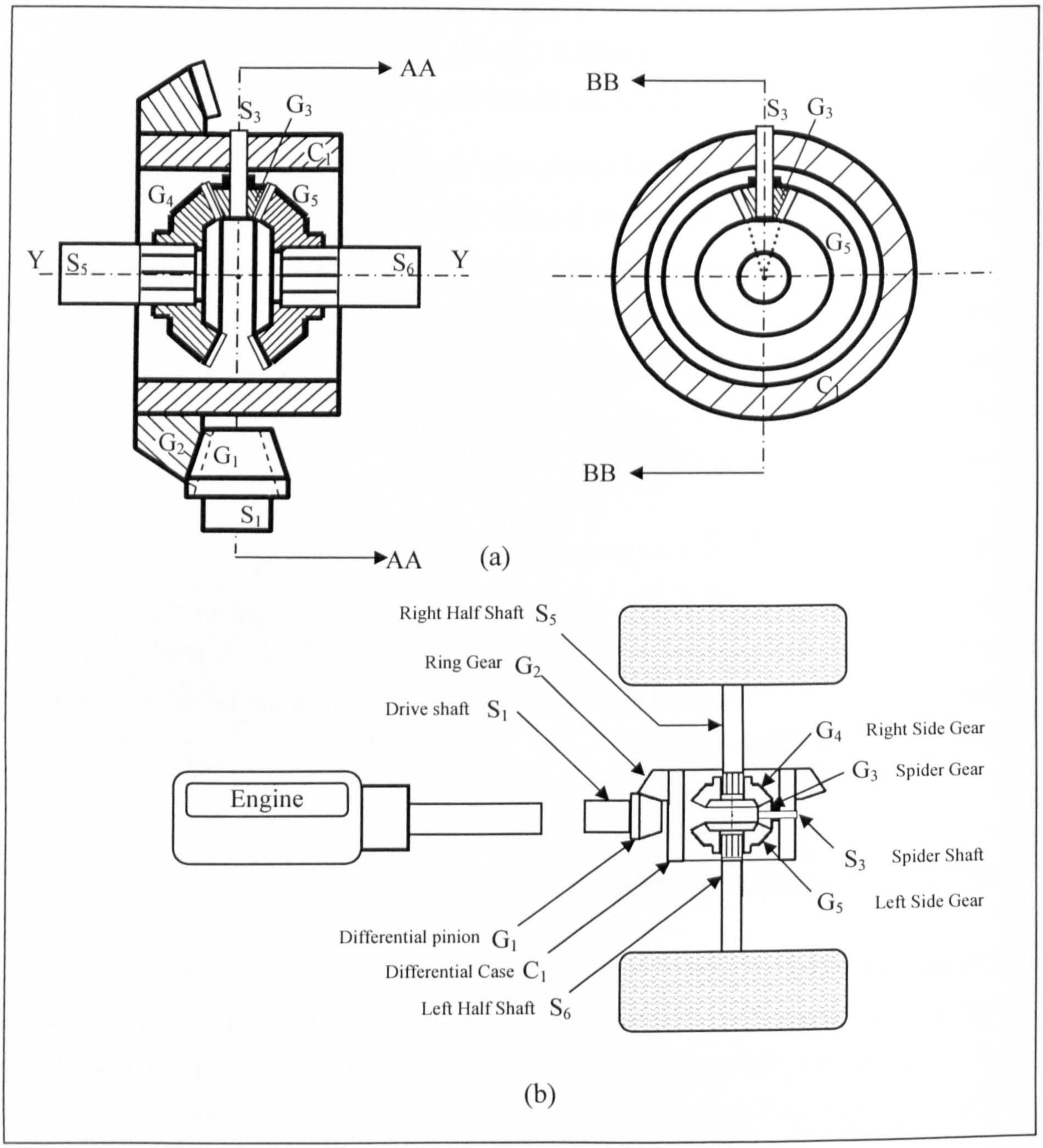

Fig (7.2) Conventional open differential layout

(a) Cross sections (b) Layout within vehicle

In straight line driving, the vehicle has equal driven wheel travelling resistances, and so, equal side gear resistance. Equal side gear resistance causes no spider rotation around its axle, which causes both wheels to run at the same speed as the differential case, while each receives half the differential case torque.

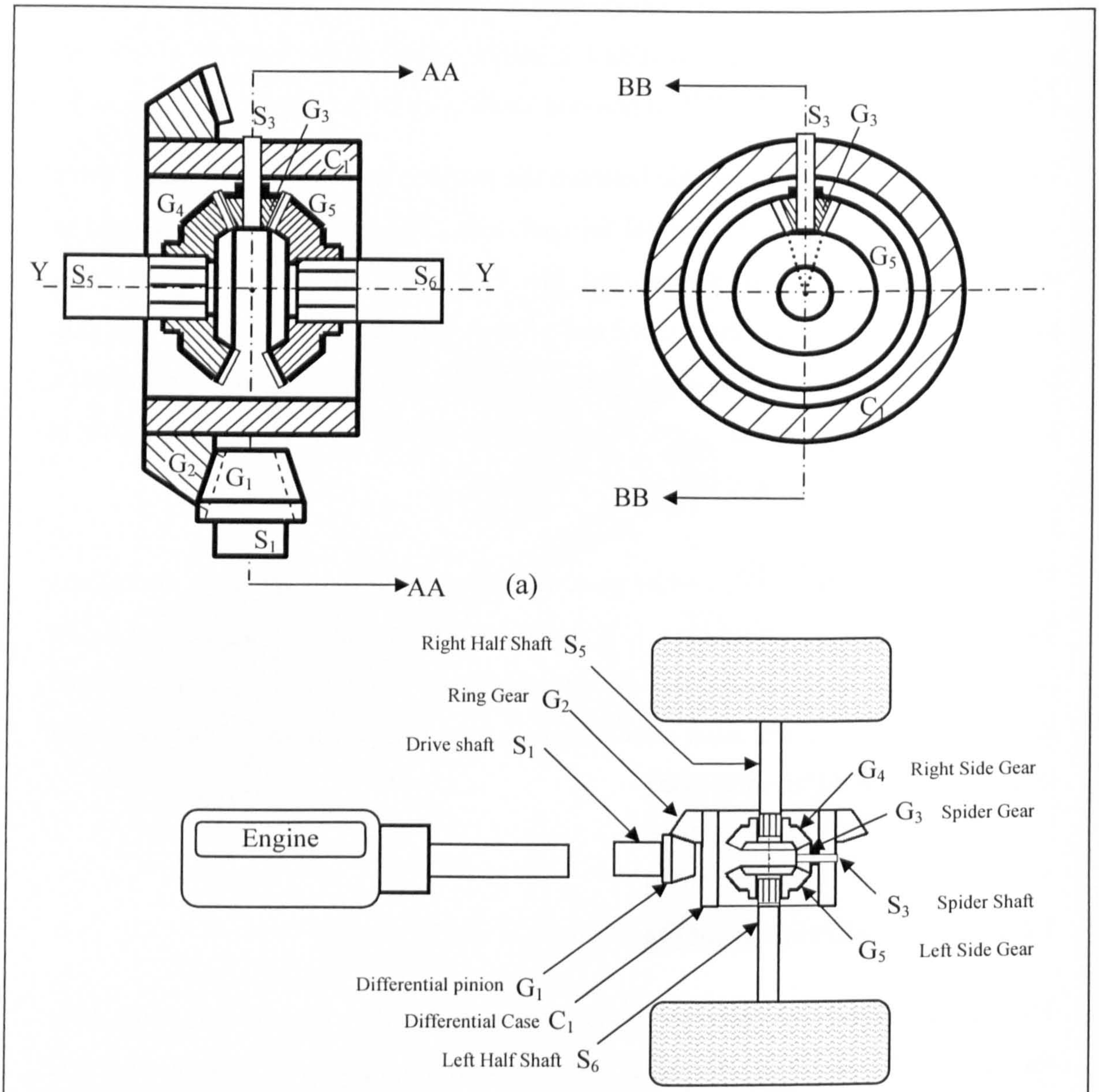

Fig (7.2) Conventional open differential layout

(a) Cross sections (b) Layout within vehicle

In straight line driving, the vehicle has equal driven wheel travelling resistances, and so, equal side gear resistance. Equal side gear resistance causes no spider rotation around its axle, which causes both wheels to run at the same speed as the differential case, while each receives half the differential case torque.

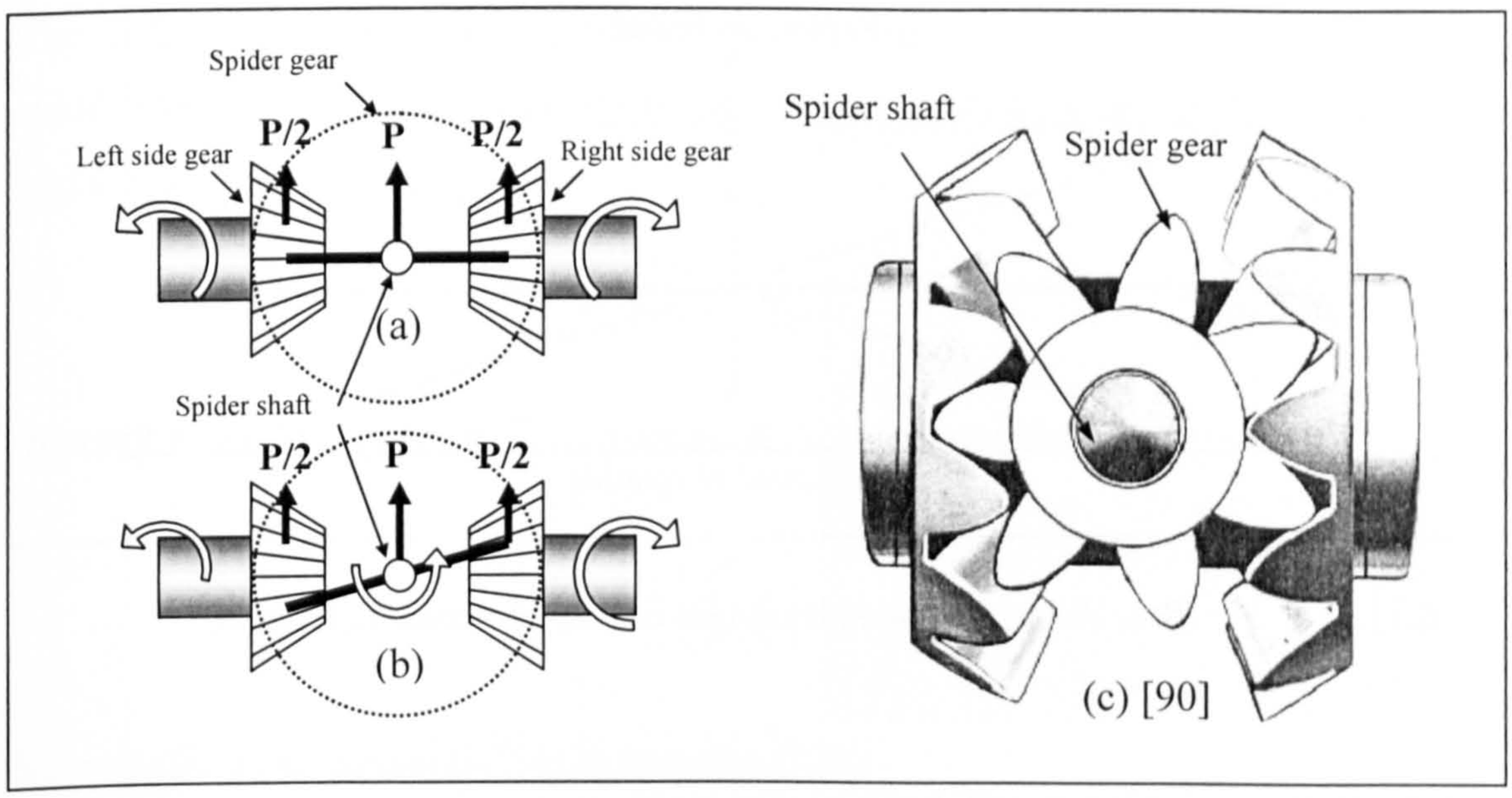

Fig (7.3) The spider gear and side gear interaction

In steady state cornering, the inner wheel resists travelling more than the outer wheel, due to the difference of path length they have to travel. If driven at the same speed, the driven wheels will scrub. The inner wheel will tend to go faster than required, while the outer wheel will attempt to go slower than required. The spider gear solves this problem by rotating around the spider shaft to force both wheels to receive equal torque rather than equal speeds. Accordingly, the more resistance of a wheel to travel, the lower the speed of this wheel. As the spider shaft is connected to the differential case, the speed differences between the wheels and the differential case are equal but with a different sign, Fig (7.4).

The open differential performance causes some problems to vehicle handling if one of the wheels suffers a degraded road holding adhesion. As the open differential delivers equal traction forces to right and left driven wheels, it limits the maximum traction force applied to a wheel to the maximum traction of the lower road holding wheel. When a wheel spins, it receives virtually zero torque, which would cause the other wheel to lose traction. This condition causes the vehicle to suffer traction loss and handing problems.

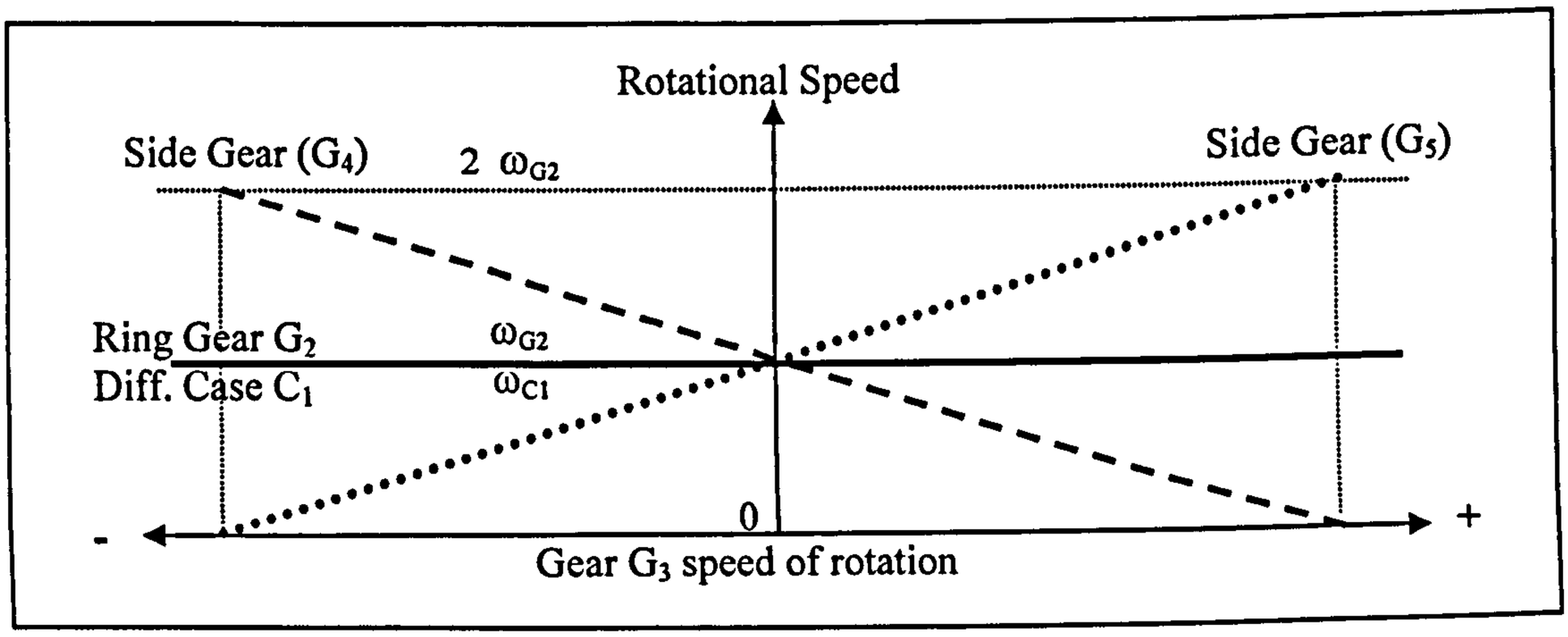

Fig (7.4) Rotational speeds outline of conventional differential

7.2.3 Differential Torque Relations

The conventional differential is designed to fulfil the main task of applying equal torque to the driven wheels. According to Fig (7.3) (b), both the side gears and therefore the driven wheels have to carry the same torque, regardless of their angular velocities.

$$T_{S5} = T_{S6} \tag{7.1}$$

Where: -

T_{Sn} Torque of shaft no. n, (n = 1, 2 ,3, 4, 5, 6)

The drive shaft S_1 supplies torque to the ring gear G_2 through the differential pinion G_1 with the following torque relation: -

$$T_{G2} = T_{S1}\left(\frac{N_{G2}}{N_{G1}}\right) \tag{7.2}$$

Where: -

N_{Gn} Number of teeth of gear no. n, (n = 1, 2 ,3, 4, 5, 6, 7, 8, 9, 10, 11 12)

The ring gear G_2 transmits this torque to the differential case C_1 as they are locked together, so: -

$$T_{C1} = T_{G2} \tag{7.3}$$

The differential case C1 in turn transmits this torque to spider gear G3 through the spider shaft S3. The spider gear splits the torque equally between the side gears G4 and G5, so: -

$$T_{C1} = T_{G4} + T_{G5} \tag{7.4}$$

Substituting from equation (7.3) in equation (7.2) and rearranging: -

$$T_{S1} = T_{C1}\left(\frac{N_{G1}}{N_{G2}}\right) \tag{7.5}$$

Substituting from equation (7.4) in equation (7.5): -

$$T_{S1} = (T_{G4} + T_{G5})\left(\frac{N_{G1}}{N_{G2}}\right) \tag{7.6}$$

Although equation (7.6) represents the input/output torque relation of the conventional differential, equation (7.1), should also be considered. According to equation (7.1) both T_{G4} and T_{G5} are equal, whilst each cannot exceed its corresponding wheel road adhesion. Accordingly they are equal and limited to the maximum working torque of the wheel with lower level of road adhesion.

7.2.4 Differential Rotational Speed Relations

As the differential pinion (G_1) is fitted on the drive shaft (S_1), Fig (7.2) so: -

$$\omega_{G1} = \omega_{S1} \tag{7.7}$$

The ring gear (G_2) is driven by the differential pinion (G_1), which leads to:

$$\omega_{G2} = \omega_{G1}\left(\frac{N_{G1}}{N_{G2}}\right) \tag{7.8}$$

Where: -

ω_{Gn} = Rotational speed of gear no. n, (n = 1, 2 ,3, 4, 5, 6, 7, 8, 9, 10, 11 12)

As the ring gear (G_2) is fitted to the differential case (C_1), they have the same speed:

$$\omega_{C1} = \omega_{G2} \tag{7.9}$$

The spider shaft (S_3) is connected to the differential case, so it rotates holding the spider gear (G_3) in orbital motion around the Y-Y axis with the same angular velocity as the differential case. As the spider gear meshes with the side gears, it causes them to rotate at a mean angular velocity equal to its pivot orbital angular velocity.

$$\omega_{C1} = \frac{(\omega_{S5} + \omega_{S6})}{2} \tag{7.10}$$

The relation between ω_{G4} and ω_{G5} is not limited by a fixed equation. Either of the side gears can take any rotational speed as long as they hold the same torque, and that the mean of their angular velocities is equal to the angular velocity of the differential case ω_{C1}.

Substituting from equation (7.7), (7.8) and (7.9) in equation (7.10): -

$$\omega_{S1}\left(\frac{N_{G1}}{N_{G2}}\right) = \frac{(\omega_{S5} + \omega_{S6})}{2} \tag{7.11}$$

Rearranging: -

$$\omega_{S1} = \left(\frac{N_{G2}}{N_{G1}}\right)\left(\frac{(\omega_{S5} + \omega_{S6})}{2}\right) \tag{7.12}$$

Equation (7.12) shows the interrelation between the half shaft speeds ω_{S5} and ω_{S6} under the governing drive shaft speed ω_{S1}. Equation (7.12) together with the torque equations (7.1) and (7.6) define the boundary of the conventional open differential performance, in that it adjusts the wheel angular velocities to comply with the equal wheel torque obligation.

7.3 WSDD Design

In this section the Wheel Speed Distribution Differential (WSDD) design targets are selected, the different design development stages are outlined and the final design is presented. Also, the WSDD fundamental equations are developed.

For a differential to allow WSDC and TFDC and also be feasible, a certain set of requirements are outlined and adhered to. The design requirements considered evolved from the drawbacks suffered by the reviewed hardware designs. Also a set of overall design targets for the new hardware is outlined and considered. This set of hardware design targets is aimed at avoiding common problems associated with current vehicle hardware components.

7.3.1 Design Targets

In order to ensure that the hardware design meets its requirements as well as avoiding the drawbacks of the reviewed systems, the required design targets for this hardware are summarised as: -

- **Capability to control speed**

To satisfy this target the hardware should allow no mechanical slippage, in order to ensure accurate adjustment of the speed. Clutches could not be used in such a system, as slippage would compromise the control of speed. Also, pullies and belt systems would not be preferred.

- **Capability to control torque**

To satisfy this target the system should be able to slip under excessive torque to prevent torque build-up. As the system would not be able to adjust the torque and speed at the same time, it should be able to allow or deny slippage.

- **Linearity**

Linearity of the hardware response to induced speeds and torques will greatly simplify the controller task. A non-linear hardware response could jeopardise the system performance. Hence, linearity of the hardware characteristics has been considered vital. Therefore, clutches are not considered as a feasible option, as the transmitted torque is not linearly proportional to the pressure between its plates.

- **Minimal speed and torque requirements**

The high speed requirement of the hardware and high torque requirement could complicate the control system components, which in turn could compromise the system feasibility. Accordingly, the torque and rotational speeds required by the hardware should be kept to a minimum.

- **Low power demand**

As the main electricity power source will be a battery, the total power required for the electrical components should be reduced to a minimal. Otherwise, a larger battery with higher charging demands would be needed and so adds to system complexity. Also, consuming a high mechanical power such as power dissipated in brakes and clutches would be a disadvantage.

- **Low controller load**

For hardware designed to enhance vehicle handling, it would be rational to spare the system or at least reduce its effort when undertaking a straight course in order to reduce the system power requirements and increase its Mean Time Between Failures (MTBF), hence adding to its feasibility. Therefore, limiting the system duties has been considered a vital requirement.

The construction targets considered for this hardware evolved from the criticism of competitor hardware. These targets could be summarised as: -

- **Development flexibility**

The hardware should allow a broad range of developments to vehicle handling behaviour, such as, allowing popular vehicle handling modes, for example, open differential mode, limited slip differential mode, TFDC, BFDC as well as WSDC.

- **Ease of manufacture**

Vehicle hardware of an unnecessarily sophisticated structure, bulky weight, and made from hard to manufacture components will lead to higher fixed and running costs. These aspects will degrade its feasibility. Consequently, simplification of the system design, without sacrificing its functionality, is considered a vital priority.

- **Small hardware size**

As the vehicle industry trend is to reduce the vehicle size and weight, reducing the proposed system size and hence weight has been considered a matter of survival for the system design.

- **Low maintenance requirements.**

A system that does not receive its proper maintenance will suffer frequent breakdowns, which could be serious in some situations. So, a trend has been adopted to design robust system hardware with low maintenance requirements. Also the ability to completely disengage the system in case of breakdown, thus allowing the vehicle to run in open differential mode has been considered vital.

7.3.2 WSDD Design Development

In the initial hardware development stage, the choice of a suitable mechanical transmission arrangement has been carried out. Candidate systems have been belt and pullies system, worm and wheel gear system and a gear train system. The investigation showed that gear train system was the only one capable of transmitting both controlled torque and controlled speed from the control system to the wheel axles.

The hardware design has been developed to reduce hardware size and complexity. Finally, the hardware has been optimised to reduce the controller duty and duty cycle resulting in the novel WSDC hardware design, Fig (7.5).

The WSDC hardware design characteristics have been thoroughly investigated to prove the system capacity to serve its designated purpose. To fulfil this task, the fundamental speed and torque equations governing its performance have been developed.

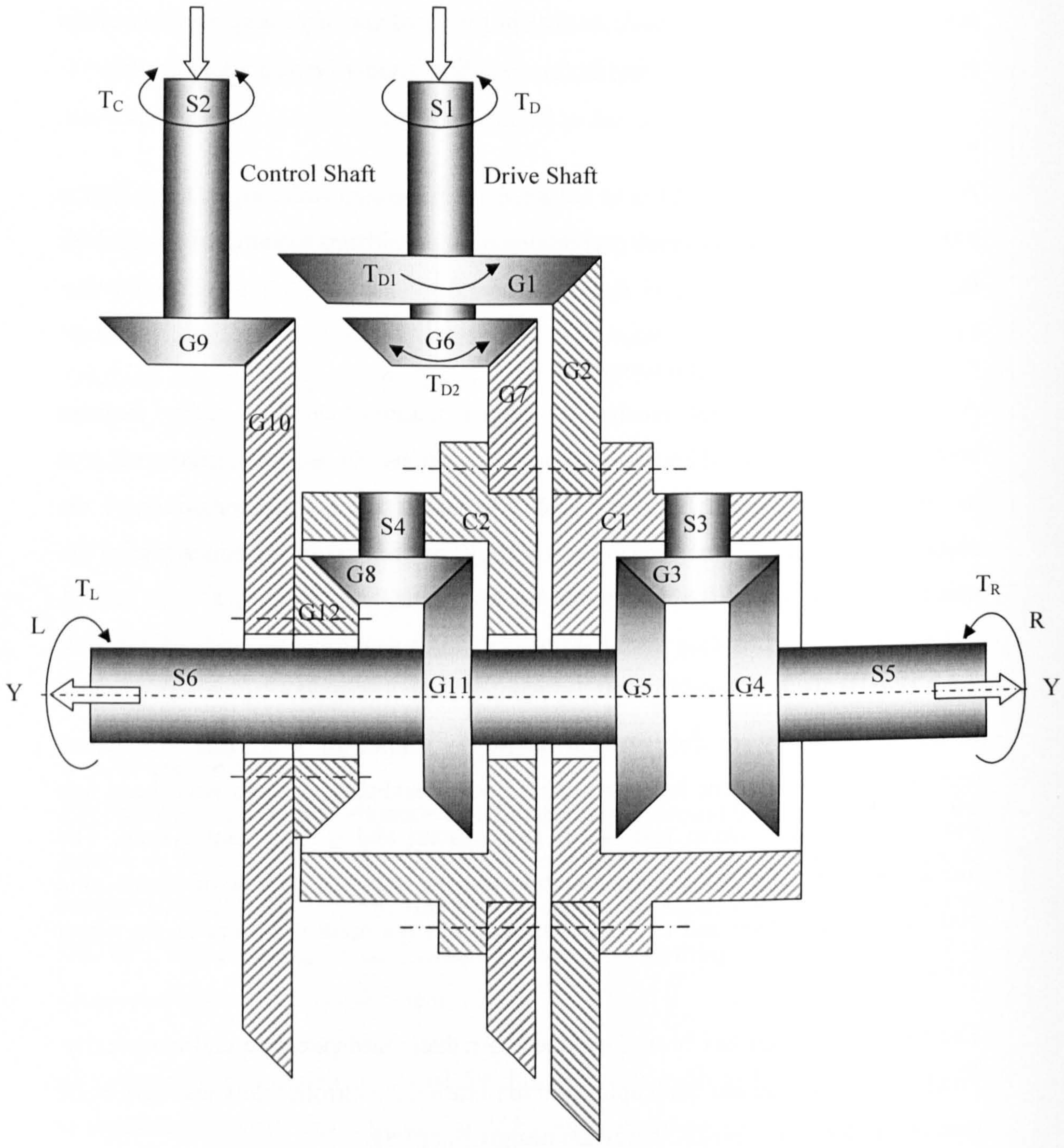

Fig (7.5) The novel WSDD design

7.3.3 Rotational Speed Relations

In this section the fundamental speed characteristic equations governing the WSDD performance are developed and discussed. The drive shaft (S1), Fig (7.5), drives the differential pinion (G1) at its rotational speed (ω_{G1}), and so: -

$$\omega_{G1} = \omega_{S1} \tag{7.13}$$

The differential pinion G1 rotates the ring gear G2: -

$$\omega_{G2} = \omega_{G1}\left(\frac{N_{G1}}{N_{G2}}\right) \tag{7.14}$$

The ring gear G2 is fitted to differential case C1, so it rotates at the same speed: -

$$\omega_{C1} = \omega_{G2} \tag{7.15}$$

The differential case rotates around the YY axis holding the spider shaft S3 and the spider gear G3. This leads to spider gear G3 rotation in a circular orbit around YY with speed equal to ω_{C1}. As G3 is meshed between the teeth of the side gears (G4, G5), it causes them to rotate at an average speed equal to its orbital speed, Fig (7.6) and Fig (7.7): -

$$\omega_{C1} = \frac{(\omega_{G4} + \omega_{G5})}{2} \tag{7.16}$$

$$\omega_{G4} = 2\omega_{C1} - \omega_{G5} \tag{7.17}$$

$$\omega_{G5} = 2\omega_{C1} - \omega_{G4} \tag{7.18}$$

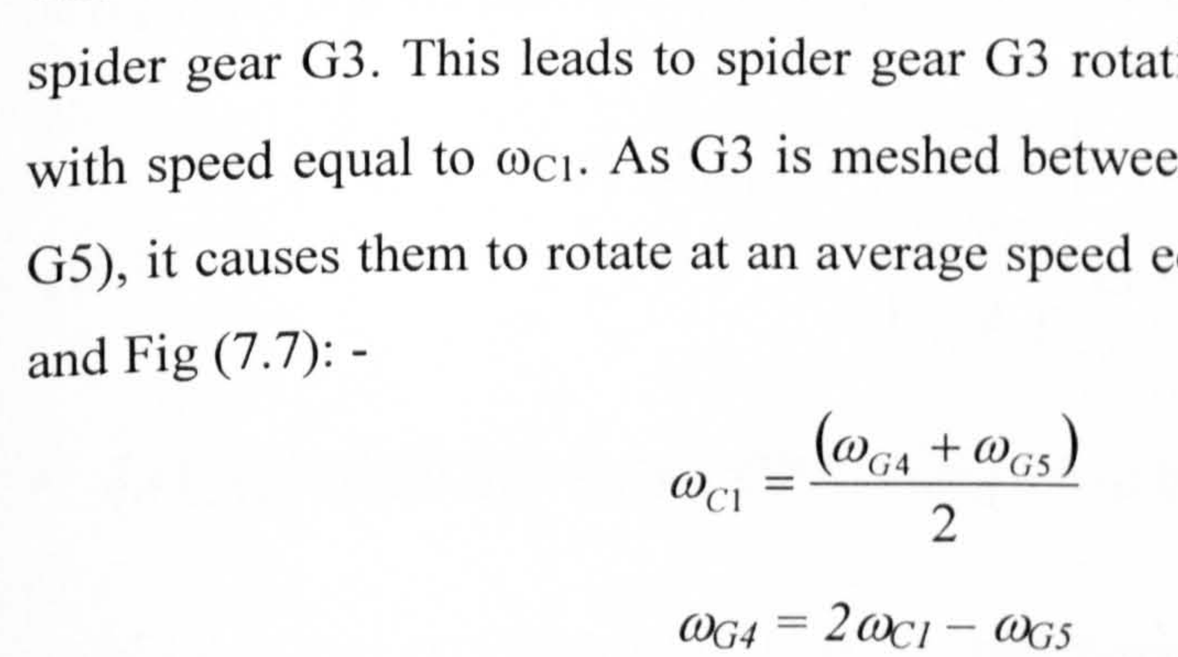

Fig (7.6) Spider gear mode of operation

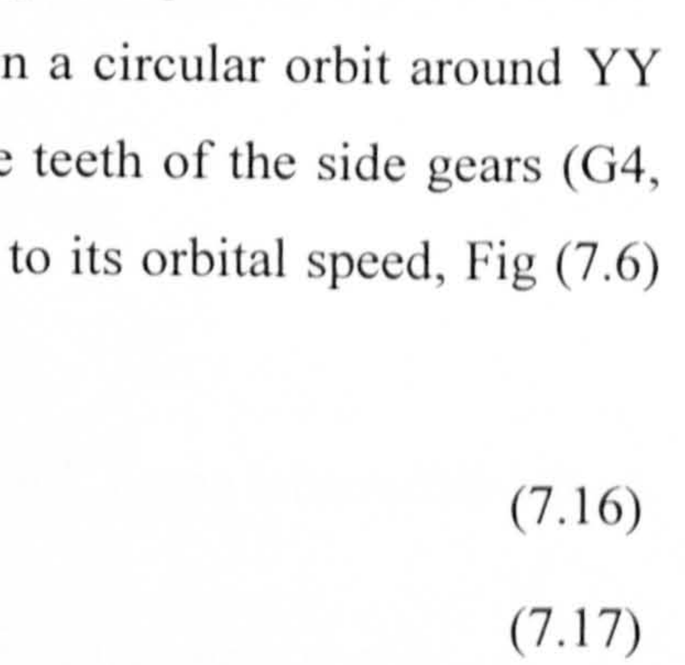

Fig (7.7) Spider gear mesh [90]

The right half shaft S5 and the left half shaft S6 rotate with the same speed as their side gears G4, G5 respectively, so: -

$$\omega_{S5} = \omega_{G4} \tag{7.19}$$

$$\omega_{S6} = \omega_{G5} \tag{7.20}$$

The above set of equations is the same as for the open differential.

In the new proposed differential, another gear, G11, is fitted to the left half shaft S6. Both G5 and G11 will rotate at the same speed as S6, Fig (7.5), so: -

$$\omega_{G11} = \omega_{G5} \tag{7.21}$$

Also, shaft S1 is fitted with pinion G6 and this rotates at the same speed as S1: -

$$\omega_{G6} = \omega_{S1} \tag{7.22}$$

The pinion G6 drives the ring gear G7. The relationship between G7 and G6 is given by: -

$$\omega_{G7} = \omega_{G6}\left(\frac{N_{G6}}{N_{G7}}\right) \tag{7.23}$$

As the differential case C2 is fitted to the gear G7, C2 rotates with speed given by: -

$$\omega_{C2} = \omega_{G7} \tag{7.24}$$

The spider shaft S4 and the spider gear G8 are connected to the differential case C2. Therefore, they rotate in a circular orbit around the YY axis, with speed equal to ω_{C2}. The spider gear G8 is in mesh with the teeth of side gears G11 and G12. Accordingly it causes them to rotate at an average speed equal to its orbital speed: -

$$\omega_{C2} = \frac{(\omega_{G11} + \omega_{G12})}{2} \tag{7.25}$$

$$\omega_{G11} = 2\omega_{C2} - \omega_{G12} \tag{7.26}$$

As gear G12 and G10 rotate at the same speed: -

$$\omega_{G10} = \omega_{G12} \tag{7.27}$$

At the same time, the control shaft S2 rotates to adjust the speed ratio between the right and left wheels by influencing ω_{G12}. The control shaft S2 drives pinion G9 with speed ω_{S2}: -

$$\omega_{G9} = \omega_{S2} \tag{7.28}$$

The relationship between the angular velocity of G10 and G9 is given by: -

$$\omega_{G10} = \omega_{G9}\left(\frac{N_{G9}}{N_{G10}}\right) \tag{7.29}$$

Substituting from equations (7.27) and (7.28) in (7.29) leads to a relationship between S2 and G12 given as: -

$$\omega_{G12} = \omega_{S2}\left(\frac{N_{G9}}{N_{G10}}\right) \tag{7.30}$$

- **Left half shaft rotational speed relations.**

As the side gear G11 is fitted on half shaft S6 they rotate at the same speed: -

$$\omega_{S6} = \omega_{G11} \tag{7.31}$$

Substituting from equation (7.26): -

$$\omega_{S6} = 2\omega_{C2} - \omega_{G12} \tag{7.32}$$

Substituting for ω_{C2} and ω_{G12} from equations (7.24) and (7.27) leads to: -

$$\omega_{S6} = 2\omega_{G7} - \omega_{G10} \tag{7.33}$$

Substituting for ω_{G7} from equation (7.23) and for ω_{G10} from equation (7.29): -

$$\omega_{S6} = 2\omega_{G6}\left(\frac{N_{G6}}{N_{G7}}\right) - \omega_{G9}\left(\frac{N_{G9}}{N_{G10}}\right) \tag{7.34}$$

Substituting for ω_{G6} from equation (7.22) and for ω_{G9} from equation (7.28), leads to the final equation of ω_{S6} as a function of the angular velocities of the drive shaft S1 and control shaft S2: -

$$\omega_{S6} = 2\omega_{S1}\left(\frac{N_{G6}}{N_{G7}}\right) - \omega_{S2}\left(\frac{N_{G9}}{N_{G10}}\right) \tag{7.35}$$

This equation demonstrates that the angular velocity of the left half shaft S6 is a function of both inputs ω_{S2} and ω_{S1}:

- **Right half shaft rotational speed relations.**

Similarly, from equation (7.19): -

$$\omega_{S5} = \omega_{G4} \tag{7.36}$$

Substituting for ω_{G4} from equation (7.17): -

$$\omega_{S5} = 2\omega_{C1} - \omega_{G5} \tag{7.37}$$

Substituting for ω_{C1} from equation (7.15) and for ω_{G5} from equation (7.21) leads to: -

$$\omega_{S5} = 2\omega_{G2} - \omega_{G11} \tag{7.38}$$

Substituting for ω_{G2} from equation (7.15) and for ω_{G11} from equation (7.26): -

$$\omega_{S5} = 2\omega_{G1}\left(\frac{N_{G1}}{N_{G2}}\right) - \left(2\omega_{C2} - \omega_{G12}\right) \tag{7.39}$$

From equation (7.13): -

$$\omega_{S5} = 2\omega_{S1}\left(\frac{N_{G1}}{N_{G2}}\right) - \left(2\omega_{C2} - \omega_{G12}\right) \tag{7.40}$$

Substituting for ω_{C2} from equation (7.24) and for ω_{G12} from equation (7.30): -

$$\omega_{S5} = 2\omega_{S1}\left(\frac{N_{G1}}{N_{G2}}\right) - \left(2\omega_{G7} - \omega_{S2}\left(\frac{N_{G9}}{N_{G10}}\right)\right) \tag{7.41}$$

Substituting for ω_{G7} from equation (7.23): -

$$\omega_{S5} = 2\omega_{S1}\left(\frac{N_{G1}}{N_{G2}}\right) - \left(2\omega_{G6}\left(\frac{N_{G6}}{N_{G7}}\right) - \omega_{S2}\left(\frac{N_{G9}}{N_{G10}}\right)\right) \tag{7.42}$$

Substituting for ω_{G6} from equation (7.22), the final equation that defines the angular velocity of the right half shaft S5, ω_{S5}, is achieved: -

$$\omega_{S5} = 2\omega_{S1}\left(\frac{N_{G1}}{N_{G2}}\right) - 2\omega_{S1}\left(\frac{N_{G6}}{N_{G7}}\right) + \omega_{S2}\left(\frac{N_{G9}}{N_{G10}}\right) \tag{7.43}$$

Equation (7.43) shows that the angular velocity of S5 is a function of inputs ω_{S1} and ω_{S2} that are associated with the angular velocities of the drive shaft S1 and control shaft S2.

- **Right / Left half shafts rotational speed cross relations.**

For the left half shaft, equation (7.35);

$$\omega_{S6} = 2\omega_{S1}\left(\frac{N_{G6}}{N_{G7}}\right) - \omega_{S2}\left(\frac{N_{G9}}{N_{G10}}\right) \tag{7.44}$$

and for the left right shaft, equation (7.43);

$$\omega_{S5} = 2\omega_{S1}\left(\frac{N_{G1}}{N_{G2}}\right) - 2\omega_{S1}\left(\frac{N_{G6}}{N_{G7}}\right) + \omega_{S2}\left(\frac{N_{G9}}{N_{G10}}\right) \tag{7.45}$$

it can be seen that the term (ω_{S2} (N_{G9}/N_{G10})) dominates the angular velocity relations. The control shaft angular velocity (ω_{S2}) term appears with a different sign in the right and left half shaft equations. This means that the angular velocity of the control shaft (ω_{S2}) will increase one half shaft speed while decreasing the speed of the other, which is a main goal of the system. The factor (N_{G9}/N_{G10}) is a linear factor and is constant for a given WSDD. This simplifies control task, which is also a main design goal.

Substituting from equation (7.35) in (7.43): -

$$\omega_{S5} = 2\omega_{S1}\left(\frac{N_{G1}}{N_{G2}}\right) - \omega_{S6} \tag{7.46}$$

This equation is the same as for right half shaft in an open differential. It shows that the new differential influences the right half shaft angular velocity, ω_{S5}, only through its influence on the left half shaft rotational speed ω_{S6}. This means that releasing the left half shaft, S6, from control turns this system to an open differential, which is an important goal.

For optimisation of control system duty cycle, the control shaft S2 angular velocity should be equal to zero when the vehicle travels in a straight line ($\omega_{S5} = \omega_{S6}$). Applying this condition in straight running: -

$$\omega_{S2} = 0 \tag{7.47}$$

Given that the basic equation for straight running is: -

$$\omega_{S5} = \omega_{S6} \tag{7.48}$$

Substituting the above into equations (7.35) and (7.43) leads to: -

$$\omega_{S6} = 2\omega_{S1}\left(\frac{N_{G6}}{N_{G7}}\right) - 0 \tag{7.49}$$

and;

$$\omega_{S6} = 2\omega_{S1}\left(\frac{N_{G1}}{N_{G2}}\right) - 2\omega_{S1}\left(\frac{N_{G6}}{N_{G7}}\right) + 0 \tag{7.50}$$

Equating equations (7.49) and (7.50) leads to;

$$2\omega_{S1}\left(\frac{N_{G6}}{N_{G7}}\right) = 2\omega_{S1}\left(\frac{N_{G1}}{N_{G2}}\right) - 2\omega_{S1}\left(\frac{N_{G6}}{N_{G7}}\right) \tag{7.51}$$

which simplifies to;

$$\omega_{S1} = (\tfrac{1}{2})\omega_{S1}\frac{\left(N_{G1}/N_{G2}\right)}{\left(N_{G6}/N_{G7}\right)} \tag{7.52}$$

and this reduces to;

$$\frac{\left(N_{G1}/N_{G2}\right)}{\left(N_{G6}/N_{G7}\right)} = 2 \tag{7.53}$$

With the gear ratio condition in equation (7.53), the control shaft S2 is stationary in straight line running. This reduces the control system duty cycle, which is an important goal of the hardware design process.

The final right and left half shaft angular velocity equations after this process are deduced by substituting from equation (7.53) in (7.35) and (7.43), resulting in half shafts equations. For the left side half shaft;

$$\omega_{S6} = \omega_{S1}\left(\frac{N_{G1}}{N_{G2}}\right) - \omega_{S2}\left(\frac{N_{G9}}{N_{G10}}\right) \tag{7.54}$$

and for the right side half shaft;

$$\omega_{S5} = 2\omega_{S1}\left(\frac{N_{G1}}{N_{G2}}\right) - \omega_{S1}\left(\frac{N_{G1}}{N_{G2}}\right) + \omega_{S2}\left(\frac{N_{G9}}{N_{G10}}\right) \tag{7.55}$$

which simplifies to;

$$\omega_{S5} = \omega_{S1}\left(\frac{N_{G1}}{N_{G2}}\right) + \omega_{S2}\left(\frac{N_{G9}}{N_{G10}}\right) \tag{7.56}$$

Equations (7.54) and (7.56) show the input/output angular velocity relations, which represent the WSDD angular velocity characteristics.

Both equations (7.54) and (7.56) have two parts, one of them is the same for both equations and is a linear function of drive shaft rotational speed (ω_{S1}). The other part of the two equations is a linear function in the control shaft rotational speed (ω_{S2}), both with different signs. This means that the control shaft rotational speed input will linearly and equally add to one of the output shafts speed and subtract from the other. The direction of control shaft rotation governs which output shaft speed is increased and which is decreased. This is the first design goal since the control shaft angular velocity should be able to increase or decrease any output shaft rotational speed, without affecting the vehicle mean forward speed.

Also, when the control shaft S2 is stationary ($\omega_{S2} = 0$), both shafts will rotate at the same speed which is governed by the drive shaft, which realises the second goal of reducing the control system load as most of the vehicle travelling is in a straight line. Accordingly, employing the new WSDD enables the dedicated control system to carry no work load in straight line driving.

7.3.4 Torque Relations

In this section the fundamental torque characteristic equations governing the WSDD are developed and discussed. To calculate the inputs/outputs torque relations of the WSDD, Fig (7.5), sign rules have been applied. The torque around the YY axis is positive when in counter clockwise (CCW) direction, looking from left to right.

Other torques are positive when in counter clockwise (CCW) direction, looking upward.

As the left half shaft S_6 is fitted with two torque inputs G11 and G5 and one torque output (left tyre torque) T_L, the governing relation is given as: -

$$T_L = T_{G11} + T_{G5} \tag{7.57}$$

The torque magnitude of G11 is equal and opposite to the G12 torque as they mesh with the freely rotating spider gear G8. The sign between them is different due to the previous rule as applying a CW torque on one of them causes a CCW torque on the other: -

$$T_{G12} = - T_{G11} \tag{7.58}$$

At the same time, the spider shaft, S_4, works as a rotating pivot between G11 and G12 and so transmits the sum of the torques of G11 and G12 to the supporting differential case C2. This torque is in the direction of T_{G12}: -

$$T_{C2} = T_{G11} + T_{G12} \tag{7.59}$$

Substituting equation (7.58) into equation (7.59) and taking into account that T_{C2} acts in the direction of T_{G12} leads to: -

$$T_{C2} = 2\, T_{G12} \tag{7.60}$$

The differential case C2 transmits torque to the ring gear G7: -

$$T_{G7} = T_{C2} \tag{7.61}$$

In turn, the ring gear G7 transmits torque to the pinion G6 according to the number of teeth N_{G6} and N_{G7} resulting in (considering the sign rule): -

$$T_{G6} = -T_{G7}\left(\frac{N_{G6}}{N_{G7}}\right) \tag{7.62}$$

As gear G1 and gear G6 are fitted on the drive shaft S1, the torque is divided between them. Gear G1 torque T_{G1} is equal to T_{D1} which is the first part of the drive shaft torque T_D. Gear G6 torque T_{G6} is equal to T_{D2}, which is the second part of the drive shaft torque: -

$$T_D = T_{D1} + T_{D2} \tag{7.63}$$

$$T_{D1} = T_{G1} \tag{7.64}$$

$$T_{D2} = T_{G6} \tag{7.65}$$

From equation (7.62) and (7.65): -

$$T_{D2} = -T_{G7}\left(\frac{N_{G6}}{N_{G7}}\right) \tag{7.66}$$

Substituting for T_{G7} from equation (7.61): -

$$T_{D2} = -T_{C2}\left(\frac{N_{G6}}{N_{G7}}\right) \tag{7.67}$$

Substituting for T_{C2} from equation (7.60): -

$$T_{D2} = -2T_{G12}\left(\frac{N_{G6}}{N_{G7}}\right) \tag{7.68}$$

As gear G10 and Gear G12 are fixed together: -

$$T_{G12} = T_{G10} \tag{7.69}$$

As gear G9 supplies the torque to gear G10 but in a different plane (considering the sign rule): -

$$T_{G10} = -T_{G9}\left(\frac{N_{G10}}{N_{G9}}\right) \tag{7.70}$$

Substituting from equation (7.69) in equation (7.70): -

$$T_{G12} = -T_{G9}\left(\frac{N_{G10}}{N_{G9}}\right) \tag{7.71}$$

As gear G9 is fitted to the control shaft S2, torque of control shaft T_C is equal to gear G9 torque T_{G9}: -

$$T_C = T_{G9} \tag{7.72}$$

Substituting from equation (7.72) in equation (7.71): -

$$T_{G12} = -T_C\left(\frac{N_{G10}}{N_{G9}}\right) \tag{7.73}$$

Substituting from equation (7.73) in equation (7.68): -

$$T_{D2} = 2T_C\left(\frac{N_{G6}}{N_{G7}}\right)\left(\frac{N_{G10}}{N_{G9}}\right) \tag{7.74}$$

Equation (7.74) shows the relation between control shaft torque and the torque contribution from the drive shaft.

From equation (7.58) and (7.68): -

$$T_{D2} = 2T_{G11}\left(\frac{N_{G6}}{N_{G7}}\right) \tag{7.75}$$

Substituting for T_{G11} from equation (7.57): -

$$T_{D2} = 2(T_L - T_{G5})\left(\frac{N_{G6}}{N_{G7}}\right) \tag{7.76}$$

As gear G4 is free to rotate and spider gear G3 registers between the open differential side-gears G5 and G4: -

$$T_{G4} = T_{G5} \tag{7.77}$$

As gear G4 is fitted on right half shaft S5 then: -

$$T_R = T_{G4} \tag{7.78}$$

The spider shaft S3 transmits the sum of the side gears torque T_{G4} and T_{G4}: -

$$T_{C1} = T_{G4} + T_{G5} \tag{7.79}$$

Substituting from equation (7.77) in equation (7.79): -

$$T_{C1} = 2T_{G5} \tag{7.80}$$

As the ring gear G2 is fitted to the differential case C1: -

$$T_{G2} = T_{C1} \tag{7.81}$$

Pinion gear G1 is engaged with gear G2 so: -

$$T_{G1} = -T_{G2}\left(\frac{N_{G1}}{N_{G2}}\right) \tag{7.82}$$

Substituting from equations (7.64) and (7.81) in equation (7.82): -

$$T_{D1} = -T_{C1}\left(\frac{N_{G1}}{N_{G2}}\right) \tag{7.83}$$

Substituting from equation (7.80) in equation (7.83): -

$$T_{D1} = -2T_{G5}\left(\frac{N_{G1}}{N_{G2}}\right) \tag{7.84}$$

Substituting from equations (7.77) and (7.78) in equation (7.57): -

$$T_L = T_{G11} + T_R \tag{7.85}$$

Rearranging: -

$$T_{G11} = T_L - T_R \tag{7.86}$$

Substituting from equation (7.58) in equation (7.73) and rearranging: -

$$T_C = T_{G11}\left(\frac{N_{G9}}{N_{G10}}\right) \tag{7.87}$$

Substituting from equation (7.86) in equation (7.87): -

$$T_C = \left(T_L - T_R\right)\left(\frac{N_{G9}}{N_{G10}}\right) \tag{7.88}$$

Considering the torque difference: -

$$\Delta T = \left(T_L - T_R\right) \tag{7.89}$$

substituting equation (7.89) into equation (7.88) and rearranging leads to: -

$$\Delta T = T_C\left(\frac{N_{G10}}{N_{G9}}\right) \tag{7.90}$$

Equation (7.90) shows that a torque applied to the control shaft will enforce a torque difference between the right and left driven wheels. It also proves that applying no control torque will enforce the condition that ΔT is to equal zero, which is the open differential mode characteristic.

Substituting from equation (7.77) and (7.78) in equation (7.76): -

$$T_{D2} = 2(T_L - T_R)\left(\frac{N_{G6}}{N_{G7}}\right) \tag{7.91}$$

Substituting from equation (7.89) in equation (7.91): -

$$T_{D2} = 2\Delta T\left(\frac{N_{G6}}{N_{G7}}\right) \tag{7.92}$$

Equation (7.92) shows that the drive shaft in this design shares the torque required to enforce the traction torque difference that reduces the control system load, which is a design goal.

Substituting equations (7.77) and (7.78) into equation (7.84) leads to an expression for T_{D1}: -

$$T_{D1} = -2T_R\left(\frac{N_{G1}}{N_{G2}}\right) \tag{7.93}$$

Finally, the total drive shaft torque is calculated by adding T_{D1} and T_{D2}, considering equations (7.91) and (7.93) along with (7.63): -

$$T_D = T_{D1} + T_{D2} = -2T_R\left(\frac{N_{G1}}{N_{G2}}\right) + 2\Delta T\left(\frac{N_{G6}}{N_{G7}}\right) \tag{7.94}$$

Which leads to: -

$$T_D = -2T_R\left(\frac{N_{G1}}{N_{G2}}\right) + 2\Delta T\left(\frac{N_{G6}}{N_{G7}}\right) \tag{7.95}$$

Equation (7.95) shows the variation in drive shaft torque resulting from a torque difference (ΔT) between left and right driven wheels. The drive shaft torque variation at the same, relatively high, running speed is meant to force the drive shaft to supply most of the power required for the traction force variation required for WSDC. This power issue is discussed in more detail in the following sections.

7.4 The WSDD Model

The novel WSDD design and its fundamental equations have shown potential to fulfil the design requirements. To further investigate this potential, the WSDD equations representing both angular velocity and torque relations have been used to build a simulation model. This model has been used to derive the new hardware performance charts.

The angular velocity performance chart, Fig (7.8), shows some important features. First, the stagnation of control shaft ($\omega_{S2} = 0$) along the line of equal half shaft speeds ω_{S5} and ω_{S6} (straight line run) demonstrates the minimisation of controller workload during straight line running. Also, the flatness of the surfaces representing speed relations illustrates the system linearity. Finally, the system symmetry is proved through the speed symmetry around the $\omega_{S2} = 0$ line. This hardware performance chart proves that the hardware fulfils its design goals and facilitates the controlling task.

In the torque performance chart, Fig (7.9), the required input torques T_{D1}, T_{D2} and T_C are plotted against the wheel output torques T_L and T_R. The figure shows the ability of the hardware to shift most of the torque required to the drive shaft T_{D2}. This reduces the power required for driving the new hardware, which therefore facilitates the control task.

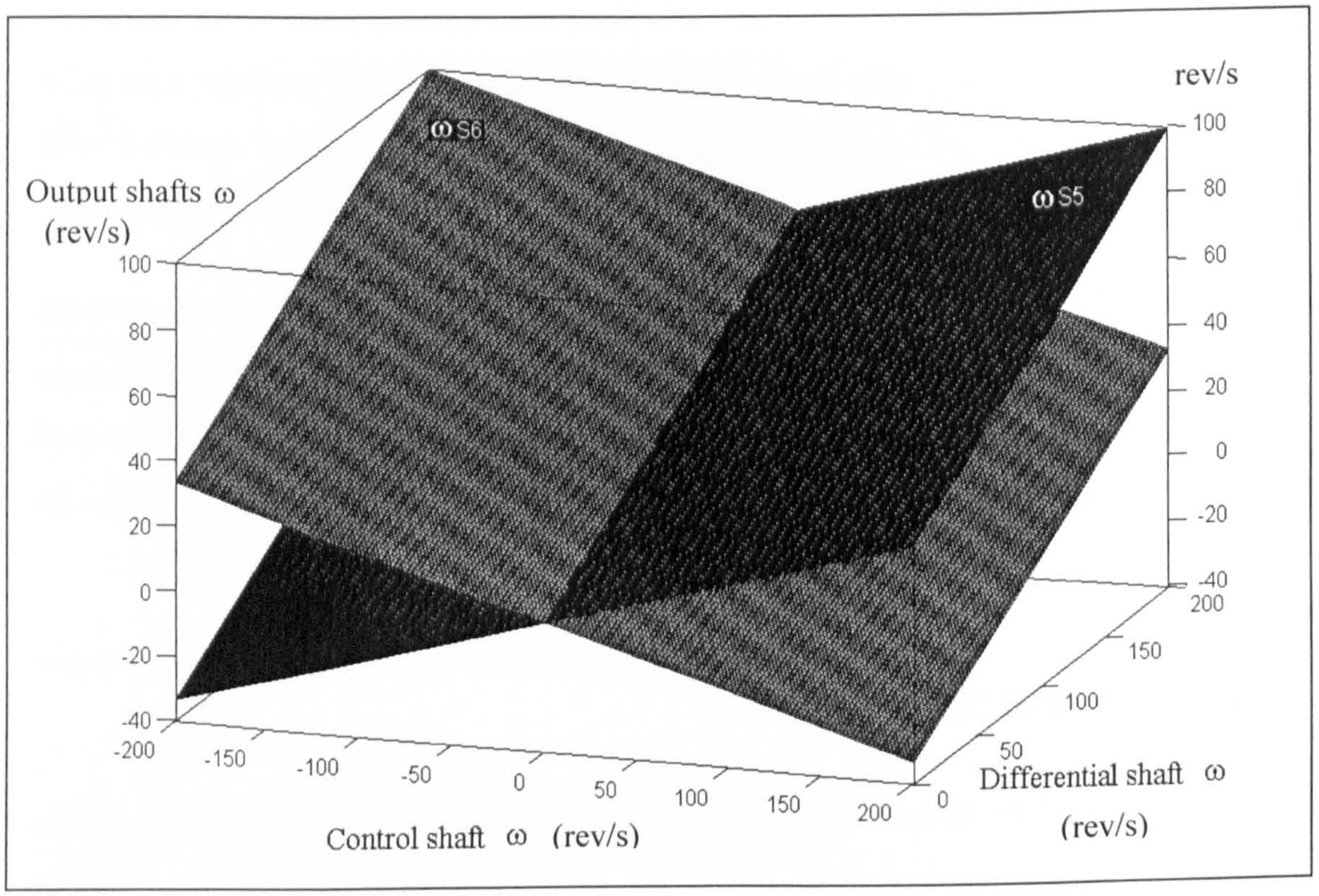

Fig (7.8) The WSDD rotational speed performance chart

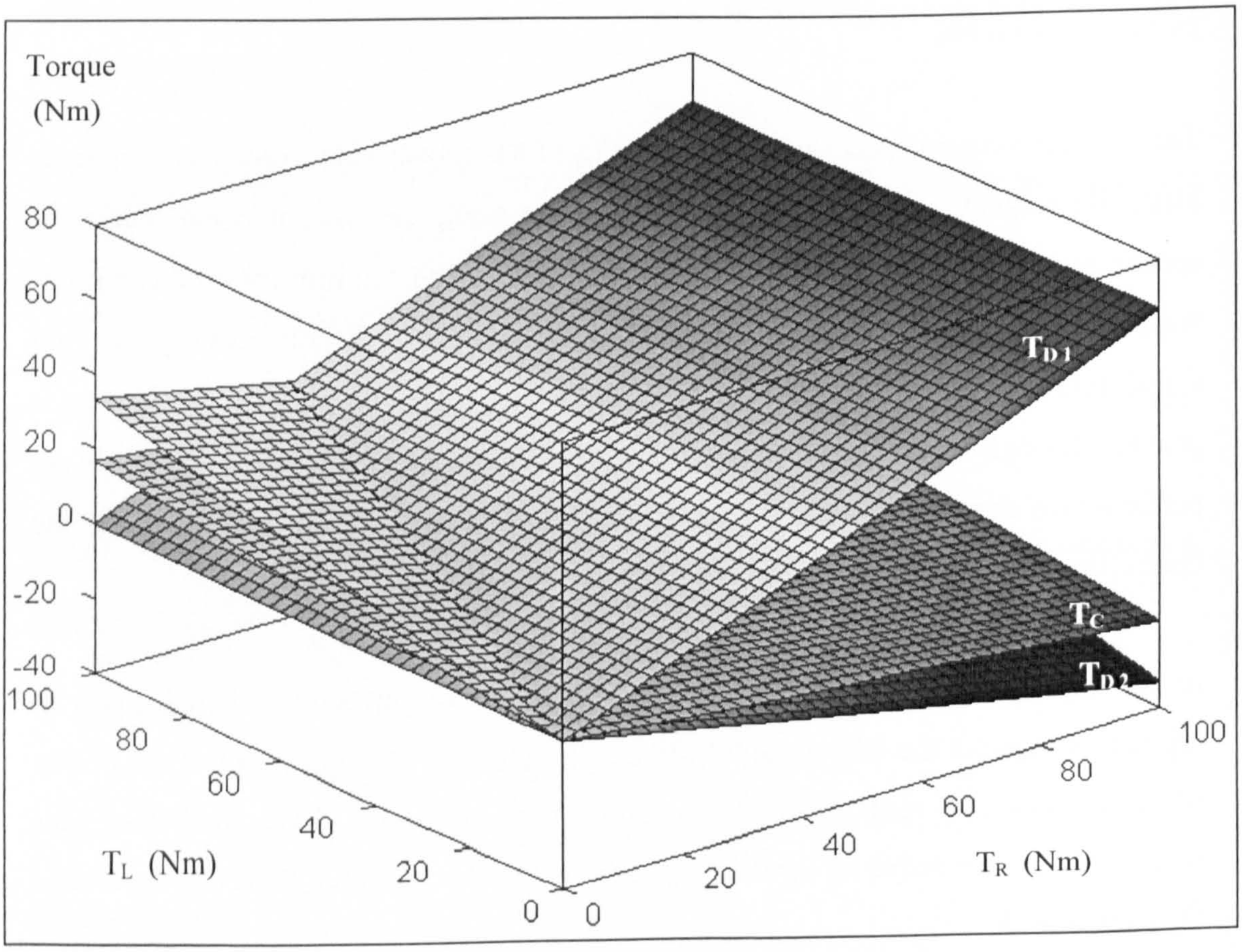

Fig (7.9) WSDD torque relation chart

7.5 WSDD Production and Maintenance

This section is dedicated to clarifying the construction of the WSDD, Fig (7.5), and demonstrates the feasibility of its production and maintenance. To achieve these tasks, the WSDD has been broken down into seven building blocks and each building block has been considered separately.

The WSDD building blocks are the two input shafts, two output shafts, two differential cases and one gear block. Each block is constructed from a small set of simple components. The two input shafts receive the driving torque from the engine and the controlling torque from the control unit, and are fitted with bevel pinions. The two output shafts deliver the torque to the driven wheels, and are fitted with bevel side gears. Each of the two differential cases is fitted with a ring gear, a spider shaft and a spider gear. The gear block consists of two bevel gears fitted together.

- **Input shafts and pinions**

The drive shaft (S1), Fig (7.10) (a), is fitted with two bevel gear pinions. This shaft delivers the vehicle engine power to the differential. The pinion (G1) is the same as that found within a conventional differential, whilst the second pinion (G6) is responsible for the support of the WSDD operation.

The control shaft (S2), Fig (7.10) (b), is fitted with pinion (G9). This shaft delivers the control torque and angular velocity input to the WSDD. The pinion (G9) is a bevel gear pinion that is used to drive the WSDD arrangement.

- **Output shafts and side gears**

The left half shaft (S6) assembly, Fig (7.11) (a), is the shaft that delivers the driving power to the left driven wheel. It is fitted with the left side gear (G5) as in a conventional differential. It is also fitted with an extra bevel side gear (G11). The side gear (G11) is used by the WSDD to influence the left half shaft torque and angular velocity.

The right half shaft (S5) assembly, Fig (7.11) (b), is the shaft that delivers the driving power to the right driven wheel. It is fitted with the right side gear (G4). In this form, they resemble the design of a conventional differential.

- **Main differential case assemblage**

The main differential case (C1), Fig (7.12), is a cylindrically shaped case. It is free to rotate around the YY axis by means of the ring gear (G2). The ring gear (G2) is a bevel gear fitted to the external surface of the main differential case (C1). Both the case and the ring gear resemble the conventional differential component.

The differential case (C1) holds the spider shaft (S3), allowing it to rotate freely around its axis. The spider shaft (S3) is fitted with a spider gear (G3) that is a small bevel gear. They are the same as in the conventional differential design.

- **Control differential case assemblage**

The control differential case (C2), Fig (7.13), is a cylindrically shaped case. It is free to rotate around the YY axis by means of the ring gear (G7), which is a bevel gear fitted to the external surface of the control differential case (C2).

The differential case (C2) holds the spider shaft (S4), allowing it to rotate freely around its axis. The spider shaft (S4) is fitted with a spider gear (G8) that is a small bevel gear. Accordingly, the design resembles that of a conventional differential.

- **Gear block**

The gear block, Fig (7.14), consists of two bevel gears (G12) and (G10). The first gear (G12) is a differential side gear, similar to side gear (G11). The second gear (G10) is a large bevel gear. Both are fitted together and are allowed to rotate around the YY axis. The influence on this block is through spider gear (G8) and pinion (G9). This block is not connected to the concentric left half shaft (S6). Accordingly, it does not represent a production complexity or need complicated maintenance, which is a design goal.

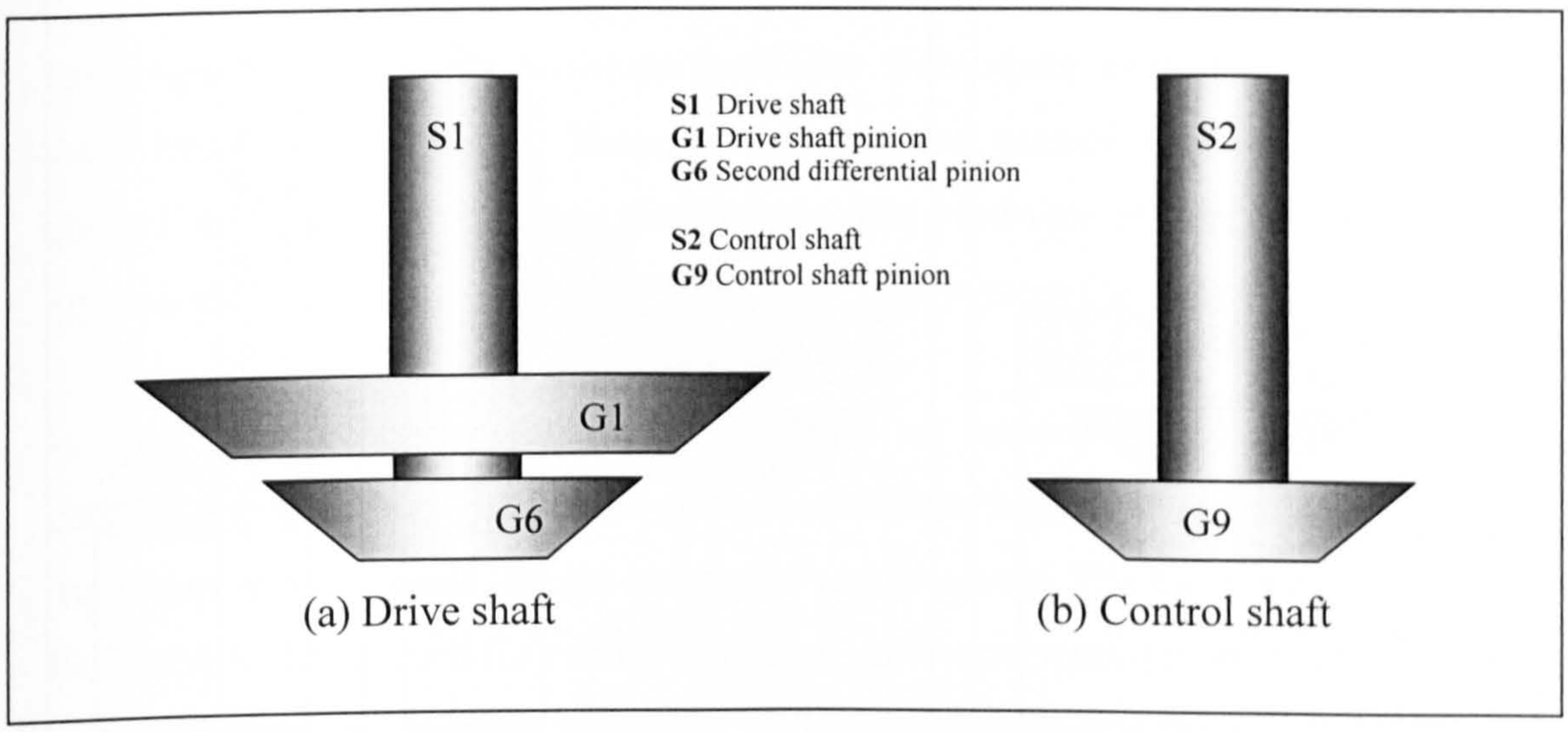

(a) Drive shaft (b) Control shaft

Fig (7.10) The WSDD input shafts

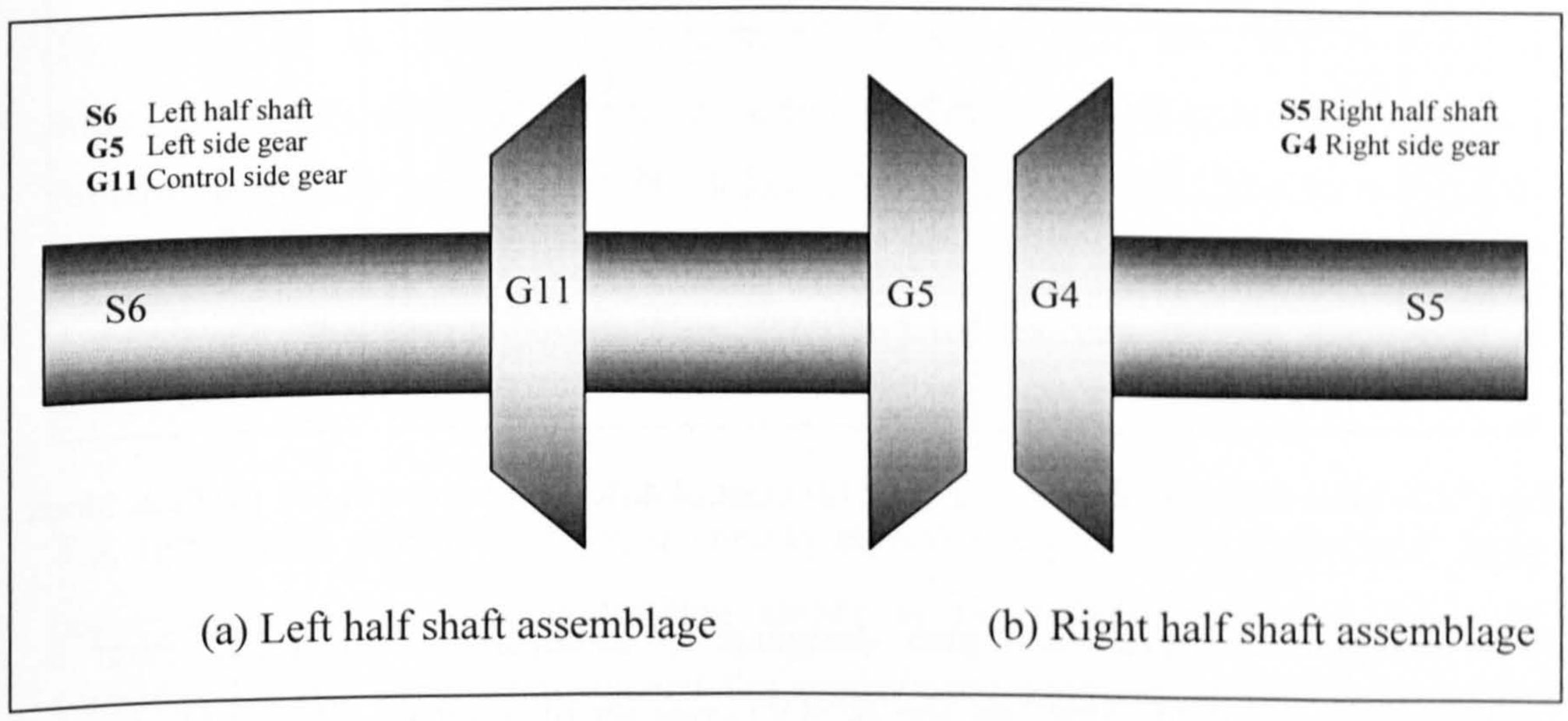

(a) Left half shaft assemblage (b) Right half shaft assemblage

Fig (7.11) The WSDD output shafts

The simplicity of the WSDD building blocks and its simple to produce components demonstrate its production feasibility. The commonality of its components, as it employs four side gears, two ring gears and two differential cases, adds to its production feasibility. The similarity of its components to conventional differential components enables it to take full advantage of all the expertise inherited from the conventional differential design and production, which means that many years of research will be available to back up its design and production.

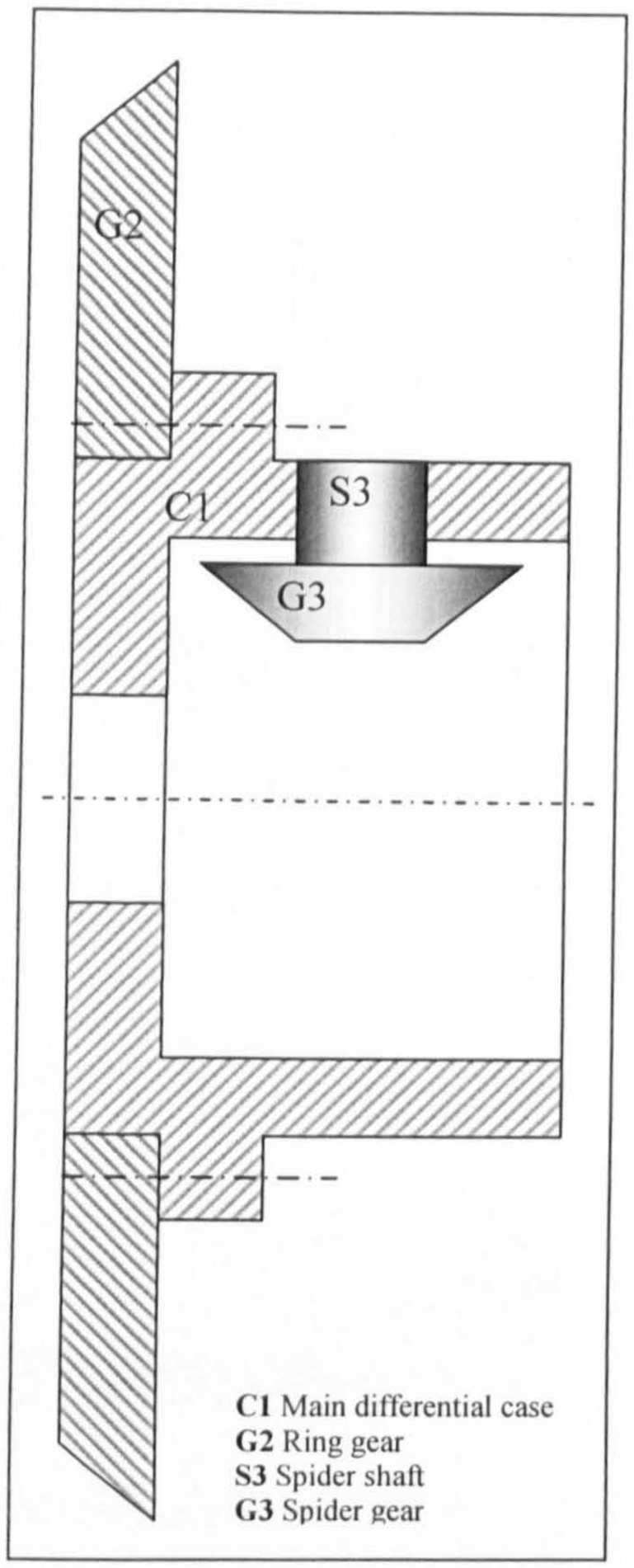

C1 Main differential case
G2 Ring gear
S3 Spider shaft
G3 Spider gear

Fig (7.12) Main differential case

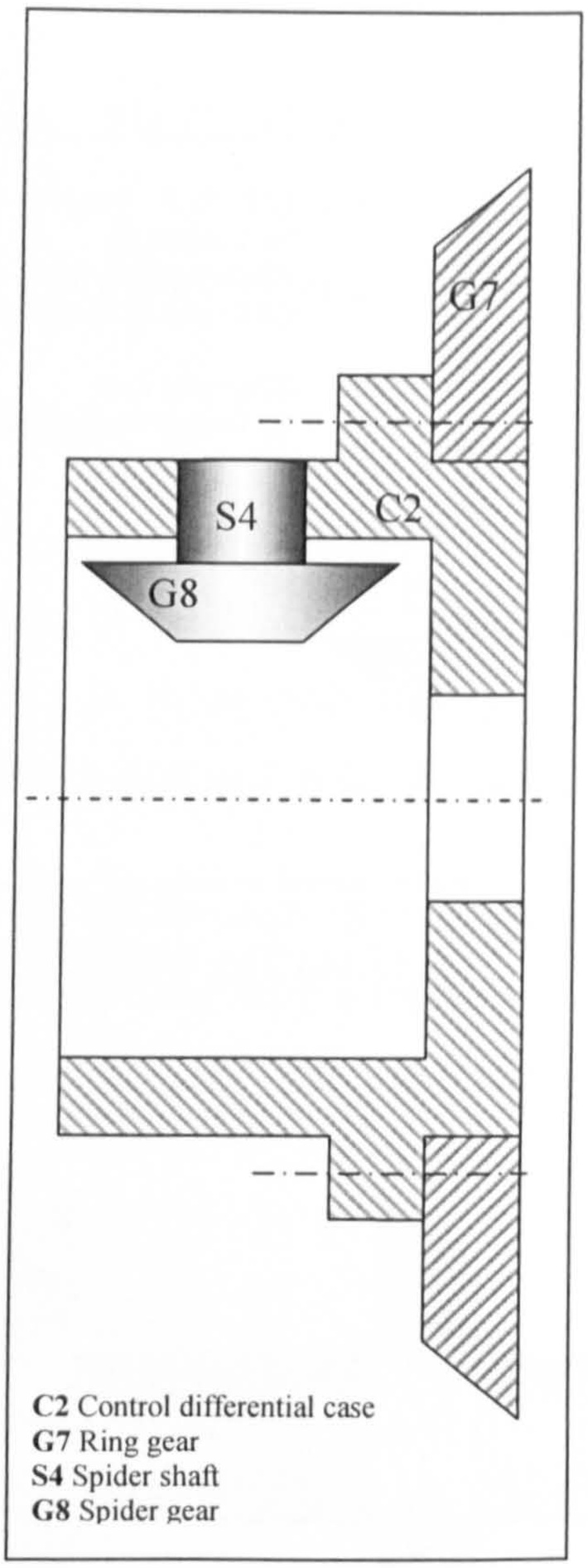

C2 Control differential case
G7 Ring gear
S4 Spider shaft
G8 Spider gear

Fig (7.13) Control differential case

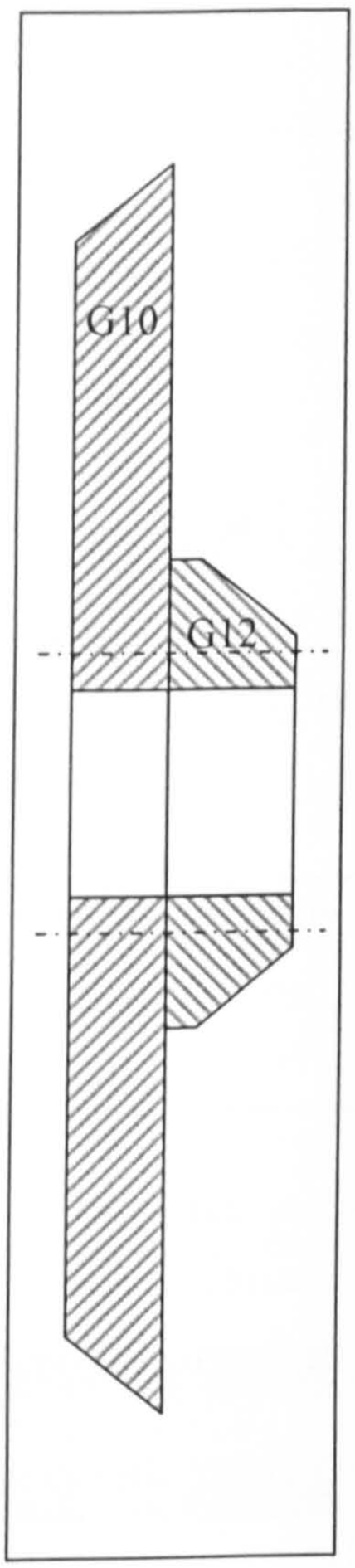

Fig (7.14) Gear block

The components have been also designed to establish its feasibility from a maintenance point of view. As the WSDD consists of a set of differential cases, gears and shafts, the maintenance needs of each is minimal. The differential cases are hollow solid containers, which need minimal maintenance throughout their lifetime. The shafts of the WSDD are the same as for the conventional differential and are known to rarely need maintenance. In addition, the WSDD gears (G1, G2, G3, G4 and G5) and (G6, G7, G8 and G11) resemble a double set from those employed in the conventional differential, known not to need neither sophisticated nor frequent maintenance. As the WSDD building components have therefore no known maintenance problems, the design has been considered feasible from a maintenance point of view.

7.6 WSDD Control Requirements

Investigation of the new hardware feasibility from some critical control points of view has been carried out. These mainly concern control shaft rotational speed, control shaft torque and control shaft power. The hardware control requirements are an essential factor, as they would greatly affect the system feasibility.

In this study of control shaft requirements, an assumption of vehicle extreme cornering and traction distribution control conditions has been used to investigate the maximum WSDD speed, torque and power requirements. The Cherokee Sport, 1997, [91] vehicle data is used for this investigation, as it represents a modern car with large mass and large yaw moment of inertia, which would challenge the new hardware.

7.6.1 Control Shaft Speed

To investigate the control shaft maximum speed required, the maximum driven wheel speed difference has been investigated. The driven wheel speed difference is a function of vehicle velocity and the radius of the negotiated turn. Smaller turn radius and higher vehicle velocity requires a higher driven wheel speed difference. Accordingly, the investigation examines the smallest turn radius achievable at different forward velocities.

The turn radius and velocity of a vehicle should not produce a centrifugal force higher than the lateral road holding ability or the vehicle will skid. Also the centrifugal force should not exceed the overturning moment or it will cause the vehicle to overturn. For the reviewed Cherokee Sport, the 2h/t factor is less than one. Accordingly, it will skid before turning over. In this test, the coefficient of friction between the road and tyres has been assumed to be equal to 1. In this condition, considering the tyre road forces, Fig (7.15), the maximum tyre lateral force would be equal to the normal reaction N, as: -

$$F_y = \mu N \tag{7.96}$$

Where: -

μ Coefficient of friction

N Road normal reaction

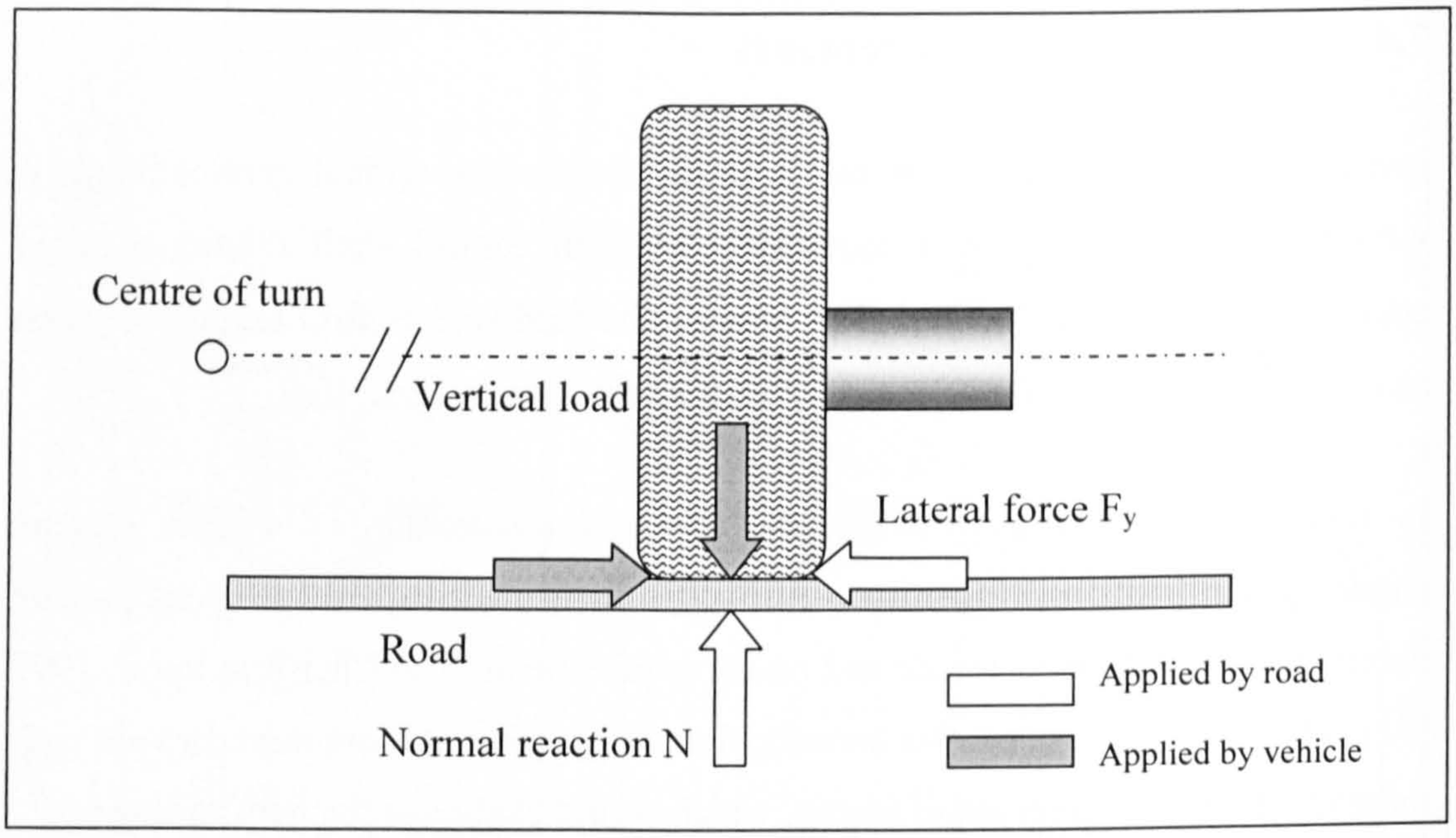

Fig (7.15) Tyre road forces

For a vehicle undertaking a turn, a centrifugal force acts through its CG in the outward direction, Fig (7.16). This force magnitude is governed mainly by three factors: the vehicle mass, velocity and the road radius of turn. For extreme handling conditions, the centrifugal force is equal to the maximum achievable tyre lateral forces. Accordingly it should not exceed the vehicle weight.

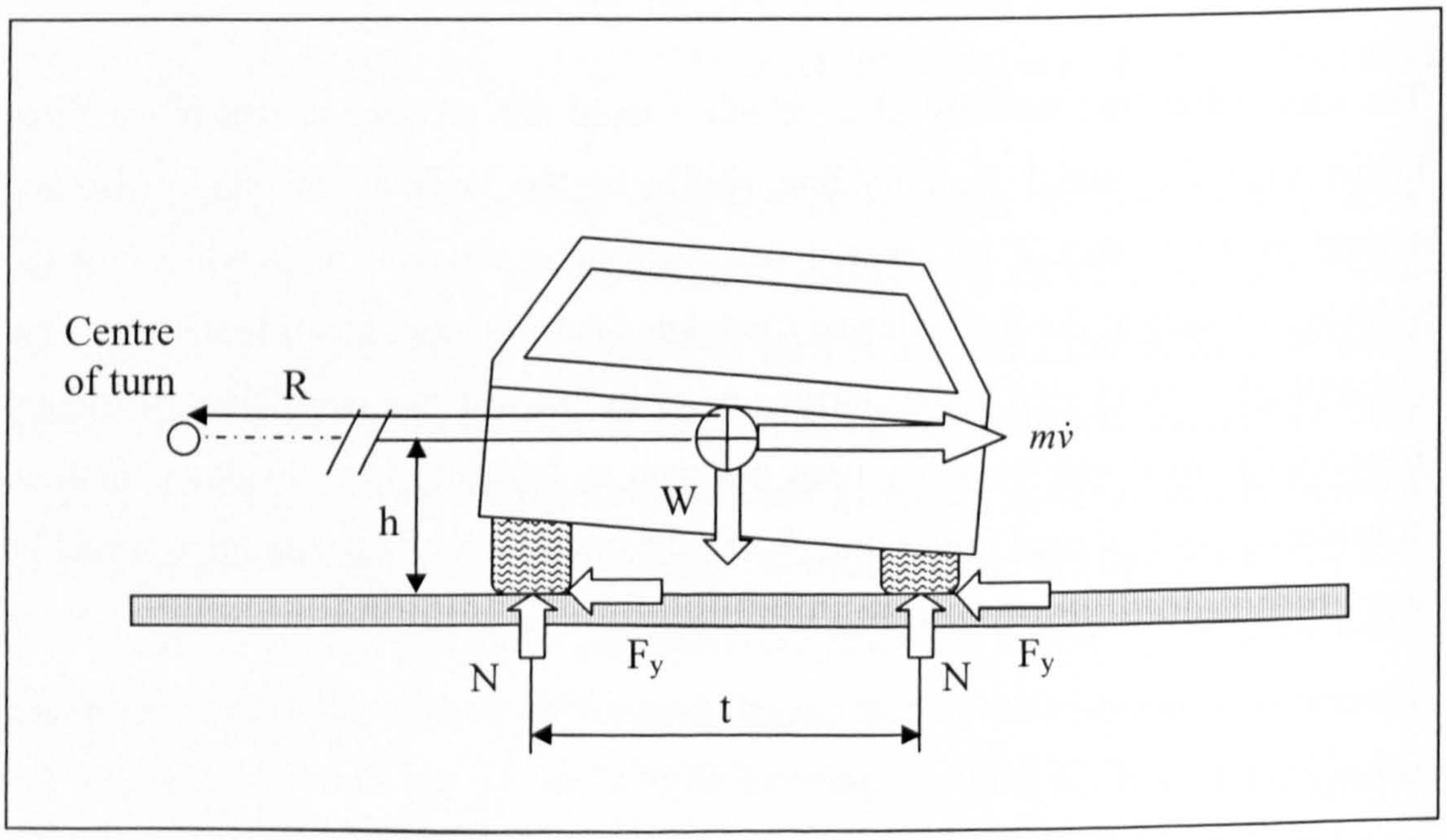

Fig (7.16) Vehicle lateral forces in turn

The lateral forces balance as: -

$$m\dot{v} = F_{yrl} + F_{yrr} + F_{yfl} + F_{yfr} \tag{7.97}$$

Under unity coefficient of friction, the maximum lateral forces are given as: -

$$m\dot{v} = W \tag{7.98}$$

Where W, vehicle weight, is given as: -

$$W = mg \tag{7.99}$$

Substituting equation (7.99) into (7.98) leads to: -

$$m\dot{v} = mg \tag{7.100}$$

Equation (7.100) shows that, at the extreme handling condition, the lateral acceleration should be less than or equal to g.

$$\dot{v} = g \tag{7.101}$$

Alternatively the lateral acceleration can be defined as: -

$$\dot{v} = \left(\frac{u^2}{R}\right) \tag{7.102}$$

Substituting equation (7.102) into (7.101) and rearranging gives: -

$$R = \left(\frac{u^2}{g}\right) \tag{7.103}$$

Equation (7.103) represents the minimum turn radius relation with forward velocity under ideal tyre road holding conditions. This equation has been used to derive the minimum turn radius at different forward velocities, Table (7.1). A smaller turn radius would cause the vehicle to skid laterally.

Vehicle forward Velocity u (m/s)	5	10	20	25	30	35	40	45	50
Road radius of turn R (m)	2.5	10.2	40.8	63.7	91.7	124.9	163.1	206.4	255

Table (7.1) Minimum vehicle turn radius at different forward velocities

For a wide range of vehicles, the minimum turning circle diameters are larger than 10 m, [13]. Hence the minimum turn radius adopted for this investigation has been taken equal to 5 m. Accordingly, the corresponding maximum vehicle forward velocity has been found equal to 7 m/s.

For a rear driven vehicle, the rotational speed difference between the outer and the inner driven wheels in a corner is mainly a function of vehicle rear track, rear axle turn radius R_r and forward velocity u, Fig (7.17).

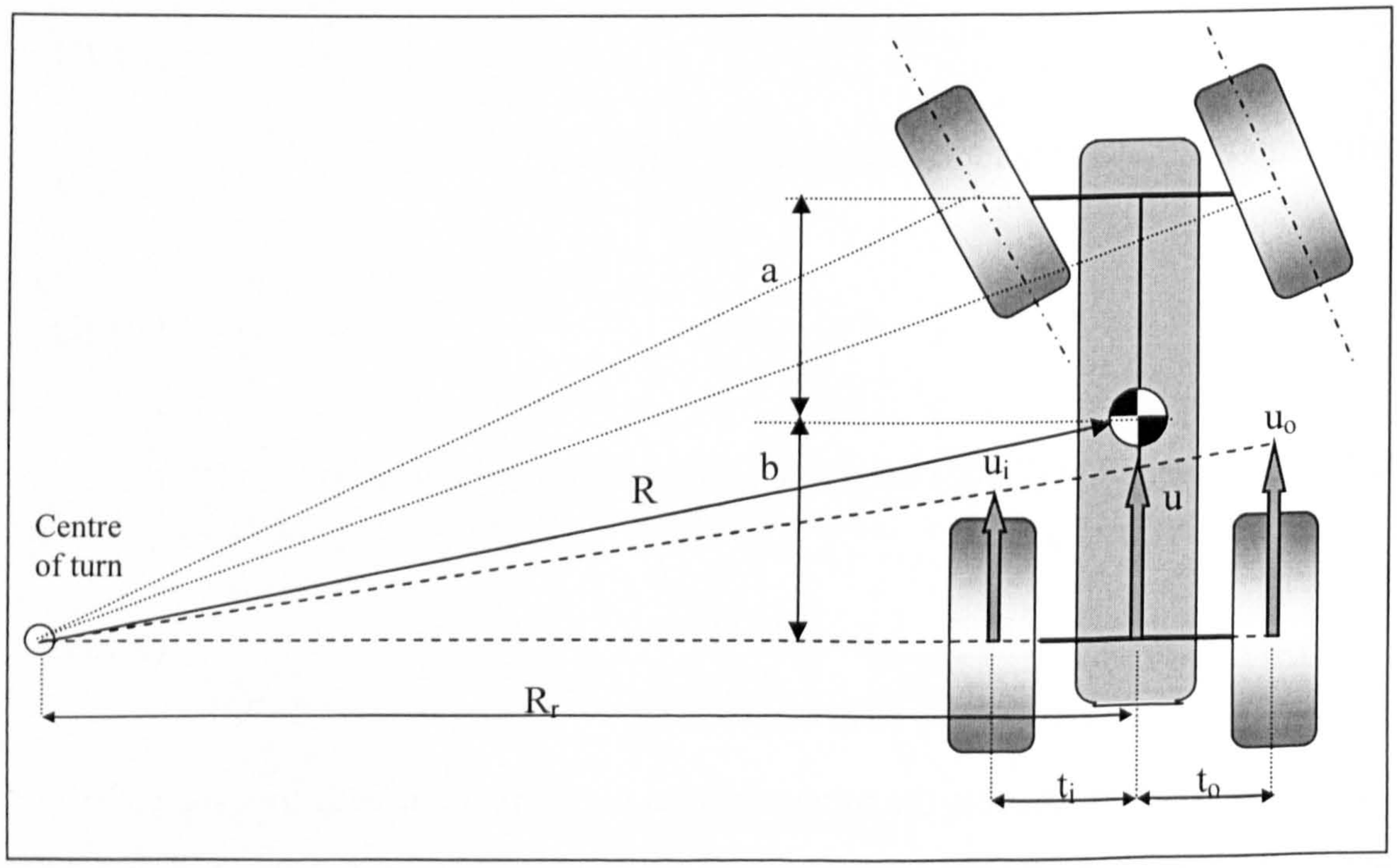

Fig (7.17) Vehicle wheel velocities in a turn

From the geometry, Fig (7.17): -

$$\frac{u}{R_r} = \frac{u_i}{(R_r - t_i)} \tag{7.104}$$

Where: -

u_i Inner wheel forward velocity

u_o Outer wheel forward velocity

Rearranging: -

$$u_i = \frac{u(R_r - t_i)}{R_r} \tag{7.105}$$

For the outer wheel: -

$$\frac{u}{R_r} = \frac{u_o}{(R_r + t_o)} \tag{7.106}$$

Rearranging: -

$$u_o = \frac{u(R_r + t_o)}{R_r} \tag{7.107}$$

Where the rear axle turn radius is given as: -

$$R_r = \sqrt{R^2 - b^2} \tag{7.108}$$

The velocity difference is given as: -

$$\Delta u = u_o - u_i \tag{7.109}$$

Substituting from equation (7.105), (7.107) and (7.108) in equation (7.109)

$$\Delta u = u\left(\frac{t_i + t_o}{\sqrt{R^2 - b^2}}\right) \tag{7.110}$$

Considering: -

$t_i + t_o$ (track)	= 1.467 m	Cherokee Sport vehicle specification [91]
b	= 1.4313 m	Cherokee Sport vehicle specification [91]
u	= 7-50 m/s	(25.2-180 km/hr)

As the control shaft angular velocity is related to the driven wheel angular velocities, the driven wheel rotational speed difference has been deduced as: -

$$\Delta\omega = \frac{\Delta u}{2\pi R_o} \tag{7.111}$$

Where: -

$\Delta\omega$ Rotational speed difference between inner and outer wheels.

R_o Wheel radius

Substituting for the vehicle range of velocities and minimum turn radius, Table (7.1), in equation (7.110) and (7.111) the maximum difference in driven wheel velocity Δu and angular speed $\Delta\omega$ was evaluated at different vehicle forward velocities, Table (7.2).

Vehicle velocity (m/s)	Vehicle velocity (km/hr)	Minimum radius of turn (m)	Δu (m/s)	$\Delta\omega$ (rev/s)
7	25.2	5	2.144	1.0905
10	36	10.2	1.453	0.7390
15	54	22.9	0.963	0.4898
20	72	40.8	0.720	0.3661
25	90	63.7	0.576	0.2930
30	108	91.7	0.480	0.2442
35	126	124.9	0.411	0.2091
40	144	163.1	0.360	0.1830
45	162	206.4	0.320	0.1627
50	180	255	0.288	0.1463

Table (7.2) Maximum driven wheels speed difference at different forward velocities

To investigate the control shaft speeds required to give the above driven wheel speed difference, the WSDD rotational speed equations has been employed.

The right and left wheel rotational speeds and their relation to the rotational speeds of control shaft and drive shaft are given as: -

$$\omega_{S5} = \omega_{S1}\left(\frac{N_{G1}}{N_{G2}}\right) + \omega_{S2}\left(\frac{N_{G9}}{N_{G10}}\right) \tag{7.112}$$

$$\omega_{S6} = \omega_{S1}\left(\frac{N_{G1}}{N_{G2}}\right) - \omega_{S2}\left(\frac{N_{G9}}{N_{G10}}\right) \tag{7.113}$$

Where: -

ω_{S1} Drive shaft speed

ω_{S2} Control shaft speed

ω_{S5} Right half shaft speed

ω_{S6} Left half shaft speed

For the current investigation the gear ratio is taken as: -

$$\left(\frac{N_{G9}}{N_{G10}}\right) = \left(\frac{1}{6}\right) \tag{7.114}$$

$\Delta\omega$ is given as: -

$$\Delta\omega = \omega_{S5} - \omega_{S6} \tag{7.115}$$

Substituting from equation (7.112), (7.113) and (7.114) in equation (7.115): -

$$\Delta\omega = \left(\frac{1}{3}\right)\omega_{S2} \tag{7.116}$$

Rearranging: -

$$\omega_{S2} = 3\Delta\omega \tag{7.117}$$

Substituting for the previously obtained values of $\Delta\omega$, the required control shaft speeds were evaluated, Table (7.3). These required control shaft rotational speeds were considered satisfactory. Therefore the next step of the investigation was to evaluate the required control shaft torque.

Vehicle velocity (m/s)	Vehicle velocity (km/hr)	Minimum radius of turn (m)	Control shaft ω (rev/s)
7	25.2	5	3.271
10	36	10.2	2.217
15	54	22.9	1.469
20	72	40.8	1.098
25	90	63.7	0.879
30	108	91.7	0.733
35	126	124.9	0.627
40	144	163.1	0.549
45	162	206.4	0.488
50	180	255	0.439

Table (7.3) Maximum control shaft rotational speeds at different forward velocities

7.6.2 Control Shaft Torque

The maximum control shaft torque has been found to be governed by the maximum applicable traction force difference between the driven wheels. Maximum traction force difference applicable has been found to be mainly a function of the driven wheel characteristics and the corresponding vertical loads.

The maximum traction torque difference is applied through the TFDD when a driven wheel applies its maximum traction force, while the other driven wheel applies no traction force.

For a typical wheel with vertical load N and assuming a coefficient of friction equal to unity, the maximum longitudinal force would be equal to N. Applying the same ratio to the current investigation, the maximum driven wheel longitudinal force would be given as: -

$$F_{xrl} = W\left(\frac{a}{a+b}\right)\left(\frac{t_r}{t_l + t_r}\right) \tag{7.118}$$

and

$$F_{xrr} = W\left(\frac{a}{a+b}\right)\left(\frac{t_l}{t_l + t_r}\right) \tag{7.119}$$

Where:-

F_{xrl} Longitudinal force of rear left wheel

F_{xrr} Longitudinal force of rear right wheel

a Vehicle CG to front axle distance

b Vehicle CG to rear axle distance

t_l Vehicle CG to left side distance

t_r Vehicle CG to right side distance

Considering the Cherokee, 1997 specifications, the static rear wheel vertical load is equal to 7254.7 N, [91]. Taking the vehicle CG at the middle of track, the driven wheel maximum applicable longitudinal forces are evaluated as: -

$$F_{xrl} = F_{xrr} = 3627\ N \tag{7.120}$$

The maximum longitudinal driving force difference is given as: -

$$\Delta F_x = F_{xrr} - F_{xrl} \tag{7.121}$$

To apply the maximum difference one of the wheels should apply the full traction force, while the other should apply no traction force, which leads to: -

$$\Delta F_x = F_{xrr} = 3627\ N \tag{7.122}$$

Also:-

$$\Delta T = \Delta F_x R_o \tag{7.123}$$

Where: -

R_o Tyre radius (taken equal to 313 mm)

ΔT Maximum torque difference

ΔF_x Maximum longitudinal force difference (3627 N)

Evaluating equation. (7.123)

$$\Delta T = 1135\,Nm \tag{7.124}$$

Substituting in the WSDD torque relations:-

$$T_C = \Delta T\left(\frac{N_{G9}}{N_{G10}}\right) \tag{7.125}$$

Where: -

$$\left(\frac{N_{G9}}{N_{G10}}\right) = \left(\frac{1}{6}\right)$$

Evaluating equation (7.125), the maximum required control shaft torque is evaluated as:-

$$T_c = 198.2\,Nm \tag{7.126}$$

This value represents the maximum control shaft torque in TFD mode. As the current hardware has been designed to work in WSD model it can control the torque difference between the inner and outer wheels including the ability to brake the inner wheel. This has been demonstrated through its ability to slow down the inner wheel as shown in Fig (7.8). In this condition, where the maximum traction and maximum braking forces are applied to the outer and the inner wheels, respectively, the maximum longitudinal force difference and hence control shaft torque would be doubled.

The maximum driven wheel torque difference is then given as: -

$$\Delta T = WR_o\left(\frac{a}{a+b}\right)\left(\frac{t_r}{t_l+t_r} + \frac{t_l}{t_l+t_r}\right) \tag{7.127}$$

Substituting with the reviewed vehicle data leads to: -

$$\Delta T = 2270\,Nm \tag{7.128}$$

$$T_c = 396.4\,Nm \tag{7.129}$$

Although this torque is not high for most vehicle applications, it could be further optimised along with the control shaft rotational speeds to match the driving motor characteristics through adjusting the WSDD size of gears or application of a gearbox between the control shaft and the motor. After the above prediction of the maximum required control shaft rotational speeds and torque, the control motor power requirement has been investigated in the next section.

7.6.3 Control Shaft Power Demand

As the WSDD control shaft power source is planned to be an electrical motor, the WSDD feasibility would be compromised if the power demands were too high. To prove the WSDD feasibility, the extreme power demand of the control shaft has been calculated as: -

$$Power = \omega_{S2}\, T_{S2} \tag{7.130}$$

Accordingly, from Table (7.3), the extreme motor power required at different vehicle travelling velocities was evaluated, Table (7.4)

Vehicle velocity (m/s)	7	10	15	20	25	30	35	40	45	50
Maximum required control motor power (Watt)	8147	5522	3659	2735	2189	1826	1562	1367	1215	1096

Table (7.4) Extreme control motor power required at different vehicle travelling velocities

For feasibility assessment, the maximum battery current requirement has been calculated for the targeted maximum velocity of 50 m/s. Assuming 100% motor efficiency the battery current is calculated as: -

$$\text{Battery current} = \frac{\text{Power demand}}{\text{Battery voltage}} \tag{7.131}$$

For a 12 v battery: -

$$\text{Current} = \frac{1096}{12} = 91 \text{ A} \tag{7.132}$$

The investigated power requirements are the theoretical most extreme and it would never be applied or needed. Accordingly the applied motor would not need to meet this power demand and a special full study is recommended for this control motor sizing. Even so, the achieved results prove that the WSDD control shaft power requirements lie within the feasible range even under the most extreme conditions.

From the required battery current point of view, the trend in the vehicle industry is to adopt the high power 42 Volt batteries, which will make the WSDD even more feasible.

For the advanced 42 volt battery: -

$$\text{Current} = \frac{1096}{42} = 26 \text{ A} \tag{7.133}$$

After investigating the WSDD feasibility from different points of view, the WSDD potential benefits are presented in the next section. Also, the schematic arrangements required to influence the WSDD different modes of operations are outlined.

7.7 WSDD Potential Benefits

As a result of achieving its design targets the WSDD differential would be able to apply a number of beneficial differential modes of operation. These modes are outlined and described in the following sections.

7.7.1 Wheel Speed Distribution Differential Mode

In the Wheel Speed Distribution Differential mode, an electrical motor controlled by a speed controller would be employed to drive the control shaft through a gearbox, Fig (7.18). The gearbox has been introduced to match both the control shaft and the motor optimum speeds. The speed controller will work under the control of the main Wheel Speed Distribution controller. This controller employs the WSD onboard model and will need input signals at least from the drive shaft speed and the steering wheel position. The hardware in this mode would facilitate the distribution of the driven wheel speeds.

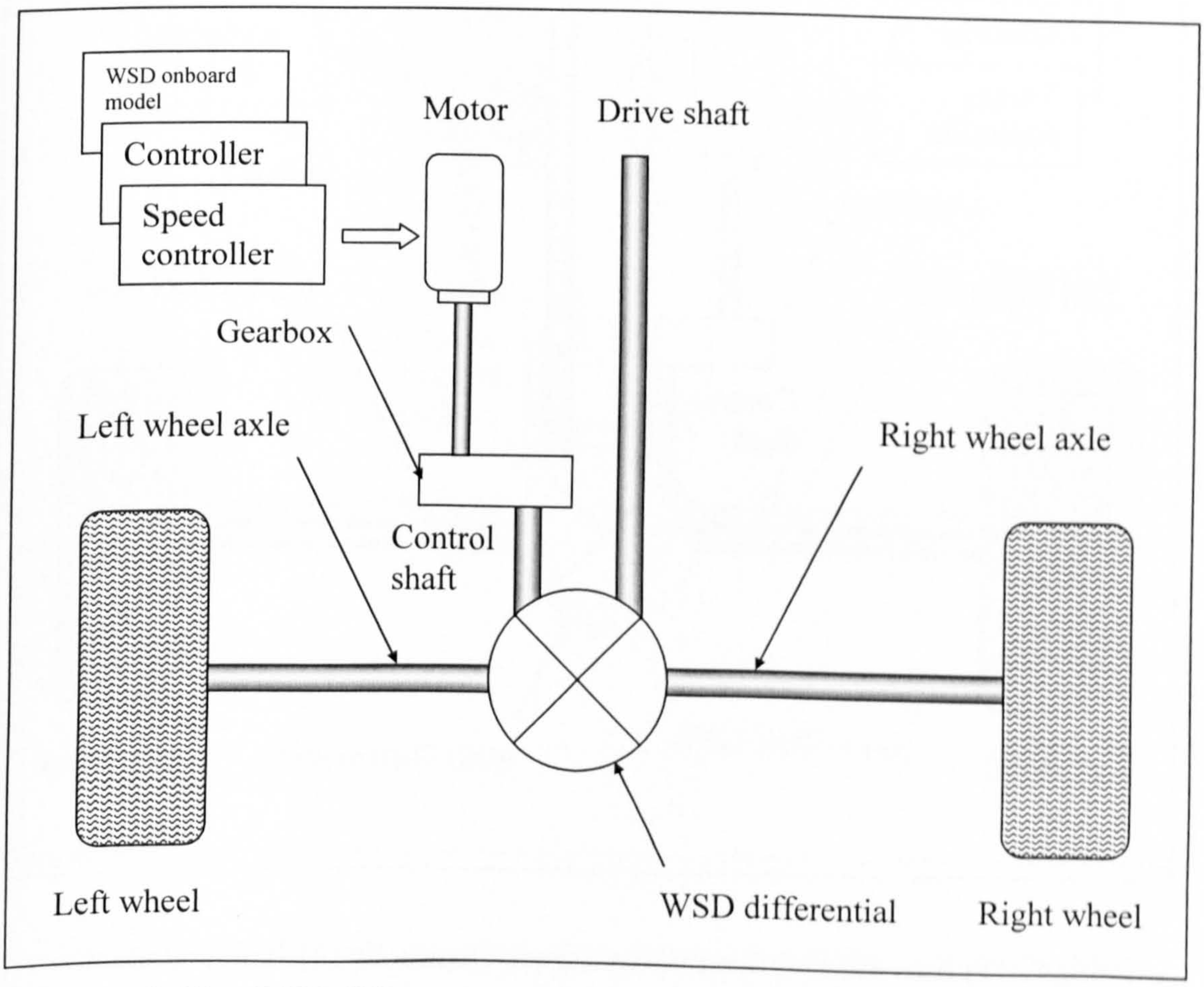

Fig (7.18) New WSD differential in Wheel Speed Distribution Differential mode

7.7.2 Torque Distribution Differential Mode

In the Torque Distribution Differential mode, an electrical motor controlled through a torque controller would be employed to drive the control shaft through a gearbox, Fig (7.19). The gearbox has been introduced to match the motor optimum torque range and the control shaft required torque. The torque controller will work under the control of a main Traction Torque Distribution controller. This controller employs the TFD onboard model and needs input signals from the steering wheel position and either lateral velocity sensor or yaw rate sensor. Both sensors could be employed together to facilitate a more robust control system. The hardware in this mode facilitates the distribution of the driving torque to the driven wheels.

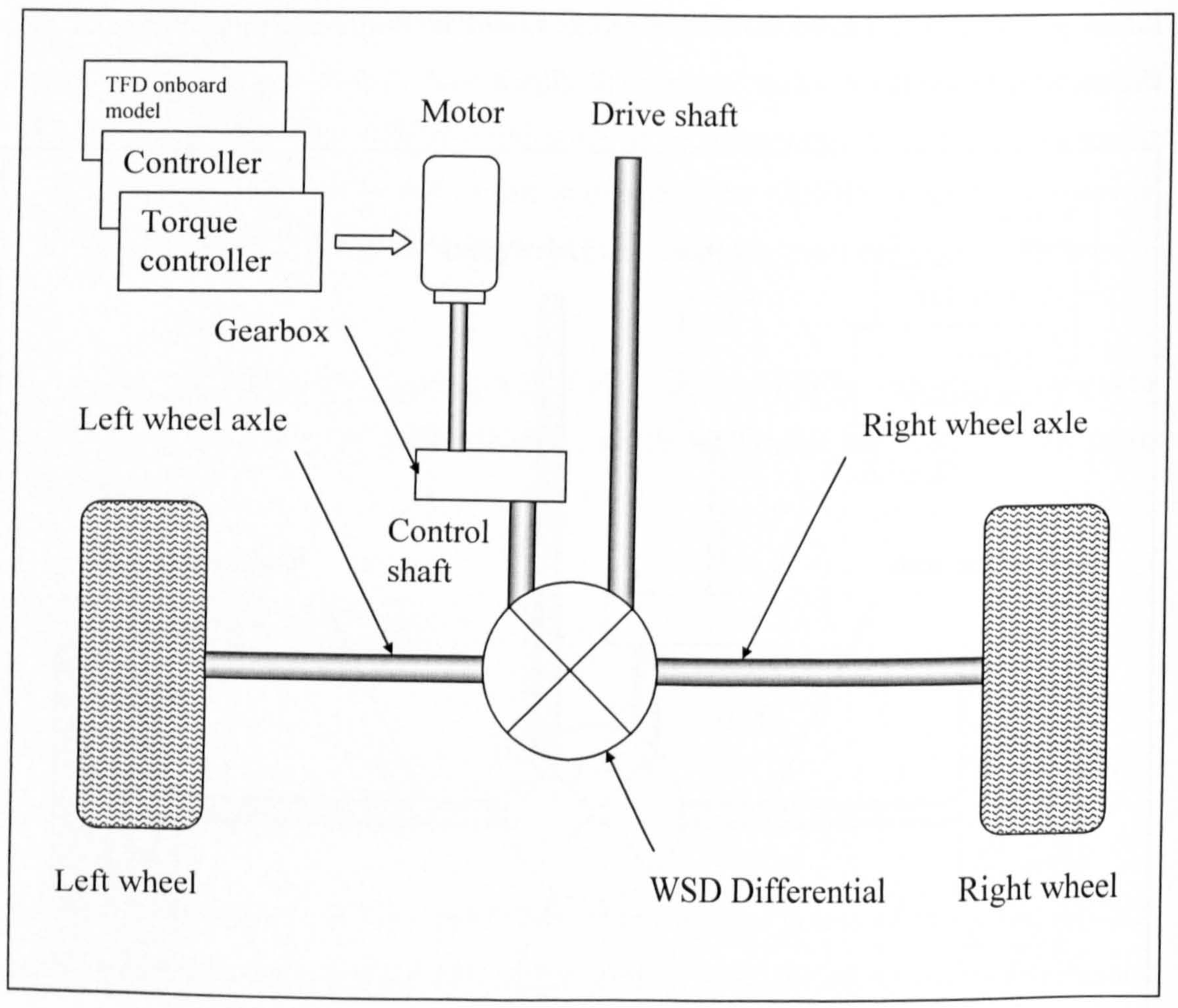

Fig (7.19) New WSD differential in Torque Distribution Differential mode

7.7.3 Controlled Limited Slip Differential Mode

In the Controlled Limited Slip Differential mode, an electrically controlled viscous coupling attached to the vehicle chassis could be used to limit the speed of the control shaft, Fig (7.20). The controller in this mode would make use of the WSD onboard model in predicting the effect of the driven wheel speed difference. A gearbox would be employed to match the optimum viscous coupling torque and speed ranges with the torque and speed ranges required for the control shaft. The controller would employ the WSD onboard model to evaluate the wheel slip limiting effect on the vehicle handling. The hardware in this mode facilitates limiting the speed difference between the right and left driven wheels.

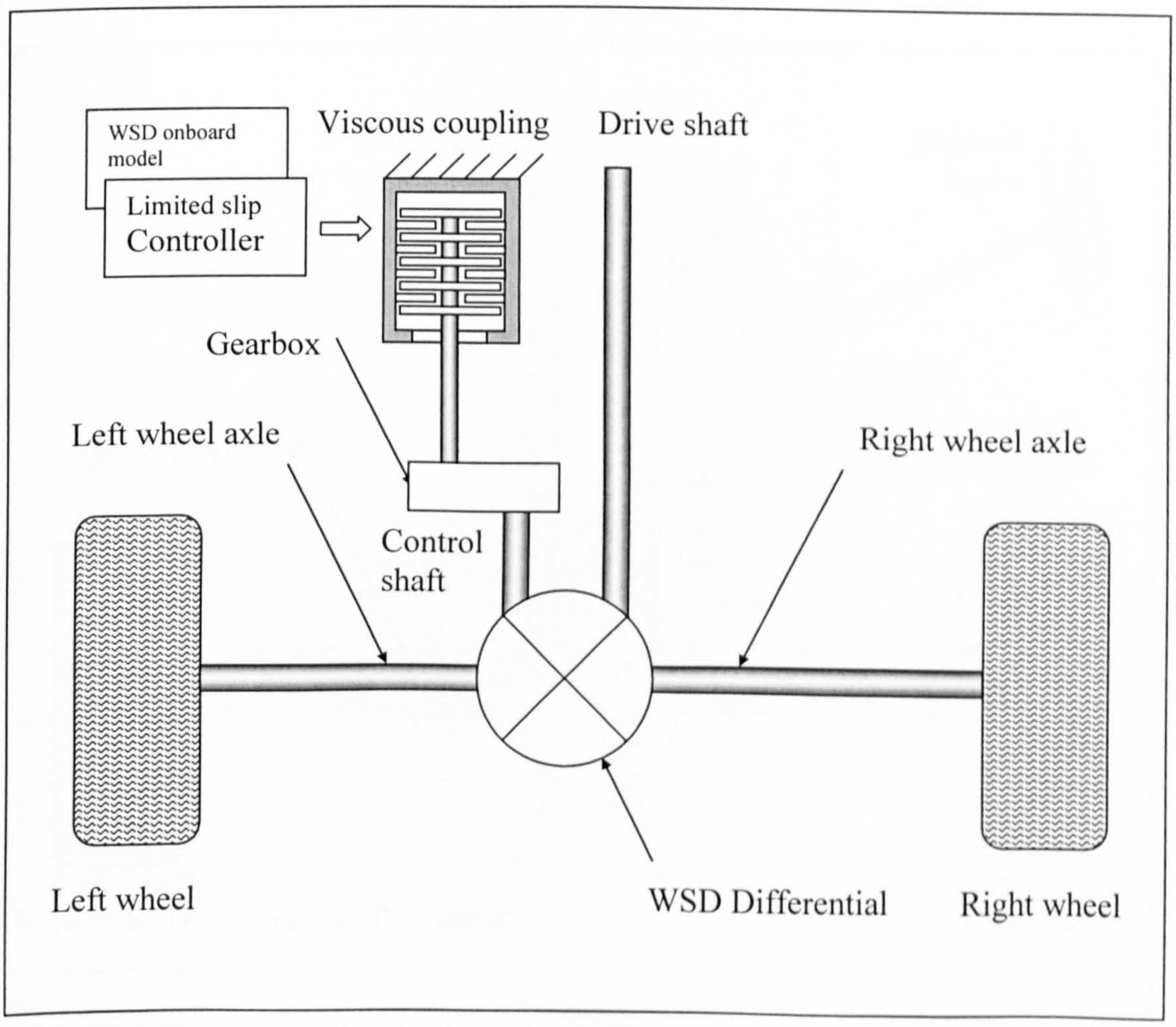

Fig (7.20) New WSD differential in Controlled Limited Slip Differential mode

7.7.4 Uncontrolled Wheel Speed Distribution Differential Mode

In the Uncontrolled Wheel Speed Distribution Differential mode, a Continuous Variable Transmission CVT would be employed to drive the control shaft through a gearbox, Fig (7.21). The gearbox is employed to match the optimum speed and torque of the CVT with the speed and torque required for the control shaft. The CVT would be controlled through a mechanical attachment to the steering wheel. This mode can be considered to be a differential lock with continuous variable speed ratio, as the driven wheel speed difference is locked at a ratio that is continuously controlled by the steering wheel angle. This mode would be suitable to develop a pure mechanical Wheel Speed Distribution that would benefit failure sensitive vehicles such as desert cruisers.

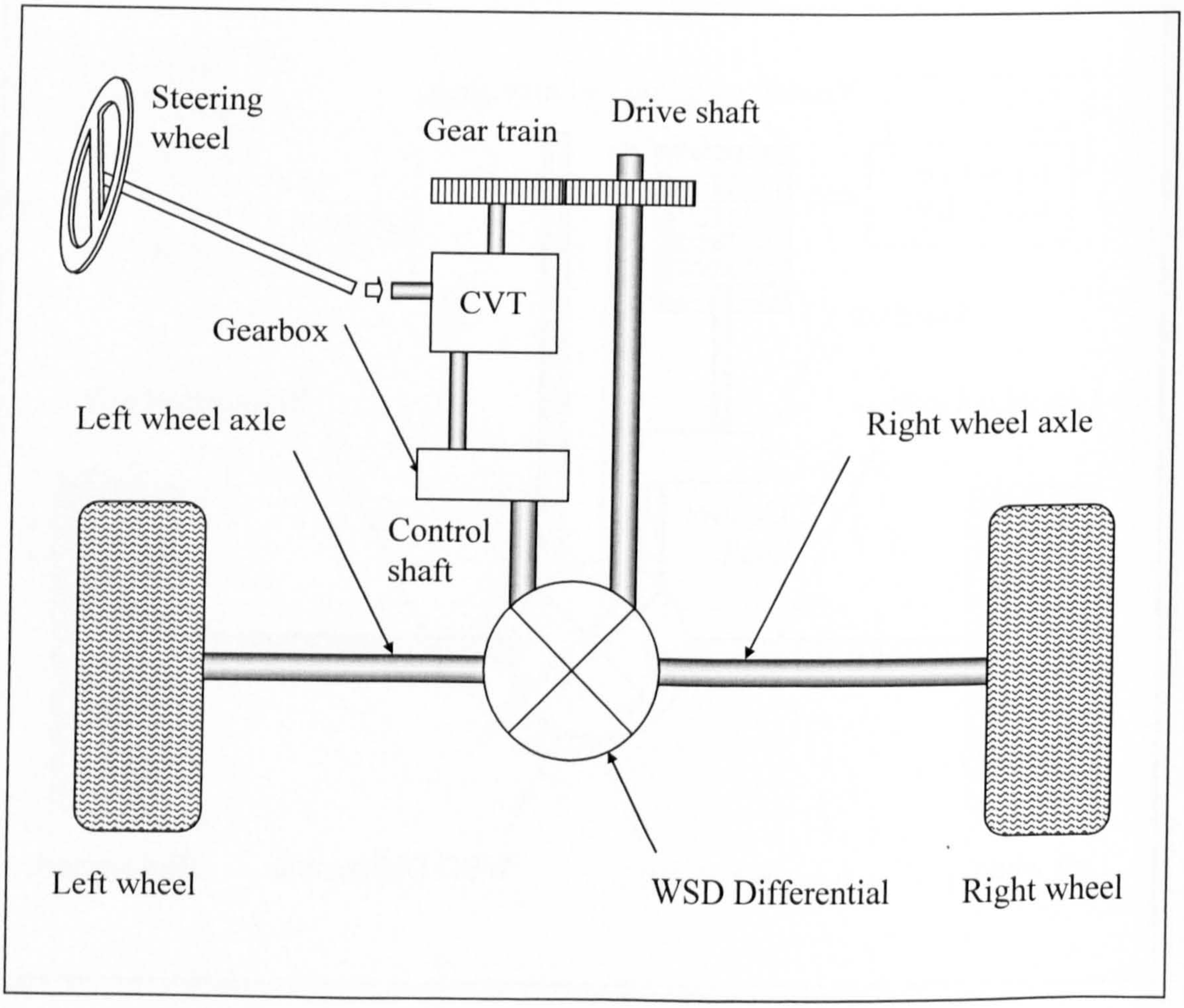

Fig (7.21) New WSD differential in uncontrolled Wheel Speed Distribution Differential mode

7.7.5 Differential Lock Mode

In the Differential Lock mode, a disc brake would be connected to the control shaft, Fig (7.22). The system controller would be allowed to brake the control shaft, forcing the right and left wheels to rotate at the same speed regardless of their torque. This mode would be beneficial when the vehicle is driven in a straight line on a slippery road. It would also facilitate off road driving. This mode could be activated either manually or through a dedicated vehicle handling controller. The WSD onboard model would be employed to investigate the effect of influencing the driven wheel speeds.

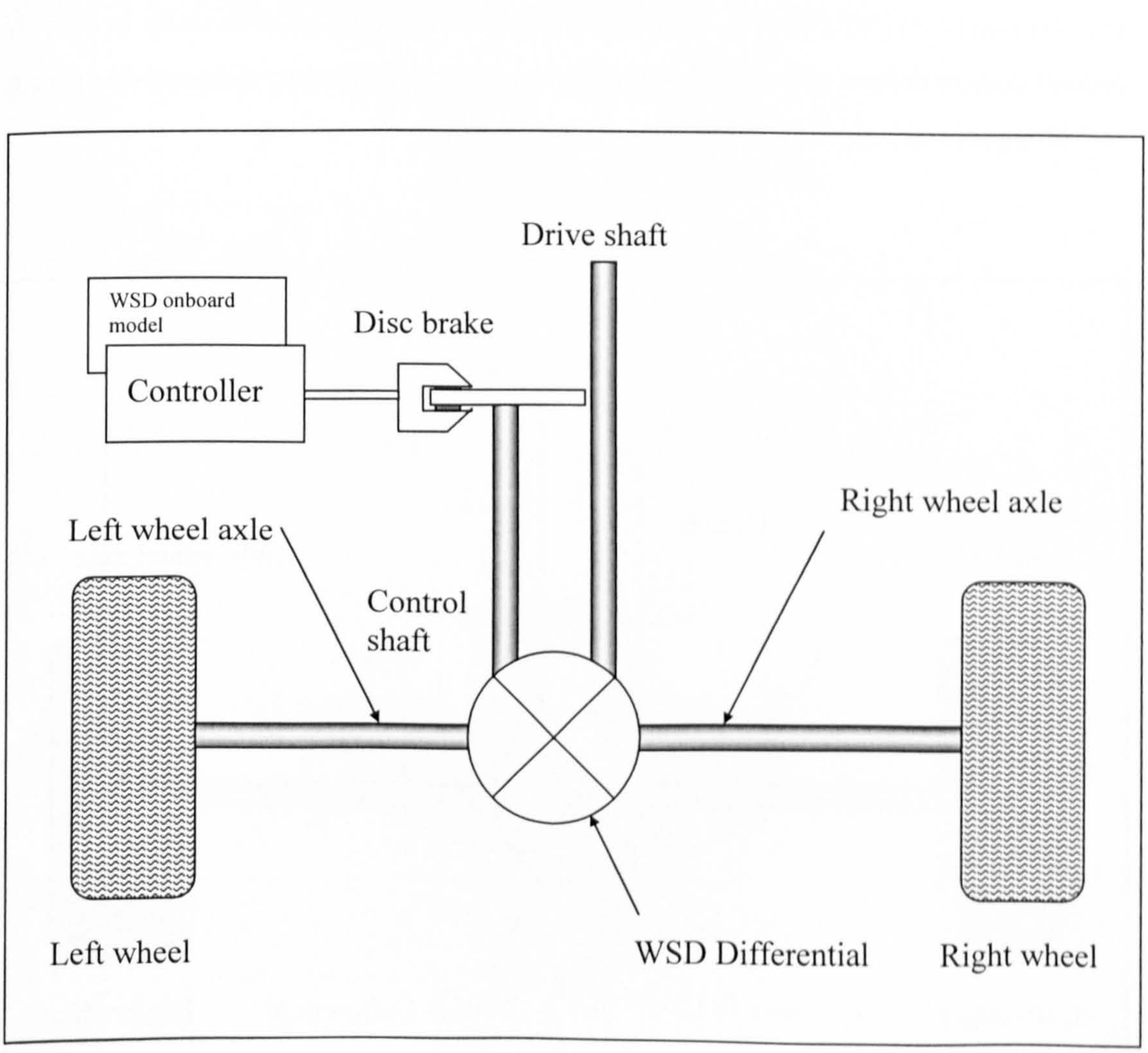

Fig (7.22) New WSD differential in Differential Lock mode

7.7.6 Open Differential Mode

For the Open Differential mode to be possible, the control shaft would be equipped with a clutch, Fig (7.23). When the clutch is disengaged, it would completely isolate the control shaft. Accordingly the left half shaft will rotate only under the influence of the drive shaft and the right half shaft. This will lead the right and left shafts to exhibit torque balance under the influence of the spider gear meshing between their side gears. The spider gear will also allow the half shafts to rotate at different rotational speeds. As both the achieved torque and speed characteristics are the same as those of an open differential, the new hardware would be functioning as a conventional open differential. This mode would be engaged automatically in case of control system failure or manually by drivers who enjoy the open differential driving feel in appropriate driving conditions.

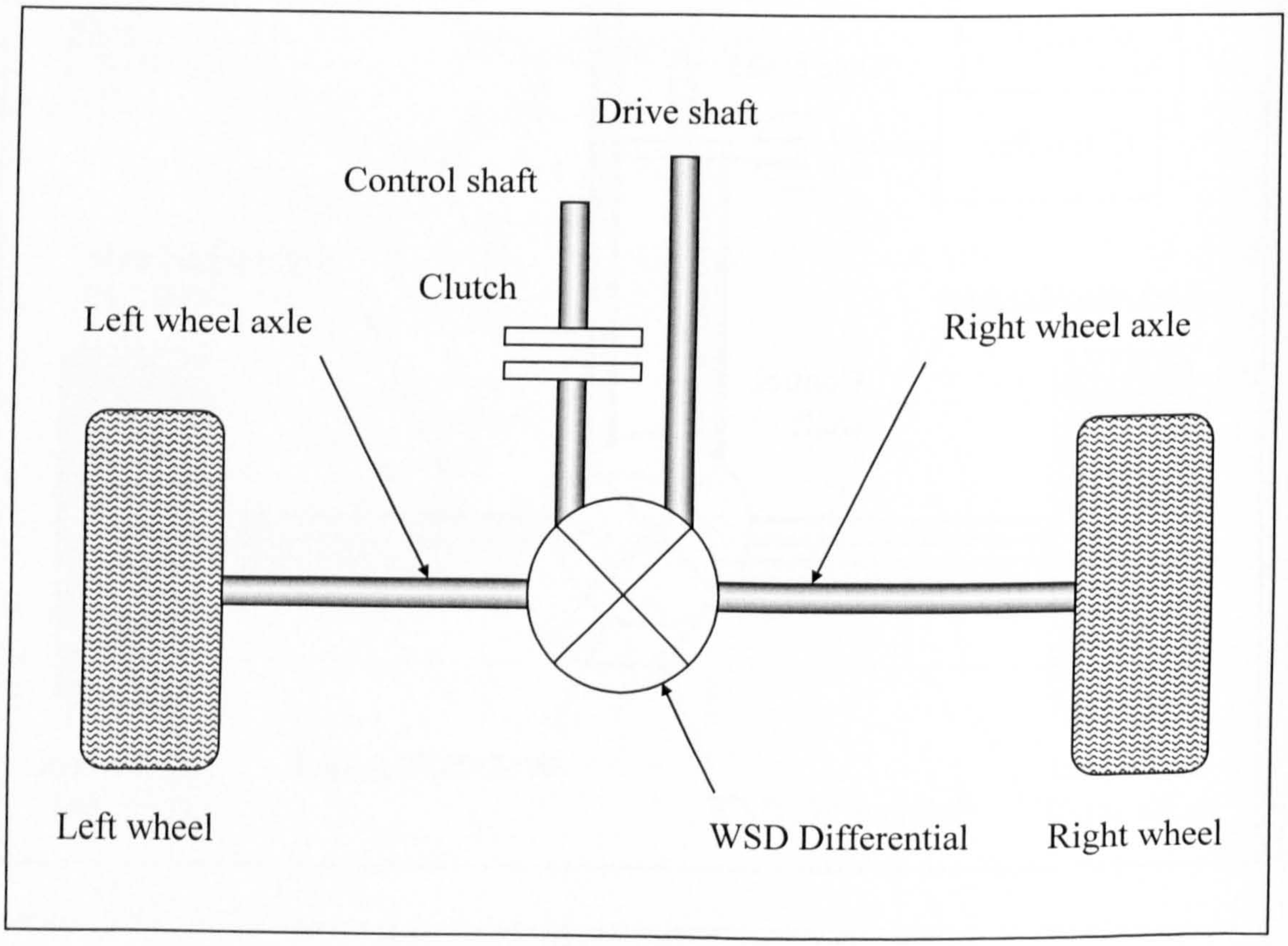

Fig (7.23) New WSD differential in Open Differential mode

7.7.7 Integrated Differential Mode

In this configuration, Fig (7.24) the WSDD would be capable of performing a set of different differential modes. However, a suitable integrated controller would be required. It would employ both TFD and WSD onboard models to investigate the effect of the control task before applying it. The controller would also allow a manual engagement of the brake and manual disengagement of the clutch. However, a proper design for the viscous coupling could eliminate the need for a separate brake and clutch. Extra care in the motor and controller design may allow for the elimination of the viscous coupling, without losing its function. This would highly simplify the system hardware while maintaining its performance benefits.

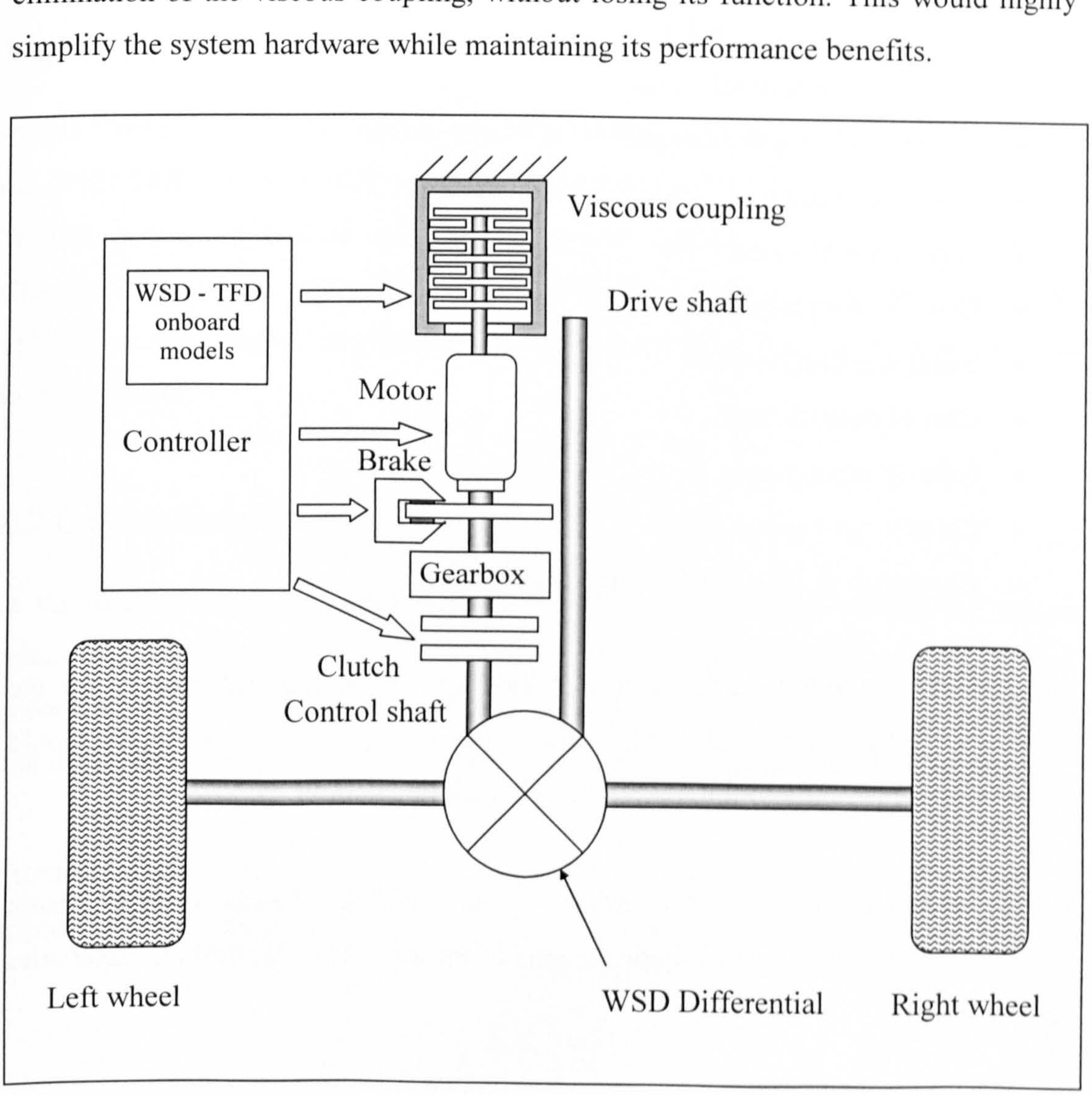

Fig (7.24) Integrated Differential configuration

7.8 Conclusions

In this chapter the hardware design goals have been laid out and the WSD hardware has been developed through different stages from first principles. The hardware speed and torque relations have been required to be linear and used to influence the design development stages.

The final Wheel Speed Distribution Differential (WSDD) has achieved the set of goals as described above that could be summarised as: -

- Capability to apply WSDC
- Linearity of speed relations
- Linearity of torque relations
- Ease of control
- Low controller load
- Low control power demand
- Small size and weight
- Ease of manufacture
- Ease of maintenance
- Capability to apply TFDC
- Capability to allow many differential modes

Accordingly the WSD hardware design has been considered satisfactory for the purpose of WSD control. Also it has many additional potential benefits and would contribute significantly to the field of vehicle handling control.

In the following chapter, conclusions of the WSDC chassis control system development and more detailed conclusions of the developed WSDD characteristics are presented.

Chapter 8

Wheel Speed Distribution Control System

8.1 Introduction

In this Chapter the WSDC vehicle handling model has been enhanced to incorporate the WSD Differential (WSDD) performance in order to investigate its effect on the WSDC system. To achieve this task, the novel WSDD performance equations of Chapter 7 have been manipulated to allow for their incorporation into the WSDC vehicle handling model. The final WSDC vehicle handling simulation model is given in Appendix G.

8.2 Conventional Differential

In this section the conventional differential drive shaft rotational speeds and torque relations presented in Chapter 7 are manipulated to accept integration with the non controlled vehicle handling model. This step is meant to demonstrate the similarities and differences of the WSDD performance with the conventional differential system.

From equations (7.12) and (7.6), the conventional differential drive shaft rotational speed and torque are given as: -

$$\omega_{S1} = \left(\frac{N_{G2}}{N_{G1}}\right)\left(\frac{\omega_{S5} + \omega_{S6}}{2}\right) \tag{8.1}$$

$$T_{S1} = (T_{G4} + T_{G5})\left(\frac{N_{G1}}{N_{G2}}\right) \tag{8.2}$$

As in Chapter 7, the gear ratio $\left(\frac{N_{G1}}{N_{G2}}\right)$ is taken to be equal to $\left(\frac{1}{3}\right)$, accordingly: -

$$\omega_{S1} = \left(\frac{3}{2}\right)(\omega_{S5} + \omega_{S6}) \tag{8.3}$$

$$T_{S1} = \left(\frac{1}{3}\right)(T_{G4} + T_{G5}) \tag{8.4}$$

Note that T_{G4} and T_{G5} are equal due to the conventional differential design.

8.3 WSDD Drive Shaft and Control Shaft Speeds

In this section the relations governing the drive shaft and control shaft of the novel WSDD are presented. These equations, developed in Chapter 7, have been treated to accept fitting in the CGT WSDC vehicle handling model.

From equations (7.54) and (7.56), the left and right differential half shafts speeds are given as: -

$$\omega_{S6} = \omega_{S1}\left(\frac{N_{G1}}{N_{G2}}\right) - \omega_{S2}\left(\frac{N_{G9}}{N_{G10}}\right) \tag{8.5}$$

$$\omega_{S5} = \omega_{S1}\left(\frac{N_{G1}}{N_{G2}}\right) + \omega_{S2}\left(\frac{N_{G9}}{N_{G10}}\right) \tag{8.6}$$

Substituting equation (8.5) from (8.6): -

$$\omega_{S5} - \omega_{S6} = 2\omega_{S2}\left(\frac{N_{G9}}{N_{G10}}\right) \tag{8.7}$$

Rearranging: -

$$\omega_{S2} = \left(\frac{\omega_{S5} - \omega_{S6}}{2}\right)\left(\frac{N_{G10}}{N_{G9}}\right) \tag{8.8}$$

As in chapter 7, the gear ratio $\left(\frac{N_{G9}}{N_{G10}}\right)$ is taken to be equal to $\left(\frac{1}{6}\right)$, accordingly: -

$$\omega_{S2} = \left(\frac{\omega_{S5} - \omega_{S6}}{3}\right) \tag{8.9}$$

Equation (8.9) represents the novel WSDD control shaft angular velocity and its relation to the driven wheel angular velocities. It demonstrates that the control shaft is stationary when the driven wheels are running at equal rotational speeds. It also demonstrates the low angular velocity required of the control shaft, which is only one third of the difference between the driven wheel angular velocity.

To investigate the drive shaft angular velocity, equations (8.5) and (8.6) have been added. Accordingly: -

$$\omega_{S5} + \omega_{S6} = 2\omega_{S1}\left(\frac{N_{G1}}{N_{G2}}\right) \tag{8.10}$$

Rearranging: -

$$\omega_{S1} = \left(\frac{\omega_{S5} + \omega_{S6}}{2}\right)\left(\frac{N_{G2}}{N_{G1}}\right) \tag{8.11}$$

Substituting for the $\left(\frac{N_{G1}}{N_{G2}}\right)$ gear ratio: -

$$\omega_{S1} = \left(\frac{3}{2}\right)(\omega_{S5} + \omega_{S6}) \tag{8.12}$$

This shows that the WSDD drive shaft rotational speed relation is the same as that of the conventional differential, which shows that there will be no need for the engine speed to be altered to facilitate the application of WSDC system. This is a positive design point.

8.4 WSDD Drive Shaft and Control Shaft Torque

In this section, the torque relations of the novel WSDD, developed in Chapter 7, are presented and manipulated for acceptance within the WSDC vehicle handling model.

The control shaft torque equation is as developed in Chapter 7, equation (7.88): -

$$T_C = (T_L - T_R)\left(\frac{N_{G9}}{N_{G10}}\right) \tag{8.13}$$

Substituting for the $\left(\frac{N_{G9}}{N_{G10}}\right)$ gear ratio: -

$$T_C = \left(\frac{T_L - T_R}{6}\right) \tag{8.14}$$

The above novel WSDD control shaft torque relation demonstrates the low torque requirement, which is only one sixth of the required driven wheel torque difference.

The drive shaft torque equation is as developed in Chapter 7, equation (7.95): -

$$T_D = -2T_R\left(\frac{N_{G1}}{N_{G2}}\right) + 2\Delta T\left(\frac{N_{G6}}{N_{G7}}\right) \tag{8.15}$$

As in chapter 7, the gear ratio $\left(\frac{N_{G6}}{N_{G7}}\right)$ has been taken to be $\left(\frac{1}{6}\right)$. Substituting for these gears ratios and rearranging: -

$$T_D = -\left(\frac{2}{3}\right)T_R + \left(\frac{T_L - T_R}{3}\right) \tag{8.16}$$

The above novel WSDD drive shaft torque relation demonstrates the extra torque the engine would have to supply. The extra torque is double the control shaft torque while at higher rotational speed. This demonstrates one of the biggest WSDC system achievements, that the engine will contribute to the power required for the vehicle yaw control without any special engine control.

To prove the WSDC system feasibility and performance, the equations representing the drive shaft and control shaft speed and torque relations have been embedded within the WSDC vehicle handling model. Accordingly, the WSDC vehicle handling model has been used to investigate the effect of the novel hardware on the WSDC vehicle handling results.

8.5 WSDC System Results

In this section the upgraded WSDC vehicle handling model has been used to investigate the control shaft torque, rotational speeds and power required for the set of vehicle manoeuvres described in Chapter 6.

In the first test the WSDD and the conventional torque requirements have been evaluated for the Buick and Ferrari WSDC vehicles in the step steer manoeuvre, Fig (8.1) and Fig (8.2). The ratio between the drive shaft torque and the control shaft torque proves that the majority of the torque required to enhance the vehicle handling performance has been extracted from the engine (drive shaft), which reduces the additional control torque requirements.

The required torque for both control shaft and drive shaft plotted in Figs (8.1) and (8.2) shows the expected increase as the vehicle velocity increased. It also shows the higher torque demand of the heavier vehicle (Buick). The comparison with the conventional differential torque showed good employment of the available engine torque that is not properly employed by the conventional differential. This good employment reflects in better handling performance of the WSDC vehicles.

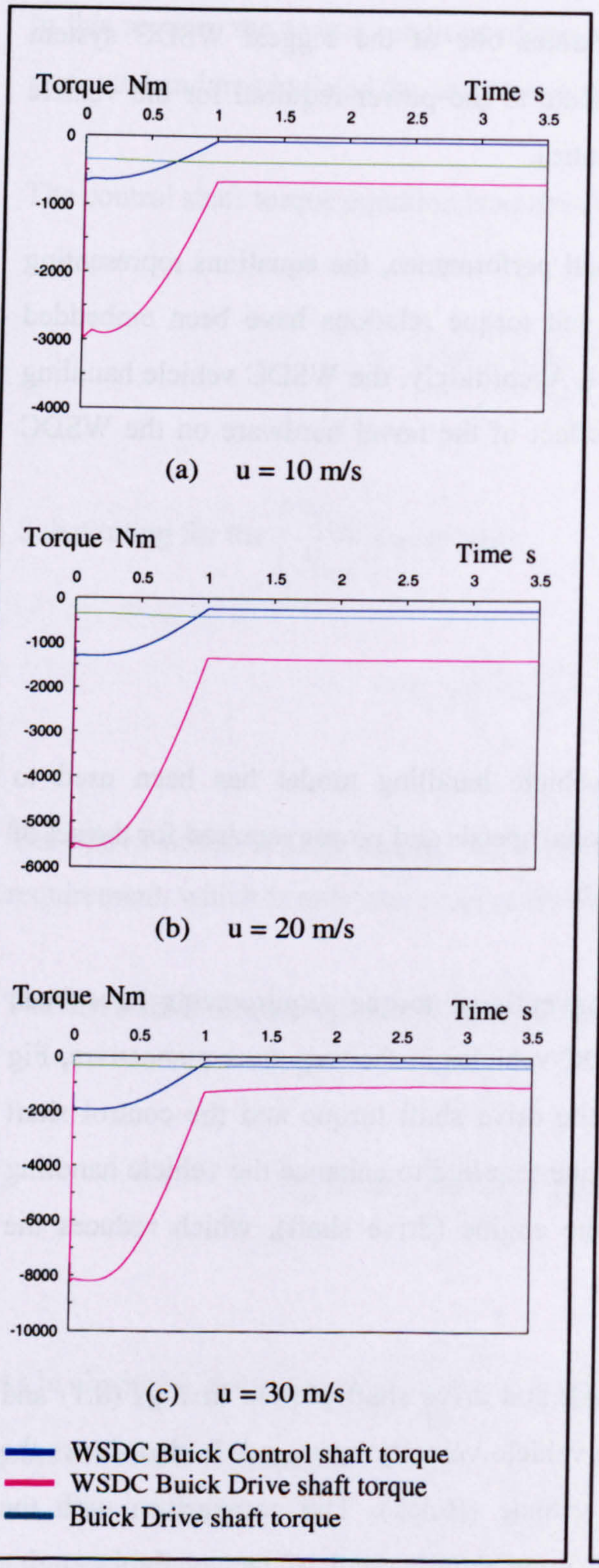

Fig (8.1) WSDD torque of Buick in step steer manoeuvre

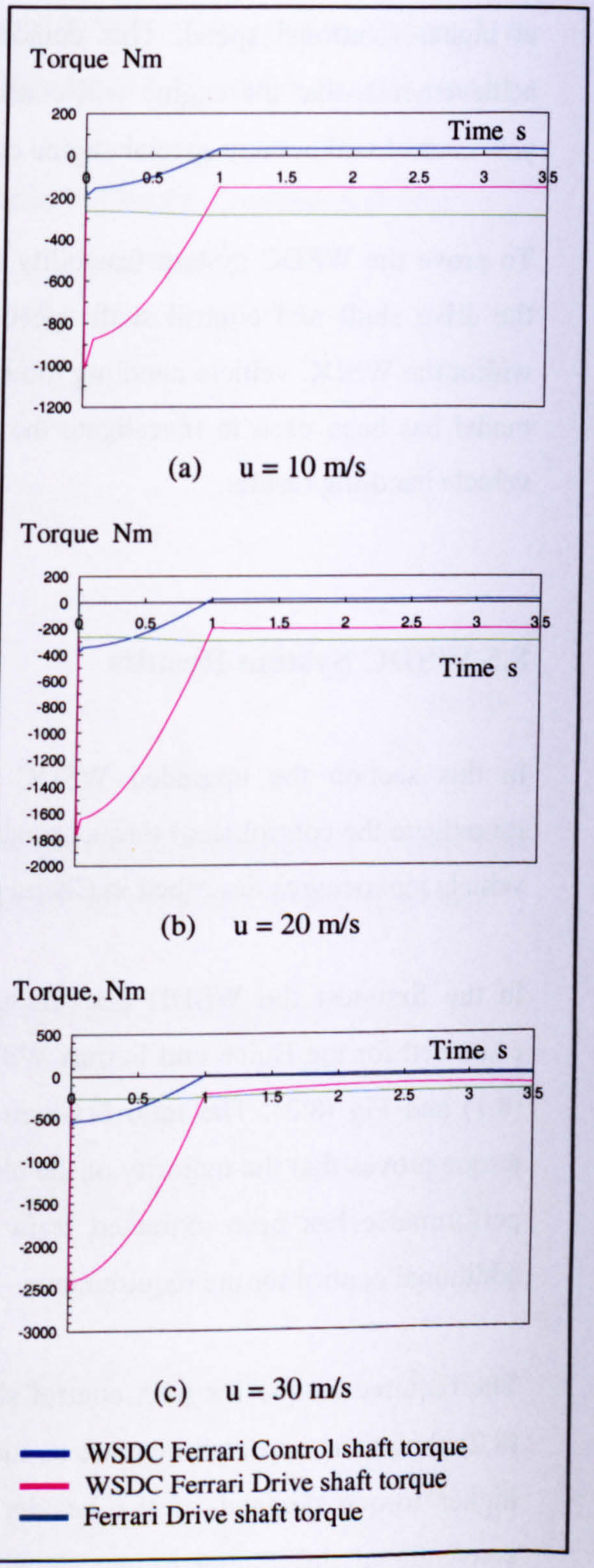

Fig (8.2) WSDD torque of Ferrari in step steer manoeuvre

To further prove the WSDC system feasibility, the control shaft rotational speeds have been evaluated for both Buick and Ferrari WSDC vehicles, Fig (8.3) and Fig (8.4) respectively. The results show that quite slow control shaft rotational speeds are required, which adds to the feasibility of the developed WSDC system.

As control power is a significant point in proving the feasibility of the WSDC system, the control shaft power requirements have also been evaluated. For Buick and Ferrari WSDC vehicles, the power requirements, Fig (8.5) and Fig (8.6), respectively have been found to be reasonable especially for the light weight Ferrari vehicle. For the heavier Buick, the peak power requirement of some 2.5 kW at 30 m/s is easily achievable by DC motor. This result further proves the WSDC system feasibility.

In the second test the WSDD and the conventional differential torque requirements have been evaluated for Buick and Ferrari WSDC vehicles in the lane change manoeuvre, Fig (8.7) and Fig (8.8). The levels of conventional differential drive shaft torque, WSDD control shaft torque and WSDD drive shaft torque, show the required torque that has been shifted to the drive shaft by the WSDD. Accordingly the control shaft torque requirements have been reduced to feasible levels.

The control shaft rotational speeds of the Buick and Ferrari WSDC vehicles in the lane change manoeuvre, Fig (8.9) and Fig (8.10), showed the feasible levels of required control shaft speeds.

Finally, the power requirements of the control shaft for the Buick and Ferrari WSDC vehicles in the lane change manoeuvre, Fig (8.11) and Fig (8.12), are reasonable especially for the Ferrari vehicle and the Buick vehicle at lower velocities. Even at the highest velocity (30 m/s) manoeuvre for the later, the peak power demand of some 6.5 kW is well within the capacity of the DC motor. As the current trend in the vehicle industry is towards lighter vehicles with lower moments of inertia, the WSDC system is therefore considered highly feasible.

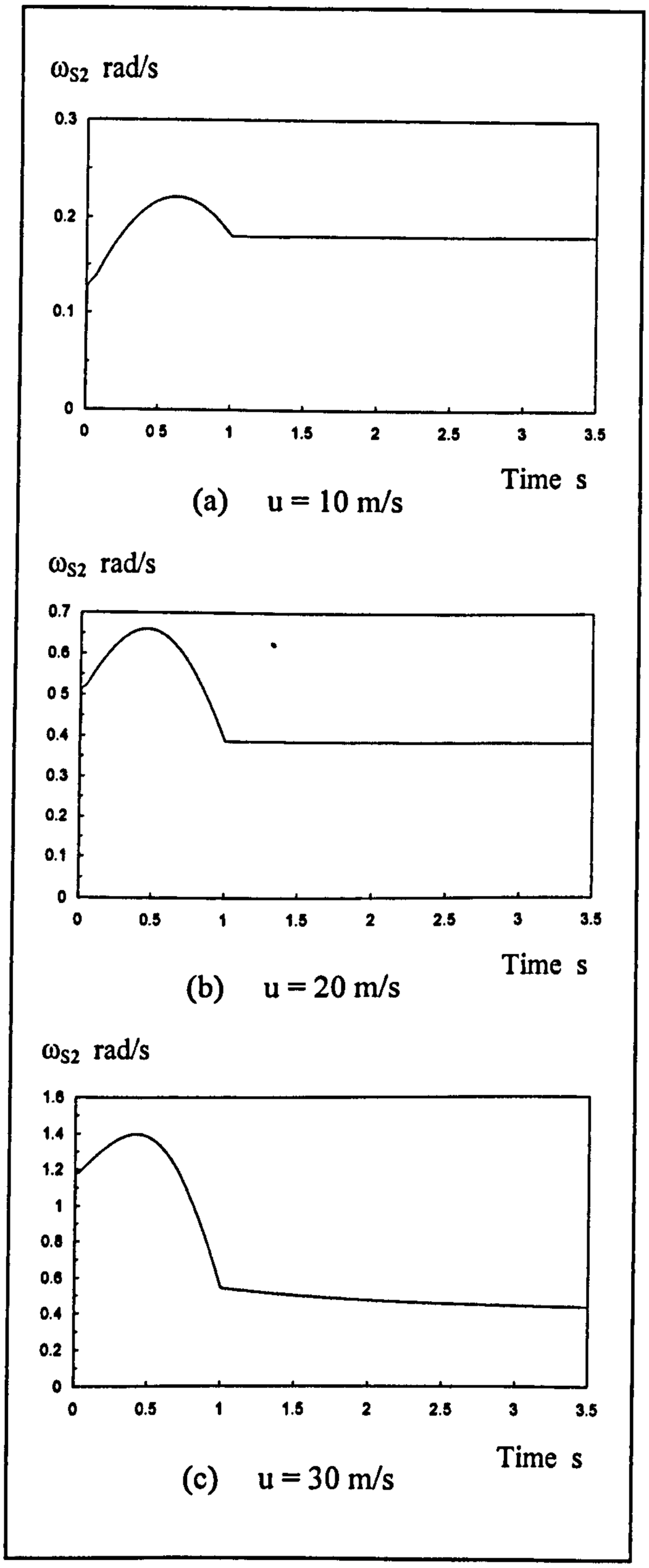

(a) u = 10 m/s

(b) u = 20 m/s

(c) u = 30 m/s

Fig (8.3) Control shaft rotational speed of Buick in step steer manoeuvre

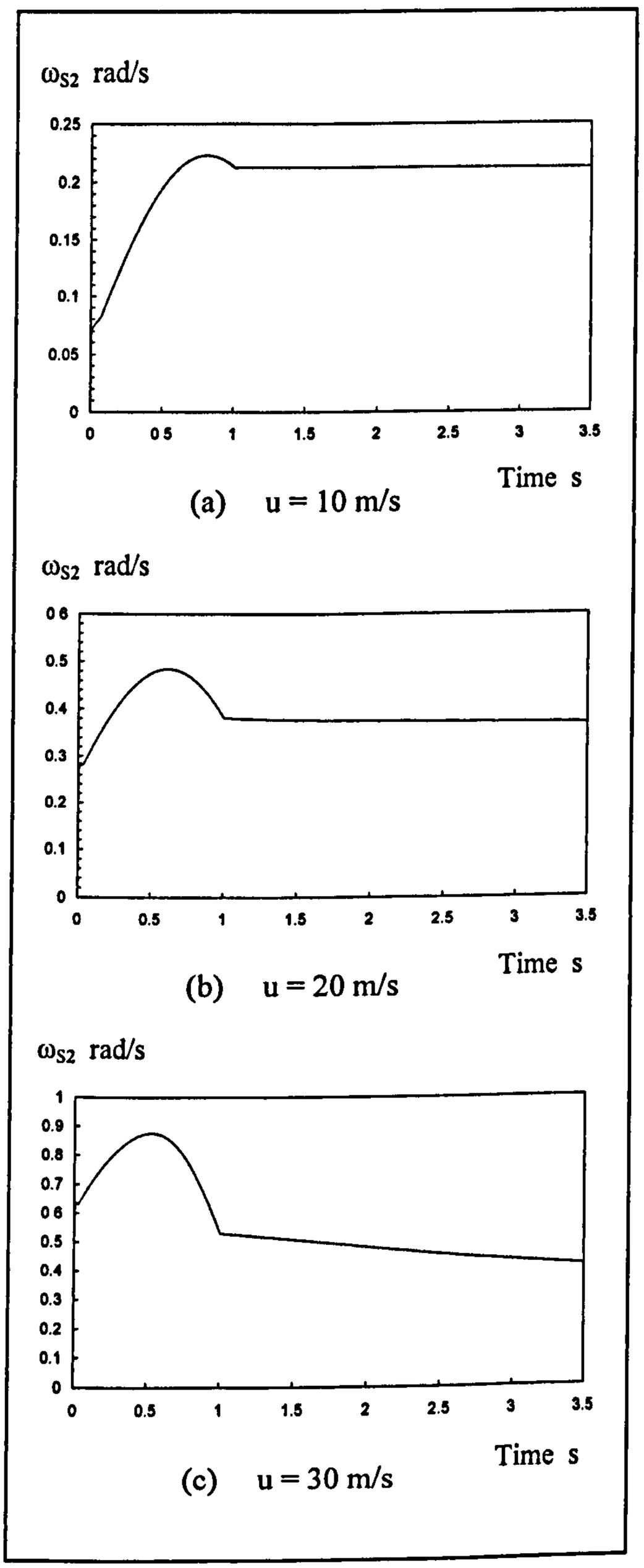

(a) u = 10 m/s

(b) u = 20 m/s

(c) u = 30 m/s

Fig (8.4) Control shaft rotational speed of Ferrari in step steer manoeuvre

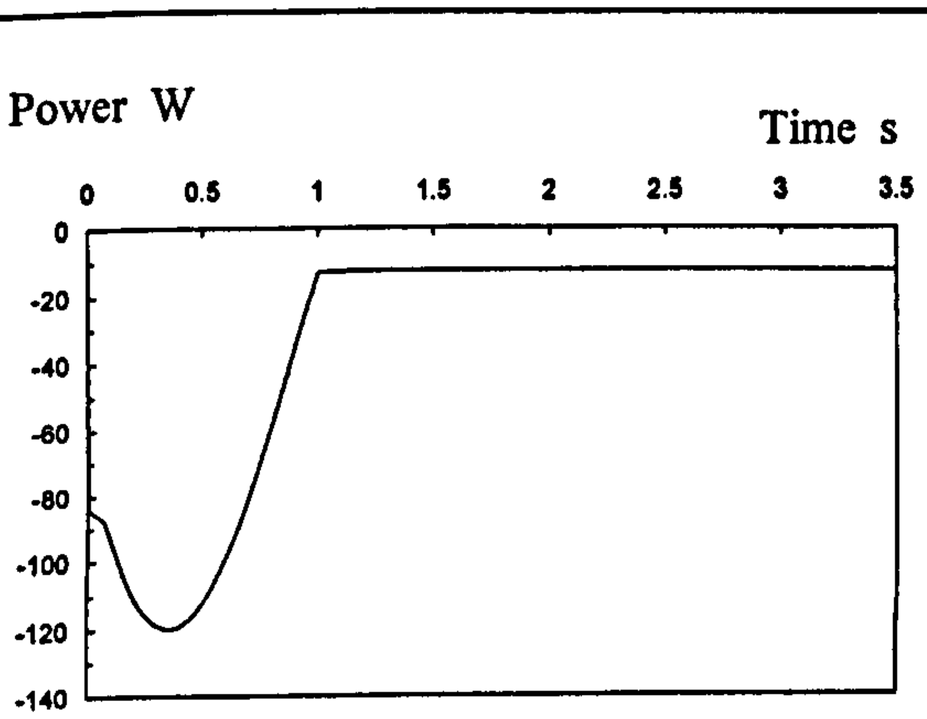

(a) u = 10 m/s

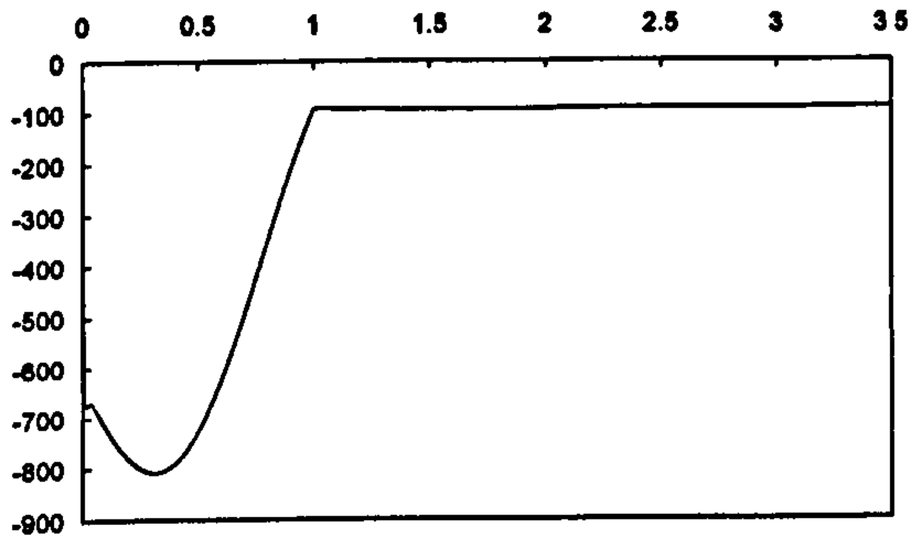

(b) u = 20 m/s

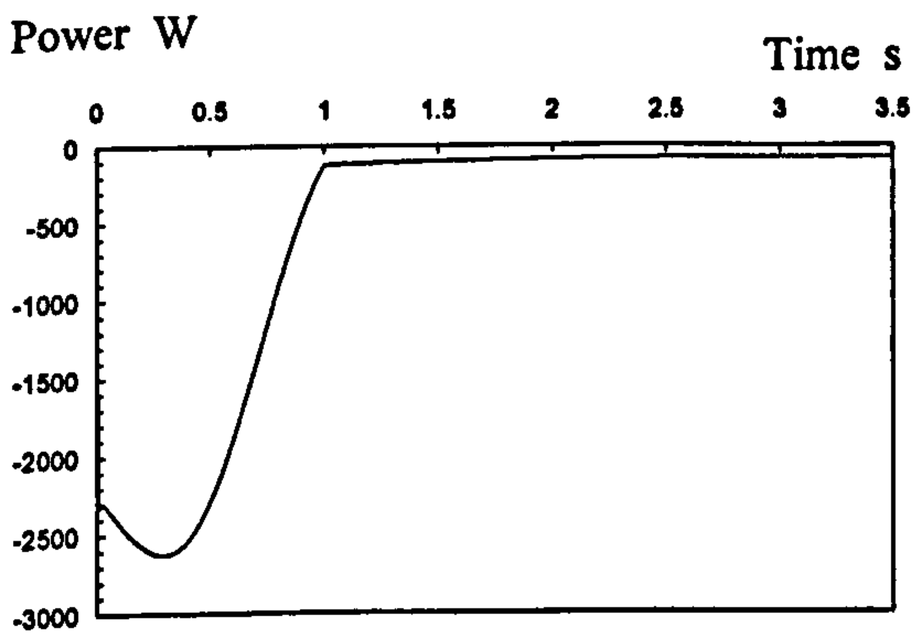

(c) u = 30 m/s

Fig (8.5) Control shaft power of Buick in step steer manoeuvre

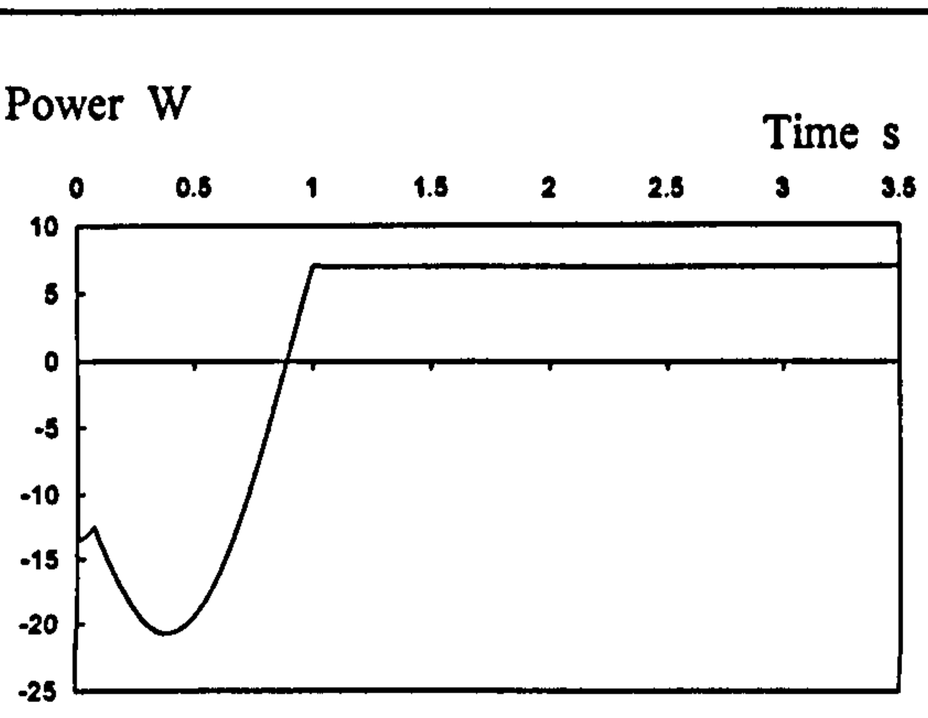

(a) u = 10 m/s

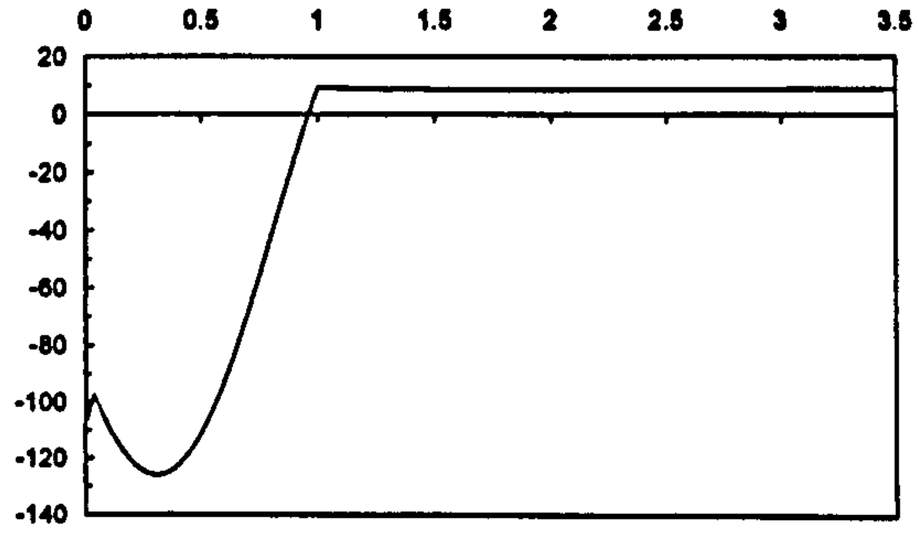

(b) u = 20 m/s

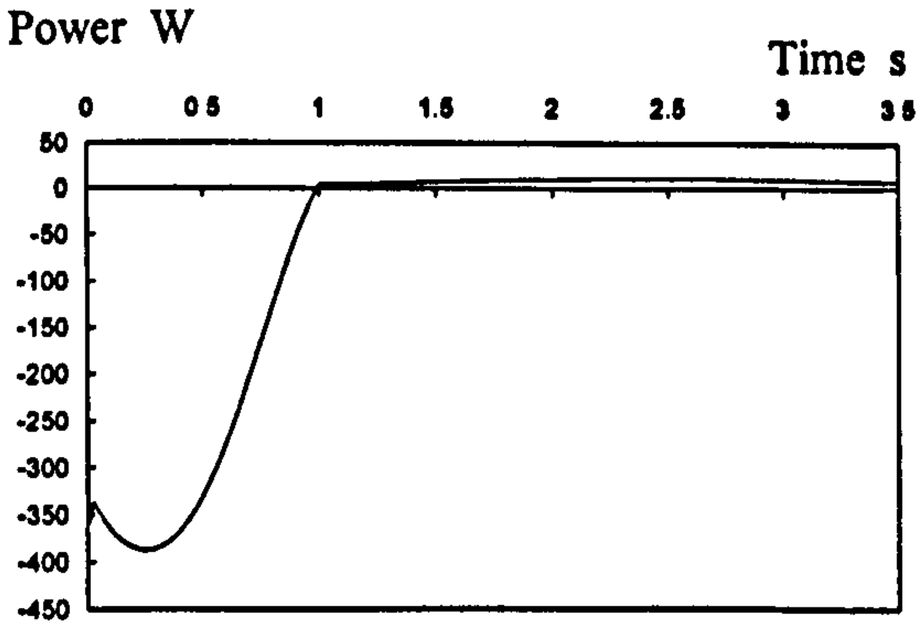

(c) u = 30 m/s

Fig (8.6) Control shaft power of Ferrari in step steer manoeuvre

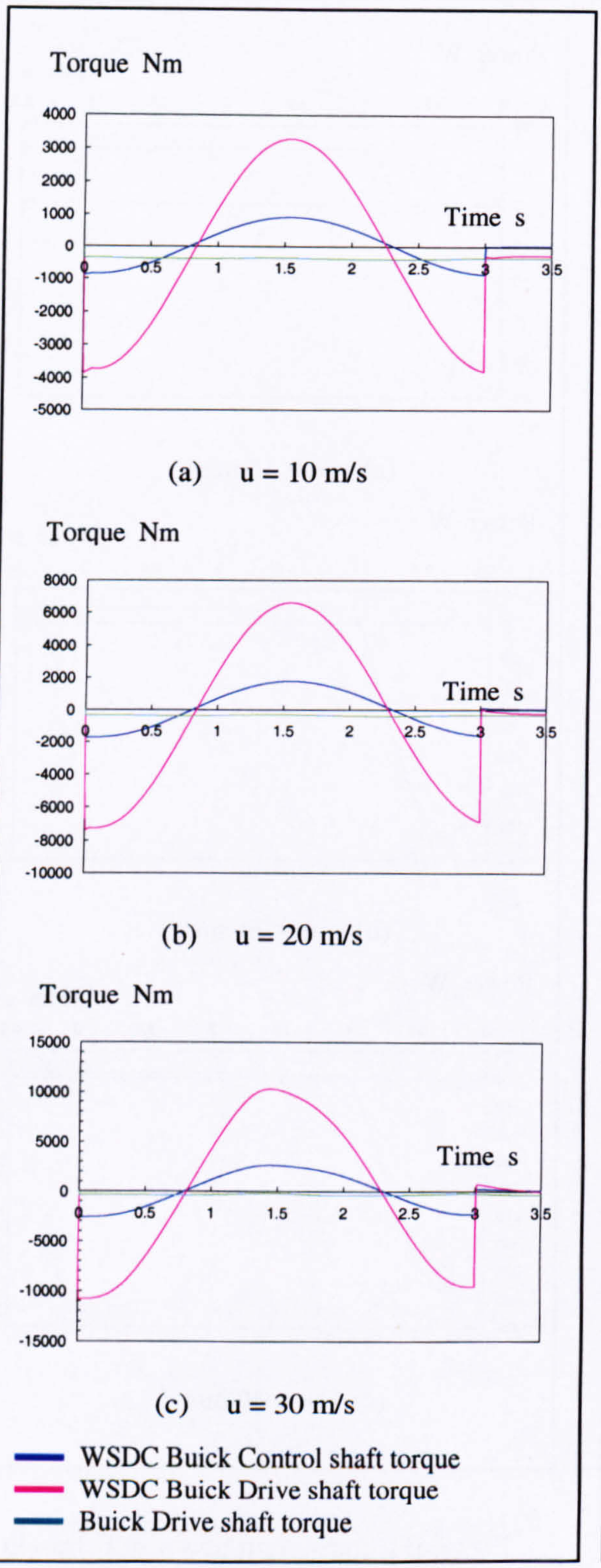

(a) u = 10 m/s

(b) u = 20 m/s

(c) u = 30 m/s

WSDC Buick Control shaft torque
WSDC Buick Drive shaft torque
Buick Drive shaft torque

Fig (8.7) WSDD torque of Buick in lane change manoeuvre

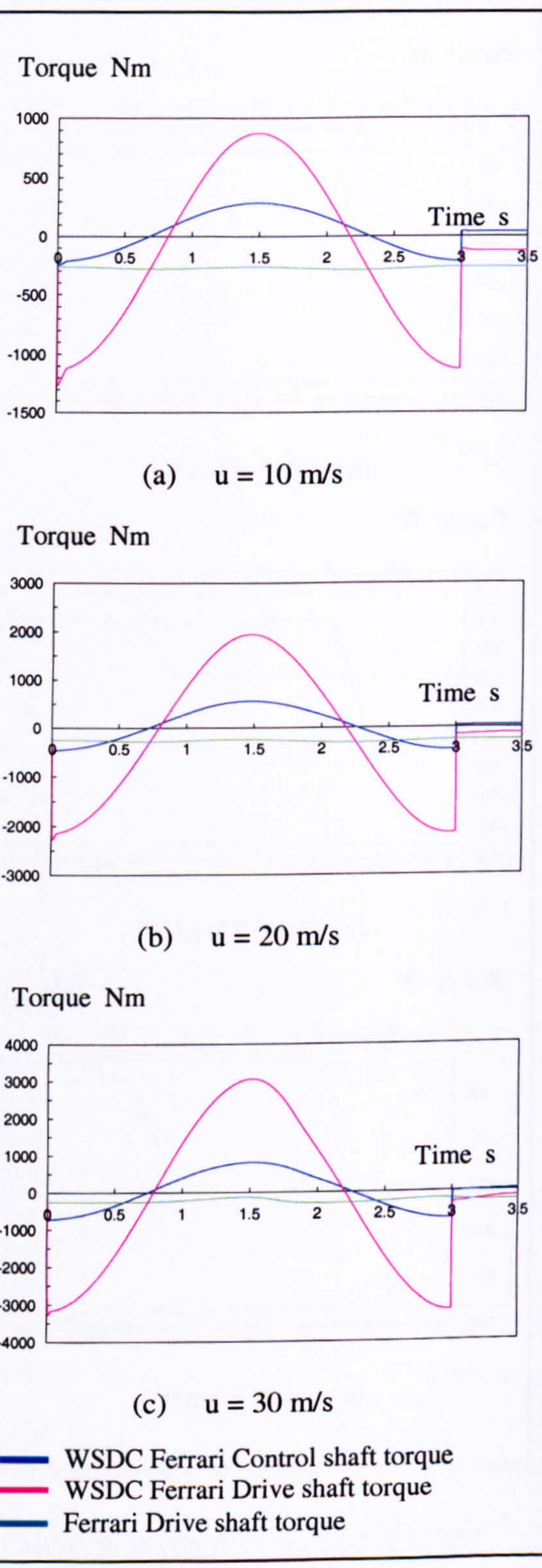

(a) u = 10 m/s

(b) u = 20 m/s

(c) u = 30 m/s

WSDC Ferrari Control shaft torque
WSDC Ferrari Drive shaft torque
Ferrari Drive shaft torque

Fig (8.8) WSDD torque of Ferrari in lane change manoeuvre

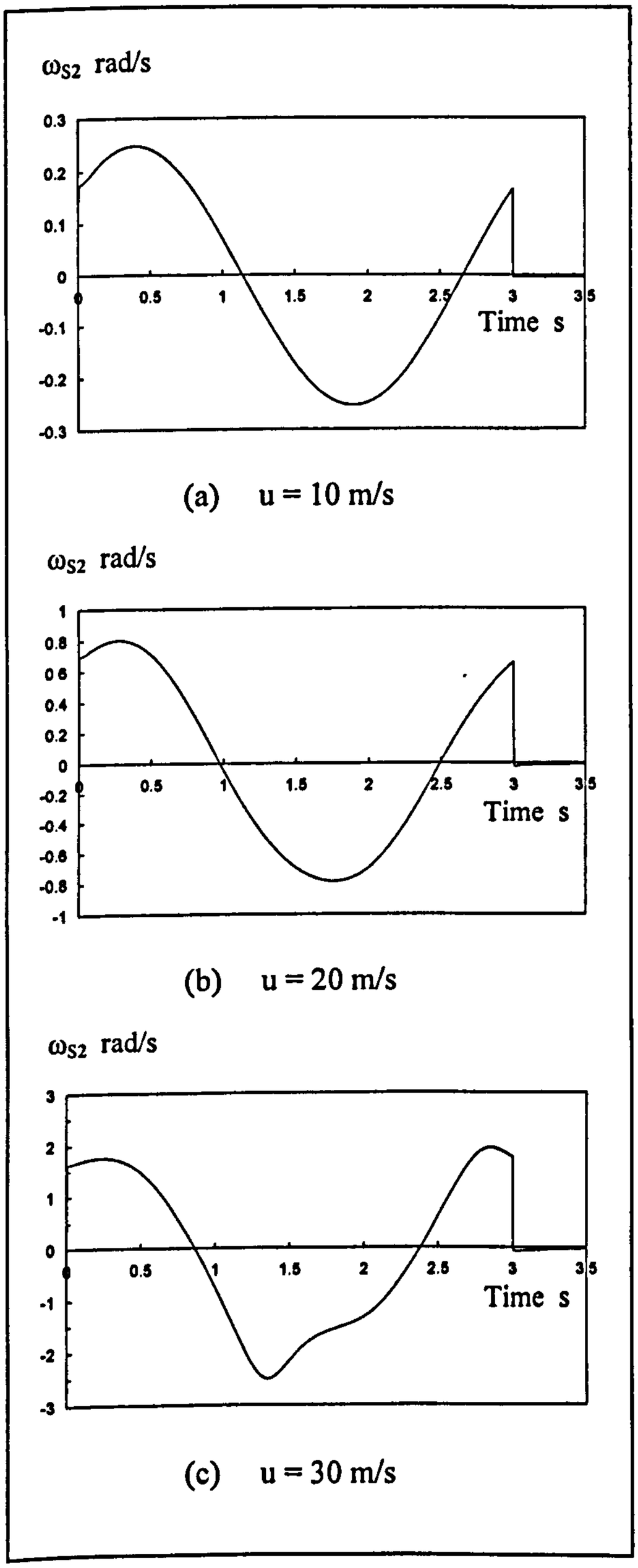

(a) u = 10 m/s

(b) u = 20 m/s

(c) u = 30 m/s

Fig (8.9) Control shaft rotational speed of Buick in lane change manoeuvre

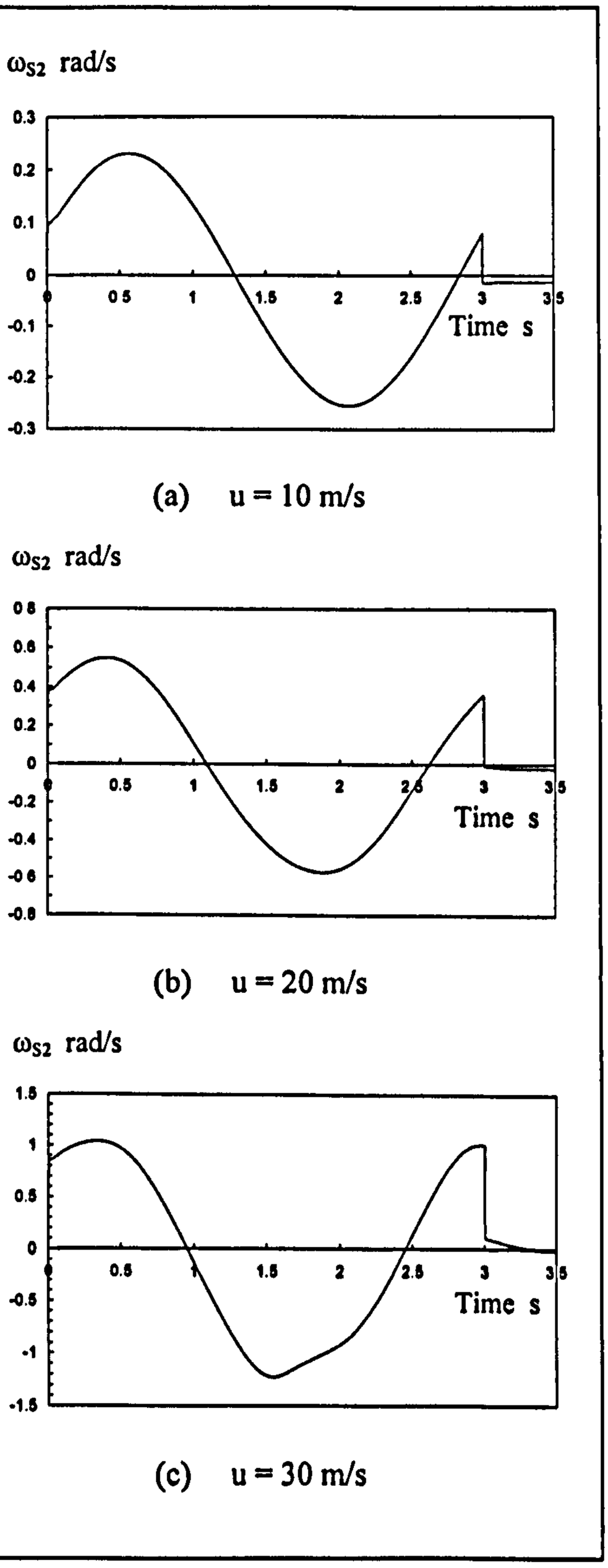

(a) u = 10 m/s

(b) u = 20 m/s

(c) u = 30 m/s

Fig (8.10) Control shaft rotational speed of Ferrari in lane change manoeuvre

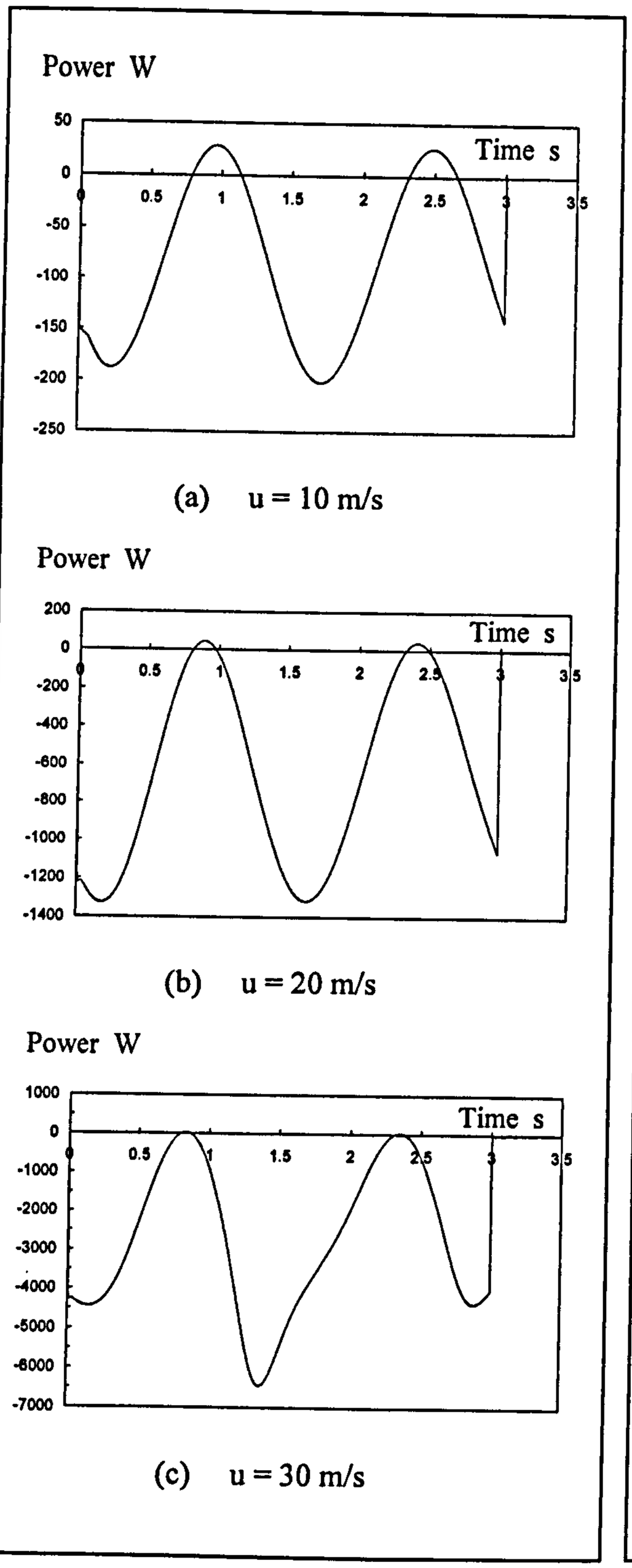

(a) u = 10 m/s

(b) u = 20 m/s

(c) u = 30 m/s

Fig (8.11) Control shaft power of Buick in lane change manoeuvre

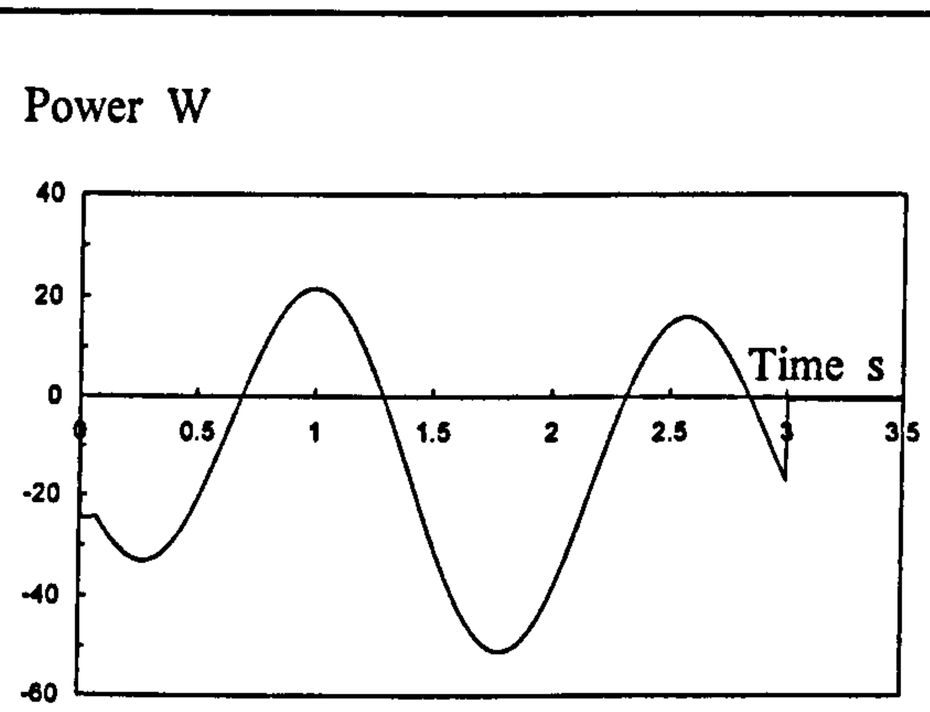

(a) u = 10 m/s

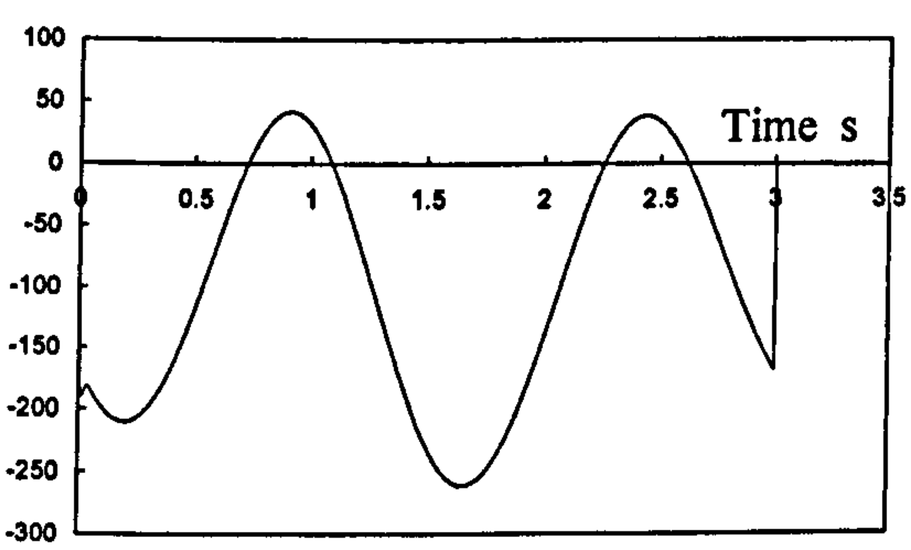

(b) u = 20 m/s

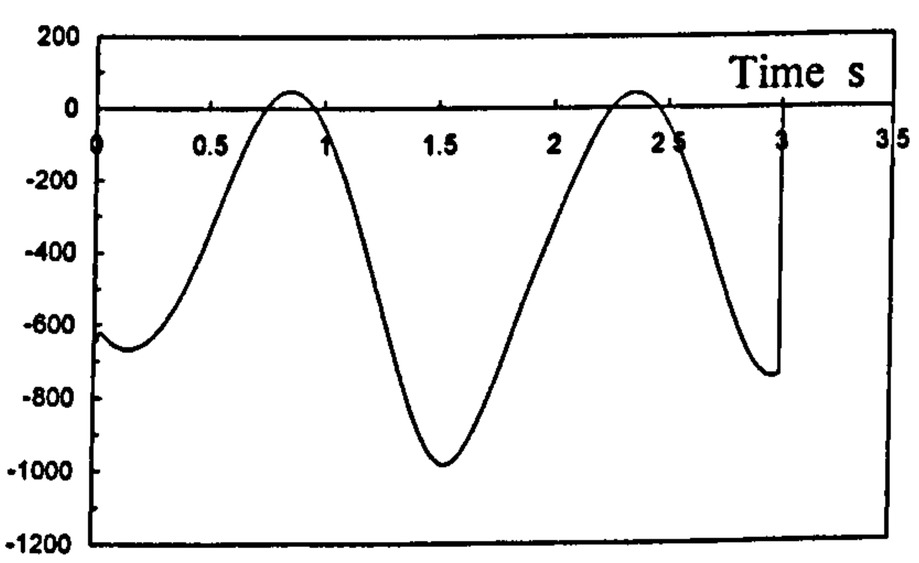

(c) u = 30 m/s

Fig (8.12) Control shaft power of Ferrari in lane change manoeuvre

8.6 Conclusions

In this Chapter, the novel WSDD performance equations have been embedded within the WSDC model to form the WSDC system. The system has been tested to investigate its control requirements to achieve the desired vehicle handling yaw rate control. Accordingly, the control shaft speed, torque and power requirements have been evaluated using the same WSDC model set of vehicle handling manoeuvres and travelling velocities stated in Chapter 6. Also the drive shaft torque has been evaluated for both the WSDC system and the conventional (non controlled) differential.

The torque predictions for both step steer and lane change manoeuvres showed that the WSDC system has been able to extract most of the required control torque from the vehicle drive shaft, without any special control applied to the vehicle. The control shaft rotational speed results showed its low speed requirements. For the tested step steer and lane change manoeuvres, control shaft rotational speeds of less than 3 rad/s have been required.

The control power results showed that for the low weight Ferrari vehicle, control shaft power demand of less than 1 kW has been required. The heavy weight Buick vehicle control shaft power demand for low velocities, up to 20 m/s, was less than 1.4 kW. For the simulated Buick manoeuvres at 30 m/s, a higher level of power was required.

As the trend of vehicle industry is biased towards reducing vehicle weight, the WSDC system power requirements will be decreased. This is will add to the WSDC system feasibility. Also, as the vehicle weight is lowered, its tyres' capacity to develop lateral forces is degraded, due to the low vertical loads, which will obligate the employment of yaw rate assisting systems. This again will add to the WSDC system feasibility.

Finally, WSDC has been considered a feasible system that can, in fact, contribute to the improvement of vehicle handling performance. It may also assist the implementation of vehicle autonomous driving.

Chapter 9

Conclusions and Recommendations

9.1 Conclusions

Road vehicles have received a lot of attention due to the high rates of accident fatalities, associated mostly with driver errors. Vehicle autonomous driving was put forward as part of the solution, but was challenged by the problems associated with vehicle handling. Vehicle handling and the systems associated with it have attracted a lot of research and a number of vehicle handling systems have been proposed with the aim of enhancing vehicle handling performance. Due to the non linear characteristics of the proposed vehicle handling system hardware, the low processing speed of the proposed controllers and the high number of non linear factors that affect vehicle handling performance, in contrast to the high safety levels required, none of the proposed systems have been widely adapted.

In this study, with the aim of enhancing vehicle handling as a precursor of vehicle autonomous driving, a novel Wheel Speed Distribution Control (WSDC) system has been developed, presented and analysed. This system evolved from the previous handling system limitations.

In the WSDC system, driven wheel speed control has been adopted in contrast to the driven wheel torque control of competitive system. Accordingly, this system takes

advantage of the more developed rotational speed measurement and control technology. To facilitate the novel WSDC system application, a high speed detailed onboard model, controller and dedicated hardware have been considered essential. The current study has been conducted in eight stages.

In the first stage, a novel high speed Cartesian Geometric Translation (CGT) modelling technique has been developed and tested. This technique employs Finite Difference Approximation (FDA) and trigonometric functions to investigate the vehicle translations in its local and global coordinates, as it undertakes consecutive time frames with 0.001 s width. With the aim of comprehensive description and testing of the CGT modelling technique, a case study in which the well established half vehicle (bicycle) handling model has been developed using the CGT technique and its results have been compared to reviewed results. As both good match and high processing speed have been achieved, the CGT technique has been considered appropriate for the current vehicle handling modelling task.

In the second stage, to upgrade the model to recognise the tyre combined slip characteristics, the empirical Magic Formula (MF) tyre model for combined slip (Bayle 1993 version) has been selected due to its established realistic estimation of tyre forces under combined slip conditions.

The Magic Formula tyre model for combined slip has been tested and found suitable for the current WSDC and has been treated to fit the requirements of the CGT modelling technique. Accordingly, an iteration routine based on "Branch and Bound" and "False Position" iteration techniques has been developed and optimised for high speed iteration, within the so-called kcal routine. This routine calculates the wheel longitudinal slip k from longitudinal force F_x and slip angle α inputs. The kcal routine has been tested using 50,000 random points and found to accurately fit its purpose with errors less than 0.01 N of the corresponding longitudinal tyre forces F_x. The developed tyre model has also been equipped with a relaxation length routine to recognise the tyre lateral forces development delay, due to time dependent rubber characteristics.

In the third stage, the CGT half vehicle handling model has been enhanced to form the CGT full vehicle handling model that takes into account lateral and longitudinal load transfer effects on tyre vertical loads. This has been tested using two different procedures.

In the first test, the model has been fitted with a linear tyre model and its results at high velocity manoeuvres have been compared with reviewed results, where a good match has been achieved. In the second test, the model was fitted with the MF tyre model for combined slip and tested in step steer manoeuvres. The achieved results have been compared with the Ackerman reference travelling path and a good match at low velocities has been achieved. As Ackerman travelling path has been developed in a mathematical way that is completely different from the vehicle dynamics employed to predict the full vehicle handling model travelling path, this result along with the first procedure result have been considered as validation of the full vehicle handling model equipped with the MF tyre model for combined slip.

In the fourth stage, the model has been fitted with the capacity to distribute the driven wheels rotational speeds (WSD). These speeds were varied with a rotational speed percentage difference ($d\omega$) around their nominal rotational speed, extracted from the vehicle nominal forward velocity. This WSD model has been used to prove the capacity of wheel speed distribution to influence both the yaw rate and travelling path of the vehicle.

The WSD model has been tested under step steer manoeuvres at different forward velocities and different $d\omega$. The travelling path and yaw rate results have been compared to reference Ackerman travelling path and yaw rates. At the start of the manoeuvre, the higher $d\omega$ showed travelling path and yaw rate closer to the Ackerman travelling path and yaw rate, due to the high yaw moment required to follow Ackerman yaw rate at the start of a step steer manoeuvre. As the yaw moment demand reached steady state, a far lower $d\omega$ was required to match the reference Ackerman travelling path and yaw rate. Accordingly, as the optimum $d\omega$ value

changes during the manoeuvres, a yaw rate controller has been considered necessary to control the variation of the driven wheels speeds.

In the fifth stage, to control the wheel speed distribution, a yaw rate controller based on Model Predictive Control (MPC) strategy has been designed and integrated into the WSD vehicle handling model to form the WSDC model. This employs finite difference approximations and inverse dynamics to control the WSD in a feedforward style. This controller acts by driving the vehicle yaw rate to match the reference Ackerman yaw rate. It has been tested in a lane change manoeuvre and found to achieve a close match to the Ackerman yaw rate. Accordingly, it has been considered fit for the purpose of controlling the vehicle driven wheel speed distribution.

In the sixth stage, the WSDC model has been used to investigate the vehicle handling performance enhancements due to the application of the WSDC concept. The investigation has been carried out for heavy and light weight vehicles under step steer and lane change manoeuvres at different forward velocities. The handling performance improvement due to WSDC adaptation showed in high correction of the controlled vehicle yaw rates in comparison to the non controlled vehicles. It also showed good correction to the vehicle travelling paths compared with the non controlled vehicles.

The WSDC high potential is awarded to its influence on the driven wheel longitudinal forces to generate the correction yaw moment. Also, it is attributed to the quick intervention to correct the deviation, typically every 0.001 s, which eliminate the chances of error propagation. The high potential of the WSDC system to enhance the vehicle handling performance has been proved, but without feasible hardware that would support it. Accordingly development of feasible WSDC hardware has been considered essential.

In the seventh stage, a novel hardware for WSDC application, the Wheel Speed Distribution Differential (WSDD) has been developed from first principles and

tested. The WSDD has been designed to enforce linear rotational speeds and torque relations. Its design has been influenced to reduce both the controller and control DC motor duty cycles and loads. It has been developed to extract most of the required control power from the vehicle drive shaft, without any especial control applied to the vehicle engine. The WSDD rotational speed, torque, power requirements, ease of production and maintenance requirements have been investigated and found feasible. Accordingly, the WSDD has been considered fit for purpose as a platform for WSDC application.

In the eighth stage, the WSDD performance equations have been fitted to WSDC model to form the complete WSDC system. The system has been tested to investigate its control requirements in order to achieve the desired vehicle handling yaw rate control. Accordingly, the control shaft speed, torque and power requirements have been evaluated under the same WSDC model set of vehicle handling manoeuvres and travelling velocities. Also the drive shaft torque has been evaluated for both the WSDC system and the conventional (non controlled) differential. The results proved the feasibility of the complete WSDC system as the control shaft speed, torque and power have forced to be been within moderate and applicable ranges. Also the results proved the system success in extracting most of the required control power from the engine drive shaft.

With respect to the objectives presented in Chapter 2, the following has been achieved: -

1. A novel modelling technique known as Cartesian Geometric Translation (CGT) has been utilised to facilitate the development of high processing speed vehicle handling simulation models and its model based controller. CGT capacity has been validated through the development of the well known half vehicle (bicycle) handling model and comparison of its predictions with published data.

2. The Magic Formula (MF) tyre model for combined slip has been adapted for employment in the validated vehicle handling model. For this purpose a MF

derivative that calculates the tyre longitudinal slip k from its longitudinal force F_x and slip angle α inputs, (kcal routine) has been developed. The routine has been tested using 50,000 random data sets and found to achieve its task with less than 0.01 N in force estimation difference from MF tyre model forces.

3. The developed half vehicle handling model has been upgraded to a full vehicle handling model, fitted with the adapted MF tyre model and with the capacity to regulate the driven wheel speeds. The developed model results proved the capacity of differential wheel speed distribution to influence vehicle handling.

4. A vehicle handling yaw rate controller based on the MPC and feedforward strategies has been developed to control the WSDC system and integrated in the validated full vehicle handling model. The WSDC vehicle handling model results of different vehicles for different manoeuvres and different travelling velocities showed that the WSDC principles could indeed enhance vehicle handling performance.

5. A novel Wheel Speed Distribution Differential (WSDD) hardware system has been developed to put WSDC theory into practice. This hardware design has been developed to have linear torque and speed characteristics and reduced speed, torque and power control requirements to facilitate its control. It also has been developed with minimised production complexity and maintenance requirements to facilitate its utilization. Finally, the WSDD system performance has been investigated through simulation and found to fulfil its objectives.

6. The WSDD hardware model has been incorporated into the developed WSDC vehicle handling model and the full WSDC system capacity to feasibly enhance vehicle handling performance has been demonstrated through simulation. The WSDC system results for different vehicles and different handling manoeuvres at different travelling velocities have demonstrated the capacity of the proposed WSDC system to feasibly enhance vehicle handling performance.

9.2 Recommendations

The model has been tested on an average PC. Although the results have been considered satisfactory, the effect of processor and memory, type and speed on the model speed requires testing on different PCs with different configurations. It is also required to investigate the means to eliminate the step variation of the model speed, which is attributed to Computer hardware characteristics. Also, investigating the possibility to fit the developed model into the Computer processor cache memory and its implication on model speed is of major importance.

Since the model running speed is quite important, as it would further enhance safety, it is a point of further research. Although the current model speed has been considered satisfactory there is still room to improve it. Also, the kcal routine, which relies on iteration, could be further optimised to reduce its processing load.

As the MF tyre model and the kcal routine represent heavy calculation loads in the model, a simpler tyre model could be tested and its results compared to the current model.

To facilitate the employment of WSDC, a dedicated control strategy would be highly desirable to control different vehicle handling situations. Although the current yaw rate controller showed excellent performance in terms of achieved yaw rates, these typical yaw rates have not produced the required vehicle travelling paths especially at high velocities, due to the increased vehicle side slip. It is a point of further research to investigate the control requirements to achieve the required travelling paths, although this is most likely to require the application of non standard Four Wheel Steering (4WS) technology.

A beneficial point of the WSDC concept is that it would allow the onboard model / controller to investigate the amount of longitudinal forces and slip exerted by the driven wheels, through yaw and longitudinal velocity sensors. This feature could be further developed to estimate the tyre-road coefficient of friction, which would

provide the WSDC vehicle handling model with updated tyre roadholding conditions.

To fully study the effect of WSDC potential, the required DC motor size has to be thoroughly investigated under different vehicle handling conditions. Also, the effect of the DC motor and controller delays and errors on WSDC vehicle handling performance should be investigated. Inclusion of the DC motor and its speed controller performance into the simulation model is a good step towards the implementation of the WSDC system.

As roads are not perfect, the model could be developed to observe suspension effects on vehicle handling. This could be considered a big step forward. In the first development stage, the road could be considered perfectly flat to test the upgraded model functionality before introducing the road roughness effect.

The high running speed WSDC model could be further developed to form a vehicle parameter optimisation tool. This tool could rapidly investigate the effect of vehicle design parameter combinations on vehicle handling performance. Accordingly, it could predict the best vehicle design parameter combination.

Feeding the simulation model with F1 racing vehicle data would reveal the WSDC potential, as these vehicles are optimised for handling. However, the required data for F1 cars and racing tyres are rarely available.

Theoretically the WSDD has proved its capacity to perform WSDC, which in turn has been shown to enhance vehicle handling performance through modelling. Accordingly, building an experimental WSDD, testing it and ultimately fitting it to a vehicle would allow a closer examination of WSDC system performance and facilitate its further development and employment.

References

1- Frank D. "Automotive Technology and its link to human life and the environment", *Seoul 2000 FISITA World Automotive Congress, paper no. F2000PH03,* 2000.

2- Aufrere R. Gowdy, J., Mertz C., Thorpe C., Wang C. C., Yata T., "Perception for collision avoidance and autonomous driving", *Mechatronics, Vol. 13, pp. 1149–1161,* 2003.

3- Bertozzi M., Broggi ., Fascioli A., "Vision-based intelligent vehicles: state of the art and perspectives", *Robotics and Autonomous Systems, Vol. 3, pp. 1–16,* 2000.

4- Provine R., Schlenoff C., Balakirsky S., Smith S., Uschold M., "Ontology-based methods for enhancing autonomous vehicle path planning", *Robotics and Autonomous Systems, Vol. 49, pp. 123–133,* 2004.

5- Balakirsky St., Scrapper C., "Knowledge representation and planning for on-road driving", *Robotics and Autonomous Systems, Vol. 49, pp. 57–66,* 2004.

6- Broucke M., Varaiya P., "A theory of traffic flow in automated highway systems", *Transpn Res-C, Vol. 4. no. 4, pp. 181-210,* 1996.

7- Kato S., Tsugawa S., "Cooperative driving of autonomous vehicles based on localization, inter-vehicle communications and vision systems", *JSAE Review, Vol. 22, pp. 503–509,* 2001.

8- Hanebutte U., Doss E., Ewing T., Tentner A., "Simulation of vehicle traffic on an automated highway system", *Mathl. Comput. Modelling, Vol. 27, No. 9-11, pp. 129-141,* 1998.

9- Iguchi M., "ITS enriches automotive technology", *Seoul 2000 FISITA World Automotive Congress, paper no. F2000P102,* 2000.

10- Russo M., Russo R., Volpe A., "Car parameter identification by handling manoeuvres", *Vehicle System Dynamics, Vol. 34, pp. 423-436,* 2000.

11- Sato K., Sugiura T., Hidekazu, "Vehicle handling simulation using mechanical dynamics analysis with modal analysis", *Proceedings of AVEC 2000,* 2000.

12- Park J., Nikravesh P., "Effect of steering-house rubber bushings on the handling responses of a vehicle", *SAE paper no. 970103,* 1997.

13- Bauer H., "Automotive handbook", *Bosch GmbH, Society of Automotive Engineers, 5th edition, ISBN 0768006694,* 2000.

14- Bellion P., "Project Y.A.M. (Yaw Analysis Methodology) vehicle testing and findings - Victoria police, accident investigation", *SAE paper no. 970955,* 1997.

15- Gillespie T., "Fundamentals of vehicle dynamics", *SAE publications, ISBN 1560911999,* 1992.

16- Bergman W., Pelargus D., "The role of steer and slip angle", *SAE paper no. 960999,* 1996.

17- Jawad B., Ziemke M., Young A., "Design of an aluminium differential for a racing style car", *SAE paper no. 2000-01-1156,* 2000.

18- Haiba M., Barton D., Brooks P., Levesley M., "Evolutionary structural optimisation with fatigue life constraints", *Sixth International Conference on Computational Structures Technology, Prague, Czech Republic,* 2002.

19- Arndt M. W., Dickerson C. P., Arndt S. M. "Influence of passenger and cargo load on the at limit handling of a mini van", *SAE, paper no. 1999-01-0449,* 1999.

20- Chace M. A., Wielenga T. J., "A test and simulation process to improve rollover resistance", *SAE paper no. 1999-01-0125,* 1999.

21- Puhn F., "How to make your car handle", *H.P. Books, ISBN 0912656468,* 1976.

22- Clover C., Bernard J., "The influence of lateral load transfer distribution on directional response", *SAE 930763,* 1993.

23- Heydinger G. J. and Bixel R. A. "Effects of loading on vehicle handling", *SAE, paper no. 980228,* 1998.

24- Marine M., Wirth J., Thomas T., "Characteristics of on-road rollovers", *SAE paper no. 1999-01-0122,* 1999.

25- Dahlberg E., "Yaw instability due to longitudinal load transfer during braking in a curve", *SAE paper no. 1999-01-2952,* 1999.

26- Kitahama K., Sakai H., "Measurement method of normalized cornering stiffness", *JASE, Vol. 21, pp. 213-217,* 2000.

27- Jones R., "Understanding vehicle roll using mechanism simulation software", *SAE paper no. 1999-01-0030,* 1999.

28- Allen R., Myers T., Rosenthal T., Klyde D., "The effect of tire characteristics on vehicle handling and stability", *SAE paper no. 2000-02-0698,* 2000.

29- Pasterkamp W., Pacejka H., "The tire as a sensor to estimate friction", *Proceedings of AVEC 1996, pp. 839,* 1996.

30- Lim E., "Introduction to all wheel drive systems" [Online]. *1999* [Accessed 2nd Feb. 2008], Available from World Wide Web: <http://www.fiction.net/~jeske/ unsolicitedDave/legacy/ awd.html>

31- Loeb J., Guenther D., Chen H., Ellis J., "Lateral stiffness, cornering stiffness and relaxation length of the pneumatic tire", *SAE paper no. 900129,* 1990.

32- Peng X., Xie Y, Guo K., "A new method for determining tire traction on ice", *SAE paper no. 2000-02-1640*, 2000.

33- Knothe K., Wille R., Zastrau B., "Advanced contact mechanics-road and rail", *Vehicle System Dynamics, Vol. 35, No. 4-5, pp. 361-407*, 2001.

34- Pacejka H. B., "Tyres and vehicle dynamics", *Oxford: Butterworth-Heinemann, ISBN 0750651415*, 2002.

35- Momiyama F., Hoshikawa K., Katou J., Hosoda T., "Tractive torque steer for on-center stability/handling augmentation with controlling differential gear for large-sized vehicles - A comparison with passive read-axle steer", *SAE paper no. 912688*, 1991.

36- Cheok K., Hoogterb F., Kobayashi K., Scaccia S., "Fuzzy logic approach to traction control design", *SAE paper no. 960957*, 1996.

37- Alberti V., Babbel E., "Improved driving stability by active braking of the individual wheels", *AVC 1996, pp. 717-732*, 1996.

38- Hoffman D. D., "The corvette acceleration slip regulation (ASR) application with preloaded limited slip differential", *SAE paper no. 920642*, 1992.

39- McKay D., Nichols G., Schreurs B., "Delphi electronic throttle control systems for model year 2000; driver features, system security, and OEM benefits ETC for the mass market", *SAE paper no. 2000-02-0556*, 2000.

40- Haskara I., Ozguner U., Winkelman J., "Wheel slip control for antispin acceleration via Dynamic Spark Advance", *Control Engineering Practice, Vol. 8, pp. 1135-1148*, 2000.

41- Bauer M., Tomizuka M., "Fuzzy logic traction controllers and their effect on longitudinal vehicle platoon system", *Vehicle System Dynamics, Vol. 25, No. 4, pp. 277-299*, 1996.

42- Holzwarth R. K., May K. A., "Analysis of traction control systems augmented by limited slip differential", *SAE paper no. 940831*, 1994.

43- Jung H., Kwak B., Park Y., "Improved directional stability in traction control system", *Proceedings of AVEC 2000*, 2000.

44- Lely C., "Torque converter", *USA Patent, 4273206*, 1981.

45- Gleasman V., Gleasman K., Gleasman J., "No-slip imposed differential reduction drive", *USA Patent, 4776235*, 1987.

46- Steiger M., "Differential drive and steering system", *USA Patent, no. 4977970*, 1990.

47- Motoyama S., Uki H., Isoda K., Yuasa H., "Effect of traction force distribution control on vehicle dynamics", *Vehicle System Dynamics, Vol. 22, pp. 455-464*, 1993.

48- Ikushima Y., Sawase K., "A study on the effects of the active yaw moment control", *SAE paper no. 950303*, 1995.

49- Sawase K., Sano Y., "Application of active yaw control to vehicle dynamics by utilizing driving/breaking force", *JSAE Review, Vol. 20, pp. 289-295,* 1999.

50- Yamamoto T., Mastsuda K., Hibi T., "Analysis of efficiency of a half-toroidal CVT", *JSAE Review, Vol. 22, pp565-570,* 2001.

51- Druten R., Tilborg P., Rosielle P., Schouten M., "Design and construction of a zero inertia CVT for passenger cars", *Seoul 2000 FISITA World Automotive Congress, paper no. F2000A058,* 2000.

52- Alex F.A., Veldpaus F. E., "New concept for control of power transients in flywheel assisted driveline with CVT", *Seoul 2000 FISITA World Automotive Congress, paper no. F2000 A129,* 2000.

53- Jung K., Lee H., Kim T., Hyunsoo Kim, Jaeshin Yi, Heebock Cho, "Dynamic characteristics of CVT electro-hydraulic control valves including shift dynamics", *Seoul 2000 FISITA World Automotive Congress, paper no. F2000 A132,* 2000.

54- Aitzetmuller H., "Steyr S-Matic - the future CVT system", *Seoul 2000 FISITA World Automotive Congress, paper no. F2000 A130,* 2000.

55- Everett N., "Integrated vehicle chassis control", *Ph.D. Thesis, School of Mechanical Engineering, University of Leeds,* 2001.

56- Besselink, B. C., "Development of a vehicle to study the tractive performance of integrated steering-drive systems", *Journal of terramechanics, Vol. 41, pp. 187-198,* 2004.

57- Hoffmann M., "The functional, digital vehicle - the backbone for integrated development of vehicle controls, chassis, and powertrain systems", *Proceedings of AVEC 2000,* 2000.

58- http://www.mscsoftware.com/support/prod_support/adams/documentation/2005/releasenotes .html?car.html.

59- Villec G.N., "Cosimulation of an automotive control system using ADAMS and Xmath", *International ADAMS User Conference,* 1998.

60- Haug E. J., "Computer aided kinematics and dynamics of mechanical systems. Vol. 1: Basic Methods", *Allyn & Bacon, ISBN 0205116698,* 1989.

61- Perera H.S., Romano R., Nunez P., "Automated methods for converting a non real-time cartesian multi-body vehicle dynamics model to a real-time recursive model", *SAE Technical Papers, no. 2006-01-1165*

62- Crolla D.A., Horton D.N.L., Brooks P.C., Firth G.R., Shuttlewood D., Woods M., Yip C.K., "A systematic approach to vehicle design using VDAS (Vehicle Dynamics Analysis Software)", *SAE International Congress and Exposition Paper* , 1994.

63- Markel T., Brooker A., Hendricks T., Johnson V., Kelly K., Kramer B., O'Keefe M., Sprik S., Wipke K. "ADVISOR: a systems analysis tool for advanced vehicle modelling", *Journal of Power Sources, Vol.110, Issue 2, 22, pp 255-266,* 2002

64- Evangelou S., "The control and stability analysis of two–wheeled road vehicles", Ph.D. *Thesis, Electrical and Electronic Engineering, Imperial College, University of London,* 2003.

65- H. Prem, E. Ramsay, J. de Pont, J. McLean, J. Woodrooffe "Comparison of modelling systems for performance-based assessments of heavy vehicles", *NRTC/Austroads Project A3 and A4), Working Paper,* October 2001.

66- http://www.mathworks.com/access/helpdesk/help/toolbox/rtw/rtw_ug/rtw_ug.html

67- Chwif L., Paul R. J., "On simulation model complexity", *Proceedings of 2000 Winter Simulation Conference, pp. 449-455,* 2000.

68- Najmi A., Mahran A., Esteve D., Vialaret G., "A scanning lidar system for obstacle avoidance in automotive field", *IEEE, paper no. 0-7803-1872-2,* 1994.

69- SAYERS M. W., "Vehicle models for RTS applications", *Vehicle System Dynamics, Vol. 32, pp.421–438,* 1999.

70- Ahamed S.V., Lawrence V.B., "Art of scientific innovation", *Prentice Hall, ISBN 0131473425,* 2004.

71- Heinke F. A., Pereira C. E., Halang W. A., "Real-time programming: extending PEARL with interfaces and active objectives", *Control Engineering Practice, Vol. 6, pp. 431-440,* 1998.

72- "SMP 2.0 Handbook:"[Online]. *European space agency directorate of operations and infrastructure, Document Reference EGOS-SIM-GEN-TN-0099, Issue 1 Revision 2, 28 October 2005,* [Accessed 2nd Feb. 2008], Available from World Wide Web: <http://www.eurosim.nl/support/manual_4_0/pdf/SMP_2.0_Handbook-1.2.pdf>

73- Dugoff H., Fancher P.S., Segal L., "An analysis of tire traction properties and their influence on vehicle dynamic performance", *SAE paper no. 700377,* 1970.

74- Pelc J., "Towards Realistic simulation of deformations and stresses in pneumatic tyres", *Applied Mathematical Modelling, Vol. 31, pp 530–540,* 2007.

75- Pacejka H.B., Besselink I.J.M. "Magic formula tyre model with transient properties", *Supplement to Vehicle System Dynamics, Vol. 27, pp 234-249,* 1997.

76- Camacho E.F., Bordons C., " Model predictive control", *Springer, ISBN 3540762418,* 1999.

77- Horiuchi S.,Okada K.,Nohtomi S., "Numerical analysis of optimal vehicle trajectories for emergency obstacle avoidance", *JSAE, Review 22, pp 495–502* ,2001.

78 Earl M.G., D'Andrea R."A decomposition approach to multi-vehicle cooperative control", *Robotics and Autonomous Systems, Article in press, accepted 23 November* 2006.

79- Li W., Cassandras C.G., "Centralized and distributed cooperative Receding Horizon control of autonomous vehicle missions", *Mathematical and Computer Modelling, Vol. 43, pp 1208–1228,* 2006.

80- Dunbar W.B., Murray R.M., "Distributed receding horizon control for multi-vehicle formation stabilization" *Automatica, Vol. 42, pp 549 – 558,* 2006.

81- Hegyi A., De Schutter B., Hellendoorn H., "Model predictive control for optimal coordination of ramp metering and variable speed limits" *Transportation Research, Part C 13, pp 185–209,* 2005.

82- Canale M., Fagiano L., Milanese M., Borodani P., "Robust vehicle yaw control using an active differential and IMC techniques" *Control Engineering Practice, Article in press, Accepted 30 November* 2006.

83- Shino M., Nagai M., "Yaw-moment control of electric vehicle for improving handling and stability",*JSAE, Review 22, pp 473–480,* 2001.

84- Crolla D., Firth G., Horton D., "An introduction to vehicle dynamics", *University of Leeds, School of mechanical engineering,* 1996.

85- "Branch and Bound" [Online]. *28 March 1996* [Accessed 2nd Feb. 2008], Available from World Wide Web: < http://www-fp.mcs.anl.gov/otc/Guide/OptWeb/discrete/ integerprog/section2_1 _1.html>

86- Craw, L, "False position" [Online]. *14 December 2003*, [Accessed 2nd Feb. 2008], Available from World Wide Web: <http://www.maths.abdn.ac.uk/~igc/tch/mx3015/ notes/node108 .html >

87- Hou Y., Hu Y., Li C., Guo K., "A study of tire lag property", *SAE, paper no. 2001-01-0751,* 2001.

88- Mancosu F., Sangalli R., Cheli F., Bruni S., "A new mathematical-physical 2D tire model for handling optimization on a vehicle", *International Congress and Exposition, Detroit, Michigan,* 1999.

89- http://www.sundevilauto.com/auto-diagrams-drive-train.asp [Accessed 2nd Feb. 2008]

90- http://www.tpub.com/content/engine/14037/css/14037_128.htm [Accessed 2nd Feb. 2008]

91- "VIMF Vehicle inertia measurement facility" [Online]. *S.E.A. Inc., 13 august 1997* [Accessed 2nd Feb. 2008], Available from World Wide Web: <http://www.ultitechcorp.com/sea/ seabrochure/VIMF.pdf>

Appendix A: CGT Half Vehicle Handling Simulation Model

```
'   ************************************************************************
'   ***************  Half Vehicle Handling Model using CGT  ****************
'   ************************************************************************
CLS
DEFDBL A-Z
'For Ferrari 50m/sec test delta = -.1663
'For Buick   50m/sec test delta = -.49
'For Ferrari 20m/sec test delta = -.965
'For Buick   20m/sec test delta = -1.624

delta = -1.624          ' Steering angle deg
prn = 0                 ' 1 print results to file, 0 don't
scr = 0                 ' 1 print results to screen, 0 don't
Sc = 1                  ' Scale on screen
IF prn THEN OPEN "F20-2.txt" FOR OUTPUT AS #1    ' output file name
u00 = 20                ' Vehicle speed m/s
ferrari = 0             ' 1 Ferrari, 0 Buick
dt = .001               ' Time interval s
St = 9                  ' Simulation time s
SS = St / dt
LOCATE 1, 1: time0 = TIMER
PRINT time0

'*****************************     Start     ***********************************
GOSUB 500     ' Set Graphics Screen
GOSUB 1000    ' Read Vehicle data
10
GOSUB 2000    ' Check end of simulation
GOSUB 3000    ' Calculate Forces and Moments
GOSUB 4000    ' Calculate Accelerations
GOSUB 5000    ' Calculate Speeds
GOSUB 6000    ' Calculate CG Movement
GOSUB 7000    ' Calculate CG Location
GOSUB 8000    ' Calculate Tyres Locations
GOSUB 9000    ' Calculate tyres Slip Angles
GOSUB 10000   ' Calculate tyres Forces
GOSUB 11000   ' Get ready for next stage
GOSUB 12000   ' Saving and Plotting Data
GOTO 10

2000 '************************  Check end of simulation  ***********************
IF aaaa < SS THEN 999
LOCATE 2, 1: PRINT TIMER
PRINT USING "#.##"; TIMER - time0
END
999
aaaa = aaaa + 1
RETURN

3000 ' ************************  Calculate Forces and Moments  ****************
Fyt = FyR + FyF * COS(delta)
mom1 = FyF * a * COS(delta)
mom2 = FyR * B * -1
Momt = mom1 + mom2
RETURN

4000 ' ************************  Calculate Accelerations  *********************
vd = Fyt / m
```

```
thetadd = Momt / I
RETURN

5000 ' ********************  Calculate Speeds  ******************************
vv = v0 + vd * dt
thetadv = thetad0 + thetadd * dt
RETURN

6000 ' ********************  Calculate CG Movement  ************************
Dux = (uv + u0) * dt / 2
Dvy = (vv + v0) * dt / 2
DvTheta = (thetadv + thetad0) * dt / 2
RETURN

7000 ' ********************  Calculate CG Location  ************************
CGx = CGx0 + Dux
CGy = CGy0 + Dvy
CGt = CGt0 + DvTheta
RETURN

8000 ' ********************  Calculate Tyres Locations  ********************
fx = CGx + a * COS(CGt)
fy = CGy + a * SIN(CGt)
rx = CGx - B * COS(CGt)
ry = CGy - B * SIN(CGt)
RETURN

9000 ' ********************  Calculate Tyres Slip Angles *******************
Sf = ATN((fy - fy0) / (fx - fx0))
Sr = ATN((ry - ry0) / (rx - rx0))
af = Sf - delta
ar = Sr
RETURN

10000 ' ********************  Calculate Tyres Forces ************************
alfa = af
FyF = -alfa * Cf
alfa = ar
FyR = -alfa * Cr
RETURN

11000 ' ********************  Get  Ready For Next Stage  ********************
v0 = vv * COS(DvTheta) - uv * SIN(DvTheta)
thetad0 = thetadv
CGyt = CGyt + CGy * COS(CGtheta) + CGx * SIN(CGtheta)
CGxt = CGxt + CGx * COS(CGtheta) - CGy * SIN(CGtheta)
CGtheta = CGtheta + CGt
RETURN

1000 ' ********************  Read Vehicle Data ******************************
pi = 3.141592654#
delta = delta * pi / 180
IF ferrari THEN
a = 1.234   'Reviewed
B = 1.022   'Reviewed
l = a + B
m = 1008
I = 1031
Cf = 117440    'N/Rad
Cr = 144930    'N/Rad
W = m * 9.81   'N

ELSE  ' Buick
```

```
a = 1.488
B = 1.712
l = a + B
m = 2045
I = 5428
Cf = 77850      'N/Rad
Cr = 76510      'N/Rad
W = m * 9.81    'N
END IF

'---------  X-Y initial locations
CGx0 = 0
CGy0 = 0
CGt0 = 0
fx0 = a
fy0 = 0
rx0 = -B
ry0 = 0

'---------  Initial Speeds and Accelerations
v0 = 0
u0 = u00
uv = u0
ud = 0
vd = 0
thetad0 = 0

'---------  Summing
CGxt = 0
CGyt = 0
CGtheta = 0
RETURN

500 '************************  Set Graphics Screen  ****************************
IF scr THEN
SCREEN 12
WINDOW (-20 * Sc, -50 * Sc)-(200 * Sc, 110 * Sc)
LINE (0, 0)-(100, 100), 5, B
LOCATE 1, 1: PRINT TIMER
END IF
RETURN

12000 '**********************  Saving and Plotting Data  **********************
'----------- Saving to File
IF prn THEN
IF Pstart = 0 THEN
PRINT #1, " ", "Time", "Delta", "CGx", "CGy", "CGt", "CGxt", "CGyt", "CGtheta",
"fx", "rx", "fy", "ry", "af", "ar", "af-deg", "ar-deg", "FyF", "FyR", "Fyt",
"Momt", "vd", "thetadd", "uv", "vv", "thetadv", "DvTheta", "thetadvdeg"
Pstart = 1
END IF
PRINT #1, USING " ########.###### "; aaaa * dt; delta * 180 / pi; CGx; CGy;
CGt; CGxt; CGyt; CGtheta; fx; rx; fy; ry; af; ar; af * 180 / pi; ar * 180 / pi;
FyF; FyR; Fyt; Momt; vd; thetadd; uv; vv; thetadv; DvTheta; thetadv * 180 / pi
END IF

'----------- Ploting to screen
IF scr THEN
PSET (CGxt, CGyt), 15
END IF
RETURN
```

Appendix B: CGT Half Vehicle Handling Simulation Model Results

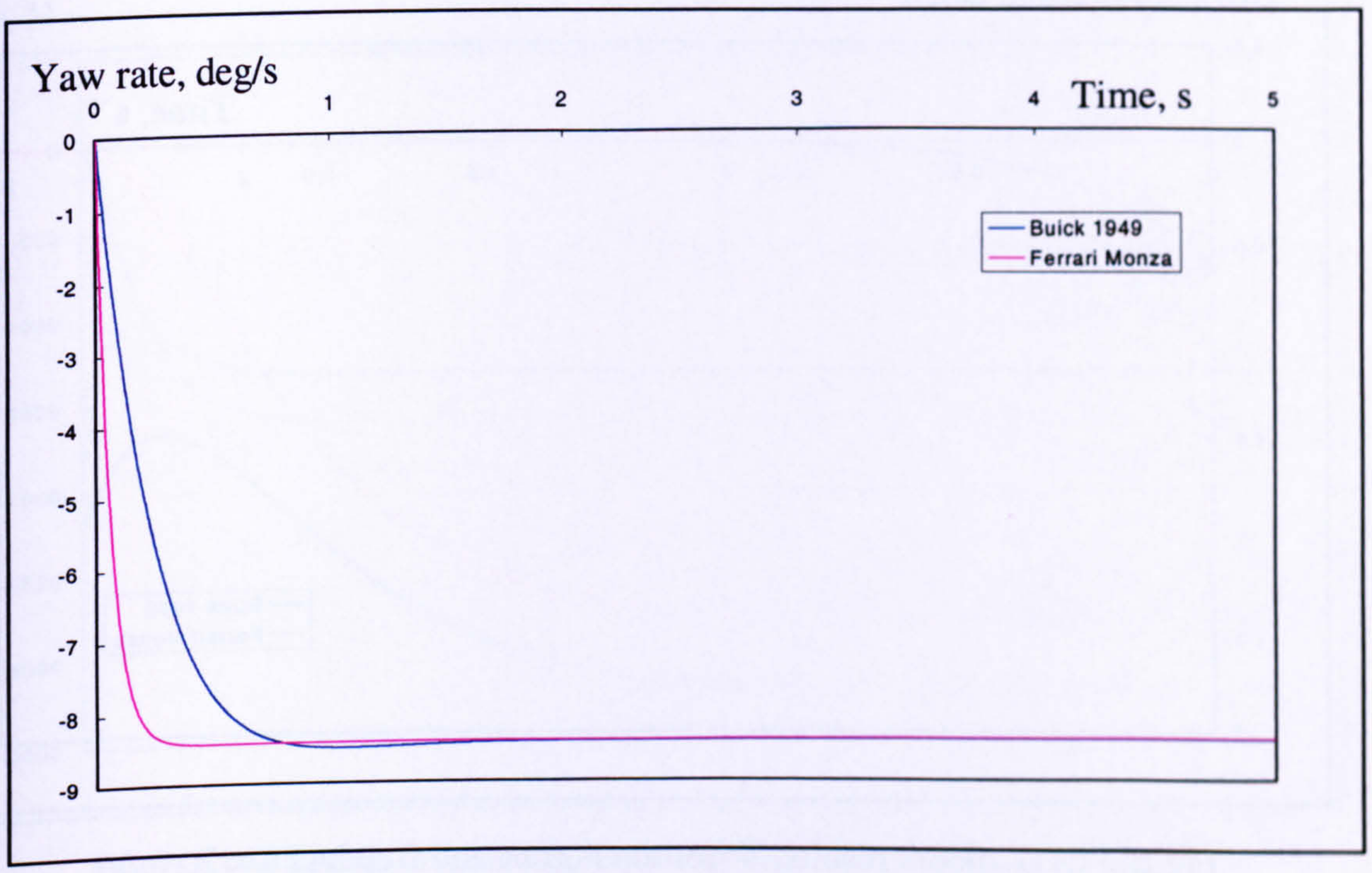

Fig B.1 CGT model results, $\dot{\theta}$ for the Buick and Ferrari at u = 20 m/s

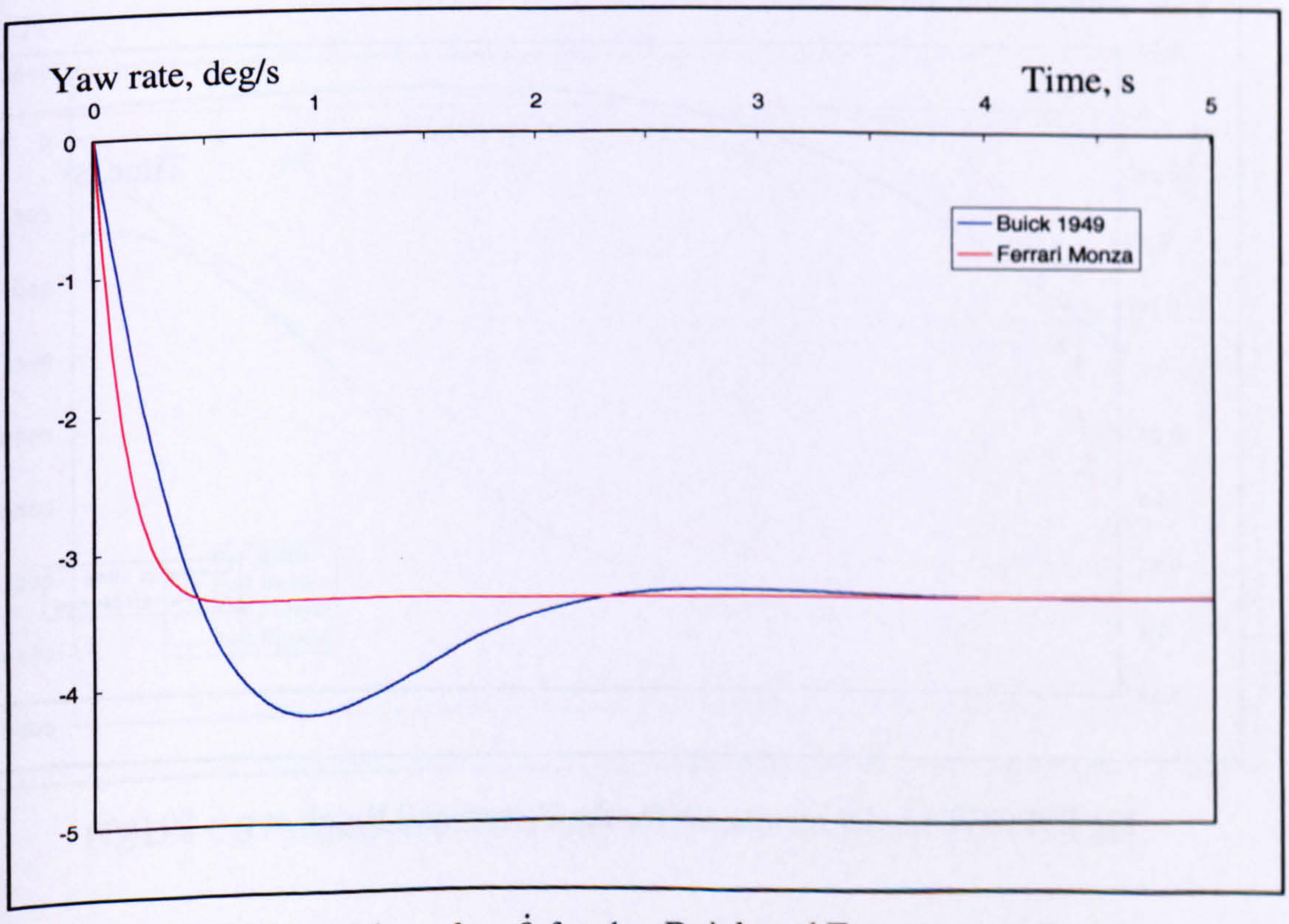

Fig B.2 CGT model results, $\dot{\theta}$ for the Buick and Ferrari at u = 50 m/s

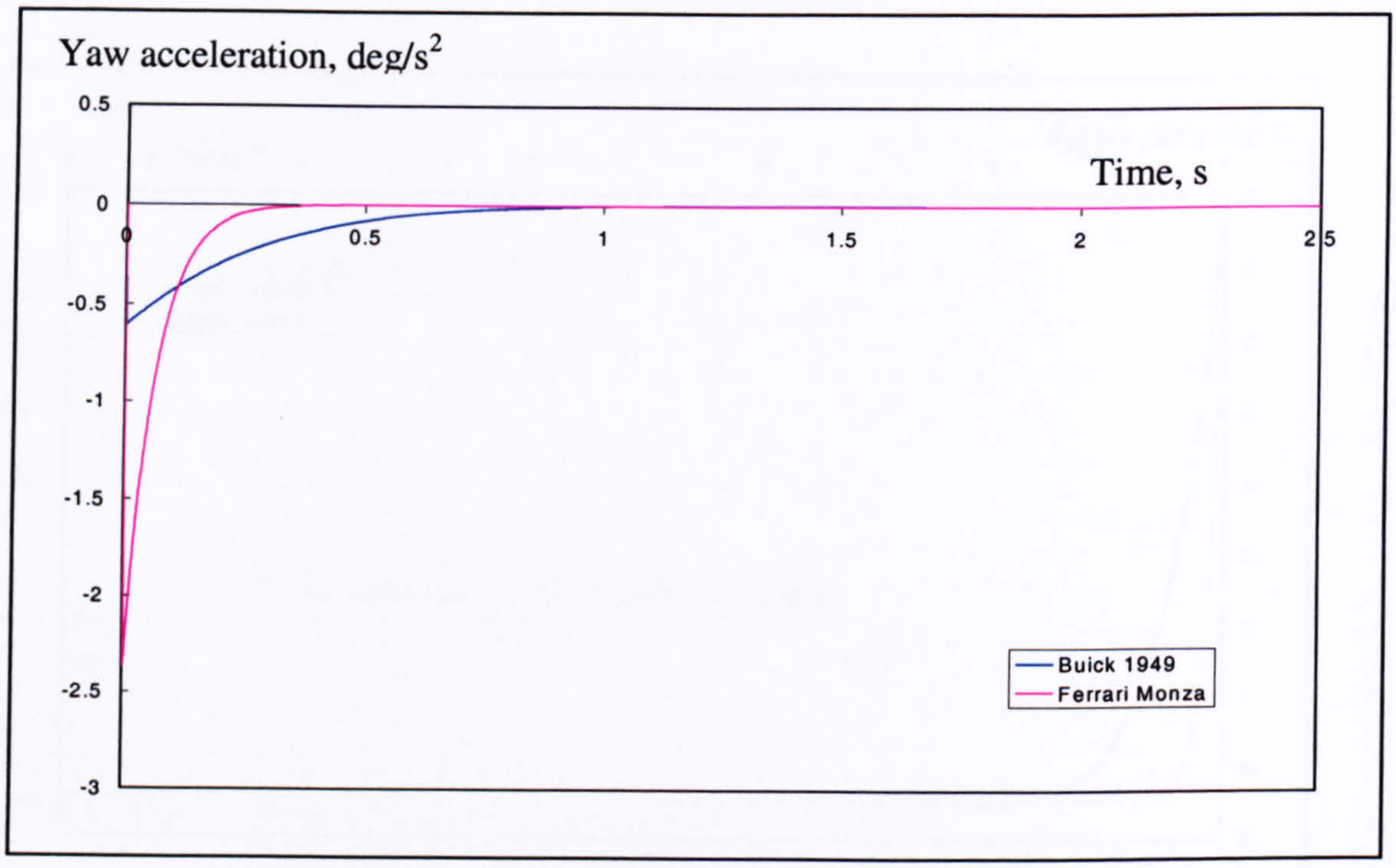

Fig B.3 CGT model results, $\ddot{\theta}$ for the Ferrari and Buick at u = 20 m/s

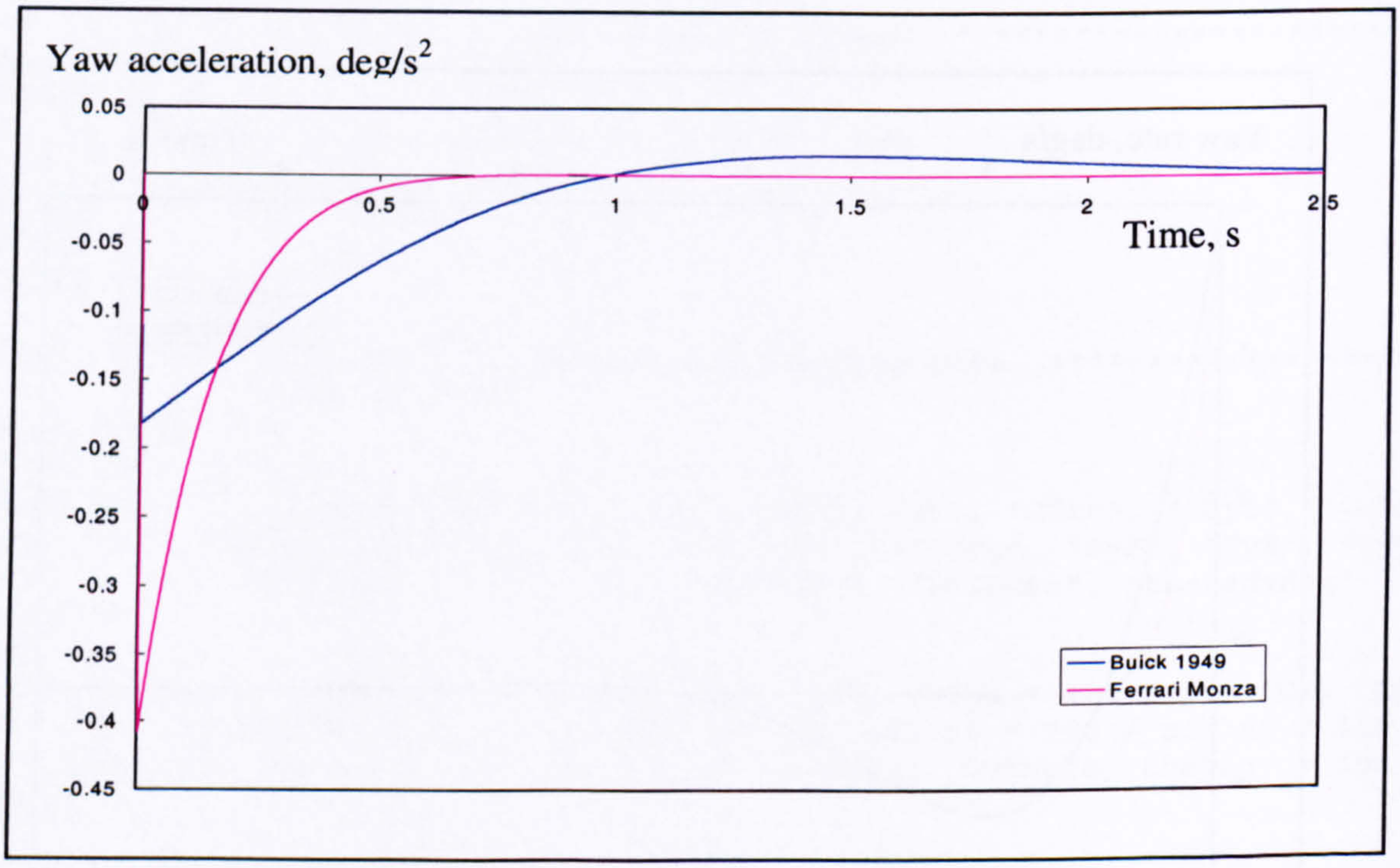

Fig B.4 CGT model results, $\ddot{\theta}$ for the Ferrari and Buick at u = 50 m/s

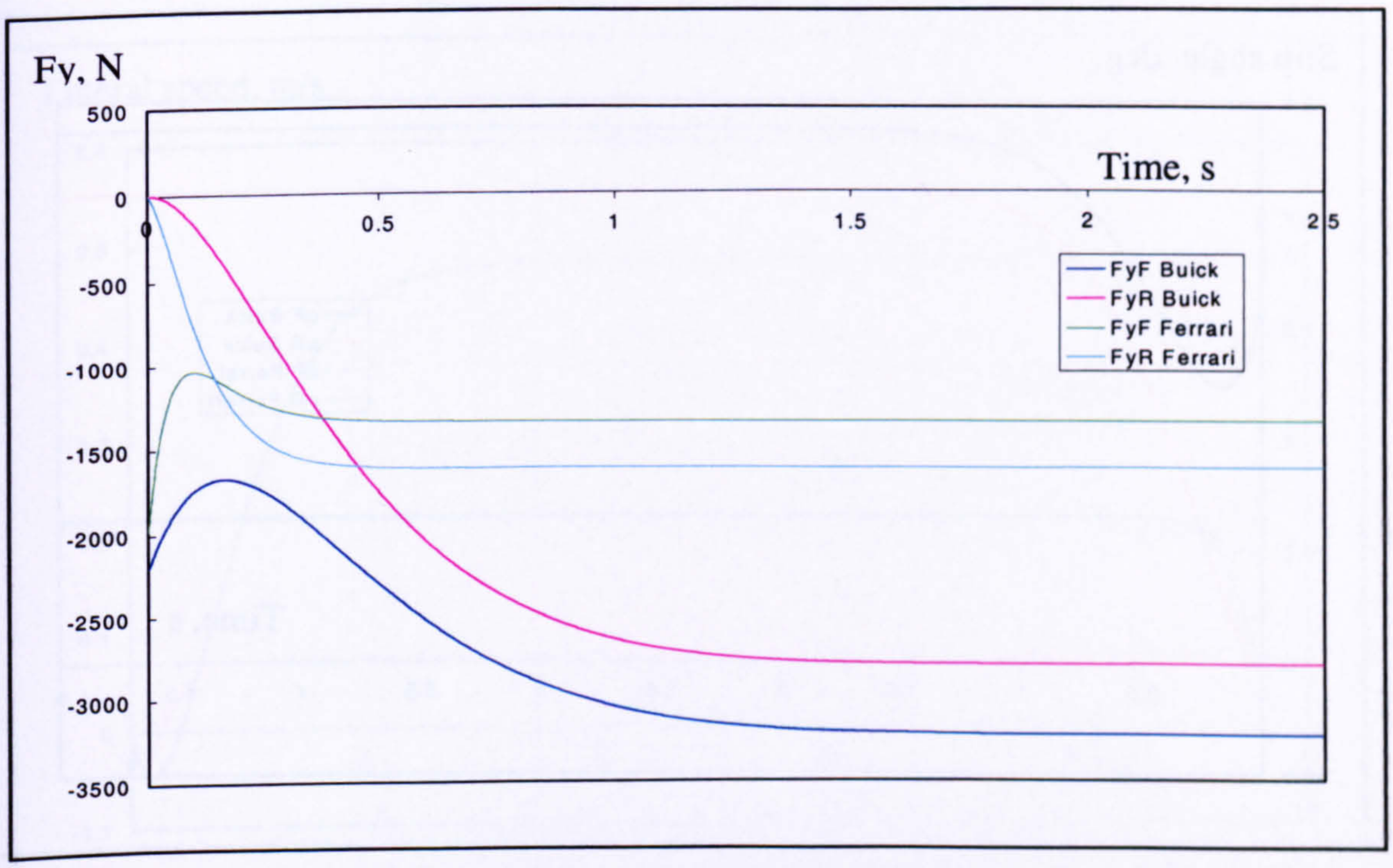

Fig B.5 CGT model results, F_y for the Ferrari and Buick at u = 20 m/s

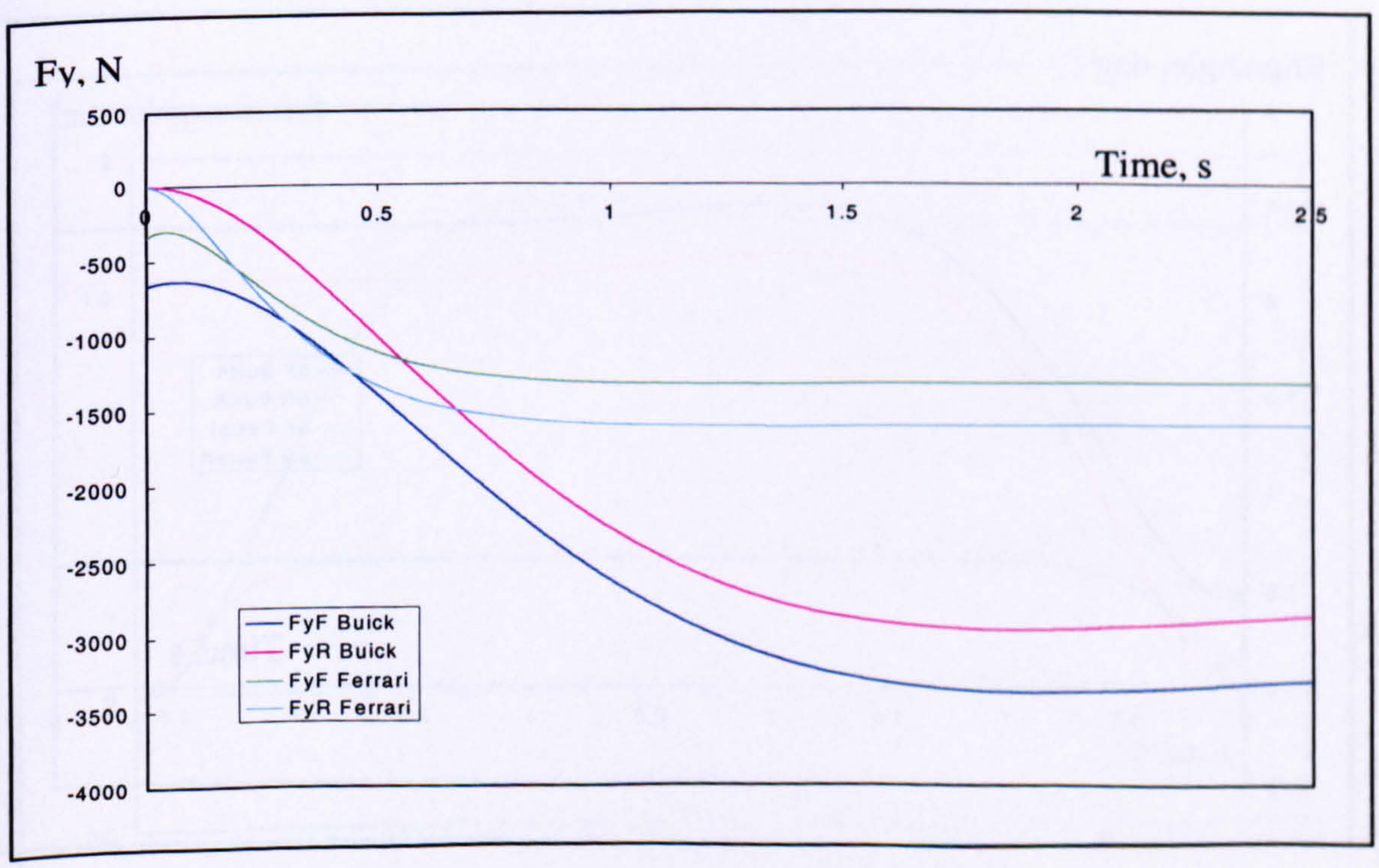

Fig B.6 CGT model results, F_y for the Ferrari and Buick at u = 50 m/s

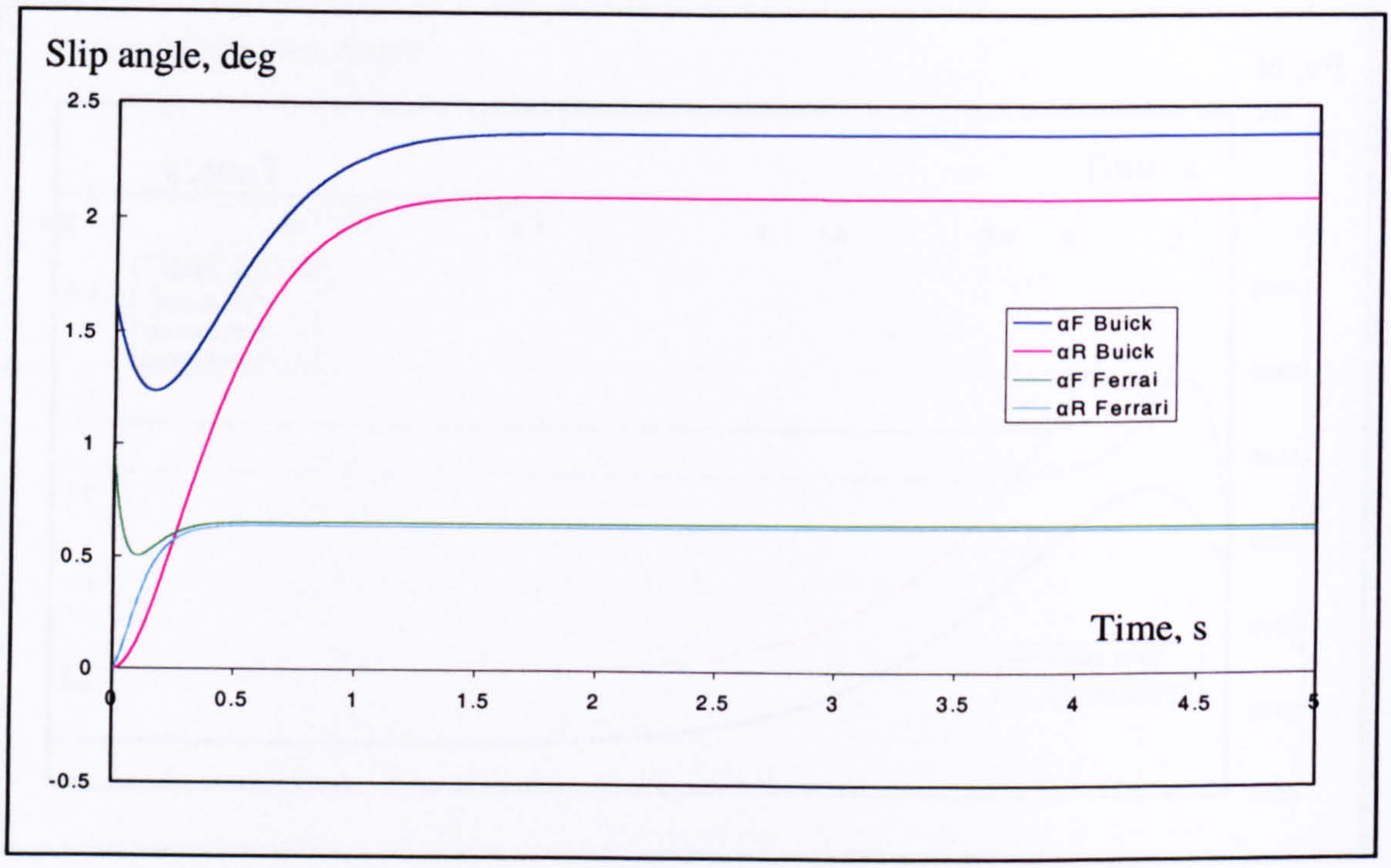

Fig B.7 CGT model results, α for the Ferrari and Buick at u = 20 m/s

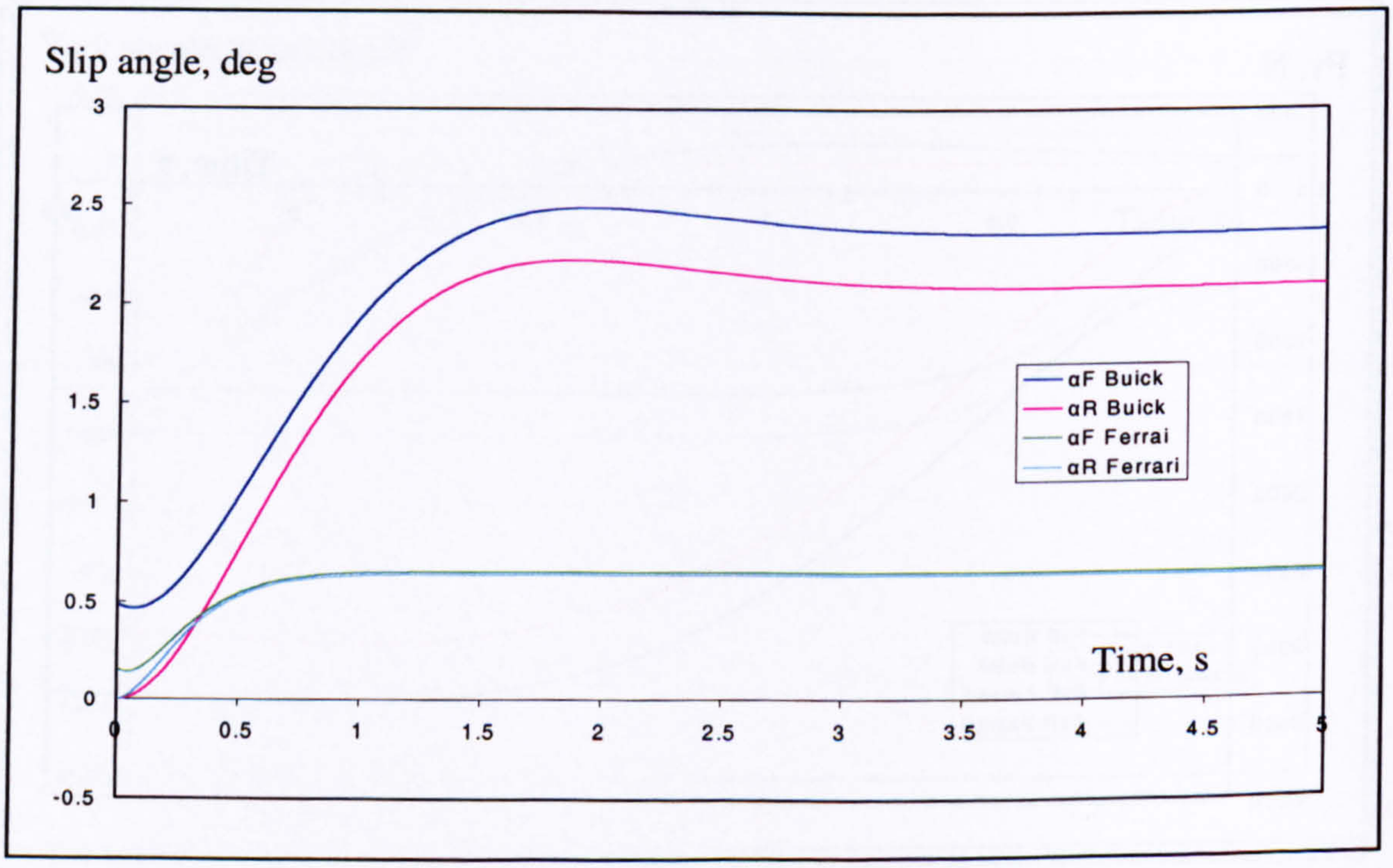

Fig B.8 CGT model results, α for the Ferrari and Buick at u = 50 m/s

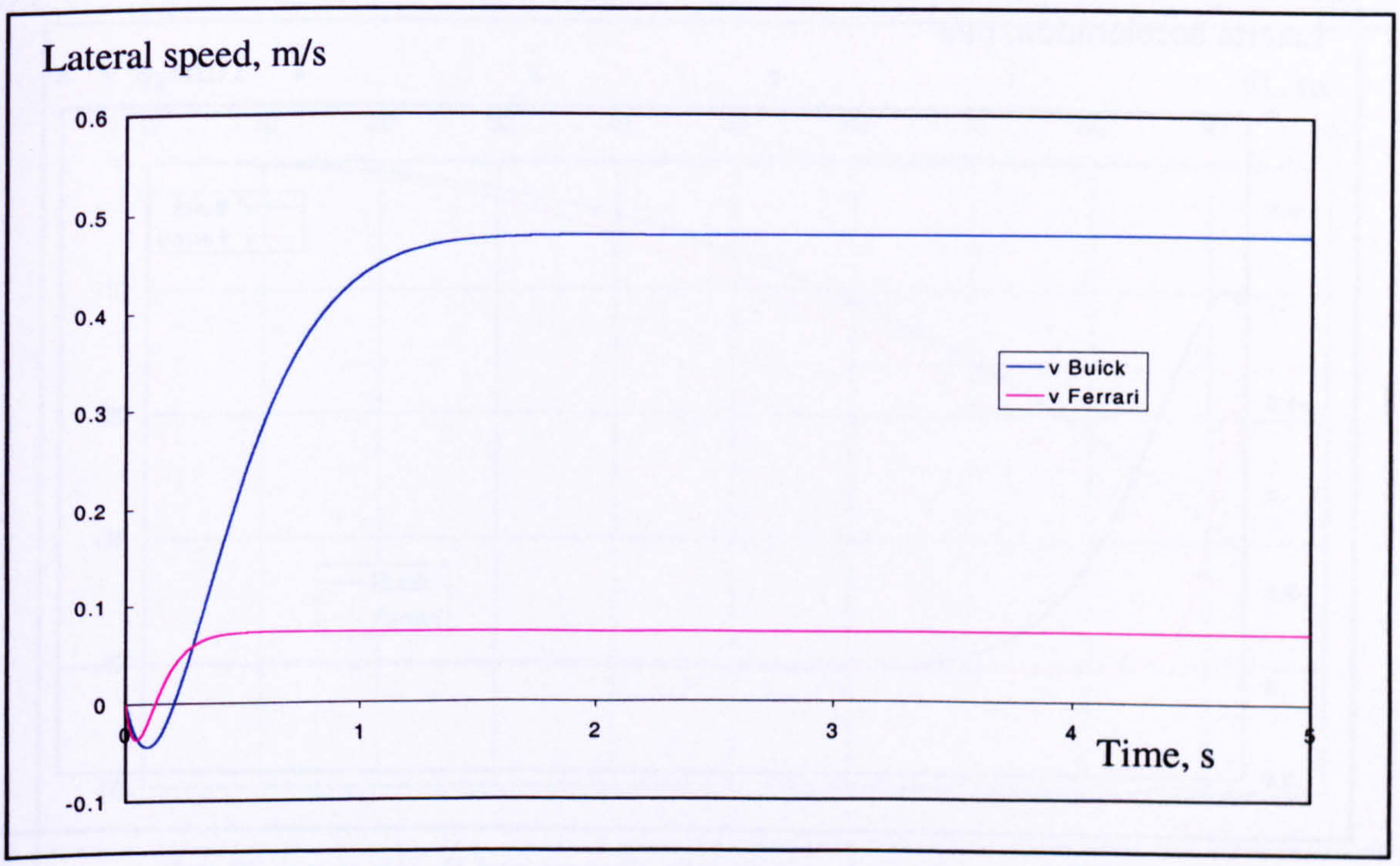

Fig B.9 CGT model results, v for the Ferrari and Buick at u = 20 m/s

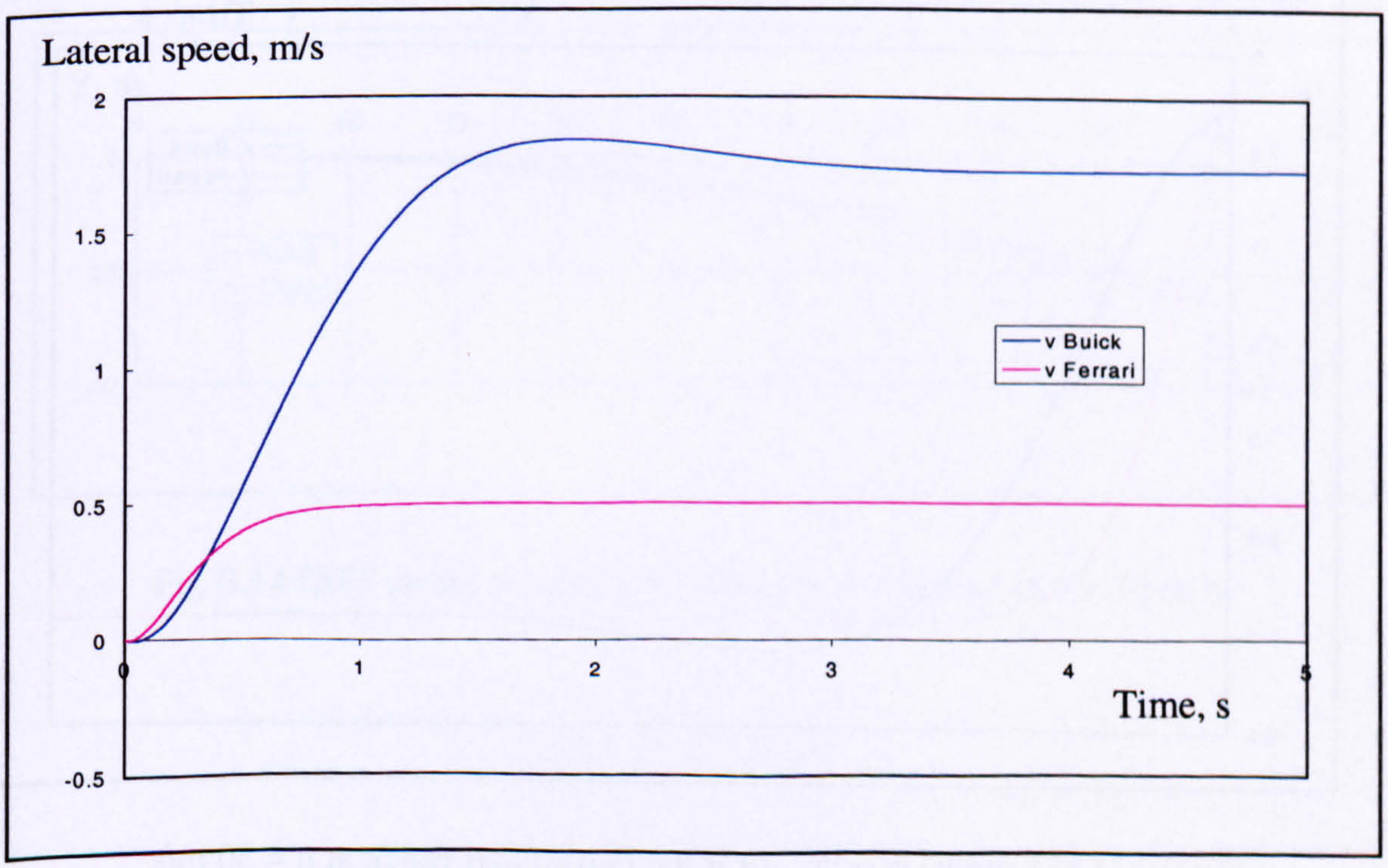

Fig B.10 CGT model results, v for the Ferrari and Buick at u = 50 m/s

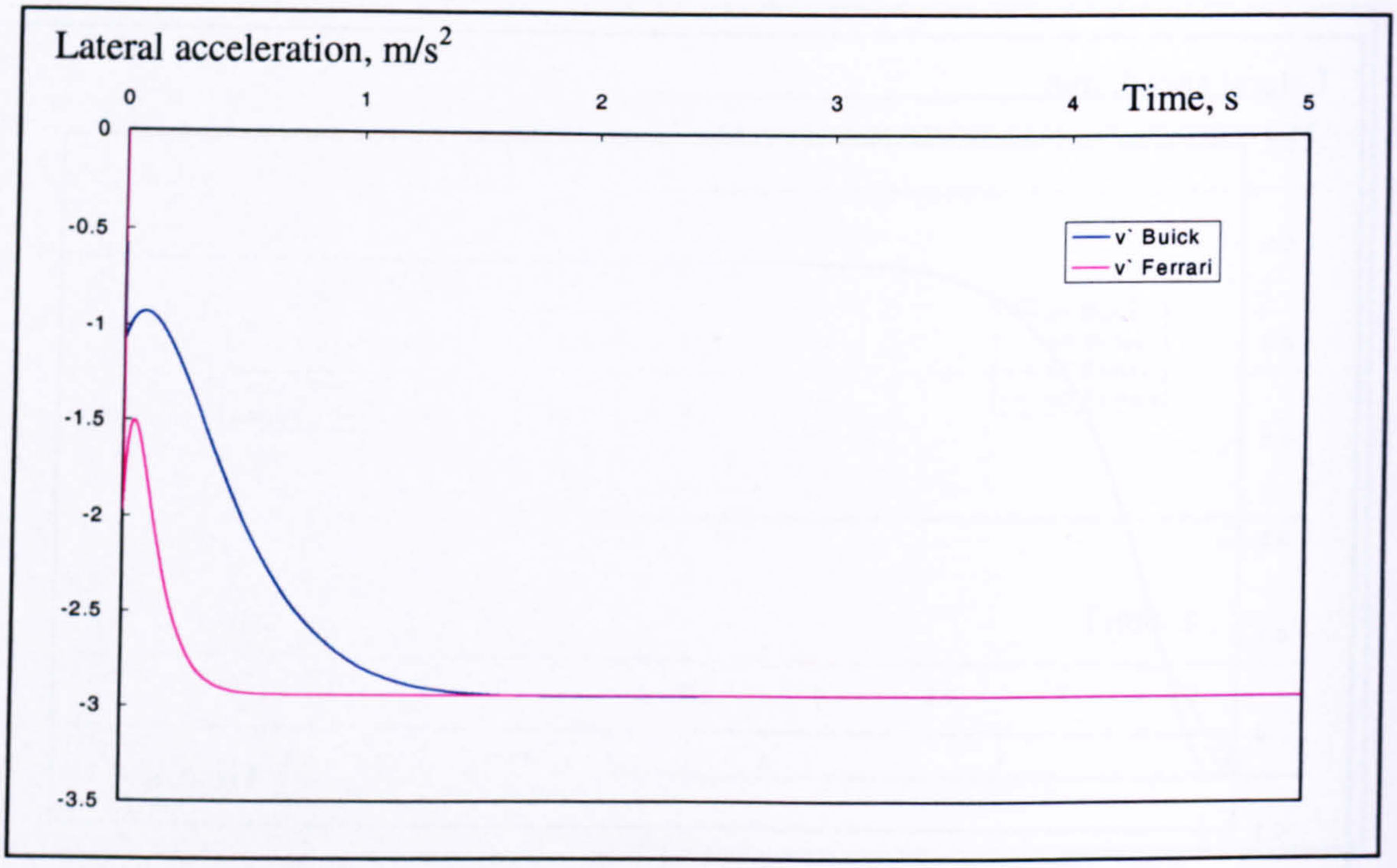

Fig B.11 CGT model results, $\dot{v}$ for the Ferrari and Buick at u = 20 m/s

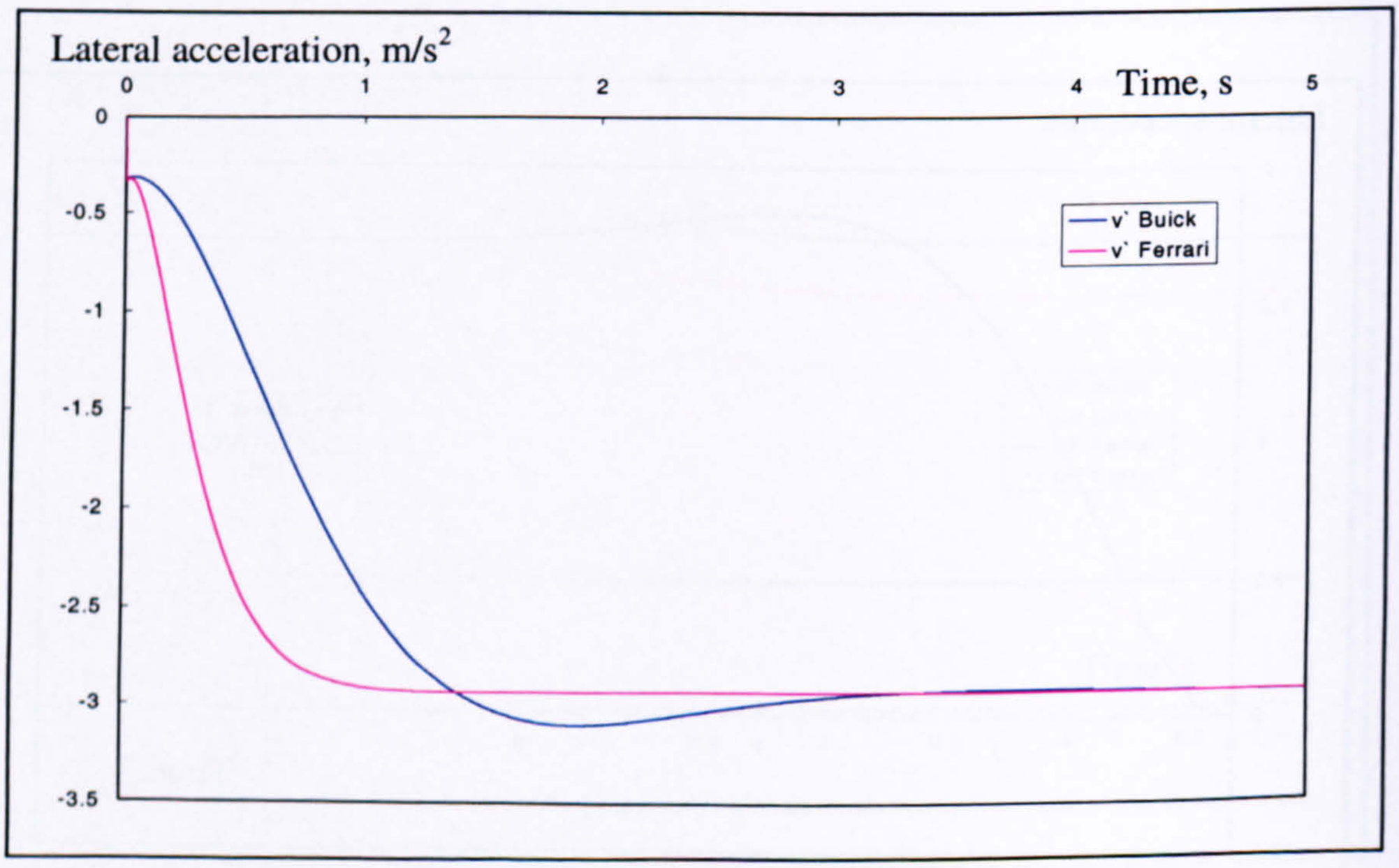

Fig B.12 CGT model results, $\dot{v}$ for the Ferrari and Buick at u = 50 m/s

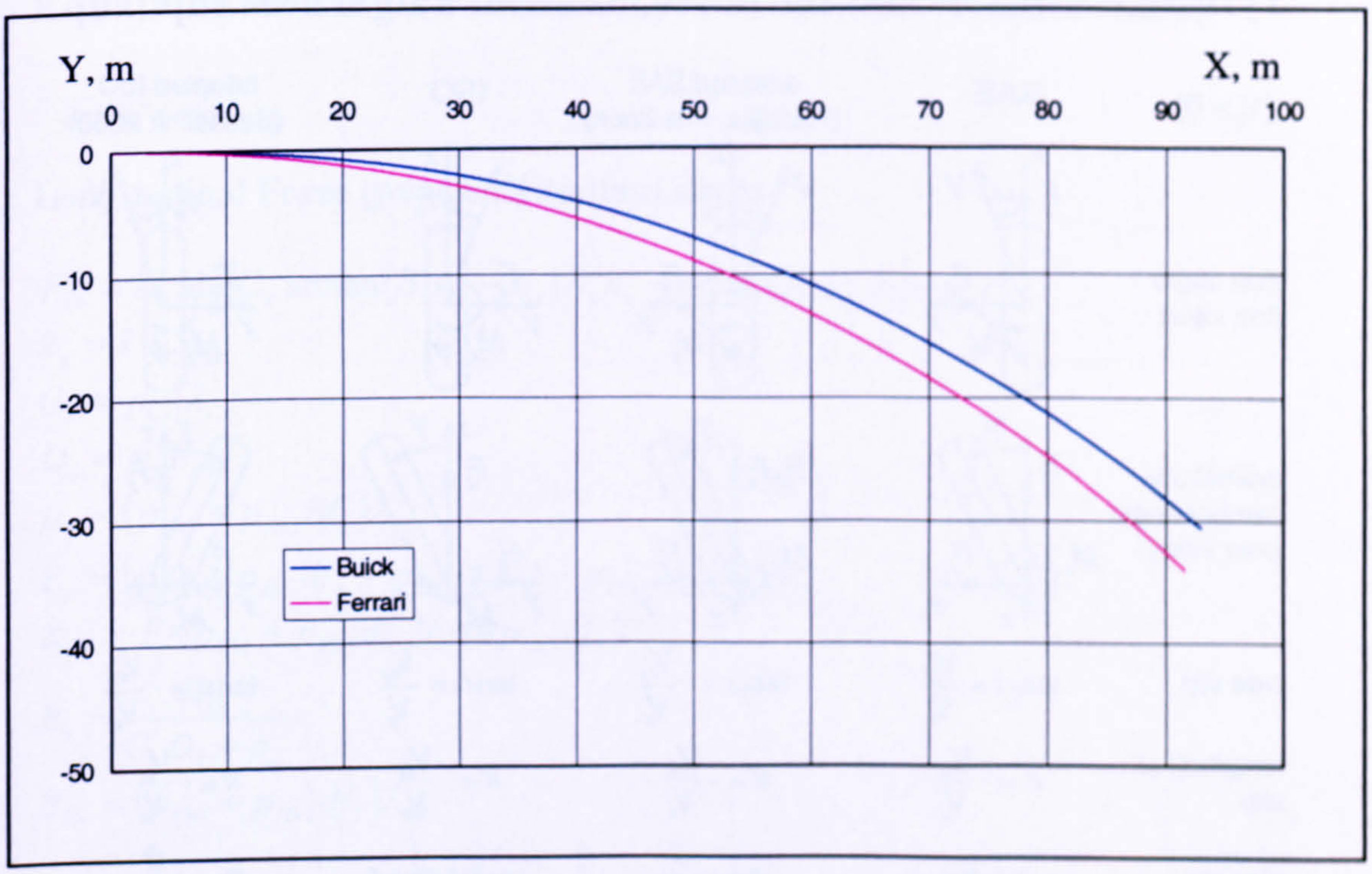

Fig B.13 CGT model results, path of the Ferrari and Buick at u = 20 m/s

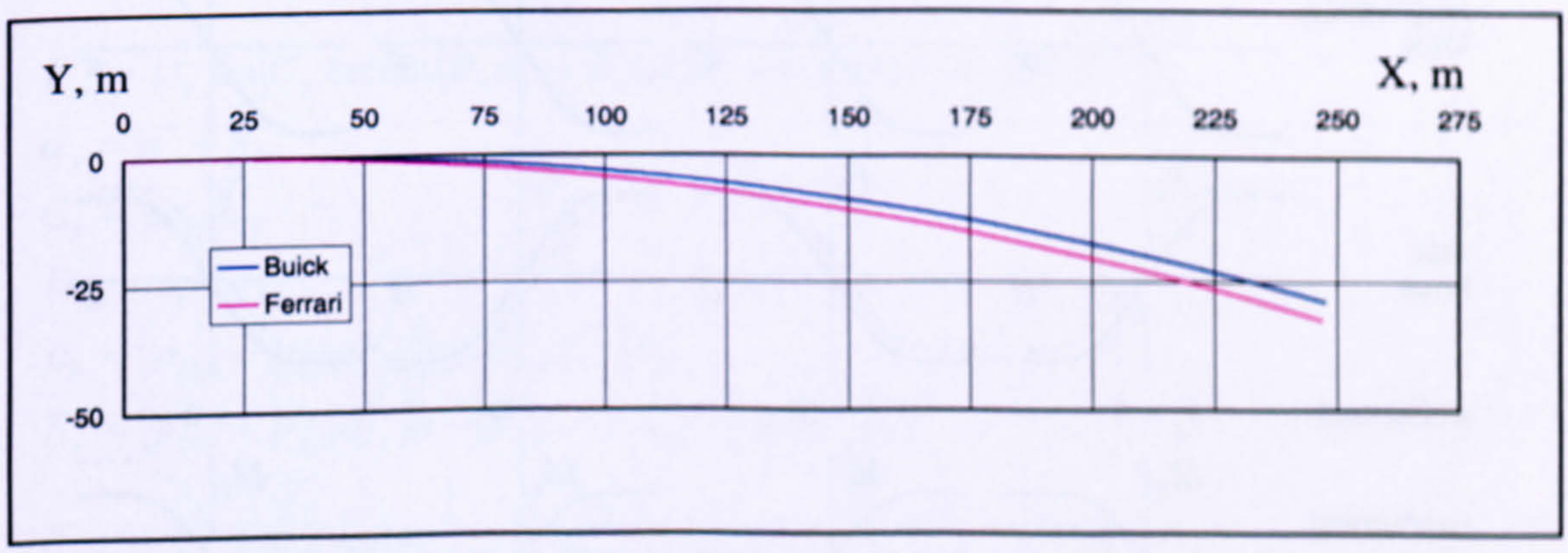

Fig B.14 CGT model results, path of Buick and Ferrari at u = 30 m/s

Appendix C

Tyre Sign Conventions for Force, Moment and Wheel Slip

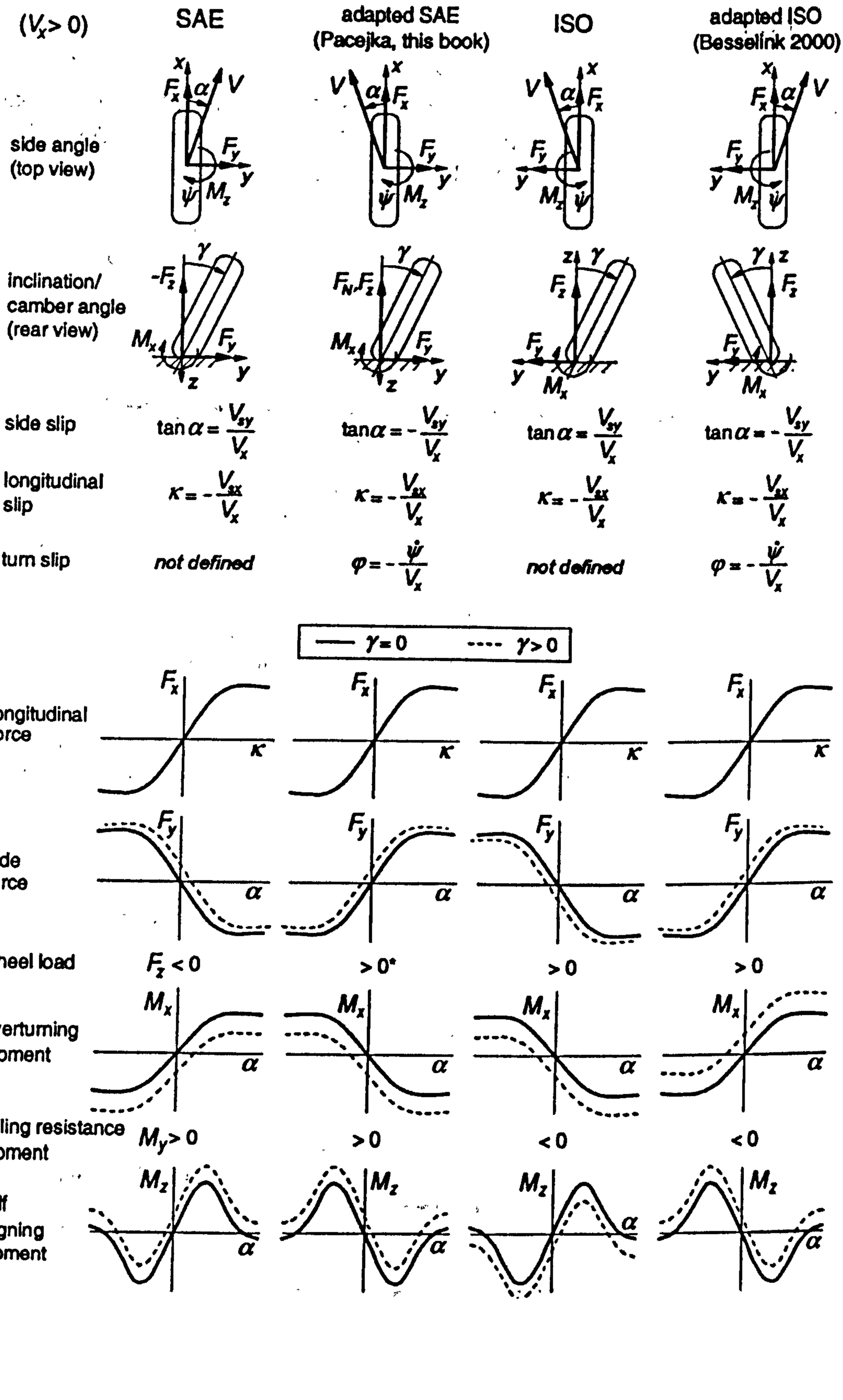

Pacejka H. B., "Tyres and vehicle dynamics", *Oxford: Butterworth-Heinemann,* 2002.

Appendix D

Equations for Magic Formula Tyre Model for Combined Slip

Longitudinal Force (pure longitudinal slip)

$$F_{xo} = D_x \sin\left[C_x \arctan\left\{B_x k_x - E_x\left(B_x k_x - \arctan(B_x k_x)\right)\right\}\right] + S_{Vx}$$

$$k_x = k + S_{Hx}$$

$$C_x = p_{Cx1}\lambda_{Cx}$$

$$D_x = \mu_x F_z \varsigma_1$$

$$\mu_x = \left(p_{Dx1} + p_{Dx2} df_z\right)\lambda_{\mu x}$$

$$E_x = \left(p_{Ex1} + p_{Ex2} df_z + p_{Ex3} df_z^2\right)\left[1 - p_{Ex4}\,\mathrm{sgn}(k_x)\right]\lambda_{Ex}$$

$$K_{xk} = F_z\left(p_{Kx1} + p_{Kx2} df_z\right)\exp\left(p_{Kx3} df_z\right)\lambda_{Kxk}$$

$$B_x = \frac{K_{xk}}{C_x D_x + \varepsilon_x}$$

$$S_{Hx} = \left(p_{Hx1} + p_{Hx2} df_z\right)\lambda_{Hx}$$

$$S_{Vx} = F_z\left(p_{Vx1} + p_{Vx2} df_z\right)\left\{\frac{|V_{cx}|}{|V_{cx}| + \varepsilon_{Vx}}\right\}\lambda_{Vx}\lambda'_{\mu x}\varsigma_1$$

Lateral Force (pure lateral slip)

$$F_{yo} = D_y \sin\left[C_y \arctan\left\{B_y \alpha_y - E_y\left(B_y \alpha_y - \arctan(B_y \alpha_y)\right)\right\}\right] + S_{Vy}$$

$$\alpha_y = \alpha^* + S_{Hy}$$

$$C_y = p_{Cy1}\lambda_{Cy}$$

$$D_y = \mu_y F_z \varsigma_2$$

$$\mu_y = \left(p_{Dy1} + p_{Dy2} df_z\right)\left[1 - p_{Dy3}\gamma^{*2}\right]\lambda^*_{\mu y}$$

$$E_y = \left(p_{Ey1} + p_{Ey2} df_z\right)\left\{1 - \left[p_{Ey3} + p_{Ey4}\gamma^*\right]\mathrm{sgn}(\alpha_y)\right\}\lambda^*_{Ey}$$

$$K_{y\alpha o} = F'_{zo}\sin\left[2\arctan\left\{\frac{F_z}{p_{Ky2}F'_{zo}}\right\}\right]\lambda_{Ky\alpha}$$

$$K_{y\alpha} = K_{y\alpha o}\left(1 - p_{Ky3}\gamma^{*2}\right)\varsigma_3$$

$$B_y = \frac{K_{y\alpha}}{C_y D_y + \varepsilon_y}$$

$$S_{Hy} = \left(p_{Hy1} + p_{Hy2} df_z\right)\lambda_{Hy} + p_{Hy3}\gamma^*\lambda_{Ky\gamma}\varsigma_0 + \varsigma_4 - 1$$

$$S_{Vy} = F_z\left\{\left(p_{Vy1} + p_{Vy2} df_z\right)\lambda_{Vy} + \left[p_{Vy3} + p_{Vy4} df_z\right]\gamma^*\lambda_{Ky\gamma}\right\}\lambda'_{\mu y}\varsigma_2$$

$$K_{y\gamma 0} = \left\{p_{Hy3}K_{y\alpha o} + F_z\left(p_{Vy3} + p_{Vy4} df_z\right)\right\}\lambda_{Ky\gamma}$$

Pacejka H. B., "Tyres and vehicle dynamics", *Oxford: Butterworth-Heinemann*, 2002 [34]

Longitudinal Force (combined slip)

$$F_x = G_{x\alpha} F_{xo}$$

$$G_{x\alpha} = \cos\left[C_{x\alpha} \arctan\left\{B_{x\alpha}\alpha_S - E_{x\alpha}\left(B_{x\alpha}\alpha_S - \arctan(B_{x\alpha}\alpha_S)\right)\right\}\right] / G_{x\alpha o}$$

$$G_{x\alpha o} = \cos\left[C_{x\alpha} \arctan\left\{B_{x\alpha}S_{Hx\alpha} - E_{x\alpha}\left(B_{x\alpha}S_{Hx\alpha} - \arctan(B_{x\alpha}S_{Hx\alpha})\right)\right\}\right]$$

$$\alpha_S = \alpha^* + S_{Hx\alpha}$$

$$B_{x\alpha} = r_{Bx1} \cos\left[\arctan\left\{r_{Bx2} k\right\}\right] \lambda_{x\alpha}$$

$$C_{x\alpha} = r_{Cx1}$$

$$E_{x\alpha} = r_{Ex1} + r_{Ex2} df_z$$

$$S_{Hx\alpha} = r_{Hx1}$$

Lateral Force (combined slip)

$$F_y = G_{yk} F_{yo} + S_{Vyk}$$

$$G_{yk} = \cos\left[C_{yk} \arctan\left\{B_{yk}k_S - E_{yk}\left(B_{yk}k_S - \arctan(B_{yk}k_S)\right)\right\}\right] / G_{yko}$$

$$G_{yko} = \cos\left[C_{yk} \arctan\left\{B_{yk}S_{Hyk} - E_{yk}\left(B_{yk}S_{Hyk} - \arctan(B_{yk}S_{Hyk})\right)\right\}\right]$$

$$k_S = k + S_{Hyk}$$

$$B_{yk} = r_{By1} \cos\left[\arctan\left\{r_{By2}(\alpha^* - r_{By3})\right\}\right] \lambda_{yk}$$

$$C_{yk} = r_{Cy1}$$

$$E_{yk} = r_{Ey1} + r_{Ey2} df_z$$

$$S_{Hyk} = r_{Hy1} + r_{Hy2} df_z$$

$$S_{Vyk} = D_{Vyk} \sin\left[r_{Vy5} \arctan\left(r_{Vy6} k\right)\right]$$

$$D_{Vyk} = \mu_y F_z \left[r_{Vy1} + r_{Vy2} df_z + r_{Vy3}\gamma^*\right] \cos\left(\arctan(r_{Vy4}\alpha^*)\right) \zeta_2$$

Definitions and descriptions of the above equations are detailed in [34]

Pacejka H. B., "Tyres and vehicle dynamics", *Oxford: Butterworth-Heinemann,* 2002 [34]

Appendix E : kcal Routine Flowchart

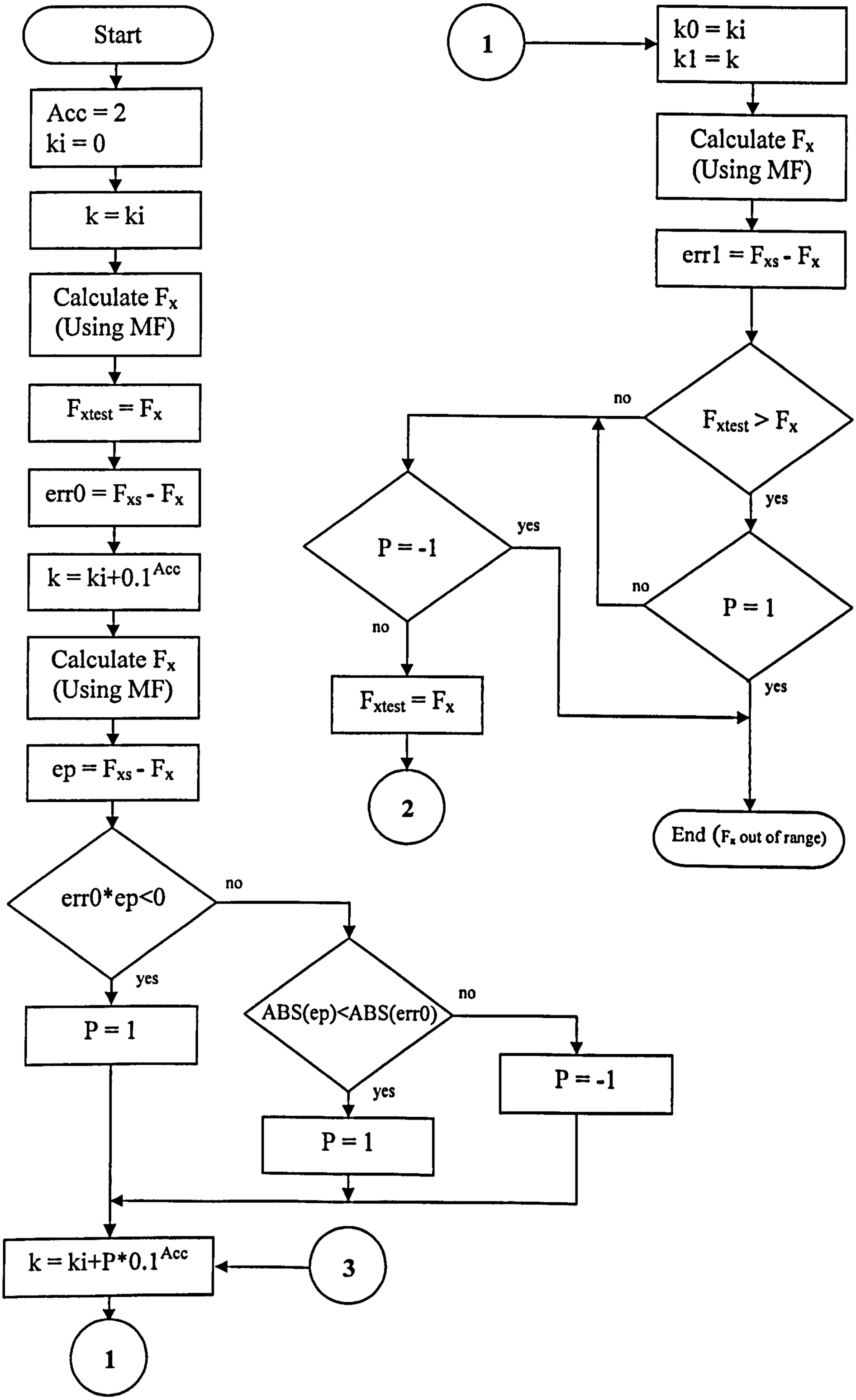

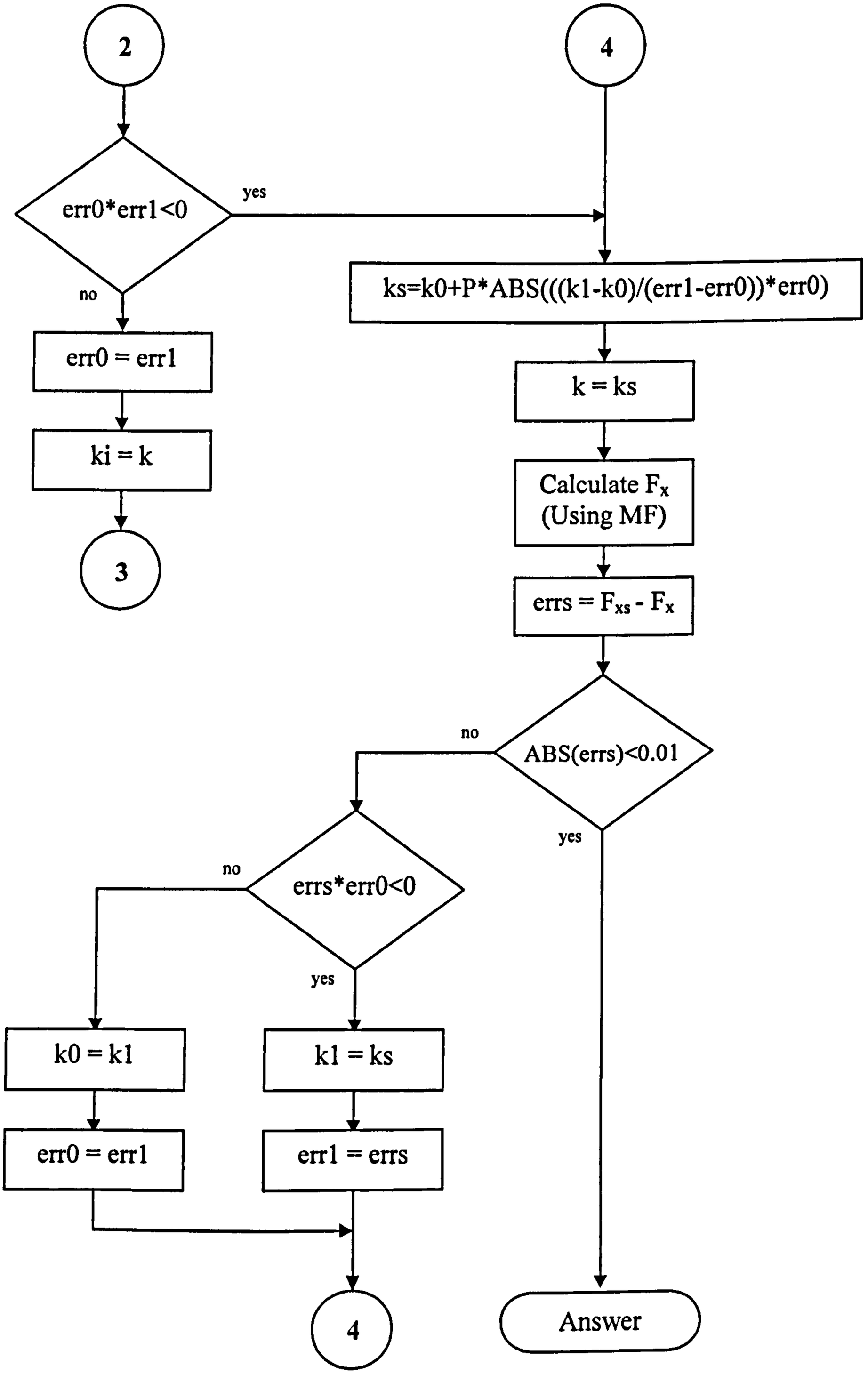
2
err0*err1<0
yes
no
err0 = err1
ki = k
3
4
ks=k0+P*ABS(((k1-k0)/(err1-err0))*err0)
k = ks
Calculate Fx
(Using MF)
errs = Fxs - Fx
ABS(errs)<0.01
no
yes
errs*err0<0
no
yes
k0 = k1
err0 = err1
k1 = ks
err1 = errs
Answer

Appendix F : Reversed Magic Formula Tyre Model Flowchart

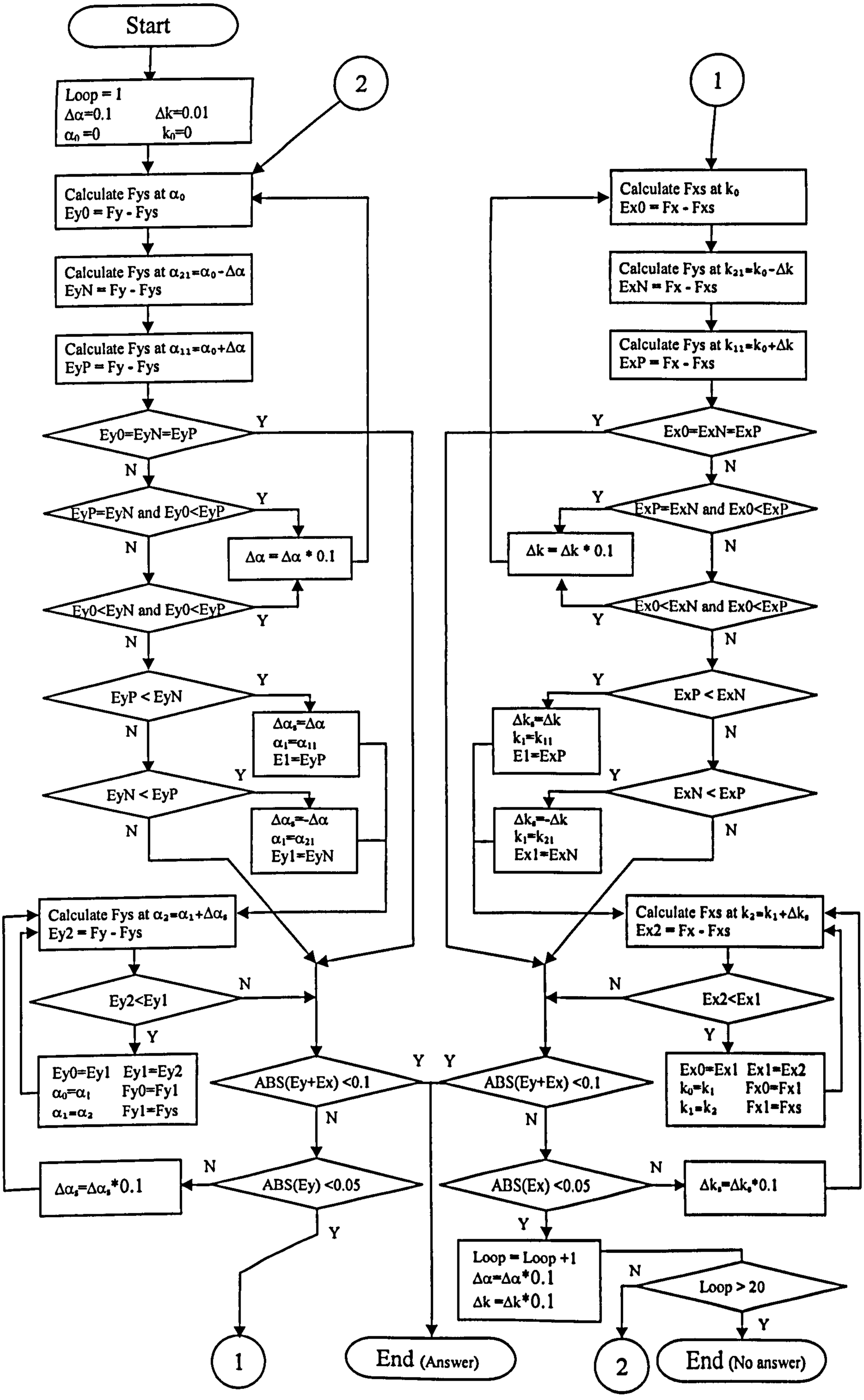

Appendix G: WSDC Vehicle Handling Simulation Model (Full Model of CH-8)

```
'   ************************************************************************
'   *** Full WSDC Vehicle Handling Model using CGT, MF,kcal, MPC and WSDD ***
'   ************************************************************************
CLS
DEFDBL A-Z
prn = 1                                    ' 1 print results to file, 0 don't
scr = 1                                    ' 1 print results to screen, 0 don't
ctrl = 0                                   ' 1 Apply Control, 0 don't
IF prn THEN OPEN "Result.txt" FOR OUTPUT AS #1          ' output file name
IF scr THEN
SCREEN 12
SS = 1                                     ' Scale on screen
WINDOW (-20 * SS, -50 * SS)-(200 * SS, 110 * SS)
LINE (0, 0)-(100, 100), 5, B
END IF
DIM FyFl(1000), FyFr(1000), FyRl(1000), FyRr(1000)
PRINT TIMER
pi = 3.141592654#
Momc = 0                                   ' External moment

u00 = 30                                   ' Vehicle speed m/s
ferrari = 1                                ' 1 Ferrari, 0 Buick
FWS = 1                                    ' 1 FWS, 0 RWS
RWD = 1                                    ' Rear  Wheel Drive Vehicle
FWD = 0                                    ' Front Wheel Drive Vehicle
AWD = 0                                    ' All   Wheel Drive Vehicle
NWD = 0                                    ' No    Wheel Drive Vehicle

u0 = u00
uv = u0
dt = .001                                  ' Time interval s
st = 5                                     ' Simulation time s
SS = st / dt                               ' simulation steps
Rl = .68                                   ' Relaxation distance m

' ************************  Manouver ***************************************
mt = 3                                     ' Time of the manouver (sec)
md = 2                                     ' Max steering angel (Degree)
ma = 360                                   ' the manouver sine wave angle
d = 0                                      ' Initial steering angle (=0)
iii = 0

' ************************  Start   ****************************************
GOSUB 1000    ' Read Vehicle data (Vehicle data inputs, line 1000)
GOSUB 2000    ' Read tyre data    (Tyre data inputs,    line 2000)
10
GOSUB 2500    ' Calculate steering angle and drive forces
GOSUB 3000    ' Calculate Forces (including the control)
GOSUB 3500    ' Calculate Wheel Speeds
GOSUB 4000    ' Calculate Accelerations
GOSUB 5000    ' Calculate Speeds
GOSUB 6000    ' Calculate CG movement
GOSUB 7000    ' Calculate tyres movement
GOSUB 8000    ' Calculate tyres locations
GOSUB 9000    ' Calculate tyres Slip angles
GOSUB 10000   ' Calculate tyres traveled distances
GOSUB 11000   ' Calculate tyres longitudinal speeds
```

```
GOSUB 12000   ' Calculate Tyre Loads
GOSUB 14000   ' Calculate tyres k
GOSUB 15000   ' Calculate tyres Forces
GOSUB 16000   ' Get ready for next stage
GOSUB 99999   ' Saving data to file
GOTO 10

999
PRINT TIMER
END

2500 ' ************  Calculating Driving Forces/Steering  ******************
FxRr = -(FyRl * SIN(delrl) - FyRr * SIN(delrr) + FxFl * COS(delfl) + FxFr *
COS(delfr) - FyFl * SIN(delfl) - FyFr * SIN(delfr)) / 2
FxRl = -(FyRl * SIN(delrl) - FyRr * SIN(delrr) + FxFl * COS(delfl) + FxFr *
COS(delfr) - FyFl * SIN(delfl) - FyFr * SIN(delfr)) / 2

Fxt0 = FxRr + FxRl

FxRl = .5 * Fxt0
FxRr = .5 * Fxt0

IF aaaa > SS THEN 999 ELSE aaaa = aaaa + 1   ' Run Number of Steps

d = (pi / 180) * md * SIN(iii * pi / 180)   'instantenious steering angle

' ****************************  Ackerman path ********************************
XA = XA + SQR((uv * dt + b * COS(ATN(uv * dt * (TAN(d) / l))) - b) ^ 2 + (uv *
dt * TAN((ATN(uv * dt * (TAN(d) / l)))) + b * SIN(ATN(uv * dt * (TAN(d) /
l)))) ^ 2) * COS(Ththet + ATN(b * TAN(d) / l) + pi / 2 - ((pi - ATN(uv * dt *
(TAN(d) / l))) / 2))

YA = YA + SQR((uv * dt + b * COS(ATN(uv * dt * (TAN(d) / l))) - b) ^ 2 + (uv *
dt * TAN((ATN(uv * dt * (TAN(d) / l)))) + b * SIN(ATN(uv * dt * (TAN(d) /
l)))) ^ 2) * SIN(Ththet + ATN(b * TAN(d) / l) + pi / 2 - ((pi - ATN(uv * dt *
(TAN(d) / l))) / 2))

vA = (uv * dt * TAN((ATN(uv * dt * (TAN(d) / l)))) + b * SIN(ATN(uv * dt *
(TAN(d) / l)))) / dt

dThthet = ATN(uv * dt * (TAN(d) / l))
Ththet = Ththet0 + dThthet
Ththetd = dThthet / dt

dthetad = Ththetd - thetadv
Ththetdd = dthetad / dt
CM = I * Ththetdd

Ththetd0 = Ththetd
Ththet0 = Ththet

'=============
IF scr THEN PSET (XA, d * 1000), 7
IF scr THEN PSET (XA, YA), 13

IF manend = 1 THEN 1234
IF iii < 0 THEN iii = -iii
iii = iii + ma * (dt / mt)
IF iii > ma THEN iii = ma: manend = 1
IF iii > 360 THEN iii = -iii

1234
```

```
'****************************** Ackerman angles ************************************
IF d = 0 THEN
r = 10000000
delfr = 0
delfl = 0
delrr = 0
delrl = 0
ELSE

IF FWS THEN
r = l / TAN(d)
IF r > 10000000 THEN r = 10000000
IF r < -10000000 THEN r = -10000000
delfr = ATN(l / (r + t / 2))
delfl = ATN(l / (r - t / 2))
delrr = 0
delrl = 0
ELSE
r = -l / TAN(d)
IF r > 10000000 THEN r = 10000000
IF r < -10000000 THEN r = -10000000
delfr = 0
delfl = 0
delrr = -ATN(l / (r + t / 2))
delrl = -ATN(l / (r - t / 2))
END IF

END IF
RETURN

3000 ' ********************  Calculating the Forces  ************************
mom1 = (FxRl * COS(delrl) - FyRl * SIN(delrl) + FxFl * COS(delfl) - FyFl *
SIN(delfl)) * tl * -1
mom2 = (FxRr * COS(delrr) - FyRr * SIN(delrr) + FxFr * COS(delfr) - FyFr *
SIN(delfr)) * tr
mom3 = (FxRl * SIN(delrl) + FyRl * COS(delrl) + FxRr * SIN(delrr) + FyRr *
COS(delrr)) * b * -1
mom4 = (FxFl * SIN(delfl) + FyFl * COS(delfl) + FxFr * SIN(delfr) + FyFr *
COS(delfr)) * a
Momt = mom1 + mom2 + mom3 + mom4 + Momc

'==========Control Start========
IF ctrl THEN
dfx = CM / t
777
Fx = FxRr + dfx / 2
Fz = FzRr
alfa = arr
Vcx = Urr1
GOSUB 1000001
IF fxout = 1 THEN
fxout = 0
dfx = dfx - (SGN(dfx) * 100)
LOCATE 1, 1
PRINT dfx
GOTO 777
END IF

Fx = FxRl - dfx / 2
Fz = FzRl
alfa = arl
Vcx = Url1
```

```
GOSUB 1000001
IF fxout = 1 THEN
fxout = 0
dfx = dfx - (SGN(dfx) * 100)
LOCATE 1, 1
PRINT dfx
GOTO 777
END IF

FxRr = FxRr + dfx / 2
FxRl = FxRl - dfx / 2
'============  Caculating Differential Torque  ==============
Tc = (FxRl - FxRr) / (Ro * 6)                    ' Control Shaft torque
Td = -(2 / 3) * (FxRr / Ro) + (FxRl - FxRr) / (Ro * 3) 'Drive Shaft torque
Tdo = -(FxRl + FxRr) / (Ro * 3)                  ' Conventional differential torque

'======
mom1 = (FxRl * COS(delrl) - FyRl * SIN(delrl) + FxFl * COS(delfl) - FyFl *
SIN(delfl)) * tl * -1
mom2 = (FxRr * COS(delrr) - FyRr * SIN(delrr) + FxFr * COS(delfr) - FyFr *
SIN(delfr)) * tr
mom3 = (FxRl * SIN(delrl) + FyRl * COS(delrl) + FxRr * SIN(delrr) + FyRr *
COS(delrr)) * b * -1
mom4 = (FxFl * SIN(delfl) + FyFl * COS(delfl) + FxFr * SIN(delfr) + FyFr *
COS(delfr)) * a
Momt = mom1 + mom2 + mom3 + mom4 + Momc
END IF
'==========  Control End ======
Fxt = FxRl * COS(delrl) + FxRr * COS(delrr) - FyRl * SIN(delrl) - FyRr *
SIN(delrr) + FxFl * COS(delfl) + FxFr * COS(delfr) - FyFl * SIN(delfl) - FyFr
* SIN(delfr)
Fyt = FyRl * COS(delrl) + FyRr * COS(delrr) + FxRl * SIN(delrl) + FxRr *
SIN(delrr) + FyFl * COS(delfl) + FyFr * COS(delfr) + FxFl * SIN(delfl) + FxFr
* SIN(delfr)
RETURN

3500 ' *********  Calculating Wheels Rotational Speeds (control) **********

'===== Calculating Orr ====
Fz = FzRr
Fx = FxRr
alfa = arr
Vcx = Urr1
GOSUB 1000001
IF fxout = 0 THEN kRr = K
Orr = (Urr1 + kRr * Urr1) / Ro

'===== Calculating Orl ====
Fz = FzRl
Fx = FxRl
alfa = arl
Vcx = Url1
GOSUB 1000001
IF fxout = 0 THEN kRl = K
Orl = (Url1 + kRl * Url1) / Ro

'=====   Calculating Differential speeds  ====
Oc = (Orr - Orl) / 3
Od = (Orr + Orl) * (3 / 2)
RETURN
```

```
4000 ' ********************  Calculating the Accelerations  ****************
ud = (Fxt) / m
vd = (Fyt) / m
thetadd = (Momt) / I
RETURN

5000 ' ********************  Calculating the Speeds  ************************
uv = u0 + ud * dt
vv = v0 + vd * dt
thetadv = thetad0 + thetadd * dt
RETURN

6000 ' ********************  Calculating CG Movement  ***********************
Dux = (uv + u0) * dt / 2
Dvy = (vv + v0) * dt / 2
DvTheta = (thetadv + thetad0) * dt / 2

7000 ' ********************  Calculate CG location  *************************
CGx = CGx0 + Dux
CGy = CGy0 + Dvy
CGt = CGt0 + DvTheta
RETURN

8000 ' ********************  Calculate tyres locations  *********************
flx = CGx + a * COS(CGt) - tl * SIN(CGt)
fly = CGy + a * SIN(CGt) + tl * COS(CGt)
frx = CGx + a * COS(CGt) + tr * SIN(CGt)
fry = CGy + a * SIN(CGt) - tr * COS(CGt)

rlx = CGx - b * COS(CGt) - tl * SIN(CGt)
rly = CGy - b * SIN(CGt) + tl * COS(CGt)
rrx = CGx - b * COS(CGt) + tr * SIN(CGt)
rry = CGy - b * SIN(CGt) - tr * COS(CGt)
RETURN

9000 ' ********************  Calculate tyres Slip angles ********************
Sfl = ATN((fly - Fly0) / (flx - Flx0))
Sfr = ATN((fry - Fry0) / (frx - Frx0))
Srl = ATN((rly - Rly0) / (rlx - Rlx0))
Srr = ATN((rry - Rry0) / (rrx - Rrx0))

afl = Sfl - delfl
afr = Sfr - delfr
arl = Srl - delrl
arr = Srr - delrr
RETURN

10000 ' ********************  Calculate tyres traveled distances ************
'TFl  = Total Distance moved by the Front Left tyre
'DFly = Distance moved by the Front Left tyre in its lateral direction

Tfl = SQR((fly - Fly0) ^ 2 + (flx - Flx0) ^ 2)
Tfr = SQR((fry - Fry0) ^ 2 + (frx - Frx0) ^ 2)
Trl = SQR((rly - Rly0) ^ 2 + (rlx - Rlx0) ^ 2)
Trr = SQR((rry - Rry0) ^ 2 + (rrx - Rrx0) ^ 2)

Dflx = Tfl * COS(afl)
Dfly = Tfl * SIN(afl)
Dfrx = Tfr * COS(afr)
Dfry = Tfr * SIN(afr)
Drlx = Trl * COS(arl)
Drly = Trl * SIN(arl)
```

```
Drrx = Trr * COS(arr)
Drry = Trr * SIN(arr)
RETURN

11000 ' ********************  Calculate tyres Speeds   **********************
' Inputs Dflx,Dfrx,Drlx,Drrx  , Dt
' Ufl1 Longitudinal speed of Front left tyre (m/sec)

Ufl1 = uv * COS(DvTheta + delfl) + vv * SIN(DvTheta + delfl) + thetadv * rfl *
COS(pi / 2 + ATN(tl / a) - delfl + DvTheta)
Vfl1 = vv * COS(DvTheta + delfl) - uv * SIN(DvTheta + delfl) + thetadv * rfl *
SIN(pi / 2 + ATN(tl / a) - delfl + DvTheta)

Url1 = uv * COS(DvTheta + delrl) + vv * SIN(DvTheta + delrl) + thetadv * rrl *
COS(pi / 2 + pi + ATN(tl / -b) - delrl + DvTheta)
Vrl1 = vv * COS(DvTheta + delrl) - uv * SIN(DvTheta + delrl) + thetadv * rrl *
SIN(pi / 2 + pi + ATN(tl / -b) - delrl + DvTheta)

Urr1 = uv * COS(DvTheta + delrr) + vv * SIN(DvTheta + delrr) + thetadv * rrr *
COS(pi / 2 + pi + ATN(-tr / -b) - delrr + DvTheta)
Vrr1 = vv * COS(DvTheta + delrr) - uv * SIN(DvTheta + delrr) + thetadv * rrr *
SIN(pi / 2 + pi + ATN(-tr / -b) - delrr + DvTheta)

Ufr1 = uv * COS(DvTheta + delfr) + vv * SIN(DvTheta + delfr) + thetadv * rfr *
COS(pi / 2 + ATN(-tr / a) - delfr + DvTheta)
Vfr1 = vv * COS(DvTheta + delfr) - uv * SIN(DvTheta + delfr) + thetadv * rfr *
SIN(pi / 2 + ATN(-tr / a) - delfr + DvTheta)
RETURN

12000 ' ********************  Calculate Tyre Loads  **********************
W = m * 9.81
FzFl = W * b / l * (tr / t) - .5 * m * ud * h / l - .5 * m * vd * h / t
FzFr = W * b / l * (tl / t) - .5 * m * ud * h / l + .5 * m * vd * h / t
FzRl = W * a / l * (tr / t) + .5 * m * ud * h / l - .5 * m * vd * h / t
FzRr = W * a / l * (tl / t) + .5 * m * ud * h / l + .5 * m * vd * h / t
RETURN

14000 ' ********************  Calculate tyres k  ***************************
' Inputs -  Alfa, Fx
'=======================
IF RWD THEN
kfl = 0
kfr = 0
'====
Fz = FzRl
Fx = FxRl
alfa = arl
Vcx = Url1
GOSUB 1000001
kRl = K
'====
Fz = FzRr
Fx = FxRr
alfa = arr
Vcx = Urr1
GOSUB 1000001
kRr = K
'====
END IF
'=========================
IF FWD THEN
'====
```

```
kRl = 0
kRr = 0
'====
Fz = FzFl
Fx = FxFl
alfa = afl
Vcx = Ufl1
GOSUB 1000001
kfl = K
'====
Fz = FzFr
Fx = FxFr
alfa = afr
Vcx = Ufr1
GOSUB 1000001
kfr = K
'====
END IF

'=========================
IF AWD THEN
'====
Fz = FzRl
Fx = FxRl
alfa = arl
Vcx = Url1
GOSUB 1000001
kRl = K
'====
Fz = FzRr
Fx = FxRr
alfa = arr
Vcx = Urr1
GOSUB 1000001
kRr = K
'====
Fz = FzFl
Fx = FxFl
alfa = afl
Vcx = Ufl1
GOSUB 1000001
kfl = K
'====
Fz = FzFr
Fx = FxFr
alfa = afr
Vcx = Ufr1
GOSUB 1000001
kfr = K
'====
END IF

'=========================
IF NWD THEN
kRl = 0
kRr = 0
kfl = 0
kfr = 0
END IF
RETURN

15000 ' ********************** Calculate tyres Forces ***************************
```

```
' Inputs -  tyres Alfa, k and Fz
nod = CINT(Rl / (uv * dt))
IF nod = 0 THEN nod = 1

Fz = FzFl
K = kfl
alfa = afl
Vcx = Ufl1
Vcy = Vfl1
Vsx = Vsxfl
GOSUB 100000 ' MF Tyre Model
FxFl = Fx
 FOR nn = nod TO 2 STEP -1
 FyFl(nn) = FyFl(nn - 1)
 NEXT nn
 FyFl(1) = Fy
 Segma = 0
 FOR nn = 1 TO nod
 Segma = Segma + FyFl(nn)
 NEXT nn
 FyFl = Segma / nod

 Fz = FzFr
 K = kfr
 alfa = afr
 Vcx = Ufr1
 Vcy = Vfr1
 Vsx = Vsxfr
 GOSUB 100000 ' MF Tyre Model
 FxFr = Fx
 FOR nn = nod TO 2 STEP -1
 FyFr(nn) = FyFr(nn - 1)
 NEXT nn
 FyFr(1) = Fy
 Segma = 0
 FOR nn = 1 TO nod
 Segma = Segma + FyFr(nn)
 NEXT nn
 FyFr = Segma / nod

 Fz = FzRl
 K = kRl
 alfa = arl
 Vcx = Url1
 Vcy = Vrl1
 Vsx = Vsxrl
 GOSUB 100000 ' MF Tyre Model
 FxRl = Fx
 FOR nn = nod TO 2 STEP -1
 FyRl(nn) = FyRl(nn - 1)
 NEXT nn
 FyRl(1) = Fy
 Segma = 0
 FOR nn = 1 TO nod
 Segma = Segma + FyRl(nn)
 NEXT nn
 FyRl = Segma / nod

 Fz = FzRr
 K = kRr
 alfa = arr
 Vcx = Urr1
```

```
Vcy = Vrr1
Vsx = Vsxrr
GOSUB 100000 ' MF Tyre Model
FxRr = Fx
FOR nn = nod TO 2 STEP -1
FyRr(nn) = FyRr(nn - 1)
NEXT nn
FyRr(1) = Fy
Segma = 0
FOR nn = 1 TO nod
Segma = Segma + FyRr(nn)
NEXT nn
FyRr = Segma / nod
RETURN
    •
1000 ' ********************  Read Vehicle Data ******************************
IF ferrari THEN
a = 1.234   'Reviewed
b = 1.022   'Reviewed
l = a + b
m = 1008
I = 1031
Cf = 117440 * dtr 'N/deg
Cr = 144930 * dtr 'N/deg
W = m * 9.81 'N
h = .4
t = 1.4
tr = .7
tl = .7
ELSE  ' Buick
a = 1.488
b = 1.712
l = a + b
m = 2045
I = 5428
Cf = 77850 * dtr 'N/deg
Cr = 76510 * dtr 'N/deg
W = m * 9.81 'N
h = .5
t = 1.5
tr = .75
tl = .75
END IF

'********************************* Initial Data ***********************************
'  X-Y Location
CGx0 = 0
CGy0 = 0
CGt0 = 0
Flx0 = a
Fly0 = tl
Frx0 = a
Fry0 = -tr
Rlx0 = -b
Rly0 = tl
Rrx0 = -b
Rry0 = -tr
rfl = SQR(tl ^ 2 + a ^ 2)
rrl = SQR(tl ^ 2 + b ^ 2)
rrr = SQR(tr ^ 2 + b ^ 2)
rfr = SQR(tr ^ 2 + a ^ 2)
```

```
'Initial Fz
FzFl = W * b / l * (tr / t)
FzFr = W * b / l * (tl / t)
FzRl = W * a / l * (tr / t)
FzRr = W * a / l * (tl / t)

' Initial Speeds and Accelerations
v0 = 0
thetad0 = 0
ud = 0
vd = 0

Ufl0 = u0
Ufr0 = u0
Url0 = u0
Urr0 = u0

Ufl1 = u0
Ufr1 = u0
Url1 = u0
Urr1 = u0

' ===========    Summing    ===========
CGtheta = 0
CGyt = 0
CGxt = 0
RETURN

2000 ' ************************  Read Tyre Data  ********************************
'============== Costants ===============
Ro = .313     '      Tyre unloaded radius
Vo = 16.67        '      reference velocity
Fzo = 4000    '      rated load
Am = 10

' X dirrection---==========
Pcx1 = 1.685
Pdx1 = 1.21
Pdx2 = -.037
Pex1 = .344
Pex2 = .095
Pex3 = -.02
Pex4 = 0
Pkx1 = 21.51
Pkx2 = -.163
Pkx3 = .245
Phx1 = -.002
Phx2 = .002
Pvx1 = 0
Pvx2 = 0
Rbx1 = 12.35
Rbx2 = -10.77
Rcx1 = 1.092
Rhx1 = .007
qsx1 = 0
qsx2 = 0
qsx3 = 0

' Y direction ====================
Pcy1 = 1.193
Pdy1 = -.99
```

```
Pdy2 = .145
Pdy3 = -11.23
Pey1 = -1.003
Pey2 = -.537
Pey3 = -.083
Pey4 = -4.787
Pky1 = -14.95
Pky2 = 2.13
Pky3 = -.028
Phy1 = .003
Phy2 = -.001
Phy3 = .075
Pvy1 = .045
Pvy2 = -.024
Pvy3 = -.532
Pvy4 = .039
Rby1 = 6.461
Rby2 = 4.196
Rby3 = -.015
Rcy1 = 1.081
Rhy1 = .009
Rvy1 = .053
Rvy2 = -.073
Rvy3 = .517
Rvy4 = 35.44
Rvy5 = 1.9
Rvy6 = -10.71

'Z Direction ========================
qbz1 = 8.964
qbz2 = -1.106
qbz3 = -.842
qbz5 = -.227
qbz6 = 0
qbz9 = 18.47
qbz10 = 0
qcz1 = 1.18
qdz1 = .1
qdz2 = -.001
qdz3 = .007
qdz4 = 13.05
qdz6 = -.008
qdz7 = .0001
qdz8 = -.296
qdz9 = -.009
qez1 = -1.609
qez2 = -.359
qez3 = 0
qez4 = .174
qez5 = -.896
qhz1 = .007
qhz2 = -.002
qhz3 = .147
qhz4 = .004
ssz1 = .043
ssz2 = .001
ssz3 = .731
ssz4 = -.238

' Other factors
qiay = .109
qma = .237
```

```
qcbxo = 121.4
qcbxz = 121.4
qkbx = .228
qkbz = .228
qcbtz = 61.96
qiaxz = .071
qmb = .763
qcby = 40.05
qkby = .284
qcbg = 20.33
qcbe = 20.33
qiby = .696
qmc = .108
qccx = 391.9
qkcx = .91
qcce = 55.82
qibxz = .357
qccy = 62.7
qkcy = .91
qkbt = .08
qic = .055
qkbg = .038
qkbe = .038
qkce = .834

qv1 = .000071
qsy1 = .01
qsy2 = 0
qa1 = .135
breff = 9
qfcx1 = .1
qv2 = 2.489
qsy3 = 0
qa2 = .035
dreff = .23
qfcy1 = .3
qfz1 = 13.37
qsy4 = 0
qbvx = 3.957
qbcz = 3.957
freff = .01
qfcx2 = 0
qfz2 = 14.35
qbvt = 3.957
qfcy2 = 0

' Lambda factors
lfzo = 1
lmx = 1
lmy = 1
lmv = 0
lkxk = 1
lkya = 1
lcx = 1
lcy = 1
lex = 1
ley = 1
lhx = 1
lhy = 1
lvx = 1
lvy = 1
lkyg = 1
```

```
lkzg = 1
lt = 1
lmr = 1

lxa = 1
lyk = 1
lvyk = 1
ls = 1

lcz = 1
lmx = 1
lmy = 1

E0 = 1
E1 = 1
E2 = 1
E3 = 1
E4 = 1
E5 = 1
E6 = 1
E7 = 1
E8 = 1

eitavx = .00000001#
eitax = .00000001#
eitay = .00000001#
RETURN

100000
IF Fz < 0 THEN PRINT aaaa, "Fz < 0": END
G = 0
alfa = -1 * alfa

' ============== Longitudinal (Pure Long. slip) ====================

' ============== Costants ===============
Ro = .313                          ' Tyre unloaded radius
Vo = uv                            ' reference velocity
Fzo = 4000                         ' rated load
Am = 10

' ********************** Precalculations
Fzodash = Fzo * lfzo
dfz = (Fz - Fzodash) / Fzodash
astar = (-1 * Vcy / ABS(Vcx)) ' ### = TAN(a) * SGN(Vcx)
Gstar = SIN(G)
lmxstar = lmx / (1 + lmv * (Vs / Vo))
lmystar = lmy / (1 + lmv * (Vs / Vo))
lmydash = Am * lmystar / (1 + (Am - 1) * lmystar)
lmxdash = Am * lmxstar / (1 + (Am - 1) * lmxstar)

' ===========  Longitudinal Pure Slip ==========
Mx = (Pdx1 + Pdx2 * dfz) * lmxstar       '(>0)
Dx = Mx * Fz * E1
Cx = Pcx1 * lcx
Kxk = Fz * (Pkx1 + Pkx2 * dfz) * EXP(Pkx3 * dfz) * lkxk
Bx = Kxk / (Cx * Dx + eitax)
Shx = (Phx1 + Phx2 * dfz) * lhx
kx = K + Shx
Ex = (Pex1 + Pex2 * dfz + Pex3 * dfz ^ 2) * (1 - Pex4 * SGN(kx)) * lex
'(<=1)
```

```
Svx = Fz * (Pvx1 + Pvx2 * dfz) * (ABS(Vcx) / (eitavx + ABS(Vcx))) * lvx *
lmxdash * E1
Fxo = Dx * SIN(Cx * ATN(Bx * kx - Ex * (Bx * kx - ATN(Bx * kx)))) + Svx

'=============== Lateral (Pure Lateral slip) ====================
My = (Pdy1 + Pdy2 * dfz) * (1 - Pdy3 * Gstar ^ 2) * lmystar  ' (>0)
Dy = My * Fz * E2
Cy = Pcy1 * lcy
kyao = Pky1 * Fzodash * SIN(2 * ATN(Fz / (Pky2 * Fzodash))) * lkya
Kya = kyao * (1 - Pky3 * Gstar ^ 2) * E3
By = Kya / (Cy * Dy + eitay)
Shy = (Phy1 + Phy2 * dfz) * lhy + Phy3 * Gstar * lkyg * E0 + E4 - 1
ay = astar + Shy
Ey = (Pey1 + Pey2 * dfz) * (1 - (Pey3 + Pey4 * Gstar) * SGN(ay)) * ley  '(<=1)
Svy = Fz * ((Pvy1 + Pvy2 * dfz) * lvy + (Pvy3 + Pvy4 * dfz) * Gstar * lkyg) *
lmydash * E2
Fyo = Dy * SIN(Cy * ATN(By * ay - Ey * (By * ay - ATN(By * ay)))) + Svy
Kygo = (Phy3 * kyao + Fz * (Pvy3 + Pvy4 * dfz)) * lkyg   ' for Mz Calculations


'=============== Longitudinal combined ====================
Exa = Rex1 + Rex2 * dfz
Bxa = Rbx1 * COS(ATN(Rbx2 * K)) * lxa
Cxa = Rcx1    ' (>0)
Shxa = Rhx1
as1 = astar + Shxa
Gxao = COS(Cxa * ATN(Bxa * Shxa - Exa * (Bxa * Shxa - ATN(Bxa * Shxa))))
Gxa = COS(Cxa * ATN(Bxa * as1 - Exa * (Bxa * as1 - ATN(Bxa * as1)))) / Gxao
Fx = Gxa * Fxo

'=============== Lateral combined ==========================
Cyk = Rcy1
Byk = Rby1 * COS(ATN(Rby2 * (astar - Rby3))) * lyk
Shyk = Rhy1 + Rhy2 * dfz    '  (<0.1 drive slip)
Dvyk = My * Fz * (Rvy1 + Rvy2 * dfz + Rvy3 * Gstar) * COS(ATN(Rvy4 * astar)) *
E2
Svyk = Dvyk * SIN(Rvy5 * ATN(Rvy6 * K))
Eyk = Rey1 + Rey2 * dfz
ks = K + Shyk
Gyko = COS(Cyk * ATN(Byk * Shyk - Eyk * (Byk * Shyk - ATN(Byk * Shyk))))
Gyk = COS(Cyk * ATN(Byk * ks - Eyk * (Byk * ks - ATN(Byk * ks)))) / Gyko

Fy = Gyk * Fyo + Svyk
Fy = -Fy    ' Test
RETURN

99999 '*****************************  Printing  *********************************
IF prn THEN
IF Pstart = 0 THEN
PRINT #1, " ", "Time", "Delta", "Delfl", "Delfr", "Delrl", "Delrr", "CGx",
"CGy", "CGt", "CGxt", "CGyt", "CGtheta", "XA  ", "YA  ", "vA  ", "Ththet",
"Ththetd", "Ththetdd", "CM", "Orl", "Orr", "dFx", "kfl", "kfr", "krl", "krr",
"xfl", "xfr", "xrl", "xrr", "yfl", "yfr", "yrl", "yrr", "afl", "afr", "arl",
"arr", "afl-deg", "afr-deg", "arl-deg", "arr-deg", "FzFl", "FzFr", "FzRl",
"FzRr", "FyFl", "FyFr", "FyRl", "FyRr", "FxFl", "FxFr", "FxRl", "FxRr", "Fxt",
"Fyt", "Momt", "ud", "vd", "thetadd", "uv", "vv", "thetadv", "DvTheta",
"thetadvdeg", "mom1", "mom2", "mom3", "mom4", "Srr", "ry/rx", "Ufr1", "Ufl1",
"Urr1", "Url1", "R", "Rv", "an", "Tc", "Td", "Tdo", "Oc", "Od"

pstart = 1
END IF
```

```
PRINT #1, USING " ########.###### "; aaaa * dt; d * 180 / pi; delfl * 180 /
pi; delfr * 180 / pi; delrl * 180 / pi; delrr * 180 / pi; CGx; CGy; CGt; CGxt;
CGyt; CGtheta; XA; YA; vA; Ththet * 180 / pi; Ththetd * 180 / pi; Ththetdd *
180 / pi; CM; Orl ; Orr; dfx; kfl; kfr; kRl; kRr; flx; frx; rlx; rrx; fly;
fry; rly; rry; afl; afr; arl; arr; afl * 180 / pi; afr * 180 / pi; arl * 180 /
pi; arr * 180 / pi; FzFl; FzFr; FzRl; FzRr; FyFl; FyFr; FyRl; FyRr; FxFl;
FxFr; FxRl; FxRr; Fxt; Fyt; Momt; ud; vd; thetadd; uv; vv; thetadv; DvTheta;
thetadv * 180 / pi; mom1; mom2; mom3; mom4; Srr; ((rry - Rry0) / (rrx -
Rrx0)); Ufr1; Ufl1; Urr1; Url1; r; Rv; an; Tc; Td; Tdo; Oc; Od
END IF
RETURN
16000 ' ********************** Get  ready for next stage  **********************
u0 = uv * COS(DvTheta) + vv * SIN(DvTheta)
v0 = vv * COS(DvTheta) - uv * SIN(DvTheta)
thetad0 = thetadv
CGyt = CGyt + CGy * COS(CGtheta) + CGx * SIN(CGtheta)
CGxt = CGxt + CGx * COS(CGtheta) - CGy * SIN(CGtheta)
CGtheta = CGtheta + CGt

Ufl0 = Ufl1
Ufr0 = Ufr1
Url0 = Url1
Urr0 = Urr1

Vfl0 = Vfl1
Vfr0 = Vfr1
Vrl0 = Vrl1
Vrr0 = Vrr1

'******************************** Printing to screen ***************************
IF scr THEN
PSET (CGxt, CGyt), 15
END IF
RETURN

1000001
'************************ Inputs *********
Fxs = Fx
'****************************************** Vehicle data
fxout = 0

'********************************* Model Test Test Test
' ======================== Initial settings for iteration
ki = 0
start = 0
acc = 2         'Starting accuracy .1^acc
K = ki

' ======================================  Iteration
7340 '---------------------------- Direction control
'     --------------- Initial error (at k=0)
K = ki
GOSUB 212000
Fxtest = Fx         'For Testing if Fx out of range
err0 = Fxs - Fx

'     --------------- Posetive direction error
K = ki + .1 ^ acc
GOSUB 212000
ep = Fxs - Fx
```

```
'      --------------- Decision
IF SGN(ep) <> SGN(err0) THEN
p = 1
GOTO 7530
END IF

IF ABS(ep) < ABS(err0) THEN
p = 1
ELSE
p = -1
END IF
7530

7540 '--------------------------------- Proceed - Crawling
K = ki + p * .1 ^ acc
k0 = ki
k1 = K
GOSUB 212000
err1 = Fxs - Fx

'----------------------------------- Check if Fx out of range
IF Fxtest > Fx THEN
        IF p = 1 THEN
        fxout = 1
        GOTO 8888
        END IF
END IF
IF Fxtest < Fx THEN
        IF p = -1 THEN
        fxout = 1
        GOTO 8888
        END IF
END IF
Fxtest = Fx
'---------------------------------- Check Signe chang
IF SGN(err0) = SGN(err1) THEN
err0 = err1
ki = K
GOTO 7540
END IF

7543 '------------------------------ Flip Flop
ks = k0 + p * ABS(((k1 - k0) / (err1 - err0)) * err0)
K = ks
GOSUB 212000
errs = Fxs - Fx
IF ABS(errs) <= .01 THEN
        GOTO 8888
ELSE
        IF SGN(errs) = SGN(err0) THEN
                k0 = ks
                err0 = errs
        ELSE
                k1 = ks
                err1 = errs
        END IF
END IF
GOTO 7543
GOTO 8888

212000 ' ************************ kcal routine  ********************************
```

```
IF start = 0 THEN
start = 1
'============== Longitudinal (Pure Long. slip) =====================
' ============== Costants ================
Ro = .313     '     Tyre unloaded radius
Vo = 16.667       '     reference velocity
Fzo = 4000    '     rated load
Am = 10

' ============== Variables ================
G = 0         '     Camber angle
' ********************** Precalculations
Gstar = SIN(G)
lmxstar = lmx / (1 + lmv * (Vs / Vo))
lmystar = lmy / (1 + lmv * (Vs / Vo))
lmydash = Am * lmystar / (1 + (Am - 1) * lmystar)
lmxdash = Am * lmxstar / (1 + (Am - 1) * lmxstar)
Fzodash = Fzo * lfzo
dfz = (Fz - Fzodash) / Fzodash
Mx = (Pdx1 + Pdx2 * dfz) * lmxstar
Dx = Mx * Fz * E1
Cx = Pcx1 * lcx
Kxk = Fz * (Pkx1 + Pkx2 * dfz) * EXP(Pkx3 * dfz) * lkxk
Bx = Kxk / (Cx * Dx + eitax)
Shx = (Phx1 + Phx2 * dfz) * lhx

'== Longitudinal combined ==
Exa = Rex1 + Rex2 * dfz
Cxa = Rcx1     ' (>0)
Shxa = Rhx1
END IF ' Of start = 0 ***************************** start = 0start = 0
astar = TAN(alfa * pi / 180) * SGN(Vcx)

' ===============  Longitudinal Pure Slip ==================
kx = K + Shx
Ex = (Pex1 + Pex2 * dfz + Pex3 * dfz ^ 2) * (1 - Pex4 * SGN(kx)) * lex
'(<=1)
Svx = Fz * (Pvx1 + Pvx2 * dfz) * (ABS(Vcx) / (eitavx + ABS(Vcx))) * lvx *
lmxdash * E1
Fxo = Dx * SIN(Cx * ATN(Bx * kx - Ex * (Bx * kx - ATN(Bx * kx)))) + Svx

'===============  Longitudinal combined ==================
Bxa = Rbx1 * COS(ATN(Rbx2 * K)) * lxa        '(>0)
Gxao = COS(Cxa * ATN(Bxa * Shxa - Exa * (Bxa * Shxa - ATN(Bxa * Shxa))))
as1 = astar + Shxa
Gxa = COS(Cxa * ATN(Bxa * as1 - Exa * (Bxa * as1 - ATN(Bxa * as1)))) / Gxao
Fx = Gxa * Fxo
RETURN

121000
' ============== Costants ================
Ro = .313         '     Tyre unloaded radius
Vo = 16.67        '     reference velocity
Fzo = 4000        '     rated load
Am = 10
' X dirrection---=========
Pcx1 = 1.685
Pdx1 = 1.21
Pdx2 = -.037
Pex1 = .344
Pex2 = .095
```

```
Pex3 = -.02
Pex4 = 0
Pkx1 = 21.51
Pkx2 = -.163
Pkx3 = .245
Phx1 = -.002
Phx2 = .002
Pvx1 = 0
Pvx2 = 0
Rbx1 = 12.35
Rbx2 = -10.77
Rcx1 = 1.092
Rhx1 = .007
qsx1 = 0
qsx2 = 0
qsx3 = 0

' Y direction ======================
Pcy1 = 1.193
Pdy1 = -.99
Pdy2 = .145
Pdy3 = -11.23
Pey1 = -1.003
Pey2 = -.537
Pey3 = -.083
Pey4 = -4.787
Pky1 = -14.95
Pky2 = 2.13
Pky3 = -.028
Phy1 = .003
Phy2 = -.001
Phy3 = .075
Pvy1 = .045
Pvy2 = -.024
Pvy3 = -.532
Pvy4 = .039
Rby1 = 6.461
Rby2 = 4.196
Rby3 = -.015
Rcy1 = 1.081
Rhy1 = .009
Rvy1 = .053
Rvy2 = -.073
Rvy3 = .517
Rvy4 = 35.44
Rvy5 = 1.9
Rvy6 = -10.71

'Z Direction ========================
qbz1 = 8.964
qbz2 = -1.106
qbz3 = -.842
qbz5 = -.227
qbz6 = 0
qbz9 = 18.47
qbz10 = 0
qcz1 = 1.18
qdz1 = .1
qdz2 = -.001
qdz3 = .007
qdz4 = 13.05
qdz6 = -.008
```

```
qdz7 = .0001
qdz8 = -.296
qdz9 = -.009
qez1 = -1.609
qez2 = -.359
qez3 = 0
qez4 = .174
qez5 = -.896
qhz1 = .007
qhz2 = -.002
qhz3 = .147
qhz4 = .004
ssz1 = .043
ssz2 = .001
ssz3 = .731
ssz4 = -.238

' Other factors
qiay = .109
qma = .237
qcbxo = 121.4
qcbxz = 121.4
qkbx = .228
qkbz = .228
qcbtz = 61.96
qiaxz = .071
qmb = .763
qcby = 40.05
qkby = .284
qcbg = 20.33
qcbe = 20.33
qiby = .696
qmc = .108
qccx = 391.9
qkcx = .91
qcce = 55.82
qibxz = .357
qccy = 62.7
qkcy = .91
qkbt = .08
qic = .055
qkbg = .038
qkbe = .038
qkce = .834

qv1 = .000071
qsy1 = .01
qa1 = .135
breff = 9
qfcx1 = .1
qv2 = 2.489
qsy3 = 0
qa2 = .035
dreff = .23
qfcy1 = .3
qfz1 = 13.37
qsy4 = 0
qbvx = 3.957
qbcz = 3.957
freff = .01
qfcx2 = 0
qfz2 = 14.35
```

```
qbvt = 3.957
qfcy2 = 0

' Lambda factors
lfzo = 1
lmx = 1
lmy = 1
lmv = 0
lkxk = 1
lkya = 1
lcx = 1
lcy = 1
lex = 1
ley = 1
lhx = 1
lhy = 1
lvx = 1
lvy = 1
lkyg = 1
lkzg = 1
lt = 1
lmr = 1

lxa = 1
lyk = 1
lvyk = 1
ls = 1

E0 = 1
E1 = 1
E2 = 1
E3 = 1
E4 = 1
E5 = 1
E6 = 1
E7 = 1
E8 = 1

eitavx = .00001
eitax = .00001
eitay = .00001
RETURN


8888
IF fxout = 1 THEN PRINT " ****************** Out ****************"
start = 0
RETURN


2100 ' ******************  Initial Tyre forces   ****************"
FzFl = W * b / l * (tr / t) - .5 * m * ud * h / l - .5 * m * vd * h / t
FzFr = W * b / l * (tl / t) - .5 * m * ud * h / l + .5 * m * vd * h / t
FzRl = W * a / l * (tr / t) + .5 * m * ud * h / l - .5 * m * vd * h / t
FzRr = W * a / l * (tl / t) + .5 * m * ud * h / l + .5 * m * vd * h / t

FxRfl = (2 / pi * (qsy1 + qsy2 * FxFl) * FzFl * ATN(u0) * lmy) / Ro
FxRfr = (2 / pi * (qsy1 + qsy2 * FxFr) * FzFr * ATN(u0) * lmy) / Ro
FxRrl = (2 / pi * (qsy1 + qsy2 * FxRl) * FzRl * ATN(u0) * lmy) / Ro
FxRrr = (2 / pi * (qsy1 + qsy2 * FxRr) * FzRr * ATN(u0) * lmy) / Ro
RETURN
```